FOSSIL ENERGY

DOE/MC/08383-45
Vol. 2 of 2

LITTLE KNIFE FIELD CO_2 MINITEST, BILLINGS COUNTY, NORTH DAKOTA

Final Report

Volume II: Appendices

Work Performed for the Department of Energy
Under Contract No. DE-AC21-79MC08383

Date Published—July 1983

Gulf Oil Exploration and Production Company
Oklahoma City, Oklahoma

National Petroleum Technology Office
U.S. DEPARTMENT OF ENERGY
Tulsa, Oklahoma

DISCLAIMER

This report was prepared as an account of work sponsored by an agency of the United States Government. Neither the United States Government nor any agency thereof, nor any of their employees, makes any warranty, expressed or implied, or assumes any legal liability or responsibility for the accuracy, completeness, or usefulness of any information, apparatus, product, or process disclosed, or represents that its use would not infringe privately owned rights. Reference herein to any specific commercial product, process, or service by trade name, trademark, manufacturer, or otherwise does not necessarily constitute or imply its endorsement, recommendation, or favoring by the United States Government or any agency thereof. The views and opinions of authors expressed herein do not necessarily state or reflect those of the United States Government.

This report has been reproduced directly from the best available copy.

DOE/MC/08383-45
Vol. 2 of 2
Distribution Category UC-92a

LITTLE KNIFE FIELD CO_2 MINITEST, BILLINGS COUNTY, NORTH DAKOTA

Final Report

Volume II: Appendices

James E. Upton, *Principal Investigator*
Gulf Oil Exploration and Production Company
P.O. Box 24100
Oklahoma City, Oklahoma 73124

Kenneth L. Spence, *Technical Project Officer*
Bartlesville Energy Technology Center
P.O. Box 1398
Bartlesville, Oklahoma 74005

Work Performed for the Department of Energy
Under Contract No. DE-AC21-79MC08383

Date Published—July 1983

UNITED STATES DEPARTMENT OF ENERGY

TABLE OF CONTENTS

		Page
APPENDIX 29 -	Little Knife Field CO_2 Minitest Water Injection Simulation, Billings County, North Dakota	1
APPENDIX 30 -	Design of a CO_2-Water Injection Program for the Little Knife CO_2 Flood Minitest	53
APPENDIX 31 -	Little Knife CO_2 Flood Residual Oil and CO_2-Water Relative Permeability Measurements	77
APPENDIX 42 -	Analysis of Observation Well #4 Pressure Core Data - Little Knife CO_2 Project	96
APPENDIX 43 -	Little Knife Field CO_2 Minitest Compositional Simulation	117
APPENDIX 44 -	An Equation-of-State Study on the Fluid Properties, Phase Behavior and Multiple-contact Miscibility in Carbon Dioxide Displacement Processes	263
APPENDIX 45 -	Analysis of Observation Well Saturation Data	329
APPENDIX 47 -	Corrosion Study for Little Knife CO_2 Minitest	389

APPENDIX 29

LITTLE KNIFE FIELD CO_2 MINITEST

WATER INJECTION SIMULATION

BILLINGS COUNTY, NORTH DAKOTA

Supervised by:

G. C. Thakur

By

R. W. Rasor
R. B. Haulenbeek
R. A. Avenshine

Reservoir Services Department
Gulf Research & Development Company
Houston Technical Services Center
Houston, Texas

TABLE OF CONTENTS

		Page
I.	Summary and Conclusions	3
II.	Introduction	4
III.	Discussion	6
IV.	Acknowledgements	17
V.	Nomenclature	17
VI.	References	17
	Sub-Appendix A	43

LIST OF TABLES

1	Well Identification	18
2	Individual Well Perforated Interval	19
3	Water Saturation Functions: Rock Type 1	20
4	Water Saturation Functions: Rock Type 2	20
5	Water Saturation Functions: Rock Type 3	21
6	PVT Properties for Oil	21
7	Problem Parameters	22
8	Factor for Allocating Production to Included Layers	22
9	Summary of Prediction Cases	23
10	Well Productivity Index Used in Declining Rate Case	24
11	Pressure Summary of Prediction Case Results	24

LIST OF FIGURES

1	Pilot Location	25
2A	Grid System Overlay	26
2B	Surface Location Map	26
3	Porosity-Permeability Relationship	27
4	Water Capillary Pressure	28
5	Oil-Water Relative Permeability	29
6	Oil Formation Volume Factor	30
7	Gas Solubility	31
8	Oil Viscosity	32
9	History Match - Well 2	33
10	History Match - Well 3	34
11	History Match - Well 5	35
12	History Match - Well 6	36
13	History Match - Well 7	37
14	History Match - Well 8	38
15	History Match - Well 9	39
16	History Match - Well 10	40
17	Calculated Field History	41
18	Prediction Case Comparison	42
A-1	Layer II Structure Top Map	43
A-2	Layer I Gross Thickness Map	44
A-3	Layer I Net Thickness Map	45
A-4	Layer I Average Porosity Map	46
A-5	Layer II Gross Thickness Map	47
A-6	Layer II Net Thickness Map	48
A-7	Layer II Average Porosity Map	49
A-8	Layer III Gross Thickness Map	50
A-9	Layer III Net Thickness Map	51
A-10	Layer III Average Porosity Map	52

I. SUMMARY AND CONCLUSIONS

A study of the water injection phase of the Little Knife CO_2 minitest has been completed using a three-dimensional, three-phase black oil simulator. The study was designed to investigate the water injection requirements for repressurization and the effects of the injection on the reservoir. An accurate reservoir characterization was necessary to accomplish this goal. It is believed that by including a detailed description of reservoir properties and production history, a good reservoir characterization was obtained. Using the resultant reservoir model, several prediction cases were run to simulate the effects of various injection plans on the minitest area. These cases included two injection start up dates and two different future production performance schedules.

The following conclusions are drawn, based upon the results of this study:

1. The pressure in the minitest area will be raised above the calculated minimum CO_2 miscibility pressure of 3400 psig, if water injection is begun on either October 1, 1980 or September 1, 1980.
2. A water injection rate of 1150 STB/D, for fifteen (15) days, will adequately repressure the pilot area if the above dates are observed.
3. The current rate of reservoir fluid withdrawal will not adversely affect the pilot area if the aforementioned injection plan is utilized.
4. Water injection in the pilot area will not strongly affect the average reservoir pressure in the D-zone of the Little Knife field.

II. INTRODUCTION

Oil production from the Little Knife field started in early 1977 and by August 1, 1978, about 2 MMSTB of oil had been produced out of an estimated 160 MMSTB of original oil-in-place. The producing zone in this field is Mission Canyon consisting of multiple reservoirs. An enhanced recovery method employing CO_2 appears to be applicable in this field. The "D-zone" in this field has been selected for investigating the applicability of CO_2 miscible flooding.

A proposal for a joint DOE-Gulf Oil Corporation minitest of a CO_2 miscible flood was submitted to DOE on September 8, 1978 (Dept. of Energy RFP No. EW-78-R-21-8383). The objective of the proposal was "...to confirm by field testing the results of laboratory displacement tests and to show that the CO_2 miscible displacement process has potential for commercialization in Southwestern U.S. and Rocky Mountain area carbonate oil reservoirs that have not been extensively waterflooded and have a high remaining oil saturation." This contract was awarded to Gulf on December 13, 1978 and the final negotiation was completed on July 17, 1979.

The minitest considers field testing of the CO_2 miscible displacement process in the Mission Canyon Formation of the Little Knife field. A WAG (water-and-gas) type injection sequence involving alternate slugs of water and CO_2 is being considered. This test is designed to establish the incremental recovery by a miscible CO_2 flood.

Little Knife reservoir fluid samples have been used to estimate the pressure at which multiple contact miscibility is developed during CO_2 displacement. This pressure is approximately equal to 3400 psig.

The minitest for this project consists of an injection well offset by three (3) observation/production wells. A fifth well will be drilled behind the front and cored with a pressure-retaining core barrel. Design of the CO_2 and water injection sequence is being conducted by a compositional simulator sensitivity study in the minitest area and by experimental laboratory tests on field cores. Log measurements of saturation changes, produced fluids analysis, and pressure measurements in the observation wells will help in interpreting the test results. These results will then be used to predict the technical and economic performance of a field demonstration test.

The work associated with this project is divided into five (5) phases:

<u>Phase I</u>: Location and Drilling of Minitest Pattern

<u>Phase II</u>: Laboratory Determination of CO_2/Water Displacement Parameters in Reservoir Cores

<u>Phase III</u>: Minitest Area CO_2 Simulation

<u>Phase IV</u>: Injection Period, Performance Data Acquisition and Interpretation

<u>Phase V</u>: Projection of CO_2 Flood Performance to Commercial Scale

This report describes the results of a part of Phase III work; namely, Little Knife CO_2 minitest water injection simulation. The work was conducted to find the volume and rate of water injection into the minitest injection well so that the pressure in this area could be raised above the minimum multiple contact miscibility pressure of 3400 psig. The injection rate, time requirement, and pilot area response were also computed during this study. In order to determine these, a

numerical reservoir simulator was utilized to match the historical performance of the minitest area and to predict the future performance of the area under various operating plans.

The report first presents reservoir description and geology. It next describes the simulation of the past history. Input data used in this model study are described in detail. Finally, a description of each prediction case is presented, together with a discussion of the results.

III. DISCUSSION

A. RESERVOIR DESCRIPTION AND GEOLOGY

1. Geologic Description

Little Knife field is located near the center of the Williston Basin and south of the Nesson Anticline in portions of Billings, Dunn, and McKenzie counties, North Dakota. Production is from the lower Mississippian Mission Canyon formation at a depth of approximately 9800 feet. The field is formed across a broad low anticlinal flexure plunging northward along a north-south axis exhibiting a subtle structural relief averaging less than one degree. The hydrocarbon accumulation is primarily a composite diagenetic-structural feature with a lesser component of stratigraphic entrapment.

The reservoir rock of interest consists primarily of dolomite and dolomitic limestone. The reservoir sequences have undergone a dissolution leaching action during dolomitization resulting in a wide range of porosities and permeabilities within each sequence.

2. Layering

Log correlations based on sonic log responses delineated the presence of key beds and helped in breaking the section into five zones: A, B, C, D and E. The central portion of the field showed multiple hydrocarbon accumulations scattered throughout the B, C and D zones. The area of interest for the Little Knife minitest water injection simulation consisted of the D-zone and some zones above. For modeling purposes, the strata were divided into three porous layers: I - the middle C zone; II - the D zone overlapping into the C; and III - the lower D zone. This division was accomplished using a 7% porosity cut off as the gross thickness delimeter. The net thickness was found using an 8% porosity limit. Vertical communication was present between layers in the southwest portion of the field. Moving toward the northeast, this communication vanished because of increased layer separation.

Modern wireline logs were run on 47 of the 49 wells penetrating the D zone reservoir. GULFLOG computer processed interpretations were performed on each well. These interpretations produced a foot-by-foot determination of lithology fractions, porosity and water saturation. Reservoir characterization maps were prepared for Layers I, II and III (above). Appendix A contains: structure top, gross and net thickness, and average porosity maps for each layer.

B. PERFORMANCE HISTORY REVIEW

The available field performance data were reviewed and qualified, before the water injection simulation phase of the minitest project was performed.

1. Area of Interest

The minitest site is located in the central portion of the field, northwest of the section center, Section 3, T144N, R98W, Billings County (Figure 1). Since the

test pattern consisted of a single injection well offset by three observation wells arranged in an inverted four-spot configuration, it was estimated that a small portion of the total field would be affected by the pilot. Therefore, only an area immediately surrounding the minitest and enclosing 2600 acres was modeled. Only eight producing wells in the area were considered to significantly influence the pilot. Thus, only these wells were included in the simulation model. The well designation, location and name are presented in Table 1.

2. Producing Ratios

The use of the water-oil and gas-oil ratios as matching parameters for the eight wells was severely restricted. The WOR was not used as a time dependent history matching characteristic, because the oil production from the included wells was essentially water free. Also, lack of information on the mobilities in various zones restricted allocation of water production. Likewise, the GOR was not useful since the reservoir remained above the saturation pressure during the period studied.

3. Production and Pressure Reports

The individual well pressure histories were the only useful time dependent history matching parameter; however, these pressures were somewhat unreliable. Because of the aforementioned A, B, C, D and E zonation, individual well performance data was recorded according to zone. It was not possible to allocate production to individual horizons because of the presence of multi-zone comple-

tions. Both production and pressure values were assigned to combinations of zones depending on the zones perforated in each wellbore. Table 2 compares the perforated intervals to the model layer definition for each well. The multi-zone completions resulted in the reported static bottom hole pressures representing an average pressure for the completed zones.

C. SIMULATION OF PAST HISTORY

1. Model Description

A three-dimensional, three-phase reservoir simulator was employed to simulate the reservoir past performance and to predict future performance. The model (Intercomp Beta II) is designed to numerically simulate two or three-phase flow in petroleum reservoirs. Solutions are obtained in one, two, or three spatial dimensions using rectangular coordinates. The program is limited to the treatment of three phases: oil, gas, and water. Gas is assumed to be soluble in oil but not in water, and neither oil nor water can exist in any phase other than its own. Water-oil (dissolved gas content is a constant) flow problems can be treated as a special subset of the general three-phase case.

For this study rectangular coordinates in three spatial dimensions were used. The project definition also permitted the use of the water-oil option since no free gas was present in the reservoir.

2. Grid Description

The development of a grid system was the initial step in the simulation study. A rectangular grid consisting of 25 x 20 x 3 cells was designed. Figure 2A depicts the grid system and overlays onto a surface location map, Figure 2B. Grid lines 6 through 19 in the x-direction and 4 through 17 in the y-direction were omitted from Figure 2A for clarity. These grid lines defined the fine mesh required in the minitest area. The three cell vertical dimension of the grid structure was necessary to depict the three layers previously discussed.

3. Input Data

Values of reservoir properties were assigned to each cell once the grid system was developed. Formation depth, gross thickness, net thickness and formation porosity were supplied by digitizing the available structure, isopachous, and iso-porosity maps (Appendix A). The required formation permeability was derived via a porosity-permeability correlation (Figure 3). This relationship was constructed using core data from wells in the Little Knife field. The most recent core analysis included directional permeability data and fracture orientation studies. Since the Beta II model allows the input of both x-direction and y-direction permeabilities, the oriented core data were easily included. To evaluate a constant directional preference, the method presented by Greenkorn[1] was used. This work led to no firm conclusions regarding directional permeability preference. However, the y-direction (northeast-southwest) permeabilities were increased by a factor of 1.75 over the x-direction (northwest-southeast) values. This alteration was done to

satisfy the fracture orientation study on the core from the injection well. Vertical permeabilities were also included where necessary. In the southwest portion of the gridded area the vertical permeability was set equal to the x-direction permeability. This was done to model the correlated permeability "window" which exists in this area. The vertical permeabilities rapidly grade down to a value of 0.3 millidarcies throughout most of the modeled area. No vertical communication was included in the northeast part of the gridded area since the thickness of the layer separation is an effective barrier to vertical flow.

Unlike location dependent properties, saturation dependent reservoir rock properties were defined in table form. Capillary pressure curves for an oil-water system were input for each layer. These curves were developed using log derived saturations at various depths. At a gravity-capillary equilibrium these curves produced initial water saturations which matched the measured in situ (log derived) reservoir saturations for each layer. The capillary pressure curves are displayed in graphical form in Figure 4 and in tabular form in Tables 3, 4 and 5. Additionally, the relative permeability-saturation relationships for each layer were required input data. These relationships for an oil-water system are presented in both Figure 5 and in Tables 3, 4 and 5. The relative permeability curves for Layers I and II were taken from an analysis done on cores from the Sabrosky No. 4-31-4C well. The curve for Layer III was obtained from calculated relationships based on a composite capillary pressure curve from the Klatt 2-19-4 and 3-19-4 wells. The composite capillary pressure curve was a combination of measured capillary pressure data at a specific value of irreducible water saturation. It must be noted at this point that although a history match was achieved using the given relative permeability curves, since only low water-oil ratios were observed the application of these relationships may not be valid in high water saturation situations.

Reservoir fluid properties were taken from a standard PVT analysis of a Little Knife oil sample. The analysis reported a saturation pressure of 2698 psig with a corresponding formation volume factor of 1.755 RB/STB. Gas solubility was measured at 1092.5 SCF/STB at the bubble point. Oil viscosity at reservoir conditions was approximately 0.23 cp. The reservoir oil properties are presented in Table 6 and Figures 6, 7 and 8.

Additional model input parameters associated with water properties and rock compressibility are presented in Table 7.

4. Production Data

Individual well production rates were retrieved from Gulf Oil Corporation's Well Historical Production System. Data from this source were in the form of oil production rates as a function of time. These rates, however, were recomputed by zone as previously discussed. It was necessary to allocate the reported rates between those physical zones which were included in the model and those which were not. This distribution was accomplished using the kh* product for each perforated interval in the individual wells. Table 8 lists the fraction of the total well rate which was apportioned to the modeled zone. Rate distribution among the three modeled layers was automatically handled by the simulator. The input rates for each well are included in Figures 9 through 16.

---

*All symbols are described in the Nomenclature section.

5. History Match

The model was initialized to a gravity-capillary equilibrium using the aforementioned input data. After initialization, a history match covering a reservoir producing period from August, 1977 to April, 1980 was attained. Given the oil production rates for this time period, the model calculated the resulting pressure history. A comparison of the historical pressure data and the calculated pressures showed good agreement. Also, the producing ratios (GOR and WOR) were acceptable. The producing gas-oil ratio was constant throughout the history period because the reservoir remained undersaturated. The observed water-oil ratio was low but was varying from point to point. This variance was not considered characteristic because of the multiple completion scheme discussed above. Therefore, the reported WOR was used only as an upper limit during the history matching. Although a good match was obtained, recently measured pressure values were in excess of those predicted by the simulator[2]. In order to match both the early history and the latest pressure data, refinements to the reservoir description were required. It was necessary to include additional reservoir volume in the model to supply more energy. This change resulted in a good match of the entire history. The individual well pressure history matches are also shown in Figures 9 through 16. In addition, the cumulative production, production rate, and average reservoir pressure for the history period are presented in Figure 17.

D. RESERVOIR PERFORMANCE PREDICTION

1. Purpose

The purpose of the performance predictions was to evaluate the volume of water required to repressure the test area in excess of the calculated CO_2 minimum miscibility pressure. Also, the injection rate, time requirement, and resulting reservoir pressures were to be found. Future prediction cases were modeled as time extensions of the characterized reservoir history.

2. Approach

A total of five prediction cases were run. Two of these cases assumed a declining future production rate. The remaining three cases assumed a constant future production rate. A description of each case is presented in Table 9.

In order to achieve a naturally declining production rate through the future prediction period, it was necessary to produce each well at a constant bottom hole flowing pressure. This method of production necessitated the calculation of individual well productivity (stock tank barrels/day/psi pressure drop) and the selection of adequate bottom hole pressures. A flowing bottom hole pressure of 2000 psig was arbitrarily chosen, to solve this problem. Combining this pressure with the respective cell pressure and flowrate from the last month of historical production, individual well PI's were calculated. Using the well PI values and the 2000 psig flowing pressure as data the simulator calculated the prediction period flow rates. The calculated PI values are listed in Table 10. Unlike the naturally

declining rate cases, the constant rate cases were an extension of the last month of historical production. The future prediction rates were held constant and equal to the last reported value.

Water injection, which was included in three of the five prediction cases, was also held at a constant rate. The injection rate was set to 1150 STB/D and was carried out for fifteen days. This resulted in approximately 20,000 STB of water being injected. These values of injection rate and volume were selected to conform to field rules. Also, the surface injection pressure was limited to a maximum of 700 psig. This was done to avoid accidental formation fracturing if the dictated injection rate required excessively high well pressures. In none of the cases was the pressure limit approached.

Comparison of prediction Cases 1 and 2 (naturally declining production rate) showed the effect of water injection beginning October 1, 1980. Table 11 lists the pressure responses of each prediction case. Reviewing Table 11 shows that water injection raised the minitest area pressure by about 350 psig resulting in an average pressure of 3717 psig. This pressure is substantially above the calculated minimum CO_2 miscibility pressure of 3400 psig. Additionally, the water injection in Case 2 did not strongly influence the average reservoir pressure which remained almost constant at 3776 psig.

Prediction Cases 3 and 4 (constant production rate) showed the same trend as the previously mentioned cases. Water injection, beginning on October 1, 1980, increased the pilot area pressure from 3315 psig to 3684 psig. This pressure exceeded the calculated minimum miscibility pressure. In Case 4 the average reservoir pressure was almost unaffected by the water injection. Slight differences in the pressure values between sets of prediction cases were attributed to the

different production rates. At the time of comparison the constant rate case produced 1733 STB/D, versus 1465 STB/D for the declining rate cases.

Prediction Case 5 started water injection on September 1, 1980, thirty days earlier than in Case 2 or Case 4. Case 5 demonstrated only a slight increase in the average reservoir pressure while the pilot area pressure rose to 3720 psig after fifteen (15) days of injection. The pilot area pressure exceeded the calculated minimum miscibility pressure. The pressure values for Case 5 were slightly higher than the other cases since less reservoir depletion had occured when injection began. Figure 18 presents a graphical comparison of all the future prediction cases.

Robert W. Rasor

R. W. Rasor

Roderick B. Haulenbeek

R. B. Haulenbeek

Robert Auvenshine

R. A. Auvenshine

Ganesh C. Thakur

G. C. Thakur

APPROVED:

M. H. Harris

M. H. Harris, Director

7/31/80

Date

William R Cook /MHH

William R. Cook, Manager

7/31/80

Date

IV. ACKNOWLEDGEMENTS

The assistance of Messrs. L. Bell and R. Lindsay of the Oklahoma City District office during the course of this study is highly appreciated.

V. NOMENCLATURE

Symbol	Definition	Units
GOR	Gas-oil Ratio	SCF/STB
kh	Permeability-Thickness Product	md-ft
PI	Productivity Index	STB/D/psi
WOR	Water-oil Ratio	STB/STB

VI. REFERENCES

1. Greenkorn, R. A., et al: "Directional Permeability of Heterogeneous Anisotropic Porous Media," Soc. Pet. Eng. Journal (June, 1964), p. 124.

2. Kingelin, G. F., et al: "Interim Report Little Knife CO_2 Minitest Project Multiwell Pulse Test Report Little Knife, North Dakota," GR&DC Production Services Department Technical Memorandum No. 444T1207, (May, 1980).

TABLE I

WELL IDENTIFICATION

LITTLE KNIFE MINITEST WATER INJECTION SIMULATION

Number	Name	Location		Type
		I	J	
2	SABROSKY 2-31-3C	23	2	Producer
3	ZABOLOTNY 4-3-1A	12	2	Producer
5	G. HURINENKO 1-2-1A	23	19	Producer
6	ZABOLOTNY 1-3-4A	3	6	Producer
7	ZABOLOTNY 2-3-3A	11	19	Producer
8	HURINENKO 2-10-1A	2	19	Producer
9	HURINENKO 1-10-2A	3	20	Producer
10	MILLER 3-10-4B	1	20	Producer
11	ZABOLOTNY INJECTION No. 1	12	11	Injector

TABLE 2

INDIVIDUAL WELL PERFORATED INTERVAL

LITTLE KNIFE MINITEST WATER INJECTION SIMULATION

Well Number	Perforated Interval * (feet)	Formation Interval (feet)*		
		Layer I	Layer II	Layer III
2**	9695-9708; 9738-44; 9750-64; 9806-12; 9822-28; 9838-44	9782-85	9810-22	9830-45
3	9725-39; 9740-59; 9795-9801; 9818-31	9796-98	9825-37	9844-62
5	9660-72; 9678-82; 9696-9708; 9723-28; 9749-51; 9763-67; 9774-80	9748-51	9763-91	9794-9811
6	9770-9810	9767-88	9791-9811	9815-23
7	9758-72; 9742-48; 9718-20; 9690-9702; 9671-75; 9662-66; 9651-54	9743-48	9756-86	9791-9801
8	9694-9700; 9708-14; 9751-72; 9802-10; 9814-34	9802-10	9814-52	9856-57
9	9752-58; 9792-9820; 9828-40; 9846-92	9846-69	9873-87	9890-93
10	9748-52; 9758-95; 9800-20; 9835-39; 9880-86	9861-63	9880-91	9894-97
11	9824-39	9795-9817	9818-40	9842-56

* Depths - Feet Below Ground Level
** No Log Available

TABLE 3

WATER SATURATION FUNCTIONS: ROCK TYPE 1

LITTLE KNIFE MINITEST WATER INJECTION SIMULATION

Water Saturation (PV)	Oil Relative Permeability	Water Relative Permeability	Water Capillary Pressure (psia)
.23	1.000	.001	22.24
.30	.935	.002	20.54
.40	.519	.003	19.76
.50	.238	.030	18.79
.55	.143	.060	18.10
.60	.083	.108	17.14
.65	.048	.170	15.76
.70	.037	.259	13.84
.75	.013	.360	11.77
.80	.004	.478	9.57
.90	0.0	.725	5.02
1.0	0.0	1.00	0.0

TABLE 4

WATER SATURATION FUNCTIONS: ROCK TYPE 2

LITTLE KNIFE MINITEST WATER INJECTION SIMULATION

Water Saturation (PV)	Oil Relative Permeability	Water Relative Permeability	Water Capillary Pressure (psia)
.27	1.0	.001	18.900
.30	.935	.002	13.650
.40	.519	.003	8.715
.50	.238	.030	7.350
.55	.143	.060	6.930
.60	.083	.108	6.516
.65	.048	.170	6.090
.70	.037	.254	5.670
.75	.013	.360	5.146
.80	.004	.478	4.620
.90	0.0	.725	3.150
1.0	0.0	1.0	0.00

TABLE 5

WATER SATURATION FUNCTIONS: ROCK TYPE 3

LITTLE KNIFE MINITEST WATER INJECTION SIMULATION

Water Saturation (PV)	Oil Relative Permeability	Water Relative Permeability	Water Capillary Pressure (psia)
.09	.990	0.0	30.00
.10	.980	0.0	28.75
.20	.868	0.0	20.00
.30	.545	0.0	16.50
.40	.277	.012	13.70
.50	.090	.039	11.60
.60	.010	.090	10.00
.70	0.0	.195	8.25
.80	0.0	.364	6.25
.90	0.0	.625	3.50
.99	0.0	1.00	.01
1.0	0.0	1.00	0.0

TABLE 6

PVT PROPERTIES FOR OIL

LITTLE KNIFE MINITEST WATER INJECTION SIMULATION

Pressure (psig)	Volume Factor (RB/STB)	Gas Solubility (SCF/STB)	Viscosity (cp)
5000	1.668	1092.5	.2779
4460	1.685	1092.5	.2665
3960	1.702	1092.5	.2564
3198	1.732	1092.5	.2383
2930	1.744	1092.5	.2325
2698	1.755	1092.5	.2302
2609	1.732	1051.0	.2359
2400	1.680	954.7	.2491
2198	1.631	862.3	.2612
1915	1.572	744.3	.2861
1670	1.524	657.1	.3078
1205	1.441	494.5	.3476
1012	1.410	429.9	.3722

TABLE 7

PROBLEM PARAMETERS

LITTLE KNIFE MINITEST WATER INJECTION SIMULATION

Geometry

Blocks in X - Direction	25
Blocks in Y - Direction	20
Blocks in Z - Direction	3
Total Number of Blocks	1500

Geology

Number of Layers	3
Number of Rock Types	3
Formation Type	Carbonate

Miscellaneous

Water Density (Standard Conditions)	(gm/cc)	1.2
Water Compressibility	(1/psi)	.000007
Water Formation Volume Factor	(RB/STB)	1.043
Water Viscosity	(cp)	.400
Rock Compressibility	(1/psi)	.000003
Reservoir Temperature	(Deg. F)	245.
Stock Tank Oil Density	(gm/cc)	.837
Oil Water Contact Depth	(ft.ss)	7325.

TABLE 8

FACTOR FOR ALLOCATING PRODUCTION TO INCLUDED LAYERS

LITTLE KNIFE MINITEST WATER INJECTION SIMULATION

Well	kh Allocation Factor
2	.299
3	.152
5	.901
6	1.00
7	.765
8	.865
9	.692
10	.109

TABLE 9

SUMMARY OF PREDICTION CASES

LITTLE KNIFE MINITEST WATER INJECTION SIMULATION

Case Number	Description
1	Naturally declining production through October 15, 1980 with no water injection.
2	Naturally declining production through October 15, 1980 with water injection beginning October 1, 1980. Injection limited by a maximum rate of 1150 STB/D and a surface tubing pressure of 700 psig.
3	Constant rate production through October 15, 1980 with no water injection.
4	Constant rate production through October 15, 1980 with water injection beginning October 1, 1980. Injection limited by a maximum rate of 1150 STB/D and a surface tubing pressure of 700 psig.
5	Constant rate production through September 15, 1980 with water injection beginning September 1, 1980. Injection limited by a maximum rate of 1150 STB/D and a surface tubing pressure of 700 psig.

TABLE 10

WELL PRODUCTIVITY INDEX USED IN DECLINING RATE CASE

LITTLE KNIFE MINITEST WATER INJECTION SIMULATION

Well Number	Productivity Index (STB/D/PSI)	Constant Bottom Hole Flowing Pressure (psig)
2	.064052	2000.
3	.034657	2000.
5	.287144	2000.
6	.283083	2000.
7	.203704	2000.
8	.170610	2000.
9	.129919	2000.
10	SHUT IN (3-1-79)	2000.
11*	1.500000	700.

* Injectivity for Injection Well No. 11
* Surface tubing pressure restriction for Well No. 11

TABLE 11

PRESSURE SUMMARY OF PREDICTION CASE RESULTS

LITTLE KNIFE MINITEST WATER INJECTION SIMULATION

Prediction Case Number	Date	Total Producing Rate (STB/D)	Volumetric Average Reservoir Pressure At Cell Depth (psia)	Minitest Area Average Pressure At Cell Depth (psia)
1	10/15/80	1445	3776	3359
2	10/15/80	1465	3781	3717
3	10/15/80	1733	3760	3315
4	10/15/80	1733	3765	3684
5	09/15/80	1733	3791	3720

FIGURE 1
PILOT LOCATION
LITTLE KNIFE MINITEST WATER INJECTION SIMULATION

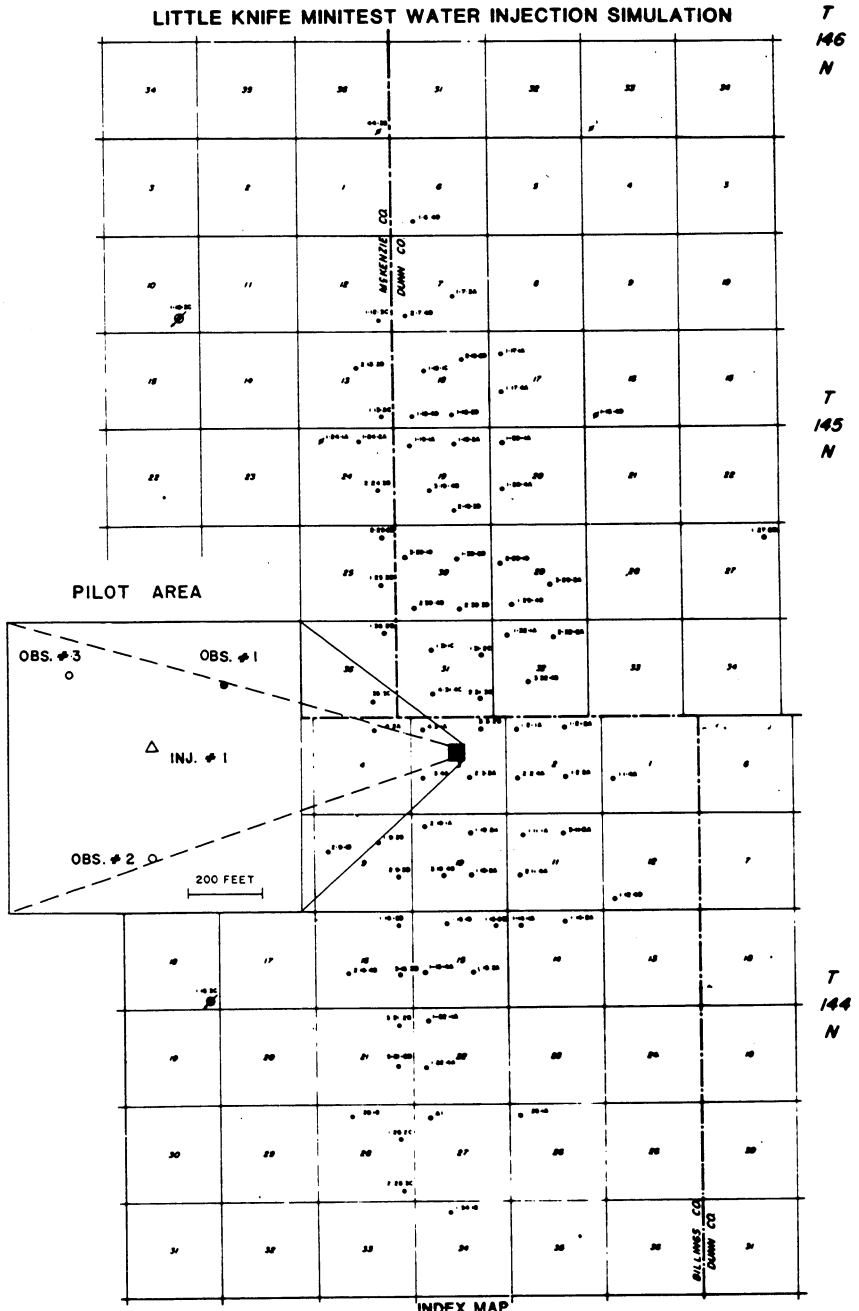

INDEX MAP
(Modified after Proctor and MacCauley, 1968 and Wittstrom and Hagemaier ,1978, 1979)

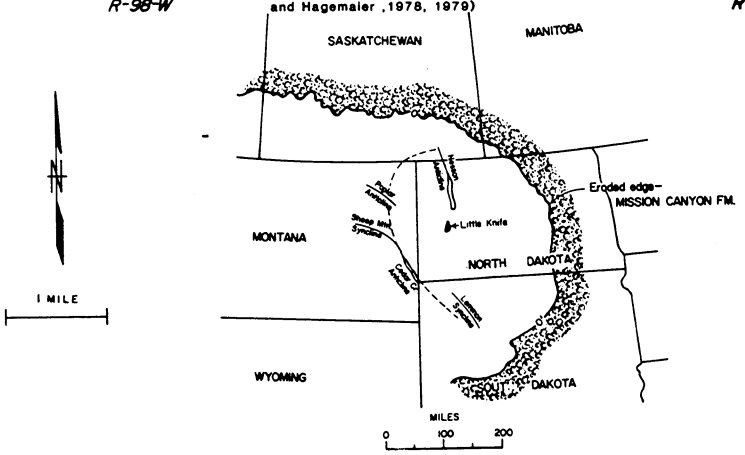

R.B.H. 6/80

FIGURE 2A

GRID SYSTEM OVERLAY

FIGURE 2B

SURFACE LOCATION MAP

LITTLE KNIFE MINITEST WATER INJECTION SIMULATION

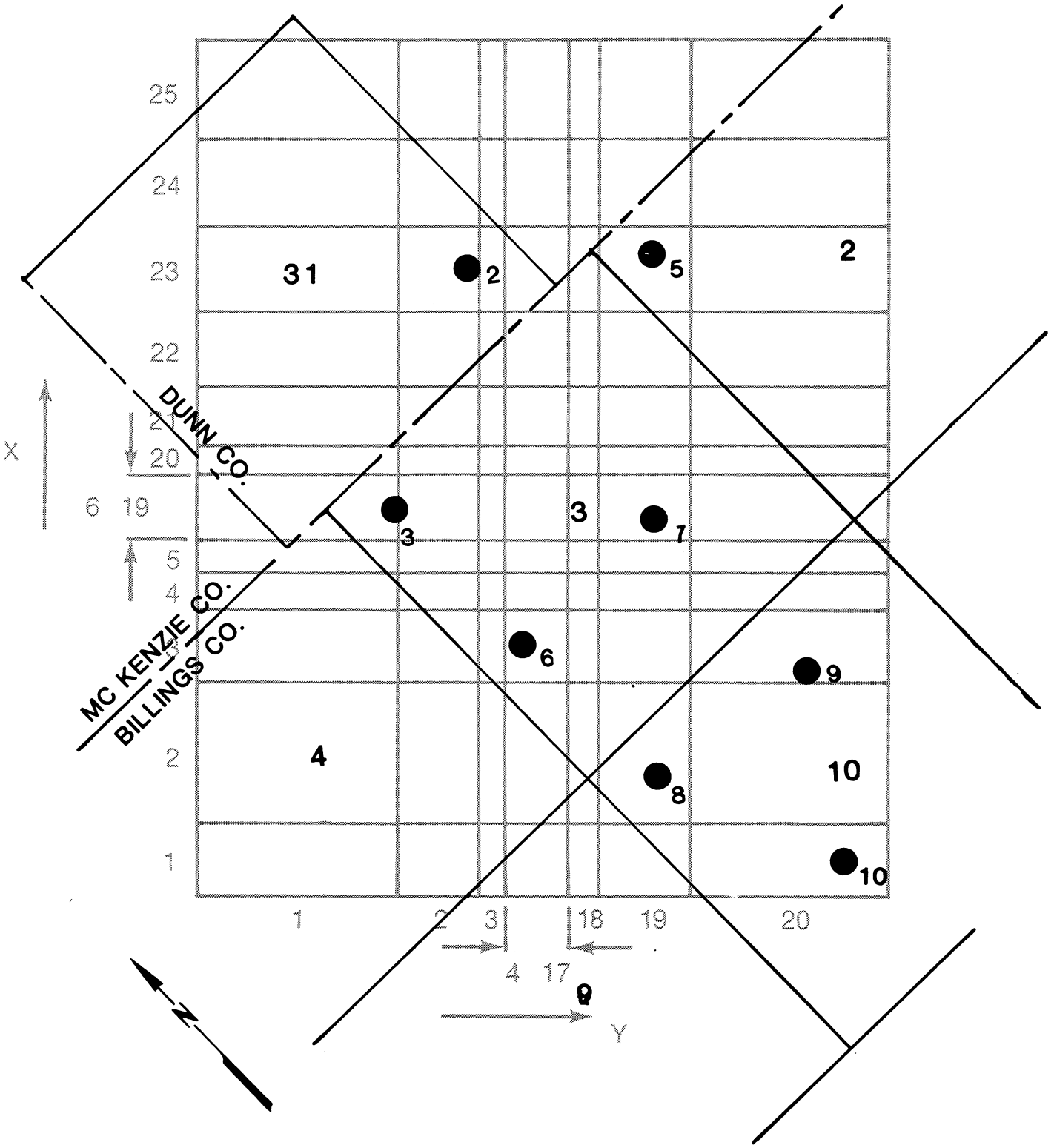

FIGURE 3

POROSITY-PERMEABILITY RELATIONSHIP

LITTLE KNIFE MINITEST WATER INJECTION SIMULATION

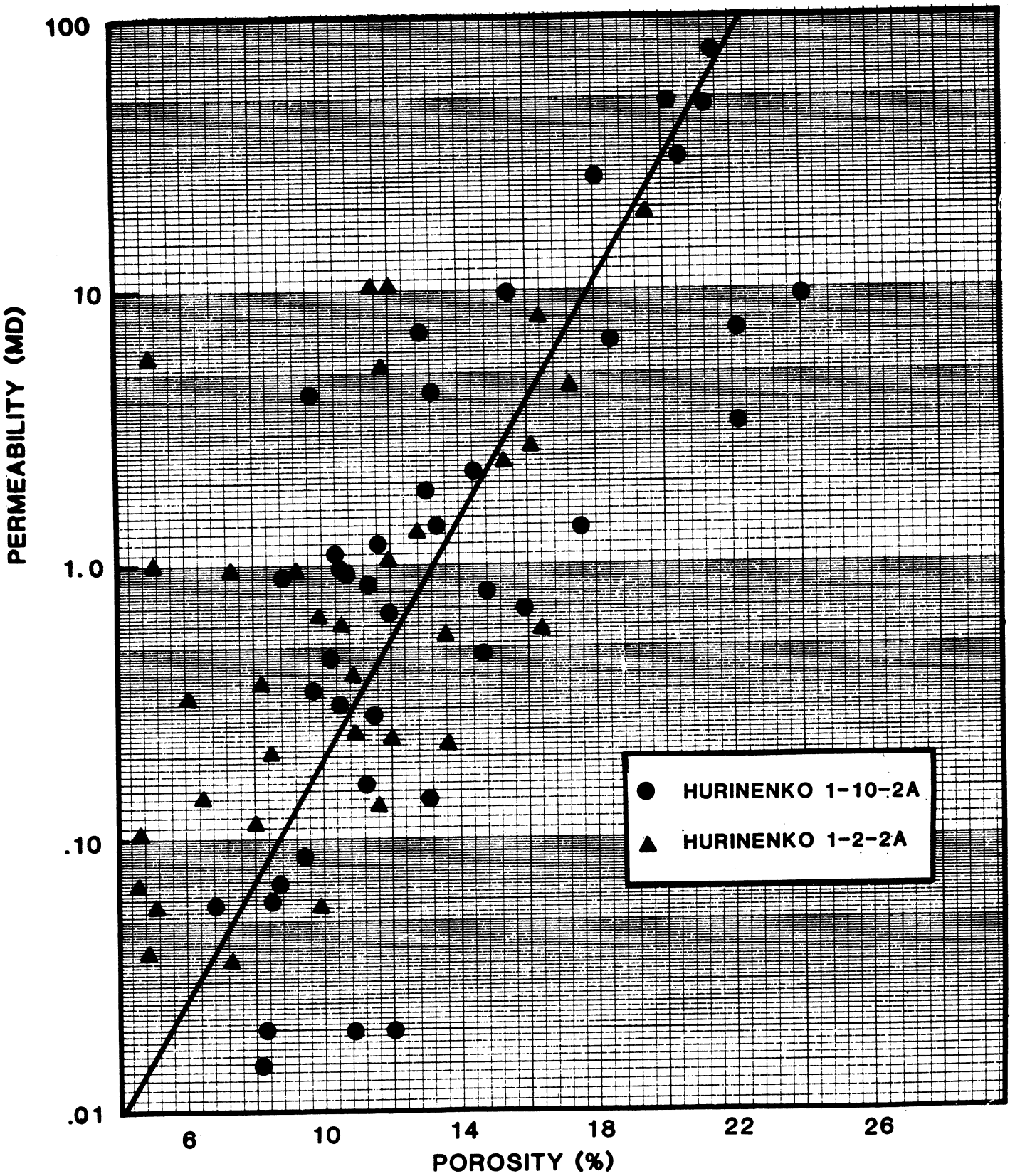

FIGURE 4

WATER CAPILLARY PRESSURE
LITTLE KNIFE MINITEST WATER INJECTION SIMULATION

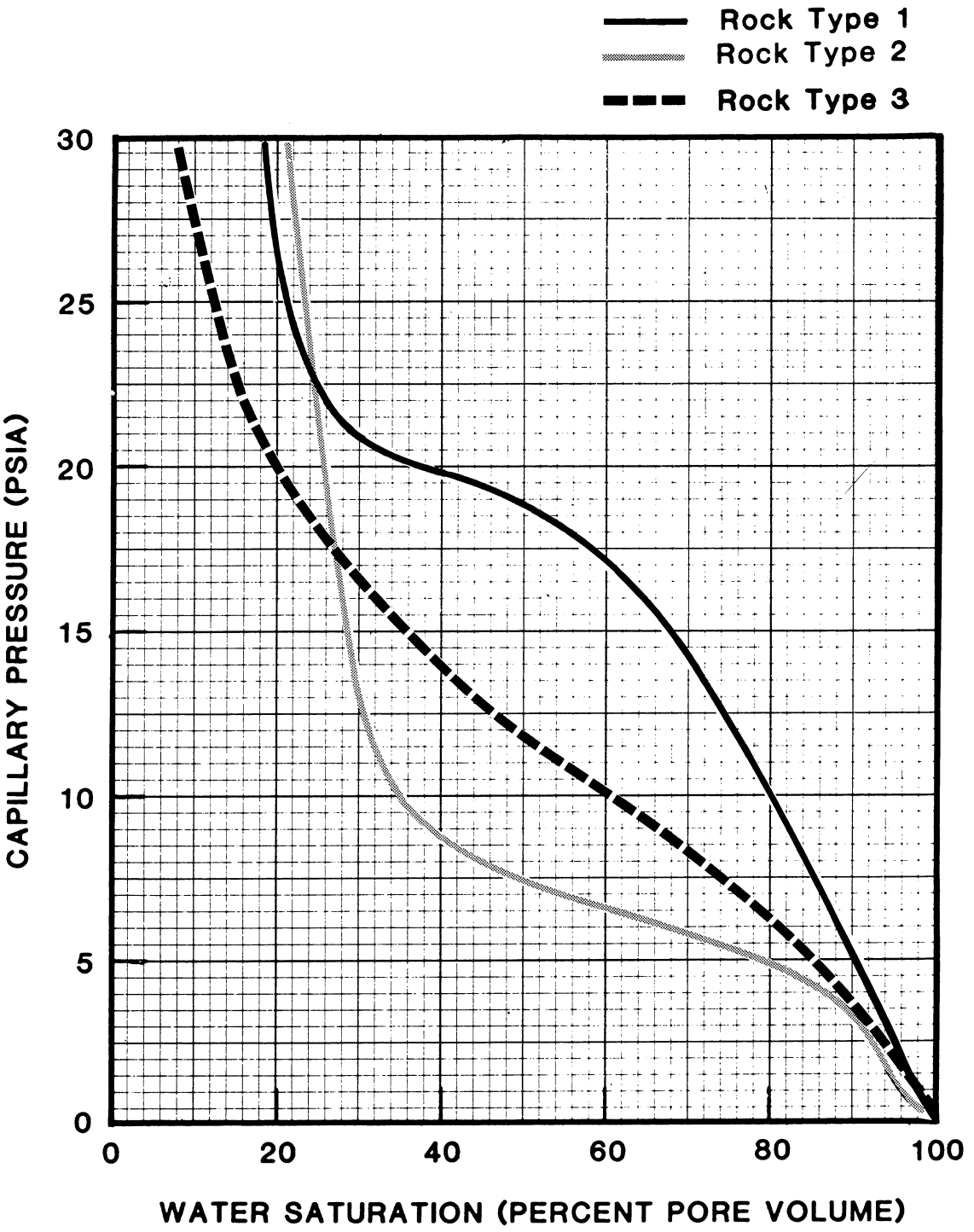

FIGURE 5

OIL-WATER RELATIVE PERMEABILITY

LITTLE KNIFE MINITEST WATER INJECTION SIMULATION

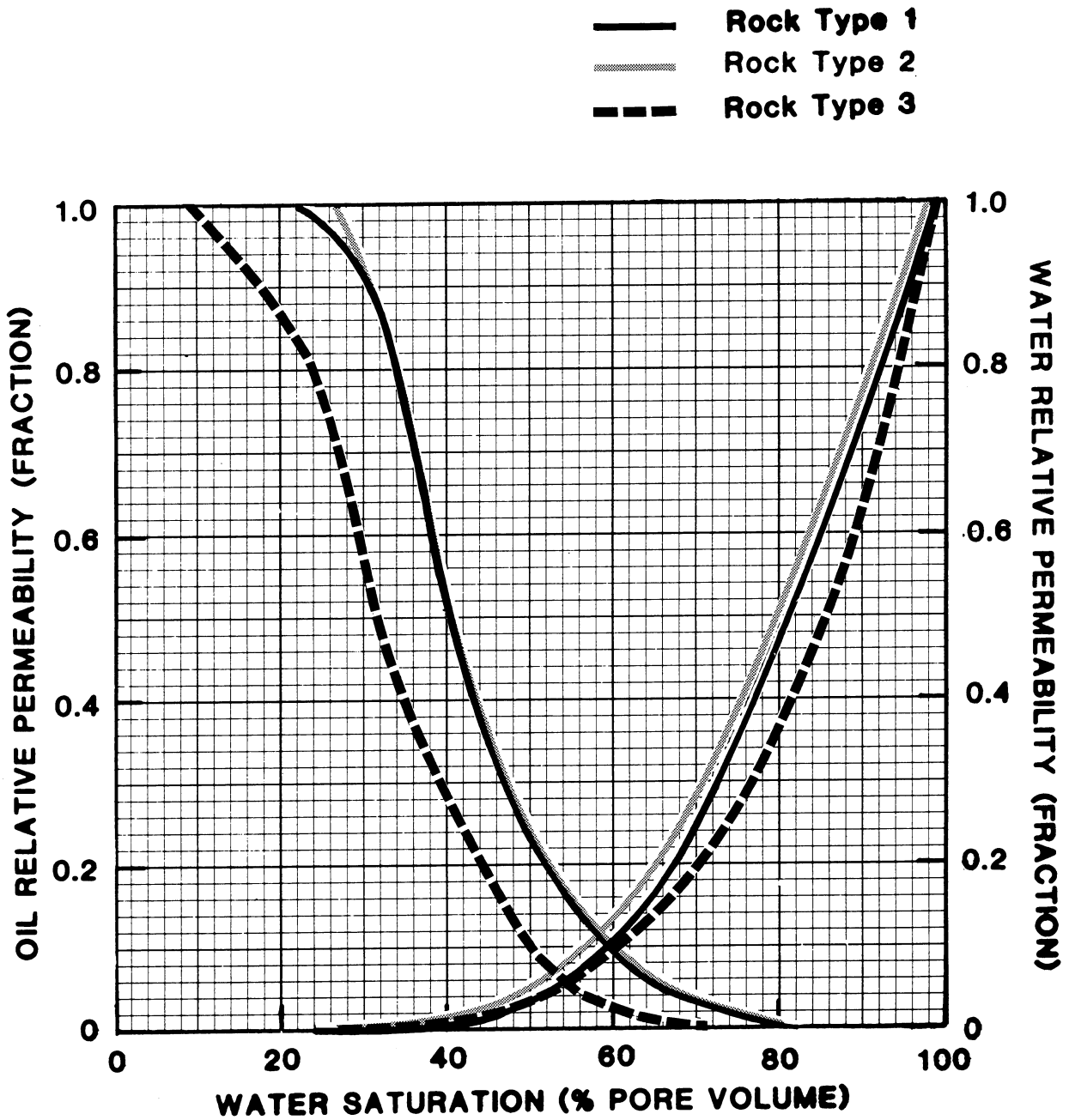

FIGURE 6

OIL FORMATION VOLUME FACTOR

LITTLE KNIFE MINITEST WATER INJECTION SIMULATION

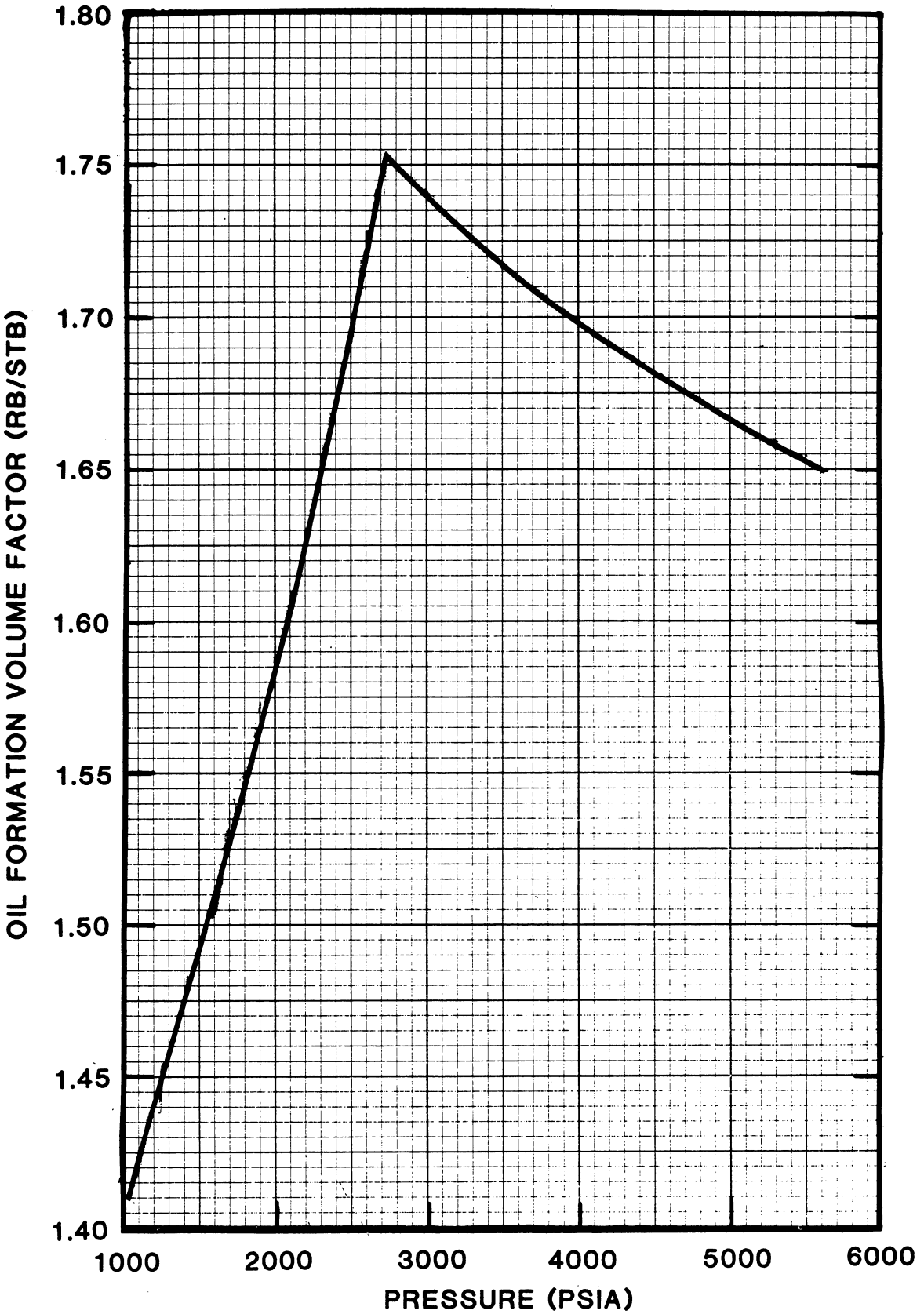

FIGURE 7

GAS SOLUBILITY

LITTLE KNIFE MINITEST WATER INJECTION SIMULATION

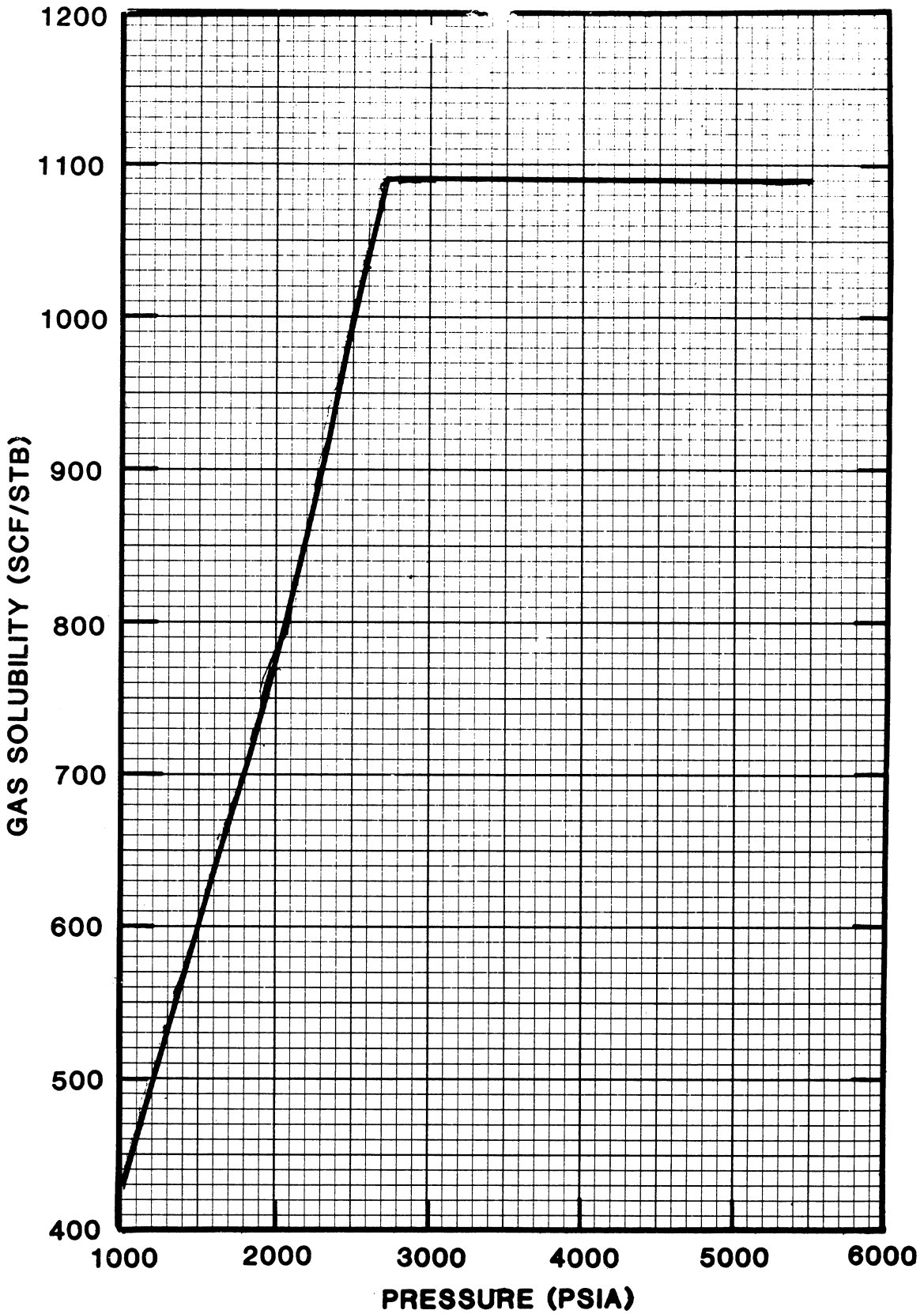

FIGURE 8

OIL VISCOSITY

LITTLE KNIFE MINITEST WATER INJECTION SIMULATION

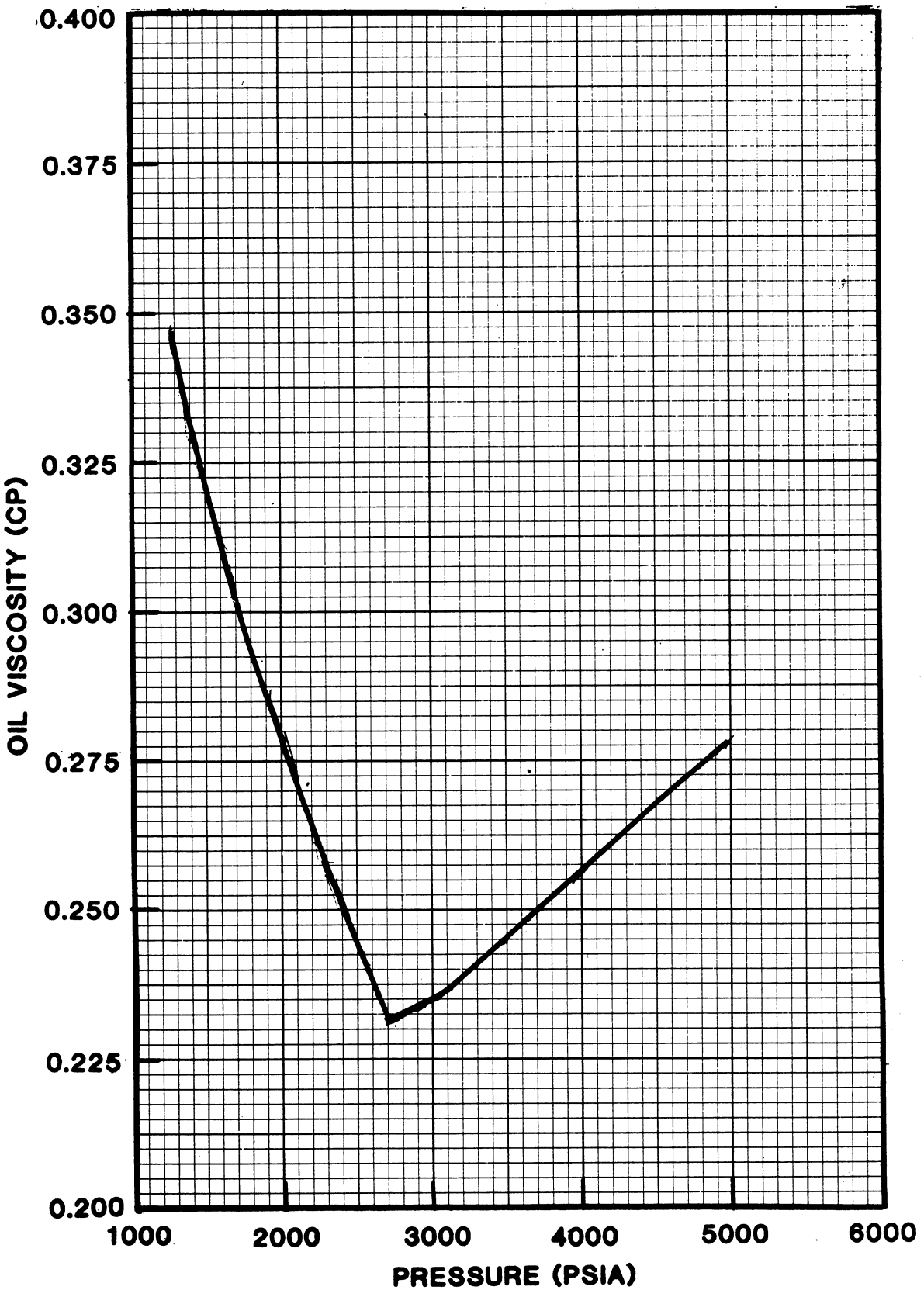

FIGURE 9

HISTORY MATCH - WELL 2 LITTLE KNIFE MINITEST WATER INJECTION SIMULATION

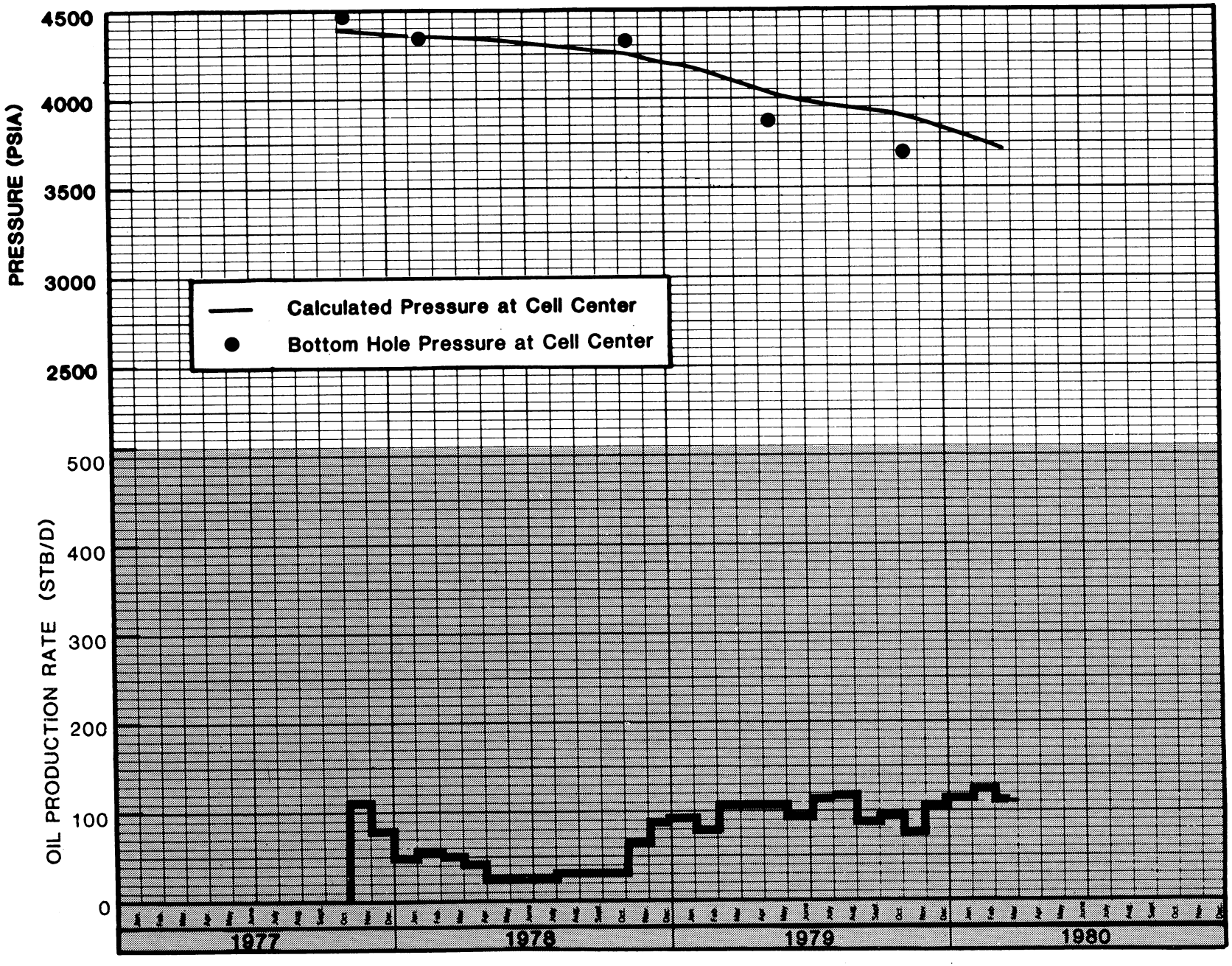

FIGURE 10

HISTORY MATCH - WELL 3 LITTLE KNIFE MINITEST WATER INJECTION SIMULATION

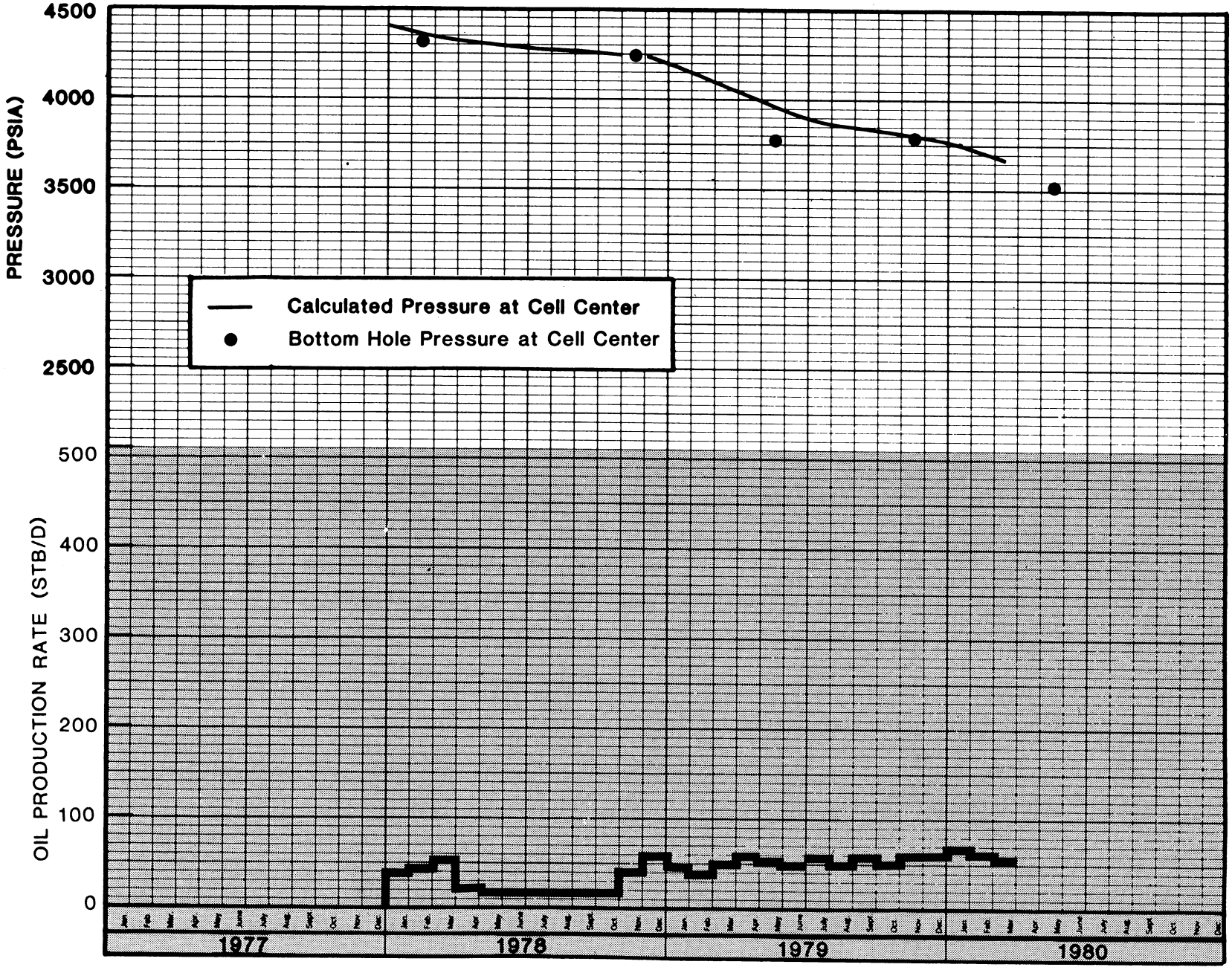

FIGURE 11

HISTORY MATCH - WELL 5 LITTLE KNIFE MINITEST WATER INJECTION SIMULATION

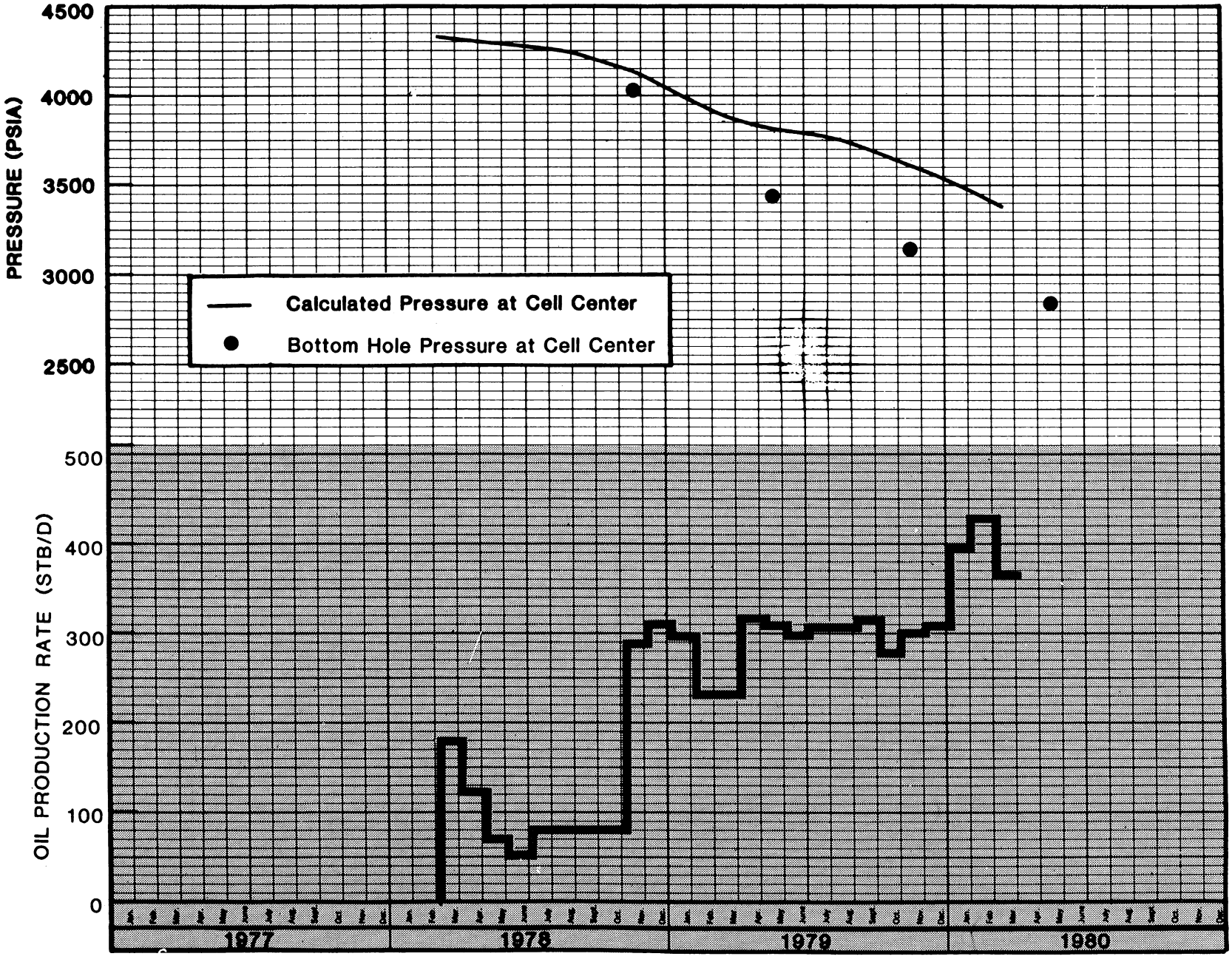

FIGURE 12

HISTORY MATCH - WELL 6 LITTLE KNIFE MINITEST WATER INJECTION SIMULATION

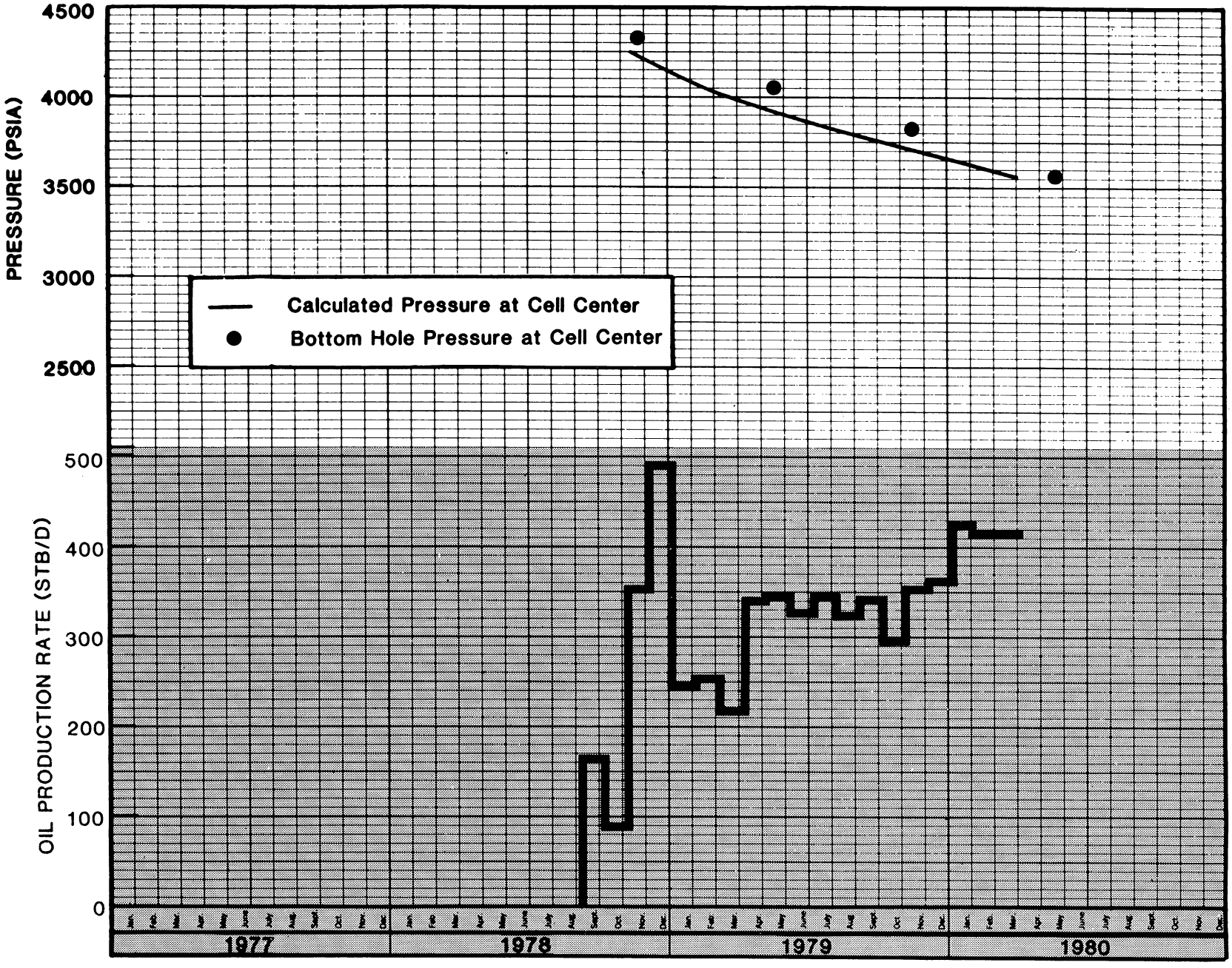

FIGURE 13

HISTORY MATCH - WELL 7 LITTLE KNIFE MINITEST WATER INJECTION SIMULATION

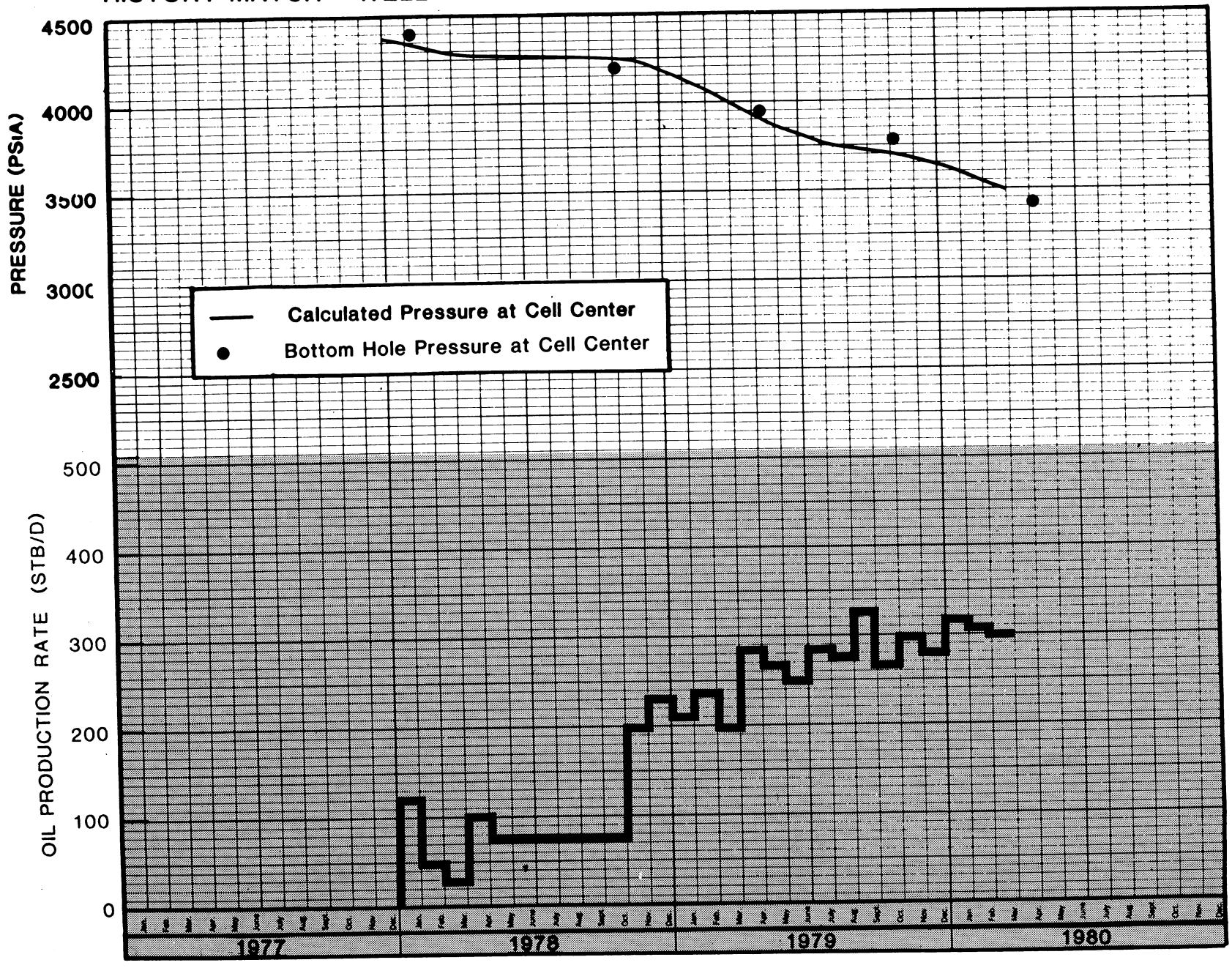

FIGURE 14

HISTORY MATCH - WELL 8 LITTLE KNIFE MINITEST WATER INJECTION SIMULATION

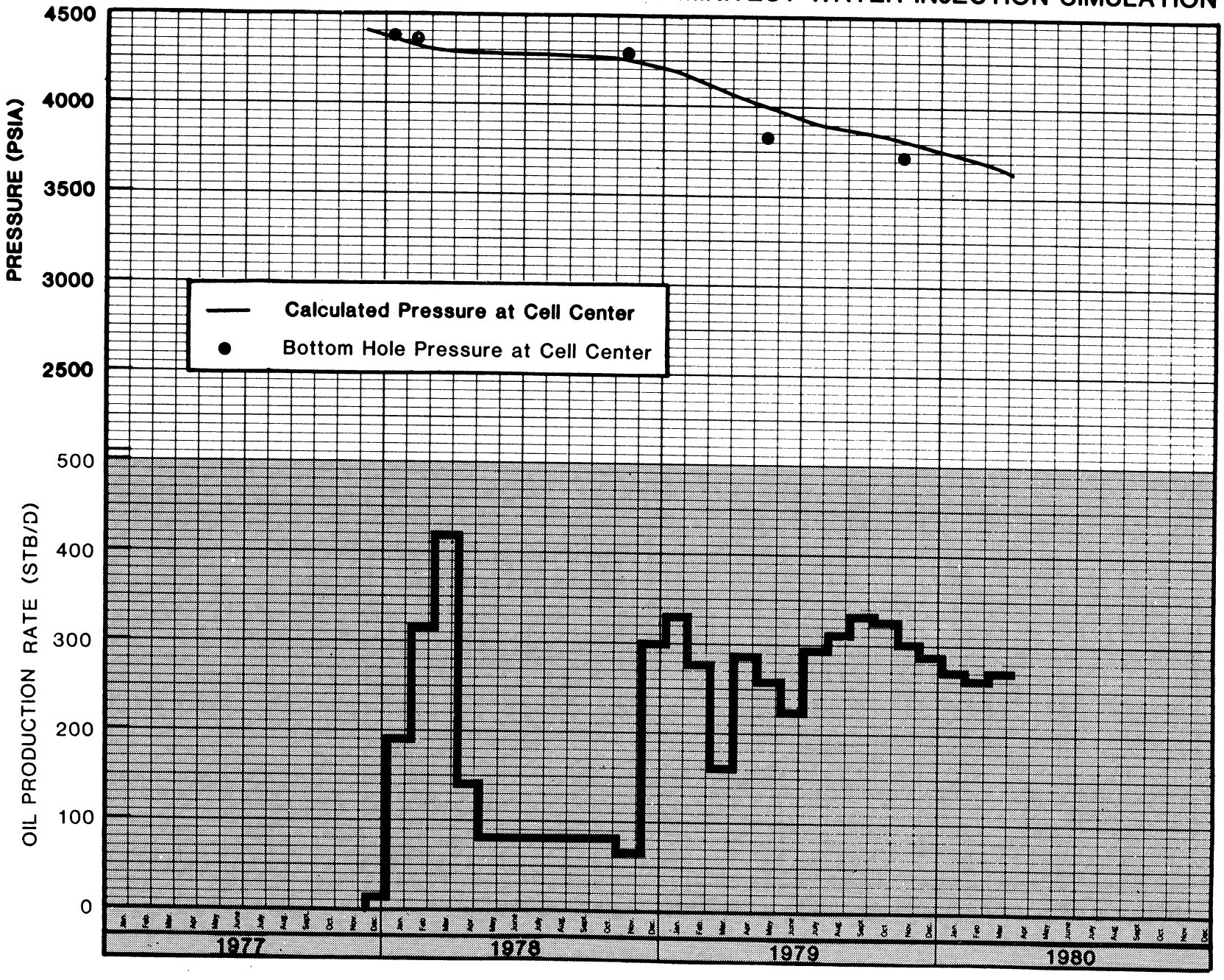

FIGURE 15

HISTORY MATCH - WELL 9 LITTLE KNIFE MINITEST WATER INJECTION SIMULATION

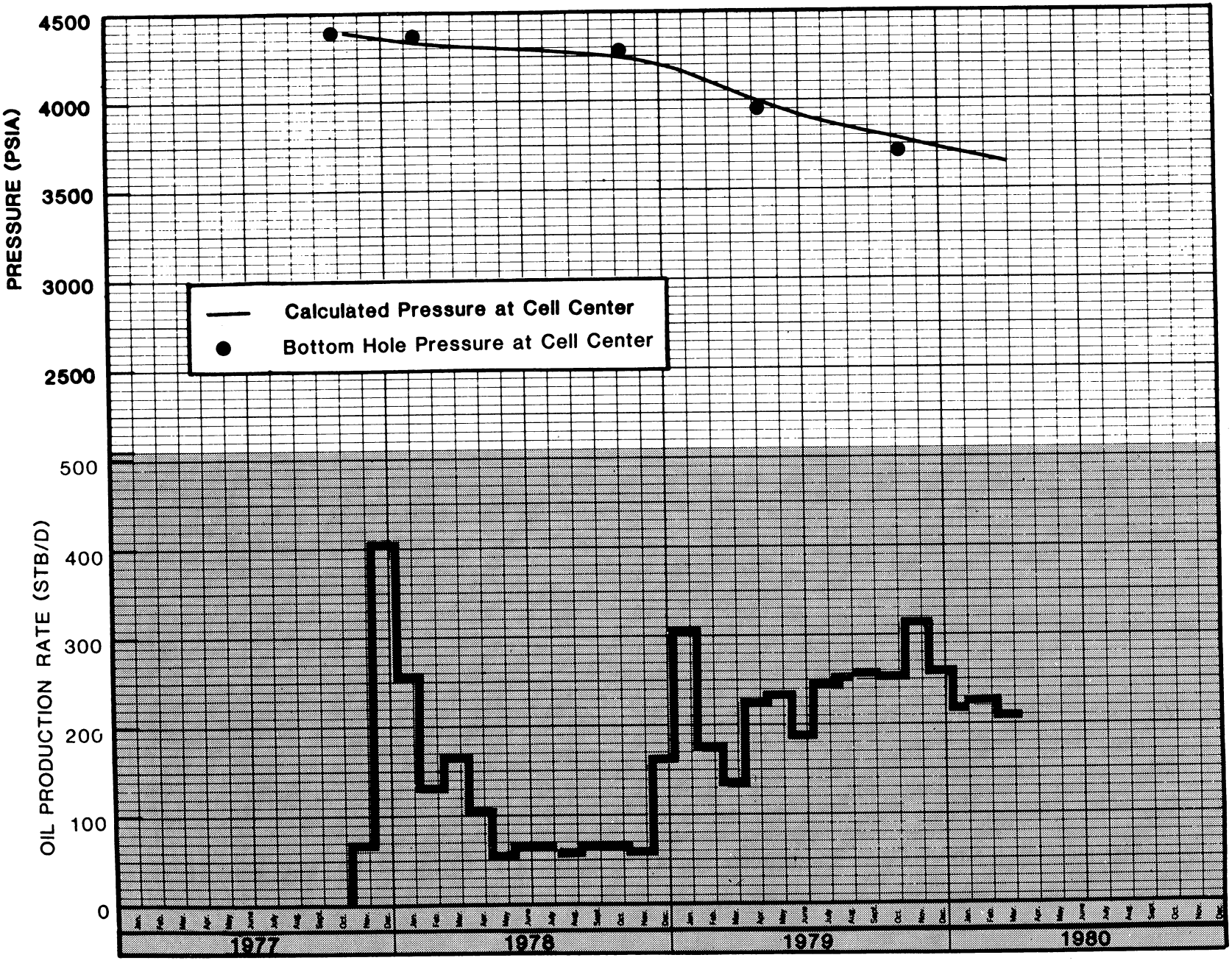

FIGURE 16

HISTORY MATCH - WELL 10 LITTLE KNIFE MINITEST WATER INJECTION SIMULATION

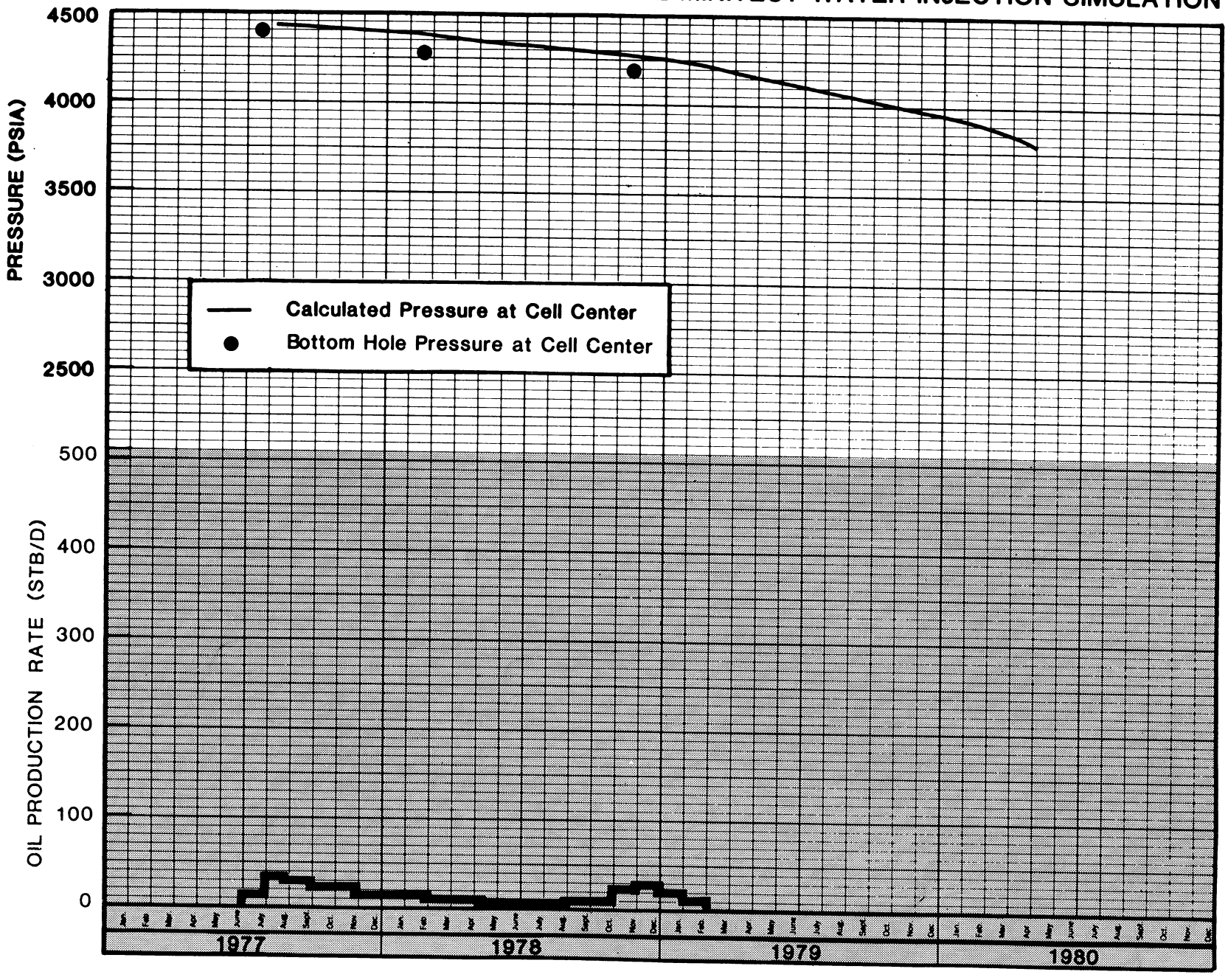

FIGURE 17

CALCULATED FIELD HISTORY - LITTLE KNIFE MINITEST WATER INJECTION SIMULATION

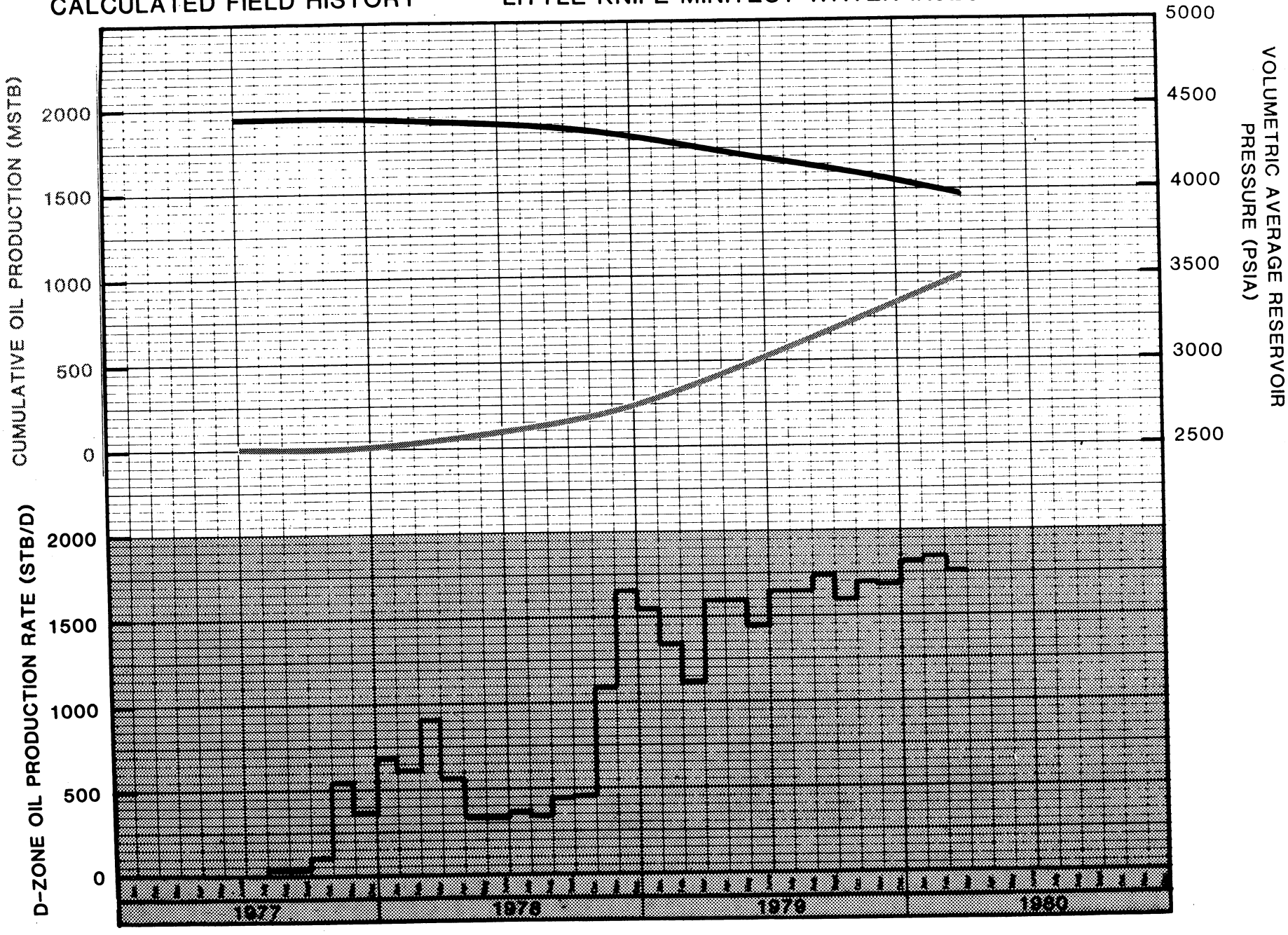

FIGURE 18
PREDICTION CASE COMPARISON
LITTLE KNIFE MINITEST WATER INJECTION SIMULATION

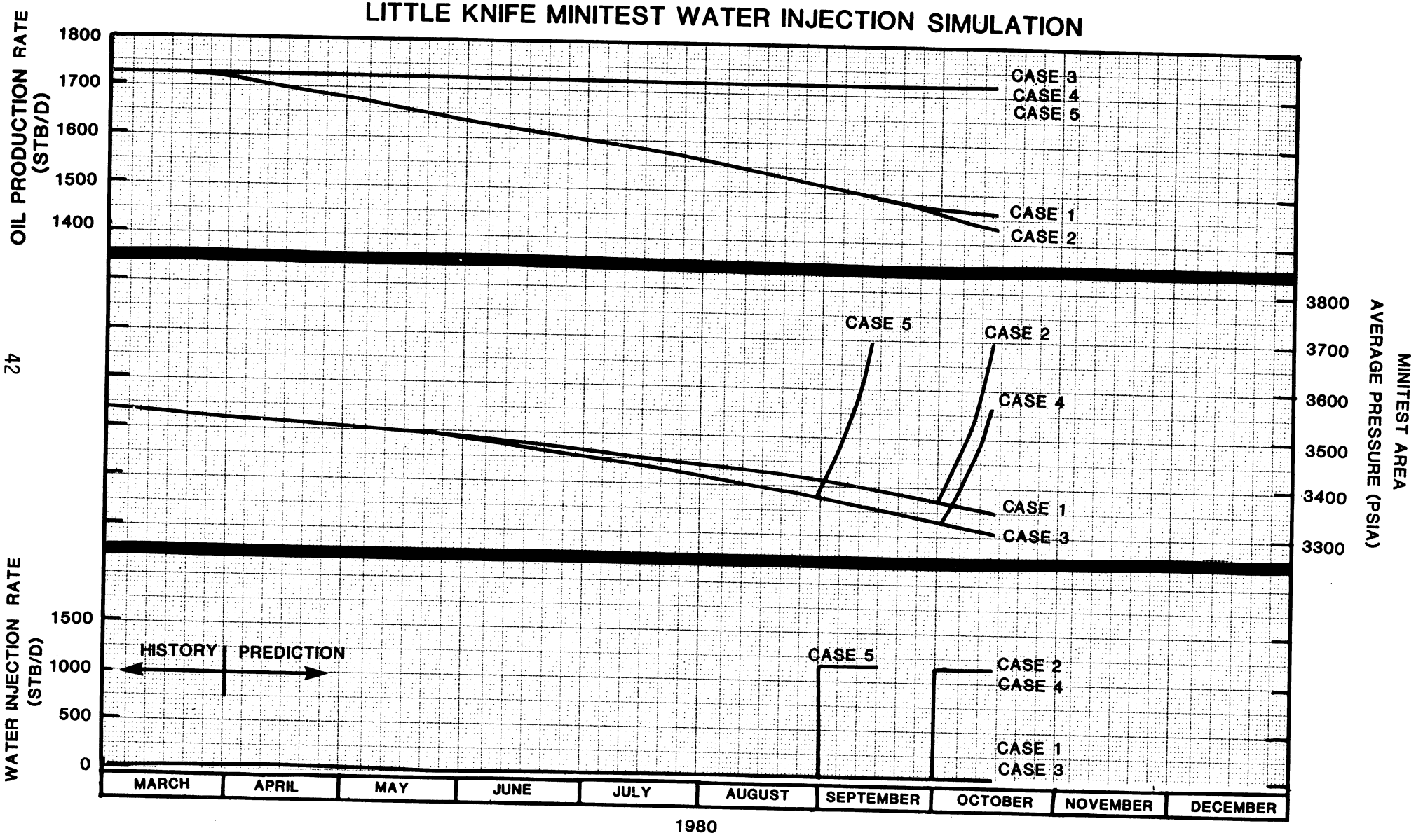

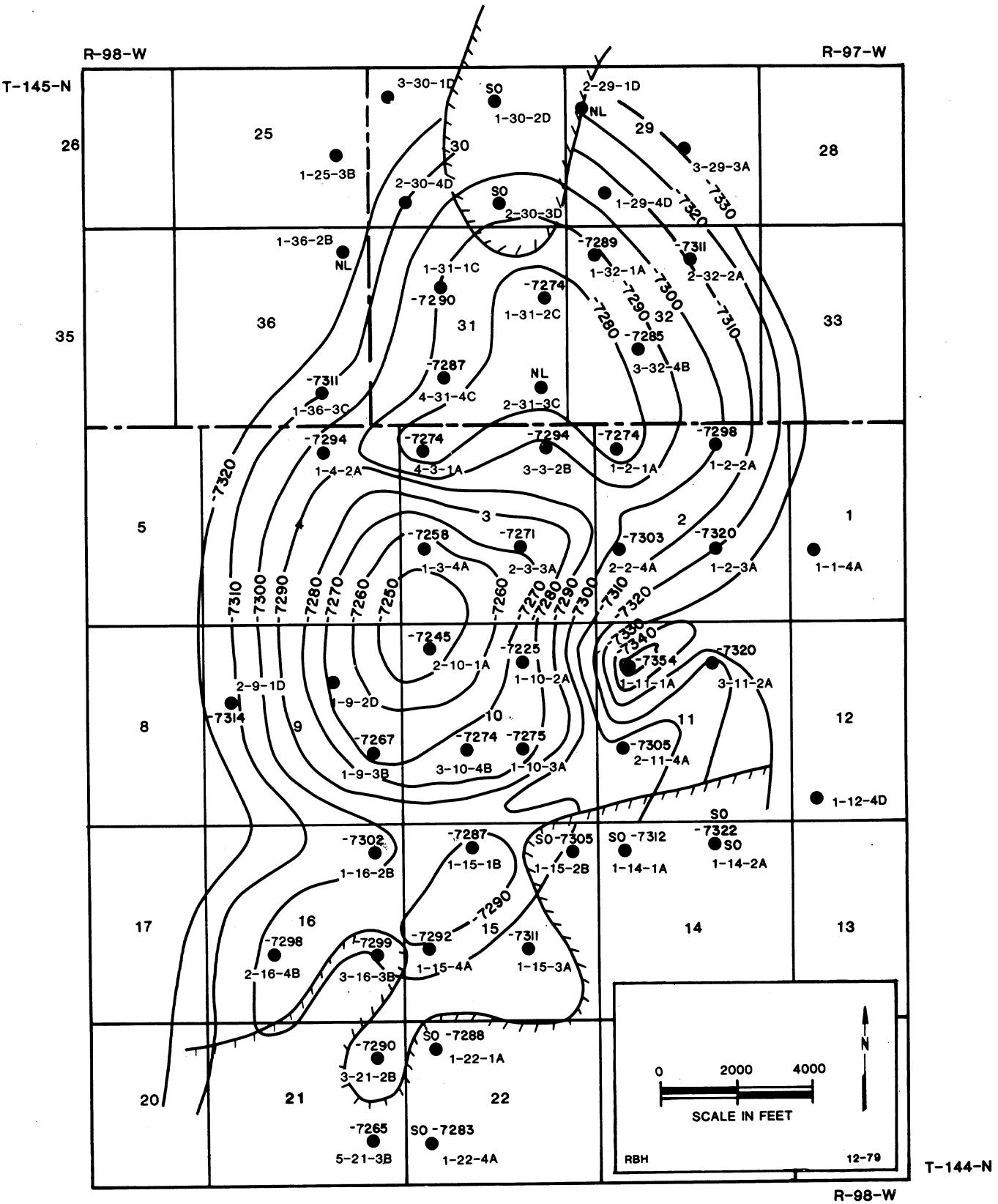

FIGURE A-1

LAYER II STRUCTURE TOP MAP

LITTLE KNIFE MINITEST WATER INJECTION SIMULATION

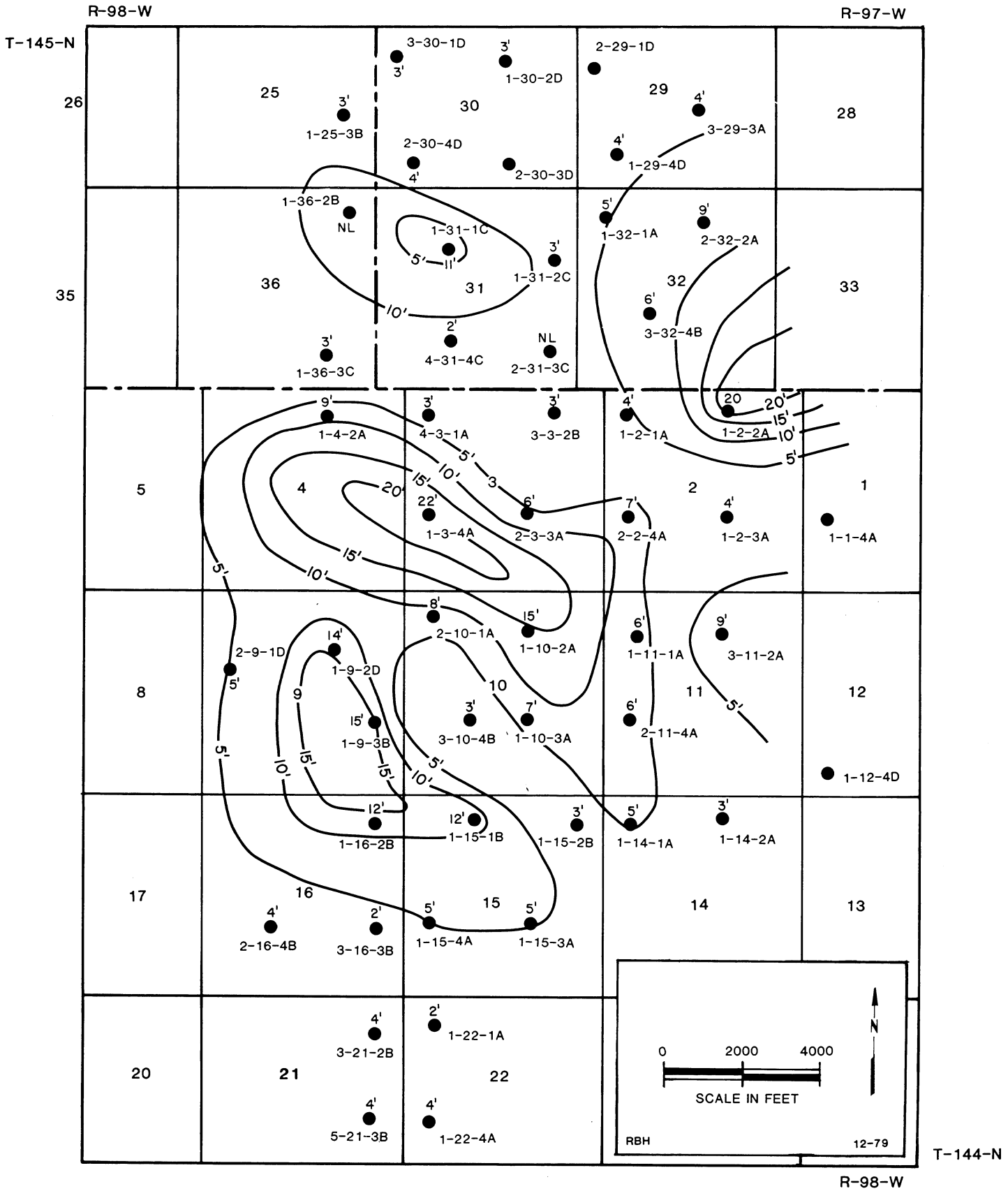

FIGURE A-2

LAYER I GROSS THICKNESS MAP

LITTLE KNIFE MINITEST WATER INJECTION SIMULATION

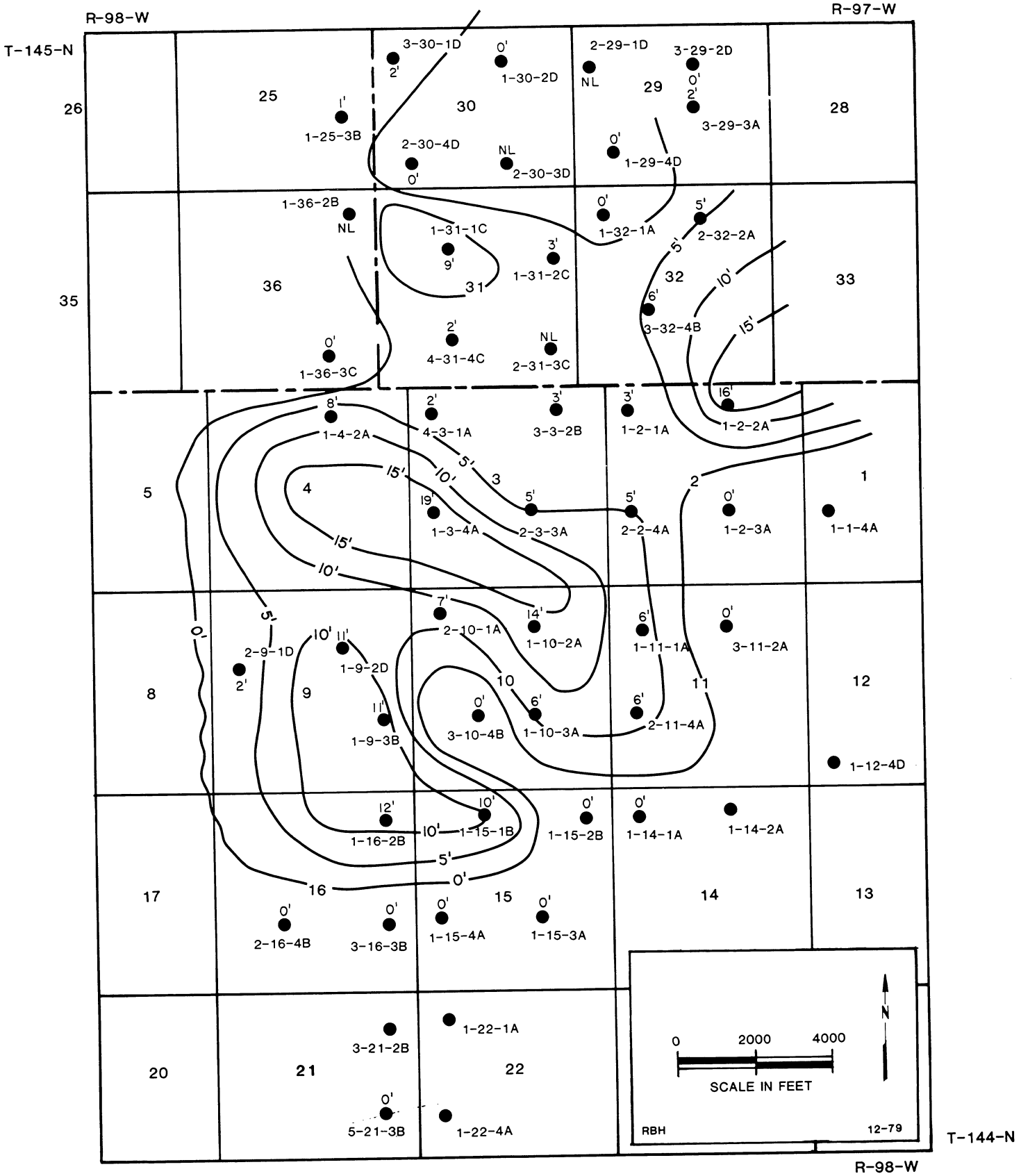

FIGURE A-3

LAYER I NET THICKNESS MAP

LITTLE KNIFE MINITEST WATER INJECTION SIMULATION

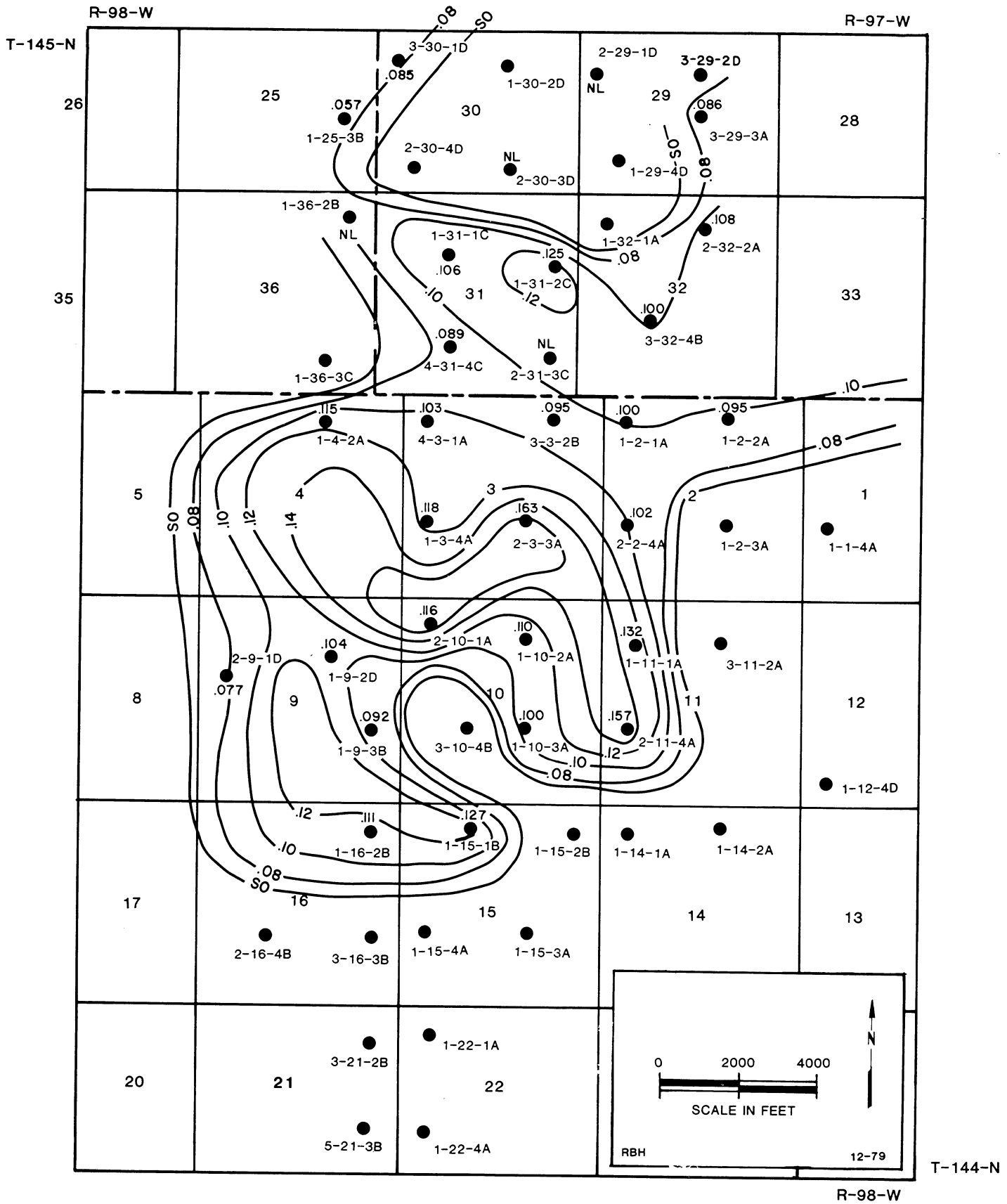

FIGURE A-4

LAYER I AVERAGE POROSITY MAP

LITTLE KNIFE MINITEST WATER INJECTION SIMULATION

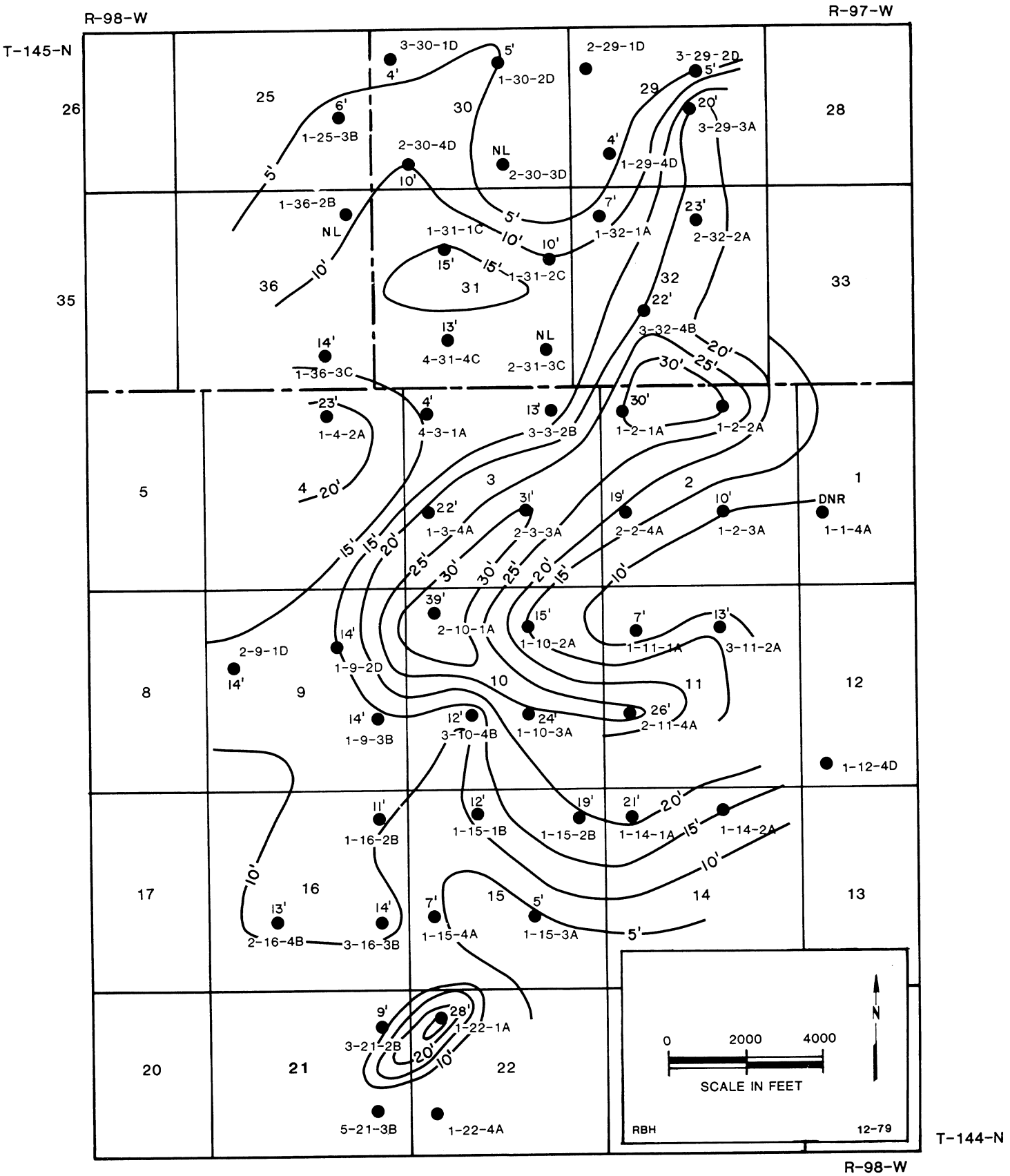

FIGURE A-5

LAYER II GROSS THICKNESS MAP

LITTLE KNIFE MINITEST WATER INJECTION SIMULATION

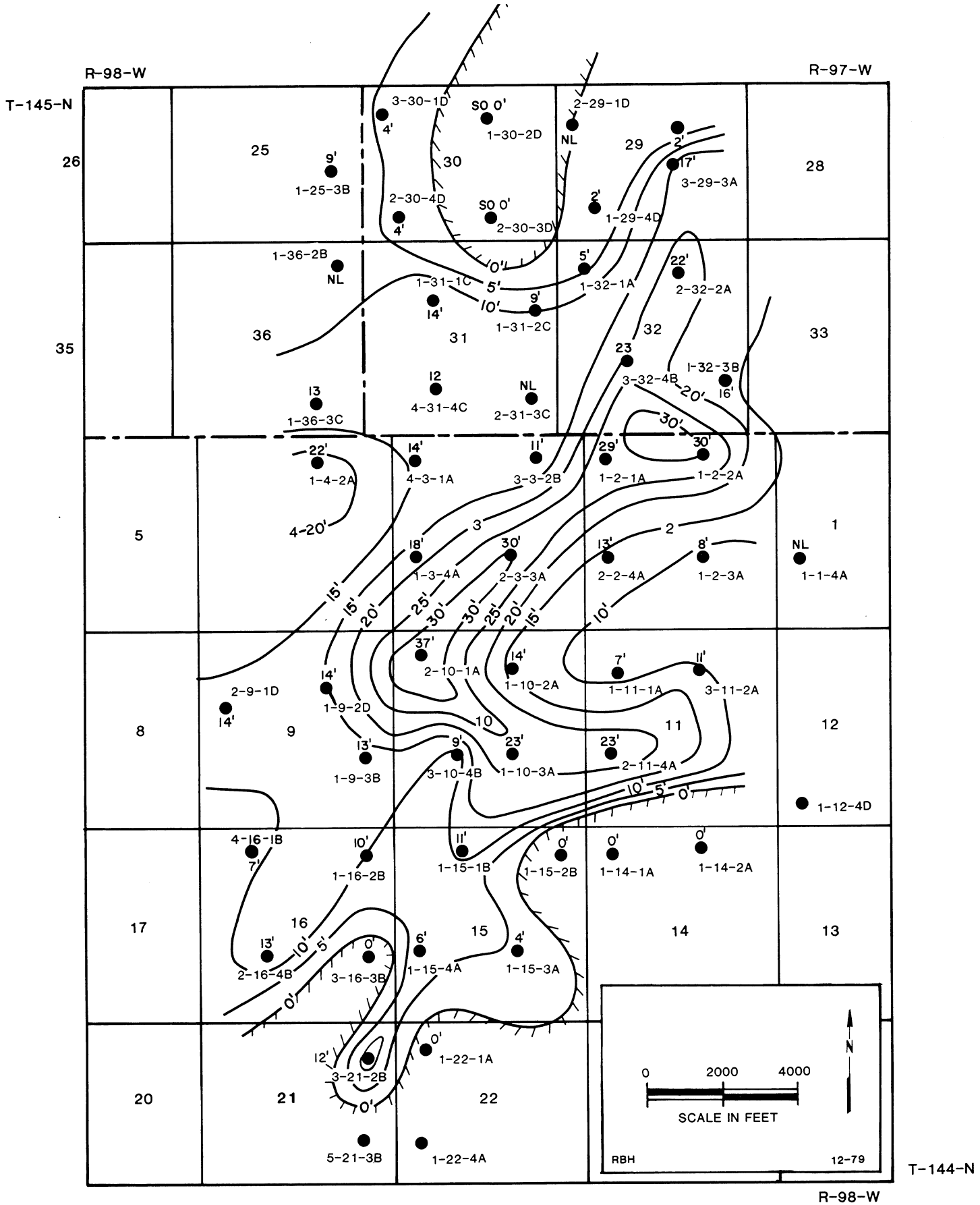

FIGURE A-6

LAYER II NET THICKNESS MAP

LITTLE KNIFE MINITEST WATER INJECTION SIMULATION

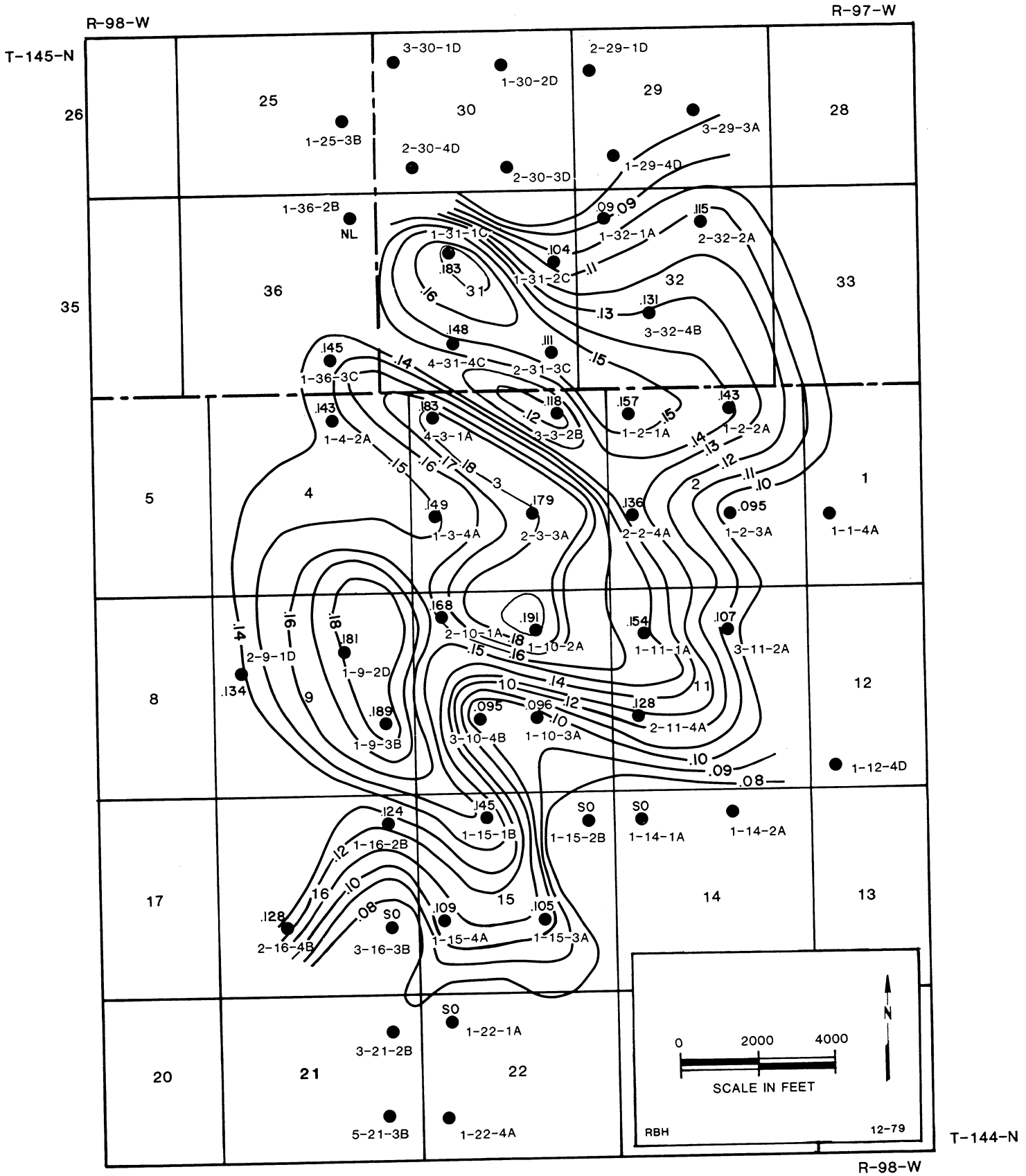

FIGURE A-7

LAYER II AVERAGE POROSITY MAP

LITTLE KNIFE MINITEST WATER INJECTION SIMULATION

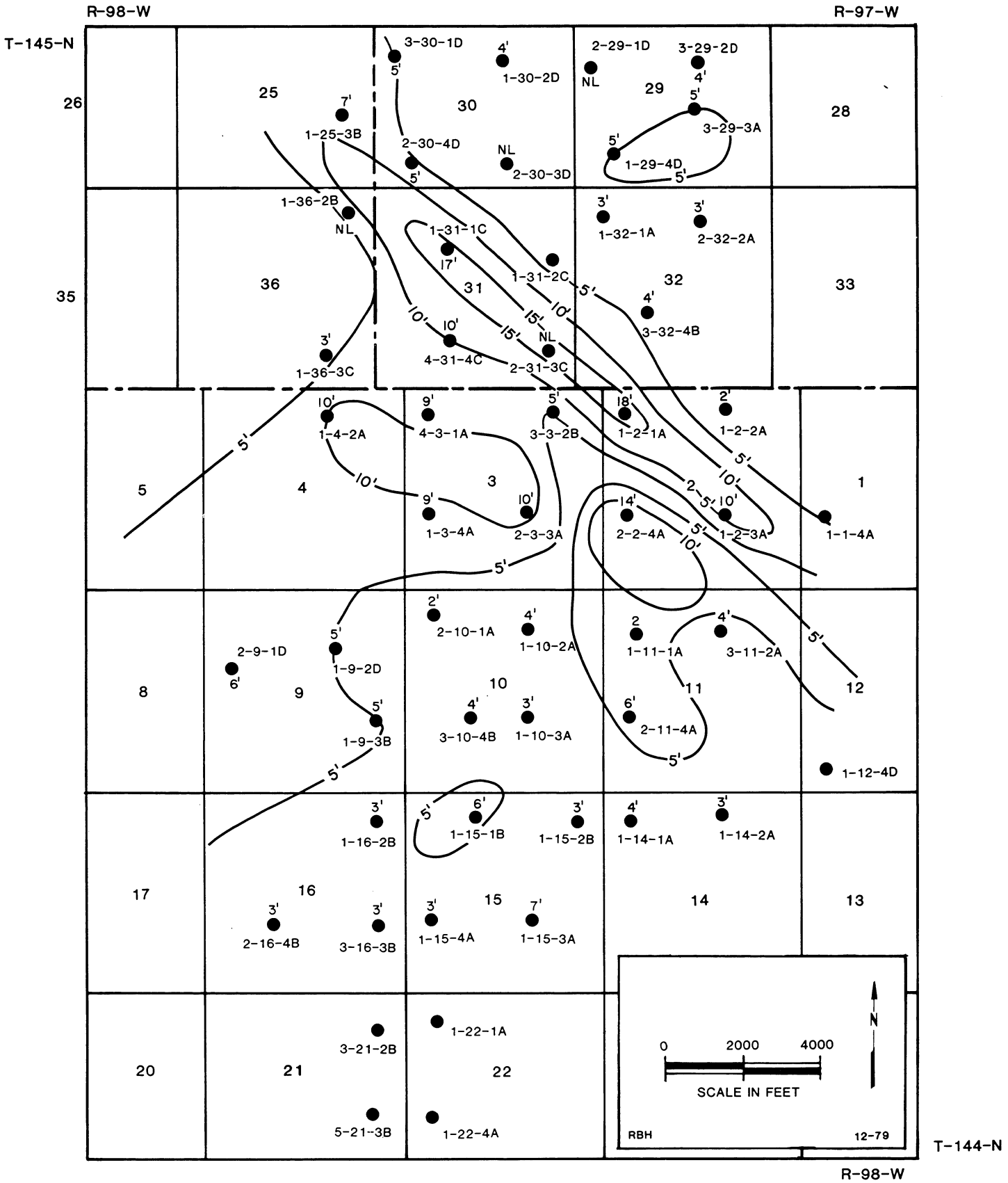

FIGURE A-8

LAYER III GROSS THICKNESS MAP

LITTLE KNIFE MINITEST WATER INJECTION SIMULATION

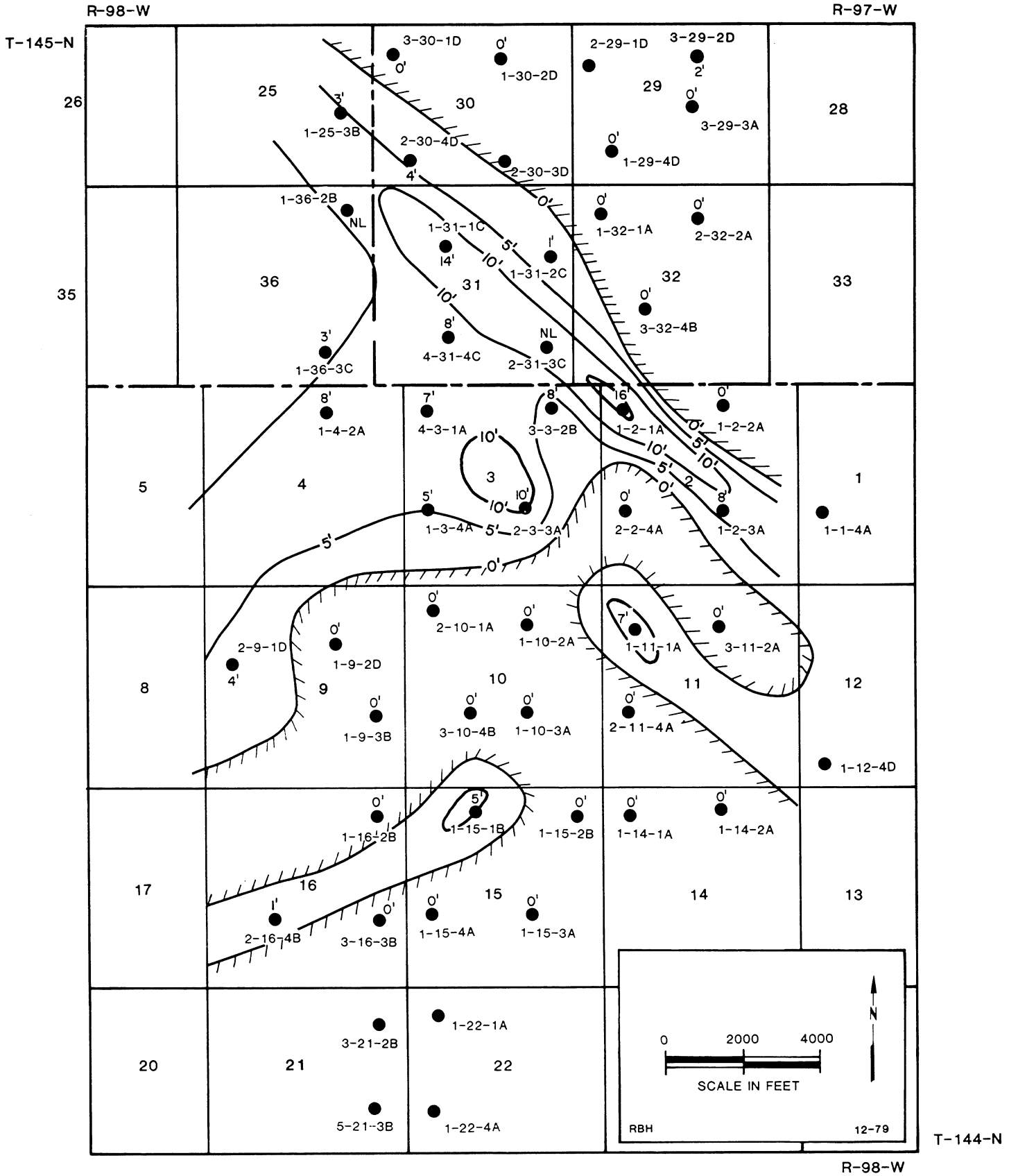

FIGURE A-9

LAYER III NET THICKNESS MAP

LITTLE KNIFE MINITEST WATER INJECTION SIMULATION

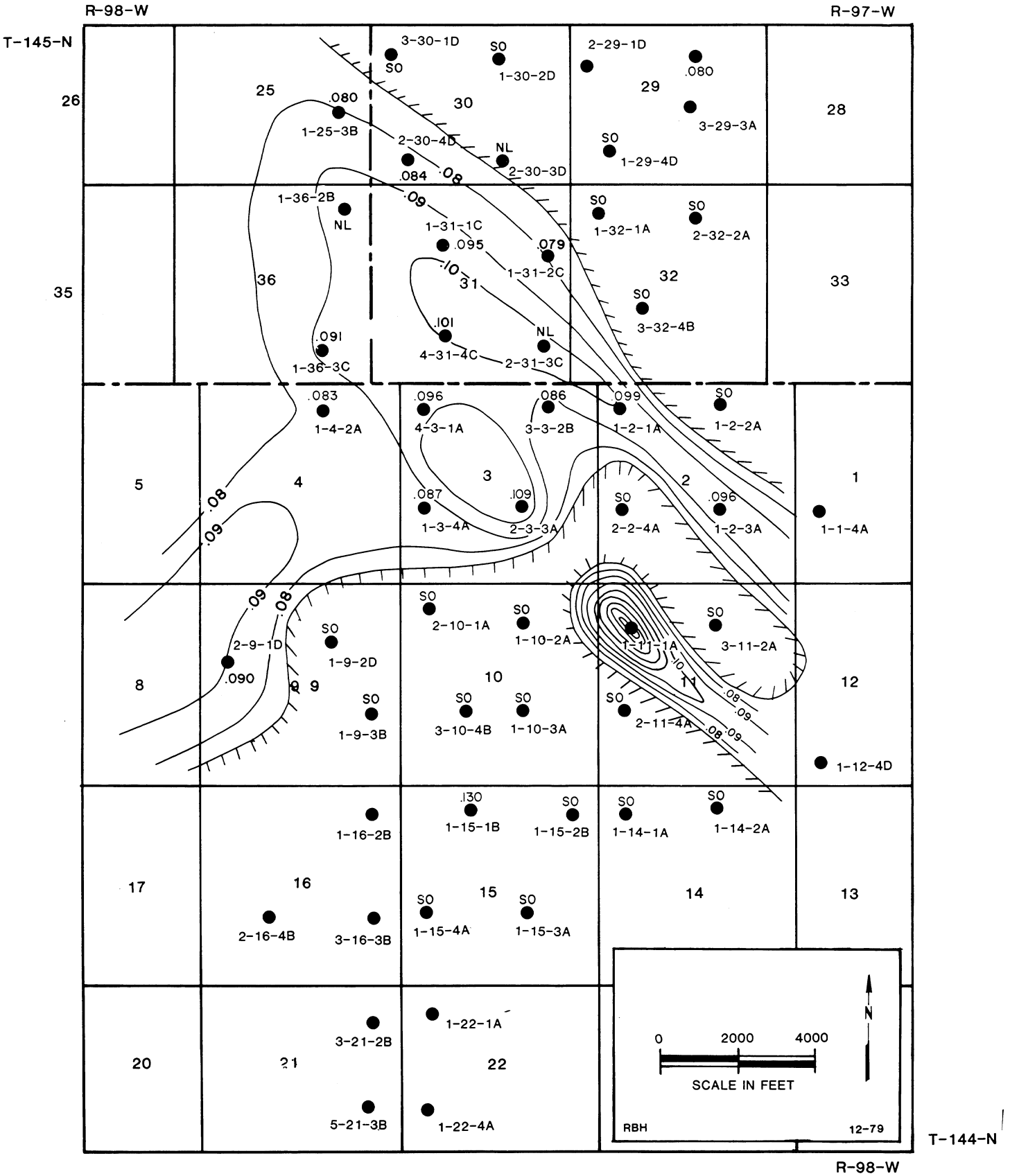

FIGURE A-10

LAYER III AVERAGE POROSITY MAP

LITTLE KNIFE MINITEST WATER INJECTION SIMULATION

APPENDIX 30

DESIGN OF A CO_2-WATER INJECTION PROGRAM FOR THE LITTLE KNIFE CO_2 FLOOD MINITEST

By
G. C. Thakur
V. Cheung
R. Ehrlich
N. M. Chaudhari
S. T. Lee

Reservoir Services Department
Gulf Research & Development Company
Houston Technical Services Center
Houston, Texas

TABLE OF CONTENTS

	Page
Summary	55
Introduction	56
Estimation of Initial Water Injection Requirements	56
Optimization of CO_2-Water Injection Scheme	57
Results	60
Conclusions	61
Future Work	61
References	62

LIST OF TABLES

Table		
1	Summary of Prediction Cases	63
2	Little Knife CO_2 Flood Minitest CO_2-Water Injection Scheme Optimization	64
3	Reservoir and Fluid Properties Used in Simulation	65
4	Measurement of CO_2-Water Residual Oil Saturation and Relative Permeability Behavior	66

LIST OF FIGURES

Figure		
1	Prediction Case Comparison	67
2	P-X Diagram for Oil Mixtures	68
3	CO_2 Displacing Crude Oil	69
4	Estimation of CO_2 Flood Minimum Miscibility Pressure	70
5	Minitest Area and Cross-section Representation	71
6	Simulation Cross-section	72
7	Simulation Cross-section	73
8	Simulation Cross-section	74
9	Simulation Cross-section	75
10	Simulation Cross-section	76

Summary

A CO_2-water injection scheme for the Little Knife CO_2 flood minitest is being designed. A three-dimensional simulation study that included several sections surrounding the minitest area and all the Mission Canyon producing zones concluded that pressure in the minitest area will decline below the estimated CO_2 flood miscibility pressure by September, 1980. Injection of water at 1150 B/D for 15 days (approximately 15% of the pattern pore volume) was found to increase the pressure to well above miscibility pressure.

A two-dimensional cross-sectional compositional simulator study of the Mission Canyon "D" zone is in progress. The injection scheme will follow the 15% pore volume of water with alternate slugs of CO_2 and water and then with water alone. Plans are to optimize this scheme with respect to the water-CO_2 ratio, the total amount of CO_2 injected, and the size of the alternating slugs. At this time, some water-CO_2 optimization work has been completed. For a 1:1 water-CO_2 ratio, an oil recovery of 57.2% PV or 76.5% OOIP (uncorrected for areal sweep or capture efficiency effects) was obtained.

Further work will complete the parameter optimization work and will test important results using a three-dimensional simulation, using relative permeability curves obtained at reservoir conditions.

INTRODUCTION

A minitest jointly funded by Gulf and DOE[1] will evaluate CO_2 miscible flooding as an enhanced recovery method for the Little Knife field. The test will be in the "D" zone of the Mission Canyon formation and will use an injection well offset by three observation wells on about five acre spacing. Analysis of cased hole logs and periodic fluid samples from the observation wells will indicate changes in fluid saturations and composition and will allow estimates and projections of process performance.

The test will consist of initial water injection to increase the minitest area pressure to above the minimum miscibility pressure, injection of a fractional pore volume of CO_2 as alternate slugs with water (WAG process), followed by injection of water alone. Parameters that must be specified in accordance with Phase III of Reference 1 in this CO_2-water injection scheme are the volume and rate for initial water injection, the total amount of CO_2 to be injected and the schedule for injecting the CO_2 (e.g., what size the alternating slugs should be; what the injection rates should be).

Numerical simulation models are being used to specify all of the above parameters. Initial water injection rate and volume are obtained using a 3-D Black Oil Simulator history matched to reservoir pressure to represent the Little Knife field in the minitest area. The CO_2-water injection parameters and recovery estimates are obtained via process performance optimization using a compositional simulator. The minitest area for this is modeled by a 2-D cross-section connecting the injection well and an observation well. Laboratory determinations of CO_2-water displacement parameters at reservoir conditions will provide residual oil saturation and relative permeability data required.

Some aspects of the design work presented here should be regarded as preliminary. As will be discussed later, performance predictions have not been made for all the required parameters. Also, conventional gas-water relative permeability curves, which are used in the reservoir simulation work given here, are being found not to describe CO_2-water flow after oil has been displaced. The final CO_2-water injection scheme will be optimized for all the critical parameters and will be based on the more realistic relative permeability curves. This work should be completed before CO_2 injection is actually begun.

ESTIMATION OF INITIAL WATER INJECTION REQUIREMENTS

A simulation study was carried out to investigate the effects of current production in the Little Knife field on pressure in the minitest area and the effects of a number of water injection schemes

on that pressure. This study used the INTERCOMP Beta II Black Oil Simulator and considered all the producing zones in the Mission Canyon formation over an area encompassing the section in which the minitest is located and four surrounding sections. Details of this study are given in Reference 2. Results and conclusions are given below.

Simulation of two possible production scenarios without initial water injection (Cases 1 and 3 in Table 1 and Figure 1) has shown that the minitest area pressure will decline below the estimated minimum CO_2 multiple contact miscibility pressure by September of 1980. Injection of water at 1150 STB/D for 15 days was shown to increase pressure to well above this miscibility pressure for either of these decline situations (Cases 2, 4 and 5).

OPTIMIZATION OF CO_2-WATER INJECTION SCHEME

Simulator and Oil Properties

Gulf's multicomponent compositional reservoir simulator is being used for prediction of the performance of various CO_2-water injection schemes. In this simulator, gas and oil are represented as being composed of discrete components with vapor-liquid equilibria governing interphase transport of these components calculated from a Peng-Robinson equation of state.

A seven-component representation of the Little Knife reservoir fluid was derived from a detailed analysis (Table 2 of Reference 1) by lumping components. The representation of the oil above its bubble point pressure is:

Component	Mole Fraction
CO_2	.0154
CH_4, N_2	.3634
H_2S	.0799
C_2H_6	.0993
C_3-C_5	.1746
C_6-C_{12}	.1777
C_{13+}	.0897
	1.0000

The ability of this type of discrete component fluid representation to adequately model CO_2-oil interactions that take place in a miscible displacement in which miscibility must be induced through multiple contacts is an important matter. Relevant experimental data available to test this are the phase behavior for the CO_2-Little Knife crude oil system obtained from single contact equilibration, the results of slim tube displacement tests at various pressures and the predicted minimum miscibility pressure from the slim tube data (Figures 5 and 6 of Reference 1).

Figure 2 shows a comparison of an experimentally determined phase envelope together with liquid volume fractions in the two-phase region (black) with that predicted from the discrete fluid representation together with the Peng-Robinson equation of state (red). Figures 3 and 4 give results of compositional simulation of one-dimensional CO_2-Little Knife displacement with rock properties that match those of the slim tube packing material. Figure 3 compares laboratory results at 3410 psi and 240°F (black) with the simulator prediction for those conditions for different numbers of grid blocks (red). Figure 4 compares laboratory oil recovery at CO_2 breakthrough and a 1.6 PV's CO_2 injection versus pressure at 240°F (black) with the simulator predictions for those conditions using 25 grid blocks (red).

These tests indicate that the fluid representation and the simulator are adequate to describe the CO_2-Little Knife crude oil phase behavior and interactions during miscible displacement. About twenty-five horizontal grid blocks appear sufficient to model the development of multiple contact miscibility.

Plans for CO_2 Water Injection Parameter Optimization

The optimum CO_2-water injection method for Little Knife will be strongly dependent on reservoir properties. The WAG ratio that gives the best mobility control will depend on the extent to which water and CO_2 will segregate in the reservoir, which will, in turn, depend on capillary, gravity and viscous force interactions over the net pay and stratification. The optimum CO_2 volume to be injected will depend on CO_2 storage behind the CO_2-water front, trapping of CO_2 by drive water, the extent to which stratification causes bypassing, and on fingering and dispersive mixing at the CO_2-oil front (the simulator does not adequately represent these last two effects).

With these considerations in mind, it was felt that simulation of CO_2-water displacement using a two dimensional vertical cross-section

representation of the Mission Canyon "D" zone in the minitest area would be sufficient to optimize these parameters. Figure 5 shows a plan view of the pilot area and the cross-section representation.

The optimization work is being carried out by choosing a base case injection scheme using what is felt are likely values for the parameters. Each parameter is then varied from the base case value and the sensitivity of recovery and process performance to it determined from simulation results. Table 2 outlines the sequence of simulation work.

The total fluid injection rate will not be optimized in this way but will be kept at the level necessary to maintain the minitest area pressure above the minimum miscibility pressure of approximately 3400 psi.

Data and Assumptions Required for Modeling Work

(a) Reservoir, Rock and Fluid Properties

From analysis of whole cores from the Mission Canyon "D" zone, porosities and permeabilities were averaged separately for the layers assumed in the cross-section model. These and other formation and fluid properties used in the simulation work are given in Table 3.

Two-phase relative permeability and capillary pressure curves were obtained from room temperature measurement using mineral oil and nitrogen to represent crude oil and CO_2 or are calculated from mercury injection data. In the simulator, required three-phase relative permeability data are calculated using Stone's approximation which assumes that water and gas are the most and least wetting phases, respectively.

(b) CO_2-Water Residual Oil and Displacement Parameters at Reservoir Conditions

Results obtained thus far in Phase II of Reference 1 have indicated that the residual oil to simultaneous flow of CO_2 and water following development of a miscible bank is low (0.8%-3.1% PV) as shown in Table 4 and insensitive to WAG ratio. For approximation purposes, residual oil saturation behind a miscible CO_2 front has been allowed to go to zero in this simulation work.

The Phase II data are also beginning to show that the conventional wetting assumptions do not hold in the water-CO_2 bank at residual oil. CO_2 appears to be the wetting phase with respect to water. This is seen in a comparison of gas saturations at approximately the same k_g/k_w before and after the CO_2 flood residual oil saturation is extracted with solvent. The much higher CO_2 saturations in the former case indicate CO_2-wetting. (This wetting by a miscible fluid in preference to water after miscible displacement has been reported previously[3]).

The optimization results given here will be somewhat sensitive to these CO_2-water relative permeability curves because they affect the mobility ratio and the CO_2 saturation at a given WAG ratio behind the CO_2-water flood front. It seems reasonable, therefore, to revise the optimization work given here once complete CO_2-water relative permeability data become available.

RESULTS

At this time, Runs 1, 2 and 3 in Table 2 -- the base case and the WAG ratio variations from it -- have been completed. The simulation results -- CO_2 and water injected and oil produced as a function of time -- are given in Figures 6, 7 and 8 for WAG ratios of 1 RBbl water/RBbl CO_2 (the base case), zero (CO_2 alone), and 3 RBbl water/RBbl CO_2, respectively. Figure 9 shows the results of a simulated waterflood (no CO_2 injected) for comparison purposes. Oil recovery and cumulative CO_2-oil ratio versus time for these runs is shown in Figure 10.

The following are considered to be significant observations from Figure 10.

(1) Although ultimate recovery is more or less the same for all the CO_2 floods, breakthrough of injected fluids is earliest for the 3:1 WAG ratio and latest for the 1:1 WAG ratio. For CO_2 alone, breakthrough is slightly earlier than for the 1:1 WAG ratio. On this basis, we would prefer the 1:1 WAG ratio. The improvements that a 1:1 WAG ratio CO_2 flood give over CO_2 alone -- 2.3% PV more oil and a small improvement in breakthrough time -- appear to be worth the extra effort involved in carrying out this type of flood.

(2) Ultimate recoveries after about 1 HCPV total fluid injection (800-1000 days) are high for all the CO_2 floods -- 76.5% OOIP for the 1:1 WAG ratio, 74.2% OOIP for CO_2 alone, and 77.5% OOIP for the 3:1 WAG ratio compared with 41.2% OOIP for the waterflood. Cumulative CO_2-oil ratios at this time are all low -- about 1 MSCF/Bbl. In looking at these numbers, it should be realized that CO_2 flood predictions in a cross-section model

which does not allow for areal sweep and capture efficiency effects, and in which such effects as viscous fingering and dispersive mixing are not adequately represented, will be optimistic. Also, some oil that is attributed to the CO_2 flood could have been recovered by primary and secondary methods. However, the fact that gravity segregation of CO_2 and water and gravity override of oil by CO_2 do not seem to be important even for the assumed $k_v/k_h = 1$ is a positive factor. Bypassing of oil because of permeability stratification appears to be limited to the bottom layer. However, because not much CO_2 enters this layer, the effect will be less on the CO_2-oil ratio. Overall, vertical sweep efficiency appears to be good.

CONCLUSIONS

1. The compositional simulator represents CO_2-Little Knife crude oil phase behavior and the development of multiple contact miscibility in slim tubes.

2. Residual oil saturation is low above the minimum miscibility pressure and does not depend on water-CO_2 ratio.

3. A 1:1 water-CO_2 ratio (RBbl/RBbl) appears on the basis of breakthrough time to be the best of those investigated. Recovery in the cross-section model of the Mission Canyon "D" zone after 1 HCPV total fluid injection is 57.2% PV or 76.5% OOIP. (These numbers include primary and secondary oil and are not corrected for areal sweep and capture efficiencies.)

FUTURE WORK

1. The simulation work outlined in Table 2 will be completed.

2. Water-CO_2 relative permeability curves in the presence of residual oil and water-oil relative permeability curves will be obtained in preserved

Mission Canyon cores at reservoir temperature and pressure.

3. Important conclusions from the simulation work will be tested using the new relative permeability curves and in a 3-D representation of the reservoir. The latter will better represent the effects of mobility ratio on recovery.

G. C. Thakur

R. Ehrlich

V. Cheung

N. M. Chaudhari

S. T. Lee

/st

REFERENCES

(1) "Technical Proposal for Enhanced Recovery Activities, Little Knife Field, North Dakota", DOE RFP No. EW-78-R-21-8383, Gulf Oil Corporation, 9/8/78.

(2) "Little Knife Field CO_2 Minitest Water Injection Simulation, Mercer County, North Dakota", Reservoir Services Report No. 445RL029, July, 1980.

(3) F. N. Schneider, W. W. Owens: "Relative Permeability Studies of Gas-Water Flow Following Solvent Injection in Carbonate Rocks", Soc. Pet. Eng. J., February, 1976, pp. 23-30.

TABLE 1

Summary of Prediction Cases

Little Knife CO_2 Flood Minitest Initial Water Injection Simulation

Case Number	Description
1	Naturally declining production through Oct. 15, 1980 with no water injection.
2	Naturally declining production through Oct. 15, 1980 with water injection beginning Oct. 1, 1980. Injection limited by a maximum rate of 1150 STB/D and a surface tubing pressure of 700 psig.
3	Constant rate production through October 15, 1980 with no water injection.
4	Constant rate production through Oct. 15, 1980 with water injection beginning Oct. 1, 1980. Injection limited by a maximum rate of 1150 STB/D and a surface tubing pressure of 700 psig.
5	Constant rate production through Sept. 15, 1980 with water injection beginning Sept. 1, 1980. Injection limited by a maximum rate of 1150 STB/D and a surface tubing pressure of 700 psig.

TABLE 2

Little Knife CO_2 Flood Minitest CO_2-Water Injection Scheme Optimization -- Sequence of Simulation for D-zone Cross-section Model

Run No.	Initial Water Inj.	CO_2 Volume	WAG Ratio	CO_2-Water Slug Size	Final Drive
1 (base case)	15% PV	25% HCPV	1.00 RBbl/RBbl	5% HCPV CO_2/5% water	Water to 1 PV total injection
2	"	"	0	25% HCPV CO_2 with no alternating water	"
3	"	"	3.00 RBbl/RBbl	5% HCPV CO_2/15% water	"
4	"	15% HCPV	**	5% HCPV CO_2/5% water	"
5	"	35% HCPV	**	"	"
6	"	***	**	2.5% HCPV CO_2/2.5% water	"
7*	"	***	**	1.25% HCPV CO_2/1.25% water	"

*Run 7 will be done only if 6 shows a difference from the base case.

**At best WAG ratio determined from 1-3.

***At best CO_2 volume determined from 4, 5 and 1, 2 or 3.

TABLE 3

Reservoir and Fluid Properties Used in Simulation

Mission Canyon "D" Zone -- 1/3 of 5-acre Pattern (Pore Volume = 42,507 Bbl)

Layer	h (ft)	Ø (%)	k_h (md)	k_v (md)	S_{wi} (% PV)	Pore Volume (Bbl)
1	4	18	25	25	22.3	9,219
2	10	20	30	30	25.4	25,606
3	4	15	1.5	1.5	28.5	7,682

Fluid Properties at 240°F, 3583 psia

Little Knife Crude Oil: ρ = 0.618 g/cc, μ = 0.22 cp, FVF = 1.73 STB/RBbl

Water : ρ = 1.151 g/cc, μ = 0.40 cp, FVF = 1.043 STB/RBbl

CO_2 : ρ = 0.515 g/cc, μ = 0.0425 cp, FVF = 1.555 MSCF/RBbl

TABLE 4

Measurement of CO_2-Water Residual Oil Saturation and Relative Permeability Behavior in Preserved Little Knife Zabolotny Injection #1 Cores at 3500 psi and 245°F

Core Data			Water-CO_2 Ratio	Final Conditions*			
Depth (ft)	K (md)	Ø (%)	(RBbl/RBbl)	S_o(% PV)	S_w(% PV)	S_g(% PV)	k_g/k_w
9823	7.3	23	0	3.1	20.0	76.9	--
9826-27	5.3	22	1.5	3.1	61.5	35.4	0.110
9814-15	39	26	3.0	0.8	63.5	35.7	0.055
(The following were obtained after extraction of residual oil.)							
9814-15	39	26	0	--	29.9	70.1	--
9814-15	39	26	1.35	--	80.3	19.7	0.124
9814-15	39	26	2.7	--	87.3	12.7	0.062

*Oil saturations are obtained gravimetrically assuming original oil density. Water and CO_2 saturations and relative permeabilities are calculated from pure component material balances and do not allow for mutual solubility.

FIGURE 1

PREDICTION CASE COMPARISON
LITTLE KNIFE MINITEST WATER INJECTION SIMULATION

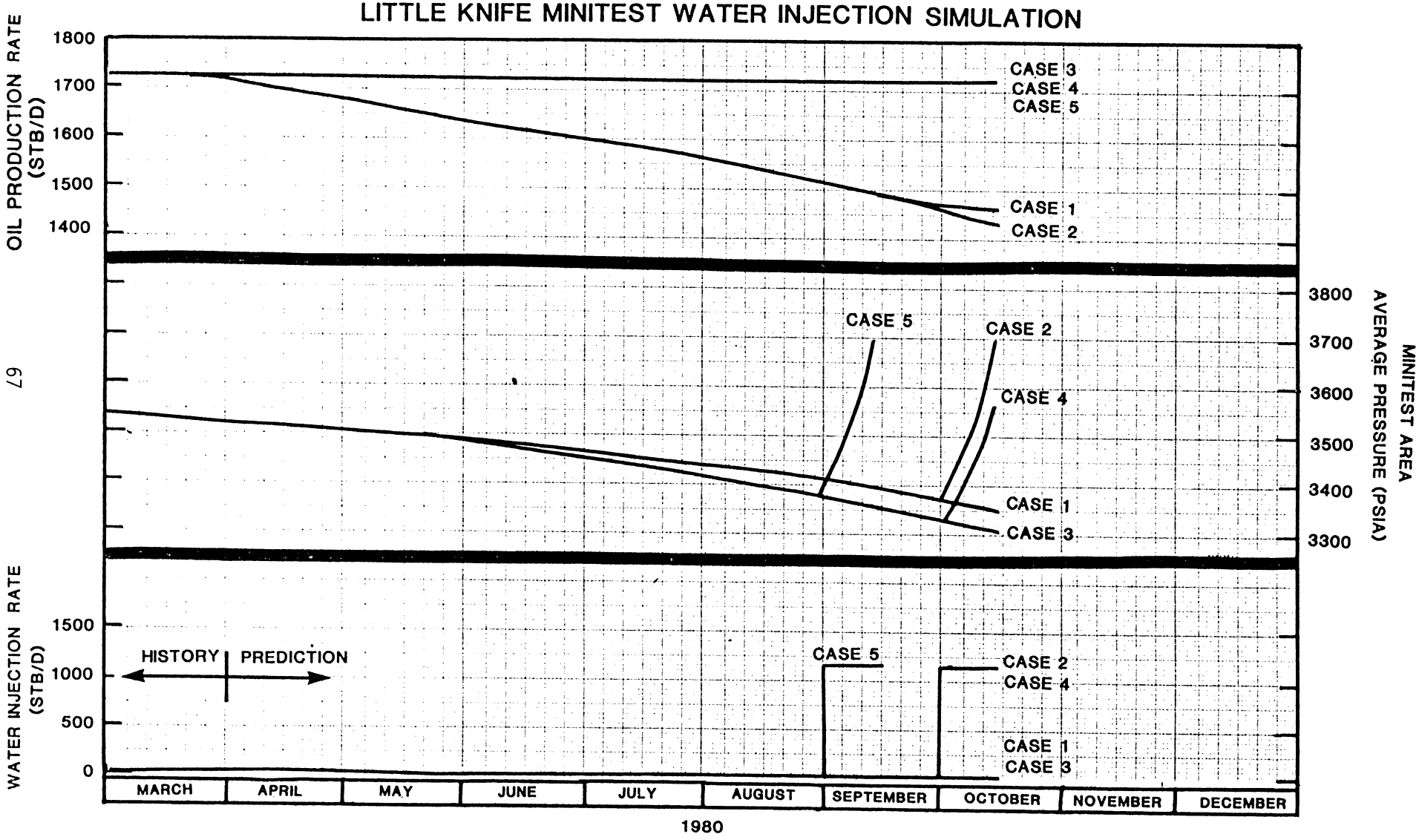

FIGURE 2

P-X DIAGRAM FOR CO_2 LITTLE KNIFE OIL MIXTURES AT 240 °F

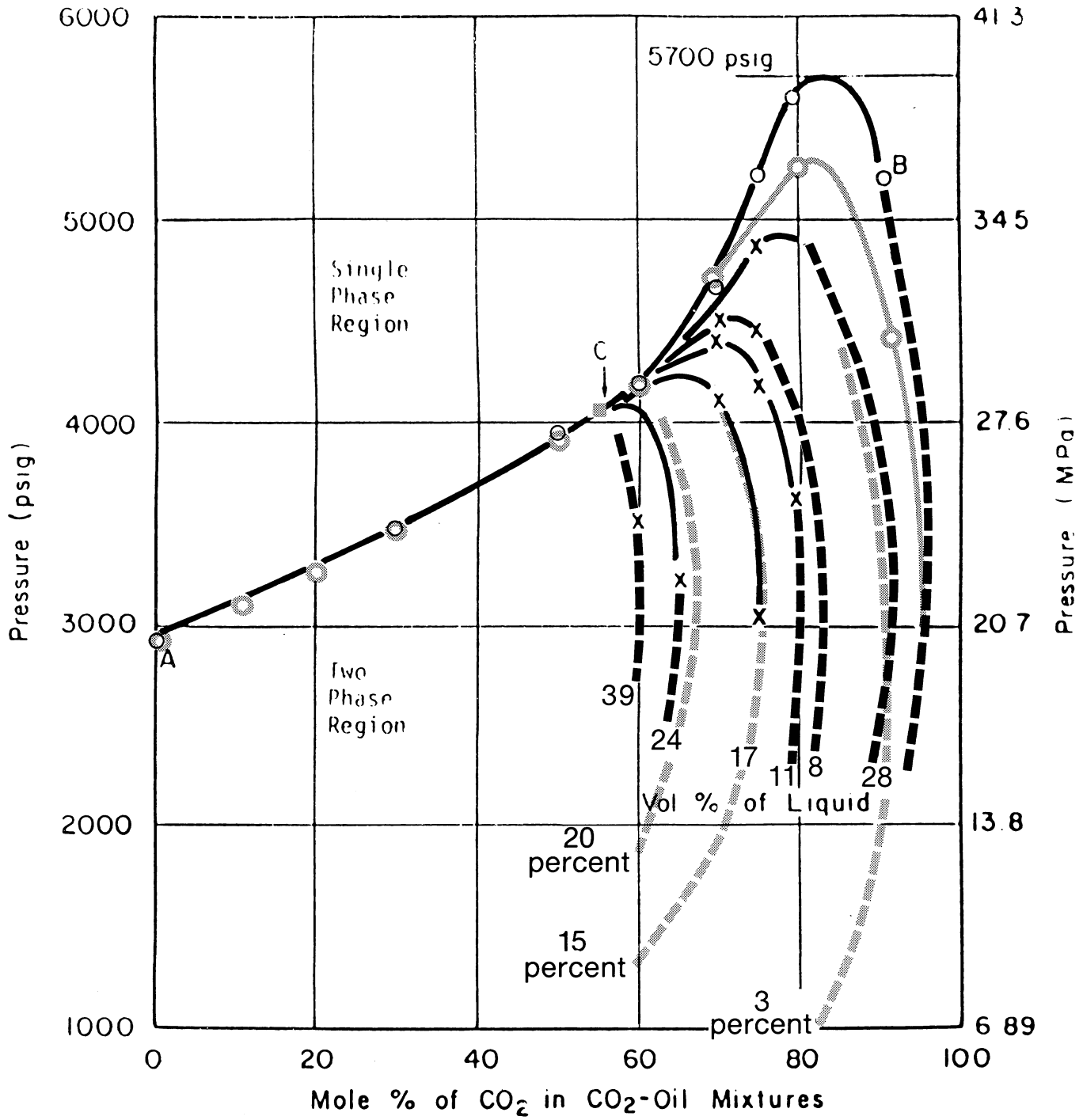

Predicted Phase Envelope

Predicted Critical Point

Predicted Constant Liquid Volume Curve

FIGURE 3

CO_2 DISPLACING LITTLE KNIFE CRUDE OIL FROM A SLIM TUBE AT 3410 psi AND 240 °F
– COMPARISON OF COMPOSITIONAL SIMULATION AND EXPERIMENTAL DATA

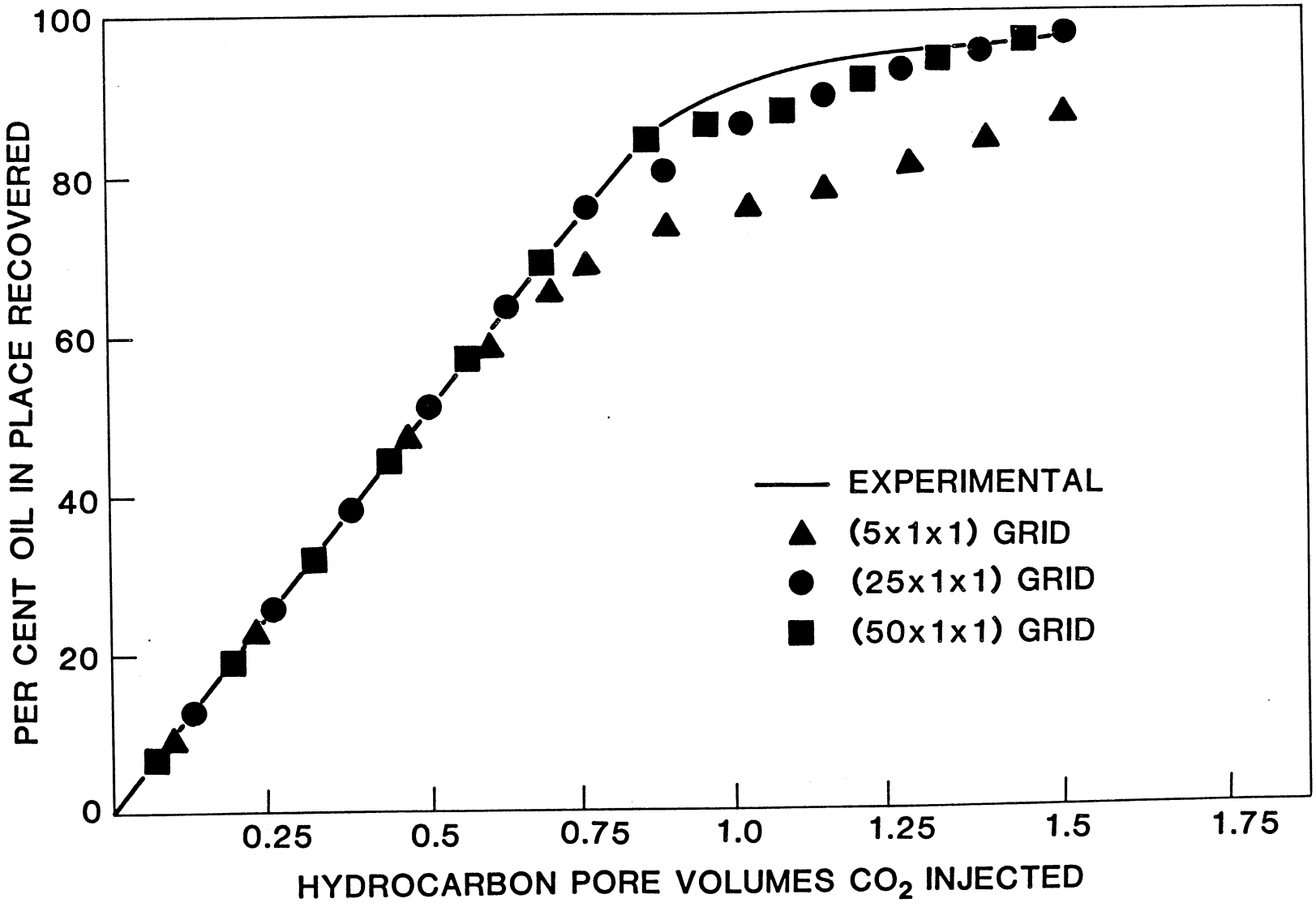

FIGURE 4

ESTIMATION OF CO_2 FLOOD MINIMUM MISCIBILITY PRESSURE FROM SLIM TUBE DISPLACEMENT TESTS FOR LITTLE KNIFE CRUDE OIL AT 240 °F - COMPARISON OF COMPOSITIONAL SIMULATION (25 GRID BLOCKS) AND EXPERIMENTAL DATA

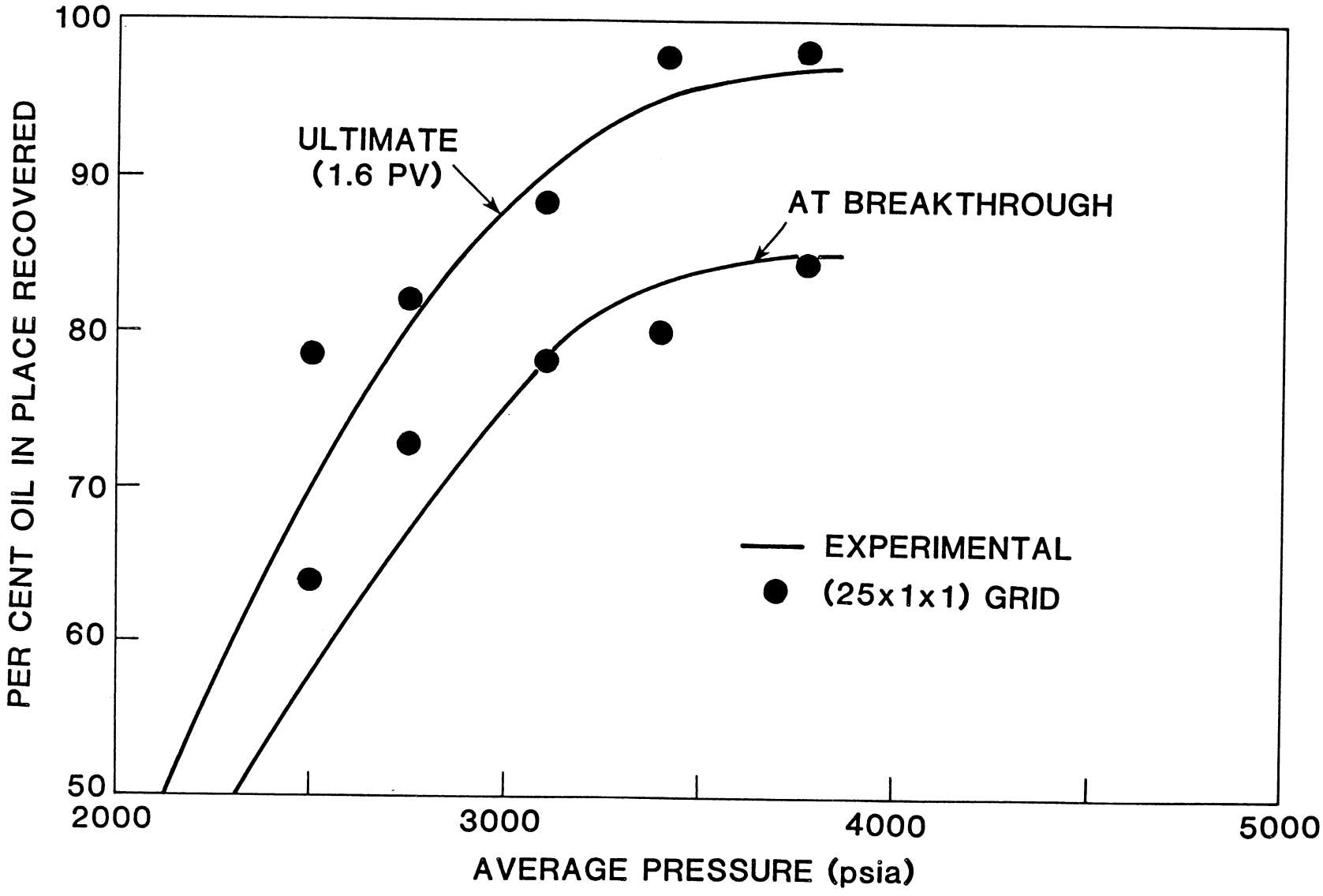

FIGURE 5

LITTLE KNIFE CO_2 FLOOD MINITEST AREA AND CROSS-SECTION REPRESENTATION OF ONE-THIRD OF THE MISSION CANYON "D" ZONE BETWEEN THE INJECTION WELL AND AN OBSERVATION WELL

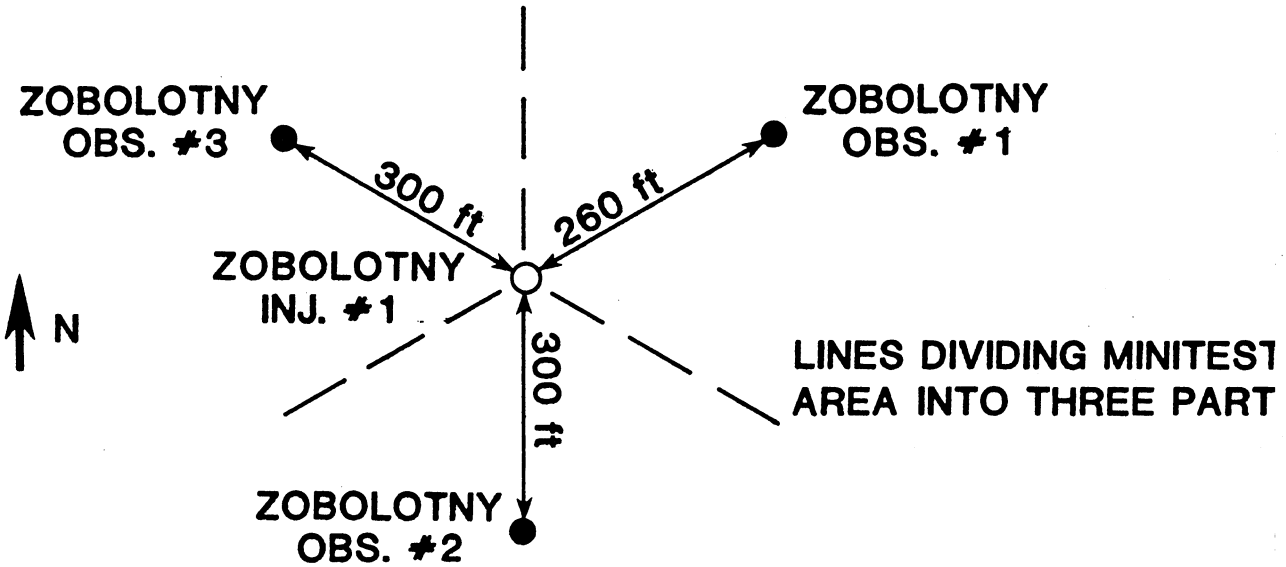

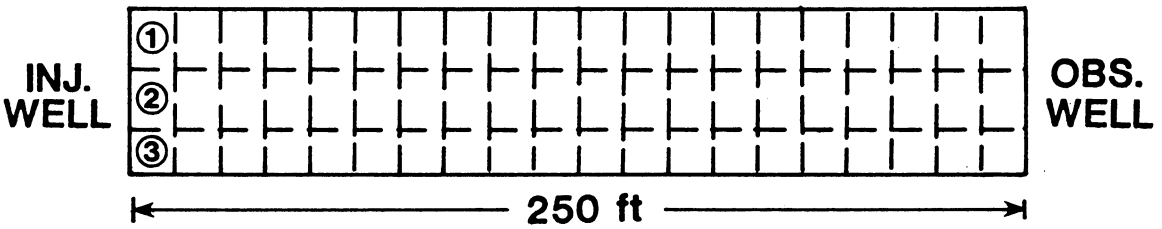

BLOCK WIDTH INCREASES WITH DISTANCE FROM INJECTION WELL TO 560 ft MAXIMUM TO SIMULATE RADIAL GEOMETRY

FIGURE 6

LITTLE KNIFE MINITEST CO_2 FLOOD SIMULATION
CROSS-SECTION OF ~ 1/3 OF 5-ACRE MISSION CANYON "D" ZONE —
25% HCPV CO_2 INJECTED AS 5% HCPV SLUGS ALTERNATING WITH
5% HCPV SLUGS OF WATER (WAG RATIO = 1:1) —
PORE VOLUME = 42,507 BBL, INJECTION RATE = 50 BBL/DAY AVG.

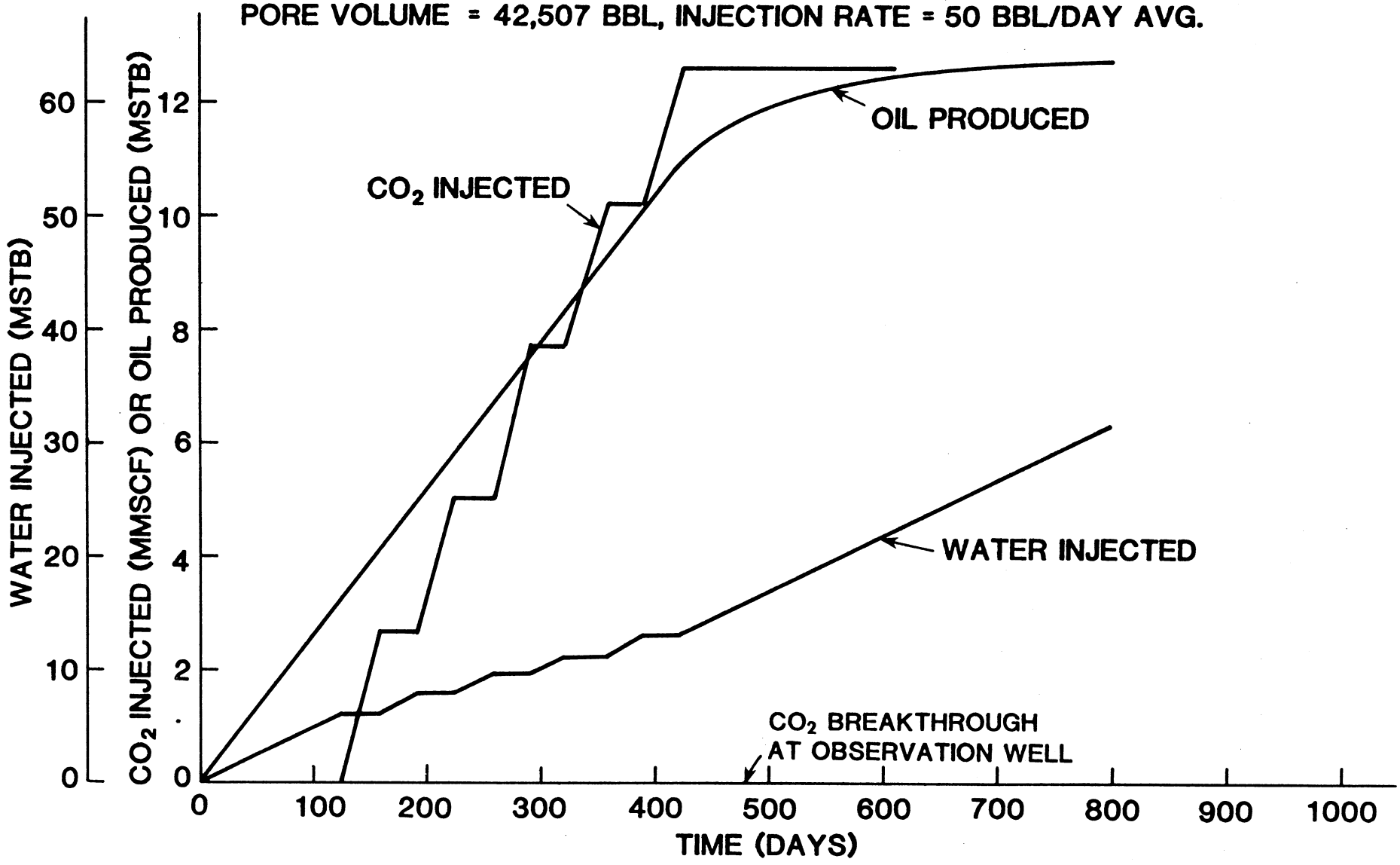

FIGURE 7

LITTLE KNIFE MINITEST CO_2 FLOOD SIMULATION
CROSS-SECTION OF ~ 1/3 OF 5-ACRE MISSION CANYON "D" ZONE —
25% HCPV CO_2 INJECTED ALONE (WAG RATIO = 0) —
PORE VOLUME = 42,507 BBL, INJECTION RATE = 50 BBL/DAY AVG.

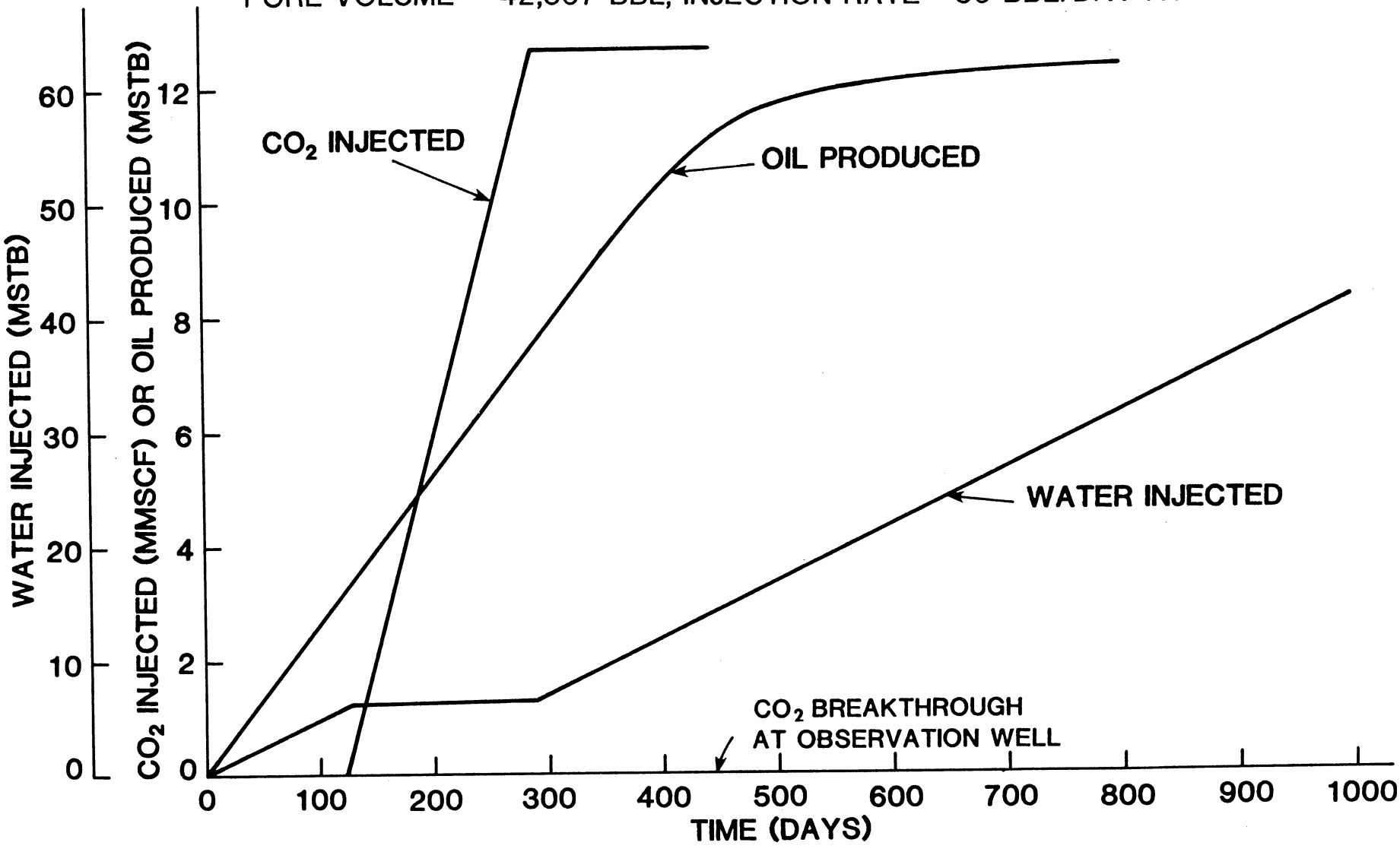

FIGURE 8

LITTLE KNIFE MINITEST CO_2 FLOOD SIMULATION
CROSS-SECTION OF ~ 1/3 OF 5-ACRE MISSION CANYON "D" ZONE —
25% HCPV CO_2 INJECTED AS 5% HCPV SLUGS ALTERNATING WITH
15% HCPV SLUGS OF WATER (WAG RATIO = 3:1) —
PORE VOLUME = 42,507 BBL, INJECTION RATE = 50 BBL/DAY AVG.

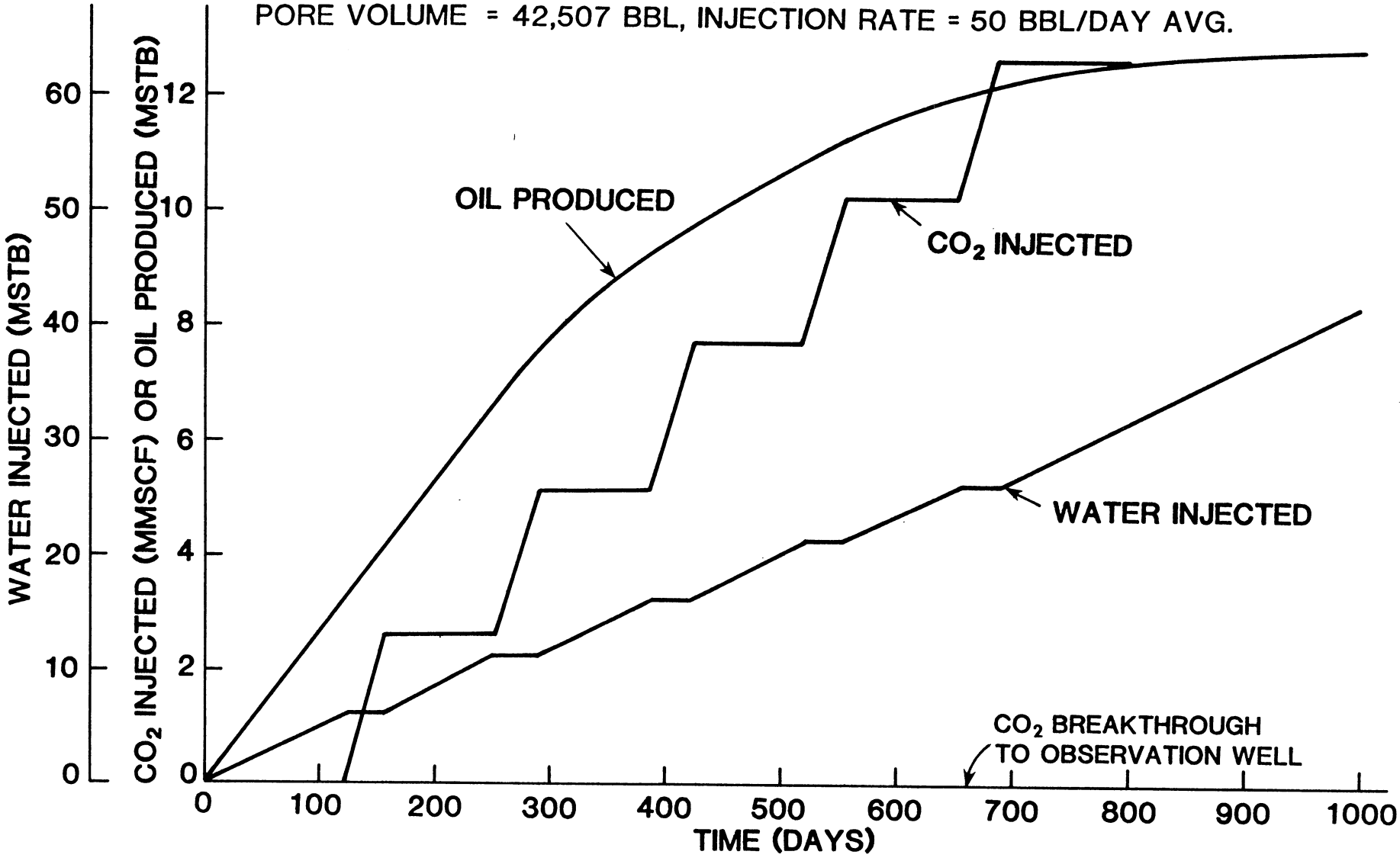

FIGURE 9

LITTLE KNIFE MINITEST CO_2 FLOOD SIMULATION
CROSS-SECTION OF ~ 1/3 OF 5-ACRE MISSION CANYON "D" ZONE —
WATERFLOOD —
PORE VOLUME = 42,507 BBL, INJECTION RATE = 50 BBL/DAY AVG.

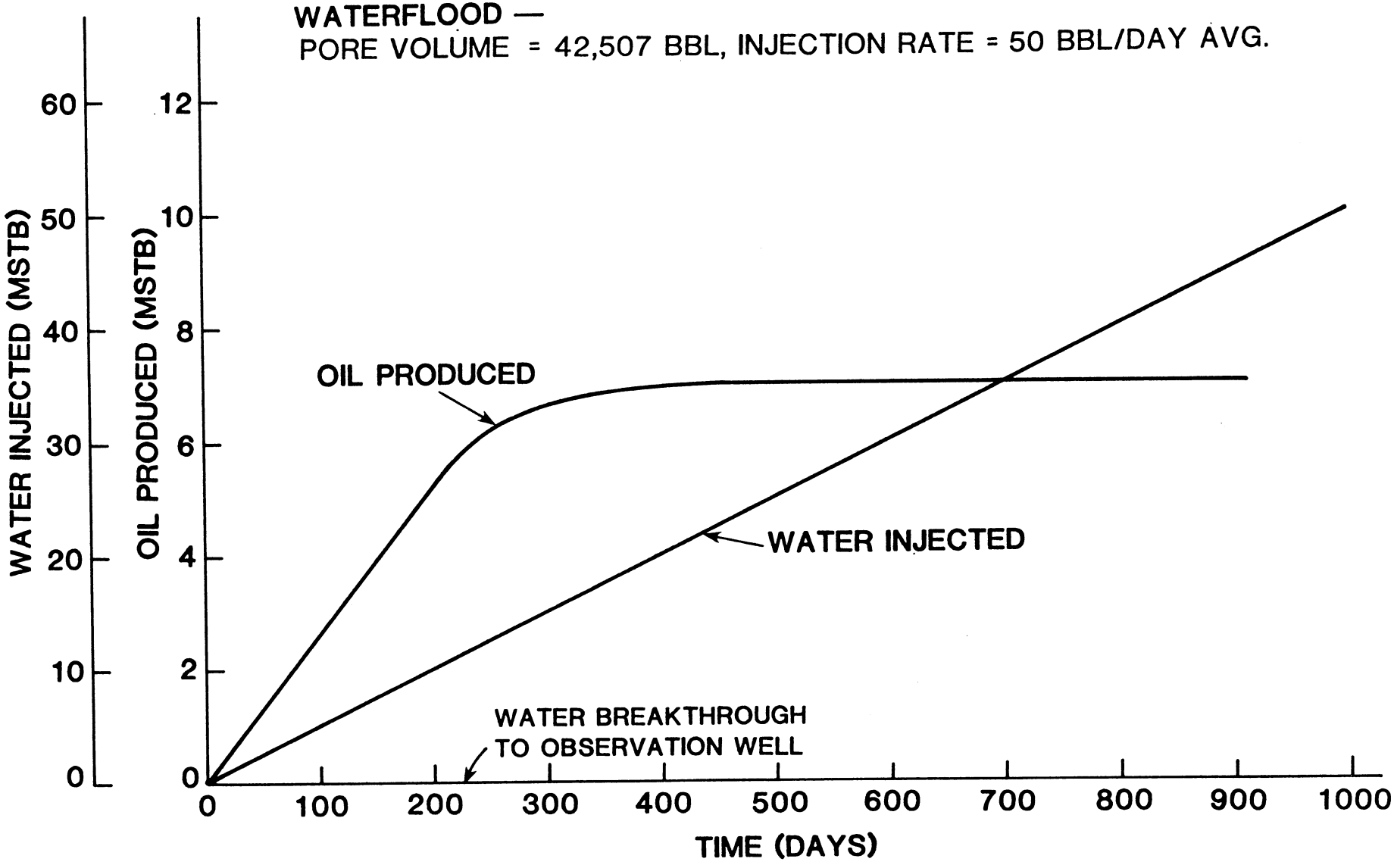

FIGURE 10

LITTLE KNIFE MINITEST CO_2 FLOOD SIMULATION
CROSS-SECTION OF ~ 1/3 OF 5-ACRE MISSION CANYON "D" ZONE —
OIL RECOVERY AND CO_2 -OIL RATIO FOR DIFFERENT WAG RATIOS

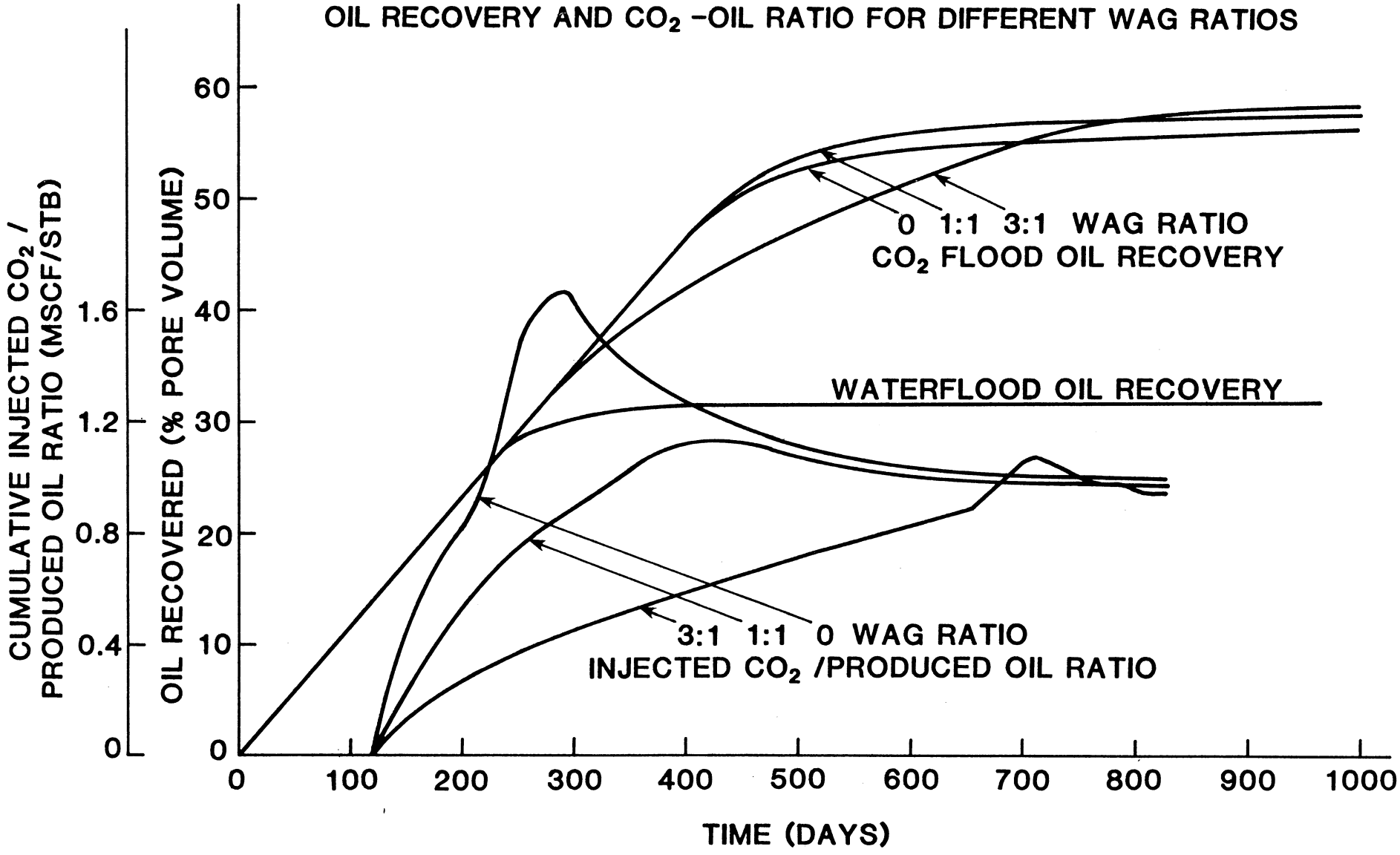

APPENDIX 31

LITTLE KNIFE CO_2 FLOOD RESIDUAL OIL AND CO_2-WATER RELATIVE PERMEABILITY MEASUREMENTS

By

R. Ehrlich
J. H. Tracht
W. W. Slack

Production Research Department
Gulf Research & Development Company
Pittsburgh, Pennsylvania

TABLE OF CONTENTS

	Page
Abstract	79
Background	79
Experimental Methods--CO_2 WAG Residual Oil and Relative Permeabilities	81
Experimental Methods--Whole Core Water-Oil and Gas-Oil Relative Permeabilities	82
Results	83
Conclusions	85
References	86

LIST OF TABLES

Table		
1	Hydrocarbon Analyses of Separator Products and Well Stream	87
2	Measurement of CO_2-Water Residual Oil Saturation and Relative Permeability Behavior	88

LIST OF FIGURES

Figure		
1	CO_2-Water Residual Oil and Relative Permeability Apparatus	89
2	CO_2-Water Relative Permeabilities	90
3	CO_2-Water Relative Permeabilities	91
4	Gas-Oil Drainage and Water-Oil Imbibition Relative Permeabilities	92
5	Gas-Oil Drainage and Water-Oil Imbibition Relative Permeabilities	93
6	CO_2-Water Relative Permeability Curves of Figure 4	94
7	CO_2-Water Relative Permeability Curves of Figure 3	95

Abstract

Residual oil saturation measurements for CO_2-water floods and CO_2-water relative permeability measurements at CO_2 flood residual oil were made in native state Little Knife Mission Canyon D zone reservoir cores. An apparatus in which a slim tube generates a multiple contact miscible bank for injection into the cores along with water was used. Results show that residual oil saturation at 3500 psi (slightly above the 3400 psi minimum miscibility pressure) and 245°F is low, 0.8% PV to 3.1% PV, for water-CO_2 ratios ranging from zero to 3.0 RBbl/RBbl. The initially strongly water-wet Little Knife cores are no longer water-wet at CO_2 flood residual oil saturation. Evidence suggests that separation of a heavy hydrocarbon phase may be responsible for this wettability change.

Background

CO_2 was shown in an earlier study[1] to be miscible in all proportions at reservoir temperature with Little Knife crude oil at pressures above 5700 psig and to develop multiple contact miscibility above 3400 psig. Reservoir pressure during a CO_2 flood in Little Knife can be above the latter but will be substantially below the former.

A CO_2 flood in Little Knife is likely to be carried out using alternating water and CO_2 slugs (WAG) for mobility control so that displacement of oil would occur in the presence of a mobile water saturation. Two uncertainties in our ability to predict the performance of this type of displacement are the extent to which mobile water shields trapped oil from CO_2 causing incomplete displacement even above the miscibility pressure and the effect of CO_2 flood residual oil on water-CO_2 relative permeabilities in the WAG bank.

Raimondi and Torcaso[2] first showed that oil trapped at high water saturation may not be accessible to a miscible flood. This result was amplified by Shelton and Schneider[3], Stalkup[4] and Griffith and Horne[5] among others. They showed that trapping and, therefore, inaccessibility does not occur in oil-wet systems and that trapped oil in water-wet systems can in fact be contacted at a rate apparently related to diffusion of solvent through water and stagnant oil films. Stalkup and Griffith and Horne reached the conclusion that propane displacement at field conditions (low rates, long contact times) can be effective despite trapping at high water saturation. This is not inconsistent with the results of Raimondi

and Torcaso, who used a heptane solvent, considering that water solubility and diffusion coefficient will be lower for heptane than for propane. If diffusion through a water film is the limiting step, the rate at which a solvent can contact trapped oil will be nearly proportional to the product of the solubility of the solvent in water and its diffusion coefficient in water.

Development of miscibility occurs somewhat differently with CO_2 than with propane or propane-enriched natural gas. In order for a multiple-contact miscible bank to develop, CO_2 dissolves in the oil and intermediate molecular weight hydrocarbons vaporize into the CO_2. All components of this intermediate-enriched CO_2 bank must be able to contact trapped oil in order for it to be miscibly displaced. Because of its high solubility and low molecular weight, transport of CO_2 through a water film will not be a problem. However, transport of intermediates* may be very slow. The ability of CO_2 to miscibly displace trapped oil under water-wet conditions even allowing long contact times at this point is uncertain.

Schneider and Owens[7] showed that initially oil-wet carbonate reservoir core samples remained hydrophobic after oil was displaced by a rich gas solvent slug which was then driven by dry gas. Water-gas relative permeabilities measured at this point were very different from the normally water-wet water-gas curves obtained after extraction of the cores with polar solvent.

Again, extrapolation of this result to CO_2 WAG floods is uncertain. It is not clear from Schneider and Owens' results that the hydrophobic water-gas relative permeability behavior was a direct consequence of the original oil-wet condition. Other explanations, such as a solid or heavy liquid phase separation on solvent-oil mixing which may have affected wettability, are possible. They did not demonstrate, for example, that solvent displacement in initially water-wet systems does not give hydrophobic water-gas behavior. The water-gas relative permeability curves are of particular importance in prediction of CO_2 WAG flood performance in that they determine mobility and CO_2 storage in the WAG bank, CO_2 and water injectivity, and the extent to which CO_2 is trapped by drive water.

This report describes a sequence of CO_2 WAG flood residual oil saturation and relative permeability measurements in preserved Little Knife Mission Canyon formation cores at reservoir conditions obtained in order to resolve these uncertainties. This work is what was described as Phase II of the Little Knife CO_2 proposal to DOE.[8]

---

*Some disagreement exists about whether intermediates in a CO_2 flood are C_3-C_6 hydrocarbons or heavier C_5-C_{30} range compounds.[6] Most likely, the important intermediate molecular weight compounds will depend on temperature, pressure and the composition of the crude oil.

Experimental Methods--CO_2 WAG
Residual Oil and Relative Permeabilities

Apparatus:

The apparatus used in these measurements consisted of a slim tube connected in series with a core holder as shown in Figure 1. The slim tube was 64 ft. long and 1/4 inch i.d. and was packed with 80-120 mesh silica sand. The rubber sleeve core holder accommodated a stack of one inch diameter plugs approximately nine inches long. This arrangement allowed a miscible bank to be developed in the slim tube and then to pass through the core plugs thus eliminating the miscibility development zone associated with CO_2 flood multiple contact miscibility that would have existed if CO_2 had been injected directly into the core plugs. In the WAG tests, water was injected into the core plugs only and not into the slim tube. Because the slim tube hydrocarbon pore volume was approximately an order of magnitude greater than that of the core plugs, miscibility development in the slim tube could be confirmed by an overall material balance. Also, the dimensions and permeabilities of the cores and slim tube were such that a valid slim tube displacement (pressure drop across the slim tube maintained at less than 100 psi) and a valid CO_2-water relative permeability measurement (pressure drop across the core plugs maintained above that necessary to minimize capillary end effects and below that which could mobilize residual satuations) could be obtained simultaneously.

In these tests, CO_2, water and oil were injected using Ruska constant rate displacement pumps. Pressure differences across the slim tube and core holder were measured using differential pressure transducers. Large fluctuations in differential pressure across the core caused by alternating CO_2 and water slug movement through a back pressure regulator were eliminated by interposing a high pressure separator between the core holder and the regulator. Only a single gas phase displaced from the nitrogen pre-pressured separator passed through the back pressure regulator, eliminating slugging and the consequent differential pressure excursions.

Core and Fluid Samples:

Preserved core samples were available for these tests from the Mission Canyon D zone in Zabolotny Injection Well #1 in the project area. This core was cut with a neutral, surfactant-free mud to maintain original reservoir wettability, was wrapped in saran and aluminum foil at the well-site and was sealed in plastic to prevent weathering.

Separator oil and gas samples were obtained from the Zabolotny 1-3-4A well and were reconstituted to the measured separator GOR. Analyses taken from Reference 9 of the separator oil, separator gas and the reconstituted fluid are given in Table 1.

Water used in these tests was a 2% NaCl brine with sufficient gypsum added to give a saturated solution at 245°F.

Procedure:

One inch horizontal plugs were cut from sections of the preserved core, encapsulated in a heat-shrinkable teflon tube, and then mounted in a high pressure core holder. The slim tube and the core assembly were both then saturated with gas-free Little Knife crude oil - the slim tube to 100% oil saturation and the core plugs to irreducible water and zero free gas saturations. These were then mounted in series in the oven as shown in Figure 1 and heated to 245°F, after which the gas-free crude oil was displaced by reconstituted reservoir oil. Following this, the core plugs only were waterflooded to residual oil saturation.

The CO_2 WAG flood was then carried out at the predetermined water-CO_2 ratio and pressure with CO_2 injected into the slim tube and water injected into the core holder along with the effluent from the slim tube. The flood was continued until a steady-state was obtained in the core plugs after CO_2 breakthrough, as indicated by no further pressure gradient changes. Following this, the core holder was removed from the oven and was blown down to atmospheric pressure. The core plugs were then removed from the core holder and a Dean-Stark extraction carried out. The volume of fluids produced into the high pressure separator was also determined. The clean and dry core plugs were then water saturated and the absolute permeability and pore volume were determined.

Steady-state water and CO_2 relative permeabilities were calculated from the injection rates corrected to reservoir conditions and the pressure drop across the core plugs. Oil and water saturations corresponding to these relative permeabilities were calculated from the Dean-Stark data (assuming the original oil density) and the volume of fluids produced during blowdown. Oil recovery from the slim tube was calculated from the volume of oil produced in the separator minus the oil produced from the core plugs.

In those tests where CO_2-water ratio was varied in the same core either at CO_2 flood residual oil saturation or with no oil present, saturation changes after steady-state was obtained with each ratio were determined gravimetrically (no extraction).

Experimental Methods--Whole Core Water-Oil and Gas-Oil Relative Permeabilities

Preserved whole cores from the Zabolotny Observation #3 Well were available for these measurements. The whole core apparatus was not capable of handling live crude oil at reservoir temperature so that gas free crude oil was used.

The cores were mounted in the core holder and flushed with crude oil with a back pressure maintained to dissolve and remove free gas and to obtain an irreducible water saturation. Steady-state water-oil imbibition relative permeabilities were measured by simultaneously flowing water and oil at various ratios starting with oil alone, then at several intermediate water-oil ratios, and finally water alone. Saturation changes were obtained at steady-state by material balance. As with the CO_2-water measurements, flow rates were maintained above a minimum necessary to control capillary end effects and below a maximum to prevent high capillary number mobilization of residual oil.

A Dean-Stark extraction was performed on each core in its final watered-out state. Pore volume and absolute permeability were then measured in the clean and dry solvent-extracted cores. Final oil and water saturations were determined from the Dean-Stark data. Intermediate and initial saturations were back calculated using the material balance data.

The cores were then saturated with a non-volatile mineral oil. Steady-state gas-oil drainage relative permeabilities were then measured by simultaneous flow of oil and nitrogen at various ratios, starting with oil alone and ending with nitrogen alone. These measurements were made at room temperature and with the core outlet maintained at 1 atm. Saturation changes were again determined by material balance.

Results

Table 2 gives the results of CO_2-water displacement tests at 3500 psi and 245°F. Over the WAG ratio range of zero to 3.0 RBbl/RBbl, CO_2 flood residual oil saturations were very low - 0.8% PV to 3.1% PV. In these tests, a material balance on the slim tube gave ~95% OIP recovery, confirming that miscibility was developed. Because the magnitude of the residual oil saturation resulting from water trapping was expected to be greatest at pressures just in excess of the 3400 psi minimum miscibility pressure (CO_2 must be enriched to the greatest extent with intermediates to develop miscibility at this point), higher pressures were not investigated. These results suggest there will be no effect of a high mobile water saturation on CO_2 flood displacement efficiency above the minimum miscibility pressure at Little Knife.

To investigate the effect of the residual oil, solvent extracted core plugs were water saturated and CO_2-water drainage relative permeabilities were measured over the same WAG ratio range. (The residual oil determinations are also drainage measurements in the sense that CO_2 saturation increases at the expense of liquid saturation.) The steady state saturations corresponding to these WAG ratios are given in Table 2 and the CO_2-water relative permeability curves are plotted in Figure 2. To obtain a direct comparison with Figure 2, preserved core plugs were CO_2 flooded to residual oil saturation and then, without extraction, completely water saturated and then subjected to a sequence of CO_2-water drainage relative permeability measurements. The results of these are shown in Figure 3.

A comparison of the data in Table 2 shows a higher gas saturation at any WAG ratio where residual oil is present. A comparison of Figures 2 and 3 shows a higher water relative permeability and a lower CO_2 relative permeability at any water saturation when residual oil is present. Both comparisons suggest that the core plugs are substantially less water-wet in the presence of the very low residual oil saturation than when the oil is extracted. On this point, we are in agreement with the observations of Schneider and Owens.

Results of whole core native-state water-oil imbibition relative permeability measurements are shown in Figures 4 and 5. Gas-oil drainage relative permeability measurements (not native state and with no water present) are also shown in these Figures. The very low water relative permeability at floodout, less than 0.1 in both cases, suggests that the Little Knife cores at native state are strongly water-wet.

Further evidence of this is offered by a comparison of the water-oil and gas-oil curves. In both Figures 4 and 5, the water curve in the water-oil system overlaps or is a continuation of the oil curve in the gas-oil system. Using the facts that the wetting phase relative permeability is not affected by hysteresis and that oil is certainly the wetting phase in a clean core gas-oil measurement, we would conclude that the native state water-oil system is strongly water-wet. (This method of comparing relative permeability curves to estimate wettability to the best of our knowledge seems to have originated with Owens and Archer[10].)

This method of comparison can be used to look again at the CO_2-water relative permeability data. Figure 6 compares the CO_2-water curves of Figure 2 (no residual oil) with the water-oil curves of Figure 4. The water curves coincide indicating that the clean cores are water-wet at reservoir conditions in the presence of CO_2. Figure 7 compares the CO_2-water curves of Figure 3 (residual oil present) with the water-oil curves of Figure 4. Here, the water curves are substantially displaced indicating again that the cores with CO_2 flood residual oil present are not water-wet with respect to CO_2 at reservoir conditions.

To summarize, the Little Knife Mission Canyon D zone carbonate reservoir rock appears strongly water-wet in native state tests. This seems to be altered in some way during a CO_2 flood so that when CO_2 flood residual oil saturation is reached, the rock is no longer water-wet even when CO_2 and water are the only mobile phases. The fact that cores can be restored to a water-wet state by extraction with polar solvents and the fact that the solvent extract was found to contain much more pigmentation (determined by light absorption) than would be contained in the solvent extract of the same amount of original Little Knife oil suggests that separation of a heavy hydrocarbon phase may be responsible for the wettability change. These observations and explanations are somewhat different from those of Schneider and Owens.

If this wettability change occurs early enough in the sequence of events leading to miscibility (i.e. if the first dilution of oil with CO_2 causes a water-wet to oil-wet shift which is then followed by displacement of oil), it would provide a sufficient explanation for the observed lack of residual oil at high WAG ratio because of the absence of trapping of oil by water in oil-wet systems.

We were not able to obtain water displacing CO_2 relative permeability measurements at residual oil saturation which would have been of interest during that part of the flood where drive water displaces CO_2. Sufficient preserved core material was not available.

We have resolved the uncertainties concerning CO_2 WAG flood performance discussed earlier in this report only for Little Knife. It is not known how general the wettability changes seen here are or, in the absence of such wettability changes, if there will then be a significant effect of water saturation on CO_2 flood residual oil saturation above the minimum miscibility pressure.

Conclusions

1. CO_2 flood residual oil saturation in Little Knife Mission Canyon D zone reservoir cores at 245°F and 3500 psi varied from 0.8% PV to 3.1% PV for WAG ratios of 0 (CO_2 alone), 1.5 RBbl water/RBbl CO_2 and 3.0 RBbl water/RBbl CO_2.

2. Native state Little Knife cores changed from strongly water-wet in the presence Little Knife crude oil to non-water-wet after displacement to CO_2 flood residual oil saturation.

R. Ehrlich

J. H. Tracht

W. W. Slack

RE:pj

References

1. Huang, E. T. S., "Miscibility Studies with Little Knife Oil", Production Research Department Technical Memorandum No. 441TJ300, January 18, 1978.

2. Raimondi, P. and Torcaso, M. A., "Distribution of the Oil Phase Obtained Upon Imbibition of Water", SPE Journal (March 1964), pp. 49-55.

3. Shelton, J. L. and Schneider, F. N., "The Effects of Water Injection on Miscible Flooding Methods Using Hydrocarbons and Carbon Dioxide", SPE Journal (June 1975), pp. 217-226.

4. Stalkup, F. I., "Displacement of Oil by Solvent at High Water Saturation", SPE Journal (December 1970), pp. 337-348.

5. Griffith, J. D. and Horne, A. L., "South Swan Hills Solvent Flood", Proc. 9th World Petroleum Congress (1975), Vol. IV, pp. 269-278.

6. Holm, L. W. and Josendal, V. A., "Mechanisms of Oil Displacement by Carbon Dioxide", Journal Pet. Tech. (December 1974), pp. 1427-1436, and the discussion by R. S. Metcalfe and L. Yarborough which follows.

7. Schneider, F. N. and Owens, W. W., "Relative Permeability Studies of Gas-Water Flow Following Solvent Injection in Carbonate Rocks", SPE Journal (February 1976), pp. 23-30.

8. Technical Proposal for Enhanced Recovery Activities - Little Knife Field, North Dakota, DOE RFP No. EW-78-R-21-8383, Minitest of Carbon Dioxide Miscible Flooding Process, Gulf Oil Corp., September 8, 1978.

9. Devaney, W. E, "GOEP-US Zabolotny 1-3-4A, Little Knife Field, Billings County, North Dakota, CO_2 Swelling Tests", HTSC Technical Memorandum No. 445TL074 (April 1980).

10. Owens, W. W. and Archer, D. L., "The Effect of Rock Wettability on Oil-Water Relative Permeability Relationships", Journal Pet. Tech. (July 1971), pp. 873-878.

TABLE I

HYDROCARBON ANALYSES OF SEPARATOR PRODUCTS AND WELL STREAM

	Separator Gas		Separator Liquid		Reservoir Fluid	
Component	Mole %	GPM @ 14.65 psia	Mole %	Volume %	Mole %	Volume %
N_2	1.93		0.12	0.03	0.93	0.27
C_1	73.28		7.51	2.51	34.01	15.25
CO_2	2.24		0.53	0.18	1.20	0.54
C_2	12.14		8.44	4.45	9.87	6.99
H_2S	4.64		5.73	1.55	4.91	1.78
C_3	4.28	1.171	8.13	4.42	6.55	4.78
IC_4	0.34	0.111	2.07	1.34	1.32	1.14
NC_4	0.70	0.219	5.90	3.68	3.68	3.08
IC_5	0.11	0.040	2.29	1.66	1.35	1.31
NC_5	0.11	0.040	2.95	2.11	1.74	1.67
C_6	0.09	0.037	4.66	3.79	3.02	3.29
C_7^+	0.14	0.068	51.67	74.28	31.42	59.90
Totals	100.00	1.686	100.00	100.00	100.00	100.00

Table 2

Measurement of CO_2-Water Residual Oil Saturation and Relative Permeability Behavior in Preserved Little Knife Zabolotny Injection #1 Cores at 3500 psi and 245°F

Core Data			Water-CO_2 Ratio	Final Conditions*		
Depth (ft)	K (md)	Ø (%)	(RBbl/RBbl)	S_o(% PV)	S_w(% PV)	S_g(% PV)
9823	7.3	23	0	3.1	20.0	76.9
9826-27	5.3	22	1.5	3.1	61.5	35.4
9814-15	39	26	3.0	0.8	63.5	35.7
(The following were obtained after extraction of residual oil.)						
9814-15	39	26	0	--	29.9	70.1
9814-15	39	26	1.35	--	80.3	19.7
9814-15	39	26	2.7	--	87.3	12.7

*Oil saturations are obtained gravimetrically assuming original oil density. Water and CO_2 saturations and relative permeabilities are calculated from pure component material balances and do not allow for mutual solubility.

FIGURE 1

CO_2-WATER RESIDUAL OIL AND RELATIVE PERMEABILITY APPARATUS

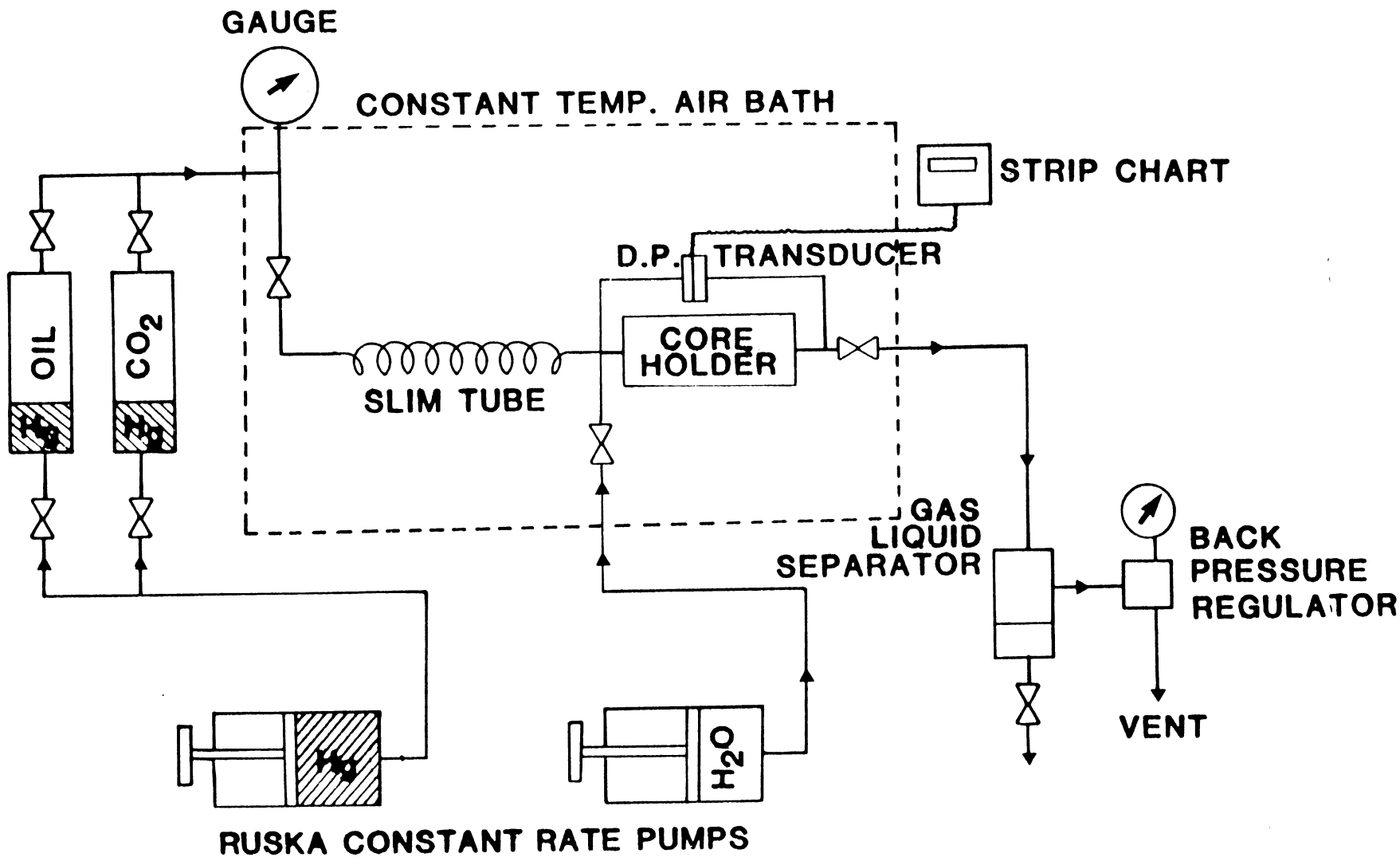

FIGURE 2

LITTLE KNIFE CO_2-WATER REALATIVE PERMEABILITIES
ZABOLOTNY INJECTION #1, 9814-9815 FT
3500 psi AND 245°F
EXTRACTED CORE-NO OIL PRESENT
(NOT CORRECTED FOR EFFECT OF CO_2 SOLUBILITY IN WATER)

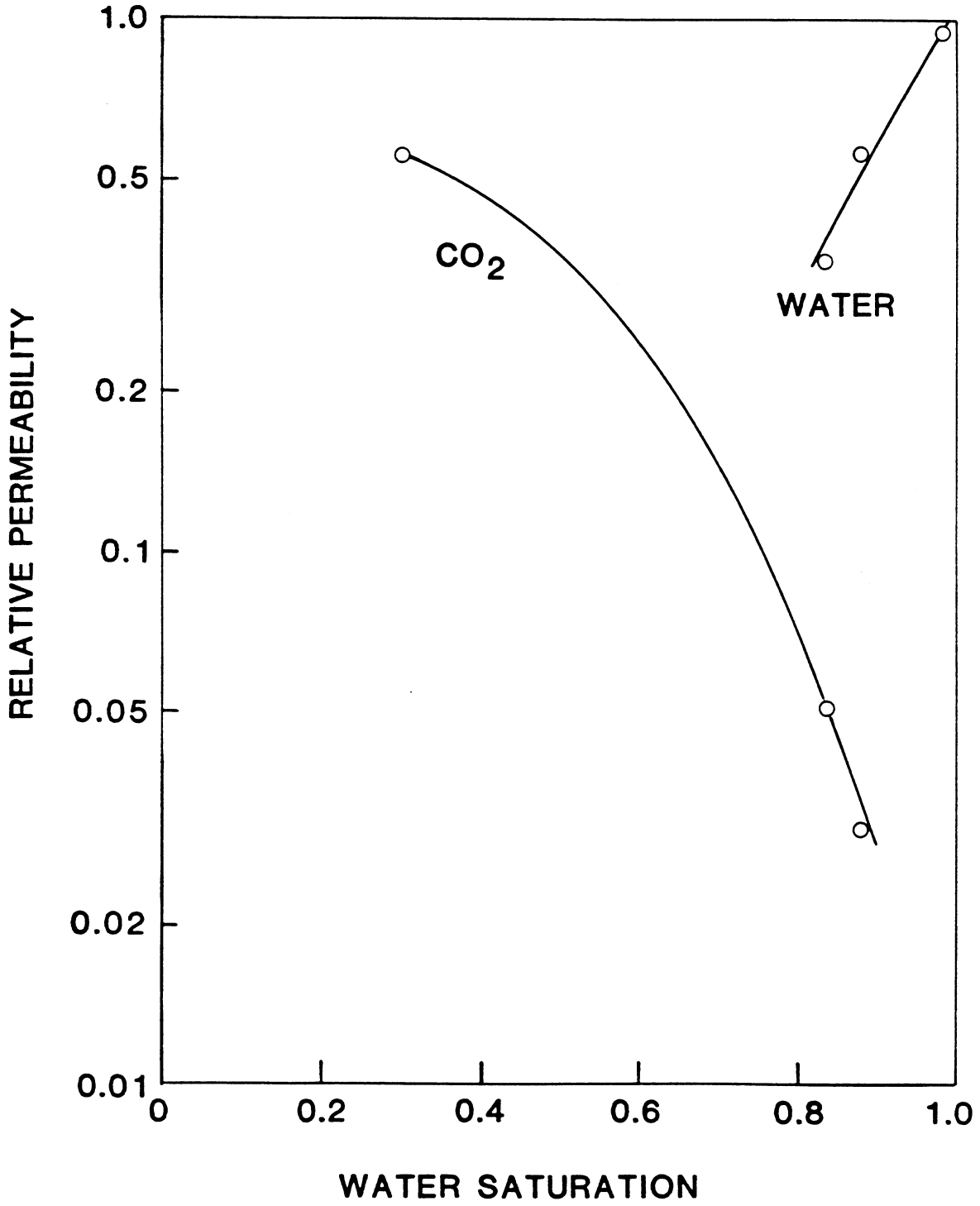

FIGURE 3

LITTLE KNIFE CO_2-WATER RELATIVE PERMEABILITIES
ZABOLOTNY INJECTION #1, 9823-9824 FT
3500 psi AND 245°F
NATIVE STATE AFTER CO_2 FLOOD
(NOT CORRECTED FOR EFFECT OF CO_2 SOLUBILITY IN WATER)

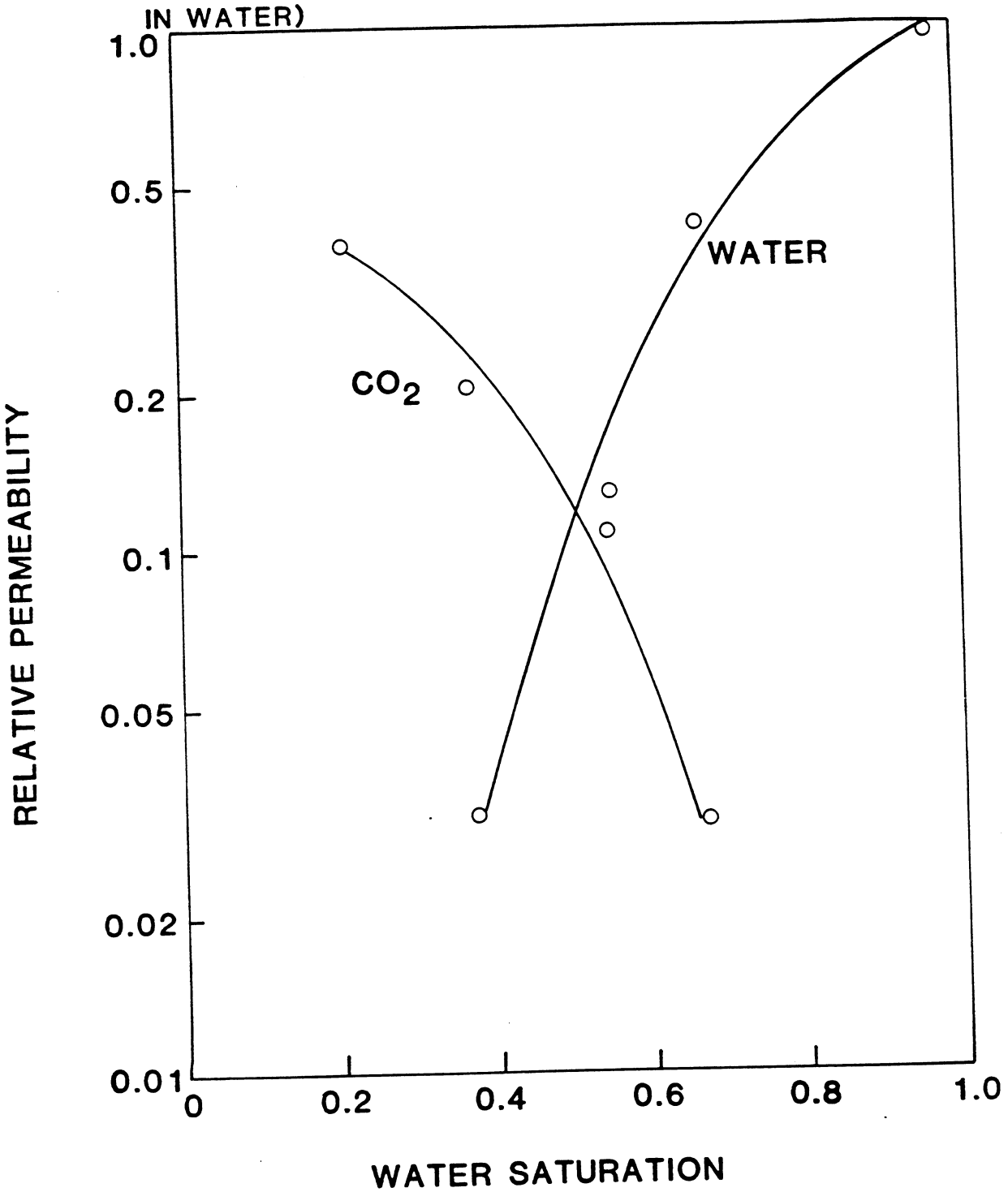

FIGURE 4

LITTLE KNIFE GAS-OIL DRAINAGE AND WATER-OIL IMBIBITION RELATIVE PERMEABILITIES

ZABOLOTNY OBSERVATION #3, 9855 TO 9856 FT ϕ = 0.23, k = 25.5 md

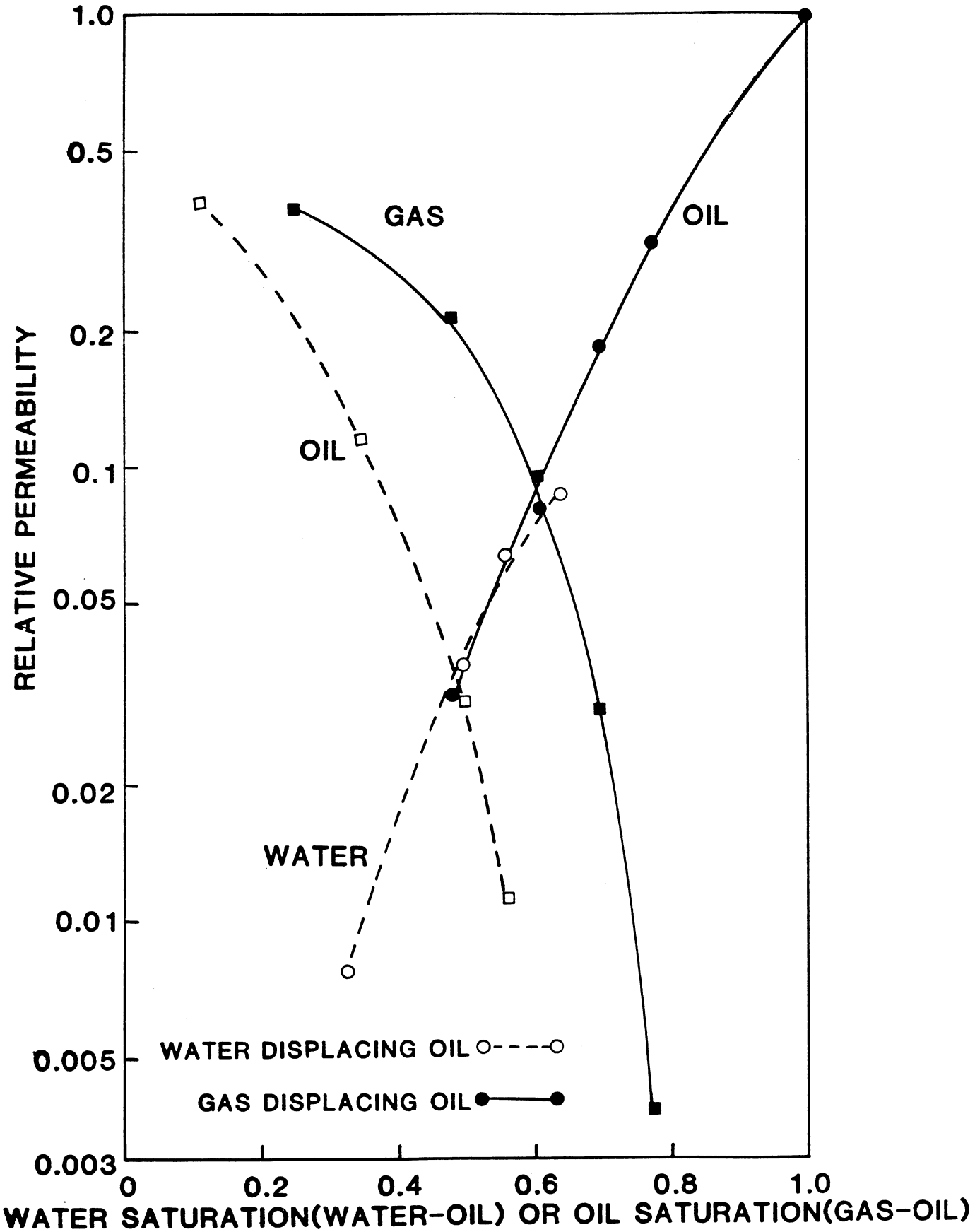

FIGURE 5

LITTLE KNIFE GAS-OIL DRAINAGE AND WATER-OIL IMBIBITION RELATIVE PERMEABILITIES
ZABOLOTNY OBSERVATION #3 9864 TO 9865 FT
k = 1.3 md ϕ = 0.124

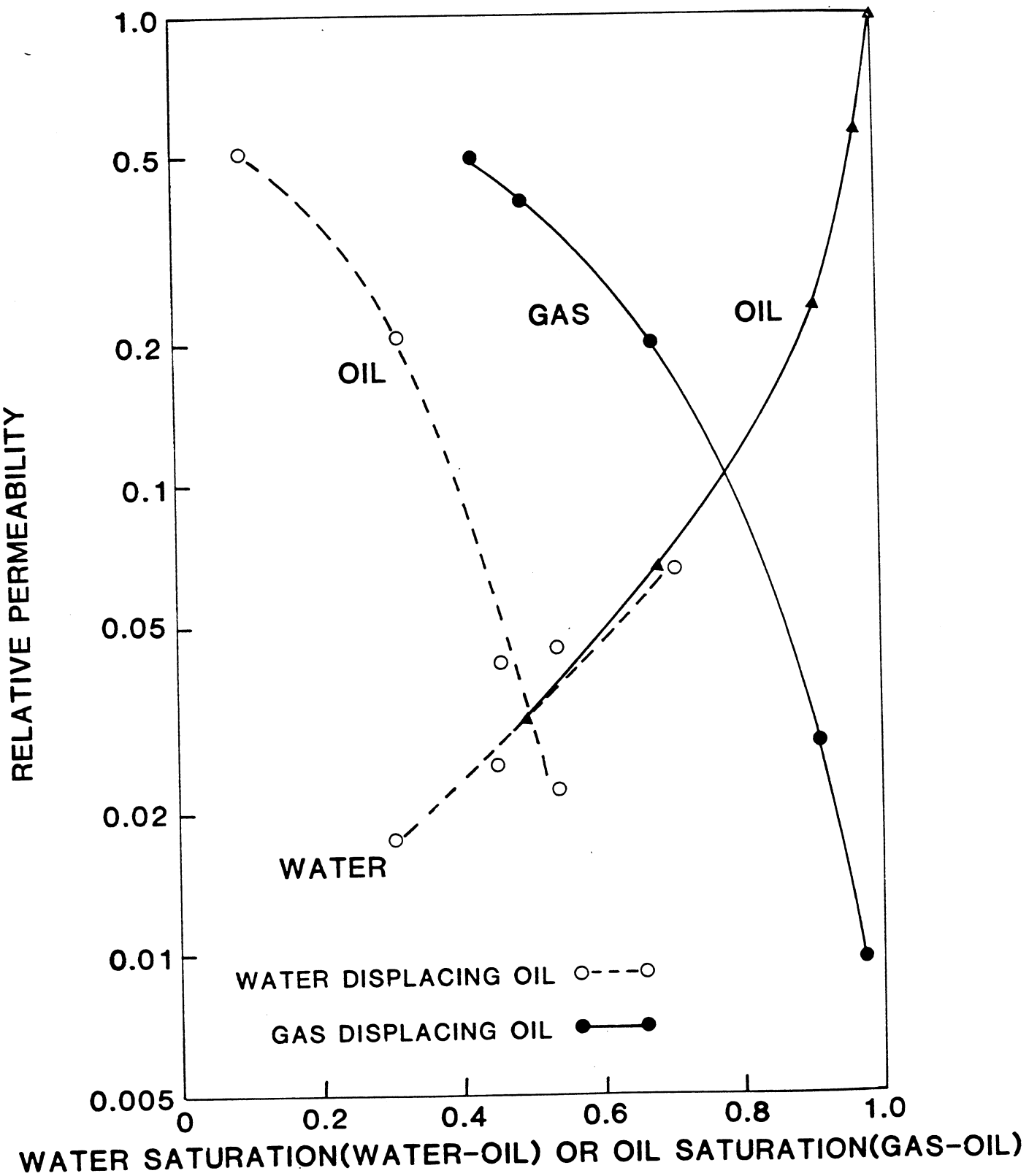

FIGURE 6

LITTLE KNIFE CO_2-WATER RELATIVE PERMEABILITY CURVES OF FIGURE 2 (NO RESIDUAL OIL) COMPARED WITH NATIVE-STATE WATER-OIL RELATIVE PERMEABILITY CURVES OF FIGURE 4

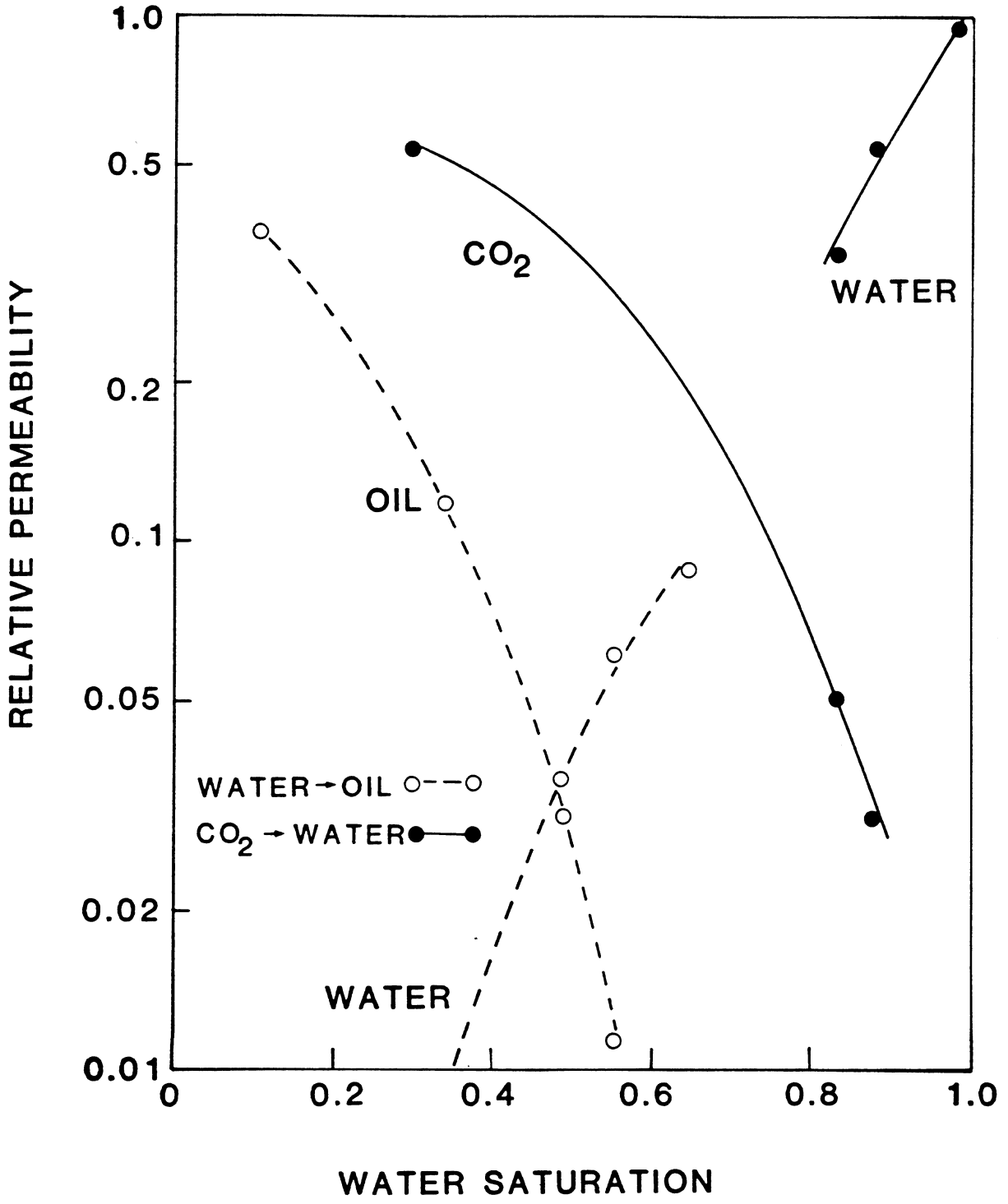

FIGURE 7

LITTLE KNIFE CO_2-WATER RELATIVE PERMEABILITY CURVES OF FIGURE 3 (RESIDUAL OIL PRESENT) COMPARED WITH NATIVE-STATE WATER-OIL RELATIVE PERMEABILITY CURVES OF FIGURE 4

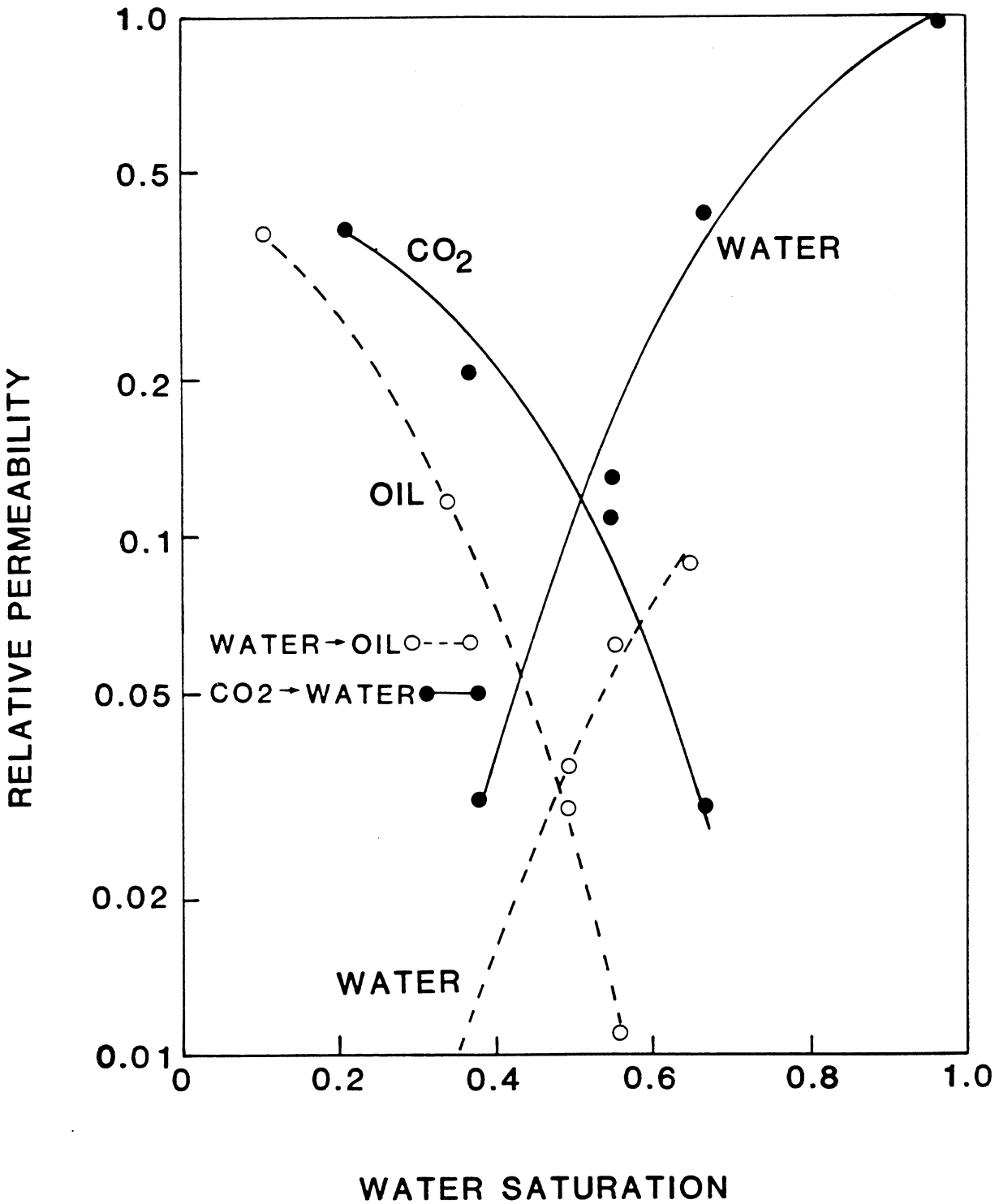

APPENDIX 42

ANALYSIS OF OBSERVATION WELL #4

PRESSURE CORE DATA - LITTLE KNIFE CO_2 PROJECT

By

R. Ehrlich

Production Research Department
Gulf Research & Development Company
Pittsburgh, Pennsylvania

TABLE OF CONTENTS

	Page
Abstract	98
Introduction	98
Pressure Core Data	98
Discussion	99
Displacement and Vertical Sweep Efficiencies	101
Conclusions	102
References	102
Sub-Appendix	106

LIST OF TABLES

Table		
1	Zabolotny Observation #4 Data	103
A-1	Cored Intervals	108
A-2	Pressure Retained Core Analysis	109
A-3	Lithological Abbreviations	111
A-4	Analysis of Liberated Gas By Gas Chromotography	112
A-5	Chloride and Bromide Data	113
A-6	Vertical Plug and Donut Data	114
A-7	Filtrate Invasion Data	115
A-8	Tritium Results From Little Knife-Gulf Oil Company	116

LIST OF FIGURES

Figure		
1	CO_2 Minitest Well Placement	104
2	Comparison of Gulflog and Pressure Core Oil Saturation	105

Analysis of Observation Well #4
Pressure Core Data - Little Knife CO_2 Project

Abstract

Data obtained from the Zabolotny Observation #4 pressure core analysis were used to estimate lower limits to oil and CO_2 saturations existing in-situ. Despite the fact that cores were flushed with mud filtrate, pressure retention was imperfect, and core recovery was incomplete, useful information was obtained. It is concluded that the very high displacement efficiencies associated with CO_2 flood multiple-contact miscibility occurred only over a part of the Y layer.

Introduction

The Little Knife CO_2 flood minitest involved a single injection well (Injection #1 in Figure 1) offset initially by three observation/sampling wells (Observation #1-#3) on an approximately five acre circle. A fourth well (Observation #4) was drilled near the end of the test for the purpose of obtaining a pressure core. Preinjection of water was begun on 12/11/80. CO_2 injection as alternating slugs with water was started on 1/7/82 and completed on 3/25/81. Final drive water injection continued to 9/24/81 at which time the project was shut in. Volumes injected as percentages of the hydrocarbon pore volumes within the five acre circle for zones X, Y and Z were: preinjection - 28% HCPV, CO_2 - 22% HCPV (accompanied by an equal volume of WAG water), and final drive water - 186% HCPV.

Observation well #4 was spudded on 5/9/81. Pressure coring in the Mission Canyon formation was begun on about 7/2/81. (It was expected that at that time, displacement would be complete at the Observation #4 location). Details of the pressure coring operation and the core analysis data as received from Core Laboratories have been given by Whiting[1]. The purpose of this memorandum is to interpret saturation and compositional data obtained from the pressure core analysis for what can be learned about CO_2 flood displacement and sweep efficiencies.

Pressure Core Data

Seven pressure cores were cut over the approximate interval, 9803-9859 ft. (core depths) with approximately 45.3 ft. of core recovered. Data obtained during pressure coring and from analysis of the cores are given in the Appendix. (Taken from Reference 1)

These are:

(1) the pressure at which each pressure core was recovered,

(2) a foot-by-foot analysis for permeability, porosity, and stock tank oil and water saturations,

(3) a foot-by-foot analysis of the gas liberated,

(4) a number of "plug and donut" analysis for water saturation and tritium concentration (tritium was used as a tracer in the coring fluid) - these would indicated the extent of filtrate invasion,

(5) a foot-by-foot analysis of water in the core for chloride and bromide content (the gel used in the core barrel contained calcium bromide) - this would presumably indicate the extent of invasion by this fluid.

Table 1 gives oil, water and CO_2 saturations along with permeability and porosity vs. depth for each pressure core. Oil and water saturations were corrected to reservoir conditions using formation volume factors (1.66 for oil, 1.056 for water). CO_2 saturations (actually the amount of CO_2 present irrespective of whether dissolved in oil or water or present as a free gas phase) were calculated from the mole fraction CO_2 in the gas, the volume of gas evolved, and the core pore volume. The estimated (by R. F. Lindsay of Oklahoma City) locations of the W, X, Y, and Z layers, as designated for the simulation work, are also shown in Table 1.

Discussion

The objective of pressure coring is to obtain core samples in which residual oil saturation is unchanged from that in the reservoir. This is done by closely balancing hydrostatic and formation pressures, using a low loss coring fluid, and maintaining reservoir pressure as the core is brought to the surface. If this is done, then water and gas saturations and the composition of the hydrocarbon phases should also be little changed.

These idealized conditions were, however, not completely met. Only one of the cores was retained at the 3800 psi reservoir pressure - the others were at pressures ranging from 0 to 3550 psi. Analysis of the water tracers indicate significant invasion from the mud filtrate. (the core water averaged ~30% filtrate with little plug-donut contrast) and from the core barrel gel (high bromide content). Gas evolved from the core was contaminated with nitrogen which could have come from the drilling mud or from various core handling steps. Pressures were, however, balanced during coring as required. The question which must be asked is how meaningful are these saturation data.

The extent to which oil saturation is changed by flushing and pressure reduction depends on a number of factors. A saturation at or below waterflood residual will not be affected by flushing in a balanced

pressure system.* Pressure reduction will be sugnificant only if it is below the bubble point pressure and gas is evolved. With no CO_2 added, this will be ∿2700 psi. At high CO_2 concentrations, the bubble point pressure can be at or close to 3800 psi. Even with some gas evolution, oil saturation reduction may be limited to shrinkage as a result of solution gas loss at least at initially low oil saturations. Oil saturations in the less than 10% PV range have to be real.

In all cases, the stock tank oil saturations represent an absolute lower limit to the actual saturation. Where compositional changes have not occurred, the volume factor - corrected oil saturation is a lower limit. Likewise, the CO_2 saturation in-situ cannot be less than that contained in the cores.

Cores #1 and #2 (W layer - 9803.0 to 9816.7 ft.)

These cores were flushed with filtrate but were retained above the bubble point pressure (2700 psi). Only trace amounts of CO_2 corresponding to that naturally occurring in the solution gas were present. Oil saturations are probably good estimates of waterflood residuals. It is uncertain, however, whether the oil saturations in-situ are actually that low. Water saturations are most likely high (as indicated by $S_w + S_o > 100\%$) because of water imbibition in the core barrel as the oil shrinks.

Core #3 (Bottom of W layer - 9819.0 to 9824.5 ft.)

This core was flushed with filtrate and was reduced below the original bubble point pressure. Even though pressure depletion must have occurred, CO_2 saturation averages 2.3% PV, well above that occurring naturally. Oil saturation averages 17.9% PV. Water saturations, again, are most likely high.

The pressure depletion introduces considerable uncertainty. The low oil saturation and the presence of CO_2, however, raises a question about the possibility of CO_2-related displacement. Core #5, which was recovered with no pressure, by comparison contains much more oil.

Core #4 (Y layer - 9827.0 to 9832.0 ft.)

Oil saturations in this core are low - 6% PV average on a stock tank basis. (The volume factor correction was used in Table 1 for consistency but is probably too high because of stripping of solution gas by CO_2.) CO_2 saturations are high and indicate free CO_2 present. The loss of pressure from 3800 psi (original pressure) to 3100 psi probably resulted in some CO_2 being lost.

*In a study of flushing during coring by Jenks et al[2], it was determined that overbalance pressures of 200 psi or less would minimize stripping of residual oil.

Core #5 (Z layer - 9835.0 to 9840.0 ft.)

This core lost all its pressure as well as being substantially flushed by mud filtrate. Despite this, oil saturations are high - 32.7% PV. This suggests that this zone was totally unaffected by CO_2 and that oil saturation is no lower than waterflood residual.

Cores #6 and #7 (9843.0 to 9859.0 ft.)

The comments made for Cores #1 and #2 apply.

Displacement and Vertical Sweep Efficiencies

The very low residual oil saturations associated with CO_2 flood multiple contact miscible displacement is seen only in a four foot zone in Core #4 in the Y layer (9828.0-31.0 ft.). Immediately above, at the very top of Core #4 and in Core #3--at the top of the Y layer and the bottom of the W layer--CO_2 saturation and CO_2 concentration in evolved gas above ambient levels together with oil saturations which appear to be below waterflood residual oil levels are present and suggest some CO_2-related displacement. However, pressure was not completely retained in Core #3 so that oil saturation data there is suspect.

The monitor log data from Zabolotny Observation #2 at the time the Observation #4 Core was cut (Figures A-18 and A-19 of Reference 5) may help in resolving this uncertainty. These show CO_2 present above the very low oil saturation zone to the same extent as seen in Observation #4. Significant oil displacement as a result of this CO_2 seems to be limited, however, to the Y layer. This may indicate that the CO_2 which has penetrated the bottom of the W layer in Zabolotny Observation #4 also did not result in important oil displacement.

A comparison of oil saturation predicted by the Gulflog with those obtained from the pressure core analysis is shown in Figure 2. Agreement is generally good over the X, Y and Z layers or at least consistent with the idea that the core data represents a lower bound to oil saturation. Agreement is less consistent in the W layer and below the Z layer.

Conclusions

1. Very low residual oil saturations associated with multiple contact miscible displacement by CO_2 are seen in a four foot interval in the middle of the Y layer (9828. - 9832. ft.).

2. Less efficient displacement (but still better than waterflooding) seems to have occurred in the Y layer above this interval. The presence of CO_2 in the W layer may not be significant in terms of oil recovery.

3. The pressure core analysis and interpretation was a worthwhile part of the Little Knife CO_2 flood minitest in terms of the information gained.

R. Ehrlich

RE:pj
Attachments

References

1. A. Whiting: " CO_2 Mini-Test Pressure Core Well" HTC Technical Memorandum No. 446TN022 (February, 1982).

2. L. H. Jenks, J. D. Huppler, N. R. Morrow, R. A. Salathial: "Fluid Flow Within a Porous Medium Near a Diamond Core Bit" J. Can. Pet. Tech. (Oct.-Dec., 1968) 172-180.

3. W. E. DeVaney: "GOEP-US Zabolotny 1-3-4A, Little Knife Field, Billings Co., ND - CO_2 Swelling Tests" HTSC Technical Memorandum No. 445TL074 (April, 1980).

4. W. C. Savre to G. C. Thakur: "Little Knife Miniflood Project Report" Ref. 4453KR03-27, 1/20/82.

5. R. Ehrlich "Analysis of Observation Well Saturation Data, Little Knife CO_2 Project" GR&DC Technical Memorandum No. 441TN387, (6/9/82).

Table 1

Zabolotny Observation #4 Data

Derived From Pressure Core Analysis

	Depth (ft)	k_{max} (md)	ϕ (%)	S_o^a (%PV)	S_w^b (%PV)	$S_{CO_2}^c$ (%PV)	CO_2 in gas (mol %) (N_2-free basis)	
Core #1 3550 psi	9803.0-04.0	12.	15.1	16.6	85.3	0.1	2.00	W
	9804.0-05.0	4.2	6.6	37.5	53.6	0.5	2.45	
	9805.0-06.0	0.58	9.2	27.7	75.5	0.3	1.94	
	9806.0-07.0	1.3	16.4	31.9	79.2	0.4	2.27	
	9807.0-08.0	3.3	12.9	32.0	72.5	0.3	1.65	
	9808.0-09.0	1.9	15.8	49.3	48.3	--	--	
	9809.0-10.0							
	9810.0-11.0			lost				
Core #2 3200 psi	9811.0-12.0	0.7	6.6	15.3	91.2		3.09	
	9812.0-13.0	3.4	10.1	39.0	65.6	0.6	2.38	
	9813.0-14.0	2.2	15.5	41.0	72.4	--	--	
	9814.0-15.0	0.42	6.7	44.2	65.7	1.3	8.56	
	9815.0-16.0	0.34	6.1	44.3	74.2	0.4	4.06	
	9816.0-16.7	1.2	9.9	39.7	67.6	0.6	2.07	
	9816.7-18.0			lost				
	9818.0-19.0							
Core #3 2000 psi	9819.0-20.0	2.6	14.0	22.2	67.0	--	--	
	9820.0-21.0	1.2	9.6	18.3	85.3	1.6	8.51	
	9821.0-22.0	1.3	6.2	12.5	89.1	1.4	9.61	
	9822.0-23.0	0.47	7.2	16.9	78.9	4.6	22.39	
	9823.0-24.0	1.6	8.5	15.6	79.5	1.6	8.05	
	9824.0-24.5	1.8	7.9	21.6	81.4	--	--	X
	9824.5-26.0			lost				
	9826.0-27.0							
Core #4 3100 psi	9827.0-28.0	454.	23.3	23.7	86.8	--	--	Y
	9828.0-29.0	63.	20.6	4.0	89.8	--	--	
	9829.0-30.0	117.	23.4	8.3	84.0	18.5	79.03	
	9830.0-31.0	567.	26.2	6.8	85.7	5.6	97.72	
	9831.0-32.0	233.	27.8	7.8	84.1	0.6	77.19	
	9832.0-33.0							
	9833.0-34.0			lost or broken				
	9834.0-35.0							
Core #5 0 psi	9835.0-36 0	617.	24.0	47.6	49.7	--	--	
	9836.0-37.0	1971.	23.6	18.6	49.9	--	--	
	9837.0-38.0	46.	21.3	28.1	37.4	--	--	
	9838.0-39.0	26.	11.8	28.9	44.1	--	--	Z
	9839.0-40.0	6.2	17.7	40.2	41.8	--	--	
	9840.0-41.0							
	9841.0-42.0			lost or broken				
	9842.0-43.0							
Core #6 3800 psi	9843.0-44.0	0.01	5.4	21.2	87.2	0.2	3.91	
	9844.0-45.0	0.38	10.5	20.6	89.4	0.1	4.38	
	9845.0-46.0	0.33	10.9	28.7	83.1	0.2	3.21	
	9846.0-47.0	0.03	9.7	6.5	96.0	0.2	12.56	
	9847.0-48.0	0.94	10.6	28.7	78.6	0.3	3.27	
	9848.0-49.0	3.9	16.7	30.9	78.6	--	--	
	9849.0-50.0	5.5	15.5	22.1	82.9	0.3	3.13	
	9850.0-51.0	3.6	10.4	20.9	89.7	0.1	3.66	
Core #7 3000 psi	9851.0-52.0	0.14	8.3	20.1	89.5	0.5	7.16	
	9852.0-53.0	0.03	5.6	11.5	97.3	0.3	5.4	
	9853.0-54.0	0.23	7.3	18.3	91.1	0.1	4.38	
	9854.0-55.0	0.24	7.3	35.7	78.7	--	--	
	9855.0-56.0	0.35	11.7	38.0	79.3	0.3	2.98	
	9856.0-57.0	0.10	4.9	16.6	85.0	--	--	
	9857.0-58.0	2.9	12.7	39.2	70.0	0.3	1.88	
	9858.0-59.0	0.67	9.5	93.3	40.3	0.3	2.32	

[a] FVF for oil at 3800 psi and 245°F ~1.66

[b] FVF for water at 3800 psi and 245°F ~1.056

[c] calculated assuming CO_2 density at retained pressure

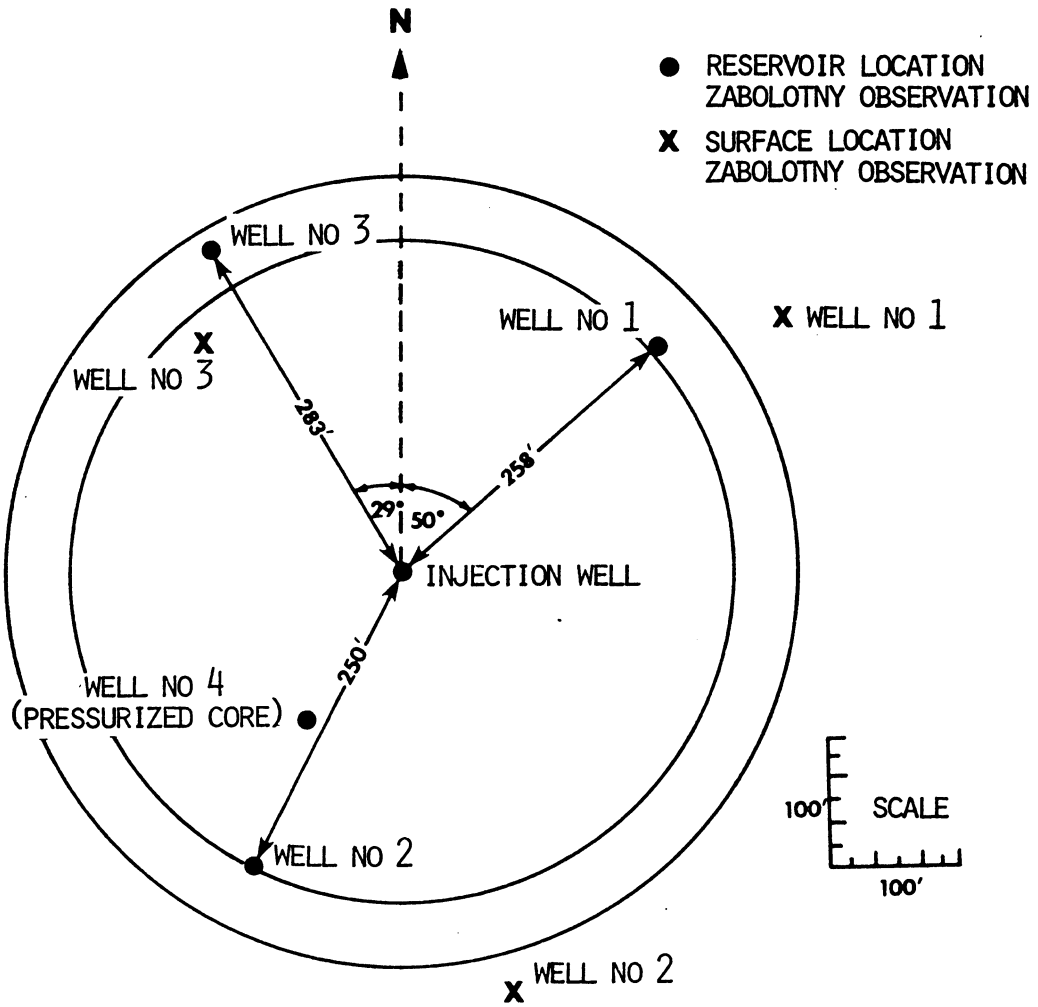

FIGURE 1
LITTLE KNIFE - CO_2 MINITEST
WELL PLACEMENT

FIGURE 2 - LITTLE KNIFE CO_2 PROJECT --
COMPARISON OF GULFLOG AND PRESSURE CORE
OIL SATURATIONS IN ZABOLOTNY OBSERVATION #4
(CORE DEPTHS ADJUSTED TO LOG DEPTHS)

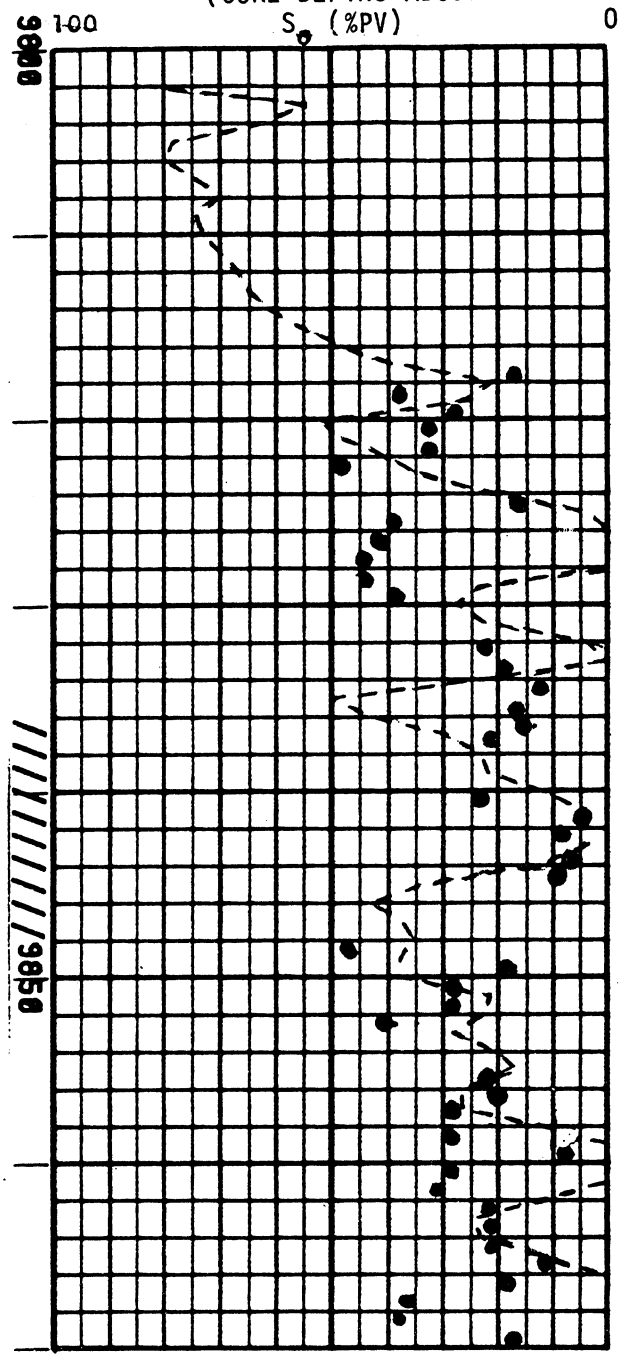

---- Gulflog 7/20/81

● Pressure core stock tank saturation corrected using FVF=1.66

SUB-APPENDIX

PRESSURE CORE ANALYSIS STUDY

FOR

GULF OIL COMPANY

Zabolotting Observation Well #4
Little Knife Field
Billings County, N. Dakota

CORE PREPARATION PROCEDURES

1. Core samples, encased in steel tubing and frozen in chests of dry ice, were submitted to our Midland laboratory.

2. Each length of tubing-encased frozen core was placed in a dry ice-filled trough attached to a milling machine. Two diametrically opposed grooves were milled down the length of the steel tubing to a depth slightly less than the wall thickness of the tubing. Liquid nitrogen was directed at the point of milling to ensure that the temperature of the tubing and core is maintained at or below that of frozen carbon dioxide.

3. The tubing was then separated into two halves and removed from the frozen core.

4. The low invasion gel that is frozen on the core was removed by chipping and abrasive action. As before, liquid nitrogen was sprayed on the core to insure that the proper cryogenic temperature was maintained.

5. The cores were then visually examined for lithological characteristics and samples were selected for analysis.

6. Both ends of each selected core segment were faced with a diamond saw using liquid nitrogen to maintain the segment in a frozen state. The faced frozen core segments were then stored under dry ice while awaiting testing.

STANDARD PRESSURE CORE ANALYSIS PROCEDURES

1. The faced frozen core segments, comprising a retort sample, were placed in a thin-walled metal thimble, quickly weighed, and placed in a gas collection cell. This cell was closed immediately.

2. The gas collection cell and its attached fluid-collecting system were evaculated for 45 seconds to remove as much air as possible before gas began to evolve from the core. The system was then sealed and the frozen core allowed to thaw to room temperature.

3. Water and oil expelled by the evolving gas were collected in a graduated receiving tube.

4. The evolved gas was collected in the void space in the cell. The system is equipped with a gauge to allow monitoring of the pressure inside the cell. If the primary cell pressure exceeded 0 psig, an attached and previously evacuated secondary cell was then opened to collect additional evolved gas. A third cell was used when neccessary.

5. Barometric pressure, room temperature, retort pressure, and produced liquid volumes were recorded periodically. Thawing of the core was considered complete when consecutive readings indicated no additional liquid and gas were being produced.

6. Portions of the evolved gas were collected separately from the primary gas collection cell and from the second and third collection cell, if used. The gas samples were analyzed to determine gas gravity and mole percent of the various components. The volumes of oil and water collected were also measured. The chloride and bromide contents of the produced water were determined.

7. Upon completion of this phase of testing, the sample and its thimble were removed from the cell, weighed, and placed in a Dean-Stark (toluene distillation) apparatus. The remaining water and oil contents of the core were removed by toluene distillation.

8. When distillation was complete, the amount of water recovered was measured volumetrically. The sample and the thimble were removed from the Dean-Stark apparatus and placed in a vacuum oven at 240° F to remove the toluene. When drying was complete, the sample and thimble were removed from the oven and allowed to cool in the presence of a desiccant and then reweighed.

9. The volume of additional oil extracted was determined gravimetrically using a stock tank oil density (corrected to room temperature) of 0.843 grams/cc as determined from the oil produced during pressure depletion. The volume of water distilled was corrected to reflect the equivalent volume of water having the same salinity as the water produced during pressure depletion.

10. The samples were then marked and placed in surgical stocking material (to minimize grain loss) and subjected to gas driven solent extraction to remove any remaining hydrocarbons. Volume of oil extracted was determined gravimetically. Those samples were then leached with methanol to remove the salts left in the pore spaces during Dean-Stark distillation.

11. Whole core porosities were then measured on each section analyzed. Two horizontal (maximum and 90°) and one vertical permeability was measured on each core segment when possible.

12. Stock tank liquid saturations as a percent of pore volume and evolved gas volumes at standard conditions were calculated for these samples.

TRACER ANALYSIS PROCEDURES
(PLUG AND DONUT ANALYSIS)

1. A cylindrical plug was drilled from each frozen core segment selected to test for filtrate invasion. Each plug was drilled concentrically to the circumference of the core segment and, hence, along its vertical axis. Liquid nitrogen was used as the bit lubricant to ensure the core remained at the proper cryogenic temperature level. The drilled plug and the remaining portion of the core segment, hereinafter referred to as the "donut" sample, were returned to the dry ice freeze chest.

2. The plugs and donut samples were removed from the freeze chest, quickly weighed, and immediately returned to the freeze chest for transport to the Dean-Stark (toluene distillation) apparatus. Metal extraction thimbles which were used with these samples to minimize grain loss were also weighed.

3. The plugs and donut samples were removed from the freeze chest, quickly inserted into their respective thimbles, and placed in their individual Dean-Stark sample chambers. The chambers were closed immediately. Heat was applied to the toluene, and distillation of the water contents from the cores commenced.

4. When distillation was complete, the volume of water recovered from each sample of core was recorded. The heat was removed from the apparatus and the samples were allowed to cool to room temperature while inside the sample chambers. The water recovered from each sample was transferred to a glass bottle which was subsequently sealed. The bottle and its contained water were submitted to Teledyne Isotopes, Inc. for determination of the tritium content of the recovered water. These samples were then leached with methyl alcohol to remove the salt.

5. After drying, the plugs and the donut samples were weighed while in their thimbles to determine their individual weight loss.

6. Porosities were run on each plug and donut with vertical permeabilities also being run on each plug sample.

7. Water saturations were calculated as a percent of pore space for each plug and donut.

8. Filtrate was calculated as a percent of total water and as a percent of total pore volume for each sample from the data supplied from Teledyne Isotopes, Inc.

Table A-1 CORED INTERVALS

Core	Depth Interval	Feet Recovered	Recovery Pressure, psi
1	9803-9811	5.9	3550
2	9811-9819	5.7	3200
3	9819-9827	5.5	2000
4	9827-9835	5.5	3100
5	9835-9843	6.4	0
6	9843-9851	7.9	3800
7	9851-9859	8.4	3000

Table A-2

GULF OIL COMPANY
CARBOLOTING OBS NO 4
LITTLE KNIFE
BILLINGS COUNTY, NORTH DAKOTA

DATE : 9-17-81
FORMATION : MISSION CANYON
DRLG. FLUID: WATER
LOCATION : SECTION 3, T144N, R98W

FILE NO : F81009
ANALYSTS : SEGREST
LABORATORY: MIDLAND TEXAS

PRESSURE RETAINED CORE ANALYSIS

	SAMPLE NUMBER	DEPTH FEET	PERM MAXIMUM	PERM 90 DEG	PERM VERTICAL	HE POR	OIL% PORE	WTR% PORE	GRAIN DEN	PORE VOL	OIL % PORE*	SAMPLE DESCRIPTION
	1	9803.0- 4.0	12.			15.1	10.0	80.7	2.81	58.0	0.2	DOL,lmy,v/f
	2	9804.0- 5.0	4.2	2.7	<0.01	6.6	22.6	50.7	2.78	27.6	2.5	DOL,lmy
	3	9805.0- 6.0	0.58	0.23	<0.01	9.2	16.7	71.4	2.81	66.0	0.1	DOL,lmy,sl/shy
	4	9806.0- 7.0	1.3			16.4	19.2	74.9	2.82	69.7	1.4	DOL,lmy,v/f
	5	9807.0- 8.0	3.3	2.8	2.3	12.9	19.3	68.6	2.83	52.3	3.3	DOL,lmy
P	6	9808.0- 9.0	1.9			15.8	29.7	45.7	2.81			DOL,lmy
		9809.0-11.0	Lost Core									
	7	9811.0-12.0	0.70	0.18	0.11	6.6	9.2	86.3	2.80	31.5	0.9	DOL,lmy,sty
	8	9812.0-13.0	3.4	2.2	0.70	10.1	23.5	62.1	2.80	51.5	10.8	DOL,lmy
P	9	9813.0-14.0	2.2			15.5	24.7	68.5	2.83			DOL,lmy
	10	9814.0-15.0	0.42	0.19	0.02	6.7	26.6	62.2	2.80	37.8	1.9	DOL,lmy
	11	9815.0-16.0	0.34	0.15	<0.01	6.1	26.7	70.2	2.81	46.0	1.3	DOL,lmy,sl/shy
	12	9816.0-16.7	1.2	0.59	0.23	9.9	23.9	64.0	2.82	48.1	10.2	DOL,lmy,carb
		9816.7-19.0	Lost Core									
P	13	9819.0-20.0	2.6			14.0	13.4	63.4	2.76			DOL,lmy
S	14	9820.0-21.0	1.2	1.0	0.45	9.6	11.0	80.7	2.74	65.3	0.0	DOL,lmy
	15	9821.0-22.0	1.3	0.44	0.20	6.2	7.5	84.3	2.76	26.7	0.0	DOL,lmy,sl/shy
	16	9822.0-23.0	0.47	0.23	0.24	7.2	10.2	74.6	2.75	38.4	0.0	DOL,lmy,sl/shy
	17	9823.0-24.0	1.6	1.0	0.31	8.5	9.4	75.2	2.75	56.5	0.0	DOL,lmy,sl/shy
	18	9824.0-24.5	1.8	1.3	0.75	7.9	13.0	77.0	2.76	26.1	0.0	DOL,lmy,sty
		9824.5-27.0	Lost Core									
P	19	9827.0-28.0	454.			23.3	14.4	82.2	2.80			DOL,lmy
	20	9828.0-29.0	63.			20.6	2.4	85.0	2.77	49.2	0.0	DOL,lmy,sl/fr
	21	9829.0-30.0	117.	96.	50.	23.4	4.9	79.6	2.82	156.5	0.4	DOL,lmy,sl/fr
	22	9830.0-31.0	567.			26.2	4.0	81.2	2.81	135.1	0.0	DOL,lmy sl/fr
	23	9831.0-32.0	233.			27.8	4.6	79.6	2.79	203.3	0.0	DOL,lmy,sl/fr
	24	9832.0-32.5	TBFA									
	25	9832.5-35.0	Lost Core									

S Indicates a Preserved Sample
P Indicates Plug Analysis

TBFA Too Broken For Analysis
* Oil Produced by Pressure Depletion

Table A-2 (cont'd.)

GULF OIL COMPANY
CABOLOTING OBS NO 4

DATE : 9-17-81
FORMATION : MISSION CANYON

FILE NO : P81009
ANALYSTS : SEGREST

PRESSURE RETAINED CORE ANALYSIS

SAMPLE NUMBER	DEPTH FEET	PERM MAXIMUM	PERM 90 DEG	PERM VERTICAL	HE POR	OIL% PORE	WTR% PORE	GRAIN DEN	PORE VOL.	OIL % PORE*	SAMPLE DESCRIPTION
P 24	9835.0-36.0	617.			24.0	28.7	47.1	2.77			DOL,lmy,sl/fr
S 25	9836.0-37.0	1971.			23.6	11.2	47.3	2.78	108.7	**	DOL,lmy,sl/fr
26	9837.0-38.0	46.	45.	37.	21.3	16.9	35.4	2.84	89.6	**	DOL,lmy,sl/fr
S 27	9838.0-39.0	26.	25.	25.	19.8	17.4	41.8	2.84	136.7	**	DOL,lmy,sl/fr
P 28	9839.0-40.0	6.2			17.7	24.2	39.6	2.81		**	DOL,lmy
	9840.0-41.0	TBFA									
	9841.0-43.0	Lost Core									
S 29	9843.0-44.0	0.01			5.4	12.8	82.6	2.81	28.1	0.0	DOL,lmy,v/f
30	9844.0-45.0	0.38	0.34	0.15	10.5	12.4	84.7	2.83	81.5	0.4	DOL,lmy,gyp inc
31	9845.0-46.0	0.33	0.27	0.78	10.9	17.3	78.7	2.82	89.4	0.6	DOL,lmy,gyp inc
32	9846.0-47.0	0.03			9.7	3.9	90.9	2.82	33.1	0.2	DOL,lmy,v/f
33	9847.0-48.0	0.94	0.75	0.32	10.6	17.3	74.5	2.82	74.1	0.7	DOL,lmy,gyp inc
P 34	9848.0-49.0	3.9			16.7	18.6	74.4	2.82			DOL,lmy
35	9849.0-50.0	5.5	5.3	4.0	15.5	13.3	78.5	2.82	73.0	0.0	DOL,lmy
36	9850.0-51.0	3.6	0.94	0.28	10.4	12.6	84.9	2.81	47.8	0.0	DOL,lmy
37	9851.0-52.0	0.14	0.12	<0.01	8.3	12.1	84.8	2.80	52.7	0.2	DOL,lmy
38	9852.0-53.0	0.03	0.03	<0.01	5.6	6.9	92.1	2.80	18.9	0.0	DOL,lmy,sl/shy
39	9853.0-54.0	0.23	0.12	0.10	7.3	11.0	86.3	2.80	29.9	0.1	DOL,lmy
40	9854.0-55.0	0.24	0.23	0.03	7.3	21.5	74.5	2.80	33.0	0.2	DOL,lmy,gyp
S 41	9855.0-56.0	0.35	0.20	0.04	11.7	22.9	75.1	2.81	76.3	0.7	DOL,lmy
P 42	9856.0-57.0	0.10			4.9	10.0	80.5	2.75			DOL,lmy
43	9857.0-58.0	2.9	2.5	1.5	12.7	23.6	66.3	2.80	46.6	1.4	DOL,lmy
44	9858.0-59.0	0.67	0.46	0.13	9.5	56.2	38.2	2.77	71.2	3.5	DOL,lmy,gyp

S INDICATES A PRESERVED SAMPLE
P INDICATES PLUG ANALYSIS

TBFA TOO BROKEN FOR ANALYSIS
* OIL PRODUCED BY PRESSURE DEPLETION
** UNPRESSURED CORE

Table A-3

LITHOLOGICAL ABBREVIATIONS

ANH (Y)	Anhydrite, Anhydritic
ARK	Arkose, Arkosic
BAN	Band, Banded
BREC	Breccia, Brecciated
CALC	Calcite, calcareous
CARB	Carbonaceous
CG	Coarse Grained
CHK (Y)	Chalk, Chalky
CHT (Y)	Chert, Cherty
CONGL	Conglomerate, Conglomeritic
CXLN	Coarsely Crystalline
DNS	Dense
DOL (C)	Dolomite, Dolomitic
F	Randomly Oriented Fractures
FG	Fine Grained
FOSS	Fossiliferous
FR	Friable
FXLN	Finely Crystalline
GAL	Galena
GLAUC	Glauconite, Glauconitic
GRAN	Granite
GYP	Gypsum, Gypsiferous
HF	Predominately Horizontally Fractured
INC	Inclusion
INTBD	Interbedded
LAM	Laminated
LM (Y)	Limestone, Limy
MG	Medium Grained
MTX	Matrix
NA	Interval Not Analyzed (At request of Client)
NOD	Nodule, Nodular
OOL	Oolitic
PISO	Pisolitic
PP	Pinpoint Porosity
PT	Parting
PYR	Pyrite, Pyritic
SD (Y)	Sandstone, Sandy
SH (Y)	Shale, Shaly
SHR	Solid Hydrocarbon Residue
SL/	Slightly
SLT (Y)	Silt, Silty
STY	Stylolite, Stylolitic
SUC	Sucrosic
SUL	Sulphur
TBFA	Too Broken For Analysis
TRIP	Tripolite
V/	Very
VF	Predominately Vertically Fractured
VGY	Vugular
XBD	Crossbedded
XLN	Medium Crystalline
XTL	Crystal

The first work in the description column of the core analysis report describes the rock type, following are rock modifiers in decreasing abundance and miscellaneous descriptive terms.

Table A-4 ANALYSIS OF LIBERATED GAS BY GAS CHROMATOGRAPHY

Depth, Feet	Component Analysis, Mole Percent												Calc. Gas Gravity (Air=1.0)	Gas Volume cc @ STP
	H_2S	CO_2	N_2	C_1	C_2	C_3	IC_4	NC_4	IC_5	NC_5	C_6	C_7+		
9803.0-9804.0	0.00	1.78	11.15	6.30	12.97	14.95	3.99	12.88	8.48	13.39	7.08	7.03	1.869	583.2
9804.0-9805.0	5.14	2.37	3.14	43.06	14.55	9.96	1.60	4.42	3.07	4.64	4.78	3.25	1.235	1469.7
9805.0-9806.0	7.29	1.47	3.65	27.38	8.45	8.61	2.98	12.47	6.43	9.54	6.72	4.99	1.594	2640.0
	7.39	2.28	3.82	49.49	12.39	7.02	0.98	2.54	1.77	4.73	3.55	4.06	1.146	
9806.0-9807.0	7.20	2.04	3.89	33.51	10.32	9.44	2.59	9.16	4.35	6.21	6.47	4.81	1.447	3227.9
	6.72	2.30	4.46	40.84	11.29	8.44	3.75	6.39	3.52	4.89	3.30	4.11	1.282	
9807.0-9808.0	5.85	1.56	4.81	34.61	8.96	7.52	3.48	4.29	4.47	7.89	8.13	8.43	1.535	248.8
	6.41	1.56	6.54	36.32	9.91	6.96	1.99	6.57	5.16	6.09	6.99	5.49	1.422	
9811.0-9812.0	7.61	2.81	9.13	40.63	10.62	6.43	2.05	2.72	2.38	4.26	6.47	4.88	1.276	745.3
9812.0-9813.0	8.36	2.06	3.44	33.56	10.73	9.95	2.54	8.34	5.11	6.36	5.05	4.51	1.421	3126.5
	8.76	2.56	2.70	45.66	12.99	7.78	1.17	3.25	2.88	5.05	4.66	2.53	1.187	
9814.0-9815.0	9.42	8.28	3.26	31.71	11.09	9.59	3.19	9.47	3.53	4.37	3.33	2.75	1.350	1471.1
9815.0-9816.0	7.56	3.79	6.70	41.39	11.42	6.47	2.25	2.44	3.78	4.12	5.55	4.52	1.269	1080.5
9816.0-9817.0	7.89	2.03	1.98	36.91	11.53	9.50	2.31	8.55	3.79	5.75	4.99	4.77	1.380	3032.9
	6.87	2.08	18.06	40.70	11.38	6.16	1.18	2.39	1.52	3.40	3.61	2.65	1.117	
9820.0-9821.0	8.69	8.27	2.82	46.34	13.30	7.42	0.92	2.29	1.48	3.88	2.54	2.07	1.107	1697.1
9821.0-9822.0	1.19	9.21	4.12	32.75	10.05	8.25	1.52	7.82	5.19	6.93	7.27	5.71	1.508	532.2
9822.0-9823.0	4.24	21.83	2.52	28.76	8.91	8.22	1.95	7.52	5.24	6.57	2.71	1.53	1.400	1051.1
9823.0-9824.0	6.45	7.85	8.61	40.27	12.31	11.03	3.33	5.61	2.21	1.11	0.80	0.44	1.098	1427.1
9824.0-9825.0*														
9828.0-9829.0	0.00	0.00	82.21	17.79	0.00	0.00	0.00	0.00	0.00	0.00	0.00	0.00	0.893	2374.7
	0.00	0.00	80.83	19.17	0.00	0.00	0.00	0.00	0.00	0.00	0.00	0.00	0.888	
9829.0-9830.0	2.60	80.41	0.44	7.87	4.53	4.15	0.00	0.00	0.00	0.00	0.00	0.00	1.410	8902.6
	3.80	76.74	0.36	9.51	4.89	4.70	0.00	0.00	0.00	0.00	0.00	0.00	1.389	
	3.20	78.97	0.41	8.36	4.72	4.35	0.00	0.00	0.00	0.00	0.00	0.00	1.403	
9830.0-9831.0	0.00	93.84	3.97	1.40	0.36	0.22	0.04	0.09	0.06	0.02	0.00	0.00	1.484	1898.0
9831.0-9832.0	0.00	47.39	38.61	1.51	5.34	3.39	0.53	1.54	0.75	0.66	0.09	0.19	1.295	349.5
9843.0-9844.0	0.00	2.90	25.76	29.54	9.00	10.14	3.34	7.49	6.28	5.54	0.00	0.00	1.216	305.4
9844.0-9845.0	11.60	4.18	4.49	31.78	8.16	9.89	2.40	10.46	6.68	6.00	2.25	2.12	1.368	639.0
9845.0-9846.0	6.13	2.85	11.18	40.41	11.07	7.29	2.06	8.16	3.98	5.21	0.71	0.95	1.161	1534.0
9846.0-9847.0	16.08	11.72	6.72	46.09	11.46	5.10	0.63	1.58	0.26	0.37	0.00	0.00	0.944	132.4
9847.0-9848.0	10.45	3.14	3.83	50.11	13.59	7.90	1.06	2.80	2.06	1.85	1.56	1.65	1.024	1601.3
9849.0-9850.0	9.85	3.10	0.90	52.37	14.76	8.80	1.23	3.29	2.16	1.50	0.88	1.16	0.997	2008.9
9850.0-9851.0	9.62	3.34	8.76	34.96	9.72	9.34	3.97	7.70	4.36	4.91	1.54	1.78	1.257	487.7
9851.0-9852.0	0.00	2.38	66.78	15.83	4.72	2.92	0.37	1.70	3.46	0.98	0.47	0.37	1.042	391.7
9852.0-9853.0	8.70	4.51	13.45	49.34	12.13	4.83	1.84	3.24	0.89	1.08	0.00	0.00	0.924	321.9
9853.0-9854.0	8.69	4.10	6.35	23.91	19.59	11.39	4.86	9.23	6.26	5.61	0.00	0.00	1.313	240.8
9854.0-9855.0*														
9855.0-9856.0	9.91	2.91	1.64	45.66	12.65	8.90	1.16	7.28	3.20	4.84	1.10	0.73	1.124	1956.4
9857.0-9858.0	6.81	1.83	2.45	35.90	10.77	8.27	2.80	10.08	8.86	9.05	1.53	1.64	1.375	1825.3
9858.0-9859.0	7.89	2.28	2.13	35.40	10.27	9.09	2.99	11.10	7.24	8.02	1.46	2.14	1.369	2753.5
	7.96	2.46	18.98	39.64	11.19	7.36	0.82	4.90	2.46	1.57	1.28	1.37	1.063	

* No sample due to equipment malfunction.

Table A-5

CHLORIDE AND BROMIDE DATA

Depth, Feet	Bromide, mg/l	Chloride, mg/l
9803.0 - 9804.0	272,300	39,280
9804.0 - 9805.0	374,100	70,650
9805.0 - 9806.0	284,200	36,850
9806.0 - 9807.0	208,400	66,310
9807.0 - 9808.0	189,000	83,470
9811.0 - 9812.0	215,500	124,200
9812.0 - 9813.0	279,400	88,660
9814.0 - 9815.0	241,500	105,500
9815.0 - 9816.0	184,200	125,300
9816.0 - 9817.0	243,900	122,900
9820.0 - 9821.0	236,800	134,600
9821.0 - 9822.0	201,300	116,300
9822.0 - 9823.0	206,000	145,500
9823.0 - 9824.0	182,300	107,700
9824.0 - 9825.0	*	*
9828.0 - 9829.0	165,800	89,540
9829.0 - 9830.0	194,200	119,490
9830.0 - 9831.0	104,700	118,100
9831.0 - 9832.0	94,720	128,300
9843.0 - 9844.0	208,400	73,410
9844.0 - 9845.0	146,800	166,100
9845.0 - 9846.0	201,300	144,700
9846.0 - 9847.0	137,300	181,700
9847.0 - 9848.0	123,100	155,400
9848.0 - 9849.0	185,200	119,200
9849.0 - 9850.0	74,830	115,800
9851.0 - 9852.0	212,200	75,980
9852.0 - 9853.0	260,500	121,200
9853.0 - 9854.0	201,300	113,500
9854.0 - 9855.0	207,900	123,300
9855.0 - 9856.0	265,200	120,500
9857.0 - 9858.0	213,100	122,400
9858.0 - 9859.0	236,800	107,600

* Insufficient water

Table A-6

VERTICAL PLUG AND DONUT DATA

Sample Number	Sample Type	Depth, Feet	Vertical Permeability, Md	Porosity, Percent	Water Saturation Percent Pore Volume
1	Plug	9803.5-9803.8	12	23.0	50.2
1	Donut			20.5	61.0
2	Plug	9806.7-9806.9	1.3	13.2	56.3
2	Donut			13.7	52.8
3	Plug	9811.4-9811.6	0.09	6.5	83.7
3	Donut			7.9	79.8
4	Plug	9819.6-9819.8	0.13	13.1	70.4
4	Donut			13.6	57.0
5	Plug	9823.8-9824.0	0.09	5.5	79.3
5	Donut			6.0	78.6
	Plug	9827.2-9827.4	4.5	15.5	84.3
6	Donut			16.5	75.0
7	Plug	9830.1-9830.3	26	23.1	79.4
7	Donut			22.9	58.9
8	Plug	9837.0-9837.2	39	23.3	31.9
8	Donut			23.1	35.7
9	Plug	9846.3-9846.6	0.06	8.6	93.1
9	Donut			7.9	92.0
10	Plug	9850.0-9850.2	0.85	13.5	86.5
10	Donut			14.0	82.9
11	Plug	9853.4-9853.6	0.17	7.9	86.7
11	Donut			8.0	92.7
12	Plug	9857.4-9857.6	1.1	14.2	66.5
12	Donut			16.0	49.9

Table A-7

FILTRATE INVASION DATA

Sample	Filtrate Percent Of Total Water	Filtrate Percent Of Pore Volume
P-1	97.4	48.9
D-1	*	*
P-2	41.4	23.3
D-2	35.1	18.5
P-3	8.4	7.0
D-3	10.3	8.2
P-4	67.9	47.8
D-4	47.8	27.2
P-5	10.6	8.4
D-5	50.4	39.6
P-6	84.1	70.9
D-6	69.6	52.2
P-7	54.6	43.4
D-7	45.8	27.0
P-8	50.2	16.0
D-8	39.9	14.2
P-9	<1.8	<1.7
D-9	<2.6	<2.4
P-10	5.4	4.7
D-10	16.8	13.9
P-11	2.3	2.0
D-11	5.8	5.4
P-12	10.4	6.9
D-12	23.7	11.8

* Sample bottle broken during shipment

Table A-8

TRITIUM RESULTS FROM LITTLE KNIFE-GULF OIL CO.

Sample	HTO pci/liter
P-1	1.11 ± 0.11 E 05
D-1	Arrived Broken
P-2	4.72 ± 0.47 E 04
D-2	4.00 ± 0.40 E 04
P-3	9.6 ± 2.0 E 03
D-3	1.17 ± 0.24 E 04
P-4	7.74 ± 0.77 E 04
D-4	5.45 ± 0.55 E 04
P-5	1.21 ± 0.22 E 04
D-5	5.74 ± 0.57 E 04
P-6	9.59 ± 0.96 E 04
D-6	7.94 ± 0.79 E 04
P-7	6.23 ± 0.62 E 04
D-7	5.22 ± 0.52 E 04
P-8	5.72 ± 0.57 E 04
D-8	4.55 ± 0.46 E 04
P-9	L.T. 2.0 E 03
D-9	L.T. 3.0 E 03
P-10	6.1 ± 1.8 E 03
D-10	1.92 ± 0.27 E 04
P-11	2.6 ± 1.6 E 03
D-11	6.6 ± 1.9 E 03
P-12	1.18 ± 0.22 E 04
D-12	2.70 ± 0.27 E 04
Mud Filtrate	(1.14 ± 0.11 E 05)

From: Andrew Carmichael
Teledyne Isotopes

APPENDIX 43

LITTLE KNIFE FIELD CO_2 MINITEST
COMPOSITIONAL SIMULATION

Supervised by:

C. J. Lin

By

Y. R. Patel
E. S. Broussard

Production Services Department
Gulf Research & Development Company
Houston Technical Services Center
Houston, Texas

TABLE OF CONTENTS

	Page
Summary and Conclusions	121
Introduction	122
Discussion	125
Acknowledgements	154
Nomenclature	155
References	156

LIST OF TABLES

Table		
1	Basic Reservoir Characteristic Data	158
2	Physical Properties of Reservoir Fluids	158
3	Hydrocarbon Analysis of Reservoir Fluids	159
4	Oil Composition and Component Parameters for the Peng-Robinson Equation of State	160
5	Binary Interaction Parameters for the Peng-Robinson Equation	160
6	K-Values vs Pressure (0.012 Mole Fraction)	161
7	K-Values vs Pressure (0.100 Mole Fraction)	162
8	K-Values vs Pressure (0.200 Mole Fraction)	163
9	K-Values vs Pressure (0.300 Mole Fraction)	164
10	K-Values vs Pressure (0.400 Mole Fraction)	165
11	K-Values vs Pressure (0.500 Mole Fraction)	166
12	K-Values vs Pressure (0.600 Mole Fraction)	167
13	K-Values vs Pressure (0.700 Mole Fraction)	168
14	K-Values vs Pressure (0.800 Mole Fraction)	169
15	K-Values vs Pressure (0.900 Mole Fraction)	170
16	Summary of Results for the CO_2 Residual Oil Saturation Tests	171
17	Core and GULFLOG Analyses for the Minitest Wells	172
18	Pattern Area Volumetric Data	173
19	Production Data in the Minitest Area	173
20	Analyses of the Responses from the Multi-Well Pulse Test	174
21	Water/CO_2 Injection Schedule for the Minitest	175
22	Volumetric Injection Data for the Minitest	176
23	Distances and Orientations of Production and Observation Wells Relative to Zabolotny Injection Well No. 1	176
24	Input Data for Reservoir Rock Properties	177
25	Water Tracer Analysis	178
26	Subsurface Sample Analysis	179
27	Separator Gas Analysis at Observation Well No. 1	180
28	Separator Gas Analysis at Observation Well No. 2	182
29	Separator Gas Analysis at Observation Well No. 3	184
30	CO_2 $^{13}C/^{12}C$ Isotope Ratio Analysis	186
31	Percentages of Oil Displaced (STB Basis)	186
32	Input Data for Reservoir Rock Properties for Layer Y	187

LIST OF FIGURES

Figure		Page
1	CO_2 Minitest Location in the Little Knife Field	188
2	Index Map of Williston Basin	189
3	Top of Mission Canyon Formation Structure Map	190
4	Stratigraphic Fence Diagram of Zones C and D	191
5	Reservoir Cross Section Grid Based on Whole Core Porosity Analysis	192
6	Whole Core Porosity and Permeability Compared to Lithology	193
7	Fractures Measured from Oriented Cores	194
8	Oil Differential Formation Volume Factor and Solution Gas-Oil Ratio	195
9	Oil Density and Oil Viscosity	196
10	Phase Boundary for Oil-CO_2 Mixtures	197
11	Pressure Volume Relationship (for Oil-CO_2 Mixtures)	198
12	Viscosity of Oil-CO_2 Mixtures	199
13	Density of Oil-CO_2 Mixtures	200
14	Coefficients of Compressibility of Reservoir Oil with CO_2 Added	201
15	Oil Recovery vs Average System Pressure	202
16	Oil Recovery vs CO_2 Pore Volumes	203
17	K-Values vs Pressure	204
18	K-Values vs Pressure (0.5 Mole Fraction)	205
19	K-Values vs Pressure (0.9 Mole Fraction)	206
20	Relative Permeability Data for Layer W	207
21	Relative Permeability Data for Layer X	208
22	Relative Permeability Data for Layer Y	209
23	Relative Permeability Data for Layer Z	210
24	CO_2-Water Relative Permeability Data with and without Residual Oil Saturation	211
25	Pressure History in the Minitest Area	212
26	Surface and Reservoir Locations	213
27	Casing and Tubing Settings in Zabolotny Injection Well No. 1	214
28	Casing and Tubing Settings in Zabolotny Observation Well No. 1	214
29	Four-Well Pulse Test Response at Observation Well No. 1	215
30	Four-Well Pulse Test Response at Observation Well No. 2	216
31	Four-Well Pulse Test Response at Observation Well No. 3	217
32	Coordinate System for the Compositional Simulation	218
33	11x11x4 Grid System	219
34	16x15x4 Grid System	220
35	Permeability - Porosity Relationship	221
36	Derived Oil-Water Capillary Pressure Data	222
37	Pressure History Match at Zabolotny Injection Well No. 1	223
38	Pressure History Match at Zabolotny Well No. 1	224
39	Pressure History Match at Zabolotny Well No. 2	225
40	Pressure History Match at Zabolotny Well No. 3	226
41	Water Saturation History Match by Layers at Zabolotny Well No. 1	227
42	Water Saturation History Match by Layers at Zabolotny Well No. 2	228
43	Water Saturation History Match by Layers at Zabolotny Well No. 3	229
44	Water Saturation History Match for Zone D at Zabolotny Well No 1	230
45	Water Saturation History Match for Zone D at Zabolotny Well No 2	231
46	Water Saturation History Match for Zone D at Zabolotny Well No 3	232
47	Measured Carbon Dioxide Contents from Logs, Separator Gas Analysis and Isotope Analysis at Zabolotny Well No. 1	233
48	Measured Carbon Dioxide Contents from Logs, Separator Gas Analysis and Isotope Analysis at Zabolotny Well No. 2	234

LIST OF FIGURES (cont'd.)

Figure		Page
49	Measured Carbon Dioxide Contents from Logs, Separator Gas Analysis and Isotope Analysis at Zabolotny Well No. 3	235
50	Swelling Factors of Oil-CO_2 Mixtures	236
51	CO_2 Saturation History Match at Zabolotny Well No. 1	237
52	CO_2 Saturation History Match at Zabolotny Well No. 2	238
53	CO_2 Saturation History Match at Zabolotny Well No. 3	239
54	Oil Saturation History Match by Layers - Zabolotny Well No. 1	240
55	Oil Saturation History Match by Layers - Zabolotny Well No. 2	241
56	Oil Saturation History Match by Layers - Zabolotny Well No. 3	242
57	Oil Saturation History Match for Zone D - Zabolotny Well No. 1	243
58	Oil Saturation History Match for Zone D - Zabolotny Well No. 2	244
59	Oil Saturation History Match for Zone D - Zabolotny Well No. 3	245
60	CO_2-Free Oil Saturation Profile at Zabolotny Well No. 4	246
61	Oil Saturation Profile at Zabolotny Well No. 4	247
62	Gas Saturation Distribution for Layer Y	248
63	Oil Saturation Distribution for Layer Y	249
64	Water Saturation Distribution for Layer Y	250
65	Gas Saturation Distribution for Layer Y	251
66	Oil Saturation Distribution for Layer Y	252
67	Water Saturation Distribution for Layer Y	253
68	CO_2-Free Oil Saturation Distribution for Layer Y	254
69	Oil Recovery from the Minitest Area	255
70	Water Saturation History Match for Layer Y	256
71	CO_2 Saturation History Match for Layer Y	257
72	Oil Saturation History Match for Layer Y	258
73	Water Saturation History Match for Layer Y	259
74	Oil Saturation History Match for Layer Y	260
75	CO_2-Free Oil Saturation Profile at Zabolotny Well No. 4	261
76	Oil Saturation Profile at Zabolotny Well No. 4	262

I. SUMMARY AND CONCLUSIONS

A reservoir simulation study of the Little Knife CO_2 Minitest was completed using Gulf's three-dimensional, three-phase, multi-component, compositional simulator.

An improved reservoir characterization in the Little Knife minitest area was developed as a result of history matching of the actual field performance. The displacement efficiency of the CO_2 minitest in the project area was evaluated. The model is to be used to predict the expansion of the CO_2 minitest to a field-wide application.

Based upon the results of this study, the following conclusions were made:

1. A satisfactory history match has been achieved. The computed bottom-hole pressures and fluid saturation changes at the observation wells are in good agreement with the observed values.
2. The amount of oil displaced (on a STB basis) as a percent of oil-in-place at the beginning of the minitest (December 11, 1980) for the straight waterflood process would be 37% from the entire project interval.
3. The amount of oil displaced (on a STB basis) as a percent of oil-in-place at the beginning of the minitest (December 11, 1980) for CO_2 flood with 1:1 WAG ratio in the minitest area is 50% from the entire project interval.
4. A small amount of CO_2 migrated to the less permeable top layer (Layer W). Ninety-five (95) percent of the CO_2 stayed in Layers X and Y.
5. The Peng-Robinson equation of state has accurately predicted physical properties of the mixtures of Little Knife crude oil and carbon dioxide.
6. The tabular K-values (equilibrium ratios) generated from the Peng-Robinson equation of state were found to be adequate in predicting the phase behavior of the CO_2 flood process for the Little Knife field.
7. Gulf's compositional simulator successfully simulated the CO_2 MCM (multiple contact miscible) process within engineering accuracy.

II. INTRODUCTION

A joint DOE-Gulf Oil Corporation minitest of carbon dioxide miscible flood process[1-3*] was conducted in the Little Knife Field, North Dakota (Figure 1) from December 11, 1980 through September 24, 1981. The objective of this minitest was to show that the CO_2 miscible displacement process has potential for commercialization in carbonate oil reservoirs in the Rocky Mountain area[4], that have not been extensively waterflooded and have a high remaining oil saturation. The purpose of this study is to monitor the field performance of the CO_2 minitest using Gulf's compositional simulator[5,6]. The model will be used to predict expansion of the CO_2 minitest to a field-wide application.

The Little Knife Field is one of the new major reservoirs found by Gulf in recent years. The first wildcat discovery well[7] was completed on February 8, 1977. The original oil-in-place (OOIP) in the Mission Canyon Formation was estimated to be 160 MMSTB. Cumulative oil production through October, 1981 was approximately 19 MMSTB (12% of OOIP). The primary recovery mechanism is solution gas drive. Currently, there are 124 producing wells on 160-acre spacing, and the average reservoir pressure has been declining from the initial reservoir pressure of 4400 psia to approximately 2750 psia. It was anticipated that waterflood residual oil saturation would be high and the CO_2 miscible process[4] would be a suitable process. However, there is no CO_2 commercially available in the area at this time. Carbon dioxide may become available from a coal gasification plant[8] to be located 50 to 60 miles east of the field. The plant has been in the planning stage since 1972 and is scheduled to be operational by 1985, producing gas at 190 MMSCF/day.

---

*All references are listed in the Reference Section.

The proposal for the Little Knife CO_2 minitest was submitted to the Department of Energy on September 8, 1978 (Department of Energy RFP No. EW-78-R-21-8383). The work associated with this minitest was divided into five phases:

Phase I: Location and Drilling of Minitest Pattern

Phase II: Laboratory Determination of CO_2/Water Displacement Parameters in Reservoir Cores

Phase III: Minitest Area CO_2 Simulation

Phase IV: Injection Period, Performance Data Acquisition and Interpretation

Phase V: Projection of CO_2 Flood Performance to Commercial Scale

This report describes the results of the reservoir simulation work conducted for Phase III and a part of Phase IV.

The Little Knife CO_2 Minitest is a non-producing, five-acre field trial of the CO_2 miscible displacement process in the Mission Canyon Formation. The test pattern consists of a single injection well offset by three observation wells arranged in an inverted four-spot configuration. A WAG-type (water-alternating-gas) injection sequence[9] involving alternate slugs of water and CO_2 was used. The test included time-lapse logging to monitor saturation changes as alternate slugs of water and CO_2 pass the observation wells. Fluid samples from the observation wells were collected periodically to check for tracers and fluid composition. At the conclusion of the drive water injection, a fifth well was drilled behind the CO_2 front and cored with a pressure-retaining core barrel to confirm the residual oil saturation to the CO_2 miscible flood. The minitest was designed to give the following information:

1. Reduction in original oil saturation due to water injection.
2. Reduction in waterflood residual oil saturation due to alternate CO_2/water injection.
3. Extent of gravity segregation within the porous zone.
4. Effect of stratification and crossflow on CO_2 displacement.
5. Influence of reservoir heterogeneity on fluid injection performance.

This information is needed to assess the potential for a full-scale fluid injection project in the Mission Canyon Formation. The compositional simulation model[5,6] was used to history match the field performance and to evaluate displacement and sweep efficiency in the project area.

The report first describes reservoir geology. Next the laboratory and field work associated with the minitest is presented. Input data used in the compositional simulation are described in detail. The incremental recovery by the miscible CO_2 flood is presented with a discussion of the results of history matching the minitest. Finally, the commercial scale applications of the miscible CO_2 process for the Little Knife Field is presented.

III. DISCUSSION

A. Reservoir Geology

1. Mission Canyon Formation

The Little Knife Field is located near the central portion of the Williston Basin (Figure 2) and south of the Nesson Anticline in portions of Billings, Dunn, and McKenzie Counties, North Dakota. Production is from the lower Mississippian Mission Canyon Formation at a depth of approximately 9,800 feet. The field is isolated within a broad, low lying, northward plunging anticlinal nose (Figure 3). Closure on the west, north, and east is created by this gentle fold, while closure on the south is a stratigraphic entrapment.

The Mission Canyon Formation is 465 feet thick, and has been subdivided into six informal zones, designated Zones A through F (Figure 4). The entire formation is interpreted as a regressive shoaling upward sequence, with Zone F having been in an open marine environment, to Zone A, which is supratidal. The various hydrocarbon bearing porosity intervals are locally well developed but deteriorate laterally. Major porosity intervals are distributed in mid to low portions of Zone B, lower portions of Zone C and upper portions of Zone D. These beds were partially-to-completely dolomitized to form fine-grained, sucrosic dolomite.

2. Minitest Project Interval

Beds utilized for the CO_2 minitest project interval (Figure 4) are the beds at the base of Zone C and at the top of Zone D, a total

thickness of 31 feet. Here the depositional environment grades upward from open to transitional, to restricted marine, where large amounts of lime mud were deposited. Higher wave energy, perhaps storms, washed skeletal fragments from more seaward regions into the low energy areas to mix with the accumulating carbonate muds. These fragments, once deposited, were thoroughly mixed with the fine carbonate muds by burrowing organisms, homogenizing the sediment. The end result was a sedimentary deposit of uniform, though low, permeability. Ion-rich brine solutions moved through the deposit, partially replacing the skeletal fragments with anhydrite. This was followed by dolomitization of the carbonate mud. Once both anhydrite replacement and dolomitization had ceased, porous beds of partially dolomitized skeletal wackestones resulted. Later, the replacing anhydrite was partially leached away, enhancing overall porosity to leave the final end product of diagenetic modifications: porous, sucrosic, calcareous dolomite.

Reservoir rock characteristics in the project interval are similar in each well (Figure 4). To perform the simulation study, the 31 foot interval has been subdivided into four layers, W, X, Y, and Z (Figure 5), based on core porosities and permeabilities. The characteristics of each layer are discussed in greater detail later in this report under "Laboratory Work: Core Analysis" (Section B, Item 4).

A stylolite is located just above Layer X throughout the minitest area, reducing porosity for approximately one foot. This stylolitized horizon serves as a marker on the sonic logs to divide the Mission Canyon into Zone C above (with Layer W) and Zone D below (with

Layers X, Y, and Z). Layer W is formed by two beds of rock. The lower bed is dolomitic limestone, containing low porosity and permeability. The upper bed is calcareous dolomite, which contains fair to good amounts of porosity and permeability. In Observation Well No. 3, only dolomitic limestone is present. This lack of a bed of calcareous dolomite is due to less dolomitization affecting the uppermost portions of the project interval at this location. Layers X, Y, and Z are composed of highly porous and permeable calcareous dolomite.

A comparison of porosity and permeability to lithology by whole core analysis[10], in all four wells, is illustrated in Figure 6. The basic reservoir data in Zone D of the Mission Canyon Formation are listed in Table I.

Some fracturing is evident in the project interval. Studies of oriented cores from the minitest wells revealed the average fracture strike directions to be in either a northwesterly (N 67° W) or northeasterly (N 69° E) direction, differing slightly from well to well (Figure 7). The fractures were found to extend vertically eighteen to twenty-four inches, and it was felt that their lateral continuity also extends only for short distances. Multi-well pulse testing[11] revealed no major contribution by fractures, but did calculate permeabilities to be 2.5 times that measured from the whole core analysis[10]. These higher average permeabilities were interpreted to be the result of the slight affect of short non-continuous fractures dispersed somewhat uniformly across the minitest area.

B. Laboratory Work

1. Fluid Properties and Phase Behavior Study

On May 12 and 13, 1979, subsurface and separator samples were obtained from the Zabolotny 1-3-4A Well which is situated about 2,000 feet from the center of the minitest area. The reservoir temperature is 245°F in the project interval. A complete oil study[12] was performed on the bottom hole samples to evaluate phase properties and engineering parameters. The saturation pressure at 245°F is 2698 psia. The results indicate that the reservoir fluid behaves as a medium shrinkage oil with a solution GOR* of 1119 SCF/STB and a formation volume factor of 1.769 RB/STB at the saturation pressure. A portion of the separator samples were recombined to obtain a representative reservoir fluid. Using this recombined reservoir fluid, CO_2 swelling tests[13] were run with various concentrations of CO_2 added to the original reservoir fluid. Viscosities were determined on two of the CO_2 enriched reservoir fluids. The addition of 50 mole percent carbon dioxide to the reservoir fluid gave a volume increase of 56 percent, a fluid density increase of 0.3 percent, and a viscosity decrease of 39 percent at a pressure of 4,000 psia.

The physical properties and the compositional analysis of the bottom hole samples and the recombined reservoir fluid are given in Tables 2 and 3. The experimental PVT data from a differential liberation study performed on the subsurface samples are shown graphically in Figures 8 and 9 as discrete points. The experimental data for

---

*All symbols are described in the Nomenclature Section.

the various CO_2-oil mixtures from the CO_2 swelling tests are presented in Figures 10-14 as discrete points.

The Peng-Robinson equation of state[14-16] has been incorporated into Gulf's Compositional Simulator to predict reservoir fluid properties and phase behavior. A modified Peng-Robinson phase package computer program[17] was used to match the laboratory measured data from the differential liberation study and the CO_2 swelling tests. The parameters for the Peng-Robinson equation of state are given in Tables 4 and 5. The fluid composition was grouped into a total of seven pseudo components: CO_2, H_2S, C_1 and N_2, C_2, C_4*, C_{10}*, and C_{14}*. Nitrogen was included in methane. Propane, butanes, and pentanes were combined as C_4*. Hexane and heptanes plus were lumped together and then divided into two components, C_{10}* and C_{14}*, according to Reference 16. The calculated values using the Peng-Robinson equation of state are shown in Figures 8-14 as smoothed lines. The phase viscosities were evaluated by the Thodos correlation[18]. Excellent agreement between the laboratory and calculated values was obtained. The deviation between the measured and the calculated stock tank oil density is about 5%. This causes a deviation between the measured and calculated differential formation volume factor (B_o) of 4% at saturation pressure. The average absolute deviation between the measured and calculated oil viscosity for 50:50 CO_2-oil mixture (near the critical region) is about 10%.

2. Minimum Miscibility Pressure Determination[3,19]

Several experimental runs[4] were performed at GR&DC to evaluate the carbon dioxide miscible flood process for the Little Knife Field. The purpose of these experiments was to determine the minimum miscibility pressure of CO_2 with reservoir oil at reservoir temperature. The experiments involved displacement of reservoir oil by CO_2 at reservoir temperature and various pressures through a slim tube packed with sands. The experimental equipment and procedure are described in Reference 19. The length of the slim tube used in the experiments was 95 feet. A total of 1.6 PV (pore volume) of CO_2 was injected into the slim tube continuously at 240°F. Figure 15 shows the oil recoveries at the CO_2 breakthrough as a function of the average system pressure at 240°F. From Figure 15 the minimum miscibility pressure (MMP) for the CO_2 displacement was estimated to be 3400 psig. The percentage of oil recovery versus CO_2 injected is shown in Figure 16 for the 3400 psig average system pressure.

A one-dimensional compositional simulation study[6] was performed to match the slim tube test performance. The linear system was divided into segments of equal length. Three different grids (5, 25, and 50 mesh blocks) were used to study the effect of grid size. The calculated oil recovery history for the 3400 psig average system pressure run is shown in Figure 16. The calculated breakthrough and ultimate recoveries for different average system pressure are shown in Figure 15. The match between the calculated and the experimental results is in good agreement, indicating the capability of the composi-

tional simulator to match the CO_2 displacement process accurately. The Peng-Robinson equation of state with the parameters listed in Tables 4 and 5 was used to calculate the hydrocarbon phase densities and K-values.

Equilibrium K-value tables (Tables 6-15) generated by the Peng-Robinson equation of state were used in this 1-D simulation study. These K-values were tabulated as functions of pressure and CO_2 composition in the hydrocarbon mixture. In evaluating the K-value data in Tables 6-15, different amounts of CO_2 were mixed (computationally) with one mole of reservoir oil and subsequently the mixture composition was normalized. The normalized CO_2-reservoir oil mixture composition was used in calculating the K-values as a function of pressure given in Tables 6-15 at reservoir temperature. The generated K-values are also plotted in Figures 17-19. The K-values were extrapolated to the convergence pressure[20] beyond the saturation pressure of a given mixture. The K-values for all the pseudo components are set equal to 1 when the system pressure is greater than the convergence pressure for that particular mixture.

3. Residual Oil Saturation Tests

The existing slim tube apparatus was modified to mount reservoir core plugs at the outlet of the slim tube. Three CO_2 residual oil saturation tests were completed at Harmarville in core plugs from the Zabolotny Injection Well No. 1. The plugs were taken from a one-foot interval at 9,823-9,824 feet (core depth) for the first test, at 9,826-9,827 feet for the second test, and at 9,814-9,815 feet for the third.

The plugs were restored to connate water saturation, waterflooded, and flooded with a CO_2-oil miscible bank developed in a slim tube at 245°F* and 3500 psia.

The summary of the results is given in Table 16. A material balance on the slim tube tests confirmed that multiple contact miscibility was developed at test conditions in each test. The very low residual oil saturations (0.8-3.1% PV) observed for the various water/CO_2 ratios were very satisfactory. However, results indicated that about 35% of the carbon dioxide was remaining in the reservoir rock.

4. Core Analysis

Conventional cores were analyzed from Injection Well No. 1, and Observation Wells No. 1, 2, and 3. Observation Well No. 4 was pressure-cored. The minitest project interval was subdivided into four layers (W, X, Y, and Z) for the simulation study. These intervals were selected based upon the porosity and permeability characteristics. The results of the core and GULFLOG analyses are displayed in tabular form in Table 17, and in graphical form in Figure 5. The properties analyzed include the log depth, thickness, porosity from cores and GULFLOGS, horizontal and vertical permeabilties from core analyses, and initial oil saturation and waterflood residual saturation from GULFLOG analyses.

5. Relative Permeability Measurements

Steady state water-oil relative permeability tests have been performed at room temperature and pressure in seven restored core

*Recent measurements indicated that the reservoir temperature is equal to 240°F.

samples from the minitest wells. Out of the seven core samples, four were taken from Layer Y and one each from Layers W, X, and Z. The results are shown in Figures 20-23.

Water-oil relative permeability measurements (no CO_2 present) in preserved cores (Layer Z) from Zabolotny Observation Well No. 3 were also obtained at reservoir conditions in an effort to determine preferential wetting at those conditions and for comparison with restored-state measurements. Results are shown in Figure 23.

CO_2-water relative permeabilities at reservoir conditions in Zabolotny Injection Well No. 1 core plugs were measured. A detailed comparison of the relative permeability with and without residual oil saturation is shown in Figure 24. The lower CO_2-water relative permeability ratio at high water saturation suggests CO_2 wetting in the presence of residual oil.

C. Field Work

1. Area of Interest

The minitest site is located in the central portion of the field, northwest of the section center, Section 3, T144N, R98W, Billings County, North Dakota (Figure 3). The minitest center is 1,800 feet from the northline and 2,460 feet from the westline of Section 3. Geological considerations for the selection of this location are based on: 1) average reservoir facies, 2) continuity of porosity, permeability, and lithology, and 3) elevated structural position.

The test pattern consisted of a single injection well offset by three observation wells arranged in an inverted four-spot configuration.

The pilot area enclosed by the minitest wells is approximately 5 acres. A 640-acre area immediately surrounding the minitest was modeled. Only three producing wells which were completed in the project interval in this area were considered to significantly influence the pilot. These three producing wells, Zabolotny 4-3-1A, Zabolotny 1-3-4A, and Zabolotny 2-3-3A, were included in the simulation model (Figure 1). The average thickness, porosity, and initial oil saturation for each layer based on core and log analysis (Table 17) are given in Table 18. The total pore volume and hydrocarbon pore volume have been calculated and are shown in Table 18.

2. Production and Pressure History

The average reservoir pressure in the minitest area was about 3350 psia when the minitest was started on December 11, 1980. Only three Zabolotny production wells 4-3-1A, 1-3-4A and 2-3-3A were assumed to have significant effects on the minitest area due to continued production. Figure 25 shows the pressure history for these three production wells.

These three wells had commingled production from Zones B, C and D. The oil production rates had to be allocated according to perforations and the well capacity (Kh) factors. Table 19 shows the perforations and the rate allocation used in the simulation. It was estimated that the average oil production rates from the project interval during the minitest period (12/11/80 - 9/24/81) for Zabolotny Wells 4-3-1A, 1-3-4A, and 2-3-3A were 31 BOPD, 237 BOPD, and 144 BOPD, respectively.

3. Drilling and Completion of Minitest Wells

Zabolotny Injection Well No. 1 was spudded on December 5, 1979, followed by Zabolotny Observation Well No. 1 on January 12, 1980, Zabolotny Observation Well No. 2 on May 15, 1980, and Zabolotny Observation Well No. 3 on July 5, 1980. A continuous directional survey was run in the injection well to locate the bottom of the hole. The gyroscopic multi-shot survey was run in the injection well to TD to compare with the continuous directional survey. Agreement between the two readings was excellent. The multi-shot survey was used in the observation wells because it was judged to be more accurate. The surface and bottom-hole locations for the injection well and three observation wells are shown in Figure 26.

The casing and tubing settings in the Injection Well No. 1 and Observation Well No. 1 are shown in Figures 27 and 28. There are only minor differences between the completions of the injection and observation wells. All observation wells are equipped with two PTS concentric pressure chambers. Gas lift mandrels with wireline retrievable gas lift valves were also employed in the observation wells.

4. Logging

The open-hole logging suite was run in Injection Well No. 1 and three observation wells and consisted of the following:

(1) Dual Laterolog - Micro - SFL with Gamma Ray and Caliper (DLL/MSFL).

(2) Compensated Neutron - Formation Density with Gamma Ray and Caliper (CNL/FDC).

(3) Borehole Compensated Sonic with Gamma Ray and Caliper (BHC).

(4)* Wave Forms - Variable Density (Wave Forms/VDL).

(5)* Fracture Identification Log with Gamma Ray (FIL).

(6) Gyroscopic Multi-Shot Survey.

The open-hole log calculations for porosity and initial oil saturation across the perforated intervals are given in Table 17.

Temperature surveys were run in the Injection Well No. 1. These surveys indicated that the injected fluid was confined to the project interval, with the majority entering approximately into the center 10 feet. This injection profile was in good agreement with the forecast from the open-hole logs which showed that portion of the project interval to be most porous. The results of communication analysis indicated that some fluid communication occurred during injection to the interval 9,806-9,824 feet, located directly above the perforations. Fluids, however, were confined within the interval 9,809-9,839 feet (31 feet), the basal portion of Zone C and top portion of Zone D, with no migration through the bottom or top of this interval.

TDT (Thermal Decay Time) logs[21] were run for monitoring changes in oil, water and CO_2 saturations with time in the observation wells.

A log-inject-log was performed on the injection well. Data from this test were compared with that obtained from the flushed zone oil saturation calculations using the micro-spherically focussed log. This comparison was then used for correlating the residual oil saturations for

*Not run in Observation Wells No. 2 and 3.

the three observation wells. The open-hole flushed zone saturations across the perforated intervals are given in Table 17.

5. Well Testing

As part of a reservoir and formation characterization program, a pulse test[22] was conducted in April and May, 1980. The injection well and Observation Well No. 1 were used in this test. By injecting filtered salt water into the injection well at a rate of 1,964 BWPD for two hours, a pulse was created in the reservoir that was monitored in Observation Well No. 1. The initial response from this pulse arrived at Observation Well No. 1 in 30 minutes and peaked in 175.8 minutes, with a maximum amplitude of 17.60 psi.

A multi-well pulse test[11] involving all four Little Knife CO_2 minitest wells was conducted on November 15, 1980. The test was conducted by pumping filtered salt water at an average injection rate of 2,297.5 BWPD into the injection well for two hours while the response to this "pulse" was monitored downhole in the three observation wells. The objective for this pulse test was to determine if a preferential direction to flow exists through the project interval in the minitest area.

The maximum response from the pulse arrived at Observation Well No. 1 (258 feet away) in 175.0 minutes with a maximum amplitude of 21.18 psia (Figure 29). The maximum response from the pulse arrived at Observation Well No. 2 (the nearest well 250 feet away) in 175.98 minutes, with a maximum amplitude of 15.835 psia (Figure 30). The maximum response from the pulse arrived at Observation Well No.

3 (the farthest well 283 feet away) in 217.5 minutes, with a maximum amplitude of 16.01 psi (Figure 31). The results provided by the analysis of the responses are given in Table 20.

The following conclusions have been derived from the multi-well pulse test:

1. All three observation wells are in good fluid communication with the injection well.
2. There are no continuous high permeability channels or fractures connecting the injection well witn any of the three observation wells.
3. There was no evidence of a free gas saturation within the confines of the four-well minitest pattern.
4. In situ effective permeabilities representing the average value between the injection well and each of the observation wells were quite similar, the maximum being 29 md and the minimum being 23 md.
5. Effective hydraulic thicknesses contacted by the pulse wave between the wells varied from 25 to 36 feet.
6. The in situ effective storage values between the injection well and the three observation wells varied from a low of 34,000 res. bbl/acre (injection well to Observation Well No. 1) to a high of 48,000 res. bbl/acre (injection well to Observation Well No. 2).

6. Water/CO_2 Injection Sequence

The water injection simulation[23] of the Little Knife CO_2 minitest has been studied to determine the volume and rate of water pre-

injection into the minitest injection well so that the pressure in the minitest area could be raised above the minimum miscibility pressure of 3400 psig. A two-dimensional, cross-sectional, compositional simulation study[24] was also performed to develop the water - CO_2 (WAG) ratio of the test. The optimum water/CO_2 injection sequence was then developed based on these two simulation studies.

The preinjection of 29,539 bbls of water (approximately 28% of Zone D hydrocarbon pore volume) started on December 11, 1980. This was then followed by 2,095 tons of CO_2 (approximately 22% of Zone D hydrocarbon pore volume) in five approximately equal slugs alternated with equal volumes of water (reservoir conditions) from January 6, 1981 through March 25, 1981. A total of 20,621 bbls of water was injected during the WAG sequence. The average water injection rate was 1,150 B/D and the average CO_2 injection rate was 40 tons/day. A total of 198,794 barrels of drive water was injected from March 25, 1981 through September 24, 1981. The actual field injection schedule and volumetric injection data were given in Tables 21 and 22 in detail. The preinjection water contained 500 ppm of isopropanol (IPA) as a water tracer. The WAG water contained 500 ppm of n-propanol (NPA). The injected CO_2 had a carbon isotope ($^{13}C/^{12}C$) value near -49o/oo, which is sufficiently different from the value of -2o/oo for the solution CO_2 to make any injected CO_2 influxing into a well easily detectable.

7. Performance Data Acquisition

As the miscible front radiated away from the injector, a series of cased-hole logs were run in each of the observation wells to monitor its

progress. This time-lapse technique[21] uses a pulsed-neutron log to detect the changes in fluid saturation around the wellbore. The tool responds directly to the changes in water saturation as measured by the thermal neutron decay rate. Any increase in CO_2 saturation between subsequent logging runs is noted as a decrease in the apparent porosity. The end result is a saturation history of the CO_2-swept region around each well.

The schedule for data acquisition during the minitest was as follows:

1. Monitor injection pressure and injection rate continuously.
2. Record bottom-hole pressure in each well continuously.
3. Sample fluid from observation wells periodically to check for tracers (IPA, NPA, and CO_2 isotope) and fluid composition.
4. Sample fluid from offset producing wells once a month.
5. Run pulsed-neutron logs in each observation well until response is noted, then increase frequency as required.
6. Run pulsed-neutron log in the injection well before injection, after water injection, and after CO_2 injection.
7. Run log-inject-log in all the observation wells to evaluate the final fluid saturations at the end of the minitest.
8. Drill the fifth well behind the CO_2 front and core with a pressure-retaining core barrel to confirm the residual oil saturation to the CO_2 flood.

D. Compositional Simulation of the Minitest

1. Compositional Simulator

Gulf's compositional simulator[6] was used in this study. The simulator calculates the distribution of all the individual components of the hydrocarbon system through space and time and also the distribution of these components in the gas and liquid phases. The simulator considers convective miscible transport of each component through the two hydrocarbon phases. The interphase mass transfer of each component between the oil and gas phases is governed by the equilibrium coefficients (K-values) under the assumption of thermodynamic equilibrium. The effects of gravity and capillary forces are included in the three-phase flow equations which are governed by a generalized form of Darcy's Law.

The hydrocarbon phase properties are computed as functions of pressure, temperature, and composition using the Peng-Robinson equation of state. A two-dimensional K-value as a function of pressure and CO_2 concentration was read in as input data and was generated externally by the Peng-Robinson equation of state.

The simulator employs the IMPES[25] (Implicit Pressure Explicit Saturation) type numerical procedure that results in an implicit pressure equation and three explicit saturation equations. The set of simultaneous pressure equations is solved by a direct method that uses an alternating diagonal ordering scheme. The saturation equations are solved explicitly.

2. Grid Description

The coordinate system used for this study is illustrated in Figure 32. The x-direction is chosen along the line connecting Zabolotny Injection Well No. 1 and Zabolotny Observation Well No. 1. This direction is along the average fracture strike direction (Figure 7). The relative well locations for the production and minitest wells are given in Table 23.

A quadrant of the minitest area (Figure 32) was divided into an 11x11 areal grid as shown in Figure 33. Three separate geological models were proposed for each observation-injection well pair (Figure 33). The early simulation runs were made with only two layers in the vertical direction. The purpose of these runs were to match the observed bottom-hole pressures at the injection well and three observation wells. The water and the CO_2 breakthrough times at the observation wells were also matched. Once the fluid breakthroughs occurred at the observation wells, it became necessary to use a four-layer model to match the fluid saturation distributions. An 11x11x6 grid system was used for a sensitivity study for the Injection-Observation No. 2 well pair.

Final simulation was run with a 16x15x4 (Figure 34) grid system to simulate the entire minitest area. This grid system included the injection well, four observation wells and three production wells as shown in Figure 34.

3. Input Data

In the preliminary simulation study using the grid systems of 11x11x2 and 11x11x4, a separate geological model was prepared for each observation-injection well pair (quadrants I, II, and III in Figure 32). Table 24 shows porosity, permeability, initial oil saturation, waterflood residual oil saturation, and thickness for each layer and each observation-injection well pair.

Final simulation runs were made using a 16x15x4 grid system. Average geological properties were assigned to each layer. The porosity, S_{oi}, S_{orw}, and the thicknesses for Layers X, Y, and Z were based on detailed information available from the logs and core analyses (Table 17). However, the thickness of Layer W, and the horizontal and vertical permeabilities were varied by matching the four-well pulse test responses at the three observation wells. The comparisons between the observed and model predicted values for the four-well pulse tests are shown in Figures 29-31. During the matching process, it was necessary to increase the thickness of Layer W. The calculated permeabilities were almost 2.5 times that of the measured values from the core analysis. These higher average permeabilities were interpreted to be the results of the effect of short non-continuous fractures dispersed somewhat uniformly across the minitest area. The permeability-porosity correlation and the core measured permeabilities are shown in Figure 35. The permeability-porosity correlation modified as a result of pulse test matching was used in the study. The vertical permeabilities between layers were found to be small compared with the

horizontal permeabilities. The x-direction (northeast-southwest) permeabilities were increased by a factor of 1.25 over the y-direction (northwest-southeast) values. This alteration was made to satisfy the fracture orientation study on the core from the injection well.

The drainage capillary pressure data were available on 12 core samples from Zabolotny Observation No. 1 Well. These data were averaged for each layer. The imbibition capillary pressure data were then deduced from the drainage capillary pressure data, connate water saturation, and waterflood residual oil saturation. The derived imbibition capillary pressure curves are shown in Figure 36. The water-oil relative permeability curves versus water saturation for each layer are presented in Figures 20-23. These relative permeability curves are based on the laboratory measured values. The end points in the curves are adjusted based upon the field observed initial oil saturations and waterflood residual oil saturations. Further adjustments were made to match water saturation profiles observed at the three observation wells. Gas-oil (drainage) relative permeability data for nitrogen and mineral oil system measured on a restored core from Zabolotny Observation No. 3 Well were used to estimate CO_2-oil (imbibition) relative permeability curves. The residual gas saturation (imbibition curve) to the waterflood was estimated to be 15%. Three phase oil relative permeability was calculated using Stone's correlation[26].

The hydrocarbon phase densities were calculated using the Peng-Robinson equation of state with the parameters listed in Tables 4 and 5. The hydrocarbon phase viscosities were calculated using Thodos corre-

lation. The equilibrium K-value tables (Tables 6-15) generated by the Peng-Robinson equation of state were used to evaluate the phase behavior of CO_2-oil mixtures under the reservoir conditions. Additional model input parameters associated with water properties and rock compressibility are presented in Tables 1 and 2.

4. Field Performance Match

a. Bottom-hole Pressure

The pressure performance matches are shown in Figures 37-40. Excellent matches are obtained between the observed and computed (model) pressures in the observation wells (Figures 38-40). No significant differences in the calculated bottom-hole pressures have been observed among the three grid systems (11x11x2, 11x11x4, 16x15x4). Field data show that the bottom-hole pressures at the injection well increased to 4800 psia during the water preinjection phase. Then bottom-hole pressures decreased to 4000 psia during CO_2 injection and 3700 psia during shut-in. A skin factor of 12 was required to match field data in the preflush phase. The maximum deviation between the observed and computed bottom-hole pressure at the injection well is about 300 psia during shut-in or CO_2 injection period. In the drive water injection phase, the bottom-hole pressure was about 4600 psia. The skin factor was reduced from 12 to 8 during the drive water injection phase. This may have been due to the leaching effect on limestone during CO_2 injection.

Excellent match between the observed and model predicted pressures at Zabolotny Observation Well No. 1 (Figure 38) was obtained

throughout the entire history. The predicted bottom-hole pressures were approximately 50 psia lower than the observed values before May 20, 1981 at Observation Wells No. 2 and 3. The maximum deviation between the observed and computed pressure was only 75 psia at Observation Wells No. 2 and 3.

b. Water Saturation

The water saturation history matches at the observation wells during the course of the minitest are shown in Figures 41-46. The comparison between the simulation results and field observed data shows good agreement. The model predicted water saturation profiles for each layer are compared with the field logging data[21] in Figures 41-43. The solid lines represent the simulation results using a 16x15x4 grid system. The discrete points represent the observed data based on pulsed-neutron logs. The initial and final water saturations calculated from pulsed neutron logs at Observation Well No. 1 are lower than the corresponding calculated values for Observation Well Nos. 2 and No. 3. The simulation results are based on the average values for all three observation wells (Table 24). The field observed water saturations for Layer Y at Observation Well No. 1 on May 18 and June 2, 1981 were too low. In matching these data, the permeability-porosity correlation was adjusted slightly and the vertical permeabilities between layers were reduced substantially.

The water saturation history matches for Zone D (Layer XYZ) at three observation wells are shown in Figures 44-46. The discrete points represent the field observed values based on TDT logs. The solid lines

represent the simulation results using a 16x15x4 grid system. The water breakthrough times are in excellent agreement with the logging data. Based on the water tracer analysis (Table 25), the water breakthrough at Observation Well No. 1 occurred before March 4, 1981, and the water breakthrough at Observation Well No. 2 and Well No. 3 occurred on or before March 27, 1981 and May 8, 1981, respectively. These data are consistent with data from pulsed-neutron logs.

c. Carbon Dioxide Saturation

Most of the injected CO_2 dissolved in the reservoir fluids and traveled to the observation wells. Part of the injected CO_2 was trapped in the CO_2-swept zone in the vicinity of the injection well. The solubility of CO_2 in the water phase was not considered in the model because of the model limitation. We estimate that 60 SCF of CO_2 would dissolve in one barrel of water under the reservoir conditions.[27]

Figures 47-49 show the CO_2 content with time at the observation wells from separator gas analysis (Table 27-29), CO_2 isotope analysis (Table 30), and logging data. Figure 47 shows CO_2 breakthrough on or about March 12, 1981 at Observation Well No. 1 from isotope analysis, separator gas analysis and logging data. Figure 48 shows CO_2 breakthrough on or about May 6, 1981 at Observation Well No. 2 from separator gas analysis, CO_2 isotope analysis, and logging data. From Figure 49, both logging data and CO_2 isotope analysis indicated that CO_2 breakthrough did occur on or about May 6, 1981. However, there was no indication of CO_2 breakthrough until July 15, 1981 at Observa-

tion Well No. 3 from separator gas analysis. The CO_2 isotope analysis is a more reliable method than the separator gas analysis because nitrogen contamination from the lift gas has little effect on the results.

A triangulation technique[21] was used to interpret TDT logging data. This technique evaluates water, CO_2-free oil, and CO_2 saturations. These saturation values were computed at various points in time and compared with the model calculated values.

Figure 50 shows the swelling factor of oil-CO_2 mixtures versus CO_2 concentration at 245°F for the Little Knife crude oil. These data were used in computing the simulator oil saturation on a CO_2-free basis.

The CO_2 saturation history matches for Layers X, Y, Z, and Zone D at the Observation wells during the course of the minitest are shown in Figures 51-53. The comparisons between the simulation results and field observed data show good agreement. The solid lines represent the simulation results using a 16x15x4 grid system. The discrete points represent the observed data based on pulsed-neutron logs. It is noted that no appreciable amount of CO_2 has been detected in Layer Z at any observation wells. However, some CO_2 did migrate to Layer X at Observation Wells No. 1 and No. 3 (and not at Observation Well No. 2). This indicates that some gravitational segregation may have occurred in the reservoir.

d. Oil Saturation

The oil saturation history matches at the observation wells during the course of the minitest are shown in Figures 54-59. The discrete

points represent the field observed values based on TDT logs. The continuous lines represent the simulation results using a 16x15x4 grid system. The model predicted oil saturation profiles for each layer are compared with the field logging data in Figures 54-56. The comparisons between the simulation results and the logging data for oil saturations in Zone D (Layer XYZ) at three observation wells are shown in Figures 57-59. As seen from these figures, satisfactory history matches have been achieved for the three observation wells.

e. Zabolotny Observation Well No. 4

The comparisons of model predicted oil saturation at Observation Well No. 4 with that obtained from pressure-core analysis and GULFLOG analysis are shown in Figures 60-61. The grid location of Observation Well No. 4 in the grid system of 16x15x4 is (5,10). The well was spudded on May 5, 1981. GULFLOG was run on July 15, 1981 and pressured-cores were taken from the project interval on July 17, 1981.

In Figures 60 and 61 the solid lines represent the observed (logging or pressure-core) data and the dashed lines represent the simulation results using a 16x15x4 grid system. The oil saturation profiles obtained from GULFLOG analysis are the CO_2-free oil saturations at reservoir conditions, while those obtained from pressure-core analysis are measured at stock tank conditions. The model predicted oil saturations are in satisfactory agreement with the observed values from both GULFLOG and pressure-core analysis for Layer Y. However, the model predicted oil saturations are somewhat low for Layer X and high

for Layer Z compared with the GULFLOG oil saturations. (These are consistent with the phenomena observed at Observation Well No. 2.)

The results indicated above imply that the actual vertical permeability between Layers X and Y should be lower than 3 md in the quadrant II of the minitest area (Figure 32).

5. Volumetric Displacement

Figures 62-64 show the model predicted fluid saturations for Layer Y at the end of CO_2 injection (March 25, 1981). Figures 65-67 show the model predicted fluid saturations for Layer Y on July 17, 1981. Figure 68 shows the calculated CO_2-free oil saturations on July 17, 1981. The radius of CO_2-swept zone (zero or very low value of residual oil saturation) in the minitest area is estimated to be 110 feet.

Simulation results show that the percentage of oil-in-place (on December 11, 1980) displaced for the straight waterflood in the minitest area is 37% (on a STB basis) from the entire project interval. The percentage of oil-in-place (on December 11, 1980) displaced for the CO_2 flood with 1 to 1 WAG ratio in the minitest area is 50% (on a STB basis) from the entire project interval. The simulation results are given in Table 31.

Simulation results show that incremental oil can be displaced for Layers X and Y using the CO_2 miscible process in the minitest area. Only 1% of additional oil can be displaced for Layer W by the CO_2 flood process over the straight waterflood. This low incremental oil displacement for Layer W is due to the low vertical transmissibility between Layers W and X. Only 0.5% of additional oil can be displaced for Layer

Z by the CO_2 flood over the straight waterflood. This low incremental oil displaced for Layer Z is due to the gravitational effect and the low vertical transmissibility between Layers Y and Z.

Figure 69 shows the amount of oil recovered (on a STB basis) as a percent of oil-in-place at the beginning of the minitest (December 11, 1980) for the CO_2 WAG process and the straight waterflood by simulating production at all three observation wells. (The fluid production in the three observation wells was maintained such that the average reservoir pressure in the minitest area was identical to the observed pressure history in the actual minitest operation.) Figure 69 shows that the waterflood and CO_2 flood recoveries are equal to 34 and 45% of oil-in-place, respectively.

Please note that the minitest was started on December 11, 1980 at an average pressure of 3350 psia; whereas, the average original reservoir pressure in the minitest area was about 4400 psia. Based upon the natural depletion from this pressure to 3350 psia, about 6% of OOIP is recovered from the reservoir. This estimate was based upon an independent simulation study of the natural depletion case.

Thus, if we base the oil recovery upon the OOIP the following recoveries are obtained:

$$\text{Waterflood} = 6\% + 0.94 \times 34\% = 38.0\%$$

$$CO_2 \text{ flood} = 6\% + 0.94 \times 45\% = 48.3\%$$

(where, natural depletion recovery = 6%, remaining OIP on 12/11/81 = 94% of OOIP, waterflood recovery = 34%, and CO_2 flood recovery = 45%).

6. Sensitivity Study (The Six-Layer Model)

An areal grid system was prepared to represent one quadrant of the minitest area including Observation Wells No. 2 and 4. This grid system is identical to the one used before except it has six rather than four layers. Layer Y has been divided into three layers Y1, Y2, and Y3. The input data for the reservoir rock properties are given in Table 32.

The results of this simulation run indicate (see Figures 70-74) that the computed CO_2 saturations are slightly less in the middle-Y zone than the observed logging data, and slightly more in the upper-Y zone than the observed logging data. However, the composite match between the observed and computed CO_2 saturations for Layer Y was essentially the same for the six and four layer models.

Figures 75 and 76 show comparisons of model predicted CO_2-free oil saturations with the saturations obtained from the logging and pressure-core data for Observation Well No. 4.

E. Commercial Scale Application

We also extended the reservoir model characterized in the minitest area to a field-wide application of the CO_2 miscible process on 160-acre spacing. We prepared a 10x10x4 rectangular grid to represent one quadrant of a five spot pattern. This grid system included only one injection well and one production well. The top layer W was not perforated in the production or the injection well.

The initial pressure distribution was determined on the basis of an initial reservoir pressure of 4,390 psi at a datum plane of 7,200 feet subsea. We calculated the original oil-in-place (OOIP) at the beginning of the

production (1-1-78) to be 2,928 MSTB for a unit well in the 160-acre five spot pattern. We assigned the average oil production from wells Zabolotny No. 1-3-4A, 2-3-3A, and 4-3-1A to the production well in the model. The current operation of natural depletion was continued until the average reservoir pressure declines to 2,500 psi as of 1-1-83. Next, water was injected at the rate of 1,200 B/D from 1-1-83 to 3-1-84 to raise the average reservoir pressure to 3,500 psi. A straight waterflood or a 1:1 CO_2 WAG process was then implemented at a constant reservoir pressure of 3,500 psi by balancing fluid withdrawal. For the 1:1 CO_2 WAG process, alternate slugs of 5 percent HCPV (based on Zone D) of CO_2 and water were injected. A constant pressure waterflood continued after a total of 25 percent HCPV CO_2 was injected in five slugs.

Simulation results show that 40% and 48% of OOIP can be recovered for the straight waterflood and 1:1 CO_2 WAG process, respectively. This gives 8% incremental oil recovery by the CO_2 WAG process over the straight waterflood. The CO_2 requirement for each incremental STB oil production is estimated to be 5 MSCF/STB. This CO_2 requirement is corrected by a factor of 1.1 to account for the CO_2 solubility in water phase. It is noted that the CO_2 WAG process was initiated early in the life of the reservoir as a secondary project for this study. The CO_2 requirement would be higher if the CO_2 WAG process was implemented as a tertiary mode. Also, the CO_2 requirement would tend to be higher if the complex reservoir heterogenities present in the Little Knife reservoir were considered in the model. The CO_2 requirement calculated in this report is optimistic because no trapping or water-blocking of oil for CO_2 flooding has been considered in this simulation. This type of information is difficult to estimate and any non-zero value of

trapped oil saturation will increase the CO_2 requirement for each incremental STB oil production. The amount of trapped oil saturation will be higher for a tertiary recovery case than for a secondary recovery case (using CO_2). This in turn, will further increase the CO_2 requirement for tertiary recovery case for the project.

Chen-jing Lin
C. J. Lin

Y. R. Patel

Ellen Broussard
E. S. Broussard

APPROVED:

Ganesh C. Thakur
G. C. Thakur, Director-Enhanced Recovery Operations

July 8, 1982
Date

William R. Cook
William R. Cook, Manager-Production Services

July 13, 1982
Date

IV. ACKNOWLEDGEMENTS

Dr. N. M. Chaudhari and Dr. S. T. Lee of Gulf Research and Development Company at Harmarville deserve a special acknowledgement for their excellent cooperation and exhaustive effort in developing and improving Gulf's Compositional Simulator. The assistance of Mrs. Anne Johnson and Mrs. C. C. Fu in preparing tables and figures for this report is highly appreciated.

A special acknowledgement and sincere gratitude are given to Dr. G. C. Thakur for his constant guidance, invaluable discussions and suggestions throughout the course of this study.

V. NOMENCLATURE

Symbol	Definition	Units
BHP	Bottom-hole Pressure	psia
c	Compressibility	psi^{-1}
FVF (or B_o)	Formation Volume Factor	RBBL/STB
GOR	Gas-Oil Ratio	SCF/STB
k_h	Horizontal Permeability	md
kh	Permeability-Thickness Product	md-ft
k_{rg}	Gas Relative Permeability	
k_{rog}	Oil Relative Permeability for the Gas-Oil System at Irreducible Water Saturation	
k_{row}	Oil Relative Permeability to the Waterflood	
k_{rw}	Water Relative Permeability	
k_v	Vertical Permeability	md
OOIP	Original Oil-in-Place	STB
P_s	Saturation Pressure	psia
P_B	Bubble Point Pressure	psia
P_D	Dew Point Pressure	psia
S_{oi}	Initial Oil Saturation	fraction
S_{orw}	Waterflood Residual Saturation	fraction
Φ	Porosity	fraction
μ	Viscosity	c.p.

VI. REFERENCES

1. Holm, L. W., "Status of CO_2 and Hydrocarbon Miscible Oil Recovery Methods", Journal of Petroleum Technology, 76, January, 1976.

2. Stalkup, F. I., "Carbon Dioxide Miscible Flooding: Past, Present, and Outlook for the Future", Journal of Petroleum Technology, 1102, August, 1978.

3. Holm, L. W. and Josendal, V. A., "Mechanisms of Oil Displacement by Carbon Dioxide", Journal of Petroleum Technology, 1427, December, 1974.

4. Huang, Edward T. S., "Miscibility Studies with Little Knife Oil" GR&DC Production Research Department Technical Memorandum No. 441TJ300, January 18, 1978.

5. Ramesh, A. B., "Compositional Reservoir Simulator Users' Manual", GR&DC Production Research Department Report No. 441, February, 1976.

6. Chaudhari, N. M., "Compositional Simulator User's Manual", GR&DC Production Research Department Report No. 441RM192, June 1, 1981.

7. Cairns, R., "Little Knife - New Field in the Williston Basin", the Orange Disc, Vol. 23, No. 1, p. 2 (Sept.-Oct., 1977).

8. The Oil and Gas Journal: "DOE Backs First Coal Gasification Plant", June 12, 1978.

9. Kane, A. V., "Performance Review of a Large-Scale CO_2-WAG Enhanced Recovery Project, SACROC Unit Kelly-Snyder Field", Journal of Petroleum Technology, 217-231, February, 1979.

10. Core Laboratories, Inc., "Special Core Analysis for Gulf Oil Exploration and Production Company, Zabolotny Minitest Wells, Billings County, North Dakota," CLI File Numbers 3402-9939, 3402-10015, 3402-10180, 3402-10275, P81005, April 7, 1981 through September 17, 1981.

11. Hickey, M. C., Hurd, T. A., Kingelin, G. F. and Lawson, W. K., "Reservoir and Formation Characterization - Little Knife CO_2 Minitest Project," Gulf Science and Technology Technical Memorandum No. 445TM093, March, 1981.

12. DeVaney, W. E., "Phase Relations Study for Zabolotny 1-3-4A Well, Little Knife Field, Billings County, North Dakota", GR&DC Production Services Department, Technical Memorandum No. 445TK065, December, 1979.

13. DeVaney, W. E., "CO_2 Swelling Test for Zabolotny 1-3-4A Well, Little Knife Field, Billings County, North Dakota", GR&DC Production Services Department, Technical Memorandum No.445TL074, April, 1980

14. Peng, D. Y. and Robinson, D. B., "A New Two-Constant Equation of State," I&EC Fund., 15 (1976), 59.

15. Robinson, D. B., and Peng, D. Y., "The Characterization of the Heptanes and Heavier Fractions," Research Report 28, GPA, Tulsa, Okla., 1978.

16. Lee, S. T., "Application of the Peng-Robinson Equation of State to Determine Reservoir Fluid Properties and Predict Equilibrium Phase Behavior," GR&DC Production Research Department Report No. 441RL186, January 30, 1980.

17. Lin, C. J., "Phase Behavior Package Computer Program Using the Peng-Robinson Equation of State," Private Communication.

18. Jossi, J. A., Stiel, L. I., Thodos, G., "The Viscosity of Pure Substances in the Dense Gaseous and Liquid Phases", A.I.Ch.E.J. (1962), Vol. 8, p. 59.

19. Huang, E. T. S. and Tracht, J. H., "The Displacement of North Ward-Estes Reservoir Oil by CO_2 from Watered-Out Linear Cores," GR&DC Production Division Report No. 441RE141, September 12, 1974.

20. NGPSA Engineering Data Book, Ninth Edition, Tulsa, Oklahoma, 1972.

21. Svor, T. R., "Little Knife CO_2 Miniflood Project Report", Production Services Department, January, 1982.

22. Kingelin, G. F., Cleland, R. B., and Barrett, D. L., "Little Knife CO_2 Minitest Project, Multiwell Pulse Test Report," Gulf Science and Technololgy Technical Memorandum No. 444TL207, May, 1980.

23. Rasor, R. W., Haulenbeek, R. B., Auvenshine, R. A., and Thakur, G. C., "Little Knife Field CO_2 Minitest Water Injection Simulation", GR&DC Production Services Department Report No. 445RL029, July, 1980.

24. Thakur, G. C. et al, "Design of a CO_2-Water Injection Program for Little Knife CO_2 Flood Minitest", GR&DC Production Services Department, Technical Memorandum No. 441TL343, SM01, September 9, 1981.

25. Kazemi, H., Vestal, C. R., and Shank, G. D., "An efficient Multi-component Numerical Simulator", Soc. of Pet. Eng. Jour. (October 1978), Vol. 12, No. 5, pp. 355-368.

26. Stone, H. L., "Estimation of Three-Phase Relative Permeability and Residual Oil Data", Jour. of Canadian Petr. Tech. (October-December, 1973), pp. 53-61.

27. Crawford, H. R., Neill, G. H., Lucy, B. J. and Crawford, P. B., "Carbon Dioxide - A Multipurpose Additive for Effective Well Stimulation", Jour. of Pet. Tech., 237, March, 1963.

TABLE 1

Basic Reservoir Characteristic Data

in Zone D of Mission Canyon Formation

Reservoir Depth, feet	9800
Thickness, feet	16
Porosity, %	21
Core Permeability, md	30
Interstitial Water Saturation, %	21
Waterflood Residual Oil Saturation, %	40
Reservoir Temperature, °F	245
Initial Reservoir Pressure, psia	4409
BHP, Dec. 1980, psia	3345
Rock Compressibility, psi^{-1}	2.63×10^{6}
Dip Angle, degree	0.5

TABLE 2

Physical Properties of Reservoir Fluids

Zabolotny 1-3-4A Well

Reservoir Temperature, °F	245
Saturation Pressure (P_s), psia	2698
Solution GOR at P_s, SCF/STB	1119.4
Oil Formation Volume Factor at P_s, RB/STB	1.769
Oil Viscosity at P_s, cp	0.20
Oil Gravity, °API	41.0
Oil Density at P_s, gm/ml	0.6043
Oil Compressibility at P_s, psi^{-1}	28.95×10^{-6}
Minimum Miscibility Pressure with CO_2, psig	3400
Water Formation Volume Factor, RB/STB	1.045
Water Viscosity, cp	0.456
Water Compressibility, psi^{-1}	3.89×10^{-6}

TABLE 3

Hydrocarbon Analysis of Reservoir Fluids from Zabolotny 1-3-4A Well

Component	Mole Percent	
	Bottom Hole Sample	Recombined Sample
Nitrogen	0.91	0.93
Carbon Dioxide	1.12	1.20
Hydrogen Sulfide	5.73	4.91
Methane	33.34	34.01
Ethane	9.85	9.87
Propane	6.66	6.55
iso-Butane	1.35	1.32
N-Butane	3.85	3.68
iso-Pentane	1.49	1.35
n-Pentane	1.96	1.74
Hexanes	3.42	3.02
Heptane-plus	30.32	31.42
Total	100.00	100.00
Properties of Heptanes Plus Fraction		
Sp. Gr. (60/60)	0.8390	0.8370
API Gravity	37.2	37.6
Molecular Weight	192	190

TABLE 4

Oil Composition and Component Parameters

for the Peng-Robinson Equation of State

Component	Mole Fraction	Molecular Weight	Critical Pressure (psi)	Critical Temperature (°R)	Critical Volume (Cu Ft/ Lb-Mole)	Accentric Factor
CO_2	.0120	44.010	1070.94	547.59	1.5051	.2250
H_2S	.0491	34.076	1305.92	672.39	1.5641	.1000
C_1N_2	.3494	16.362	663.10	339.98	1.5860	.0112
C_2	.0987	30.070	707.76	549.78	2.3695	.0986
C_4*	.1464	54.809	565.12	733.36	3.5420	.1860
C_{10}*	.0668	135.000	375.22	1149.90	8.6030	.3705
C_{14}*	.2776	192.000	292.49	1298.30	12.5000	.5485

TABLE 5

Binary Interaction Parameters for

the Peng-Robinson Equation of State

	CO_2	H_2S	C_1N_2	C_2	C_4*	C_{10}*	C_{14}*
CO_2	0.						
H_2S	0.100	0.					
C_1N_2	0.100	0.088	0.				
C_2	0.130	0.080	0.001	0.			
C_4*	0.131	0.072	0.020	0.	0.		
C_{10}*	0.129	0.034	0.034	0.	0.	0.	
C_{14}*	0.127	0.003	0.065	0.	0.	0.	0.

TABLE 6

K-Values vs Pressure at 245° F for CO_2

Composition of 0.012 Mole Fraction

Pressure (psia)	K-Values						
	CO_2	H_2S	C_1N_2	C_2	C_4*	C_{10}*	C_{14}*
1000	3.1167	1.3238	5.1353	1.8249	0.6230	0.0186	0.0021
2000	1.8417	0.8998	2.7677	1.2225	0.5422	0.0373	0.0071
2500	1.5945	0.8332	2.2947	1.1172	0.5544	0.0547	0.0130
2740	1.5089	0.8143	2.1276	1.0832	0.5653	0.0656	0.0172
2900	1.4565	0.8107	2.0186	1.0630	0.5731	0.0741	0.0208
3100	1.3970	0.8081	1.8950	1.0410	0.5846	0.0865	0.0264
3300	1.3437	0.8079	1.7839	1.0223	0.5978	0.1012	0.0336
3550	1.2848	0.8106	1.6605	1.0031	0.6172	0.1236	0.0456
3800	1.2336	0.8168	1.5521	0.9885	0.6399	0.1516	0.0621
4050	1.1892	0.8263	1.4566	0.9779	0.6661	0.1868	0.0849
4300	1.1508	0.8391	1.3721	0.9711	0.6960	0.2310	0.1165
4500	1.1238	0.8516	1.3115	0.9682	0.7227	0.2744	0.1505
4700	1.0998	0.8662	1.2562	0.9674	0.7520	0.3267	0.1948
5000	1.0687	0.8918	1.1819	0.9697	0.8013	0.4260	0.2879
5250	1.0466	0.9165	1.1268	0.9746	0.8473	0.5331	0.3999

TABLE 7

K-Values vs Pressure at 245° F for CO_2

Composition of 0.100 Mole Fraction

Pressure (psia)	K-Values						
	CO_2	H_2S	C_1N_2	C_2	C_4*	C_{10}*	C_{14}*
1000	3.1314	1.3260	5.1307	1.8233	0.6236	0.0188	0.0021
2000	1.8502	0.9069	2.7386	1.2215	0.5485	0.0396	0.0079
2500	1.6010	0.8430	2.2593	1.1169	0.5643	0.0596	0.0149
2740	1.5143	0.8255	2.0895	1.0832	0.5770	0.0722	0.0201
2900	1.4645	0.8173	1.9910	1.0648	0.5870	0.0820	0.0244
3100	1.4052	0.8169	1.8698	1.0448	0.6005	0.0963	0.0312
3300	1.3518	0.8185	1.7604	1.0277	0.6158	0.1133	0.0399
3550	1.2924	0.8235	1.6385	1.0103	0.6377	0.1394	0.0546
3800	1.2403	0.8317	1.5307	0.9970	0.6629	0.1721	0.0750
4050	1.1946	0.8429	1.4353	0.9874	0.6916	0.2133	0.1033
4300	1.1545	0.8573	1.3504	0.9813	0.7241	0.2652	0.1429
4500	1.1260	0.8709	1.2891	0.9786	0.7528	0.3165	0.1855
4700	1.1004	0.8865	1.2329	0.9779	0.7843	0.3783	0.2414
5000	1.0664	0.9134	1.1570	0.9800	0.8366	0.4962	0.3596
5250	1.0418	0.9391	1.1004	0.9844	0.8853	0.6236	0.5025

TABLE 8

K-Values vs Pressure at 245° F for CO_2

Composition of 0.200 Mole Fraction

Pressure (psia)	K-Values						
	CO_2	H_2S	C_1N_2	C_2	C_4*	C_{10}*	C_{14}*
1000	3.1441	1.3257	5.1243	1.8191	0.6226	0.0189	0.0022
2000	1.8558	0.9116	2.7032	1.2172	0.5534	0.0420	0.0086
2500	1.6041	0.8509	2.2154	1.1131	0.5733	0.0650	0.0172
2740	1.5160	0.8352	2.0420	1.0798	0.5884	0.0800	0.0236
2900	1.4651	0.8283	1.9412	1.0617	0.6001	0.0918	0.0292
3100	1.4085	0.8230	1.8282	1.0428	0.6164	0.1090	0.0378
3300	1.3533	0.8269	1.7189	1.0273	0.6344	0.1296	0.0491
3550	1.2918	0.8348	1.5968	1.0118	0.6600	0.1615	0.0683
3800	1.2376	0.8457	1.4888	1.0001	0.6891	0.2019	0.0954
4050	1.1896	0.8597	1.3928	0.9920	0.7219	0.2533	0.1336
4300	1.1473	0.8768	1.3072	0.9870	0.7587	0.3188	0.1877
4500	1.1169	0.8926	1.2452	0.9852	0.7912	0.3841	0.2470
4700	1.0892	0.9103	1.1883	0.9852	0.8266	0.4635	0.3255
5000	1.0521	0.9404	1.1111	0.9881	0.8853	0.6164	0.4941
5250	1.0248	0.9687	1.0532	0.9930	0.9397	0.7836	0.7013

TABLE 9

K-Values vs Pressure at 245° F for CO_2

Composition of 0.300 Mole Fraction

Pressure (psia)	K-Values						
	CO_2	H_2S	C_1N_2	C_2	C_4*	C_{10}*	C_{14}*
1000	3.1542	1.3233	5.1188	1.8133	0.6204	0.0188	0.0022
2000	1.8586	0.3133	2.6683	1.2103	0.5560	0.0439	0.0093
2500	1.6042	0.8556	2.1713	1.1064	0.5796	0.0700	0.0194
2740	1.5144	0.8416	1.9940	1.0732	0.5970	0.0875	0.0273
2900	1.4625	0.8360	1.8907	1.0554	0.6104	0.1015	0.0342
3100	1.4041	0.8325	1.7745	1.0368	0.6292	0.1223	0.0453
3300	1.3515	0.8327	1.6699	1.0219	0.6504	0.1475	0.0601
3550	1.2864	0.8438	1.5464	1.0084	0.6805	0.1870	0.0855
3800	1.2287	0.8581	1.4372	0.9987	0.7145	0.2379	0.1222
4050	1.1775	0.8755	1.3402	0.9924	0.7527	0.3036	0.1753
4300	1.1320	0.8961	1.2536	0.9892	0.7955	0.3888	0.2521
4500	1.0992	0.9149	1.1908	0.9886	0.8331	0.4748	0.3378
4700	1.0690	0.9355	1.1331	0.9898	0.8740	0.5808	0.4535
5000	1.0283	0.9702	1.0548	0.9944	0.9419	0.7881	0.7075
5250	1.0000	1.0000	1.0000	1.0000	1.0000	1.0000	1.0000

TABLE 10

K-Values vs Pressure at 245° F for CO_2

Composition of 0.400 Mole Fraction

Pressure (psia)	K-Values						
	CO_2	H_2S	C_1N_2	C_2	C_4*	C_{10}*	C_{14}*
1000	3.1629	1.3194	5.1153	1.8064	0.6172	0.0187	0.0022
2000	1.8606	0.9124	2.6368	1.2017	0.5563	0.0453	0.0099
2500	1.6033	0.8573	2.1305	1.0975	0.5831	0.0742	0.0214
2740	1.5119	0.8448	1.9492	1.0644	0.6024	0.0940	0.0307
2900	1.4585	0.8403	1.8434	1.0466	0.6174	0.1102	0.0391
3100	1.3983	0.8386	1.7242	1.0284	0.6384	0.1346	0.0528
3300	1.3434	0.8408	1.6163	1.0138	0.6624	0.1648	0.0715
3550	1.2799	0.8493	1.4932	1.0003	0.6973	0.2142	0.1055
3800	1.2162	0.8679	1.3806	0.9929	0.7380	0.2794	0.1561
4050	1.1598	0.8900	1.2810	0.9891	0.7837	0.3658	0.2317
4300	1.1096	0.9157	1.1925	0.9885	0.8350	0.4805	0.3450
4500	1.0732	0.9387	1.1284	0.9901	0.8802	0.5988	0.4753
4700	1.0397	0.9639	1.0696	0.9934	0.9295	0.7476	0.6561
5000	1.0000	1.0000	1.0000	1.0000	1.0000	1.0000	1.0000
5250	1.0000	1.0000	1.0000	1.0000	1.0000	1.0000	1.0000

TABLE II

K-Values vs Pressure at 245° F for CO_2

Composition of 0.500 Mole Fraction

Pressure (psia)	K-Values						
	CO_2	H_2S	C_1N_2	C_2	C_4*	C_{10}*	C_{14}*
1000	3.1708	1.3142	5.1142	1.7988	0.6131	0.0185	0.0022
2000	1.8624	0.9094	2.6094	1.1916	0.5543	0.0461	0.0102
2500	1.6028	0.8562	2.0948	1.0868	0.5834	0.0772	0.0229
2740	1.5102	0.8450	1.9105	1.0538	0.6042	0.0990	0.0335
2900	1.4558	0.8415	1.8028	1.0361	0.6203	0.1169	0.0432
3100	1.3939	0.8412	1.6814	1.0181	0.6432	0.1443	0.0592
3300	1.3369	0.8452	1.5714	1.0040	0.6694	0.1789	0.0815
3550	1.2700	0.8464	1.4456	0.9915	0.7082	0.2367	0.1234
3800	1.2039	0.8760	1.3264	0.9844	0.7571	0.3218	0.1936
4050	1.1382	0.9048	1.2204	0.9842	0.8145	0.4395	0.3047
4300	1.0799	0.9381	1.1270	0.9878	0.8795	0.6024	0.4812
4500	1.0379	0.9679	1.0601	0.9930	0.9375	0.7771	0.6952
4700	1.0000	1.0000	1.0000	1.0000	1.0000	1.0000	1.0000
5000	1.0000	1.0000	1.0000	1.0000	1.0000	1.0000	1.0000
5250	1.0000	1.0000	1.0000	1.0000	1.0000	1.0000	1.0000

TABLE 12

K-Values vs Pressure at 245° F for CO_2

Composition of 0.600 Mole Fraction

Pressure (psia)	K-Values						
	CO_2	H_2S	C_1N_2	C_2	C_4*	C_{10}*	C_{14}*
1000	3.1785	1.3081	5.1158	1.7907	0.6084	0.0182	0.0021
2000	1.8655	0.9045	2.5877	1.1806	0.5503	0.0462	0.0104
2500	1.6043	0.8527	2.0661	1.0750	0.5806	0.0787	0.0239
2740	1.5107	0.8424	1.8793	1.0418	0.6021	0.1018	0.0353
2900	1.4557	0.8397	1.7706	1.0241	0.6189	0.1209	0.0458
3100	1.3929	0.8403	1.6482	1.0063	0.6427	0.1502	0.0635
3300	1.3349	0.8454	1.5381	0.9928	0.6700	0.1873	0.0881
3550	1.2662	0.8584	1.4126	0.9814	0.7109	0.2499	0.1348
3800	1.1973	0.8804	1.2943	0.9763	0.7632	0.3435	0.2146
4050	1.1189	0.9178	1.1701	0.9793	0.8401	0.5109	0.3811
4300	1.0444	0.9650	1.0631	0.9902	0.9315	0.7639	0.6797
4500	1.0000	1.0000	1.0000	1.0000	1.0000	1.0000	1.0000
4700	1.0000	1.0000	1.0000	1.0000	1.0000	1.0000	1.0000
5000	1.0000	1.0000	1.0000	1.0000	1.0000	1.0000	1.0000
5250	1.0000	1.0000	1.0000	1.0000	1.0000	1.0000	1.0000

TABLE 13

K-Values vs Pressure at 245° F for CO_2

Composition of 0.700 Mole Fraction

Pressure (psia)	K-Values						
	CO_2	H_2S	C_1N_2	C_2	C_4*	C_{10}*	C_{14}*
1000	3.1862	1.3010	5.1205	1.7822	0.6031	0.0178	0.0021
2000	1.8704	0.8979	2.5720	1.1688	0.5144	0.0458	0.0104
2500	1.6085	0.8469	2.0445	1.0620	0.5745	0.0787	0.0241
2740	1.5149	0.8371	1.8567	1.0285	0.5960	0.1021	0.0359
2900	1.4598	0.8347	1.7477	1.0108	0.6127	0.1215	0.0467
3100	1.3970	0.8358	1.6260	0.9931	0.6364	0.1510	0.0647
3300	1.3392	0.8414	1.5175	0.9799	0.6635	0.1883	0.0897
3550	1.2708	0.8547	1.3956	0.9694	0.7038	0.2502	0.1364
3800	1.2030	0.8765	1.2833	0.9657	0.7548	0.3406	0.2137
4050	1.1276	0.9121	1.1697	0.9708	0.8278	0.4947	0.3659
4300	1.0277	1.2929	1.0349	0.9919	0.9571	0.8527	0.7969
4500	1.0000	1.0000	1.0000	1.0000	1.0000	1.0000	1.0000
4700	1.0000	1.0000	1.0000	1.0000	1.0000	1.0000	1.0000
5000	1.0000	1.0000	1.0000	1.0000	1.0000	1.0000	1.0000
5250	1.0000	1.0000	1.0000	1.0000	1.0000	1.0000	1.0000

TABLE 14

K-Values vs Pressure at 245° F for CO_2

Composition of 0.800 Mole Fraction

Pressure (psia)	K-Values						
	CO_2	H_2S	C_1N_2	C_2	C_4*	C_{10}*	C_{14}*
1000	3.1945	1.2929	5.1290	1.7734	0.5972	0.0174	0.0020
2000	1.8777	0.8895	2.5628	1.1562	0.5363	0.0447	0.0101
2500	1.6165	0.8385	2.0310	1.0478	0.5650	0.0769	0.0236
2740	1.5236	0.8288	1.8429	1.0137	0.5856	0.0997	0.0351
2900	1.4693	0.8263	1.7347	0.9957	0.6014	0.1184	0.0455
3100	1.4076	0.8273	1.6149	0.9779	0.6237	0.1464	0.0625
3300	1.3512	0.8325	1.5095	0.9648	0.6490	0.1810	0.0857
3550	1.2856	0.8447	1.3938	0.9545	0.6858	0.2367	0.1271
3800	1.2223	0.8639	1.2909	0.9510	0.7309	0.3134	0.1911
4050	1.1564	0.8927	1.1942	0.9555	0.7903	0.4292	0.3006
4300	1.0904	0.9291	1.1118	0.9689	0.8619	0.5913	0.4746
4500	1.0434	0.9624	1.0535	0.9830	0.9267	0.7665	0.6862
4700	1.0006	0.9994	1.0007	0.9997	0.9989	0.9961	0.9945
5000	1.0000	1.0000	1.0000	1.0000	1.0000	1.0000	1.0000
5250	1.0000	1.0000	1.0000	1.0000	1.0000	1.0000	1.0000

TABLE 15

K-Values vs Pressure at 245° F for CO_2

Composition of 0.900 Mole Fraction

Pressure (psia)	K-Values						
	CO_2	H_2S	C_1N_2	C_2	C_4*	C_{10}*	C_{14}*
1000	3.2043	1.2830	5.1449	1.7644	0.5907	0.0169	0.0019
2000	1.8891	0.8785	2.5630	1.1426	0.5259	0.0429	0.0096
2500	1.6303	0.8266	2.0282	1.0319	0.5514	0.0732	0.0222
2740	1.5392	0.8163	1.8407	0.9968	0.5698	0.0941	0.0327
2900	1.4862	0.8134	1.7336	0.9783	0.5838	0.1110	0.0419
3100	1.4268	0.8135	1.6165	0.9599	0.6034	0.1357	0.0567
3300	1.3732	0.8174	1.5152	0.9461	0.6251	0.1652	0.0760
3550	1.3123	0.8270	1.4067	0.9349	0.6558	0.2103	0.1083
3800	1.2418	0.8442	1.3150	0.9352	0.6958	0.2693	0.1548
4050	1.1806	0.8660	1.2354	0.9401	0.7419	0.3466	0.2225
4300	1.1271	0.8924	1.1658	0.9493	0.7945	0.4481	0.3210
4500	1.0891	0.9168	1.1162	0.9595	0.8416	0.5520	0.4317
4700	1.0546	0.9440	1.0712	0.9720	0.8936	0.6814	0.5819
5000	1.0084	0.9901	1.0110	0.9949	0.9812	0.9383	0.9142
5250	1.0000	1.0000	1.0000	1.0000	1.0000	1.0000	1.0000

TABLE 16

Summary of Results for the CO_2 Residual Oil Saturation Tests

Interval, Core Depth, feet*	Porosity,%	Permeability, md	Water/CO_2 Ratio	Final Saturations after 1.2 PV of CO_2 Injected, % PV				
				S_o	S_w	S_{co_2}	K_{rw}	K_{rco_2}
9823 - 9824	23.0	7.0	0:1	3.1	20.0	76.9		
9826 - 9827	21.7	5.3	1.5:1	3.1	61.5	35.4	0.295	0.033
9814 - 9815	26.0	39.0	3:1	0.8	63.5	35.7	0.597	0.033

*Zabolotny Injection Well No. 1

Pressure = 3,500 psia

Temperature = 245°F

TABLE 17

Core and GULFLOG Analyses for the Mintest Wells

Layer	Log Depth (ft)	Thickness (ft)	Core Φ(%)	Log Φ(%)	K_h (md)	K_v (md)	S_{oi} (%)	S_{orw}* (%)
Zabolotny Inj. No. 1								
W	9809-24	15	11.4	9.6	2.3	2.4	---	---
X	9824-27	3	17.0	18.1	9.5	30.6	79.8	42.5
Y	9827-35	8	22.7	22.2	58.7	38.1	81.8	39.7
Z	9835-40	5	15.6	16.6	11.7	8.5	70.0	50.5
		31						
Zabolotny Obs. No. 1								
W	9798-10	12	10.2	8.4	2.9	.9	---	---
X	9810-13	3	18.3	16.0	5.0	32.0	79.6	44.7
Y	9813-21	8	22.2	23.4	16.5	32.3	84.4	40.2
Z	9821-25	4	14.9	14.0	1.2	5.8	72.9	59.9
		27						
Zabolotny Obs. No. 2								
W	9842-57	15	11.2	10.9	1.5	.8	---	---
X	9857-59	2	20.5	17.4	4.1	20.0	74.8	47.9
Y	9859-68	9	24.4	25.0	25.6	36.9	78.2	38.2
Z	9868-73	5	14.9	17.4	2.8	4.2	74.9	54.7
		31						
Zabolotny Obs. No. 3								
W	9823-38	15	9.6	5.5	.9	.4	---	---
X	9838-41	3	18.0	17.8	18.0	---	76.8	---
Y	9841-50	9	21.9	23.0	34.0	21.2	79.8	37.1
Z	9850-54	4	14.9	14.4	13.8	.7	71.9	49.2
		31						
Zabolotny Obs. No. 4								
W	9821-35	14	9.3	---	1.5	.3	---	---
X	9835-38	3	21.9**	15.8	63.0	---	---	---
Y	9838-46	8	25.0**	23.4	96.0	50.0	---	---
Z	9846-51	5	19.6**	14.3	29.6	31.0	---	---
		30						

* Based upon flushed zone water saturation correlation (micro-resistivity logs).

** Portions of the core samples were broken and hence not analyzed or pressure was too low.

TABLE 18

Pattern Area Volumetric Data

(Radius = 283 feet)

Layer	Thickness (ft)	Porosity (%)	Pore Volume (bbl)	S_{oi}	HCPV (bbl)
W	15.0	0.106	71,200	0.680	48,400
X	3.0	0.184	24,700	0.778	19,200
Y	8.5	0.228	86,800	0.810	70,300
Z	4.5	0.149	30,000	0.724	21,700
XYZ	16.0	0.198	141,500	0.786	111,200
WXYZ	31.0		212,700		159,600

TABLE 19

Production Data in the Minitest Area

During the Test Period (12/11/80 - 9/24/81)

Well Name	Perforated Interval (Feet)	Total Production Rate (BOPD)	kh Allocation Factor	Production Rate from Project Interval (BOPD)
Zabolotny 4-3-1A	9725-39; 9740-59; 9795-9801; 9838-44	204	0.152	31
Zabolotny 1-3-4A	9770-9810	237	1.000	237
Zabolotny 2-3-3A	9651-54; 9662-66; 9671-75; 9690-9702; 9718-20; 9742-48; 9758-72	188	0.765	144
	Average Production Rate (BOPD)	210		137

TABLE 20

Analyses of the Responses for the Multi-Well Pulse Test

DATE: November 15, 1980
PULSE TYPE: Water Injection
PULSE DURATION: 1.9933 Hours
PULSE RATE: 2297.5 B/D

	WELL PAIR		
	Z1 - ZO1	Z1 - ZO2	Z1 - ZO3
Maximum Response Time (minutes)	175.0	176.0	217.5
Maximum Response Pressure (psi)	21.180	15.835	16.010
Transmissibility (md-ft/cp)	3,482.5	4,712.0	3,189.6
Diffusivity, $k/\mu\Phi c$ (md-psi/cp)	39.578×10^{-6}	37.638×10^{-6}	32.054×10^{-6}
Storage Capacity, Φch (ft/psi)	87.990×10^{6}	125.190×10^{6}	99.507×10^{6}
Effective Hydraulic Thickness (ft)	25.2	36.5	29.4
Effective Permeability (md)	29.3	27.4	23.0
Storage (RB/acre)	33,610	47,820	38,010

Z1 - Zabolotny Injection Well No. 1
ZO1 - Zabolotny Observation Well No. 1
ZO2 - Zabolotny Observation Well No. 2
ZO3 - Zabolotny Observation Well No. 3

TABLE 21

Water/CO_2 Injection Schedule for the Minitest

Date	t Days	Water B/D	Carbon Dioxide Tons/Day	Cumulative Time, Days
12/11/80 - 01/06/81	26	1136.12	--	26
01/07/81 - 01/12/81	6	--	39.35	32
01/13/81 - 01/18/81	6	Temporarily Shut-in		38
01/19/81 - 01/23/81	5	--	36.88	43
01/24/81 - 01/27/81	4	1251.75	--	47
01/28/81 - 02/05/81	9	--	46.72	56
02/06/81 - 02/10/81	5	992.80	--	61
02/11/81 - 02/14/81	4	--	38.47	65
02/15/81 - 02/19/81	5	Temporarily Shut-in		70
02/20/81 - 02/26/81	7	--	39.73	77
02/27/81 - 03/02/81	4	1218.50	--	81
03/03/81 - 03/11/81	9	--	44.74	90
03/12/81 - 03/16/81	5	1155.20	--	95
03/17/81 - 03/25/81	9	--	46.57	104
03/26/81 - 08/31/81	159	1141.09	--	263
09/01/81 - 09/09/81	9	809.90	--	272
09/10/81 - 09/11/81	2	1617.50	--	274
09/12/81 - 09/18/81	7	Temporarily Shut-in		281
09/19/81 - 09/24/81	6	1139.35	--	287
09/24/81		Complete Shut-in		
TOTAL		248,954 BBLS	2,095 tons	

TABLE 22

Volumetric Injection Data for the Minitest

Injected Fluid	Cumulative Injected Volume BBLS	Tons	RB	W-Z %PV	W-Z %HCPV	XYZ %PV	XYZ %HCPV
Preflush Water	29,539		30,700	14.44	19.25	21.71	27.63
Carbon Dioxide		2095	24,700	11.62	15.48	17.46	22.21
WAG Water	20,621		21,446	10.08	13.43	15.16	19.29
Drive Water	198,794		206,746	97.20	129.54	146.11	185.92
TOTAL	248,954	2095	283,592	133.34	177.70	200.44	255.05

WAG Ratio = 1.08:1

Avg. Injection Rate: Water - 1150 B/D

CO_2 - 40 tons/day

Formation Volume Factor: Water - 1.04 RB/Bbl

CO_2 - 11.8 RB/ton

TABLE 23

Distances and Orientations of Production Wells and Observation Wells Relative to Zabolotny Injection No. 1 Well

Well	Distance, feet	Azimuthal Angle θ, Degree
Zabolotny 4-3-1A	2015	90
Zabolotny 1-3-4A	1915	180
Zabolotny 2-3-3A	1713	270
Observation No. 1	258	0
Observation No. 2	250	201
Observation No. 3	283	78.9
Observation No. 4	136	196.7

TABLE 24

Input Data for Reservoir Rock Properties

Well Pair	Distance (ft)	Layers	Thickness (ft)	Porosity	Permeability, md k_h	k_v	S_{oi}	S_{orw}
ZI-ZO1	258	W	10	0.105	4.2	3.0	0.680	0.55
		X	3	0.180	34.0	3.0	0.796	0.45
		Y	8	0.223	112.0	3.0	0.844	0.41
		Z	4	0.149	14.2	1.0	0.729	0.60
		*XYZ	15	0.195	50.1	3.0	0.811	0.46
ZI-ZO2	250	W	20	0.112	5.0	3.0	0.680	0.55
		X	2	0.196	50.3	3.0	0.748	0.45
		Y	9	0.240	180.0	3.0	0.782	0.33
		Z	5	0.149	14.2	1.0	0.749	0.55
		*XYZ	16	0.206	70.0	3.0	0.770	0.40
ZI-ZO3	283	W	15	0.100	3.6	3.0	0.680	0.55
		X	3	0.178	32.0	3.0	0.768	0.45
		Y	9	0.221	105.0	3.0	0.798	0.37
		Z	4	0.149	14.2	1.0	0.719	0.50
		*XYZ	16	0.195	50.1	3.0	0.778	0.41
**Average		W	15.0	0.106	4.3	3.0	0.680	0.55
		X	3.0	0.184	38.8	3.0	0.771	0.45
		Y	8.5	0.228	132.3	3.0	0.808	0.38
		Z	4.5	0.149	14.2	1.0	0.732	0.55

*For 11x11x2 grid system.
**For 16x15x4 grid system.

TABLE 25

Water Tracer Analysis (ppm)

Date 1981	Obs. No. 1		Obs. No. 2		Obs. No. 3	
	IPA	NPA	IPA	NPA	IPA	NPA
3-4	41	0	-	-	-	-
3-27	43	1	52	1	-	-
4-9	72	1	41	1	-	-
4-28	108	1	56	1	-	-
5-8	107	67	107	0	27	0
5-22	42	108	98	61	70	0
6-5	44	102	94	87	127	0
6-18	25	61	45	180	36	0
7-3	25	74	27	144	76	61
7-20	23	40	19	74	35	107
7-31	17	3	18	35	28	120
8-14	18	0	18	28	24	65
8-28	2	1	12	1	11	18
9-21	7	1	13	8	14	37

IPA - isopropyl Alcohol

NPA - normal propyl Alcohol

TABLE 26

Subsurface Sample Analysis

	Date: Component	Mole Percent 12/17/80	1/28/81	2/25/81	3/12/81	3/25/81	4/9/81	4/28/81
Obs. Well No.2	N_2	0.89	0.92	0.92	0.77			
	CO_2	1.28	1.27	1.22	1.45			
	H_2S	4.82	5.63	6.63	5.20			
	C_1	35.47	34.51	34.57	33.90			
	C_2	10.50	11.43	10.20	9.90			
	C_3	6.99	7.23	7.03	6.75			
	iC_4	1.37	1.58	1.12	1.09			
	nC_4	3.92	4.10	4.06	3.85			
	iC_5	1.60	1.66	1.37	1.25			
	nC_5	1.85	1.85	2.01	2.13			
	C_6	5.26	4.81	4.20	3.30			
	C_7^+	26.05	25.01	26.67	30.41			
	Mole wt.	223	225	220	193			
	Sp. Gr.	0.8433	0.8488	0.8460	0.8407			
	P(SAT)	1870 @ 76°	1850 @ 76°	1820 @ 76°	1825 @ 67°			
Obs. Well No.3	N_2	2.30			0.73	0.75	0.79	0.91
	CO_2	1.36			1.48	1.45	1.48	2.15
	H_2S	4.07			5.22	5.07	5.15	5.22
	C_1	45.28			33.66	33.14	33.58	33.93
	C_2	8.86			9.89	9.86	9.94	10.02
	C_3	4.56			6.58	6.43	6.75	6.56
	iC_4	0.80			1.01	0.93	1.32	1.17
	nC_4	2.22			3.71	4.40	3.81	3.91
	iC_5	0.80			1.30	1.18	1.28	1.17
	nC_5	0.97			1.94	2.06	1.91	1.29
	C_6	9.47			3.31	1.88	2.38	2.83
	C_7^+	19.28			31.17	32.82	31.61	30.84
	Mole wt.	198			190	193	190	193
	Sp. Gr.	0.8382			0.8392	0.8375	0.8338	0.8345
	P(SAT)	5100+ @ 76°			1840 @ 65°	1757 @ 70°	1821 @ 68°	1842 @ 69°

TABLE 27

Separator Gas Analysis (N_2 and H_2S Free, Mole Percent)

Observation Well No. 1

Date	12/17/80	1/28/81	2/25/81	3/12/81	3/26-27/81
Sep. Press.				96	50
CO_2				11.67	13.20
C_1				59.81	46.48
C_2				16.03	20.24
C_3				8.40	13.49
iC_4				1.07	1.10
nC_4				2.36	3.01
iC_5				0.35	1.07
nC_5				0.31	1.43

Date	4/9/81	4/22-29/81	5/6-11/81	5/20-26/81	6/2-4/81
Sep. Press.		30	30	10	18
CO_2		5.84	12.09	46.99	60.21
C_1		43.44	53.42	38.61	19.15
C_2		23.92	27.59	8.04	9.31
C_3		21.39	5.48	3.38	6.92
iC_4		2.27	0.48	0.62	1.19
nC_4		2.50	0.79	1.84	3.21
iC_5		0.28	0.09	0.26	-
nC_5		0.37	0.05	0.26	-

TABLE 27 (Cont'd)

Separator Gas Analysis (N_2 and H_2S Free, Mole Percent)

Observation Well No. 1

Date	6/20/81	7/2/81	7/16/81	7/28/81	8/11-13/81
Sep. Press.	5	-	38	20	30
CO_2	2.85*		53.34	52.92	31.34
C_1	4.13		33.44	33.25	49.35
C_2	2.28		7.19	6.45	10.23
C_3	-	All	3.16	3.66	5.62
iC_4	23.79	Nitrogen	0.53	1.12	0.95
nC_4	44.02		1.39	1.80	2.84
iC_5	10.68		0.32	0.42	0.29
nC_5	12.25		0.18	0.38	0.18

Date	8/25-27/81	9/13-21/81
Sep. Press.	10	-
CO_2		94.6*
C_1		4.56
C_2		0.80
C_3	All	
iC_4	Nitrogen	
nC_4		
iC_5		
nC_5		

*Extremely high nitrogen concentrations before calculating N_2 free basis.

TABLE 28

Separator Gas Analysis (N_2 and H_2S Free, Mole Percent)

Observation Well No. 2

Date	12/17/80	1/28/81	2/25/81	3/12/81	3/26-27/81
Sep. Press.	-	58	110	100	41
CO_2	2.55	2.49	2.52	2.49	2.68
C_1	67.49	69.78	72.30	64.79	64.70
C_2	17.33	16.91	15.57	16.08	18.27
C_3	8.57	7.05	6.70	10.84	9.70
iC_4	1.04	0.84	0.91	1.62	1.69
nC_4	2.29	2.23	1.63	2.88	1.96
iC_5	0.37	0.28	0.24	0.57	0.49
nC_5	0.35	0.25	0.18	0.73	0.51

Date	4/9/81	4/22-29/81	5/6-11/81	5/20-26/81	6/2-4/81
Sep. Press.	30	40	40	40	12
CO_2	4.75*	1.04	32.08	26.40	13.93
C_1	62.76	84.09	42.13	44.06	59.14
C_2	9.65	0.52	16.88	6.20	9.16
C_3	14.20	3.19	7.23	6.14	5.90
iC_4	2.34	3.64	0.58	2.91	1.79
nC_4	5.25	4.81	0.89	9.36	5.89
iC_5	0.52	1.27	0.13	2.43	2.46
nC_5	0.53	1.44	0.08	2.52	1.74

*Extremely high nitrogen concentrations before calculating N_2 free basis.

TABLE 28 (Cont'd)

Separator Gas Analysis (N_2 and H_2S Free, Mole Percent)

Observation Well No. 2

Date	6/20/81	7/2/81	7/16/81	7/28/81	8/11-13/81
Sep. Press.	11	30	-		
CO_2	7.41	11.91	13.92		
C_1	63.91	69.99	68.43		
C_2	7.96	9.26	9.13		
C_3	4.16	4.53	4.67	Sample	Sample
iC_4	3.40	1.61	1.07	Container	Container
nC_4	9.18	2.25	2.41	Empty	Empty
iC_5	1.75	0.28	0.25		
nC_5	2.24	0.17	0.12		

Date	8/25-27/81	9/13-21/81
Sep. Press.	20	-
CO_2	26.53	25.3*
C_1	50.60	18.3
C_2	5.99	16.0
C_3	7.08	13.5
iC_4	2.79	7.8
nC_4	5.68	12.0
iC_5	0.70	3.3
nC_5	0.63	3.8

*Extremely high nitrogen concentrations before calculating N_2 free basis.

TABLE 29

Separator Gas Analysis (N_2 and H_2S Free, Mole Percent)

Observation Well No. 3

Date	12/17/80	1/28/81	2/25/81	3/12/81	3/26-27/81
Sep. Press.	42			100	46
CO_2	2.61			2.33	2.51
C_1	61.26			69.90	62.38
C_2	18.42			16.30	17.64
C_3	10.31			6.77	10.88
iC_4	1.65			1.22	1.73
nC_4	4.26			2.99	3.29
iC_5	0.49			0.37	0.76
nC_5	0.70			0.13	0.80
C_6	0.30				

Date	4/9/81	4/22-29/81	5/6-11/81	5/20-26/81	6/2-4/81
Sep. Press.	30	100	98	44	14
CO_2	2.36	2.65	3.43	2.84	3.85
C_1	85.10	69.57	68.68	78.60	73.13
C_2	8.02	17.27	17.20	8.76	11.03
C_3	3.39	6.79	7.18	5.65	4.62
iC_4	0.06	0.87	0.73	1.84	1.75
nC_4	0.47	1.84	2.10	2.31	2.59
iC_5	0.33	0.38	0.34	-	1.67
nC_5	0.28	0.64	0.33	-	1.36

TABLE 29 (Cont'd)

Separator Gas Analysis (N_2 and H_2S Free, Mole Percent)

Observation Well No. 3

Date	6/20/81	7/2/81	7/16/81	7/28/81	8/11-13/81
Sep. Press.	12	10	22		10
CO_2	4.77	1.95	15.31		30.84
C_1	49.80	28.87	61.90		36.08
C_2	28.76	0.89	13.20		15.05
C_3	11.29	-	5.66	All	-
iC_4	1.83	-	-	Nitrogen	-
nC_4	3.00	8.09	0.89		4.39
iC_5	0.39	34.77	2.25		10.74
nC_5	0.17	9.55	0.49		0.97
C_6		15.88	0.30		1.93

Date	8/25-27/81	9/13-21/81
Sep. Press.	10	
CO_2	58.01	
C_1	32.01	
C_2	4.64	
C_3	-	All
iC_4	-	Nitrogen
nC_4	-	
iC_5	3.83	
nC_5	1.51	
C_6	-	

TABLE 30

CO_2 $^{13}C/^{12}C$ Isotope Ratio Analysis

Date	Inj. CO_2	Obs. No.1	Obs. No.2	Obs. No.3	Well Z1	Well Z2	Well Z3
12-17-80	-48.8	-	-2.3	-2.4	-1.6	-1.7	-1.6
1-28-81	-48.9	-	-2.5	-	-1.8	-2.1	-2.3
2-25-81	-	-	-2.1	-	-	-	-
3-12-81	-	-38.3	-1.6	-2.1	-	-0.1	-
3-25-81	-	-40.3	-2.7	-2.8	-	-	-2.3
4-9-81	-	-	-	-1.6	-	-2.0	-
4-22-81	-	-34.6	+0.4	-2.1	-	-	-
5-6-81	-	-43.6	-45.2	-12.7	-1.9	-	-
5-20-81	-	-45.6	-43.7	-11.8	-	-	-
6-2-81	-	-46.8	-40.1	-14.8	-	-	-
6-27-81	-	-	-37.5	-22.8	-	-	-
7-1-81	-	-	-39.6	-	-	-1.6	-
7-15-81	-	-47.8	-39.2	-36.3	-	-	-
7-28-81	-	-49.9	-	-	-	-	-
8-11-81	-	-49.2	-	-15.2	-	-	-
8-25-81	-	-	-44.8	-	-	-	-
9-17-81	-	-49.6	-45.9	-	-	-	-

Z1 - Zabolotny 1-3-4A

Z2 - Zabolotny 2-3-3A

Z3 - Zabolotny 4-3-1A

TABLE 31

Percentages of Oil Displaced (STB Basis)

(Radius = 283 Feet)

Layer	OIP*(STB)	Waterflood	CO_2 WAG=1:1	Incremental
W	27,360	15	17	2
X	10,854	39	58	19
Y	39,740	57	79	22
Z	12,267	21	24	3
TOTAL	90,221	37	50	13

*Oil-in-place on December 11, 1980

TABLE 32

INPUT DATA FOR RESERVOIR ROCK PROPERTIES FOR LAYER Y (SIX-LAYER MODEL)

Layers	Depth	Thickness (Ft)	Porosity	S_{oi}	S_{orw}	S_o (9-16-81)	Permeability, md K_h	Permeability, md K_v
Y1	9859		.241	.723		.283		
		2			.370		50	1
	9860		.240	.784		.244		
	9861		.320	.825		.085		
Y2	9862	3	.228	.804	.320	.056	200	100
	9863		.256	.784		.015		
	9864		.255	.793		.105		
Y3	9865	3	.256	.786	.320	.138	100	3
	9866		.270	.760		.139		
Y (Combined)		8	.246	.782	.330	.133	125	

FIGURE 1

CO_2 MINITEST LOCATION IN THE LITTLE KNIFE FIELD , NORTH DAKOTA

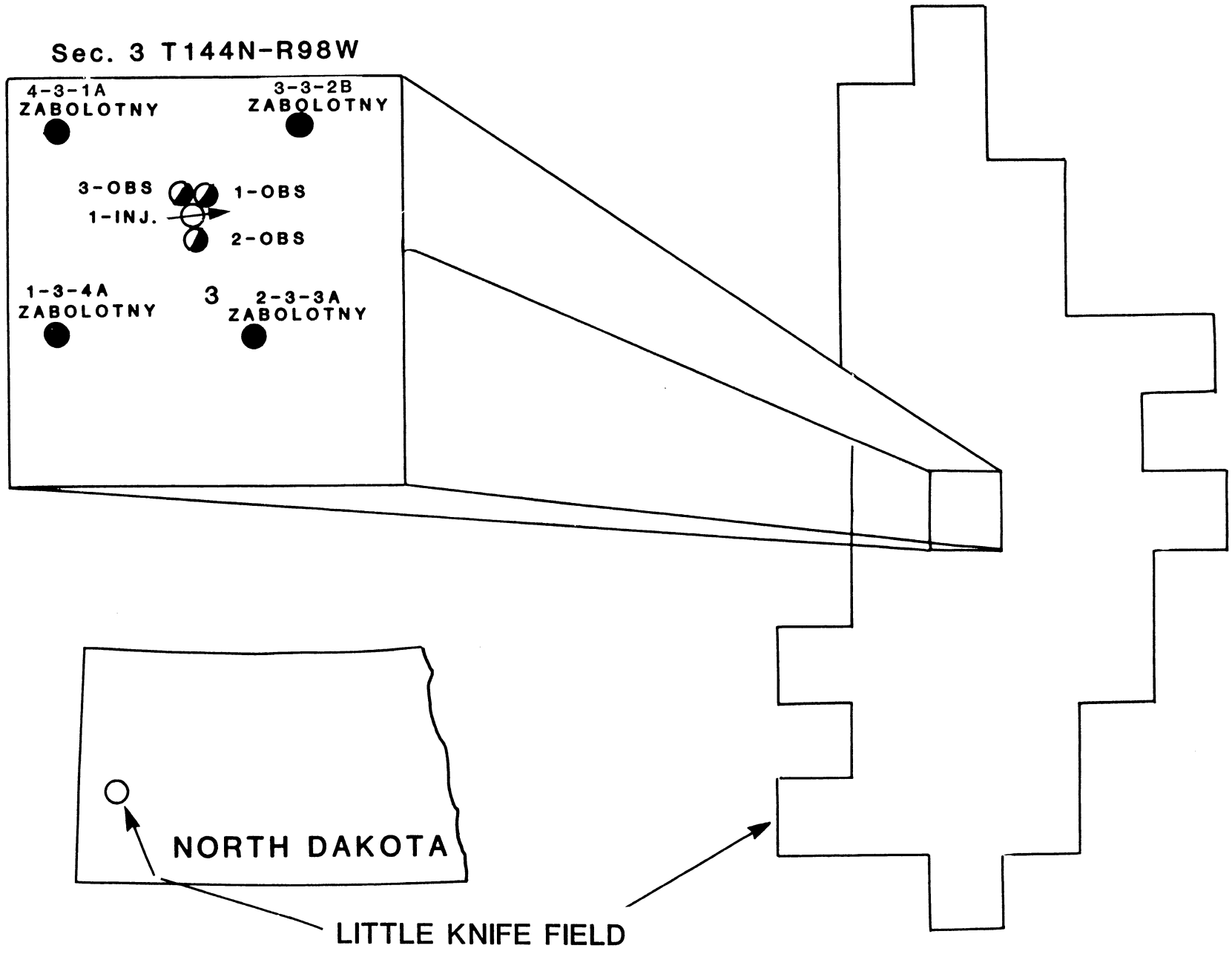

FIGURE 2

INDEX MAP OF WILLISTON BASIN

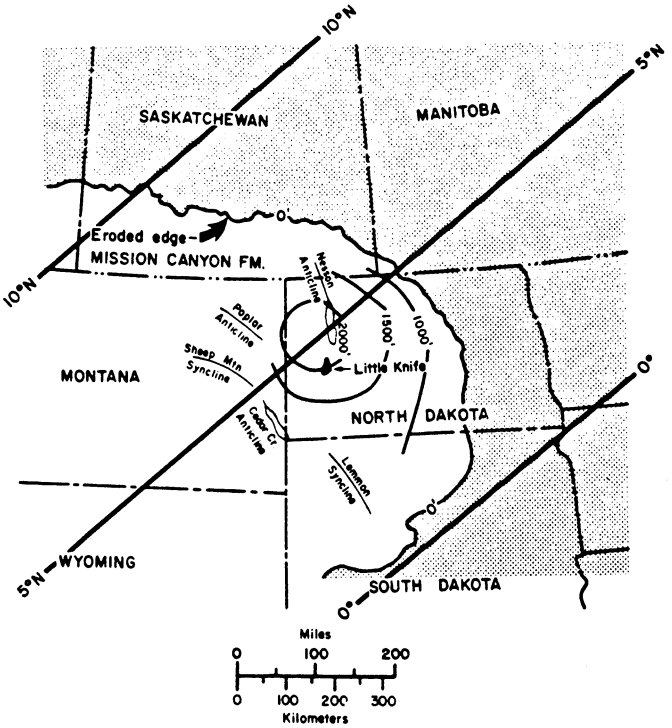

FIGURE 3

TOP OF MISSION CANYON FORMATION STRUCTURE MAP

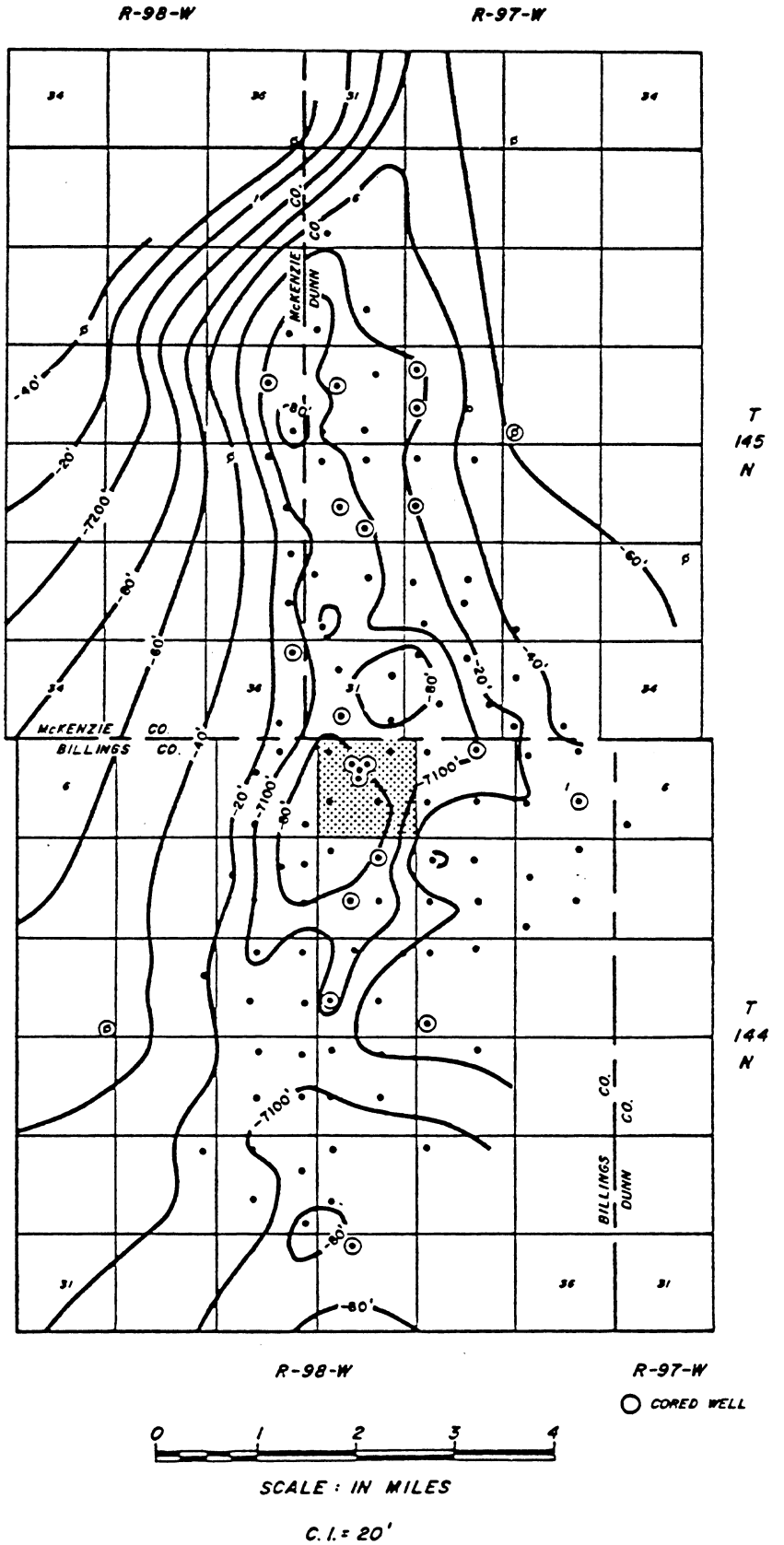

CO_2 Minitest Pattern's Located In Central Portion Of The Field Within Shaded Section

FIGURE 4

STRATIGRAPHIC FENCE DIAGRAM OF ZONES C AND D OF THE MISSION CANYON FORMATION THROUGH ALL MINITEST WELLS

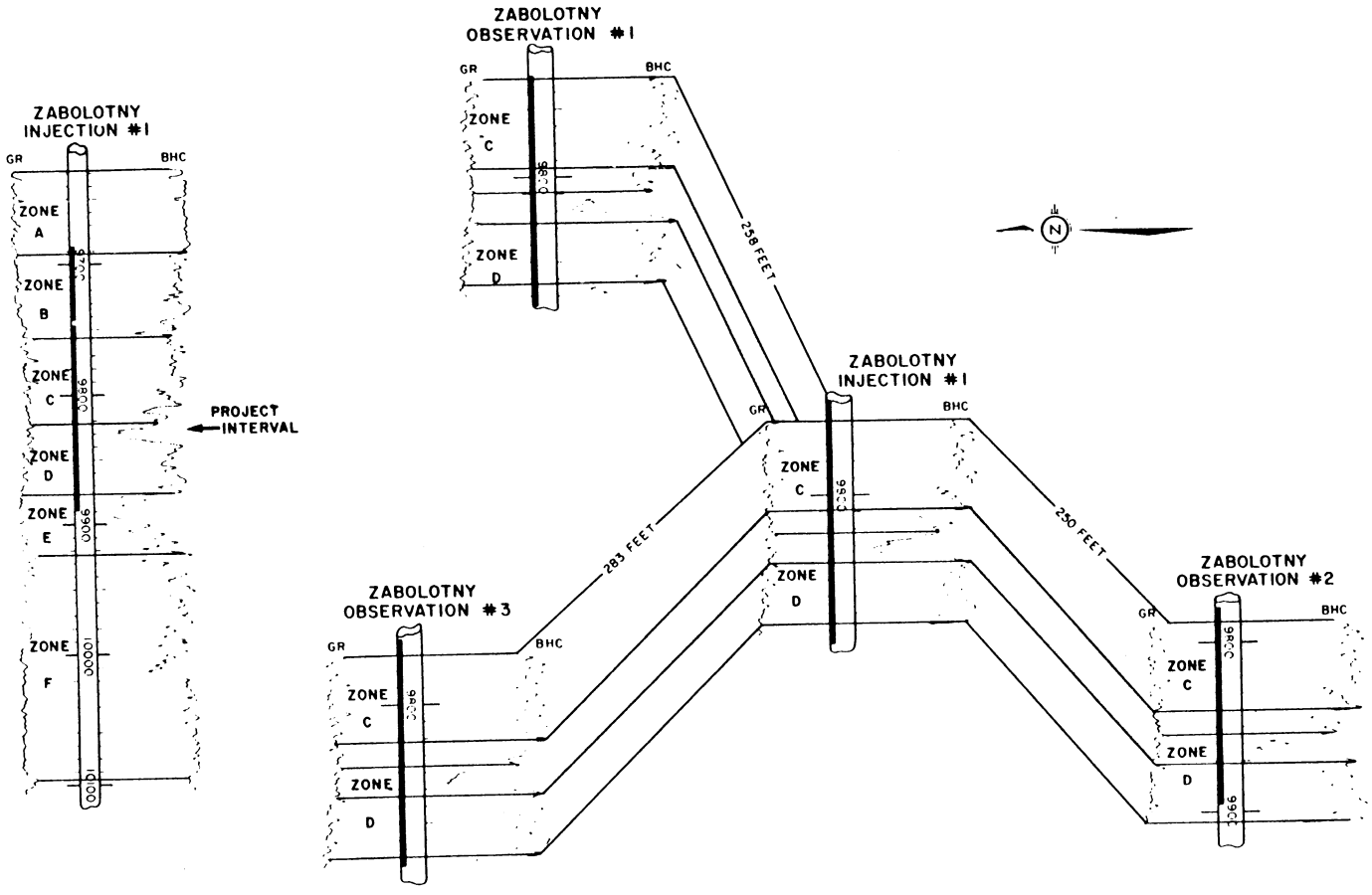

FIGURE 5
RESERVOIR CROSS SECTION GRID BASED ON WHOLE CORE POROSITY ANALYSIS

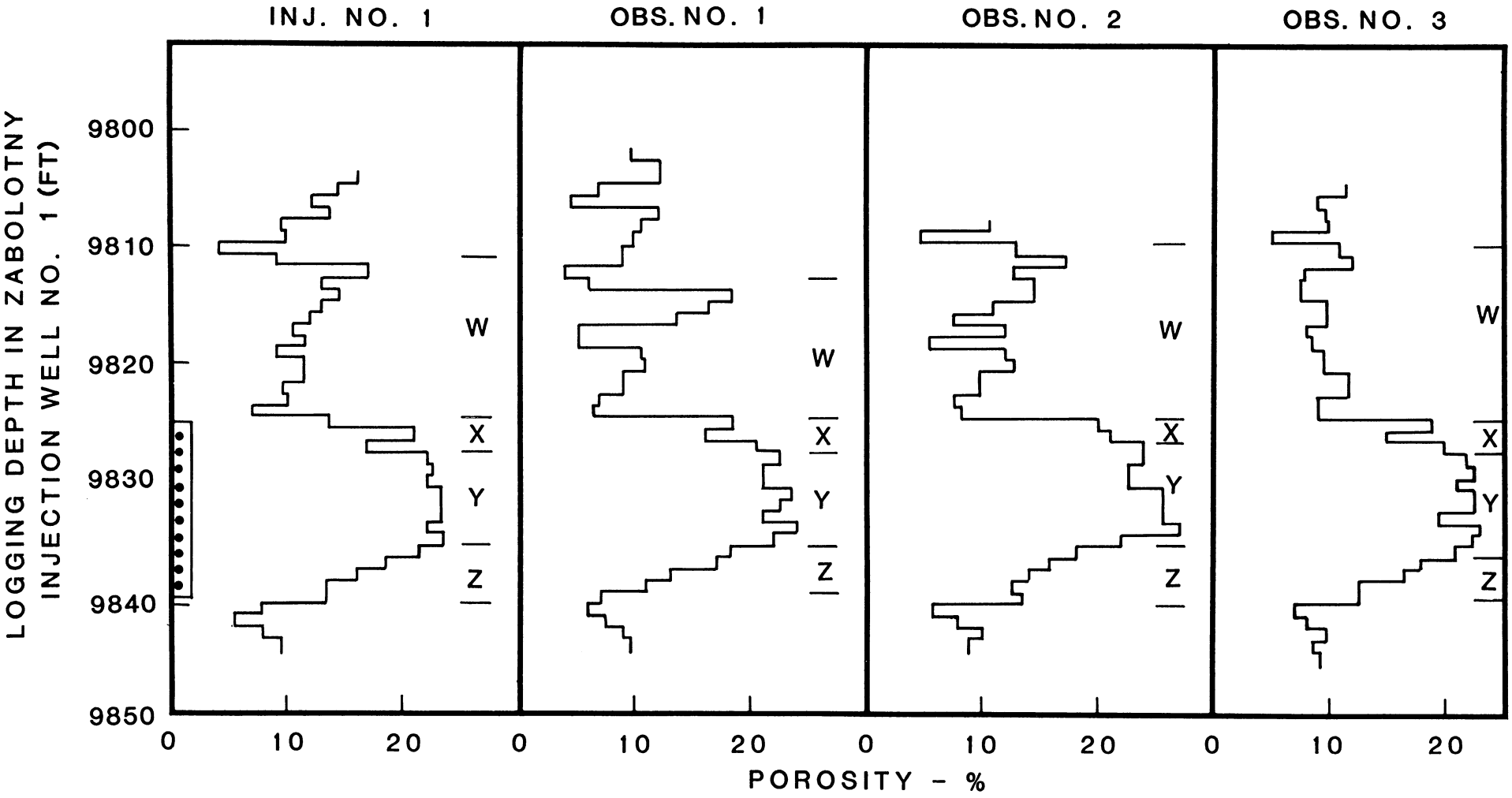

FIGURE 6
WHOLE CORE POROSITY AND PERMEABILITY COMPARED TO LITHOLOGY IN EACH MINITEST WELL

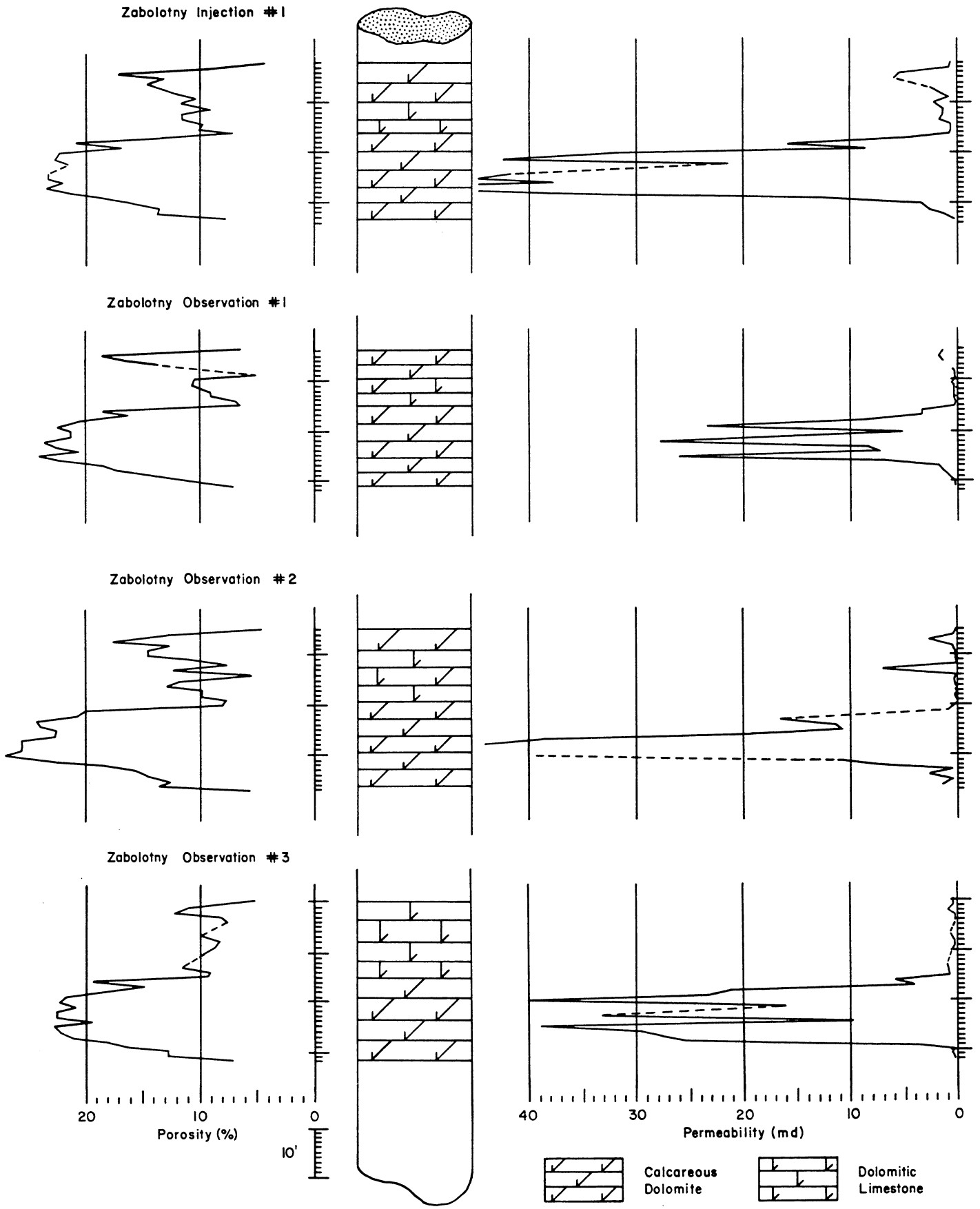

FIGURE 7

FRACTURES MEASURED FROM ORIENTED CORES IN THE MINITEST PROJECT INTERVAL

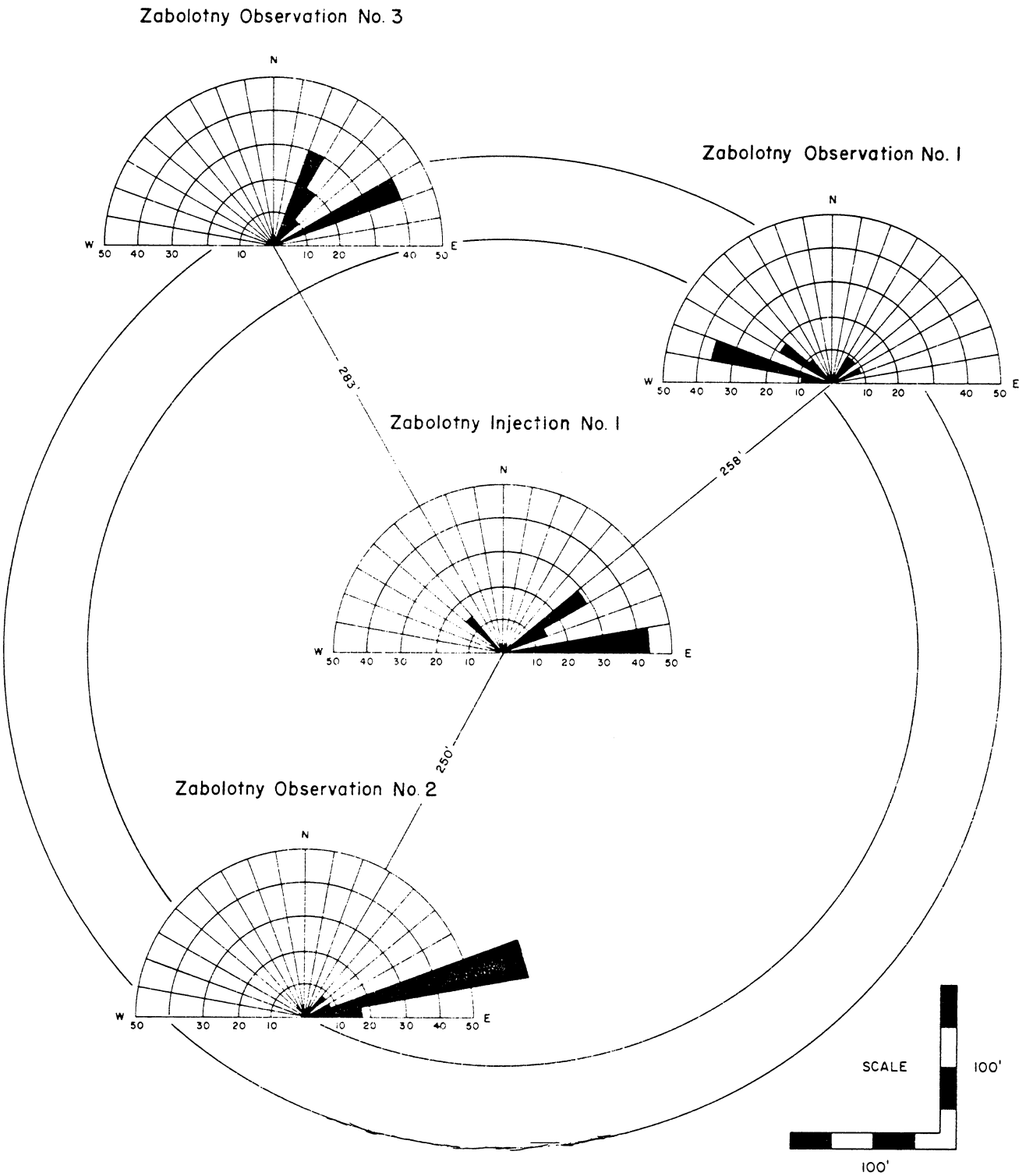

FIGURE 8

LITTLE KNIFE ZABOLOTNY 1-3-4A OIL DIFFERENTIAL FVF AND SOLUTION GAS OIL RATIO AT 245°F

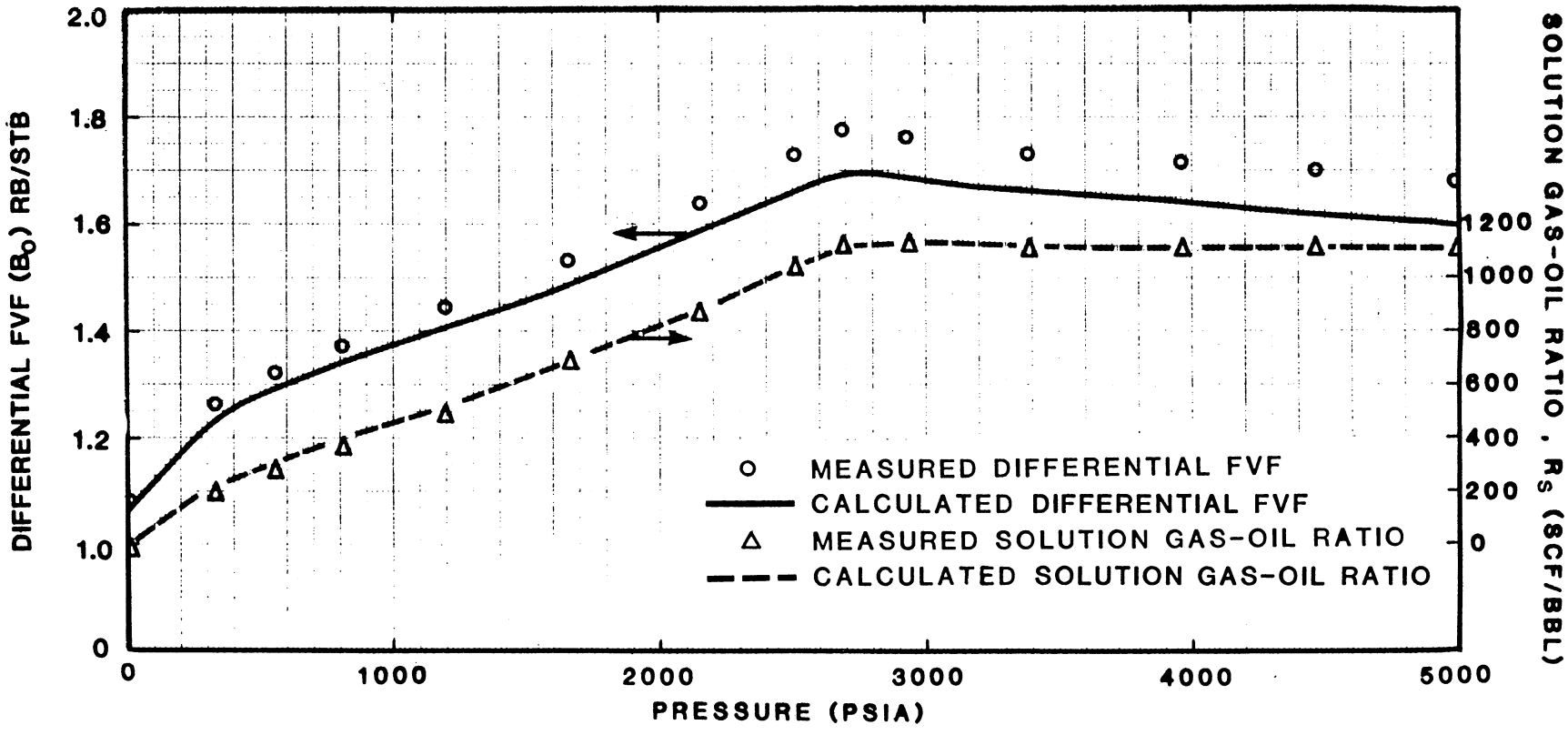

FIGURE 9

LITTLE KNIFE ZABOLOTNY 1-3-4A

OIL DENSITY AND VISCOSITY AT 245° F

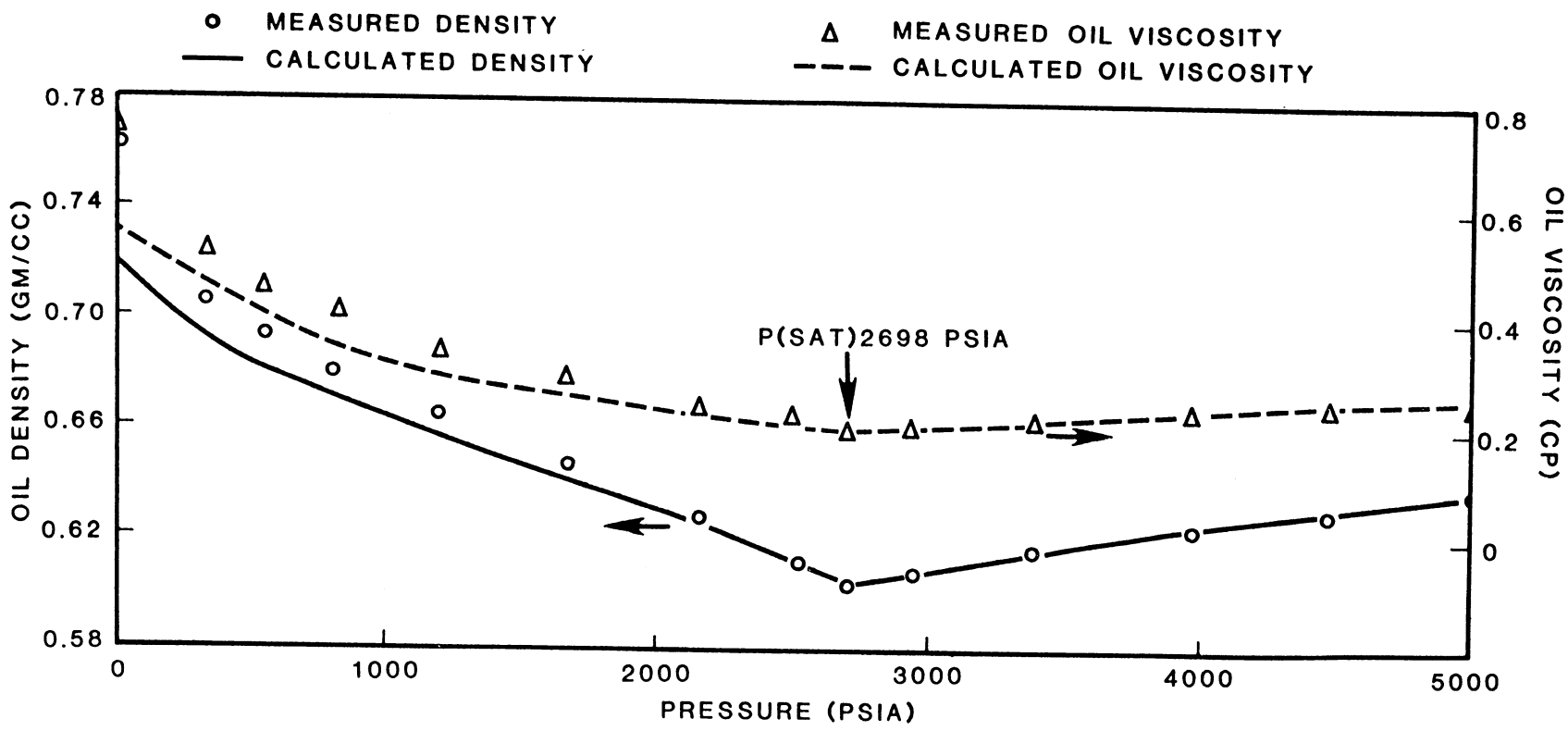

FIGURE 10

LITTLE KNIFE ZABOLOTNY 1-3-4A

PHASE BOUNDARY FOR OIL-CO_2 MIXTURES AT 245°F

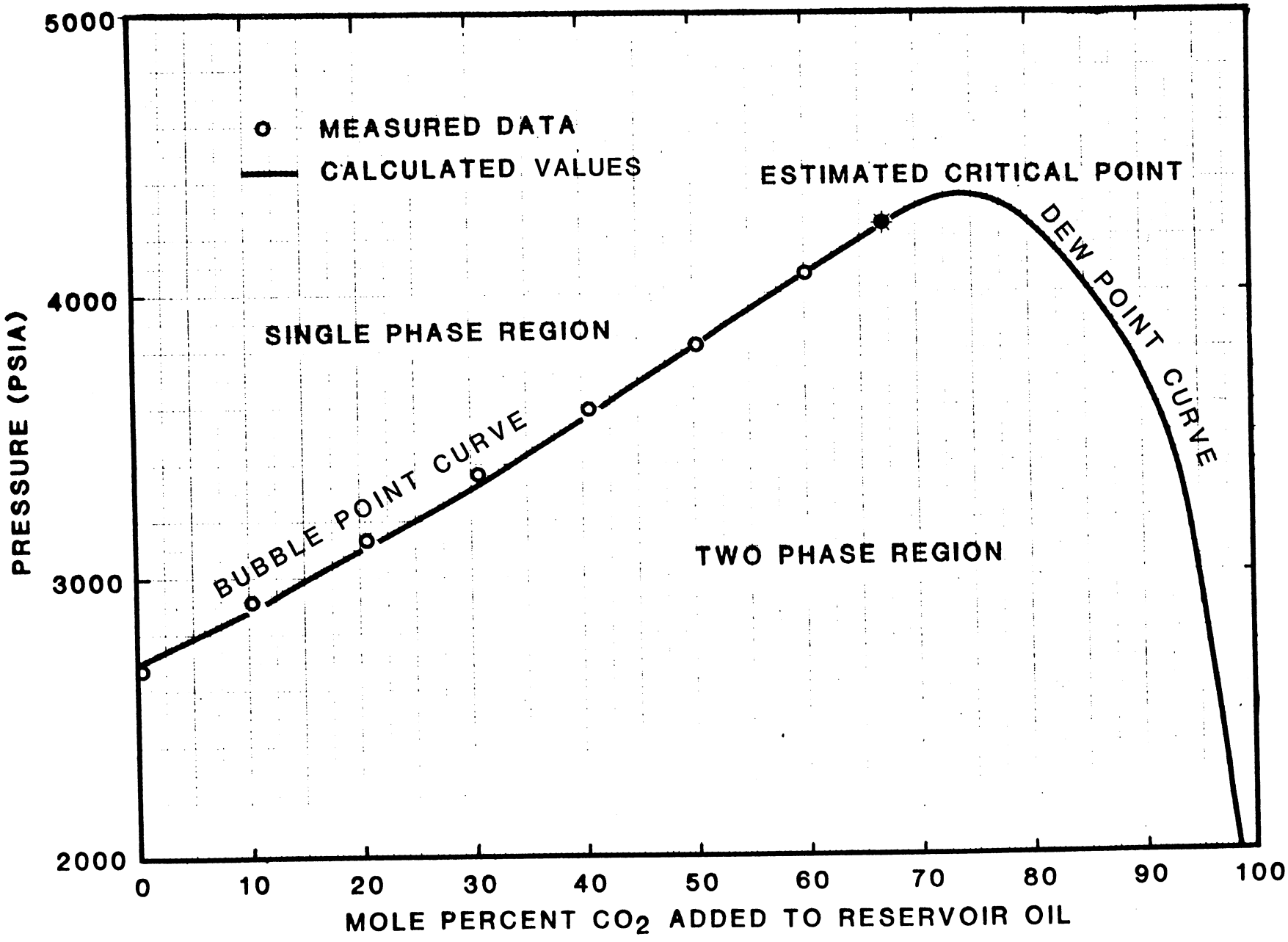

FIGURE 11

LITTLE KNIFE ZABOLOTNY 1-3-4A

PRESSURE VOLUME RELATIONSHIP AT 245°F

FOR OIL-CO_2 MIXTURES

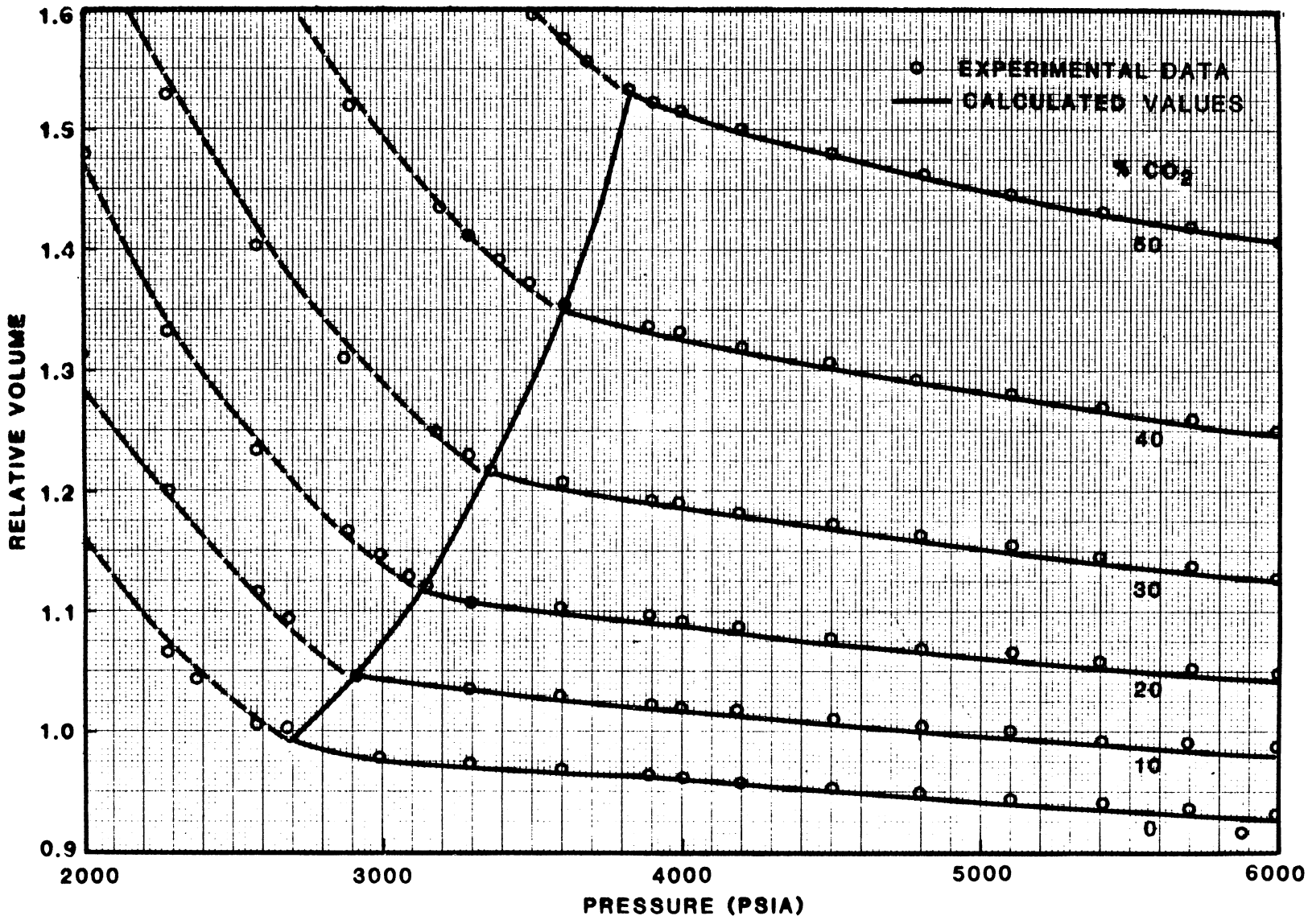

FIGURE 12
LITTLE KNIFE ZABOLOTNY 1-3-4A
VISCOSITY OF OIL-CO_2 MIXTURES AT 245°F (RECOMBINED SAMPLE)

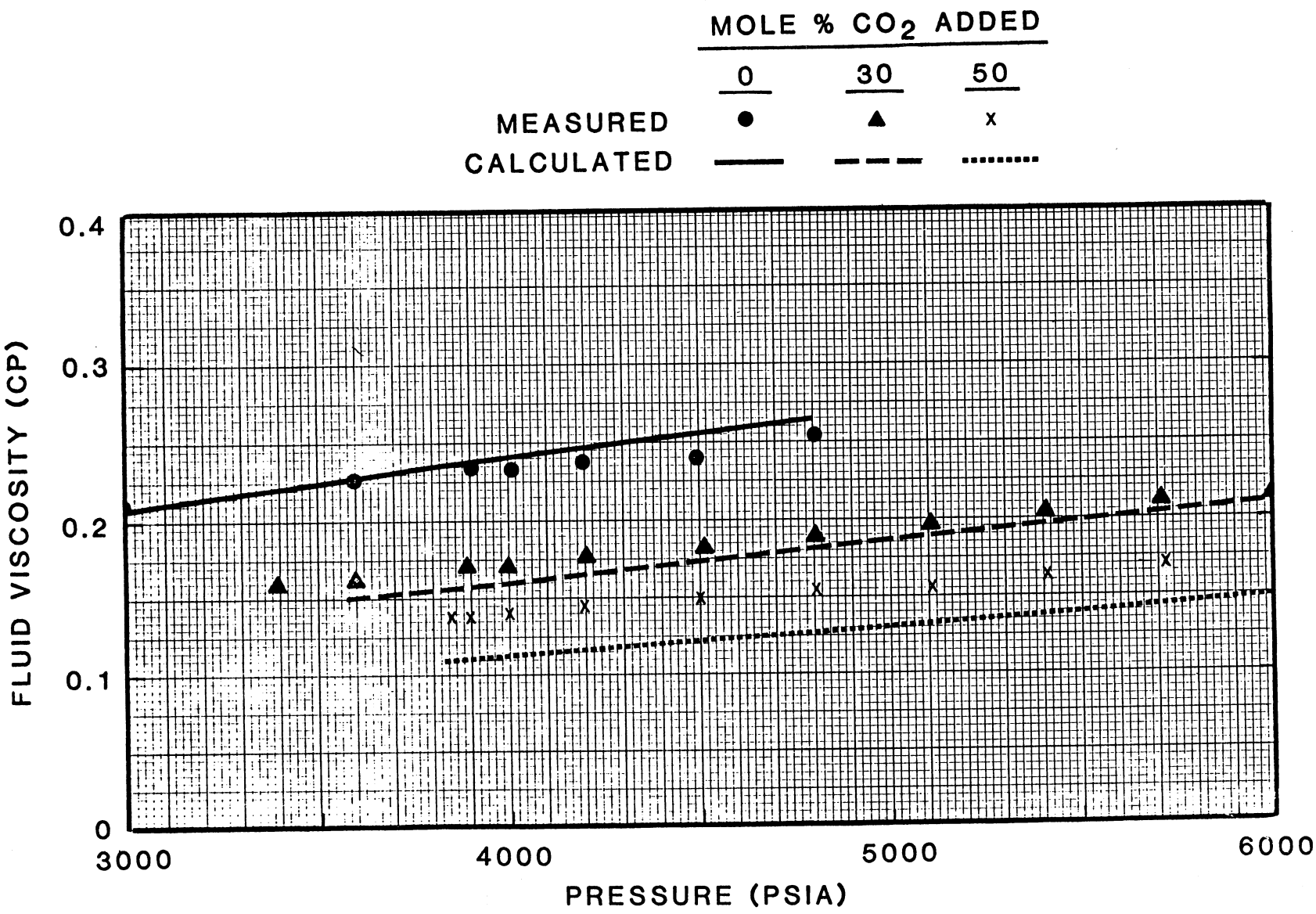

FIGURE 13

LITTLE KNIFE ZABOLOTNY 1-3-4A

DENSITY OF OIL - CO_2 MIXTURES AT 245° F

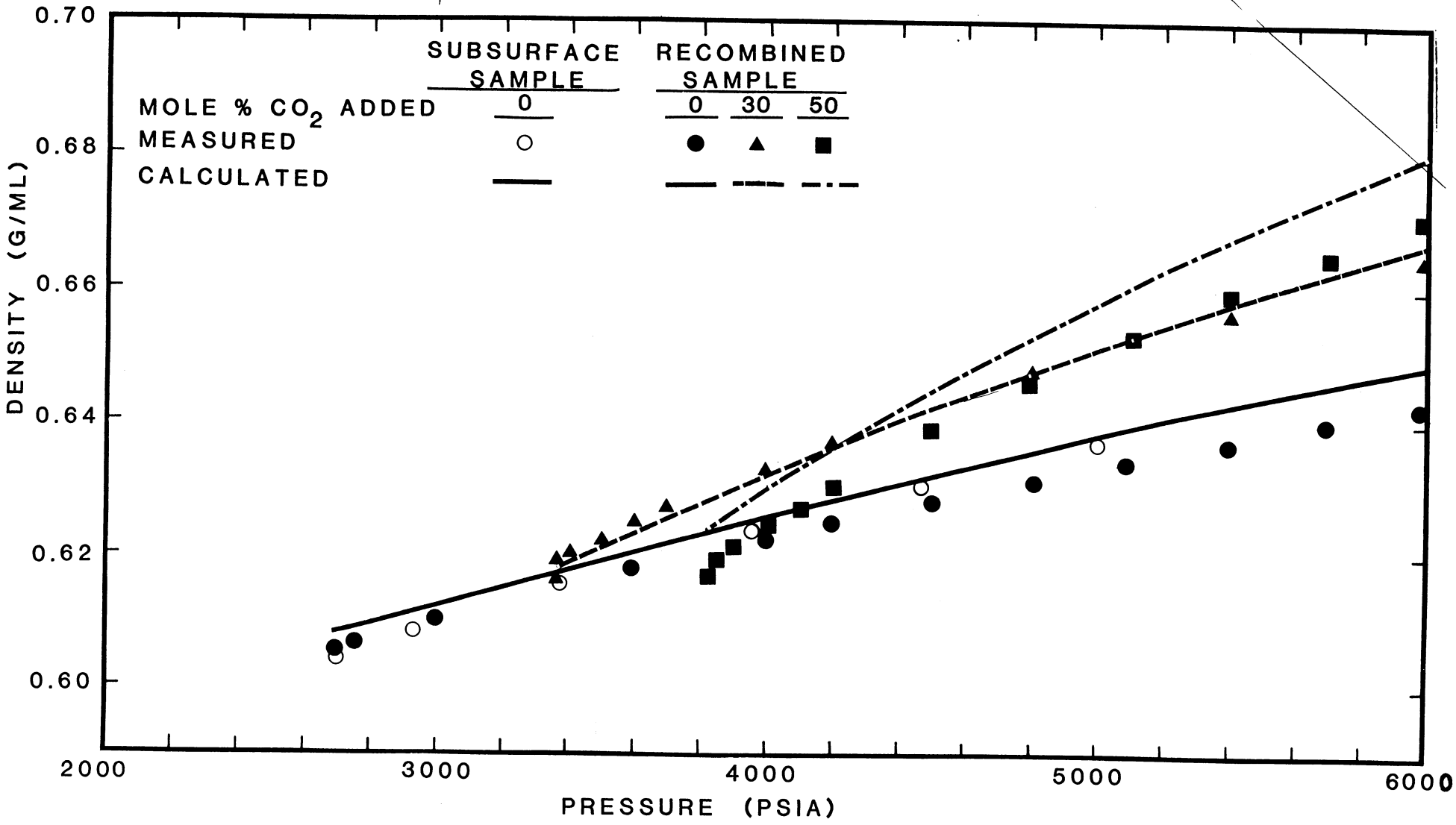

FIGURE 14

LITTLE KNIFE ZABOLOTNY 1-3-4A

COEFFICIENTS OF COMPRESSIBILITY OF RESERVOIR OIL WITH CO_2 ADDED AT 245°F

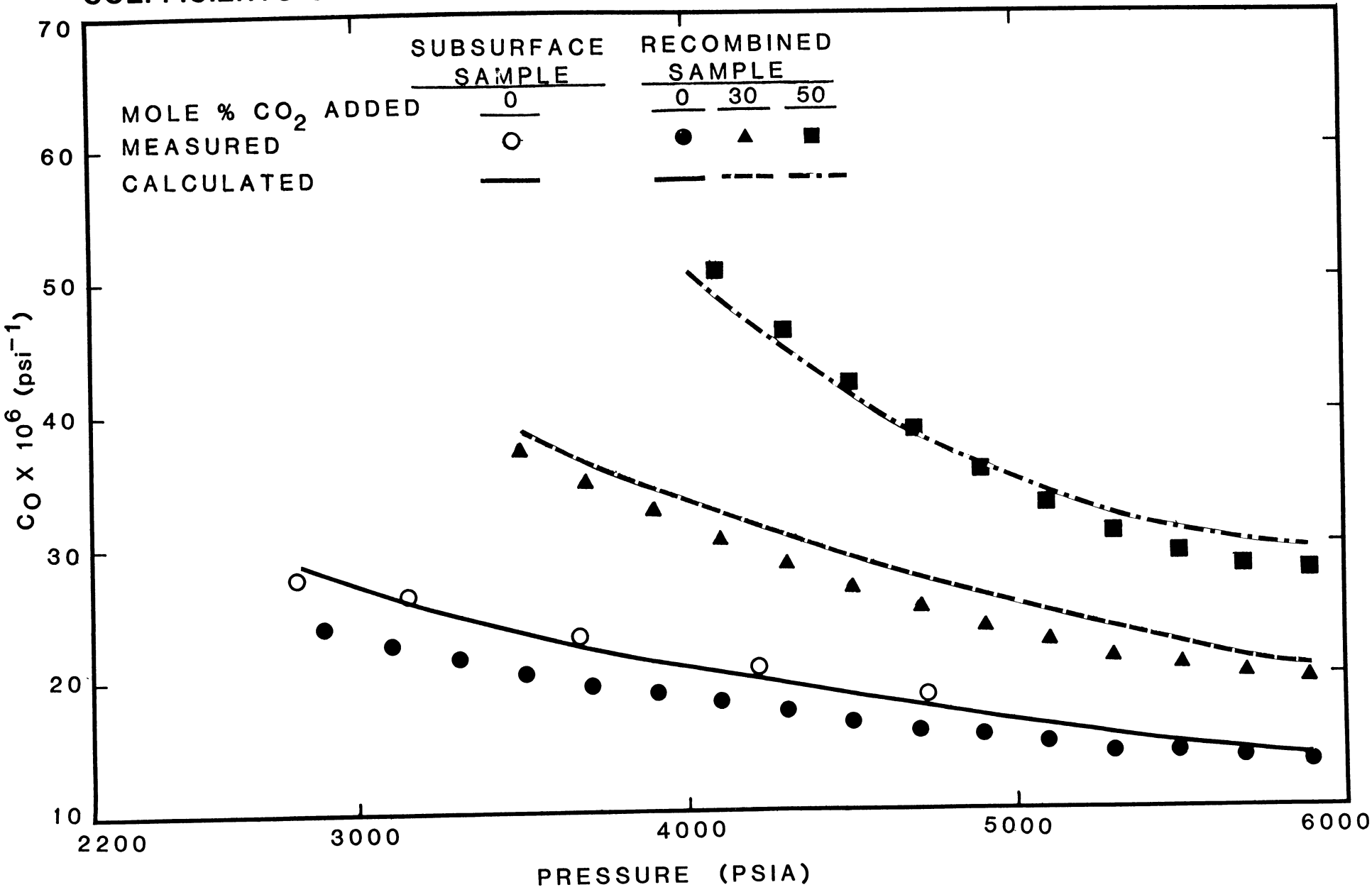

FIGURE 15

OIL RECOVERY VS. AVERAGE SYSTEM PRESSURE AT 240°F FROM THE SLIM TUBE TEST

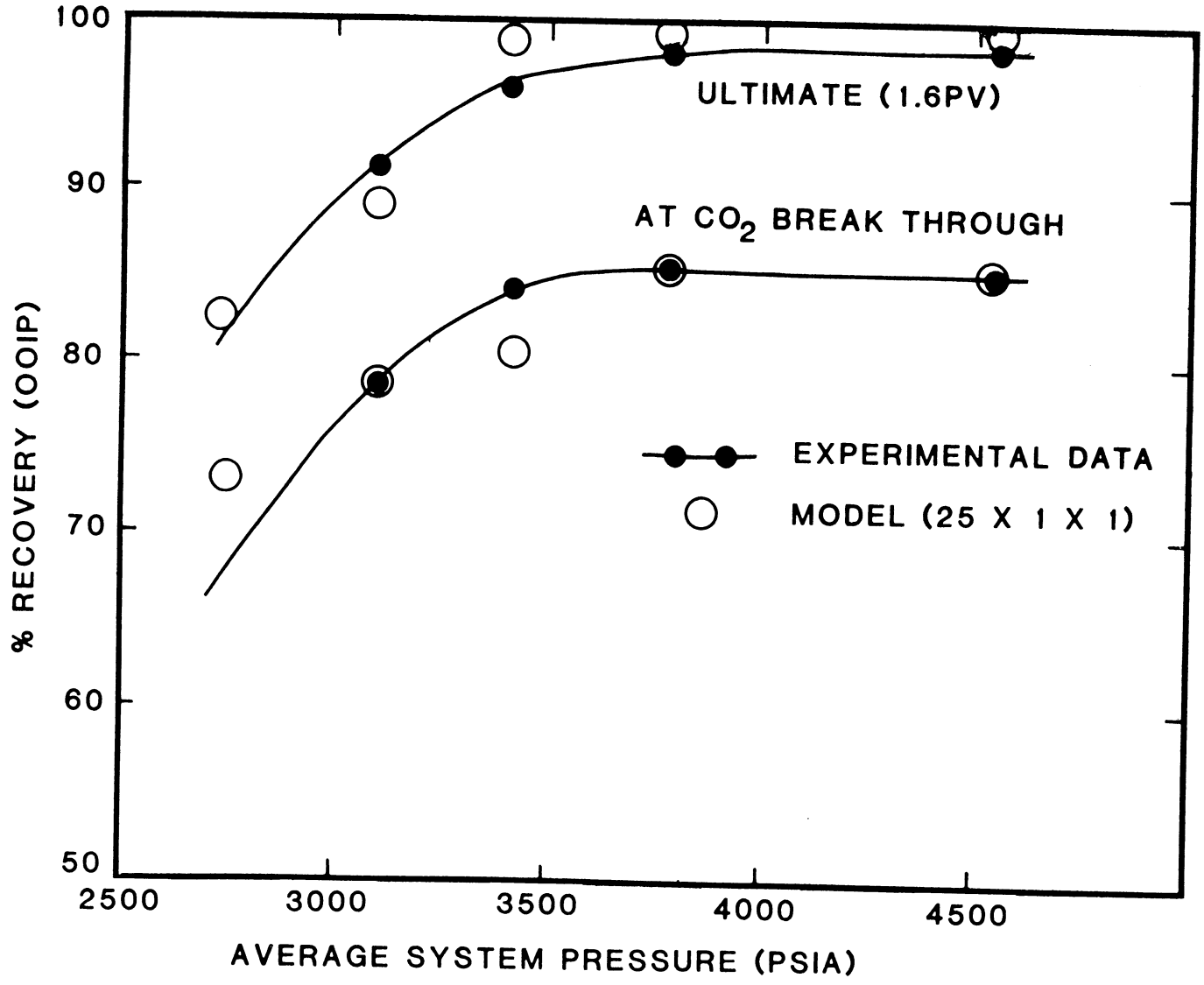

FIGURE 16

OIL RECOVERY VS. CO_2 PORE VOLUMES INJECTED FROM THE SLIM TUBE TEST AT 240° F AND 3400 PSIG

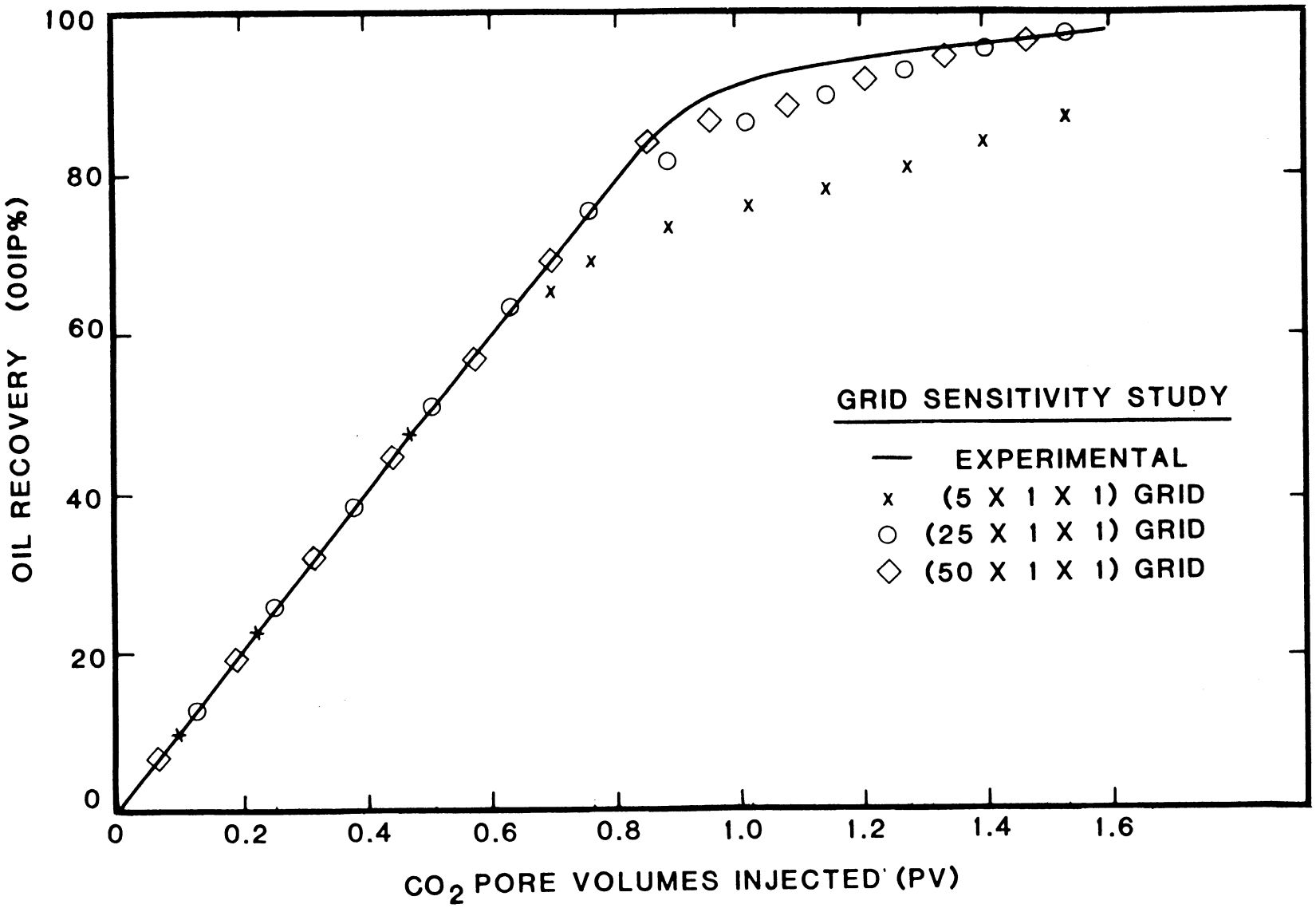

FIGURE 17

K-VALUES VS. PRESSURE AT 245°F FOR LITTLE KNIFE RESERVOIR FLUID

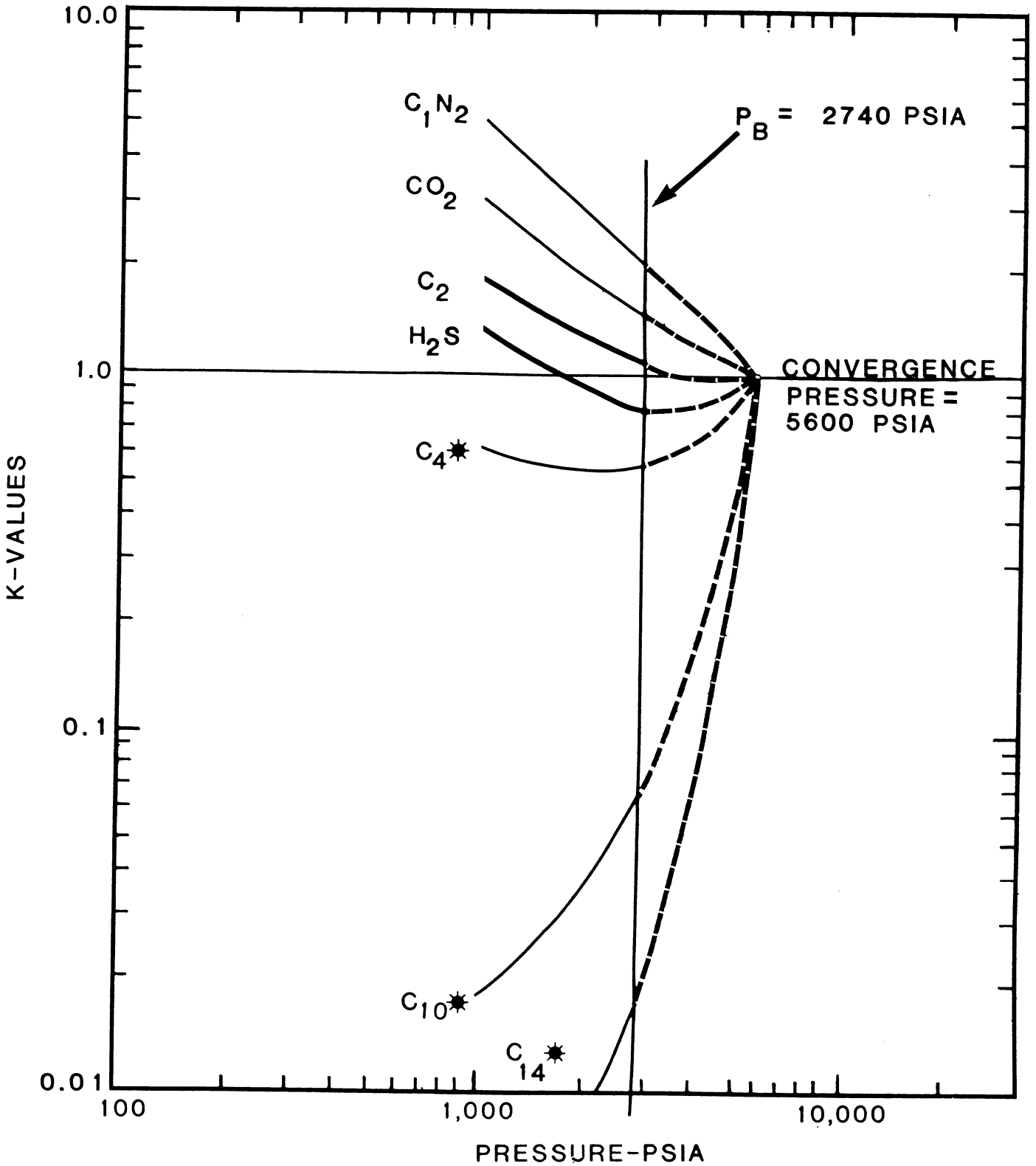

FIGURE 18

K-VALUES VS. PRESSURE AT 245°F FOR CO_2 COMPOSITION OF 0.500 MOLE FRACTION

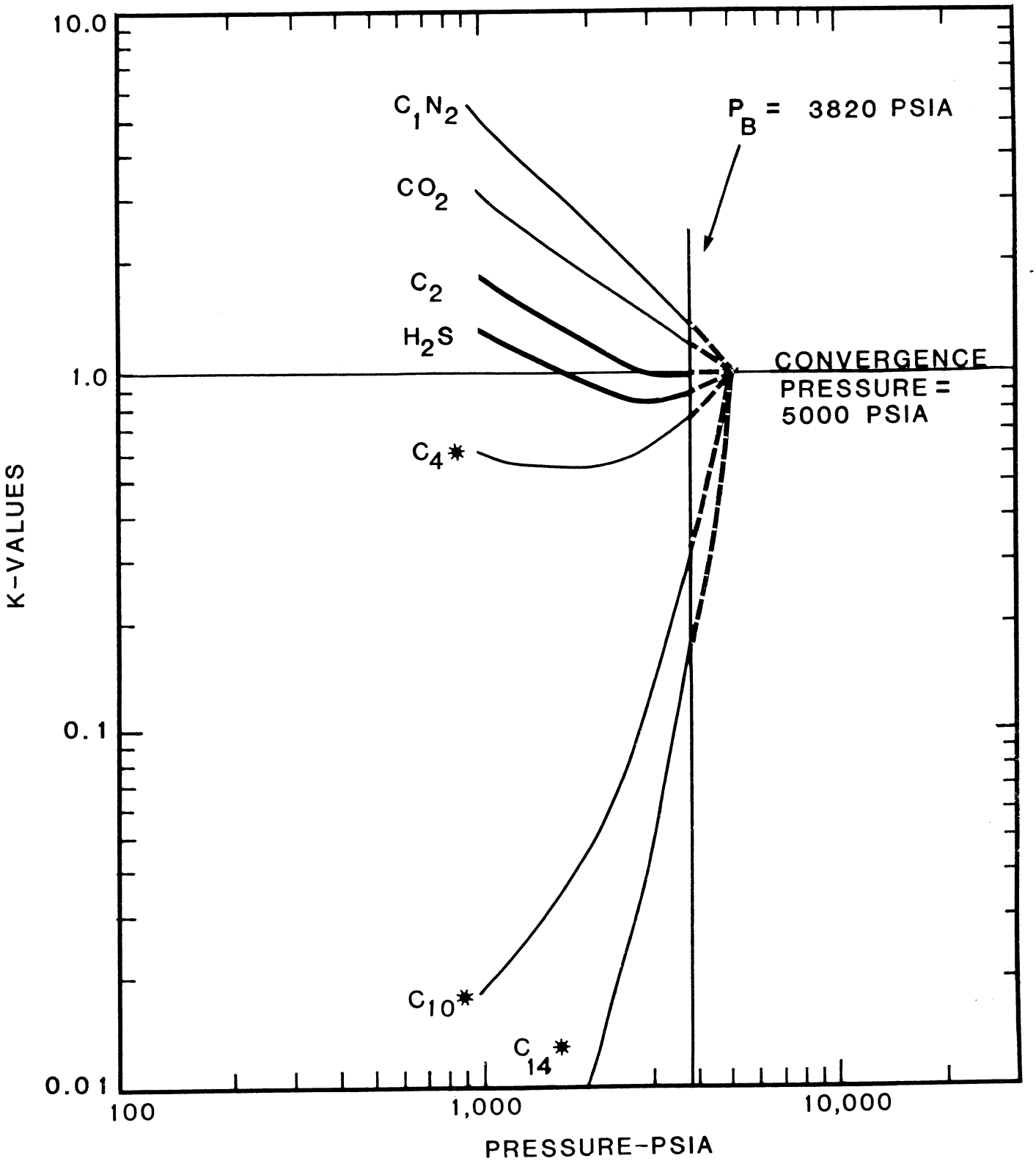

FIGURE 19

K-VALUES VS. PRESSURE AT 245°F FOR CO_2 COMPOSITION OF 0.900 MOLE FRACTION

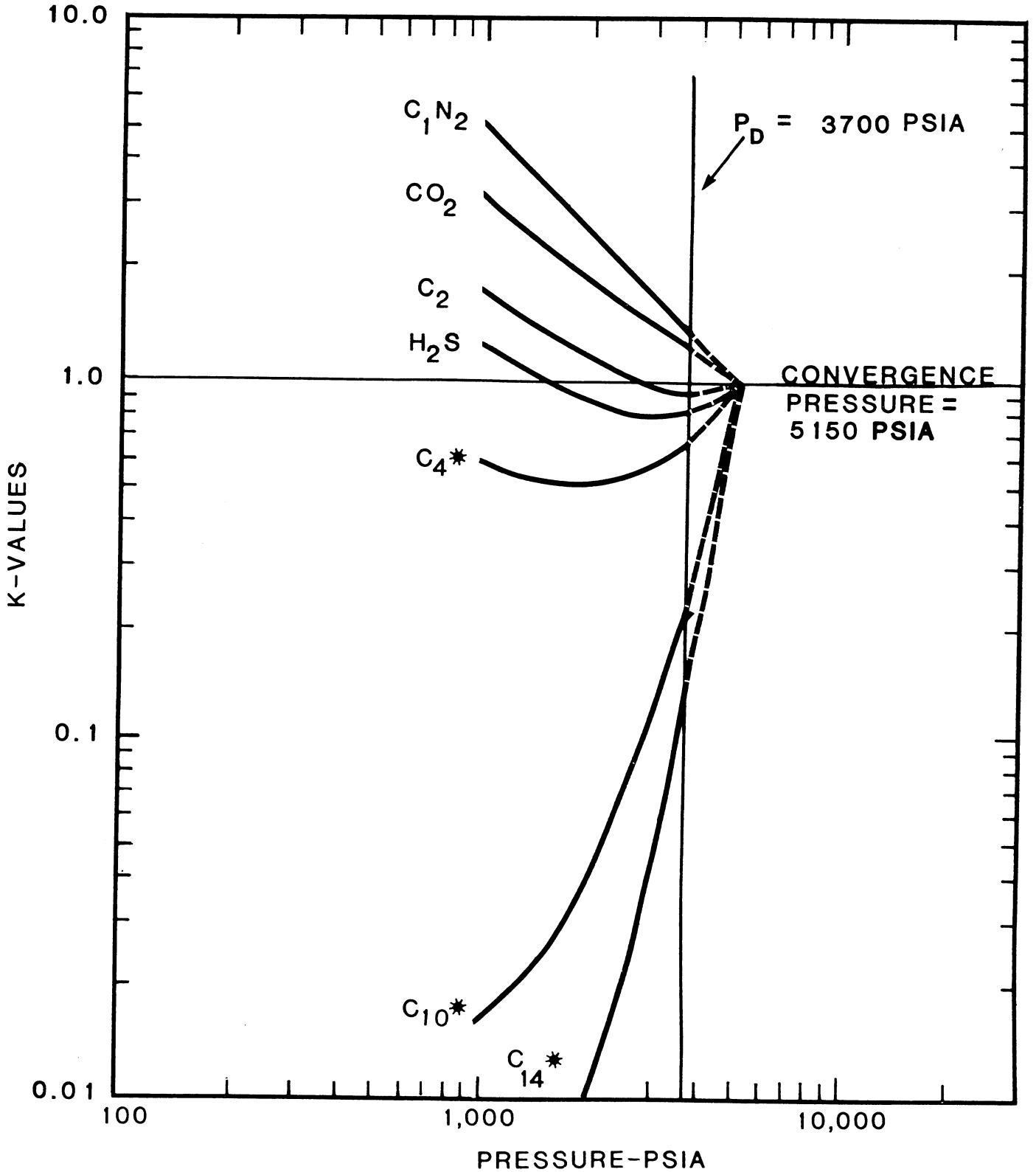

FIGURE 20

RELATIVE PERMEABILITY DATA FOR LAYER W

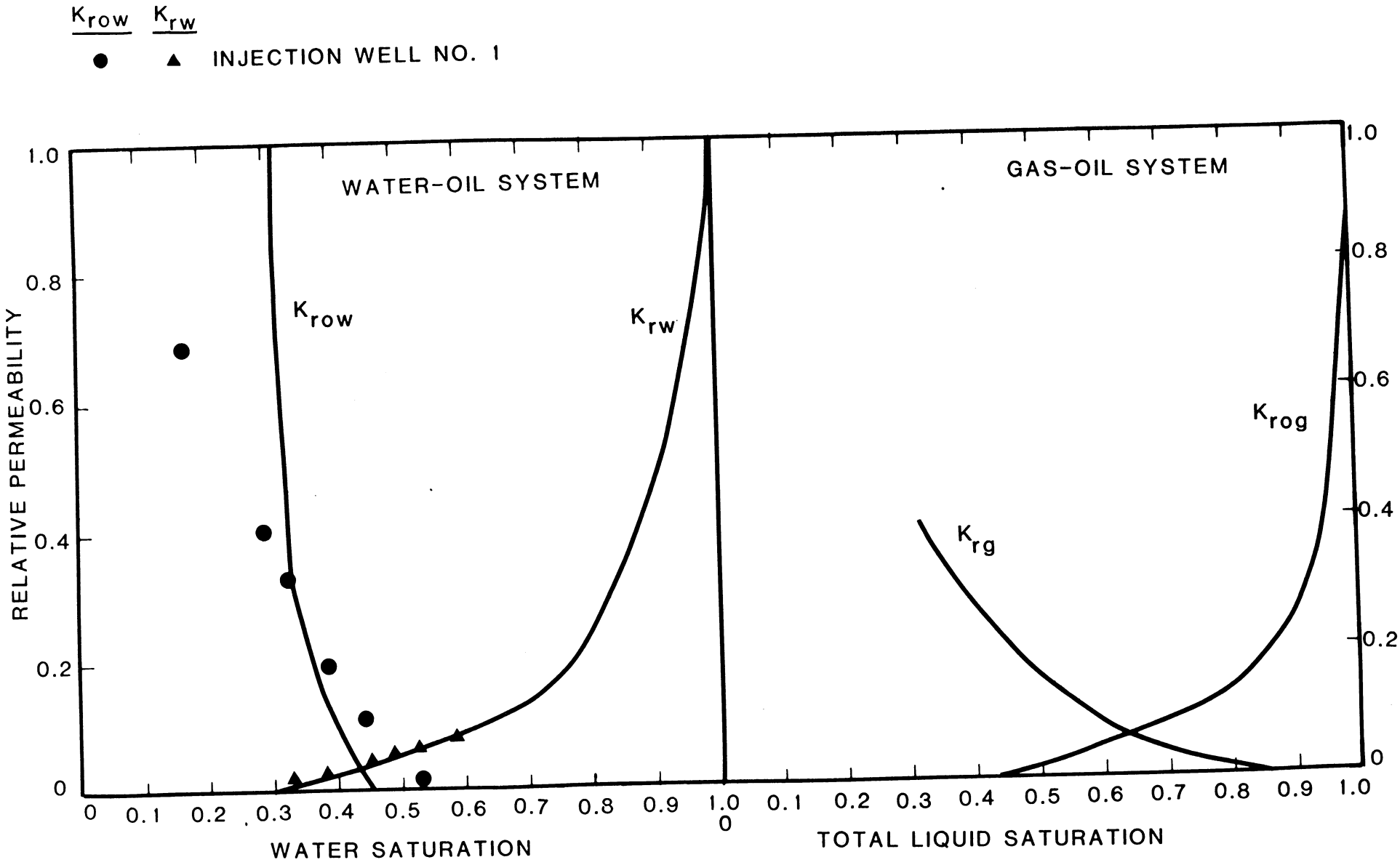

FIGURE 21

RELATIVE PERMEABILITY DATA FOR LAYER X

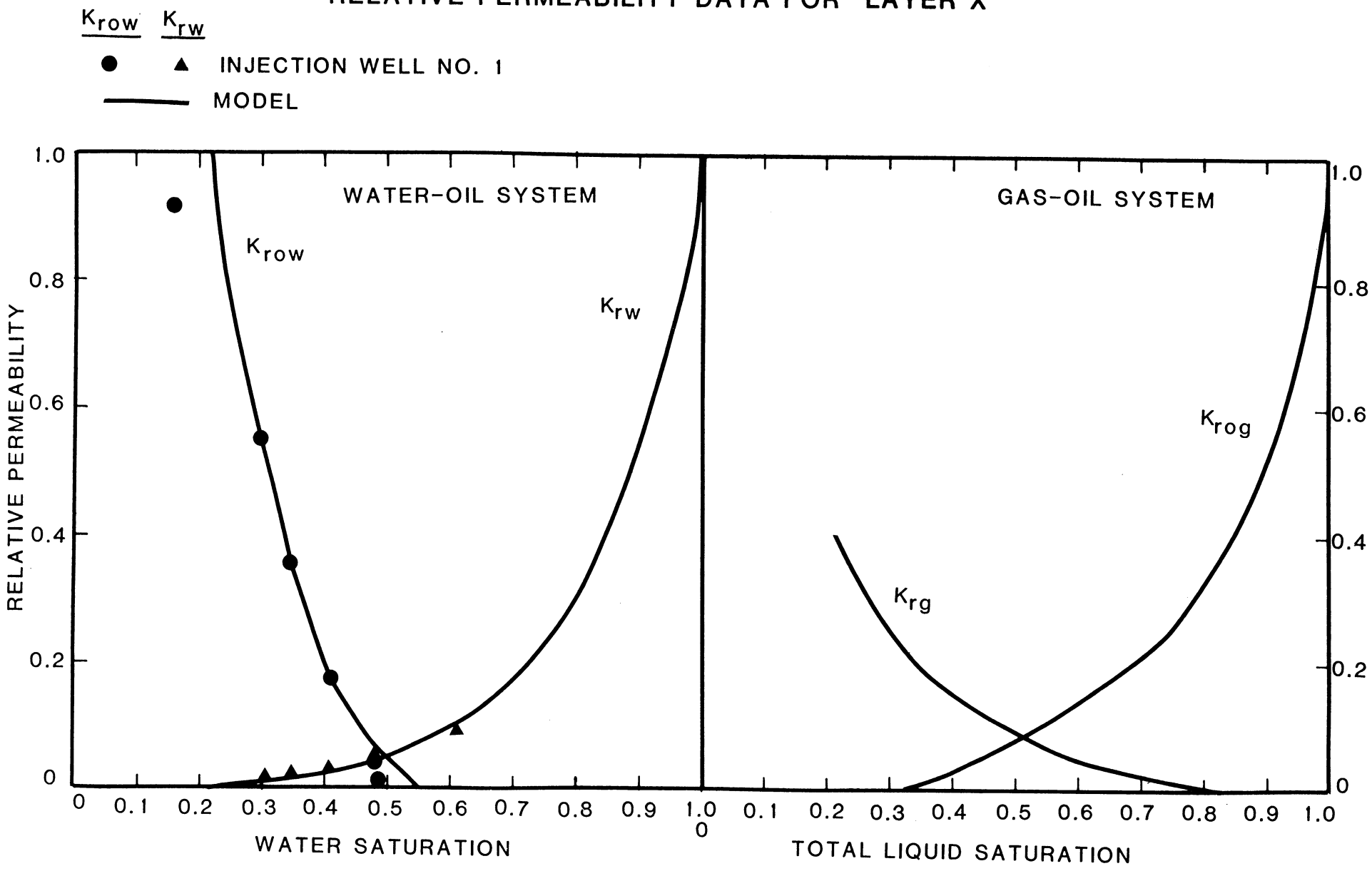

FIGURE 22

RELATIVE PERMEABILITY DATA FOR LAYER Y

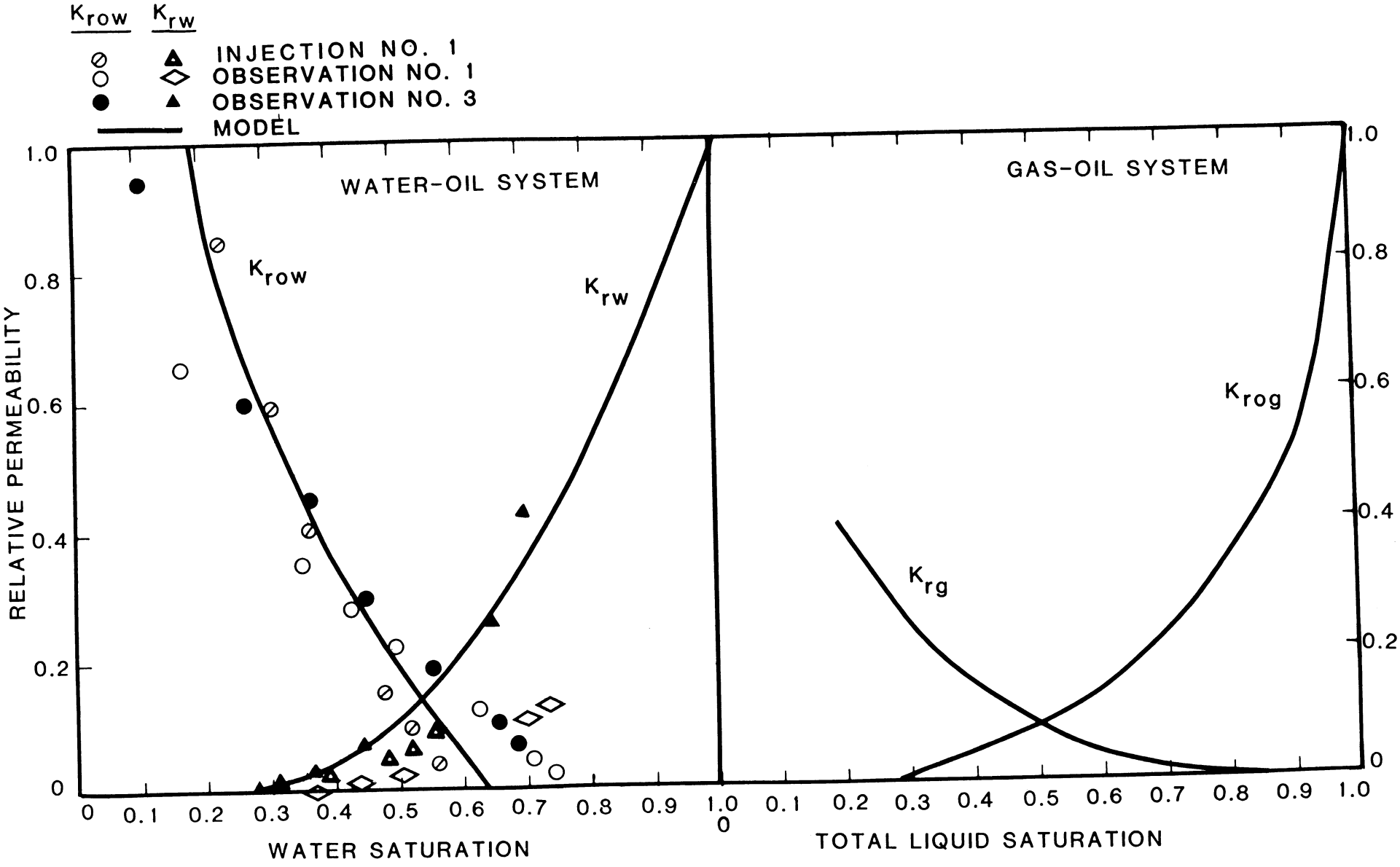

FIGURE 23

RELATIVE PERMEABILITY DATA FOR LAYER Z

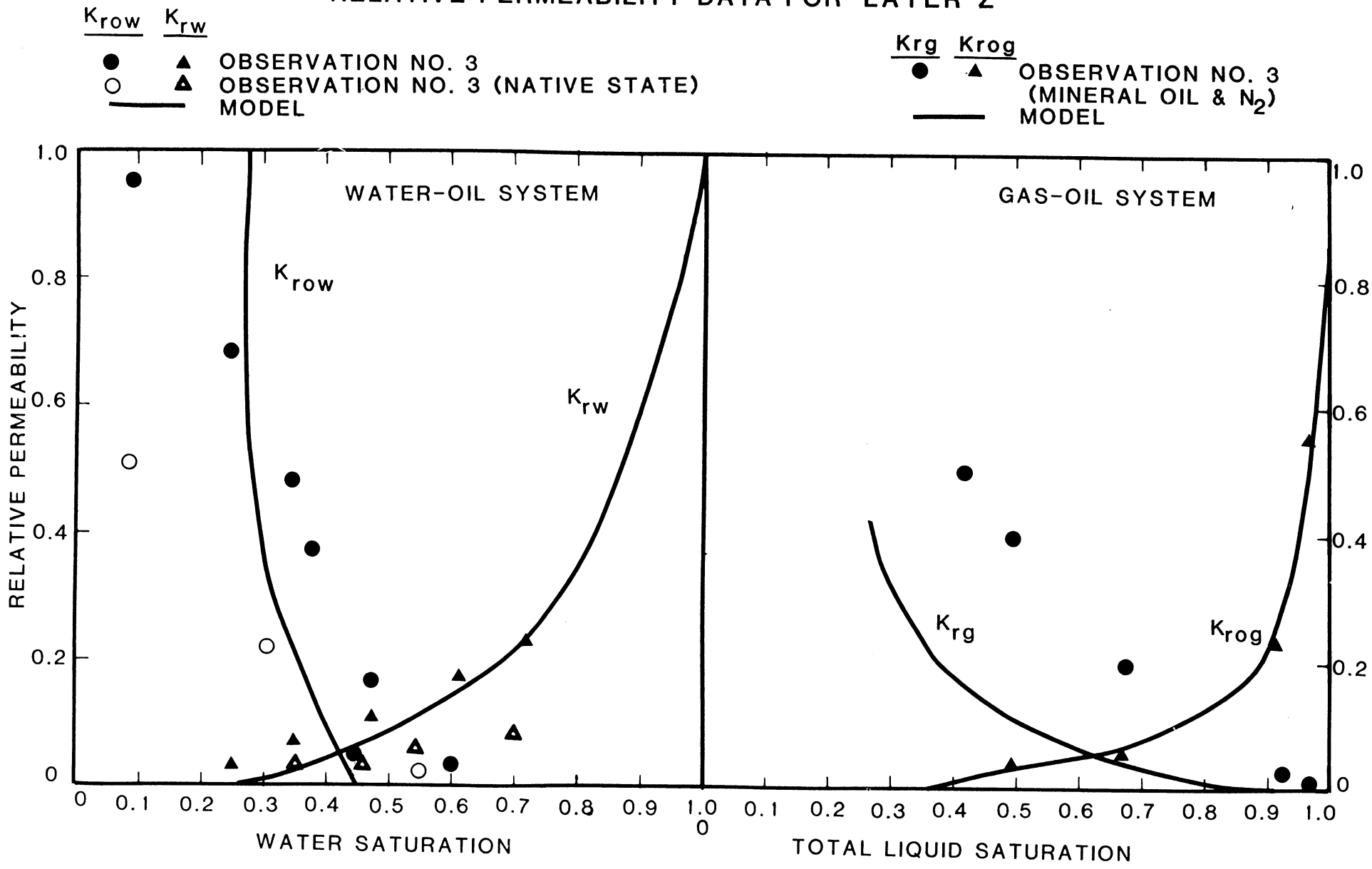

FIGURE 24

CO_2 - WATER RELATIVE PERMEABILITY DATA WITH & WITHOUT RESIDUAL OIL SATURATION

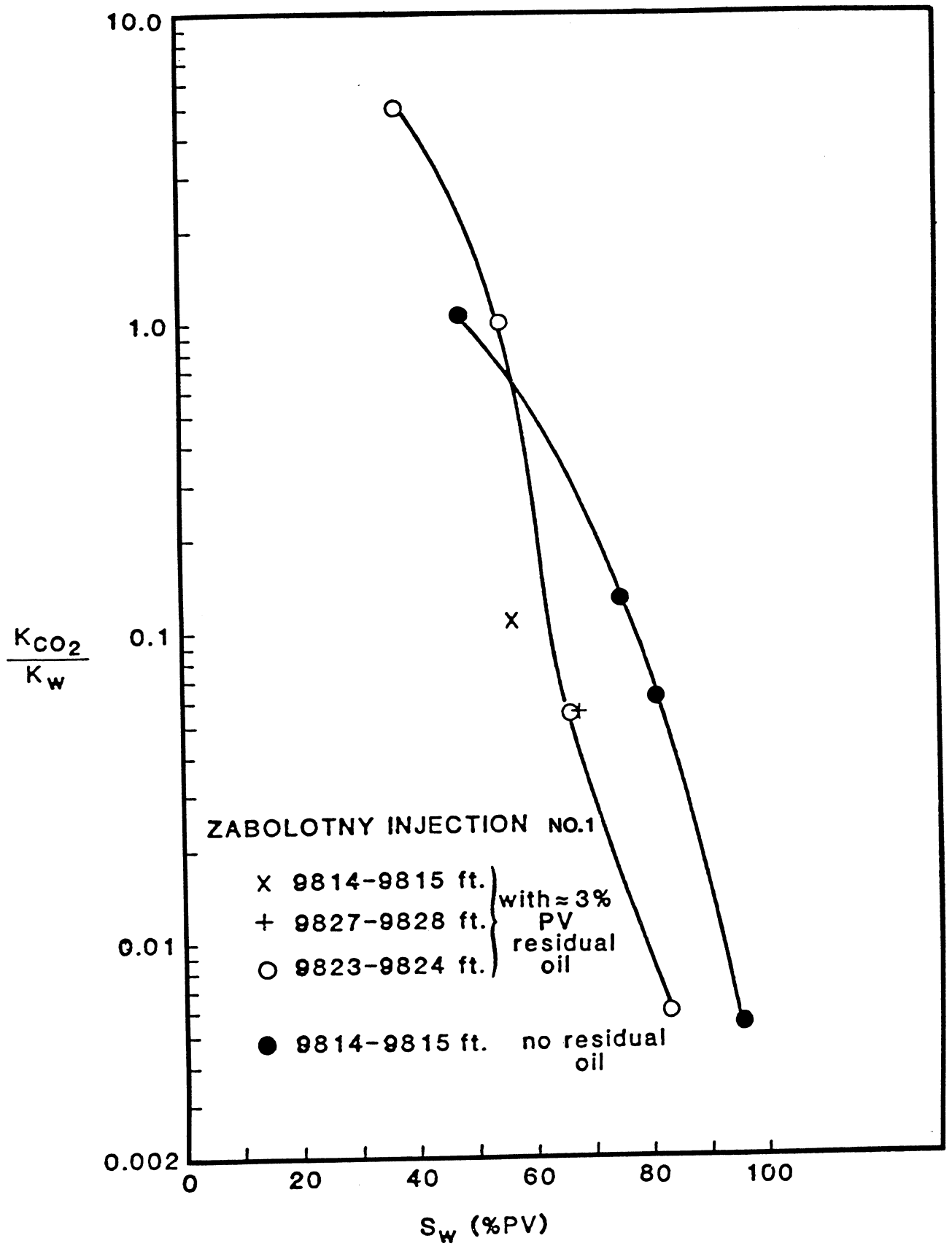

FIGURE 25

PRESSURE HISTORY IN THE MINITEST AREA

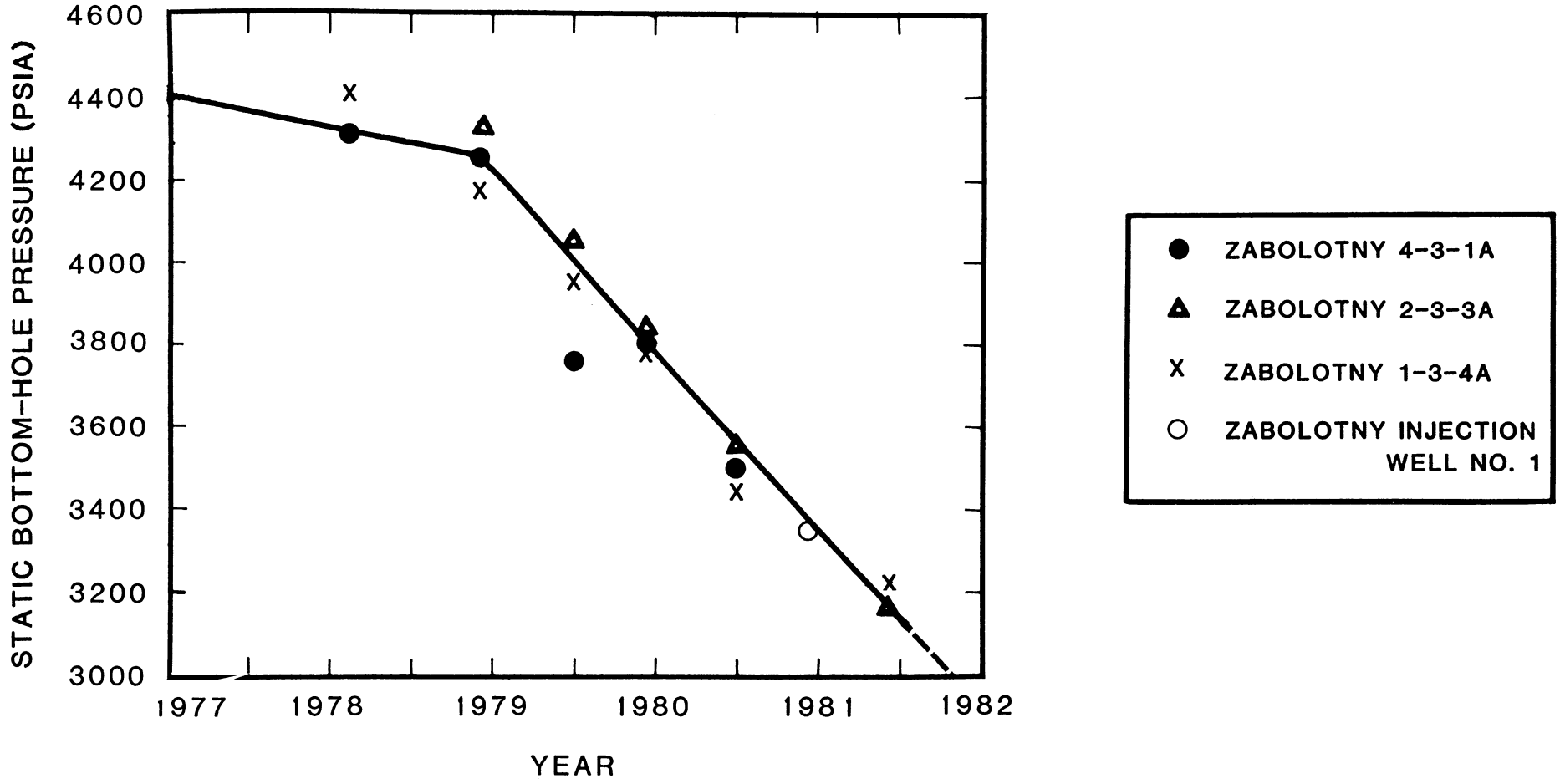

FIGURE 26

SURFACE AND RESERVOIR LOCATIONS OF LITTLE KNIFE CO_2 MINITEST WELLS

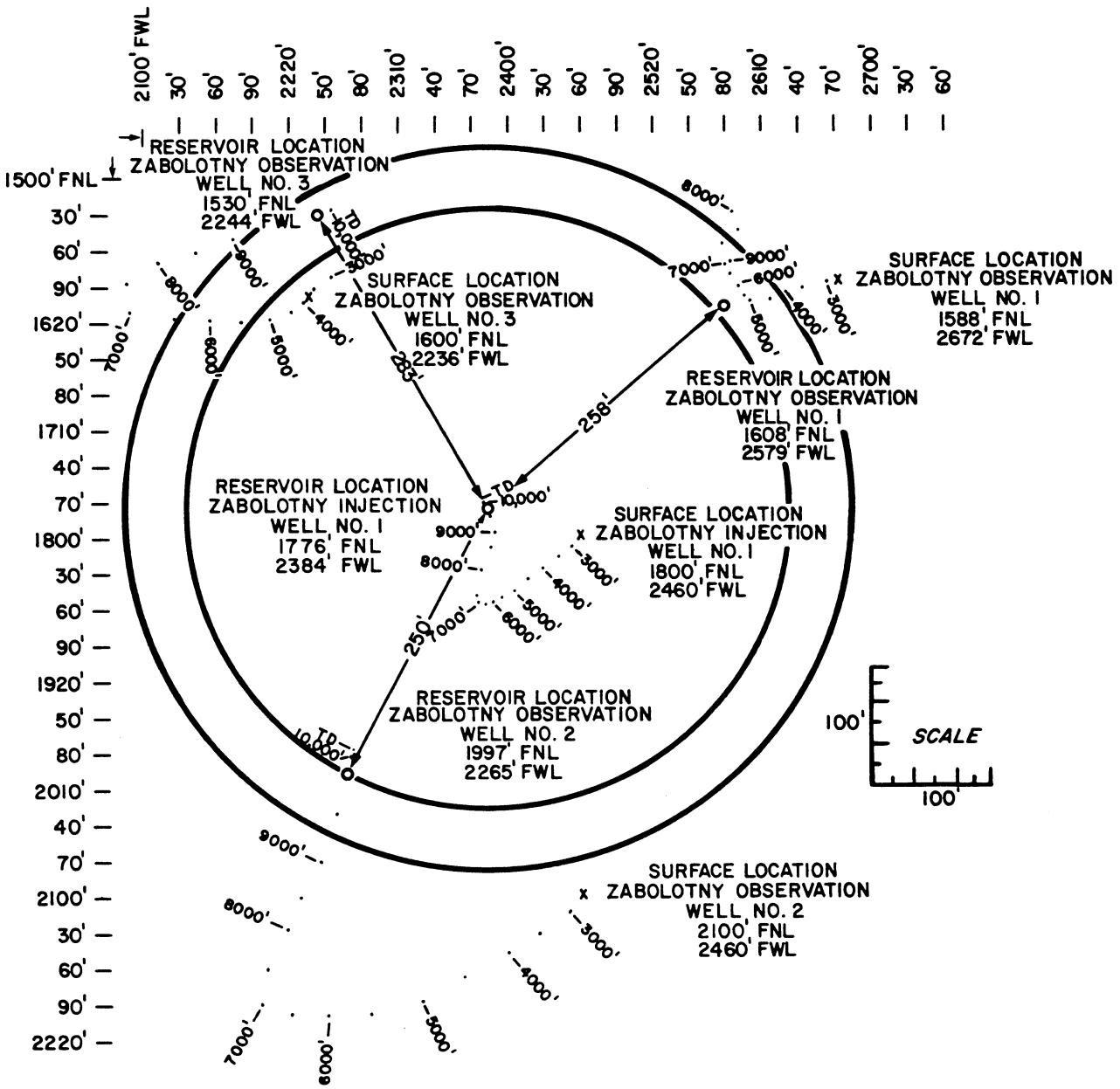

FIGURE 27

DOWN HOLE ASSEMBLY
ZABOLOTNY INJECTION #1
TUBING SETTING

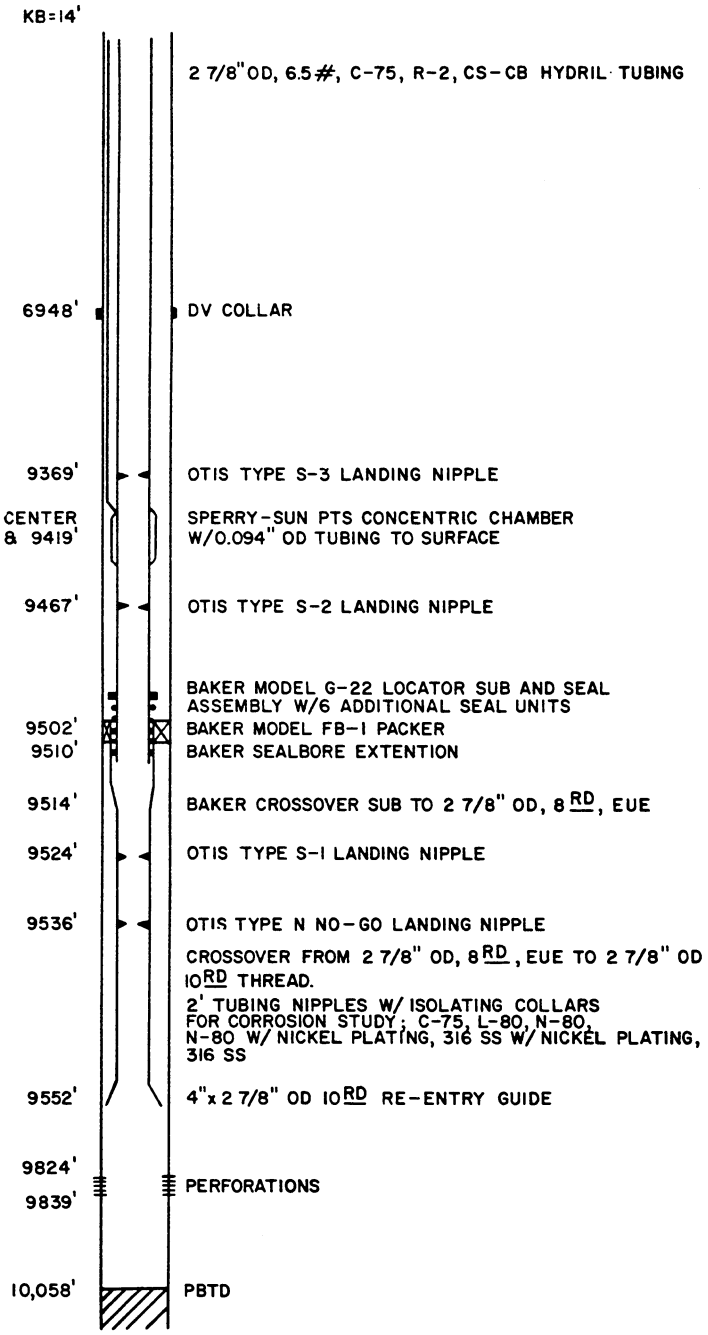

FIGURE 28
DOWNHOLE ASSEMBLY
ZABOLOTNY OBSERVATION # 1
TUBING SETTING

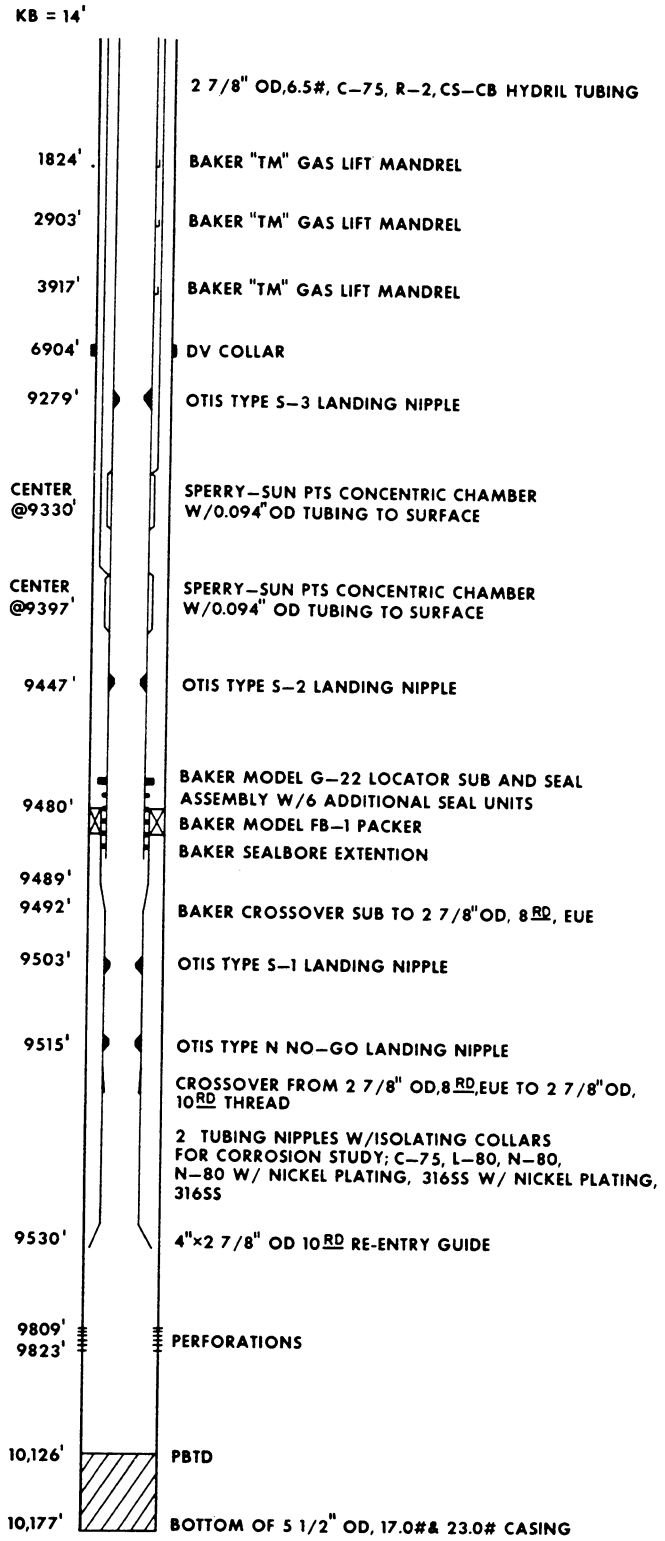

FIGURE 29

FOUR-WELL PULSE TEST RESPONSE AT OBSERVATION NO. 1

NOVEMBER 15, 1980

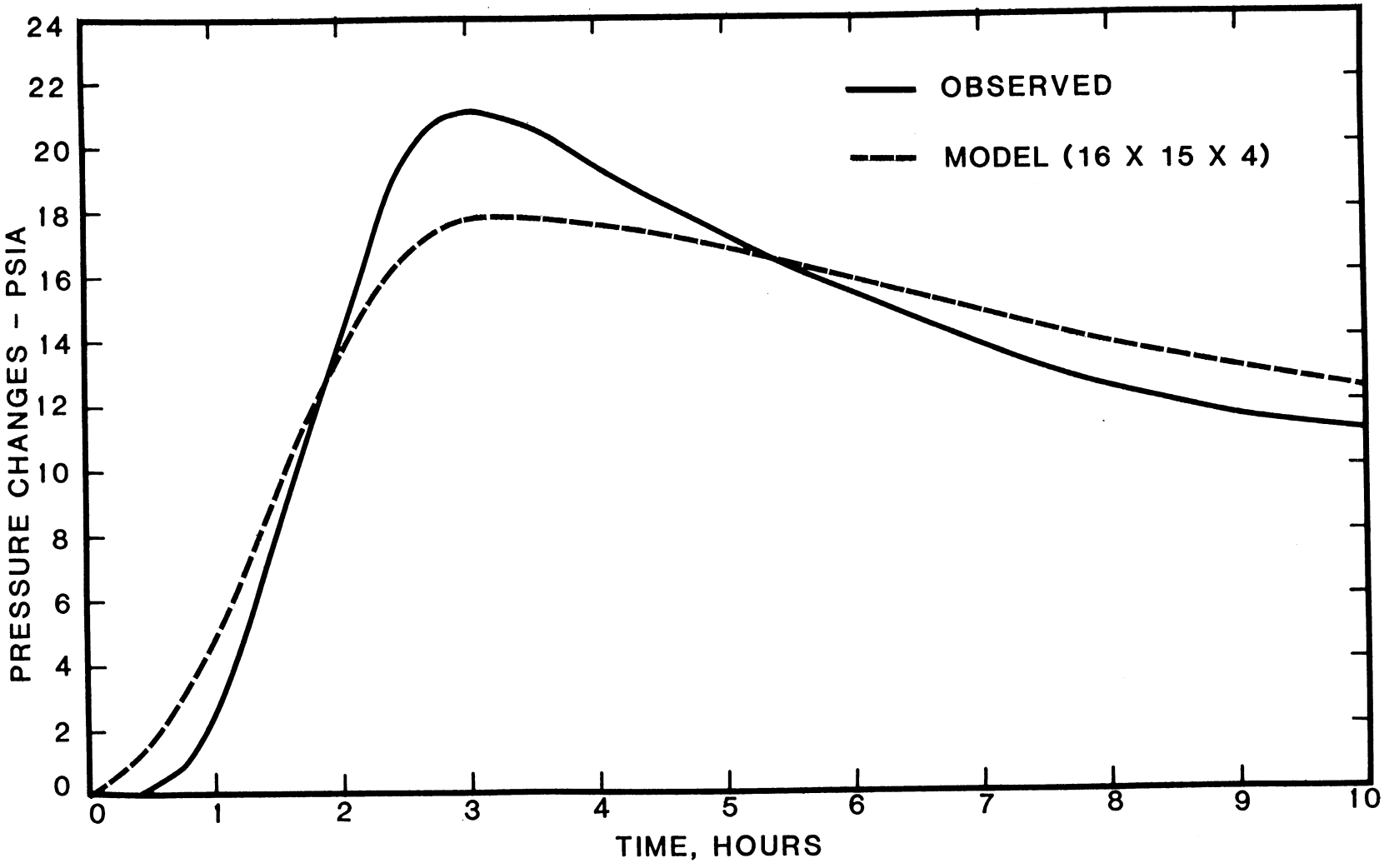

FIGURE 30

FOUR-WELL PULSE TEST RESPONSE AT OBSERVATION NO. 2

NOVEMBER 15, 1980

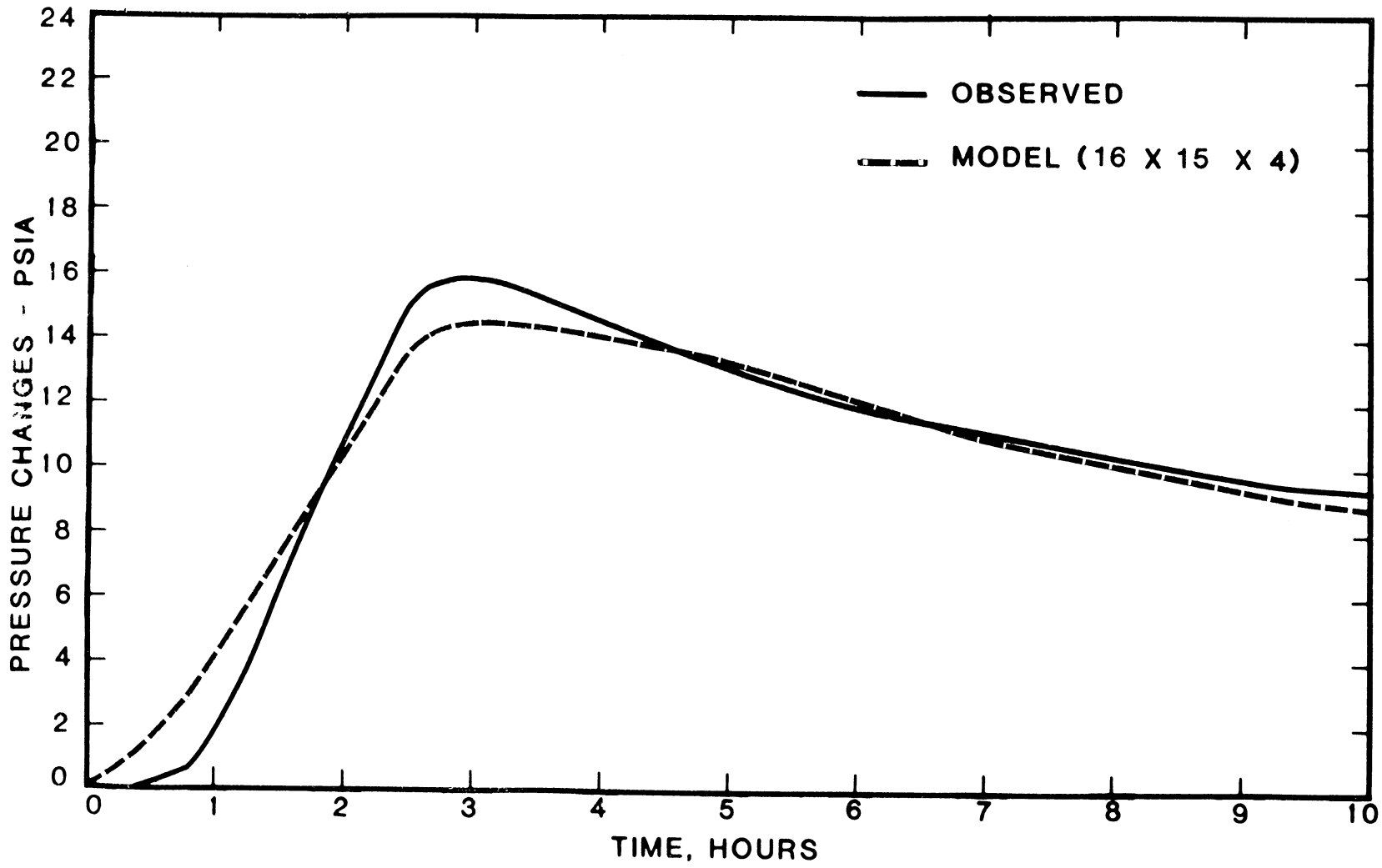

FIGURE 31

FOUR-WELL PULSE TEST RESPONSE AT OBSERVATION NO. 3

NOVEMBER 15, 1980

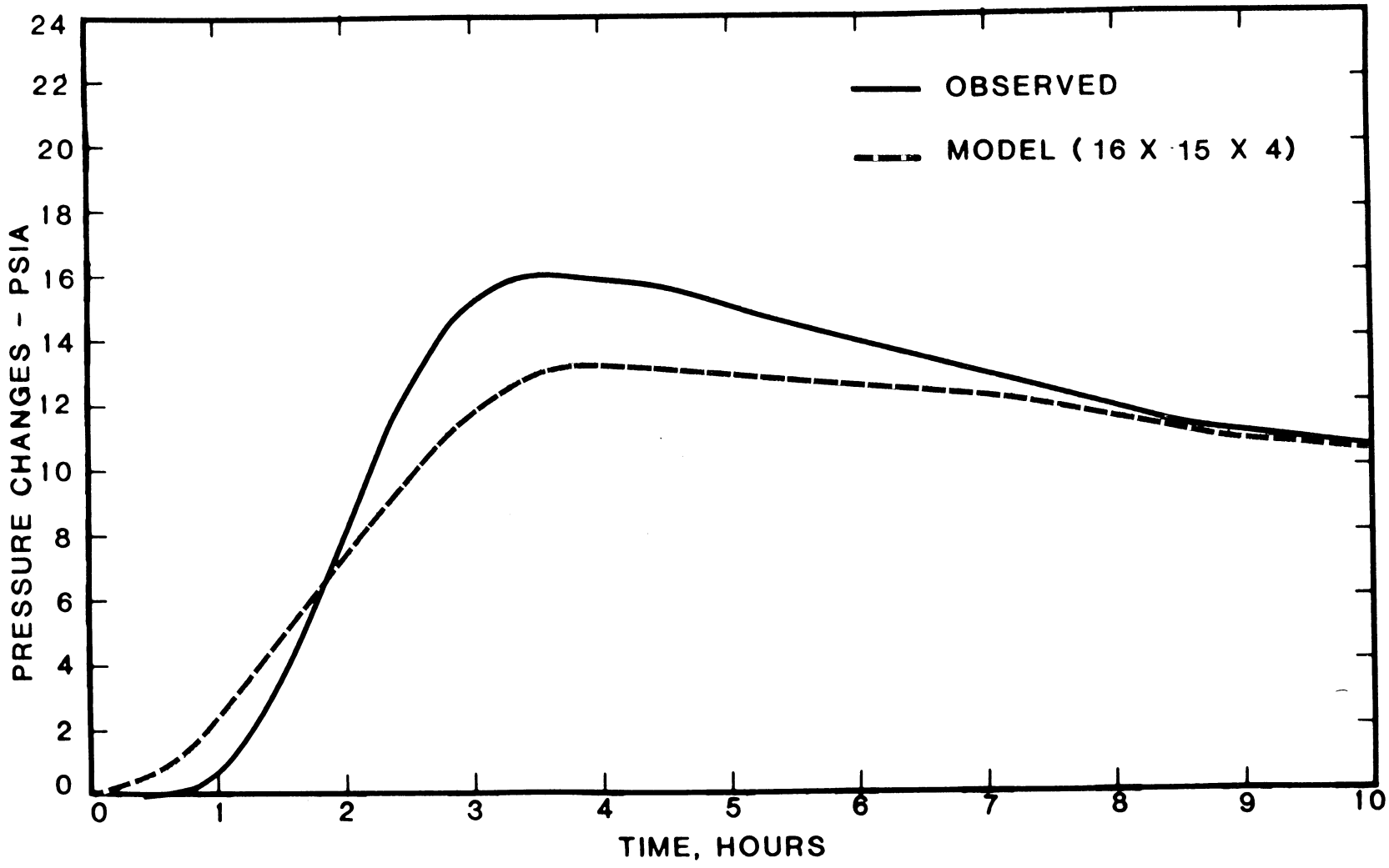

FIGURE 32

COORDINATE SYSTEM FOR THE COMPOSITIONAL SIMULATION

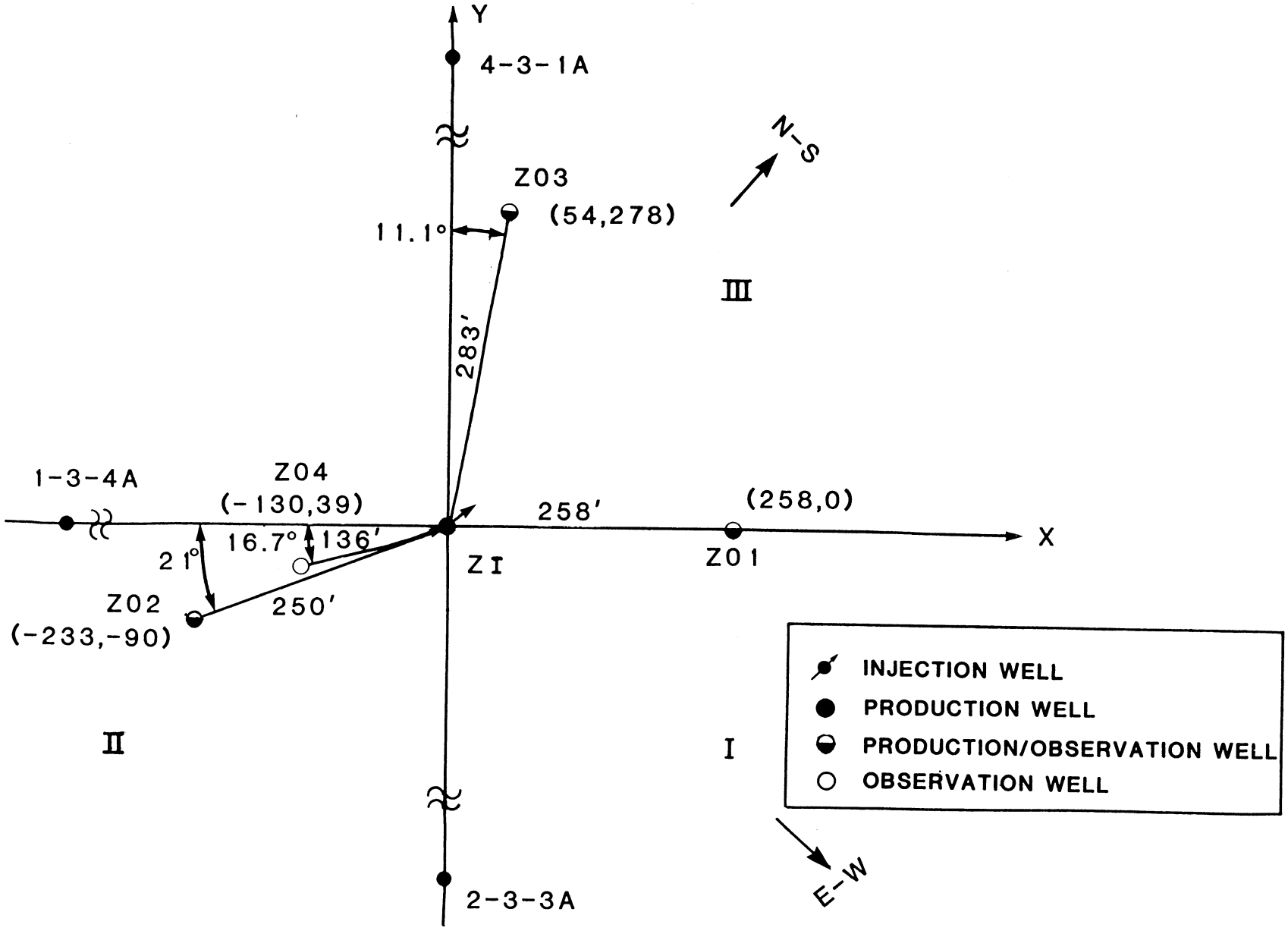

FIGURE 33

11 X 11 X 4 GRID SYSTEM

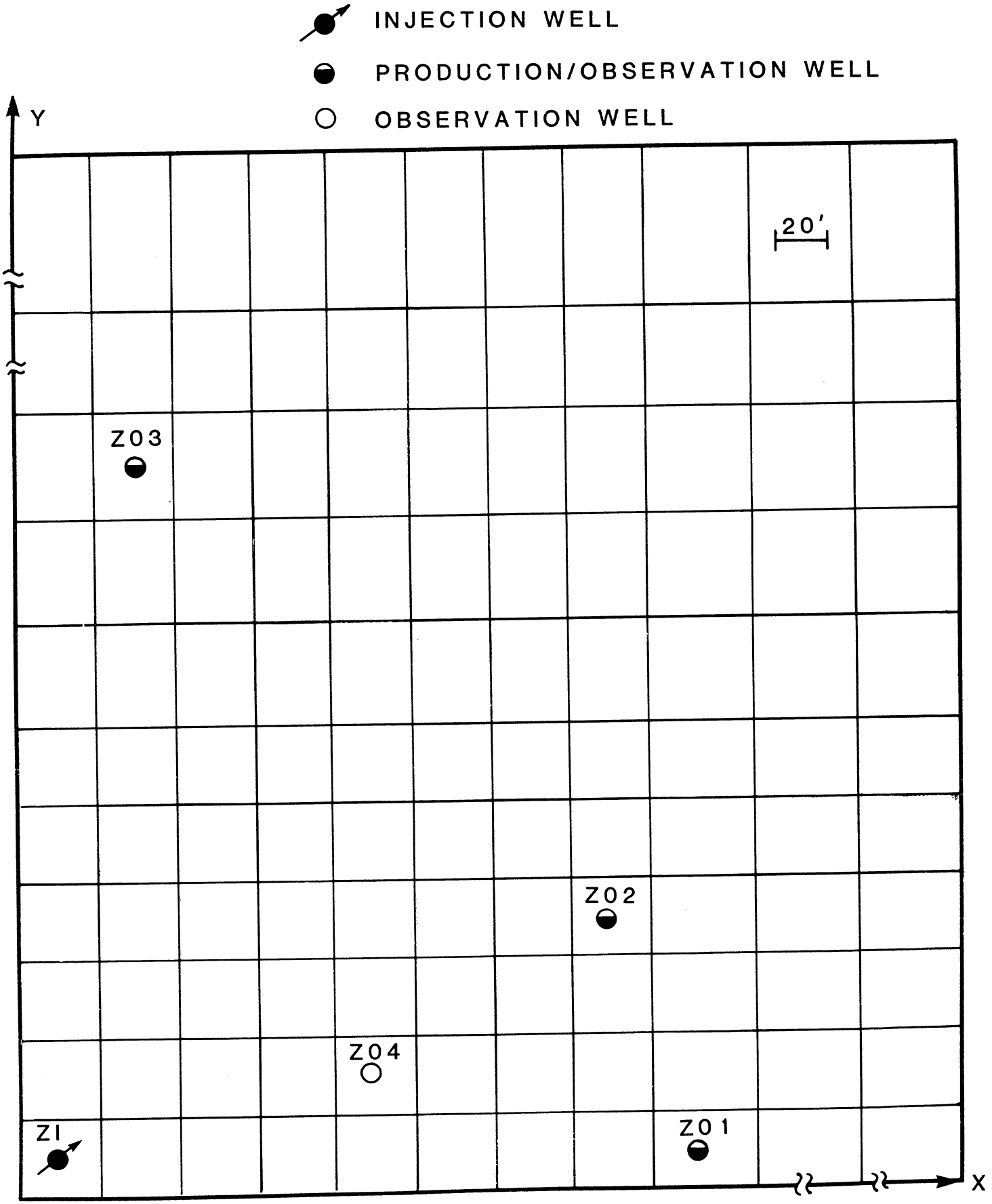

FIGURE 34
16 X 15 X 4 GRID SYSTEM

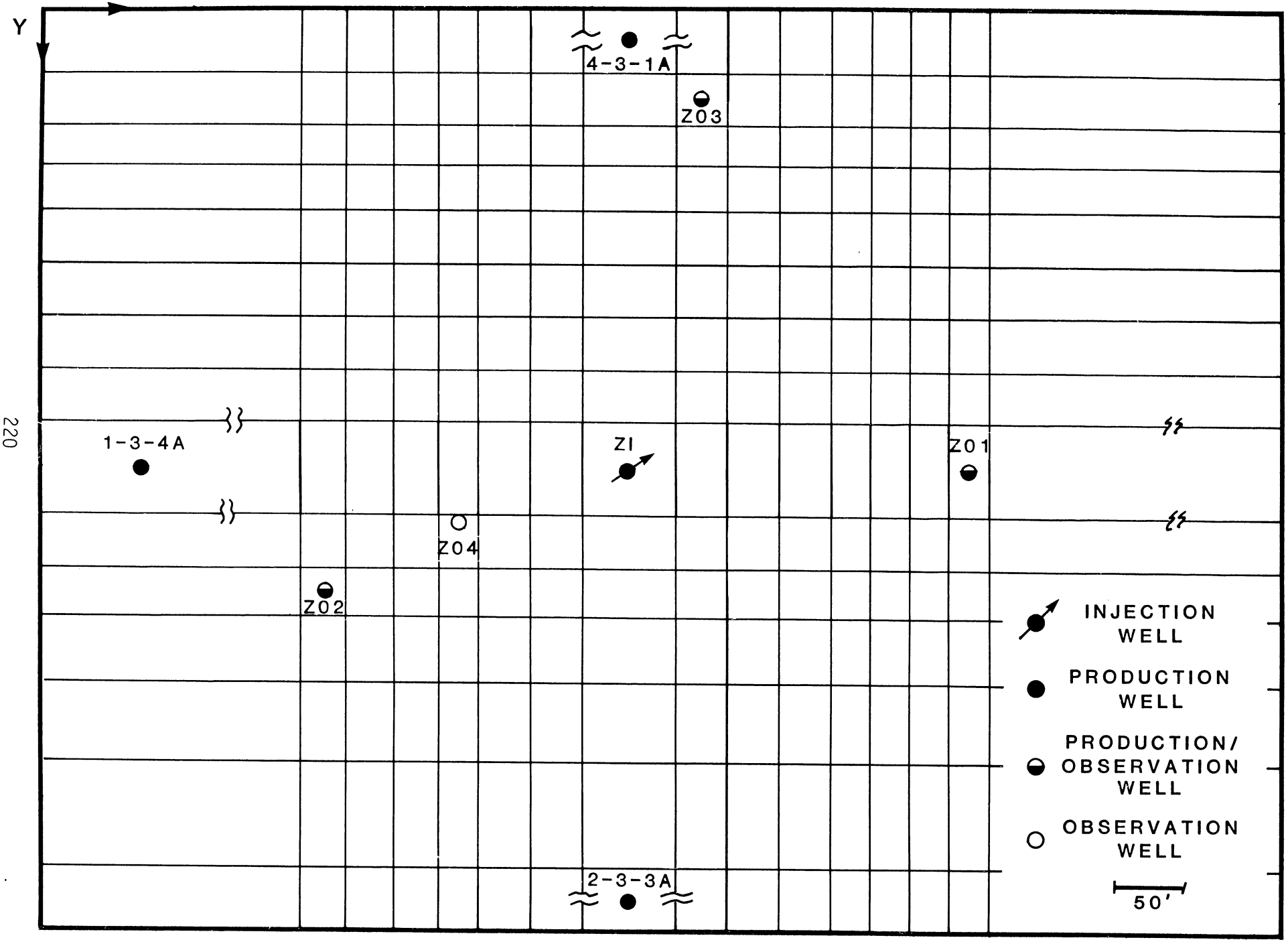

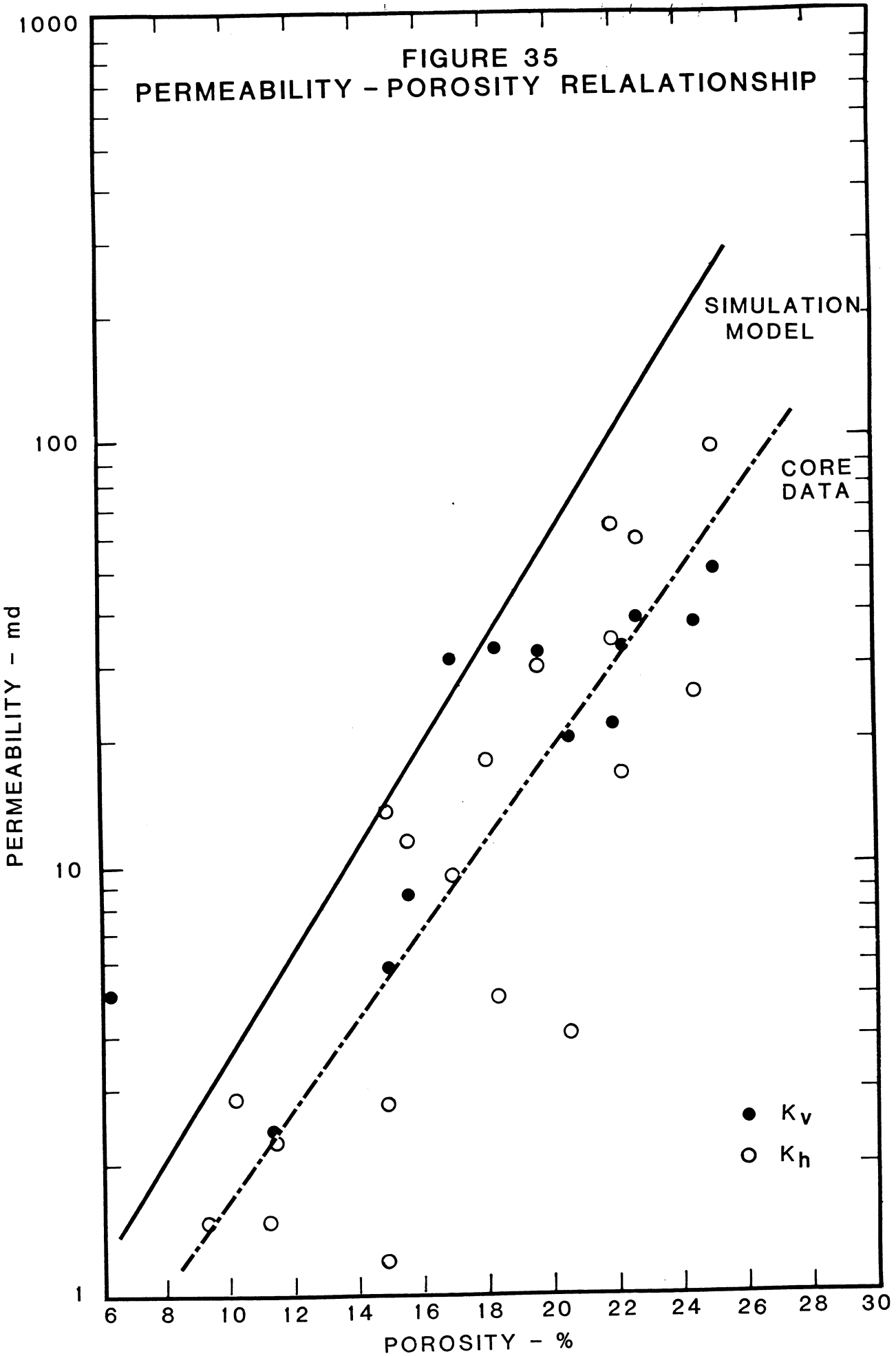
FIGURE 35
PERMEABILITY - POROSITY RELALATIONSHIP
SIMULATION MODEL
CORE DATA
Kv
Kh
PERMEABILITY - md
POROSITY - %
1000
100
10
1
6
8
10
12
14
16
18
20
22
24
26
28
30

FIGURE 36

DERIVED OIL-WATER CAPILLARY PRESSURE DATA

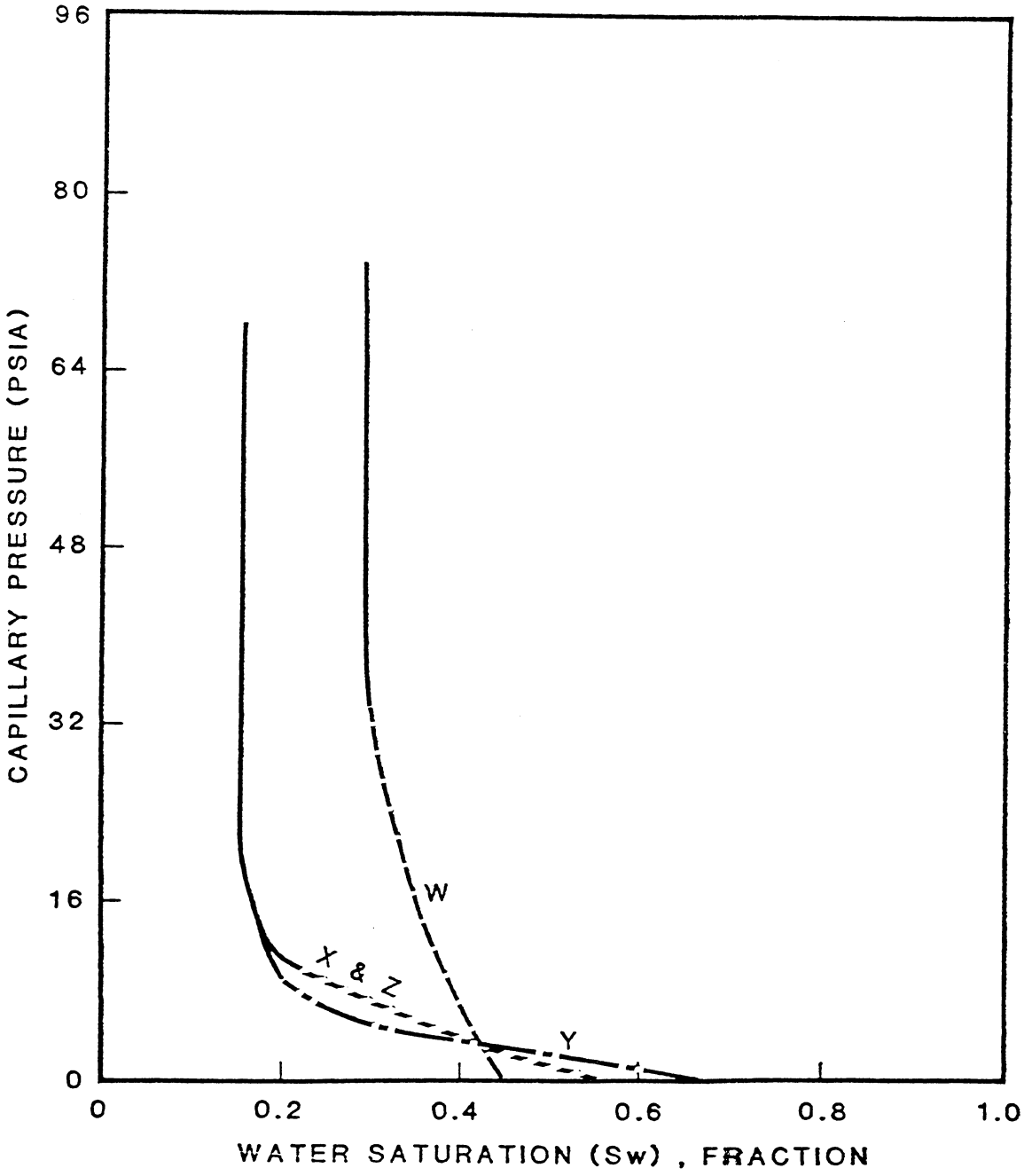

FIGURE 37
PRESSURE HISTORY MATCH (12-11-80 TO 10-7-81)
ZABOLOTNY INJECTION WELL NO. 1

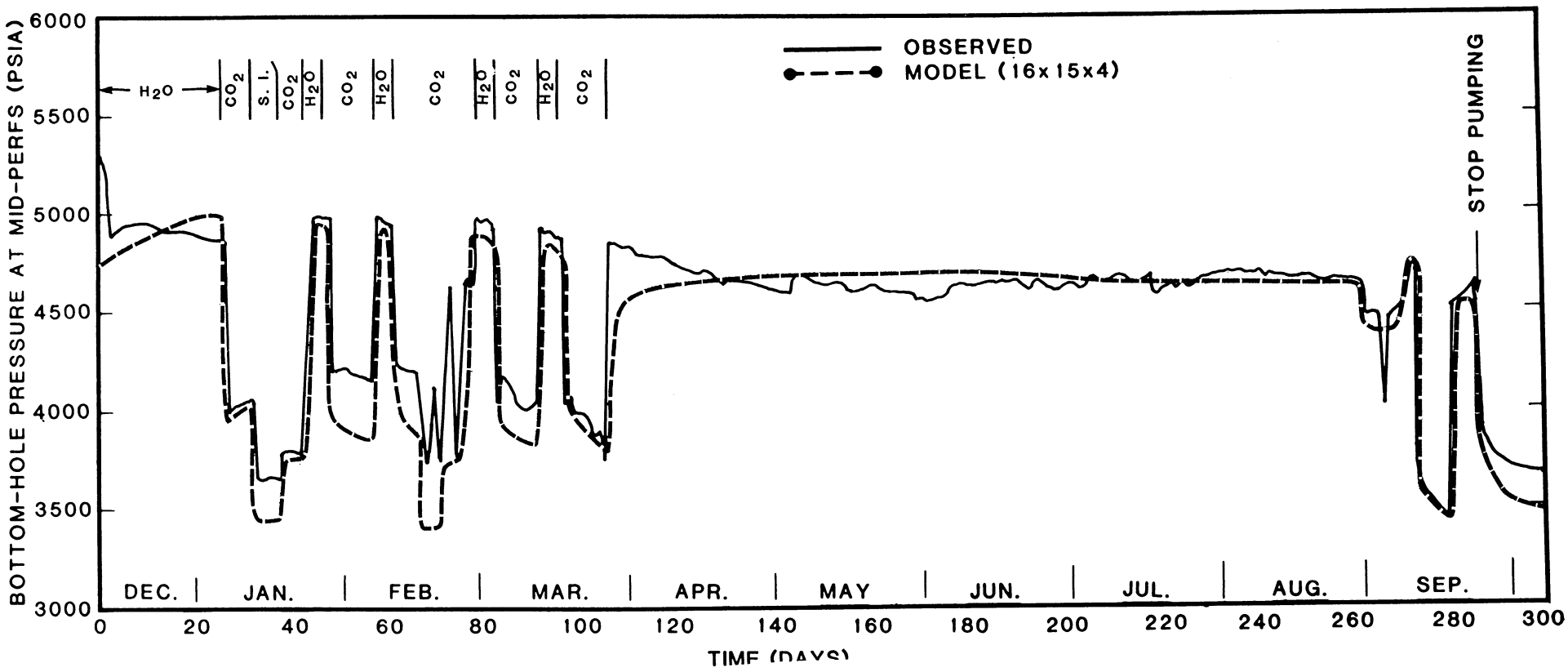

FIGURE 38
PRESSURE HISTORY MATCH (12-11-80 TO 10-7-81)
ZABOLOTNY OBSERVATION WELL NO. 1

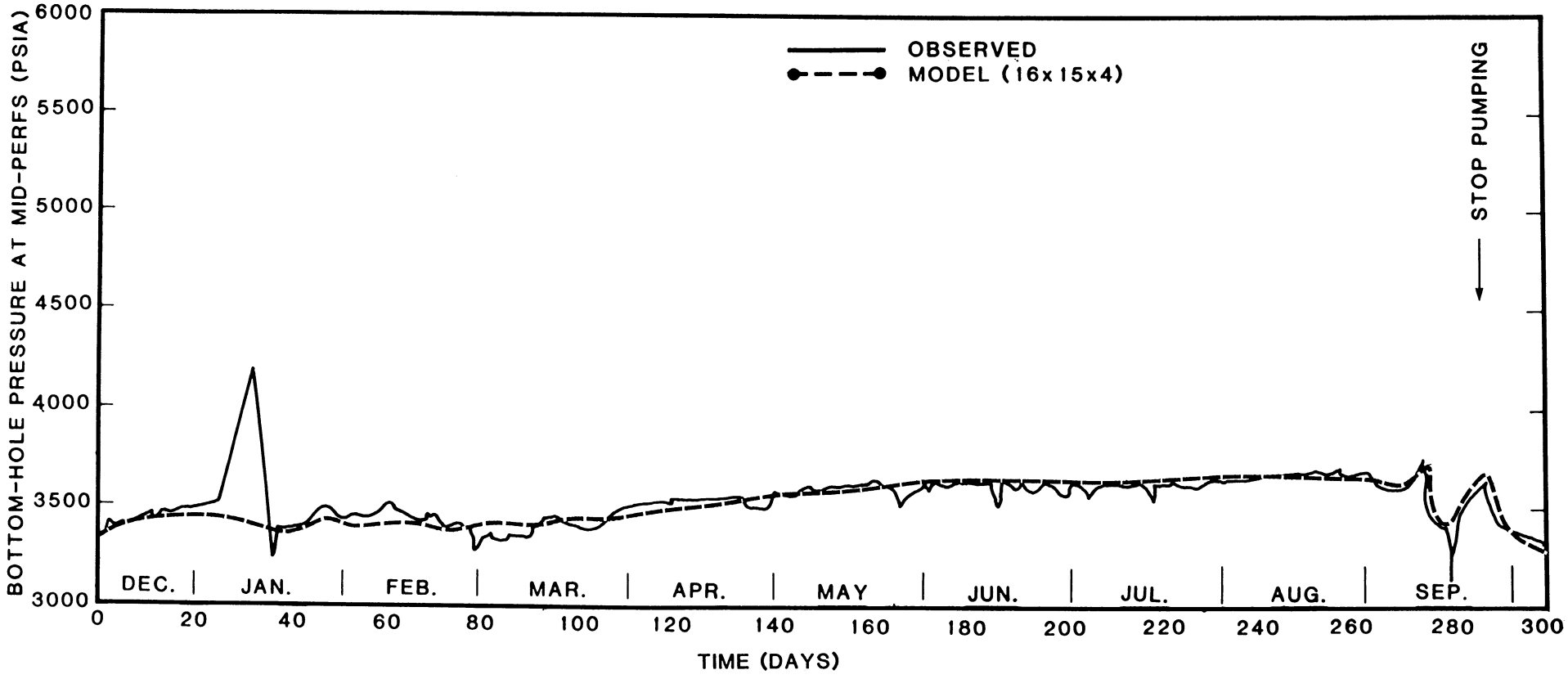

FIGURE 39
PRESSURE HISTORY MATCH (12-11-80 TO 10-7-81)
ZABOLOTNY OBSERVATION WELL NO. 2

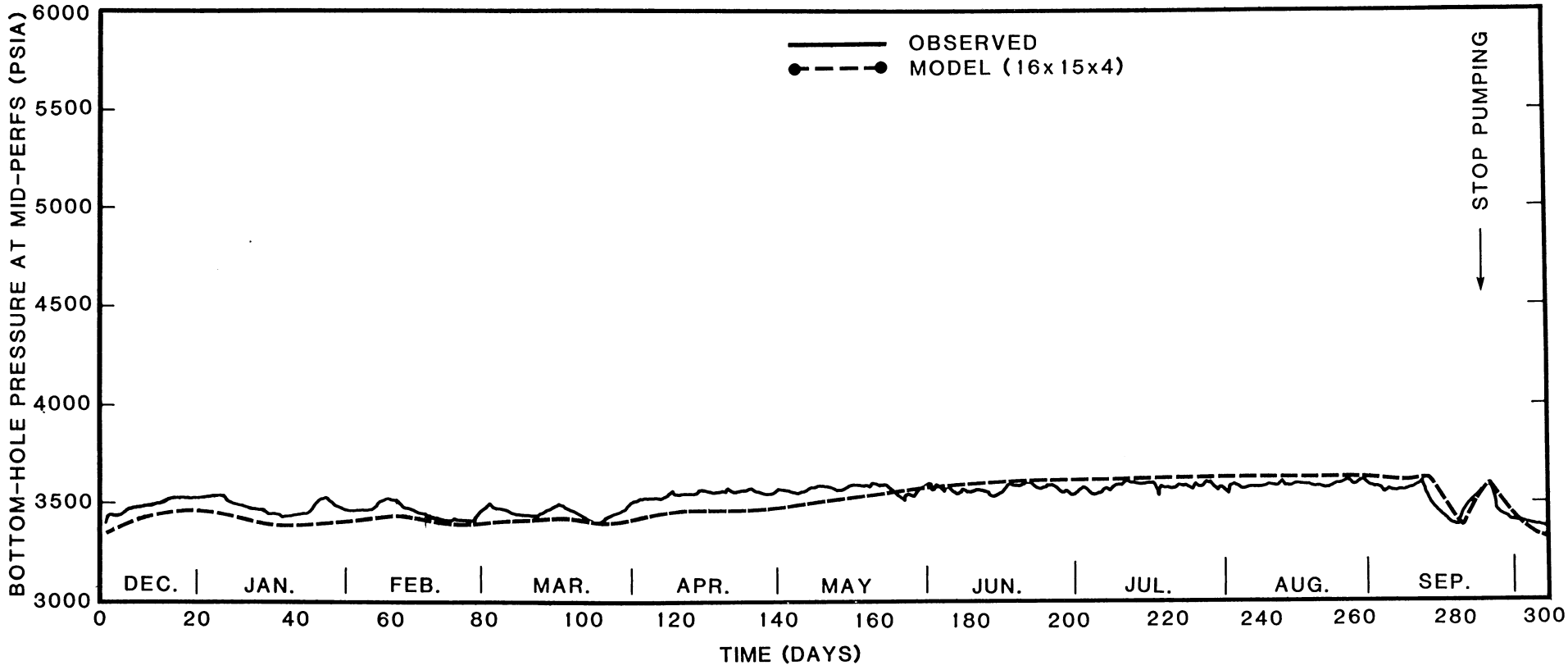

FIGURE 40
PRESSURE HISTORY MATCH (12-11-80 TO 10-7-81)
ZABOLOTNY OBSERVATION WELL NO. 3

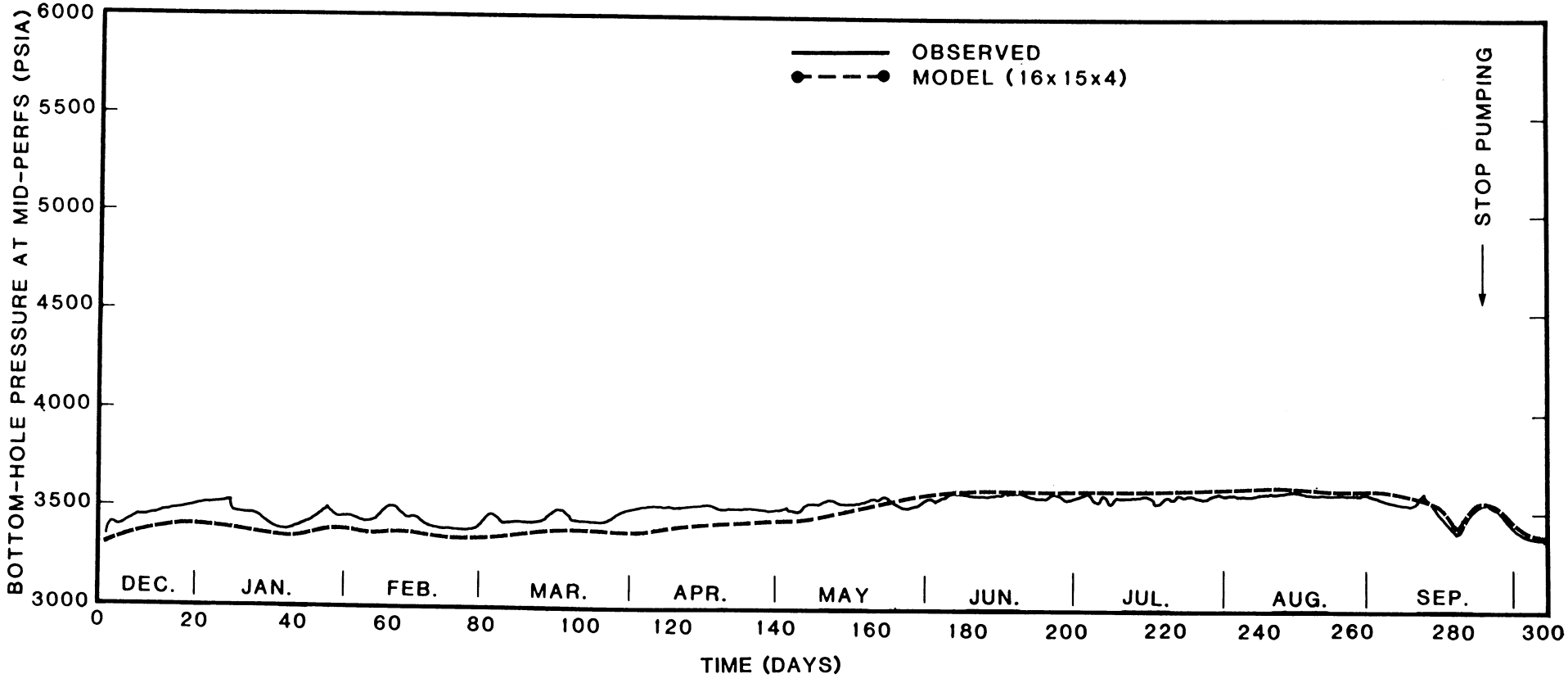

FIGURE 41

WATER SATURATION HISTORY MATCH BY LAYERS (12-11-80 TO 9-17-81)

ZABOLOTNY OBSERVATION WELL NO. 1

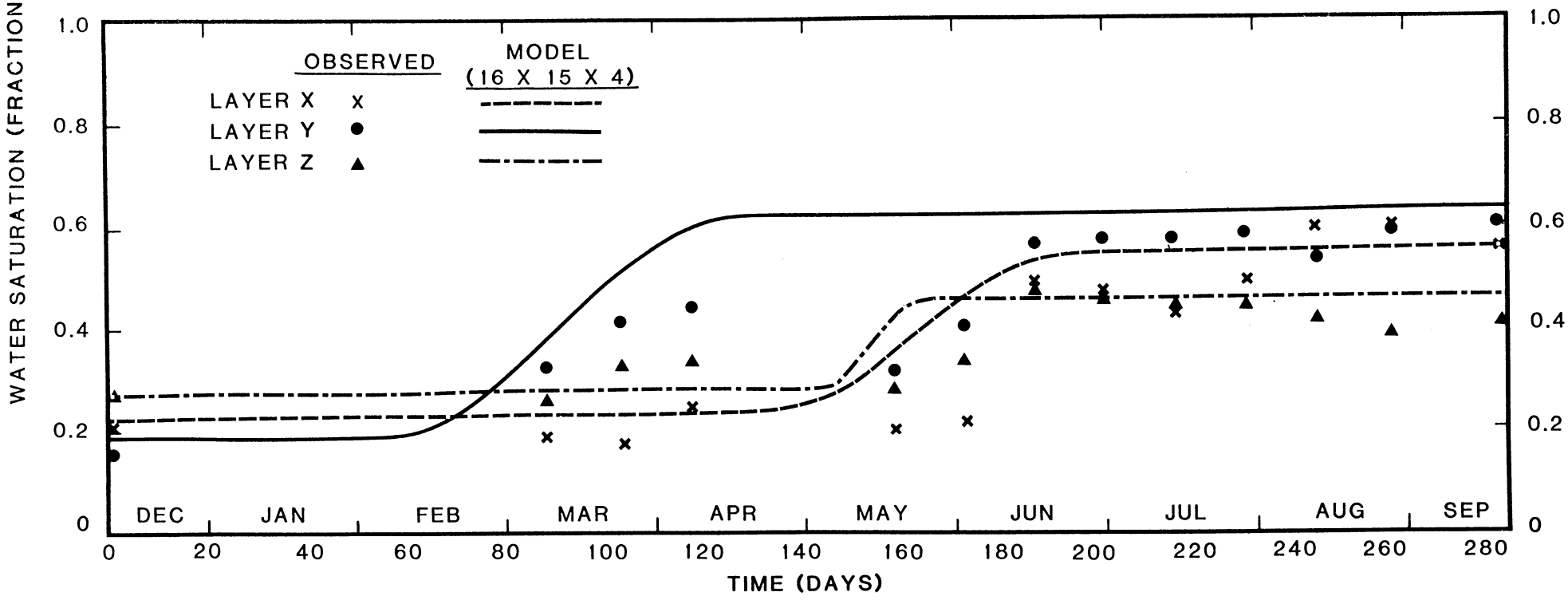

FIGURE 42
WATER SATURATION HISTORY MATCH BY LAYERS (12-11-80 TO 9-17-81)
ZABOLOTNY OBSERVATION WELL NO. 2

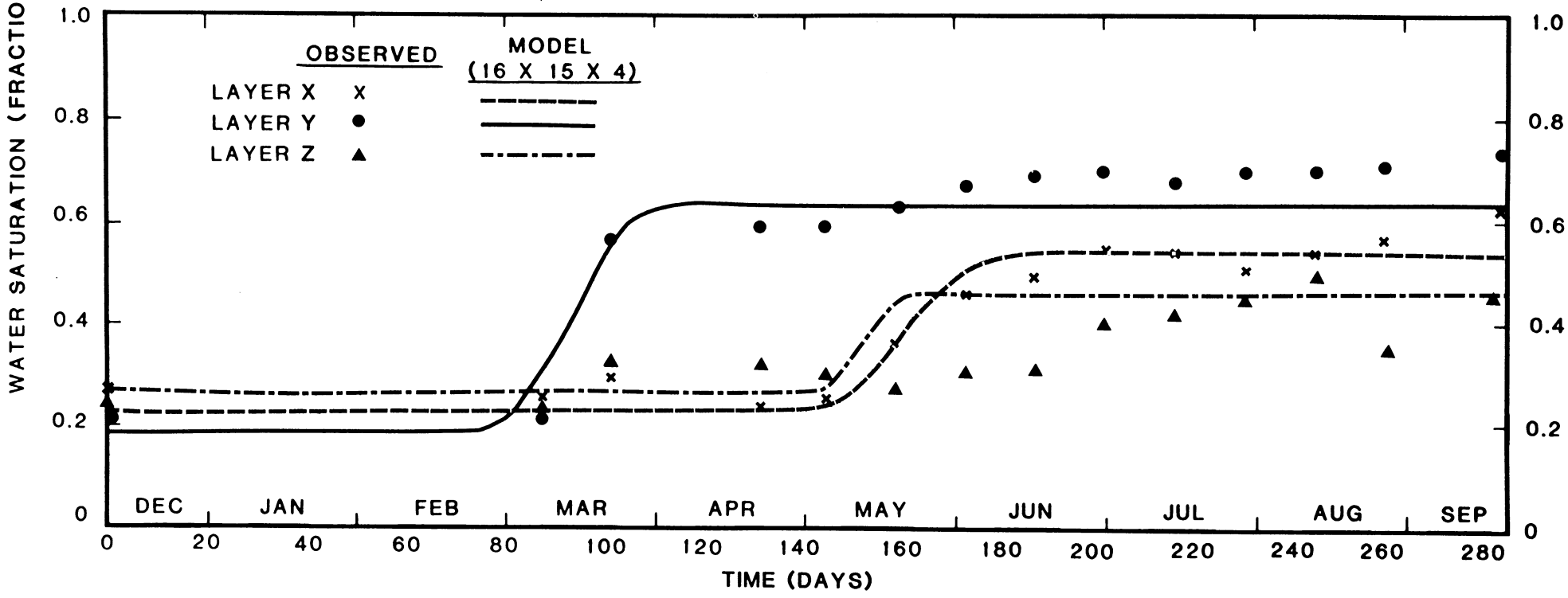

FIGURE 43

WATER SATURATION HISTORY MATCH BY LAYERS (12-11-80 TO 9-17-81)

ZABOLOTNY OBSERVATION WELL NO. 3

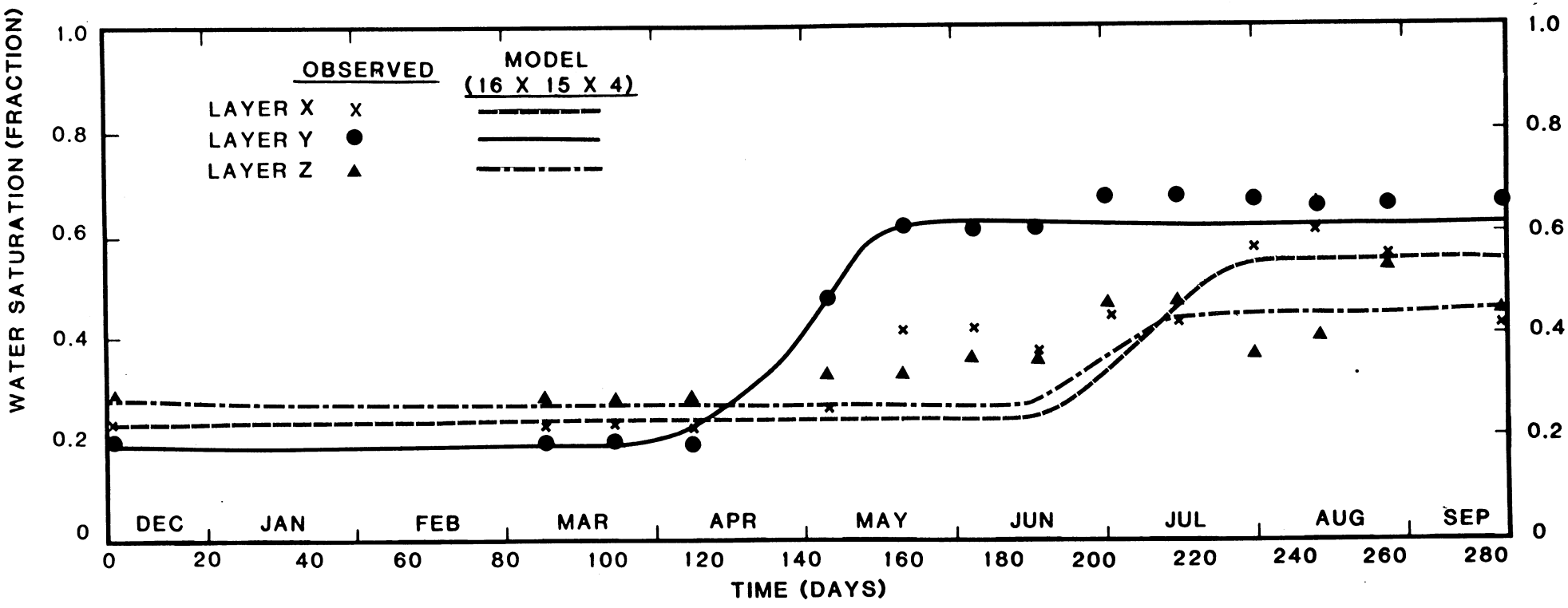

FIGURE 44

WATER SATURATION HISTORY MATCH FOR ZONE D (12-11-80 TO 9-17-81)

ZABOLOTNY OBSERVATION WELL NO. 1

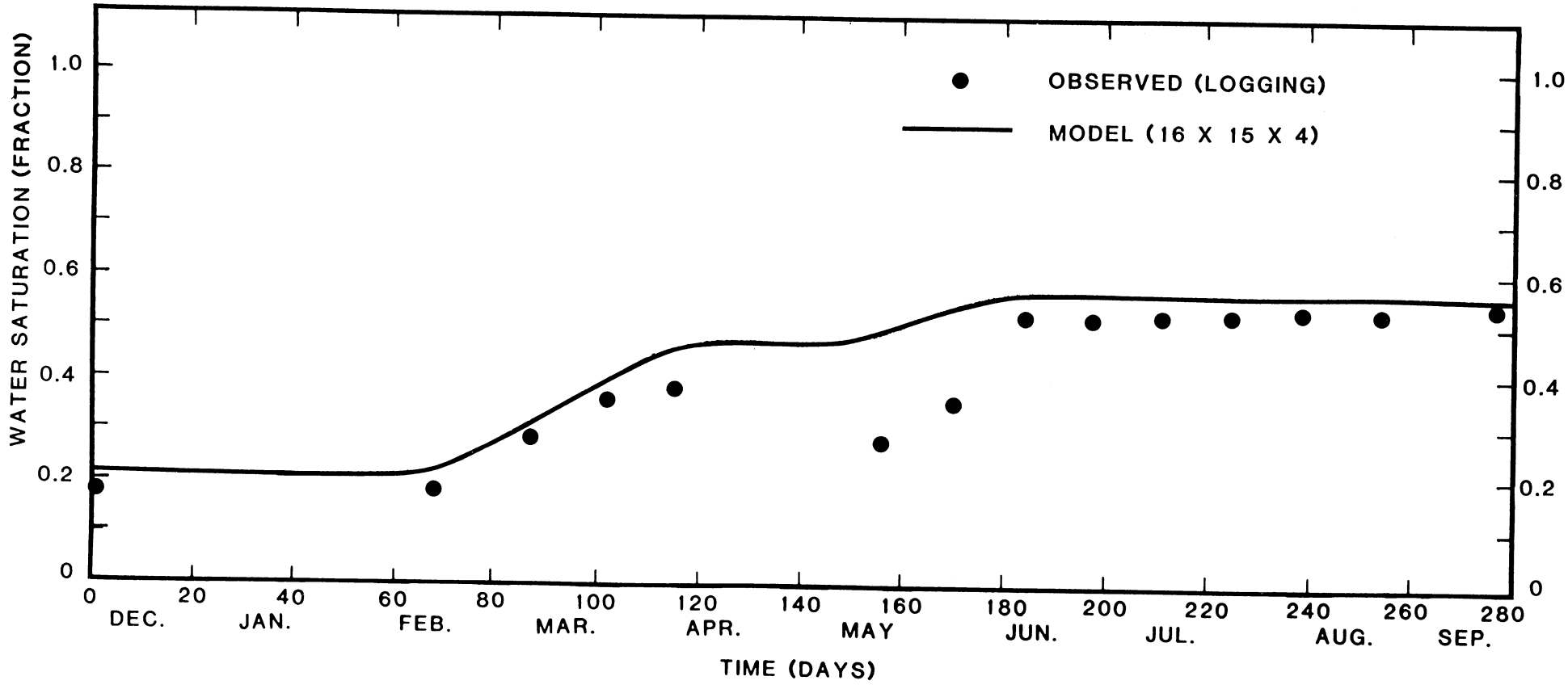

FIGURE 45

WATER SATURATION HISTORY MATCH FOR ZONE D (12-11-80 TO 9-17-81)

ZABOLOTNY OBSERVATION WELL NO. 2

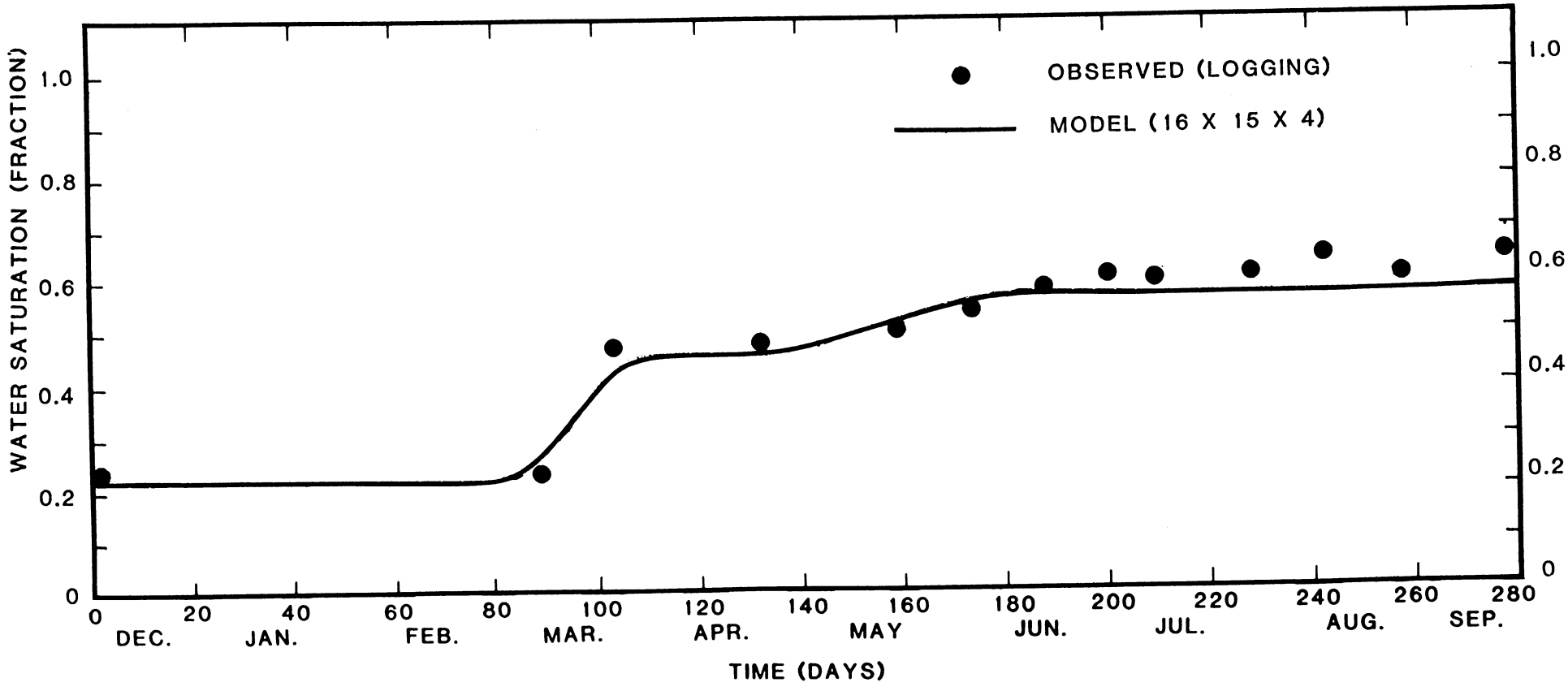

FIGURE 46

WATER SATURATION HISTORY MATCH FOR ZONE D (12-11-80 TO 9-17-81)

ZABOLOTNY OBSERVATION WELL NO. 3

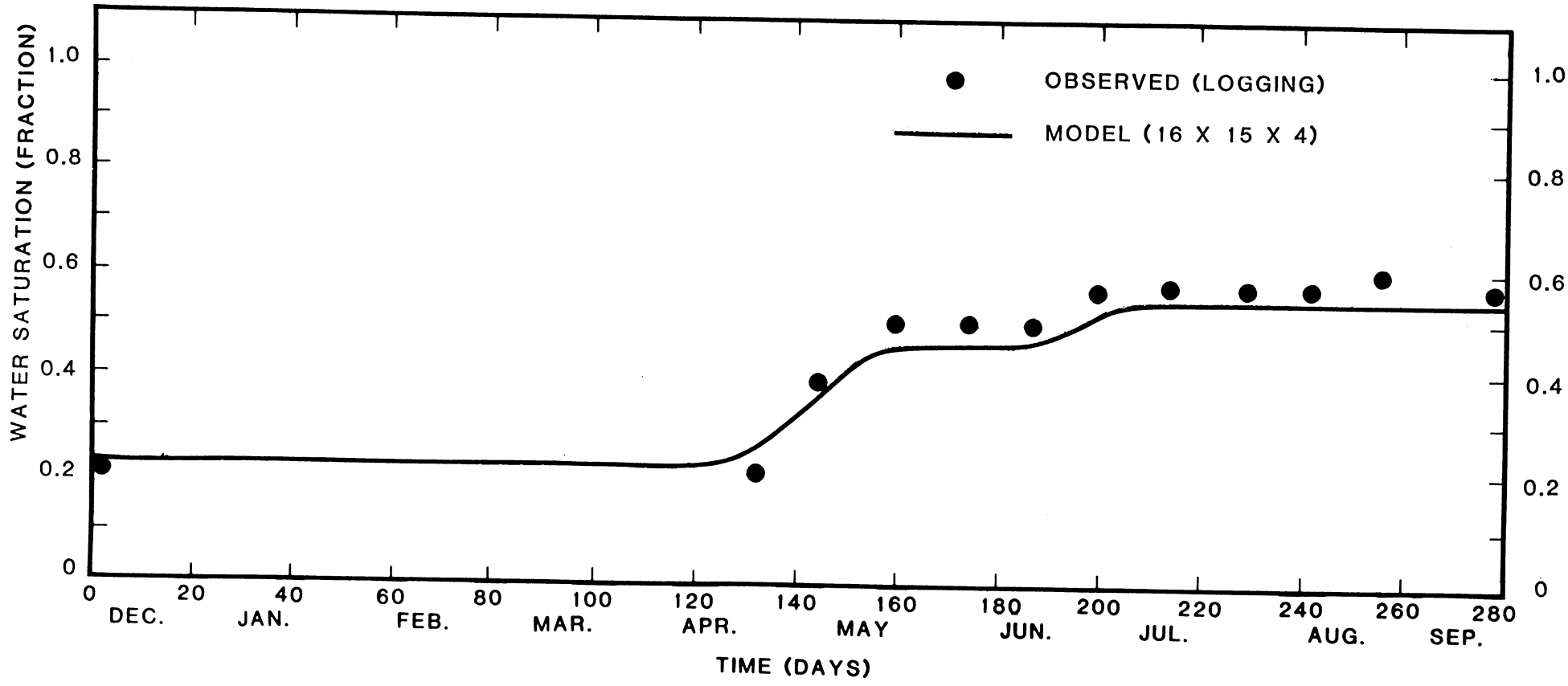

FIGURE 47

MEASURED CARBON DIOXIDE CONTENTS FROM

LOGS,SEPARATOR GAS ANALYSIS,AND ISOTOPE ANALYSIS

ZABOLOTNY OBSERVATION WELL NO. 1

(12-11-80 TO 9-17-81)

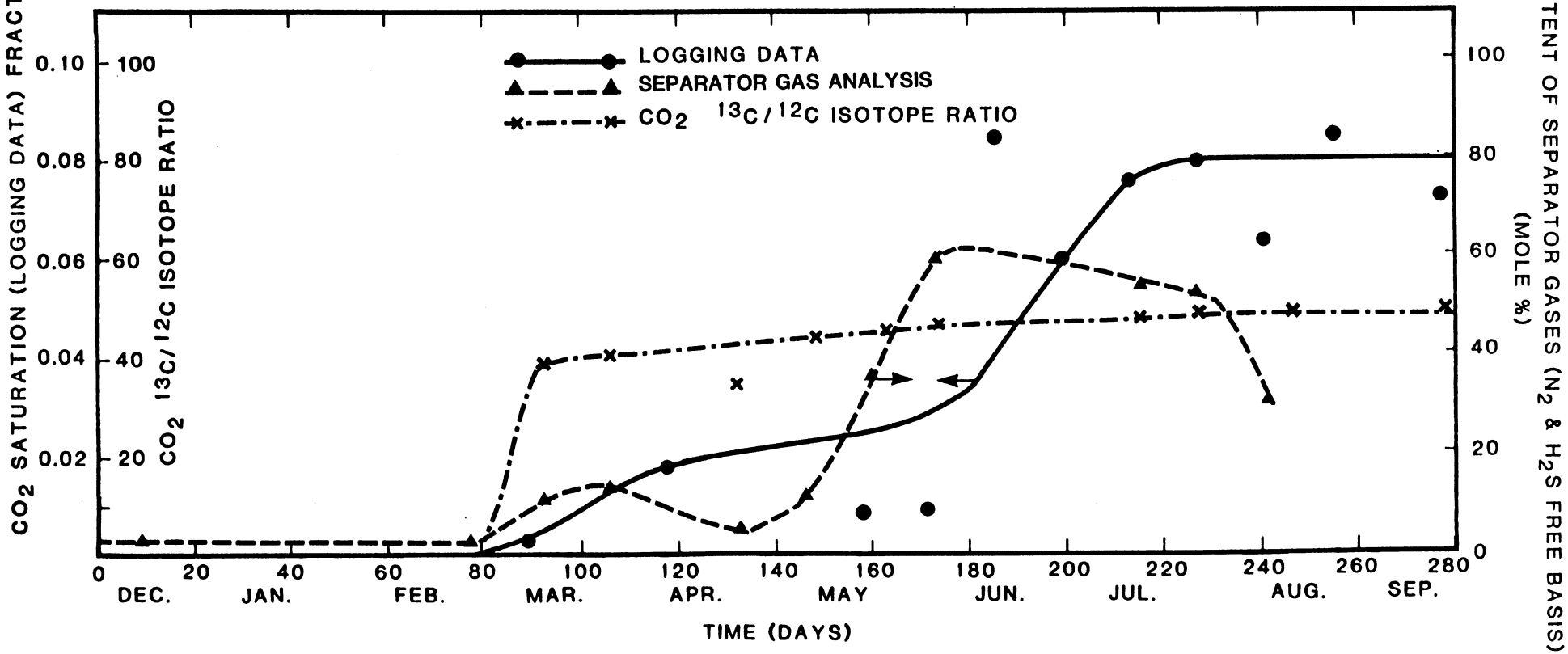

FIGURE 48

MEASURED CARBON DIOXIDE CONTENTS FROM LOGS,SEPARATOR GAS ANALYSIS,AND ISOTOPE ANALYSIS

ZABOLOTNY OBSERVATION WELL NO. 2

(12-11-80 TO 9-17-81)

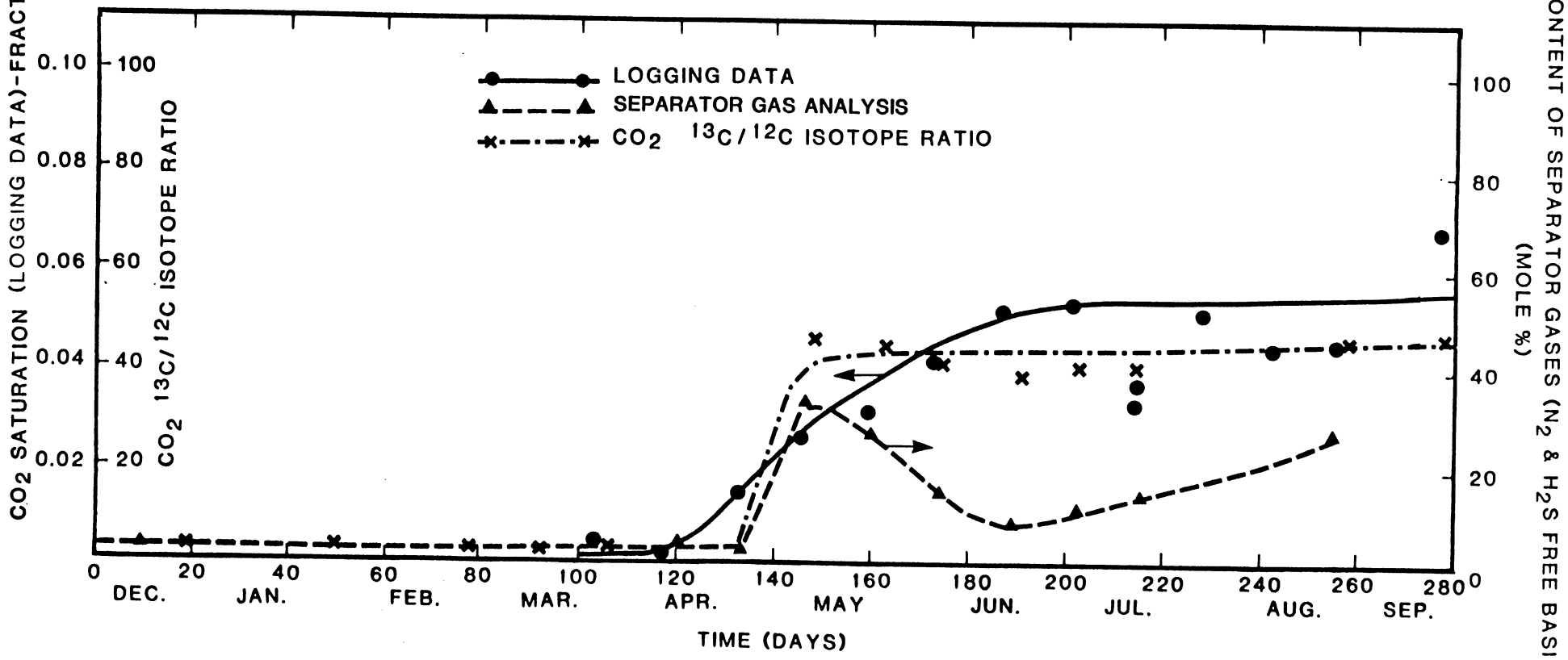

FIGURE 49

MEASURED CARBON DIOXIDE CONTENTS FROM LOGS, SEPARATOR GAS ANALYSIS, AND ISOTOPE ANALYSIS

ZABOLOTNY OBSERVATION WELL NO. 3

(12-11-80 TO 9-17-81)

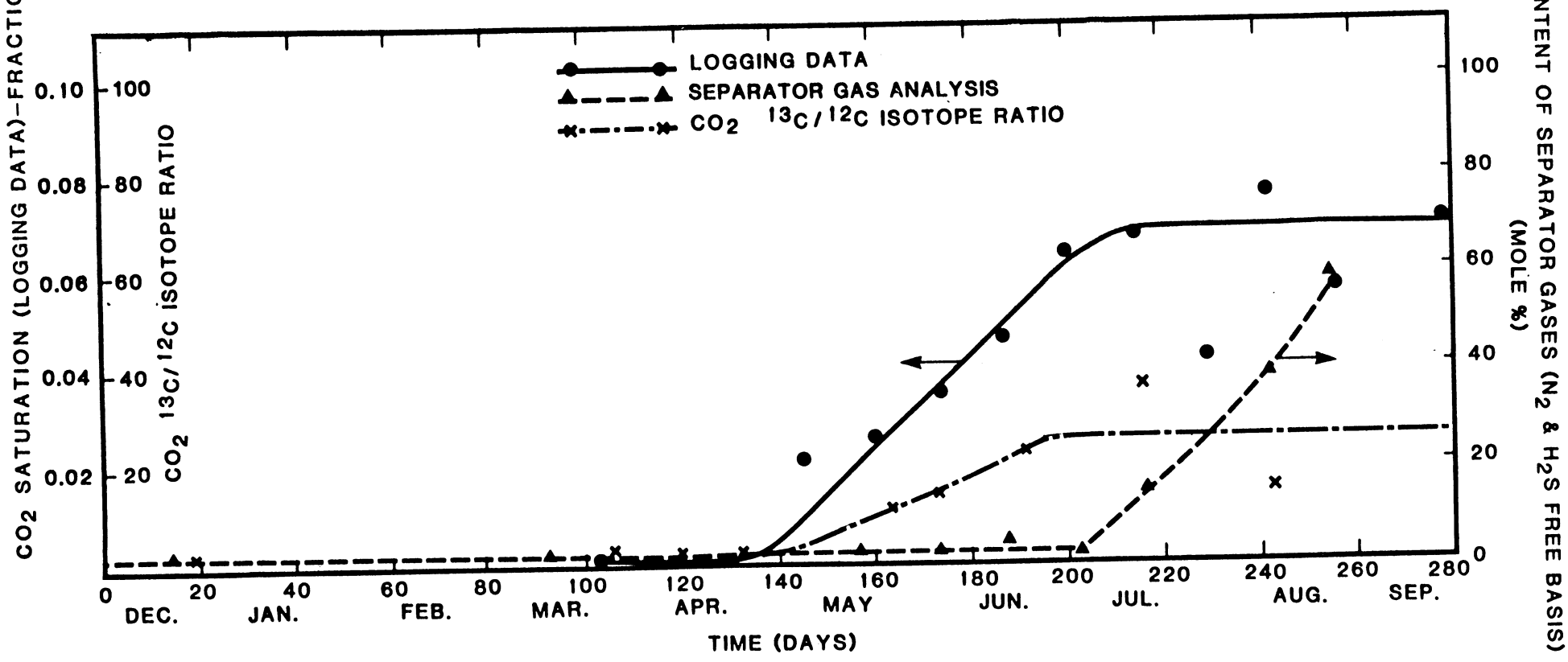

FIGURE 50

SWELLING FACTORS OF OIL-CO_2 MIXTURES AT 245°F

ZABOLOTNY 1-3-4A WELL

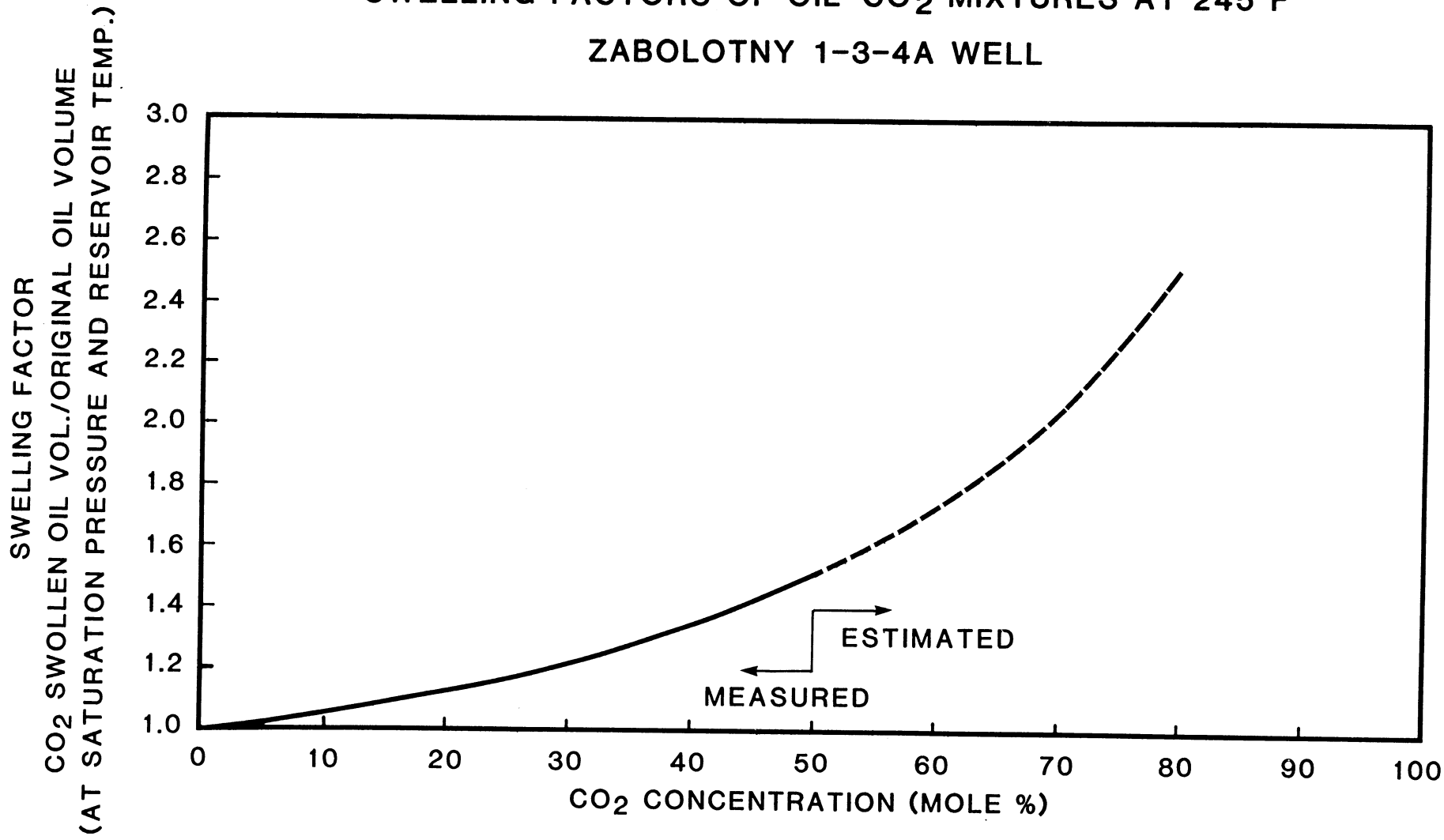

FIGURE 51

CO_2 SATURATION HISTORY MATCH (12-11-80 TO 9-17-81)

ZABOLOTNY OBSERVATION WELL NO. 1

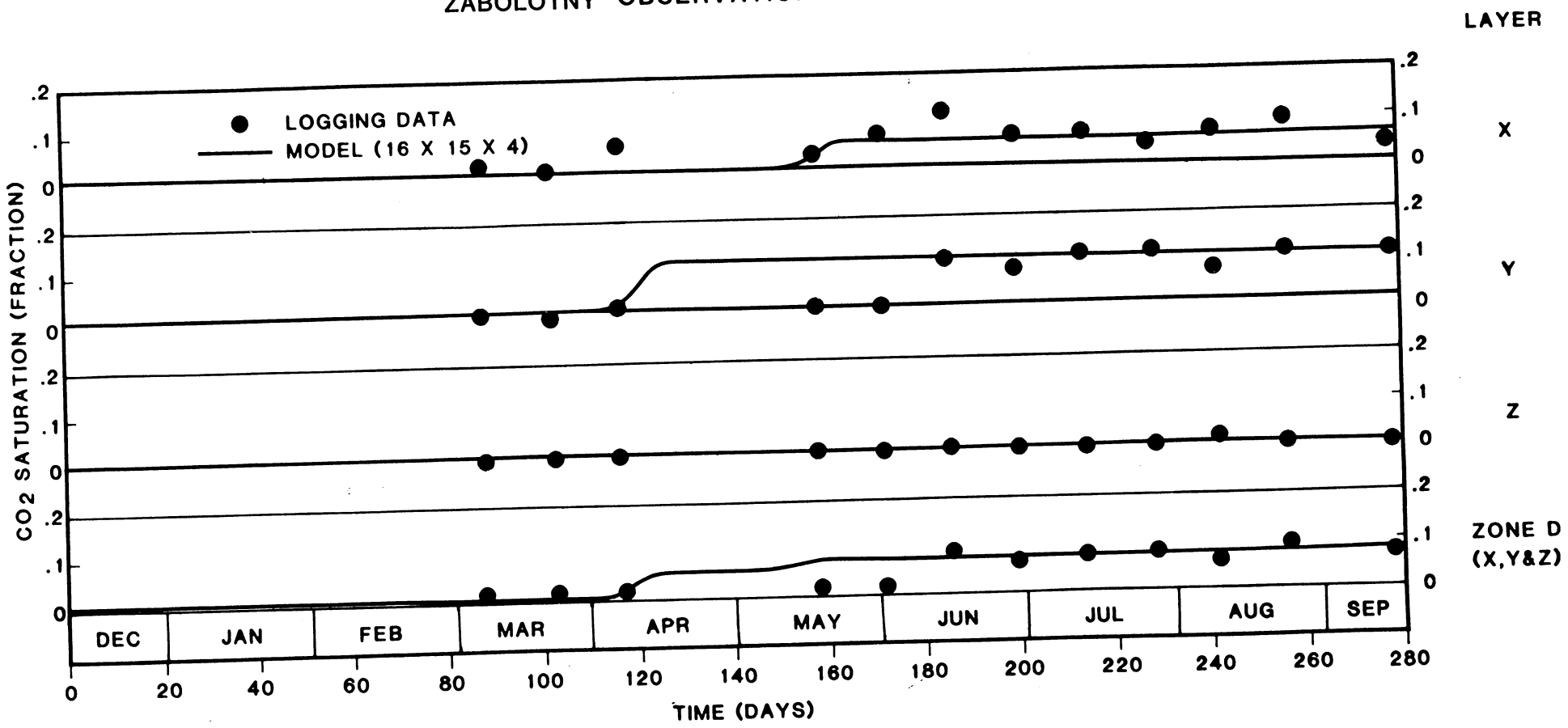

FIGURE 52

CO_2 SATURATION HISTORY MATCH (12-11-80 TO 9-17-81)

ZABOLOTNY OBSERVATION WELL NO. 2

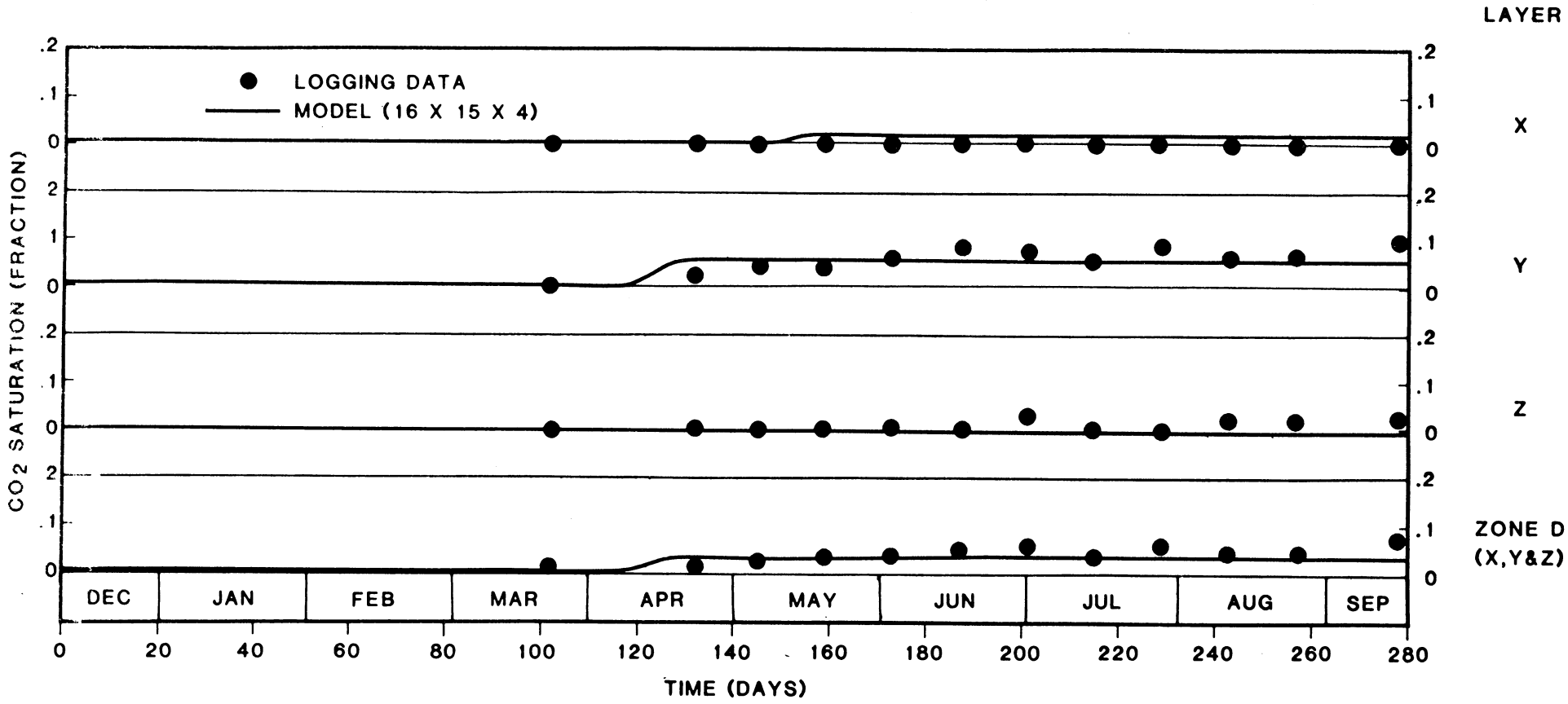

FIGURE 53

CO_2 SATURATION HISTORY MATCH (12-11-80 TO 9-17-81)

ZABOLOTNY OBSERVATION WELL NO. 3

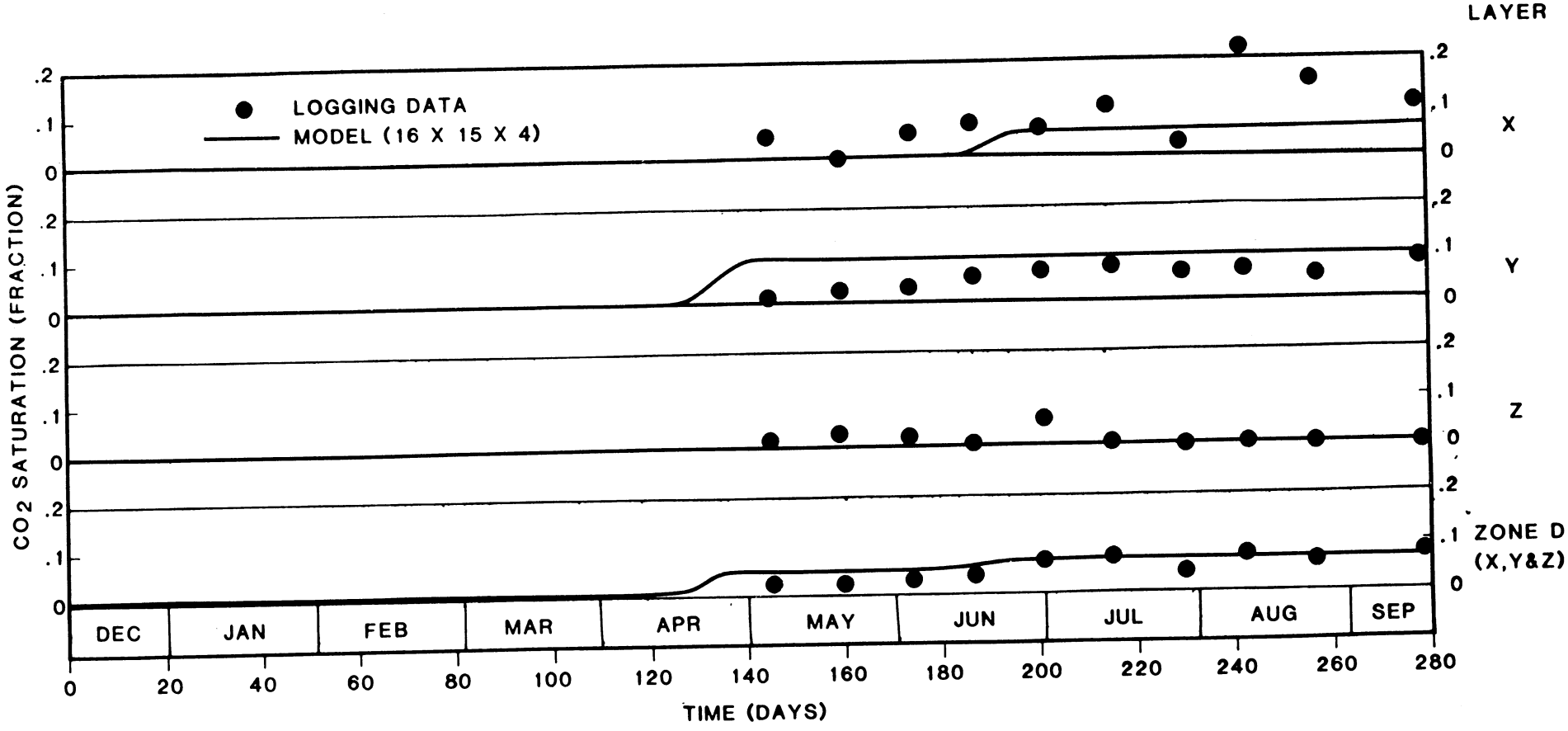

FIGURE 54

OIL SATURATION HISTORY MATCH BY LAYERS (12-11-80 TO 9-17-81)

ZABOLOTNY OBSERVATION WELL NO. 1

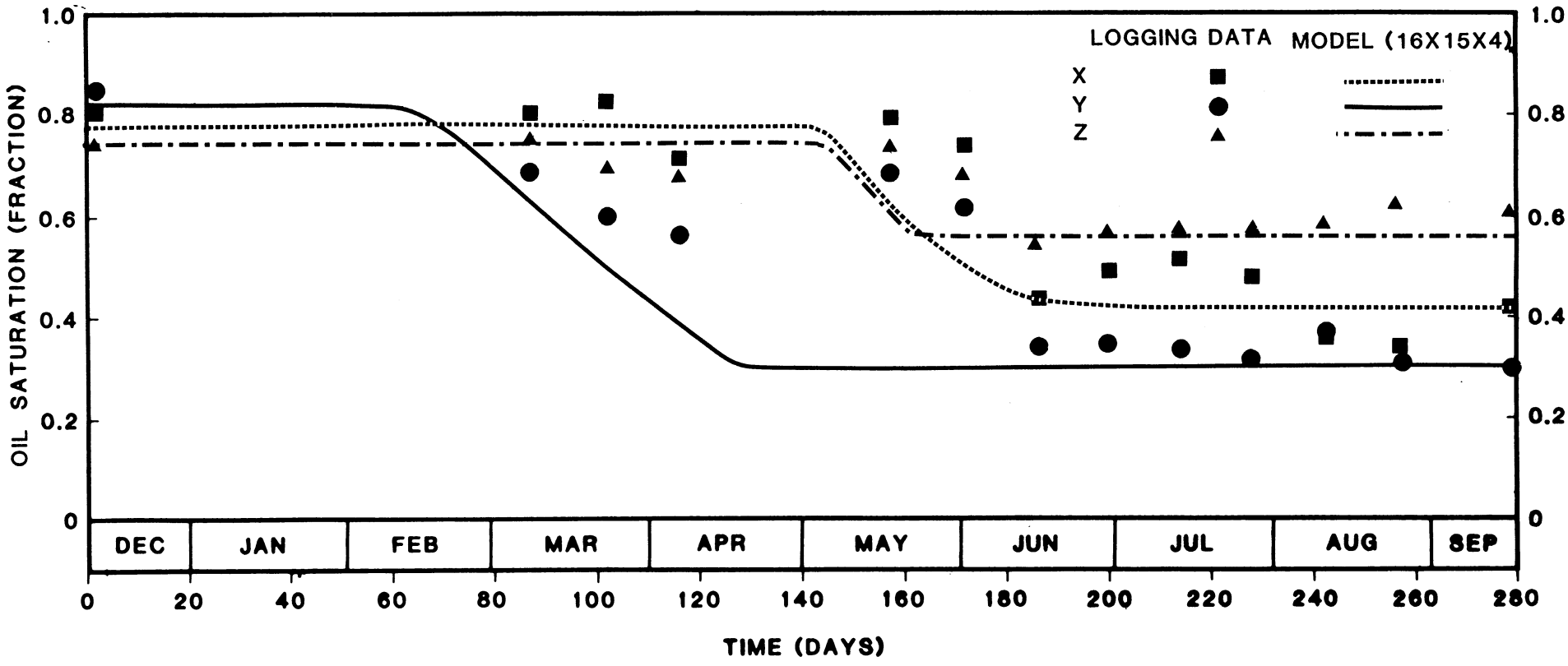

FIGURE 55

OIL SATURATION HISTORY MATCH BY LAYERS (12-11-80 TO 9-17-81)

ZABOLOTNY OBSERVATION WELL NO. 2

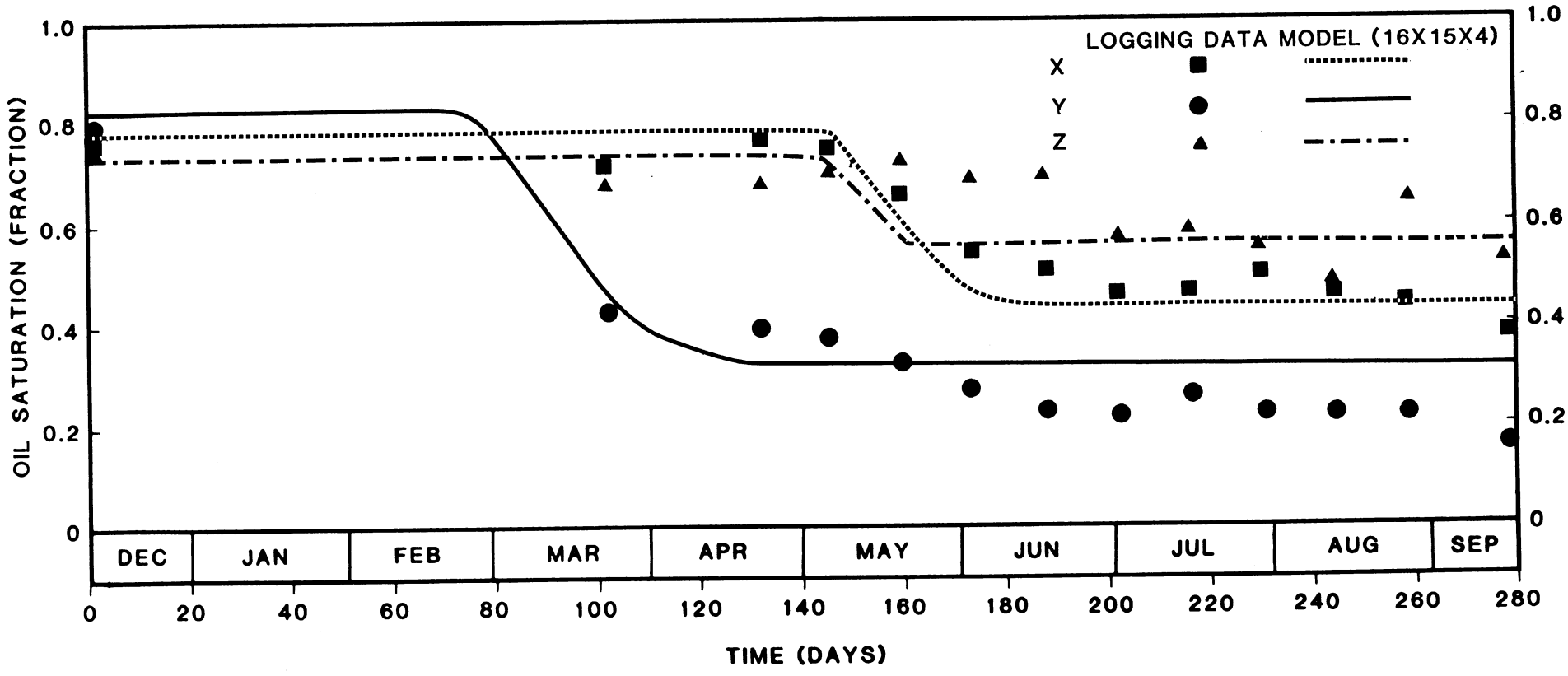

FIGURE 56

OIL SATURATION HISTORY MATCH BY LAYERS (12-11-80 TO 9-17-81)

ZABOLOTNY OBSERVATION WELL NO. 3

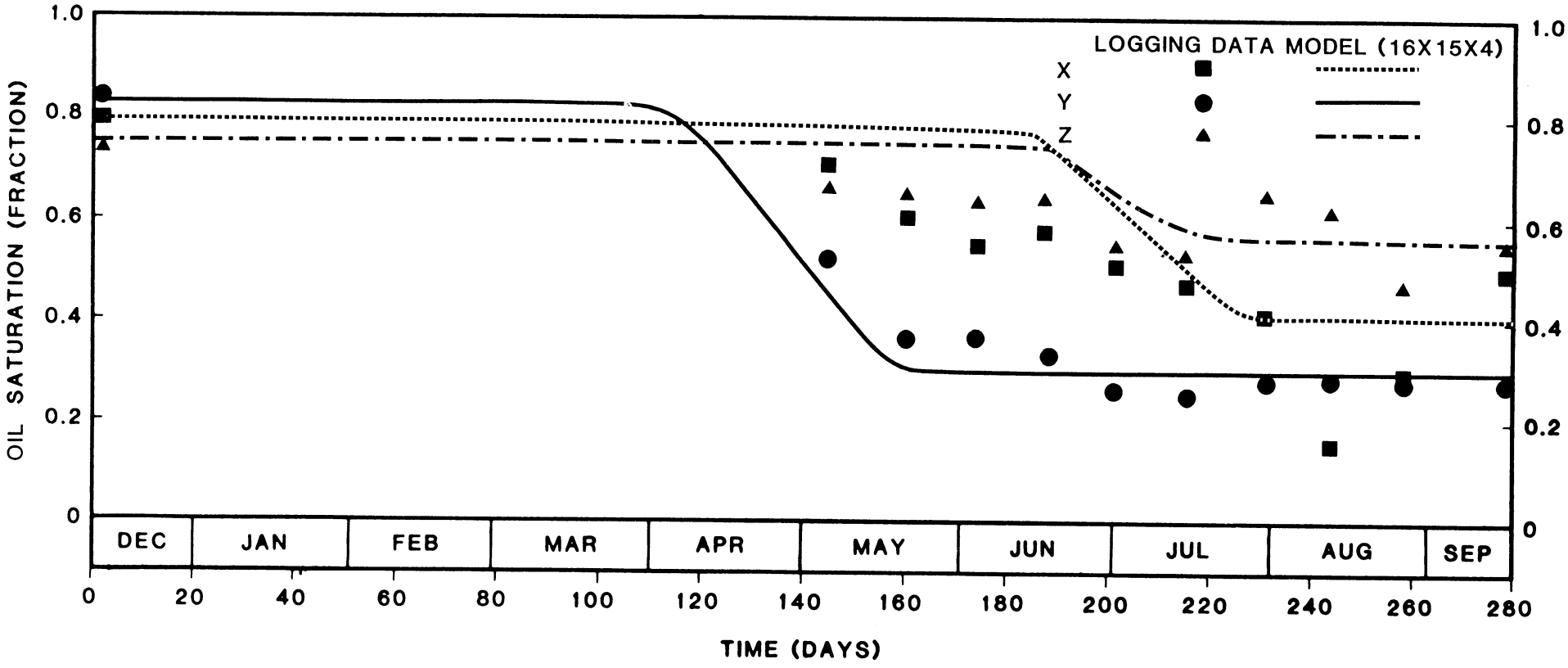

FIGURE 57

OIL SATURATION HISTORY MATCH FOR ZONE D (12-11-80 TO 9-17-81)

ZABOLOTNY OBSERVATION WELL NO. 1

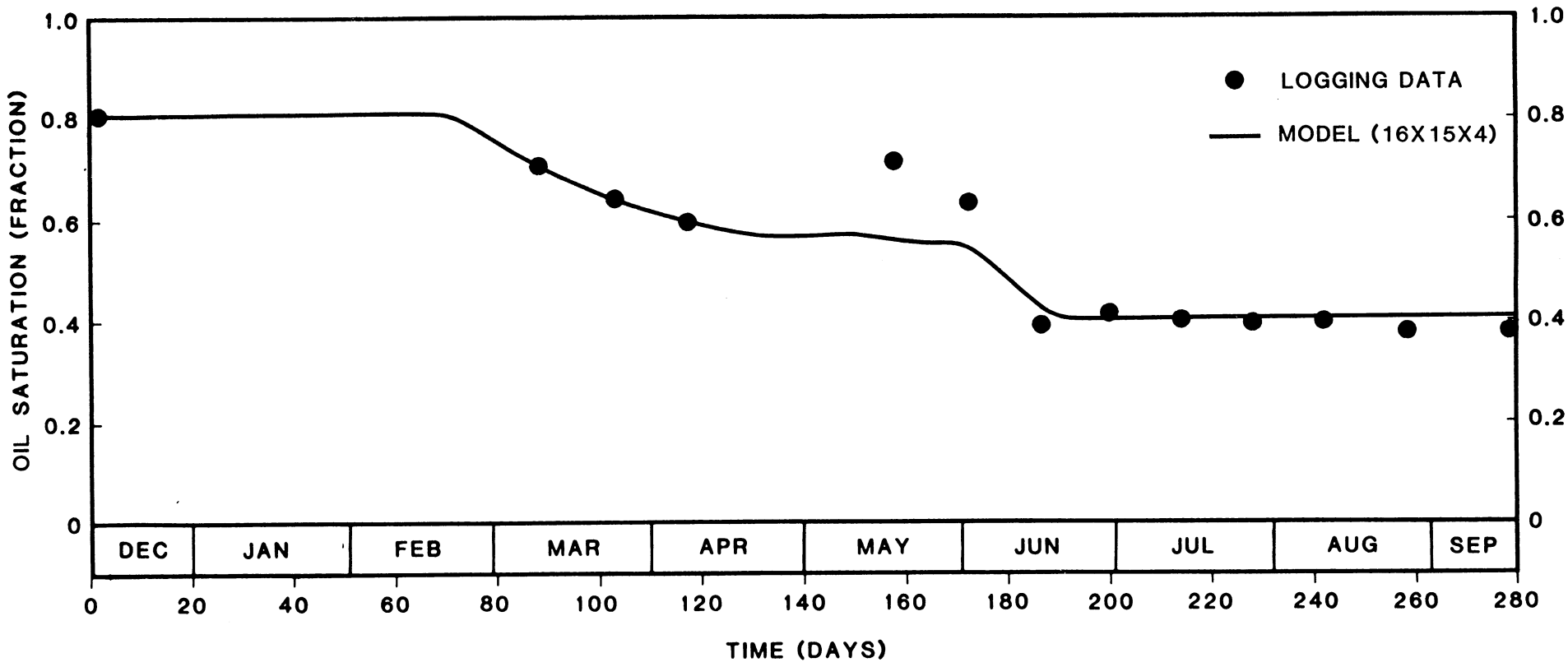

FIGURE 58

OIL SATURATION HISTORY MATCH FOR ZONE D (12-11-80 TO 9-17-81)

ZABOLOTNY OBSERVATION WELL NO. 2

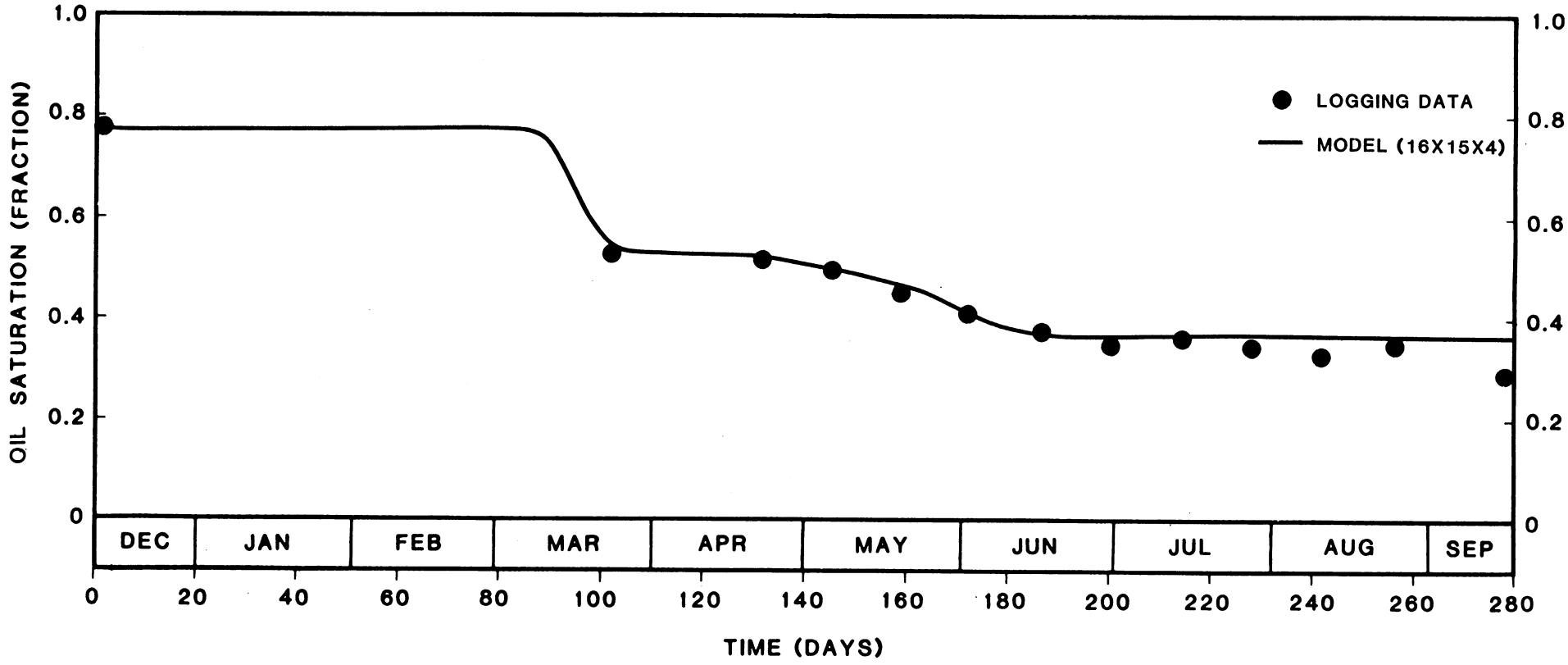

FIGURE 59

OIL SATURATION HISTORY MATCH FOR ZONE D (12-11-80 TO 9-17 -81)

ZABOLOTNY OBSERVATION WELL NO. 3

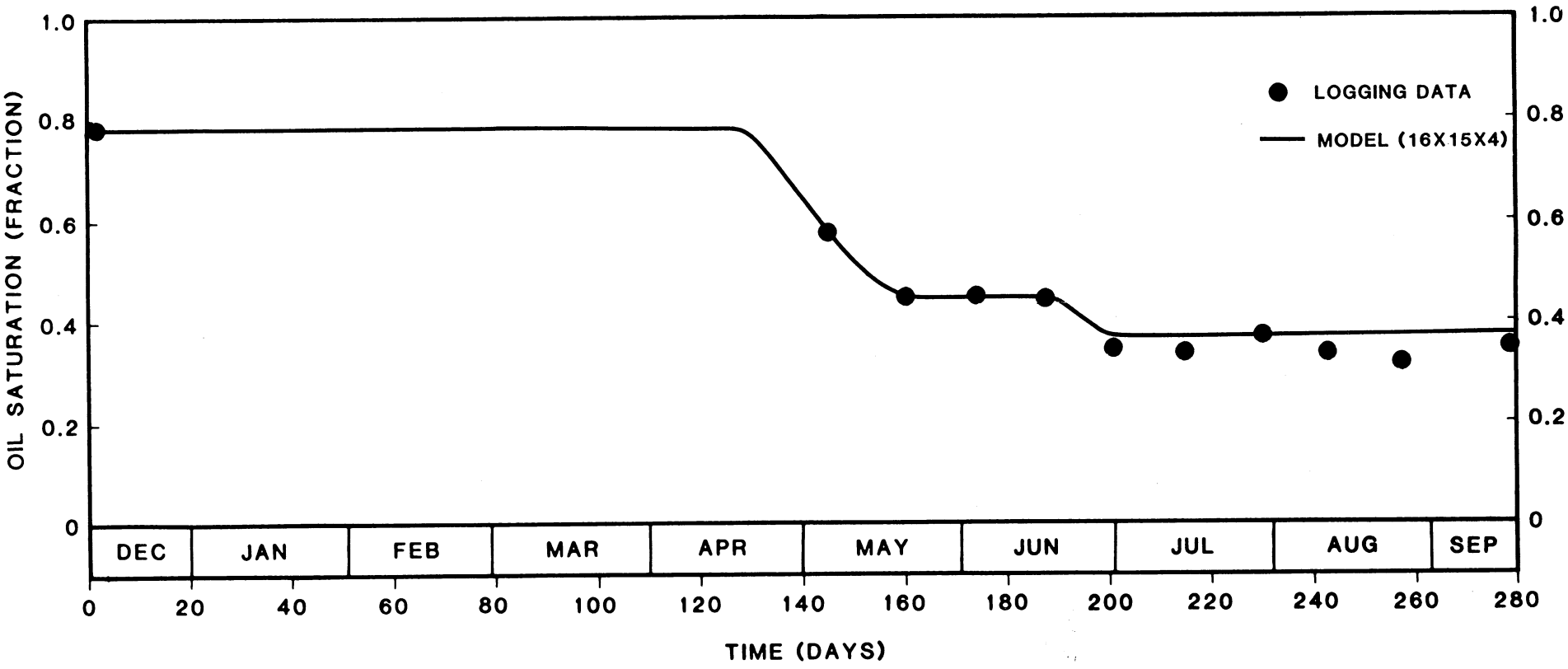

FIGURE 60

CO_2-FREE OIL SATURATION (AT RESERVOIR CONDITIONS)
PROFILE ON JULY 17,1981
FOUR LAYER MODEL
ZABOLOTNY OBSERVATION WELL NO. 4

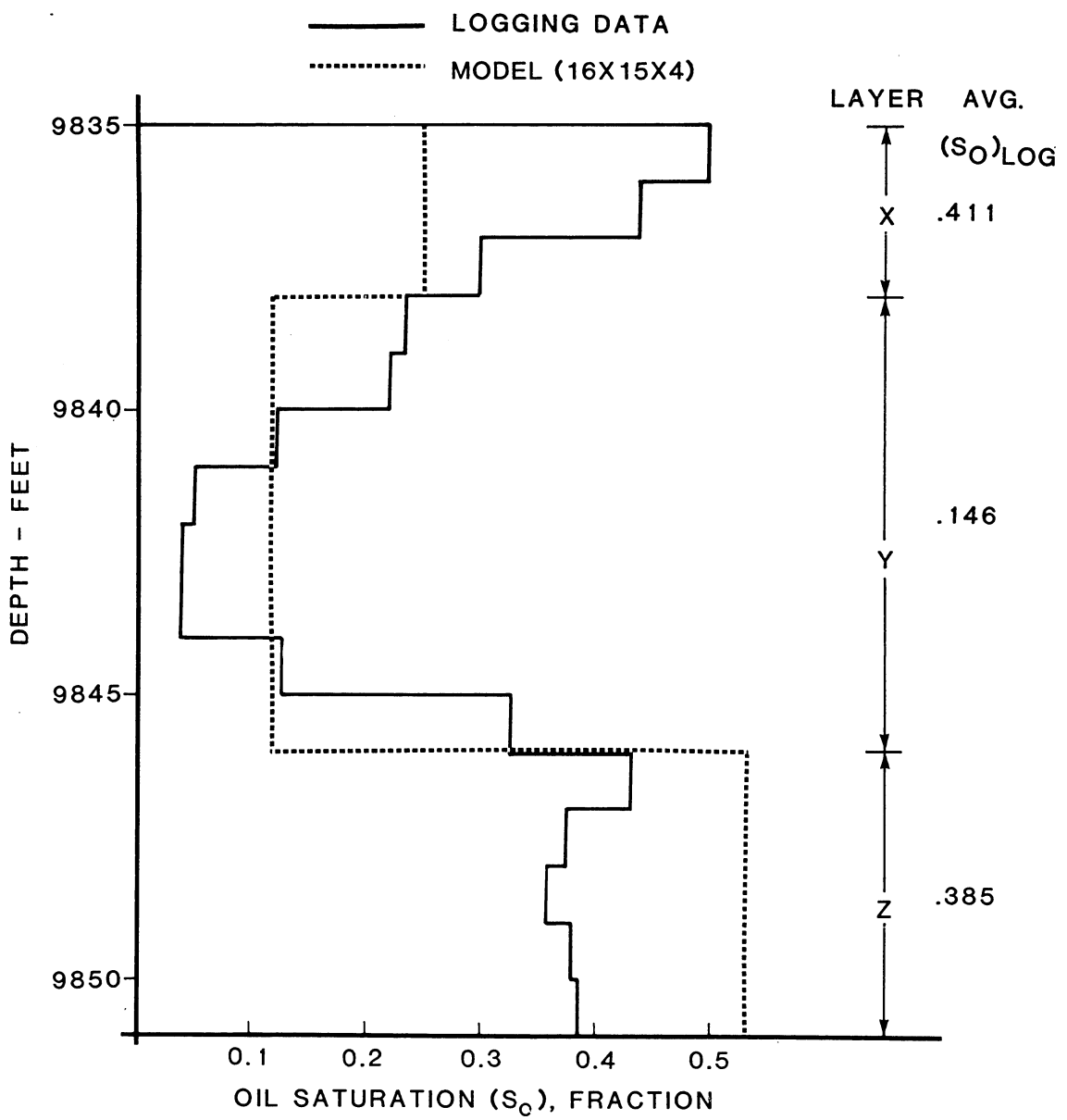

FIGURE 61

OIL SATURATION (AT STOCK TANK CONDITIONS) ON JULY 17,1981
FOUR LAYER MODEL
ZABOLOTNY OBSERVATION WELL NO. 4

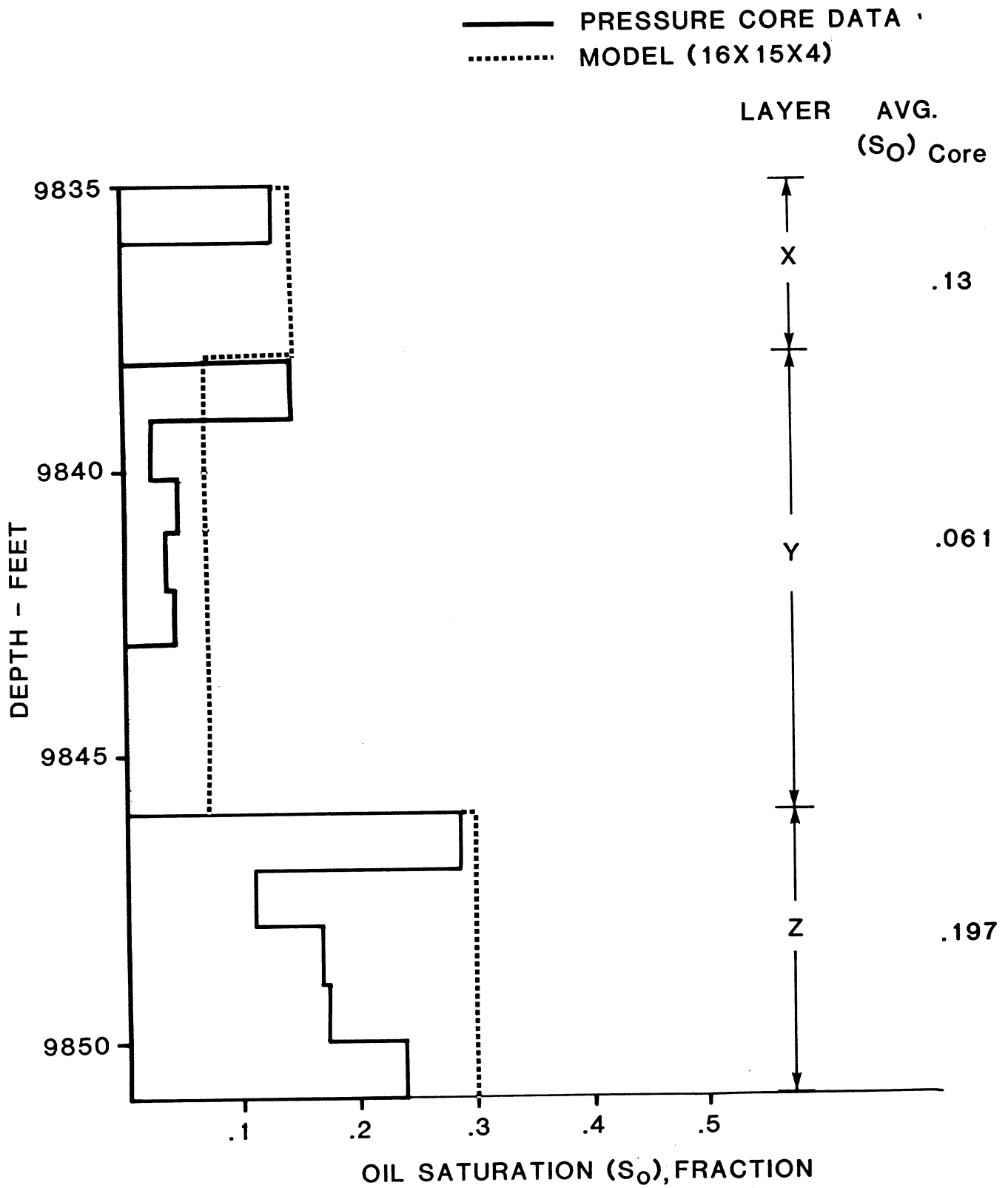

FIGURE 62

GAS SATURATION DISTRIBUTION FOR LAYER Y AT THE END OF CO_2 INJECTION

(March 25,1981)

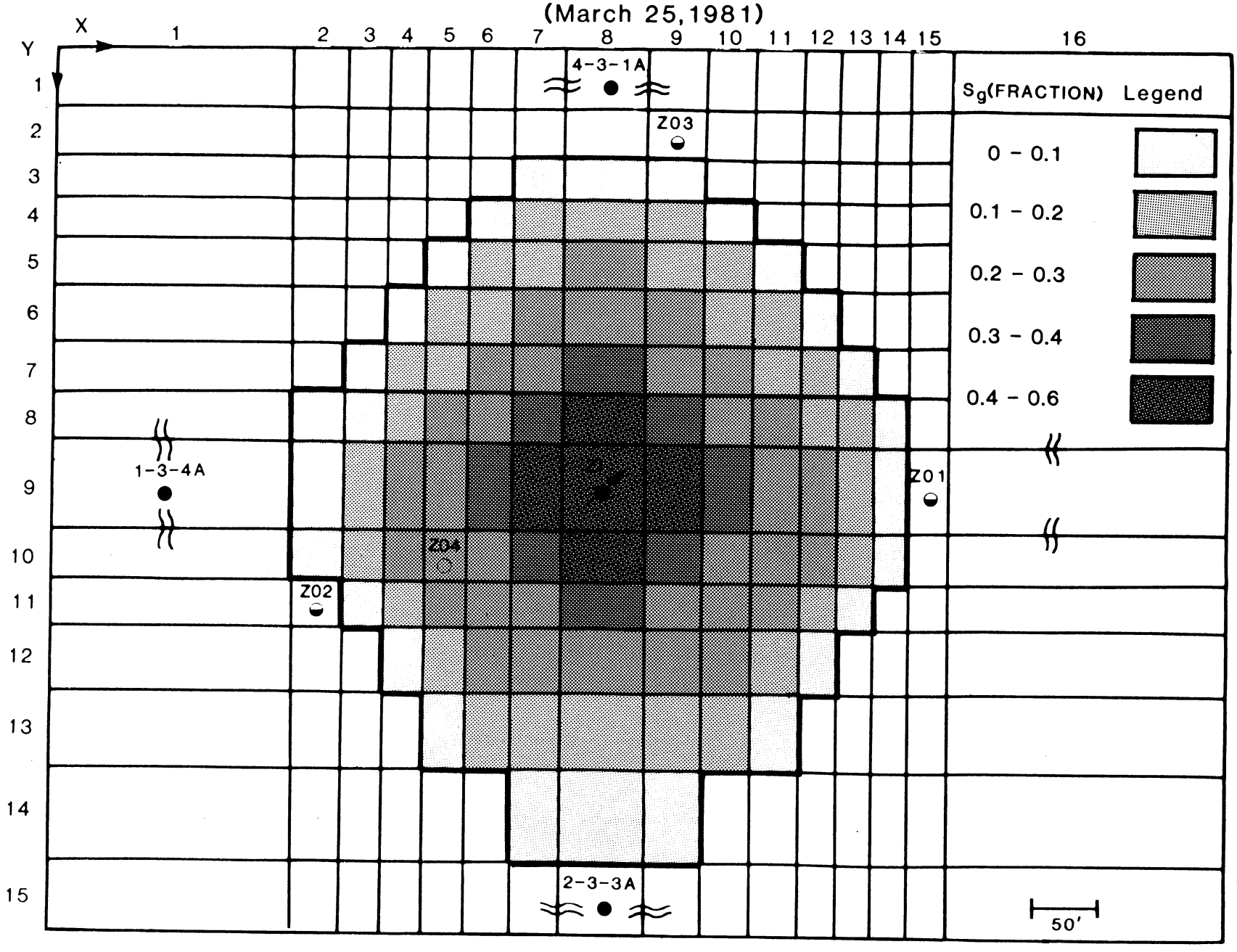

FIGURE 63

OIL SATURATION DISTRIBUTION FOR LAYER Y AT THE END OF CO_2 INJECTION

(March 25,1981)

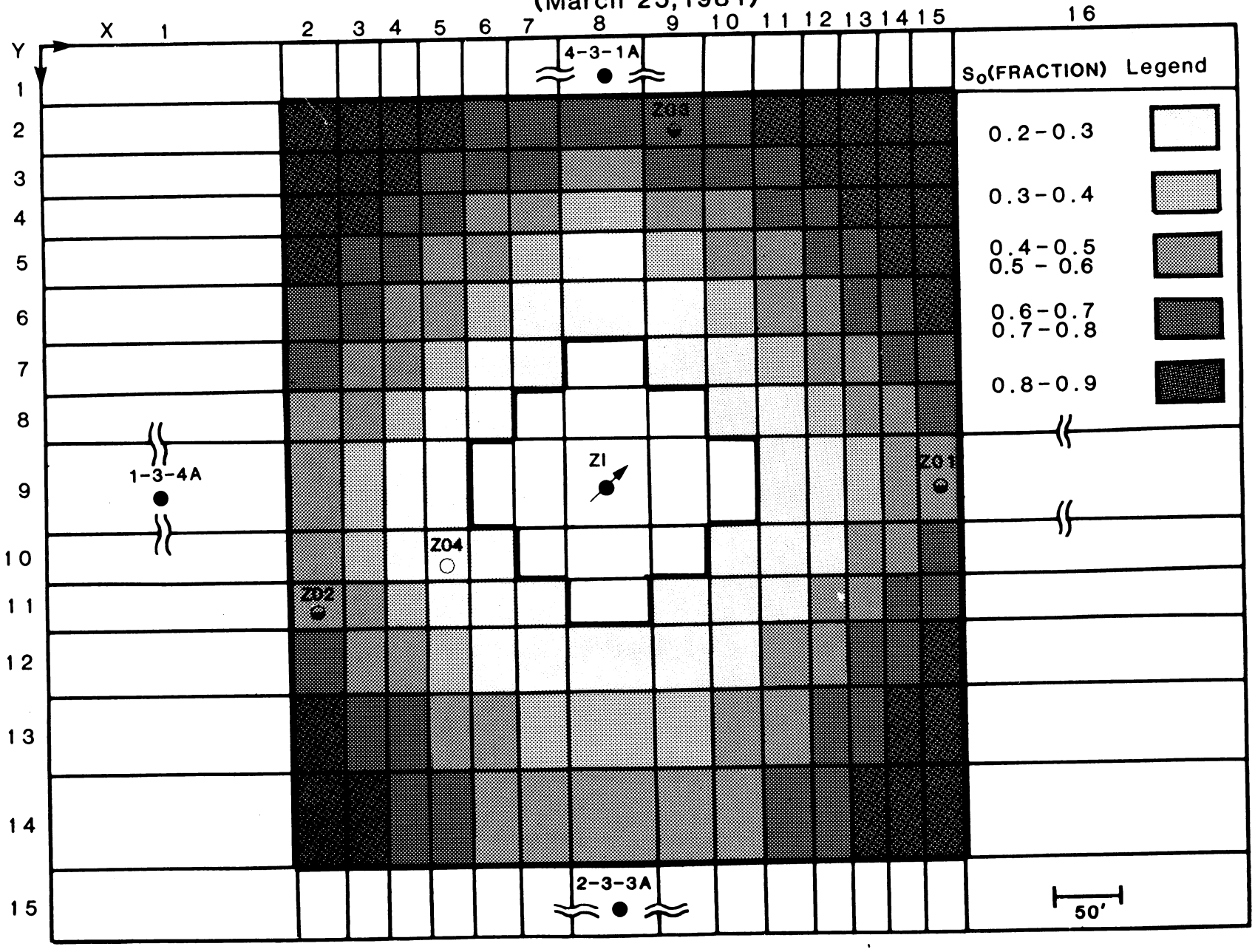

FIGURE 64

WATER SATURATION DISTRIBUTION FOR LAYER Y AT THE END OF CO_2 INJECTION

(March 25,1981)

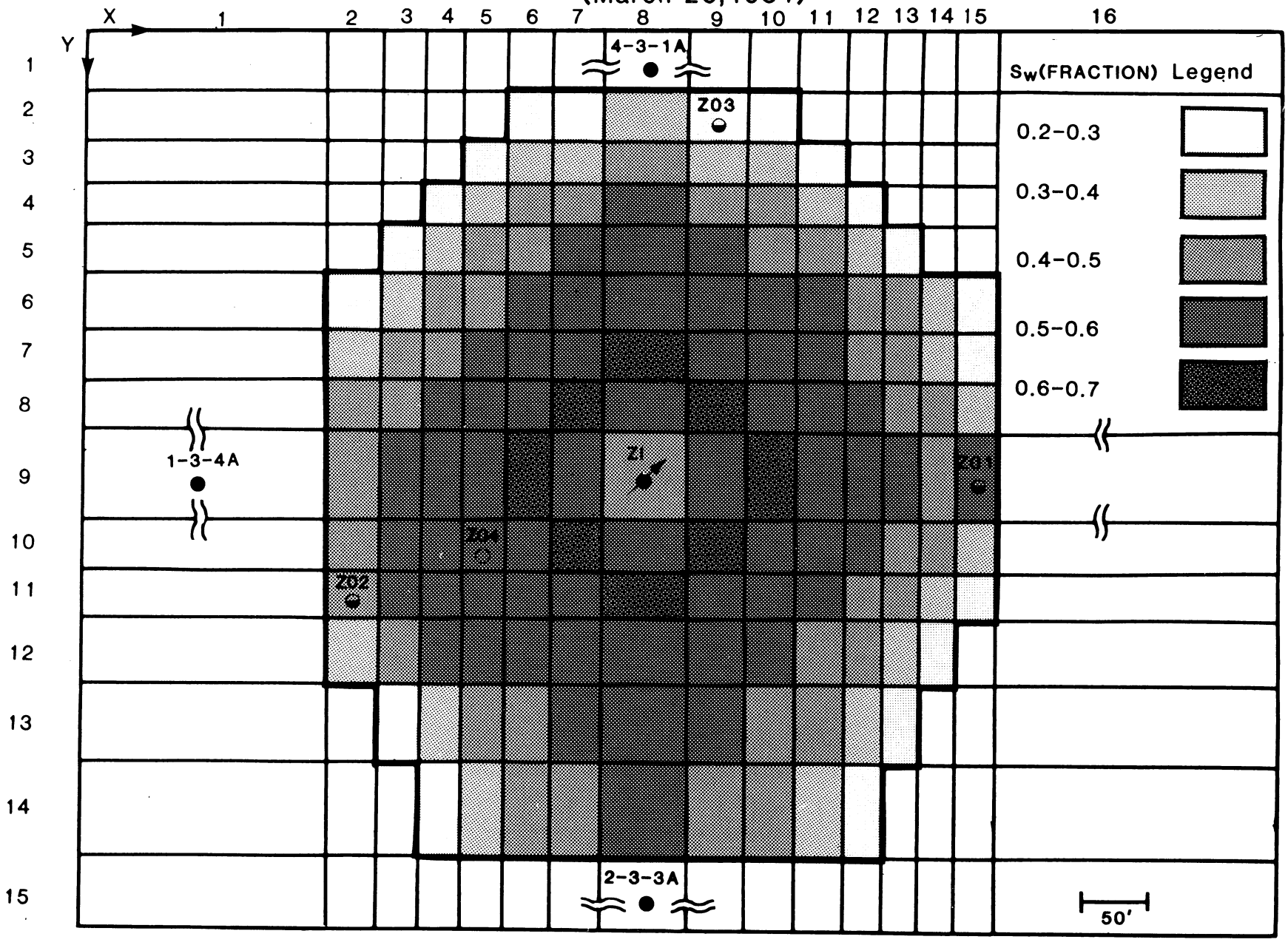

FIGURE 65

GAS SATURATION DISTRIBUTION FOR LAYER Y

(JULY 17, 1981)

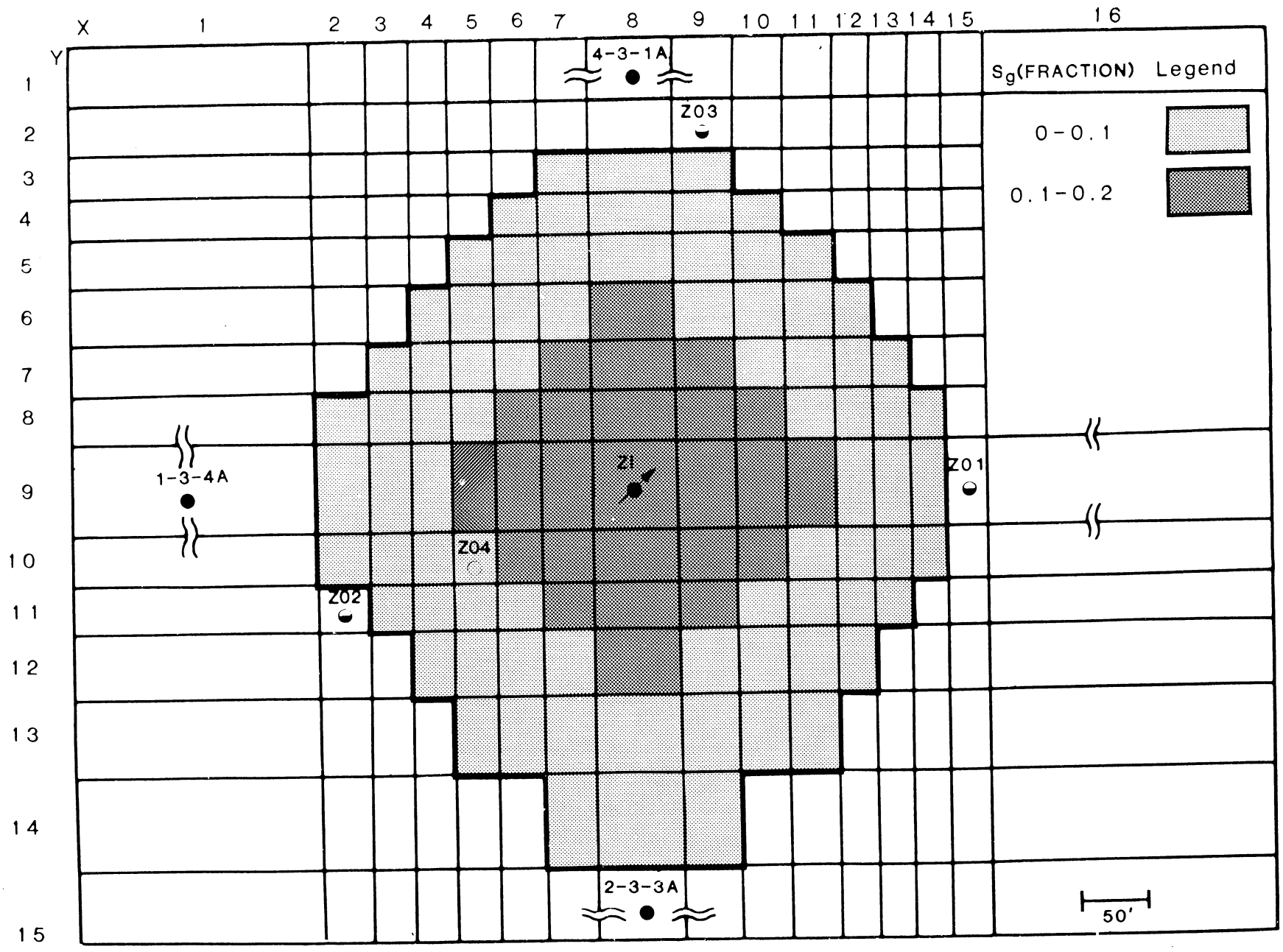

FIGURE 66

OIL SATURATION DISTRIBUTION FOR LAYER Y ON July 17,1981

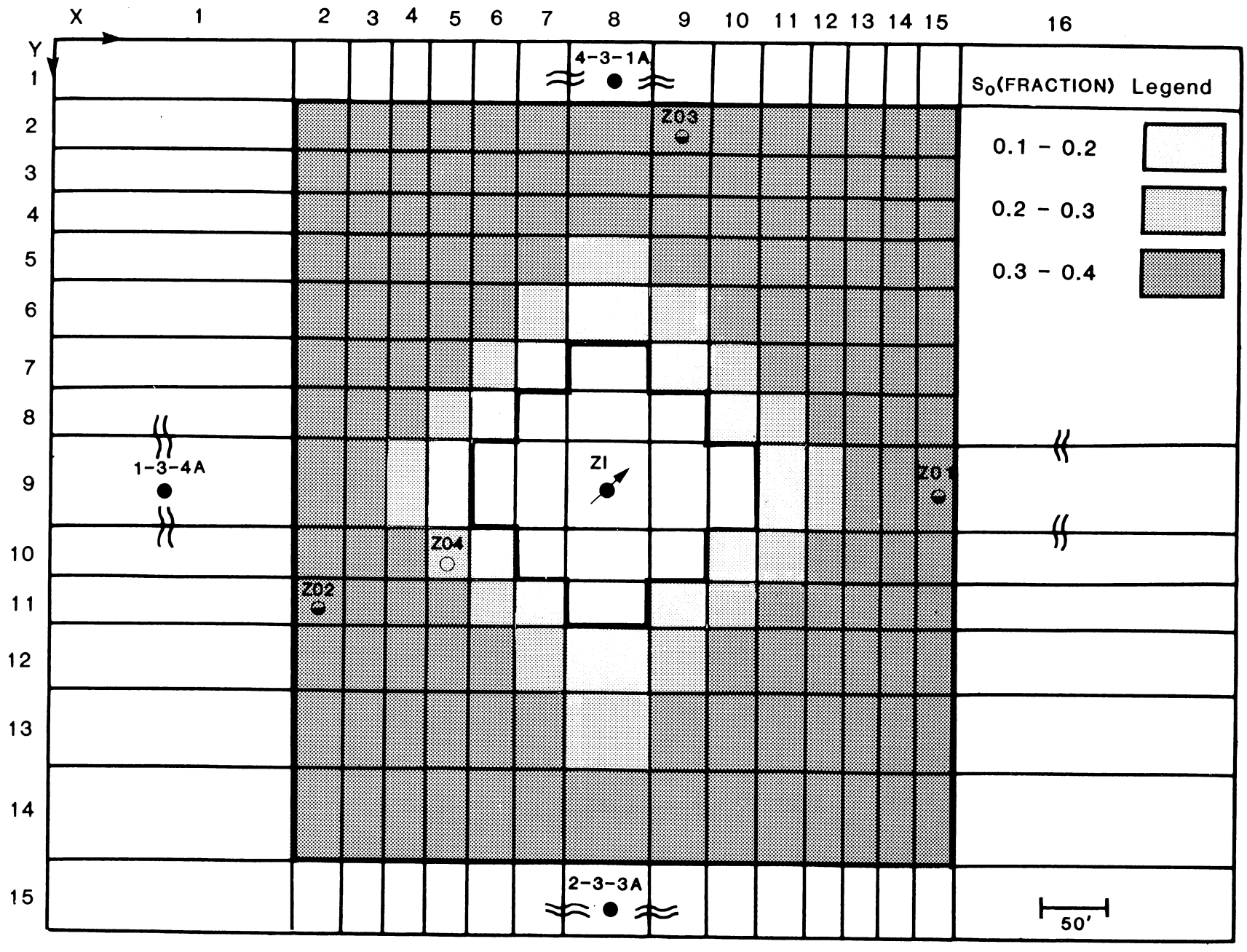

FIGURE 67

WATER SATURATION DISTRIBUTION FOR LAYER Y

(JULY 17, 1981)

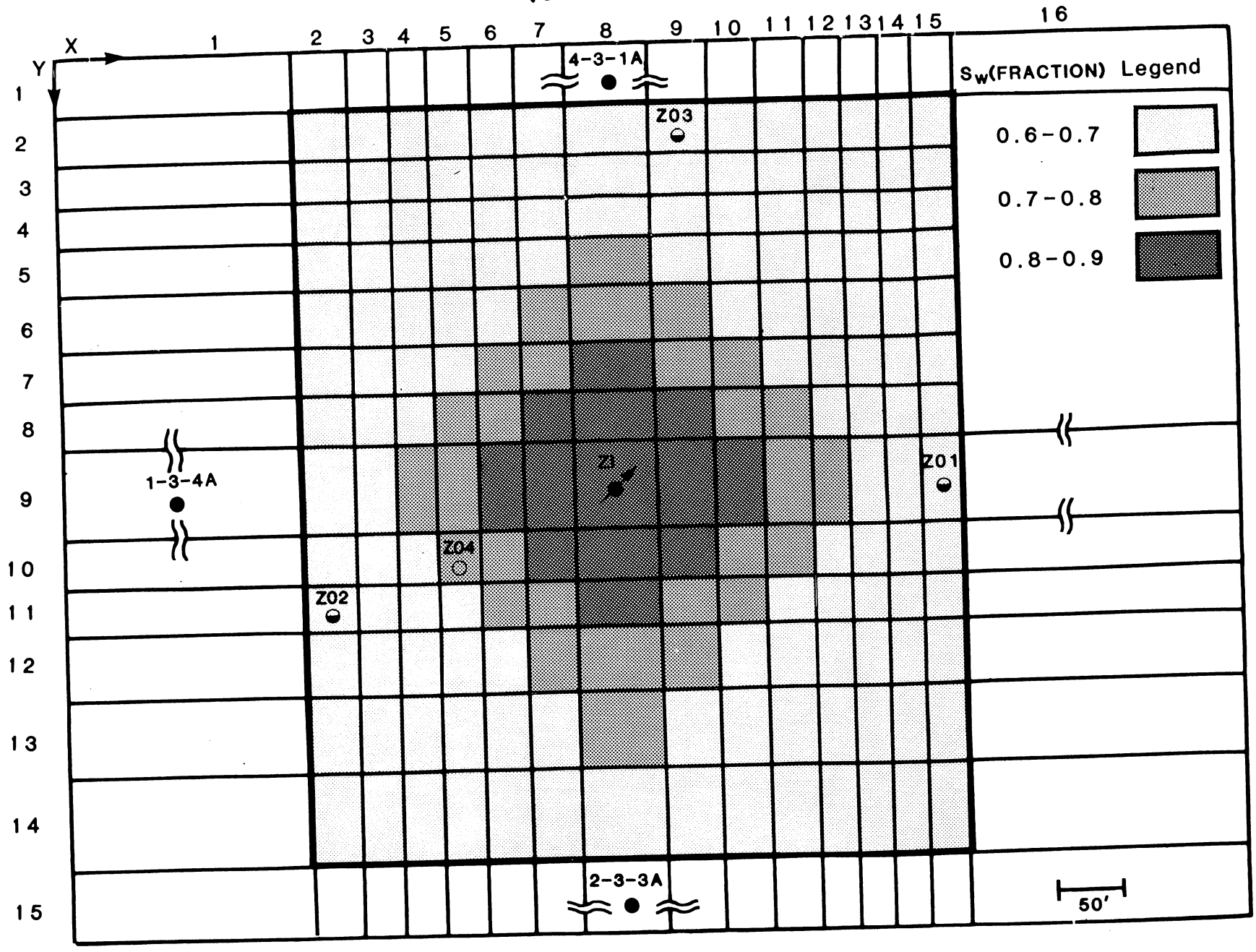

FIGURE 68
CO_2 - FREE OIL SATURATION DISTRIBUTION (PERCENTAGES) FOR LAYER Y
(July 17 , 1981)

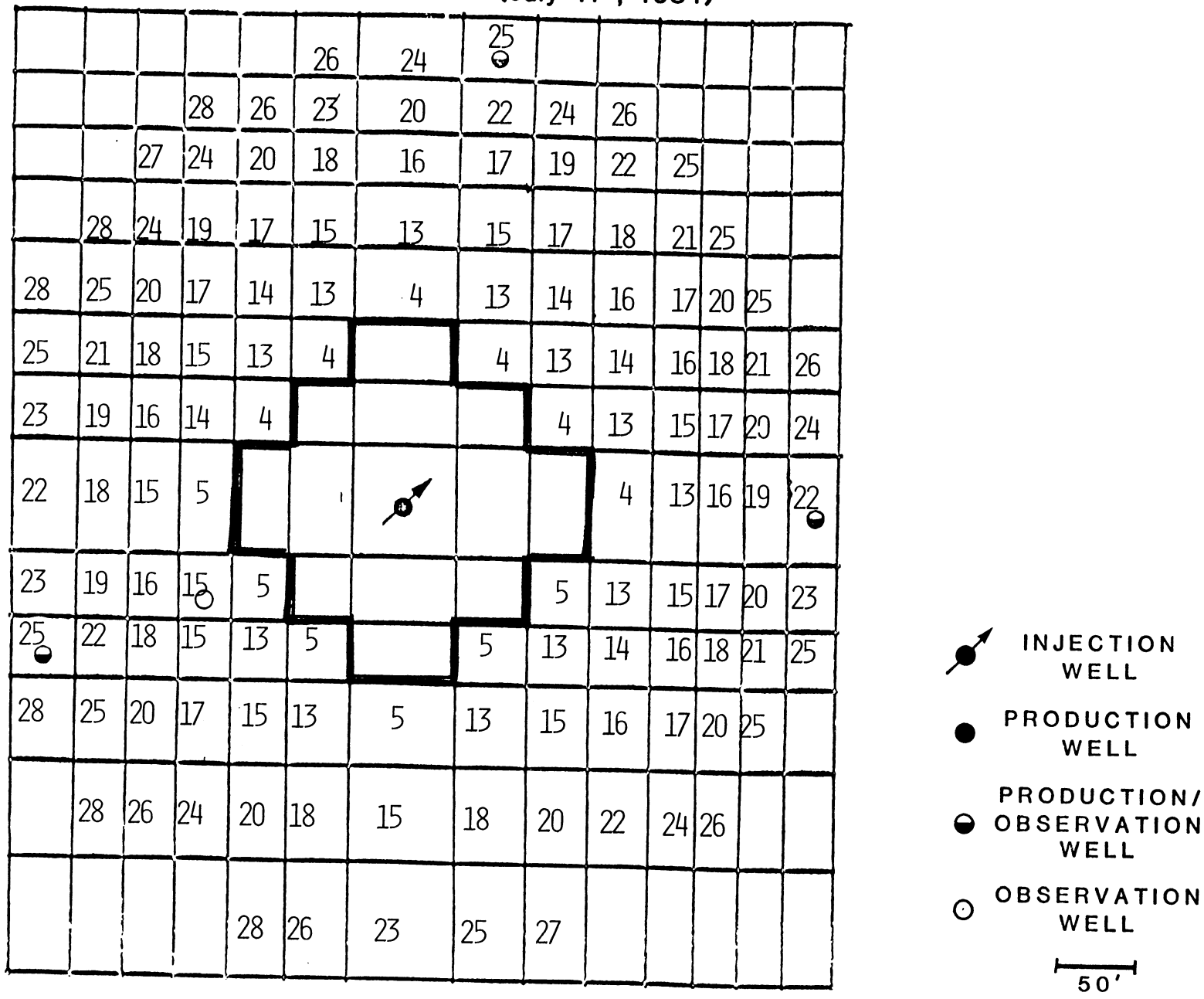

FIGURE 69

OIL RECOVERY FROM THE MINITEST AREA

BY PRODUCING ALL THREE OBSERVATION WELLS

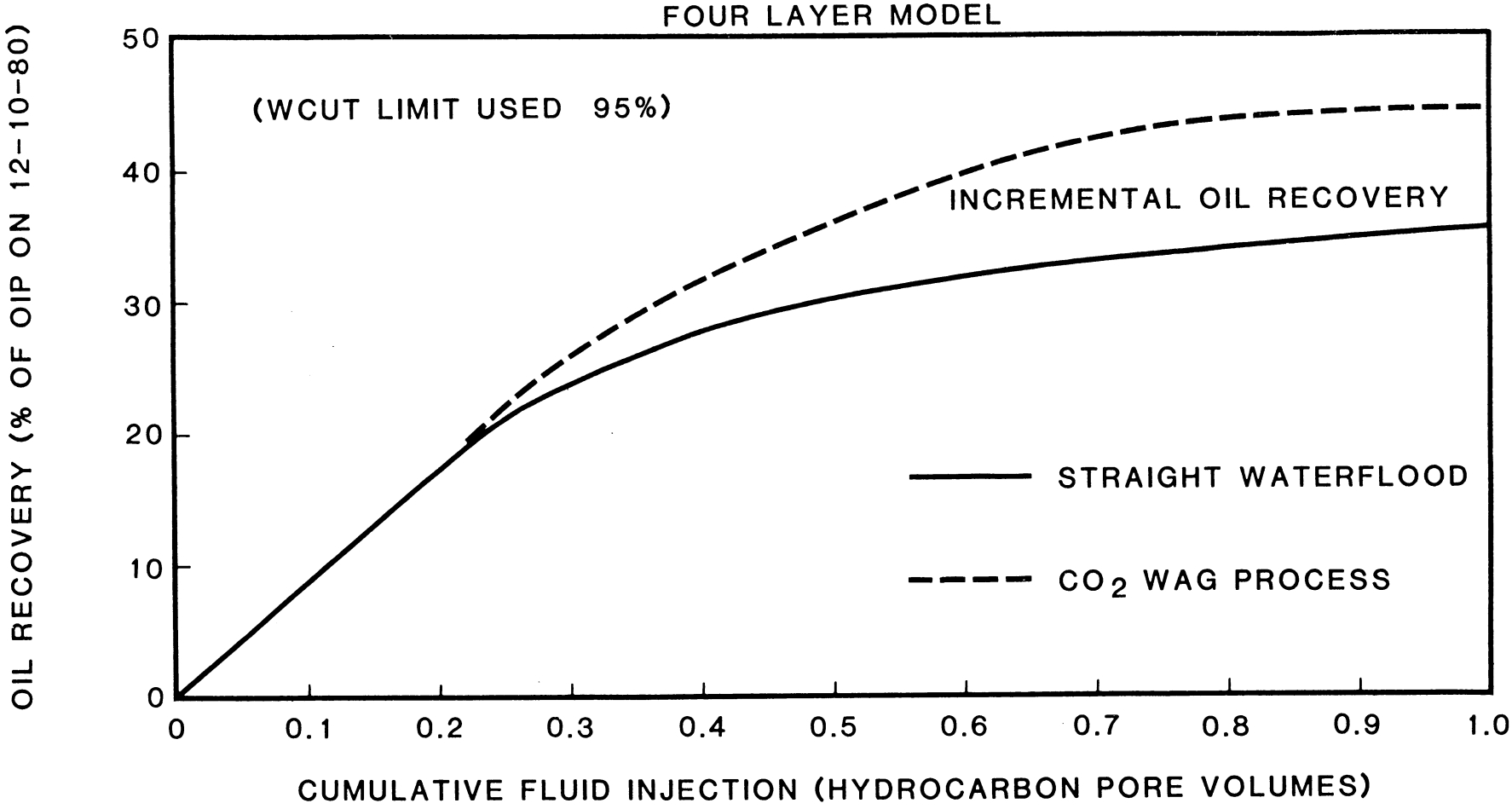

FIGURE 70

WATER SATURATION HISTORY MATCH FOR LAYER Y (12-11-80 TO 9-17-81)

SIX LAYER MODEL

ZABOLOTNY OBSERVATION WELL NO. 2

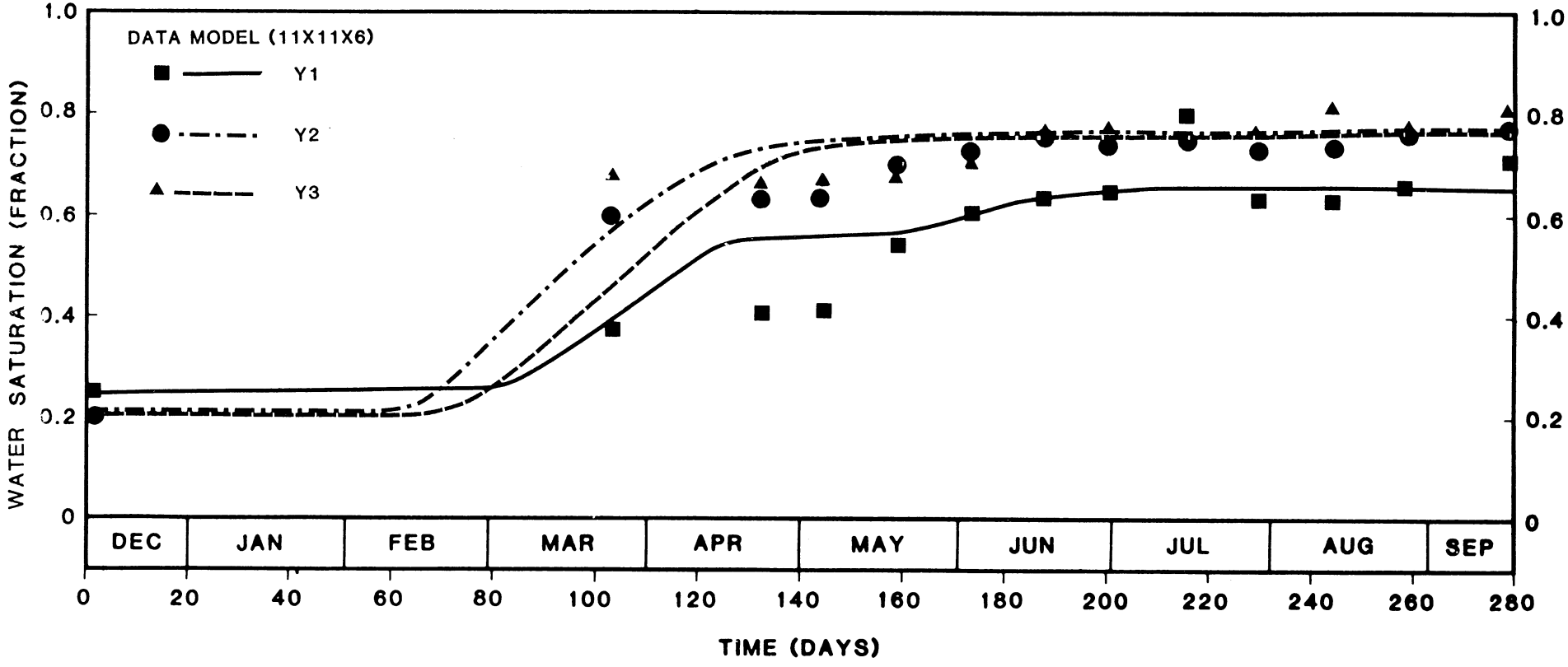

FIGURE 71

CARBON DIOXIDE SATURATION HISTORY MATCH FOR LAYER Y (12-11-80 TO 9-17-81)

ZABLOTNY OBSERVATION WELL NO. 2

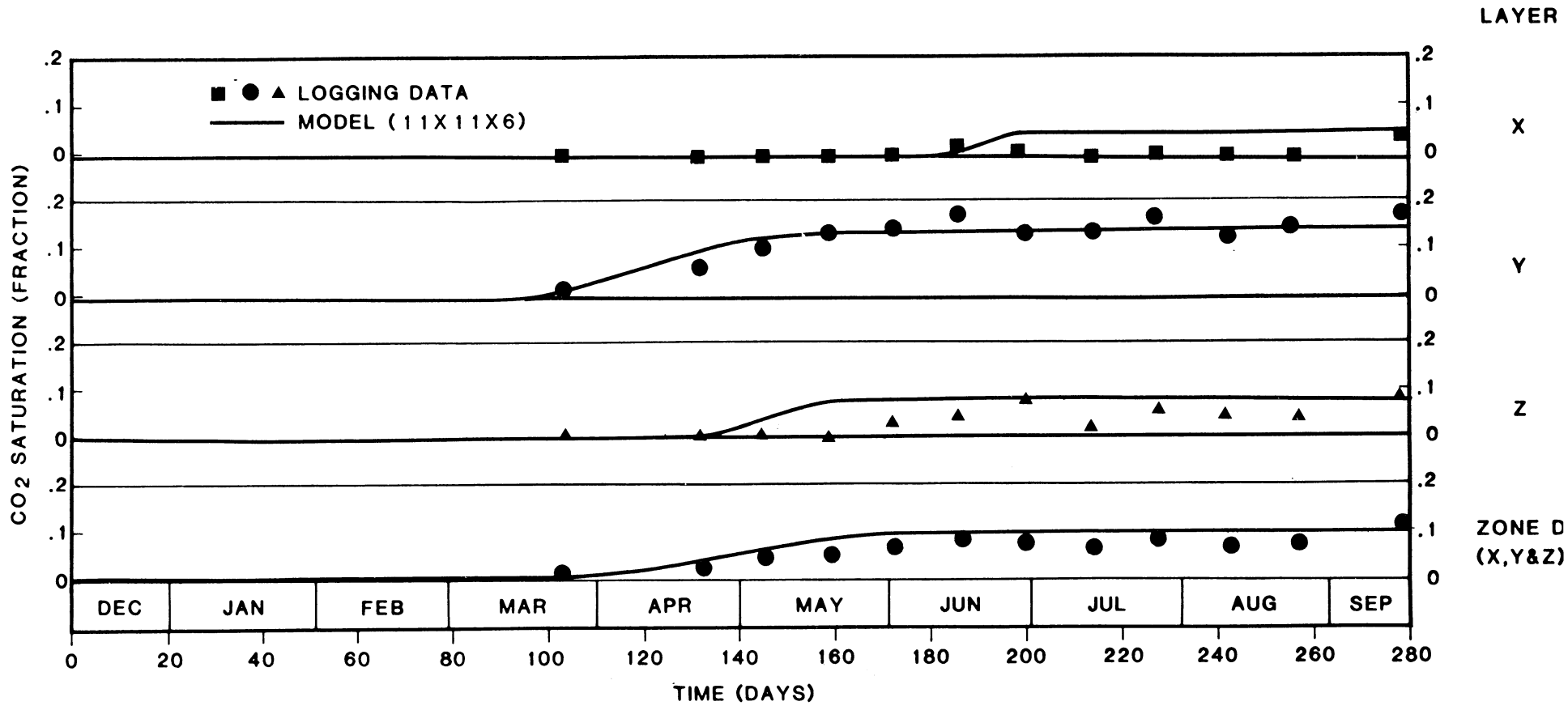

FIGURE 72

OIL SATURATION HISTORY MATCH FOR LAYER Y (12-11-80 TO 9-17-81)

SIX LAYER MODEL

ZABOLOTNY OBSERVATION WELL NO. 2

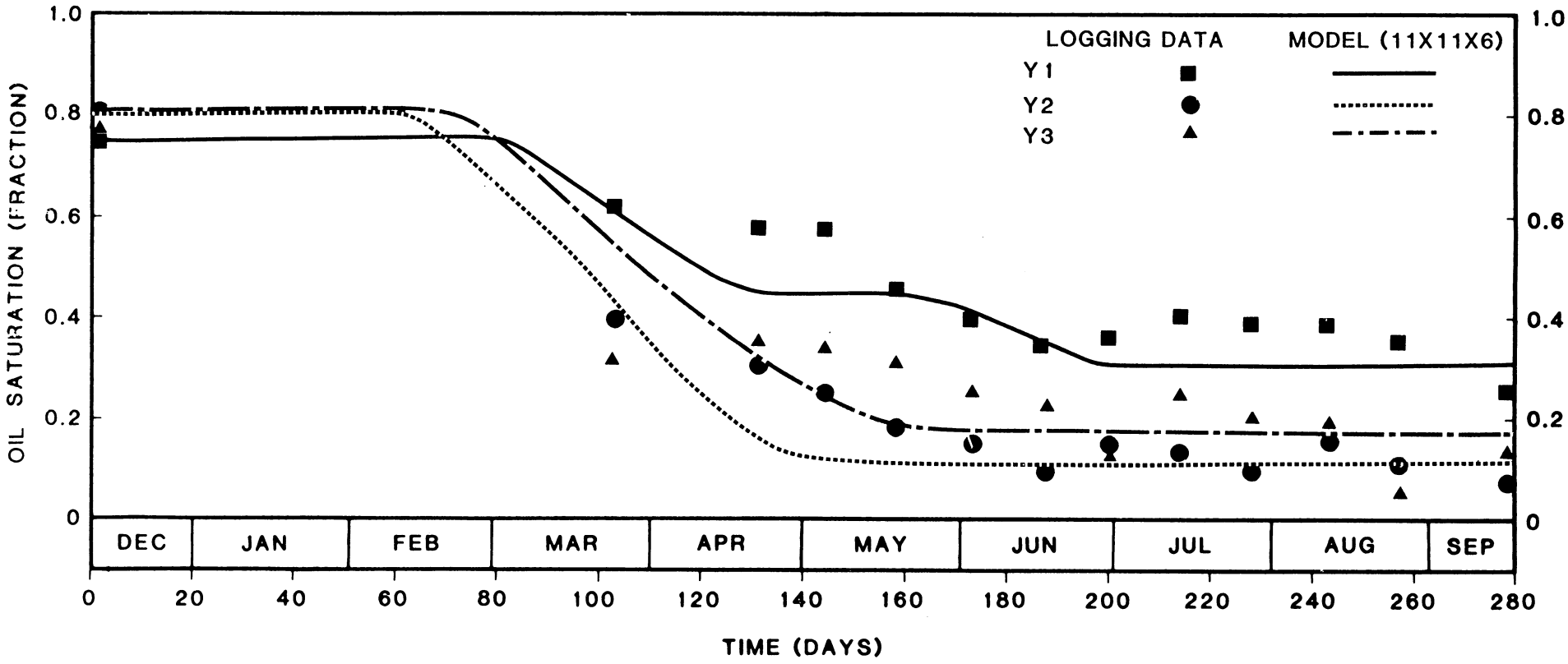

FIGURE 73

WATER SATURATION HISTORY MATCH FOR LAYER Y (12-11-80) TO 9-17-81)

SIX LAYER MODEL

ZABOLOTNY OBSERVATION WELL NO. 2

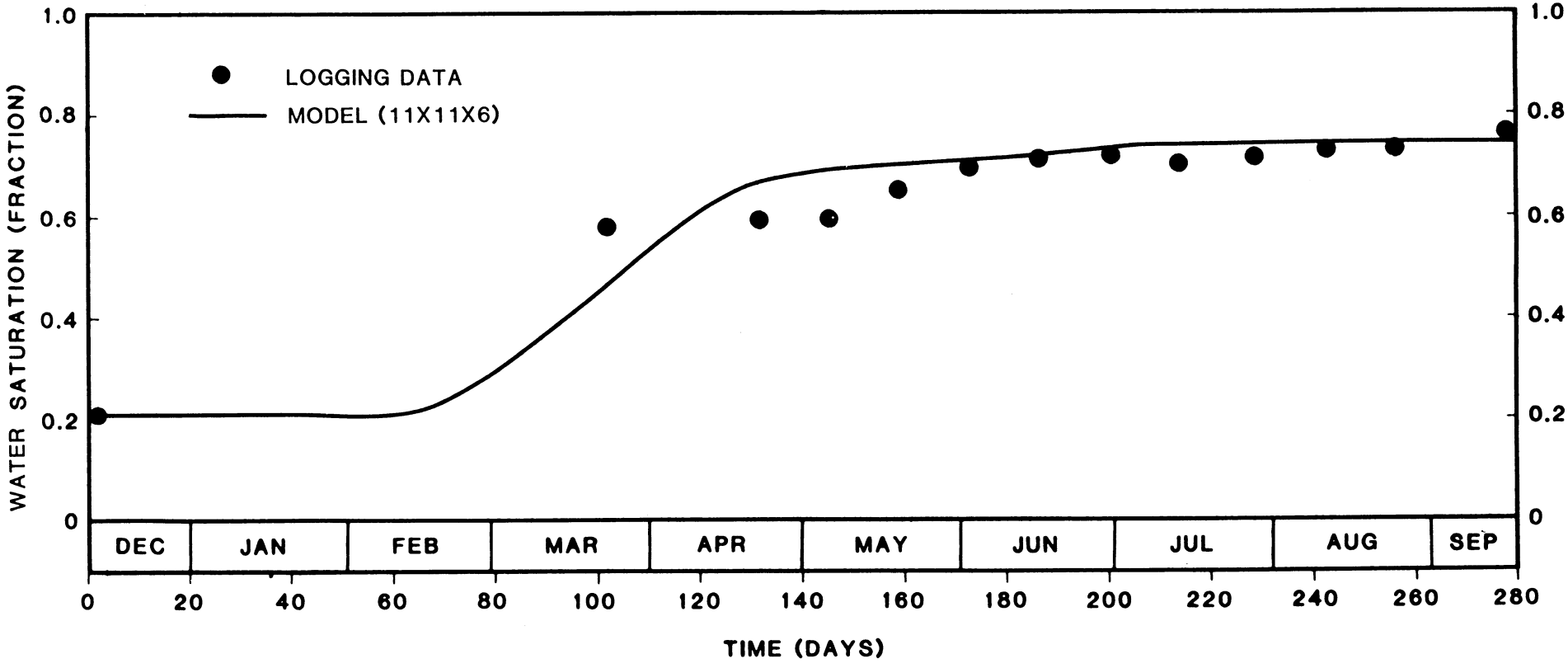

FIGURE 74

OIL SATURATION HISTORY MATCH FOR LAYER Y (COMBINED) (12-11-80 TO 9-17-81)

SIX LAYER MODEL

ZABOLOTNY OBSERVATION WELL NO. 2

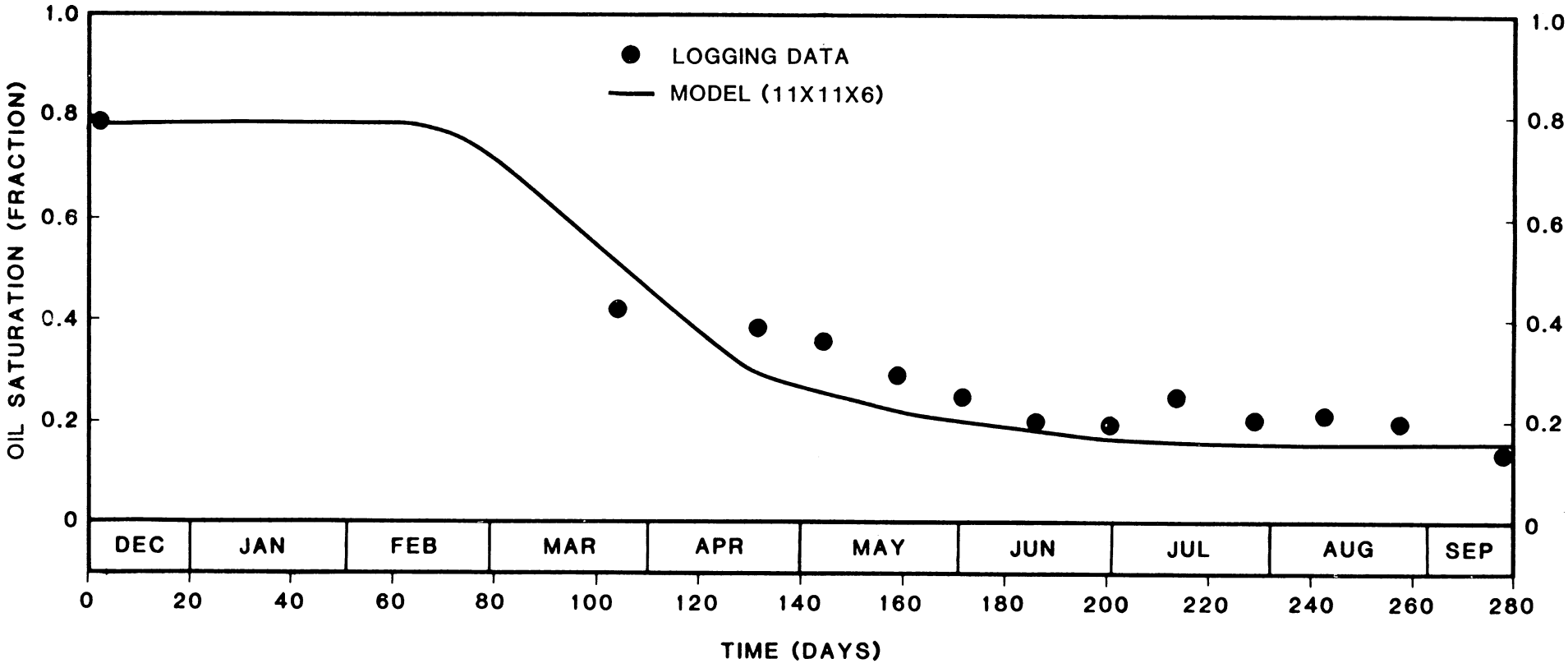

FIGURE 75

CO_2-FREE OIL SATURATION (AT RESERVOIR CONDITIONS)

ON JULY 17,1981

SIX LAYER MODEL

ZABOLOTNY OBSERVATION WELL NO. 4

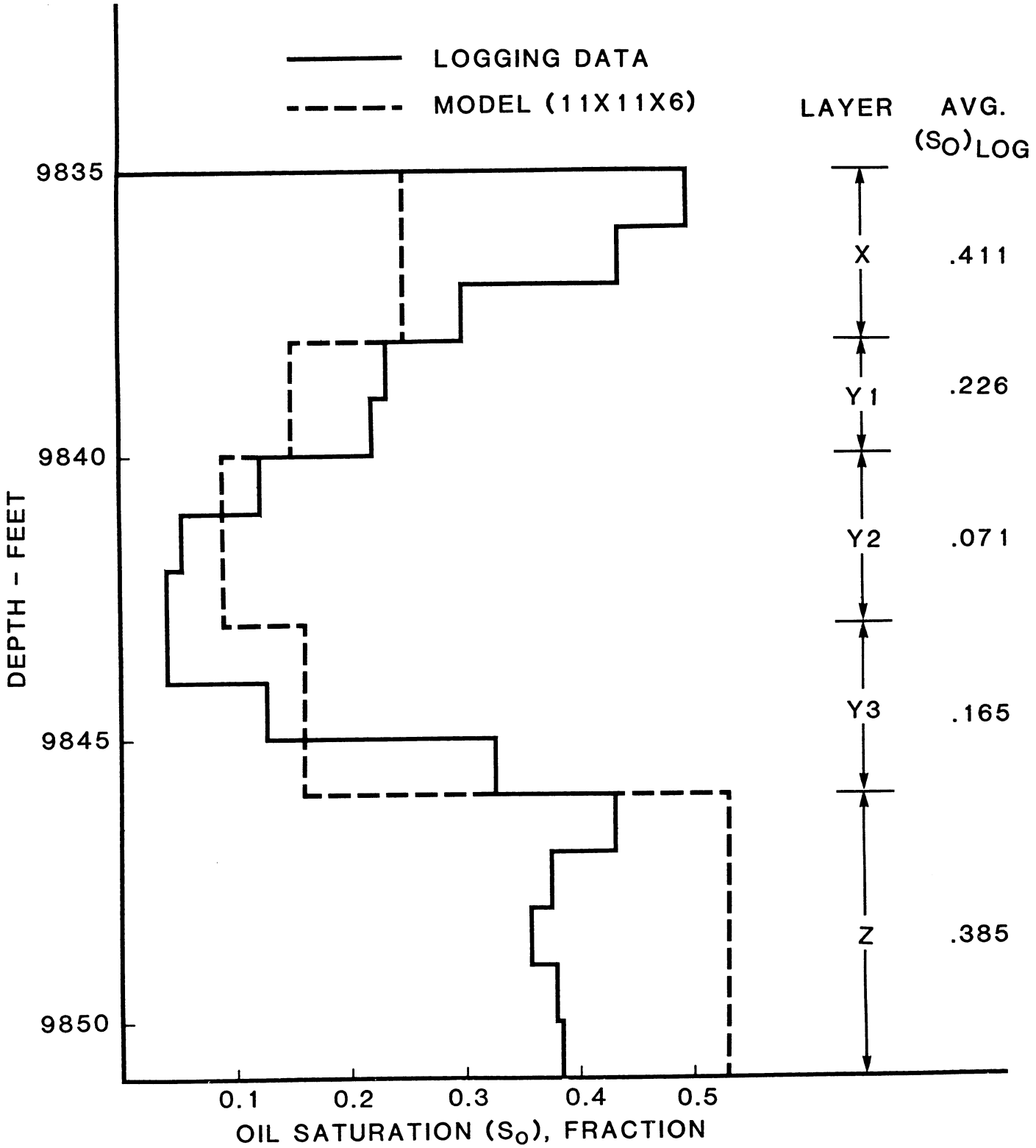

FIGURE 76

OIL SATURATION (AT STOCK TANK CONDITIONS) PROFILE

ON JULY 17 , 1981

SIX LAYER MODEL

ZABOLOTNY OBSERVATION WELL NO. 4

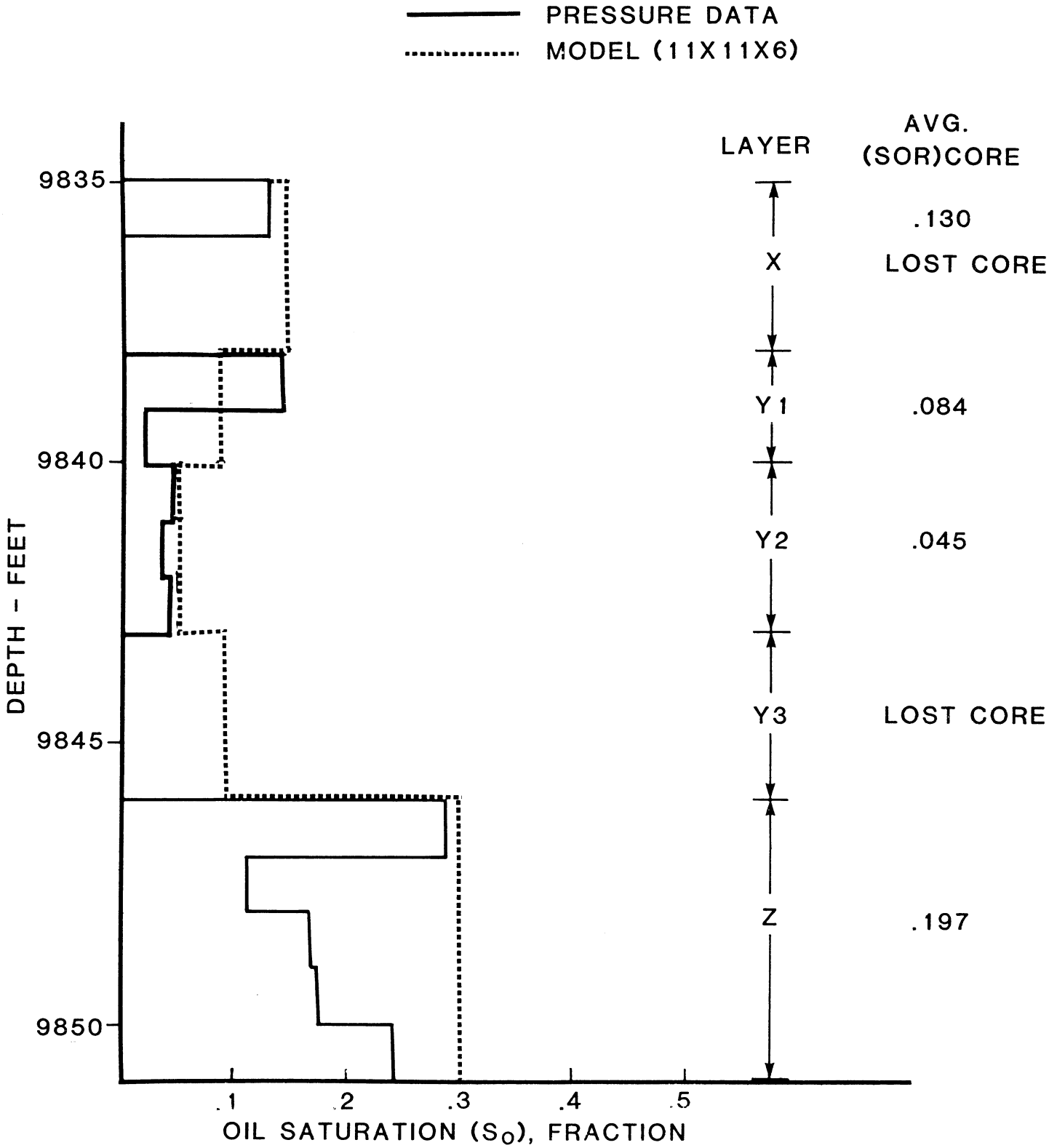

APPENDIX 44

AN EQUATION-OF-STATE STUDY ON THE FLUID PROPERTIES, PHASE BEHAVIOR AND MULTIPLE-CONTACT MISCIBILITY IN CARBON DIOXIDE DISPLACEMENT PROCESSES

By

Sheng-Tai Lee
John J. Komlenic

Production Research Department
Gulf Research & Development Company
Pittsburgh, Pennsylvania

TABLE OF CONTENTS

	Page
Abstract	265
Introduction	266
Prediction of Single-Contact Fluid Properties and Phase Behavior	268
Discussion on Representation of Multiple Contact Processes via Ternary Diagrams and Proposition of a Procedure to Study Development of Miscibility	280
Example Calculations and Discussions of Results	296
Conclusions	305
Acknowledgements	306
References	307

LIST OF TABLES

Table		
1	Compositional Analyses of Two Reservoir-Fluid Samples	310
2	Comparison of Experimental and Predicted Saturation Pressure	311
3	Comparison of Experimental and Predicted Swelling Factors	311
4	Volume Change upon Mixing for CO_2 and B Fluid System	312
5	General Distinctions of the Two Gas Injection Processes	313
6	General Information on the A Reservoir Fluid Slim-Tube Experiment	314
7	Hydrocarbons Compositions of Synthetic Oil	315

LIST OF FIGURES

Figure		
1	Pressure - Composition Diagram for A Mixtures	316
2	Stable, Meta-Stable and Unstable State of a Pure Substance	317
3	Prediction of Phase Stability for A Reservoir Fluid System	318
4	Triangular Representation for a Pure Ternary System	319
5	Tetrahedral Representation of a Four-Component System	320
6	Pseudo-Ternary Phase-Composition Representation of a Four-Component System	321
7	Slim-Tube Multiple Contact Process	322
8	Slim-Tube Multiple Contact Process	323
9	Effect of Mixing Ratio on the Minimum Miscibility Pressure	324
10	Effect of H_2S on MMP for CO_2 Injection Process	325
11	Pressure Composition Diagram for CO_2-Synthetic Oil System	326
12	Pseudo Ternary Representations of Compositional Path	327
13	Ternary Phase Envelope for IPA - Brine - Oil System	328
14	Dual Critical - Point Pseudo Ternary Phase Envelope	328

ABSTRACT

The purpose of this work is to demonstrate that an equation of state can be effectively utilized to generate sufficient and quite accurate information that could serve as a basis for designing laboratory experiments and field projects related to hydrocarbon recovery processes via gas injection. The study consists of two major parts. In the first part, we show that the single-contact data, such as the swelling factors and the pressure-composition phase envelopes, needed for preliminary evaluations of process feasibility can be predicted with reasonable accuracy using the Peng-Robinson equation of state. In addition, the volume change of mixing and the thermodynamic stability of the CO_2-Little Knife reservoir fluid system are investigated using the same equation of state and relevant thermodynamic relations. For the systems investigated and at practical reservoir conditions, we have found that the volume change of mixing cannot be neglected and that the CO_2-Little Knife reservoir fluid mixtures can exist as a single phase fluid in a metastable state without phase splitting if the mole fraction of CO_2 in the mixture exceeds 0.86.

In the second part, the use of pseudo-ternary phase-composition diagrams to represent the multicomponent processes is first discussed from a thermodynamic standpoint. Then, a simple procedure is presented to study the development of miscibility for high-pressure vaporization processes. This procedure utilizes a set of explicit finite difference flow equations together with the Peng-Robinson equation to compute the compositional changes and phase redistributions occurring in the front of the transition zone between the frontal fluid and the in-place reservoir fluid. The relative permeability characteristics of the porous medium is also taken into consideration in the procedure. The procedure presented is computationally simple.

Results from a previous slim-tube experiment were used to verify the proposed procedure. Good agreement was obtained between the experimental and the predicted minimum miscibility pressures. We have also found that the proposed procedure is capable of predicting the effect of various process variables, such as pressure, temperature and injected gas compositions, on the performance of a given recovery process.

I. INTRODUCTION

The design of miscible-displacement processes requires an accurate knowledge of the complex phase behavior and properties of the fluid systems involved. The most rigorous and convenient approach of examining the influences of the various factors on a given recovery process is by means of a fully compositional simulator containing an equation of state capable of describing, in detail, the phase equilibrium related to the process [2a]. The reliability of a simple van-der-Waals-type equation of state to predict the phase behavior and equilibrium properties of natural reservoir fluid systems has been greatly enhanced by the recent introduction of the Soave-Redlich-Kwong [23] and the Peng-Robinson equations of state [19].

This work was initiated as a summer project in 1980. The objectives were:

(1) To demonstrate the applicability of the Peng-Robinson equation of state in predicting fluid properties and phase behavior for mixtures resulting from mixing reservoir fluids with injection gases, generally called the single-contact data.

(2) To develop a simple procedure that utilizes the Peng-Robinson equation to examine the development of miscibility for hydrocarbon recovery processes via gas injection.

The single-contact data, such as the pressure-composition phase envelopes and the swelling factors, are useful for preliminary evaluation of potential reservoir fluids suitable for a particular kind of miscible-gas process. In addition, correct interpretation of the development of multiple-contact miscibility between the injection fluid and the original reservoir fluid is important in designing laboratory and field-wide projects.

Consistent with the objectives, this report contains two major sets of results. In the first part, we show that it is possible to use the Peng-Robinson equation of state to predict the single-contact fluid properties. We also examine the volume change upon mixing CO_2 and the Little Knife reservoir fluid at reservoir conditions. The magnitude of the volume change upon mixing not only will indicate the thermodynamic ideality of the fluid mixture involved, but also could shed light on the appropriateness of deriving the governing transport equations of a compositional process based on the volume-conservation principle [5]. Finally in this part, the Gibbs' criterion of fluid phase stability [6] is applied in connection with the Peng-Robinson equation to study the thermodynamic stability of the CO_2 and Little Knife reservoir fluid systems.

In the second part, a discussion of the use of pseudo-ternary diagram in describing the composition path of a multi-component multiple-contact process is presented. Then, a simple procedure is presented to calculate the compositional changes resulting from mixing, separation and flow at the front of the transition zone for high-pressure vaporization processes. This procedure is based on a set of explicit finite-difference material conservation equations and on the Peng-Robinson equation. Examples are also provided to illustrate the applications of the procedure.

II. PREDICTION OF SINGLE-CONTACT FLUID PROPERTIES AND PHASE BEHAVIOR

1. Fluid Systems Investigated

Two fluid mixtures from the Little Knife field, designated here respectively as the Little Knife A and the Little Knife B samples were used in this study. Compositions of both samples are given in Table 1 along with the respective reservoir temperatures. For the Little Knife B sample, the component analysis beyond the heptanes (C_7) was not available. In a compositional process, a lumped C_{7+} fraction may affect the computed development of miscibility. This is because as the critical region is approached, the K-values of the individual components in the fluid system approach one. In this situation representing the C_{7+} fraction by only one pseudocomponent could underestimate the vaporization tendency of the heavier components in the C_{7+} fraction.

2. Prediction of the Phase Behavior of the CO_2-Little Knife A Fluid System

An overall view of the phase envelope of the CO_2-Little Knife A mixtures at T = 240°F is provided in Figure 1 in the form of pressure versus CO_2 concentration diagram. This is a high-temperature CO_2-crude oil system, involving only two coexisting hydrocarbon phases and neglecting possible small amount of precipitated solid. The phase

behavior of the low-temperature CO_2-crude oil system is more complicated. It occurs at a reservoir temperature slightly above the critical temperature, 87.89°F (31.05°C), of CO_2 and generally exhibits a three-phase (vapor, light liquid and heavy liquid) behavior at CO_2 overall concentration above approximately 60 mole percent [18].

The predicted phase envelope (bubble-point, dew-point curves and the critical point) and the constant-liquid curves are shown in Figure 1 together with experimental data. The matches of the predicted versus the experimental data are quite satisfactory. Except for the binary interaction coefficient for CO_2 and the C_{12+} fraction, the equation of state parameters, e.g. the pseudo critical properties, acentric factors and binary interaction coefficients of the hydrocarbon pseudocomponents, were generated through the correlations that we developed earlier [13]. It is well known that the multiple-contact miscible displacement of the reservoir hydrocarbon depends on the formation of a critical solution in-situ. In this connection, the match of the experimental single-contact data at the near-critical retrograde region is particularly important. The phase behavior of the fluid at this particular region is influenced strongly by the molecular interactions among the light molecules (C_1), the heavy molecules (C_{12+}) and the dominant molecules (CO_2). Therefore, in addition to proper characterization of the parametric properties of the heavy hydrocarbons required by the equation of state, the binary interaction coefficients for the pairs involving C_1, CO_2 and C_{12+} must be given properly. Based

on our experience, for light-oil systems, the semi-theoretical equation [13, Chapter 4] that we developed to correlate the binary interaction coefficients involving hydrocarbon pseudocomponents can serve as good initial values to obtain a match with available experimental data.

In the rest of the section, we will focus our discussion on the predictions of the following fluid properties:

(1) the swelling factors of the CO_2-Little Knife B fluid system,

(2) the volume of mixing of the CO_2-Little Knife B fluid system, and

(3) the thermodynamic stability of the CO_2-Little Knife A fluid system.

3. Prediction of the Swelling Factors for CO_2-Little Knife B Fluid System

When CO_2 and oil are mixed, the following physical changes could occur that contribute to increased oil recovery: (1) the reduction in oil viscosity, (2) the extraction of oil to the light phase, and (3) the swelling of oil. The swelling factors of CO_2 and oil mixtures, being easily measured experimentally in a single-contact fashion, is therefore an important criterion in selecting prospective candidates for CO_2-flooding projects. By definition, the swelling factor is related to the fluid properties as follows:

$$\text{swelling factor} = \frac{\rho_0^s(\text{original oil at T})}{\rho_\ell(\text{oil} + CO_2 \text{ at T})} \times \frac{1}{1 - x_{CO_2}} \qquad (1)$$

where, in the numerator, ρ_0^s is the molar density, g mole/c.c., of the original oil at saturation pressure and reservoir temperature, T. The denominator contains the molar density, ρ_ℓ, of the CO_2 and oil mixture at the same temperature and x_{CO_2} is the mole fraction of CO_2 in the mixture containing CO_2 and oil. Based on the definition given in Equation (1), the swelling factor can be easily calculated through an equation of state. As the experimental swelling factors for the CO_2 and Little Knife B fluid system are available [4], the equation of state is now used to predict the swelling factors of this system. The predicted results will then be compared with the corresponding experimental data.

The procedure that we adopted to obtain the match of the swelling factors is now described. By adjusting only the interaction coefficient for CO_2 and C_{7+} fraction of the Little Knife B fluid, and leaving the rest of the equation-of-state parameters associated with the C_{7+} fraction to be generated through the correlations that we earlier developed, we were able to obtain a very good agreement between the experimental and calculated saturation pressures for mixtures containing CO_2 up to 50 mole percent (see Table 2). It is noted from the table that as the amount of CO_2 increases from 40% to 50% by mole, the deviation of the predictions changes from negative to positive. This could be ascribed to the fact that as the mole fraction of CO_2

approaches 0.5, the bubble point condition is near the critical state. At such conditions even the heaviest component has a considerable vaporization tendency. It is inappropriate then to represent the C_{7+} fraction by only one pseudocomponent. Simultaneous with the predictions of the saturation pressures, the molar densities and consequently the swelling factors for the CO_2-Little Knife B fluid system are calculated through the equation of state. The predicted swelling factors are compared with the corresponding experimental data for three CO_2 concentrations in Table 3. The overall absolute average deviation for 17 data points was 1.01% and the maximum deviation was -1.84%. This is quite acceptable because as stated earlier, the only adjusted parameter, associated with the equation of state, was obtained not from matching the swelling-factor data, but from matching the experimental data of the saturation pressures.

Simon and Graue [26] earlier developed a graphical correlation for determining the swelling factors of CO_2-crude oil systems, based purely on experimental data. Their correlation expresses the swelling factors as a function of the amount of CO_2 dissolved in oil and of the molar volume of the CO_2-oil mixture. The nine oils used by the above authors to develop their correlation all had vapor pressures less than 1 atm at the temperatures of their study (110°F-200°F). This indicates that these oils were depleted of the light hydrocarbons, i.e. C_1 to C_3. As a result, the application of the Simon-Graue correlation is limited. Furthermore, in comparison with Simon and Graue's approach,

the approach using the equation of state has sound theoretical basis, and its extrapolation to fluid systems and conditions, for which experimental data are not available, are more reliable.

Most recently, Mulliken and Sandler [17] used the Peng-Robison equation of state and the CO_2-crude oil solubility data published by Simon and Graue [26] to obtain a correlation of the interaction coefficients, denoted here as δ_{ij}, for CO_2 and the pseudocomponent representing the whole crude oil. The equation of state, together with the δ_{ij}'s determined, was then used to calculate the swelling factors, for the same CO_2-crude oil systems that Simon and Graue studied. It is noted that, in Mulliken and Sandler's work, only one pseudocomponent was used to represent the crude oil, and the Watson characterization factor [27] was used to relate the average boiling point and the specific gravity of the oil pseudocomponent needed as parameters in the equation of state. According to Mulliken and Sandler, the overall average deviation was reported to be 1.4% for 37 data points with a maximum deviation of 6.7%. Regarding Mulliken and Sandler's work, our comments are as follows:

1. The Watson characterization factor is used primarily as an indication of the paraffin content of a hydrocarbon fraction [27]. It is very insenstive to a wide range of values of the average boiling point and the specific gravity of the hydrocarbon fraction [13]. As a result, using the Watson characterization factor to relate the basic properties of hydrocarbon fractures is inappropriate.

2. For the CO_2-crude oil systems, CO_2 will preferentially extract the intermediate hydrocarbons (C_3-C_5) into the vapor phase. In this respect, it is improper to represent the hydrocarbons by a single pseudocomponent. Another argument regarding the representation of the heavy hydrocarbons by one pseudocomponent has been discussed in Section II.2.

4. Change of Volumes Upon Mixing CO_2 with the Little Knife B Fluid Sample

The changes of thermodynamic properties upon mixing two or more substances at constant temperature and pressure are generally called the thermodynamic functions of mixing [21]. The magnitudes of these functions are generally indicative of the degree of interactions and the similarities of the component molecules of the resulting mixture system. A solution, or mixture, is said to be perfect only if the molecular interaction, mass and size of the constituent molecules are sufficiently similar [21]. In such a case, all the thermodynamic functions of mixing are zero. The most easily measured and physically realizable thermodynamic function of mixing is the volume of mixing, denoted here as V^m. For a system of n_c components, V^m is defined as [21].

$$V^m \equiv V(P, T, x_1, \ldots x_{n_c}) - \sum_i x_i V_i^o(P,T) \qquad (2)$$

The superscript 'o' in Equation (2) refers to pure component properties and x_i is the mole fraction of the ith component in the single-phase mixture. The variable, V, is the molar volume of the mixture.

In studying the CO_2-crude oil mixtures, it is interesting from a theoretical point of view to know the magnitude of V^m. Another motivation for investigating the V^m for CO_2-crude oil systems is that, in a one-dimensional compositional numerical simulator for CO_2 recovery processes developed by the Shell Development Company [5], the conservation of volume was assumed in the governing transport equations; in other words, the volume of mixing is neglected in the transport processes. We have shown earlier in Section II.3 that the Peng-Robinson equation of state is accurate in predicting the volumetric properties of the CO_2-Little Knife B mixtures. Therefore, for the same fluid system, the equation of state should also provide reliable information regarding the change of volume upon mixing, V^m.

To compute V^m for the CO_2-Little Knife B fluid mixtures according to Equation (2), one needs, in addition to the molar volume of the mixture, V, the molar volume of each component, V_i^o, at the same condition. As some of the experimental pure component data at the desired reservoir conditions are not available, the equation of state was utilized to generate the needed data. Comparing the predicted pure-component molar volumes with the corresponding experimental data available [25], we found that for about 60 conditions, the average deviations for the light components, i.e. CO_2, C_1, C_3 and C_4 were about 2%, and those for the heavy components, i.e. C_5 and C_6 were about 4%. The errors involved in predicting the pure component data will reduce the reliability of the predicted V^m. Table 4 details the calculated

V, V_i^o and V^m for two mixtures of the CO_2 and Little Knife B fluid system at six pressure conditions. It is shown in the Table that in the single phase undersaturated region as pressure decreases toward the bubble-point curve, V^m/V increases steadily for both mixtures. In other words, as the liquid mixture becomes more compressible, the volume change upon mixing becomes more significant. Also judging from the numerical values of V^m/V given in Table 4, we have learned that in deriving the basic material balance equations for CO_2-related compositional processes, it is improper to neglect the volume change upon mixing.

5. Thermodynamic Stability of CO_2-Crude Oil Systems

Introduction. Thermodynamic systems can be considered as being either stable or unstable. By definition, unstable fluid systems will spontaneously change to form different stable fluid systems. As the thermodynamic variables, such as pressure, temperature and compositions, vary, it is important to have the criteria that can be used to judge when a stable system may become unstable. Although several thermodynamic textbooks [16,24] have introduced such criteria and some recent technical publications have applied the criteria for simple binary and ternary systems, a general treatment on the subject, nevertheless, is still to be found in Gibbs' original work [6].

The primary purpose of our study here is to apply Gibbs' general criteria of fluid-phase stability to the CO_2-Little Knife A

fluid system. To fix some basic concepts, a simple case of single-component phase stability is examined first.

A Simple Example of Phase Stability. Let us focus our attention on a particularly simple example, taken in part from [22]. Consider a subcooled single-phase, pure liquid in an isothermal environment (see point a in Figure 2). As the pressure is reduced to the bubble-point pressure (point b in the Figure), one might expect boiling to occur. Usually this will occur, as expected, and vapor at g occurs. However, if the liquid is reasonably free of impurities and the experimental equilibrium cell is ideally smooth [2], we can superheat the liquid by passing into the phase envelope toward point d. The path from b to d is termed "metastable", indicating that there exists a more stable phase (i.e. vapor), but with small perturbations on the system, no phase transition will occur. Although the lowest attainable pressure depends on the experimental conditions, there exists a thermodynamic limit where even a slight reduction in pressure leads to a phase change. This condition is called "the limit of intrinsic stability*" [16]. On Figure 2, it is shown schematically at point e. It is emphasized here that in this simple example the liquid phase is intrinsically stable in the region from points a through b and d up to e. At point e, the stability criterion is violated. For the simple example considered

* Equivalent terminologies include diffusional stability [22], and material stability [24].

here, this is because between points 'e' and 'f', $(\frac{\partial p}{\partial v})_T > 0$, which is physically unrealizable in practice.

Similar reasoning can be applied for isothermal compression of saturated vapor at point g to a limit at point f at which a slight increase in pressure would result in the disappearance of vapor phase.

Thermodynamic Stability of CO_2-Little Knife - A Fluid System. It was shown by Gibbs[6] that a necessary and sufficient condition for a multicomponent mixture (of n_c component) to be intrinsically stable is that the symmetric matrix, G, of the second partial derivatives

$$\left(\frac{\partial^2 g}{\partial x_i \, \partial x_j}\right)_{T,P,x_k,k\neq i,j} \qquad \begin{array}{l} i = 1, 2, \ldots, n_c-1 \\ j = 1, 2, \ldots, n_c-1 \end{array} \tag{3}$$

be positive definite, where g is the molar Gibbs free energy. Therefore, the limit of intrinisic stability is the locus of the points at which the matrix, G, ceases to be positive definite. Since G is a symmetric matrix, the condition of the stability limit is equivalent to

$$\text{determinant } (G) = 0 \quad . \tag{4}$$

The partial derivatives of Equation (3) can be obtained in accordance with any specific thermodynamic model used. Peng and Robinson [20], in their work on predicting the critical state of

multicomponent mixture, derived explicit expressions of the second partial derivatives of the molar Gibbs free energy, based on their equation of state. The expressions of $\frac{\partial^2 g}{\partial x_i \, \partial x_j}$, derived by Peng and Robinson, are used here to investigate the thermodynamic stability of the CO_2-Little Knife A fluid system. The pressure limits of intrinsic stability of the CO_2-Little Knife A fluid system at a reservoir temperature of 240°F are now calculated based on the Gibbs criterion (Equation 4) and the Peng-Robinson equation of state. The results are plotted in Figure 3 together with the predicted bubble-point, dew-point curves and the critical point. According to the Gibbs criteria for stability of fluid phases and for the critical state of fluid systems, the envelope of intrinsic stability and the conventional bubble-point and dew-point phase envelope should coincide at the critical point of the fluid system (see Figure 3). Consequently, as the state of fluid is closer to the critical state, the region of the single-phase metastability shrinks, as indicated in the Figure. Also, according to the prediction in Figure 3, it is interesting to note that as the mole fraction of CO_2 exceeds about 0.86, and if the experimental process is ideally smooth, then the fluid system can exist as a single-phase vapor state throughout all pressure ranges without undergoing phase split. To our knowledge, the analysis on the stability of fluid phases for multicomponent fluid systems involving natural hydrocarbons has not been seen in the published literature. On the other hand, it must be noted that in a real field recovery process, the metastable state of the fluid system is unlikely to be encountered. This is because in a recovery process phase, equilibrium occurs simultaneously with continuous fluid flow in the porous medium; also some impurities, such as inorganic compounds, may exist in the fluid mixture.

III. DISCUSSION ON REPRESENTATIONS OF MULTIPLE CONTACT PROCESSES VIA TERNARY DIAGRAMS AND PROPOSITION OF A PROCEDURE TO STUDY DEVELOPMENT OF MISCIBILITY

1. Introduction

Currently in the area of tertiary recovery processes, the multiple-contact miscible processes generally include two broad categories: the chemical (surfactant) process and the miscible process via gas injection. The basic differences of both types of processes are discussed briefly here. In a surfactant process, the solubility of the two immiscible liquid phases (oil and water) is enhanced with the existence of surfactant; more importantly, under certain conditions, a middle phase can be developed between the oil and water phases so that the interfacial tensions between the existing phases are drastically reduced. On the other hand, in the miscible gas processes, the most significant mechanism responsible for the development of miscibility is via the preferential extraction, or condensation, of the fluid components involved to form a critical solution; the change of interfacial activity is only gradual.

Among the gas injection recovery processes, two types of processes are generally conceived: (1) the condensing-gas, or rich gas, drive, and (2) the vaporizing, or high-pressure, gas drive. The distinctions between these two processes are detailed in Table 5. The objectives of this section are:

(1) to examine the validity of using the pseudoternary phase-composition diagrams to describe the development of multiple contact miscibility, and

(2) to present a simple method, which utilizes a set of material balance equations and the Peng-Robinson equation to predict the development of miscibility for gas injection processes.

2. A Discussion on Representation of Multiple Contact Processes via Ternary Diagrams

Hutchinson and Braun [10], Beham, et al. [1] and several other authors have used the ternary diagrams with grouped components as a means of studying the phase relationship and development of miscibility for systems with more than three components. Most recently, Williams, et al. [31] presented a method of utilizing the Peng-Robinson equation of state and the ternary diagram to predict the development of multiple-contact miscibility. According to the above authors, the phase envelope in the ternary diagram was constructed based on the following procedure:

> "A three-component composition (C_1, C_{2-6}, C_{7+}) was arbitrarily selected from within the envelope for initial flash. Then a detailed composition was constructed using the same proportions of individual hydrocarbons within the pseudocomponent grouping as found in the reservoir fluid."
>
> "The flash calculation was then performed providing equilibrium gas and liquid composition. These compositions were reduced to the pseudocomponent compositions for display (in the ternary diagram). Additional flashes were performed in a similar manner to fill out the envelope."

William, et al.'s procedure to predict the development of miscibility oversimplified the multicomponent multiple contact processes in two important aspects:

(1) By arbitrarily selecting a composition point within the two phase region of the pseudoternary diagram and then performing the flash calculations, the multiple contact process is not properly accounted for in the calculation procedure. The overall composition path of a multiple-contact front, plotted in a pseudoternary diagram, is a smooth curve extending from the composition point of the injection fluid to that representing the original fluid.

(2) By setting the proportions of the constituent components, grouped as the intermediate and heavy pseudocomponents, to be the same as those of the original oil, the effect of preferential extraction, or condensation, is neglected. Because of the above mentioned mass-transfer effect, the relative amounts of the constituent components in the displacement front are different from those of the original oil.

To acquire a sound theoretical basis on the validity of the triangular representation of the phase-composition relations for multiple contact processes, a discussion, based mainly on thermodynamic principles, is made in Sections II-3 and II-4 to follow.

3. Thermodynamic Considerations for Miscible Processes Having Three Pure Components at Fixed Temperature and Pressure

The phase-composition relations and the conditions of multiple contact miscibility for fluid systems containing three pure components have been well documented in the literature [10]. We recall here only

the basic results. In the ternary diagram (see Figure 4) representing the phase equilibrium of the three pure components, C_L, C_I and C_H, where subscripts L, I and H refer respectively light, intermediate and heavy components, the saturation curve, s, together with the tangent, t, to this curve at the critical point c, divide the diagram into four regions:

(1) the two-phase region, denoted as I;

(2) the super-critical gas region, denoted as II, which is bounded by the tangent, t, and the dew-point envelope,

(3) the undersaturated liquid region, denoted as III, which is bounded by the tangent, t, and the bubble-point envelope; and

(4) the region IV, bounded by the tangent, t, and the triangular apex, C_I. In this region, the state of the fluid will change continuously from the near critical liquid state (the part close to III) to a supercritical gas state (the part close to II).

As is well-known, for miscibility to occur, at least one fluid (injected or reservoir fluid) must have the composition point inside region IV. If the fluid is the displacing fluid, the displacement will be by condensing-gas drive; if the fluid is the displaced fluid, the process is the high-pressure gas drive.

Based on Gibbs' phase rule for a three-component system with two phases, the degree of freedom, f, is f = number of components-number of phases + 2 = 3. Thus, if temperature and pressure are specified, as

is the case here, the thermodynamic degree of freedom is one. An important implication of the observation above is that for a three-component system at fixed temperature and pressure, the phase envelope together with the critical point is unique. Since the tie line passing through the critical point determines the minimum miscibility pressure (hereafter denoted as MMP) of the entire displacement process, the condition of miscibility depends completely on the thermodynamic phase behavior and mass transfer of the fluid system and is independent of the characteristics of the porous medium (e.g. permeability) and of the rate of displacement. In such cases, the characteristics of the porous medium and the displacement rate only affect the length of the mixing zone. The conclusion elaborated above for multiple contact miscibility of fluid systems containing three pure components is based on the premises that the fluid phases are always in thermodynamic equilibrium and the gas injection is continuous. If, however, the injection is of finite slug size and in the second slug a different gas is injected, then the three-component constraint is violated and the conclusion drawn here is no longer valid. The above observation, based on thermodynamic principles and physical judgements, is consistent with numerical simulation results obtained via separate compositional-type simulators by Corteville, et al. [3a] and Metcalfe, et al. [15] for fluid systems containing three-pure components. The above authors did not simulate the case with continuous injection of miscible gases.

4. Thermodynamic Considerations for Miscible Processing Having Four or More Components at Fixed Temperature and Pressure

We now examine the case where four pure components are present in the fluid system. As before, the components are designated respectively as C_L, C_{I1}, C_{I2} and C_H, where I1 and I2 represent the first and second intermediate hydrocarbon components. Following [30], a tetrahedral diagram is used to represent the phase composition relations of the four-component system (see Figure 5). The principles to be discussed here are basically the same as in the case of the three-component system. Each point inside the regular tetrahedron of Figure 5 represents an overall component composition in the mixture, the mole fraction of each point being proportional to the distance from the point to the triangular surface opposite to the corner representing the pure component. At a given temperature and pressure, a saturation surface separates the system into two-phase and single-pnase regions. A critical line, c, divides the surface into two parts: the bubble-point and the dew-point surfaces. The set of the tangent lines passing through the critical line, c, generates a surface, designated as t_s, which separates the tetrahedron into four regions, I, II, III, and IV. The phase states and the miscibility relations of these four regions are the same as their counterparts in the three-component case.

It is worth noting that different critical compositions on the critical locus, c, will yield different MMP's. In other words, for the four-component case, the composition path from which the critical point

is approached could alter the development of miscibility at specified temperature and pressure. To discuss the above observation from a different point of view, we now replot the phase envelopes of the quaternary system in a ternary triangular diagram by combining C_{I1} and C_{I2} as a pseudocomponent. Figures 6a and 6b show qualitatively the resulting ternary diagram. In both figures, the parameter used in the phase envelopes is the fraction of C_{I1} in the $C_{I1} + C_{I2}$ pseudocomponent, designated as f. From the figures, it is clear that for a four-component system, at fixed temperature and pressure, the phase envelope, or equivalently the location of the critical points, is not unqiue. For the case examined here, the spread of the phase envelopes depends on the molecular similarity of components C_{I1} and C_{I2}. If C_{I1} and C_{I2} are of similar molecular species, e.g. n-C_4 and i-C_4 respectively, then the spread of the envelope will be narrow (Figure 6b) and the range of critical compositions is small. Under such condition, and for a continuous injection process, the MMP will be <u>insensitive</u> to the path from which the critical point is approached. We recall here that at a specified temperature and pressure, the composition path of a displacement process is affected by two major factors, namely the relative permeabilities and the displacement rate, in addition to being a function of the equilibrium phase behavior. Thus, for a four-component system with at least two molecularly similar components, the MMP determined is insensitive to the relative permeabilities of the porous medium and to the displacement rate. The opposite is true if the

component species in the quaternary system are quite different from each other (Figure 6a).

The above observations can be extended to fluid systems containing five, or more, pure components and to real reservoir fluid systems. With fluid systems containing a wider spectrum of molecular species of hydrocarbons, the degree of similarity among the components is reduced. As a result, the influence of the reservoir characteristics and the displacement rate on the development of miscibility becomes more pronounced.

5. A Simple Procedure to Predict Development of Miscibility in Linear Cores

Basic Assumptions. The approach being proposed here is a simplified version of the one-dimensional compositional simulator. It is applicable to the high-pressure gas drive processes, such as the CO_2 process, in which the miscibility is generally developed at the front of the transition zone. Similar algorithm, however, can be developed for the condensing-gas drive processes. The key feature of this approach is that a set of finite-difference material balance equations is used in conjunction with the Peng-Robinson equation of state to calculate the phase saturation and the compositions of the fluid at the front of the transition zone. Other basic assumptions made are as follows:

(1) the flow is one-dimensional;

(2) the flow is isothermal with a maximum of two fluid phases;

(3) the porous medium is isotropic and homogeneous;

(4) mechanisms taken into account include convective flow according to relative permeabilities and equilibrium mass transfer between the moving phases;

(5) the interphase mass transfer is achieved instantaneously, so that both phases are always in thermodynamic equilibrium;

(6) molecular diffusion, hydrodynamic dispersion and viscous fingering are neglected; (For gas-oil displacement processes in the porous medium, the molecular diffusion and hydrodynamic dispersion are both in the order of 10^{-5} cm^2/sec [23]. The effect of the diffusion-dispersion mechanism is to smear the displacement front. To precisely estimate the importance of this mechanism, one must use a numerical simulator, which includes the diffusion-dispersion term, but is free of the numerical dispersion effect);

(7) gravity and capillary-pressure effects are neglected.

The Procedure Proposed. We shall start from the familiar transport equations of the conventional compositional simulator. Based on the assumptions listed above, the material conservation equation for component i can be written as

$$\frac{\partial}{\partial x} \sum_{j=1}^{n_p} V_j \rho_j X_{ij} + \phi \frac{\partial}{\partial t} \sum_{j=1}^{n_p} \rho_j X_{ij} S_j = 0 \qquad i = 1, \ldots, n_c \qquad (5)$$

where $V_j = \frac{K k_{rj}}{\mu_j} \frac{\partial p}{\partial x}$ is the Darcy's velocity of the jth phase, cm/sec,

ρ_j = the molar density of the jth phase, g-mole/c.c.,

X_{ij} = mole fraction of the ith component distributed in the jth phase; for the vapor phase $X_{ij} \equiv y_i$, for the liquid phase, $X_{ij} \equiv x_i$,

n_p = total number of phases present,

S_j = volumetric phase saturation,

ϕ = porosity

To further simplify the discussions, the total amount of component i at a given in the porous media, i.e. $\sum_{j=1}^{n_p} \rho_j X_{ij} S_j$, can be rewritten as equilibrium grid block

$$\sum_{j=v,L} \rho_j X_{ij} S_j = \rho_v y_i S_v + \rho_L x_i S_L = \rho z_i \tag{6}$$

where ρ = molar volume of the mixture, g-mole/c.c.,

z_i = mole fraction of component i in the mixture,

and subscripts, v, L represent vapor and liquid phases respectively. Also the molar flow rate of the jth phase, q_j, g-mole/sec, is related to V_j according to

$$q_j = V_j \rho_j A \phi \quad . \tag{7}$$

Substituting Equations (6) and (7) into Equation (5), we obtain

$$\frac{1}{A\phi} \frac{\partial}{\partial x} \sum_j q_j X_{ij} + \frac{\partial}{\partial t} \rho z_i = 0 \qquad i = 1, \ldots, n_c \ . \tag{8}$$

Equation (8) is now approximated by explicit finite difference expressions in both x and t to give

$$(\rho\ z_i)_{t+\Delta t,x} = (\rho\ z_i)_{t,x} + \frac{\Delta t}{A\phi\Delta x} \left[(q_L x_i + q_v y_i)_{t,x-\Delta x} - (\sum_{j=L,v} q_j X_{ij})_{t,x}\right] \tag{9}$$

As mentioned earlier, the primary purpose of the derivation is to obtain an expression that allows us to calculate the composition of the transition front as it travels across the linear core. To this end, let us assume that at time t after the injection, the front is located at $x-\Delta x$. At the same time, the fluid at axial position x, just downstream of the front, is approximated as the original fluid. This approximation follows from the assumption that the mechanisms of diffusion-dispersion and viscous fingering are negligible. Therefore, the flow is piston-like and little of the injected fluids has penetrated beyond the front of the transition zone. At time step, $t+\Delta t$, the front has been moved to axial position x with a new fluid composition. Using Equation (9) and based on the argument made in this paragraph, the new fluid composition at the front is calculated as

$$(\rho\ z_i)_{t+\Delta t,x} = (\rho^o\ z_i^o)_{t,x} + \frac{\Delta t}{A\phi\Delta x} \left[(q_L x_i + q_v y_i)_{t,x-\Delta x} - (q^o\ z_i^o)_{t,x}\right] \tag{10}$$

where the superscript o refers to the condition of the original reservoir fluid. At the reservoir condition, the original fluid is a single-phase fluid. Therefore, only one term is needed to represent the density and flow of the original fluid at condition (t,x). However, for the flow at condition (t,x-Δx), multiphase flow will occur prior to the formation of the critical solution. The multiphase flow rates are represented in Equation (7) by q_v and q_L, which can be further related to the Darcy's Law according to

$$q_L = -\frac{K\ k_{rL}}{\mu_L}\ \rho_L \frac{dp}{dx}\ A\phi \tag{11}$$

$$q_v = -\frac{K\ k_{rv}}{\mu_v}\ \rho_v \frac{dp}{dx}\ A\phi \tag{12}$$

where k_{rL} and k_{rv} are, respectively, relative permeabilities of the vapor and liquid phases in the transition front.

For a slim-tube linear process in which the pressure gradient is generally about 1 psi/ft, it is reasonable to assume that the linear velocity V is constant. According to the Darcy's law,

$$V = \left(\frac{K\ k_{rL}}{\mu_L}\ \frac{dp}{dx} + \frac{K\ k_{rv}}{\mu_v}\ \frac{dp}{dx} \right) \tag{13}$$

from which the pressure gradient, dp/dx, is obtained as

$$\frac{dp}{dx} = - \frac{V}{K\left(\frac{k_{rL}}{\mu_L} + \frac{k_{rv}}{\mu_v}\right)} \tag{14}$$

Substituting Equation (14) into Equations (11) and (12), we are able to express explicitly the frontal molar flow rates in terms of the relative permeabilities, fluid properties of the phases, injection rate and the characteristics of the linear core. Equation (10), which calculates the frontal fluid composition, is now further rearranged. First, we defined q_T, the total molar flow rate across x,

$$q_T \equiv q_L + q_v$$

and the fractional molar flow rates,

$$f_L \equiv q_L/q_T,$$

$$f_v \equiv q_v/q_T,$$

and

$$f^o \equiv q^o/q_T$$

Substituting f_L, f_V and f^o into Equation (10) and rearranging, we obtain

$$(\rho\ z_i)_{t+\Delta t,x} = \frac{q_T\ \Delta t}{\Delta x A\phi}\ \left[(f_L x_i + f_V y_i)_{t,x-\Delta x} + \left(\frac{\rho^o \Delta x A\phi}{q_T\ \Delta t} - f^o\right)_{x,t}\ z_i\right] \tag{15}$$

Equation (15) is the final form of the equation being used to calculate the overall component composition, z_i, at condition $(t+\Delta t,x)$. Once the new fluid composition, z_i, is calculated, a flash calculation using this composition is performed to obtain x_i, y_i and the volumetric phase saturations, i.e. S_V and S_L, and other needed fluid properties, e.g. ρ_V, ρ_L, μ_V and μ_L. The above data are then stored at condition $(t,x-\Delta x)$. Furthermore, for a given set of values of S_V and S_L, the relative permeabilities, k_{rV} and k_{rL} can be determined. With the above description, it is clear that the fluid and rock data needed on the right-hand side of Equation (15) are calculated, and the computation of the frontal fluid composition can be advanced to a new step in both time and axial position. Two additional points are noted here regarding Equation (15):

(1) The quantity, $\frac{\rho^o \Delta x A\phi}{q_T\ \Delta t} - f^o$, represents the amount of the original oil at the downstream of the displacement front that will be mixing with the frontal fluid from upstream to form a new front at $t+\Delta t$

and x. Physically, this quantity must be positive, and its magnitude is determined by the input values of Δx and Δt and by the injection rate, V. The above statement can be clarified by rearranging the quantity, namely,

$$\left(\frac{\rho^o \, \Delta x A\phi}{q_T \, \Delta t} - f^o\right)_{t,x} = \frac{\rho^o \, A\phi}{q_T \, \Delta t} \left[\Delta x - V\Delta t\right]_{t,x}$$

Hence, $(\Delta x - V\Delta t)$ is proportional to the <u>net</u> amount of the original fluid which will be mixing with the invading frontal fluid. If the values of Δx, Δt and V chosen are such that $(\Delta x - V\Delta t)$ becomes negative, then, physically, there will be no solution and, numerically, the solution will be unstable.

(2) If we assume that $f_L \equiv 0$ at condition (t,x) in Equation (15), then the approach of studying the development of miscibility presented here is similar to that used by Hutchinson and Braun [10], Beham, et al. [1] and several other authors. With $f_L \equiv 0$, it is implied that the liquid phase is always immobile at the displacement front. As was discussed earlier in this section and will further be discussed later via an example, the relative mobility of the existing fluid phases has certain influence on the development of miscibility for fluid system having more than three components.

Another point noteworthy here is that the conventional Hutchinson and Braun's approach does not specify the relative amounts of the frontal fluid and the original oil mixing at the displacement front. It is clear that different mixing ratios of the two fluids at the displacement front will yield different component distributions in the phases, and eventually lead to different miscibility conditions. In the preceding paragraph, we have noted that the mixing ratio is related to the displacement rate, V, the time and grid sizes, Δt and Δx, and the local fluid properties and rock characteristics. For a given displacement rate, proper values of Δt and Δx must be taken so that thermodynamic equilibrium is attained at each mixing stage. In an example in the following section, we shall demonstrate that using Hutchinson and Braun's approach with different mixing ratios of the fluids in the displacement front could lead to different MMP's.

IV. EXAMPLE CALCULATIONS AND DISCUSSIONS OF RESULTS

The numerical procedure proposed in the preceding section is applied here to several examples. The slim-tube CO_2-miscibility experiment with the Little Knife A fluid [9] is used as a basis for the examples presented here. The input data required by the proposed numerical procedure, viz., the slim-tube data, the injection rate, the reservoir temperature, and the time and the space sizes, Δt and Δx, are given in Table 6. In all but one of the examples presented here, pseudoternary diagrams are used to examine the composition path of the frontal fluid and the development of miscibility. The fluid compositions, after each flash calculation, are combined into three groups of components: (1) the injection fluid, (2) the light-to-intermediate hydrocarbons, including methane to pentanes, and (3) the heavy hydrocarbons, namely the hexanes and plus fraction.

Example 1: Effects of Pressure and Phase Mobility on the Development of Miscibility

Figure 7 displays the pseudoternary phase diagram and the composition path of the displacement front for the multiple contact process at P = 3200 psia and T = 240°F. A key feature of this figure is that at the given condition, no critical solution is formed and the frontal fluid stays in the two-phase region. The contact and

equilibration process at the front generates a progression of tie lines that terminates at the one, which, when extended through the phase envelope intersects the composition point of the original oil. Further contacts of the frontal fluid with respect to the original oil downstream yield exactly the same phase compositions given by the intersections between this tie line and the phase envelopes. At the same time, the overall composition will move along the tie line toward the original oil. It will take an unrealistically long linear core and a large amount of the injection fluid for the fluid at the displacement front to move out of the two-phase region. As a result, under the given conditions, the displacement is an immiscible process.

For the same conditions as in Figure 7, but at P = 3480 psia, the composition path and the phase envelope are shown in Figure 8. It is seen that at this pressure level a critical solution has been formed. The tie line through the critical point passes to the left of the composition point of the original oil, indicating that the frontal fluid, after passing through the critical point, will contact miscibly with the original oil. The closeness of this tie line with respect to the composition point of the original oil suggests that the operating pressure is close to the MMP. With certain degree of uncertainty in the relative-permeability correlations used in the study, the operating pressure, i.e. 3480 psia can be accepted as the predicted MMP. The predicted MMP compares very favorable with the experimentally determined value of 3420 psia.

Also plotted in Figure 8 in dotted curve is the frontal composition path for the case with infinite gas-phase relative mobility at the front. It is clear from the Figure that the frontal composition paths for both cases studied in Figure 8 are very close prior to the near-critical region which is characterized by a shrinkage of the two-phase region and by the closeness of the bubble-and dew-point curves. This is because at the early mixing stages, the fluid at the front is dominated by the gas phase. According to the relative-permeability characteristics (see Table 6), then, the frontal fluid that moves downstream is nearly the gas-phase fluid. As a result, the effect of relative-permeability curves plays a minor role in the fluid flow when the frontal fluid is dominated by the gas-phase fluid. However, as the frontal fluid is close to the near-critical region, liquid phase becomes comparable in amount with the gas phase. The function of the relative-permeability characteristics is to allow certain amounts of the liquid phase, which is rich in the intermediate hydrocarbons, to move simultaneously with the gas phase at the front. Consequently, the miscibility between the frontal fluid and the original oil at the new mixing stage is enhanced, and a critical solution is formed for the case with relative-permeability treatment for the frontal fluid advancement.

To summarize the discussion here, we note that as the fluid at the displacement front is near the critical region, the formation of a miscible (critical) solution depends, in addition to pressure and temperature, on the overall composition of the fluid mixture at each

mixing stage; the local overall composition is strongly affected by the relative-permeability characteristics of a porous medium. Assuming infinite gas-phase relative mobility at the front, as Hutchinson and Braun [10] and others did, will reduce the amount of intermediate hydrocarbon in the fluid mixture at near-critical region, and consequently, overestimate the MMP for a CO_2 recovery process.

Finally in this example, another deficiency of the Hutchinson and Braun's approach is discussed. As pointed out in the later part of the preceding section, the mixing ratio of the displacing fluid versus the residing original fluid at each frontal mixing stage was never explicitly specified, or discussed, in Hutchinson and Braun's paper[10], or in other publications [1,5,31]. To illustrate the influence of the mixing ratio, Figure 9 is presented. Using the Hutchinson and Braun's approach, the MMP's obtained are plotted in the Figure against their corresponding mixing ratios. It is noted that in each numerical multiple-contact calculation to determine an MMP, a fixed value of the mixing ratio is used. From Figure 9, it is shown clearly that different mixing ratios could result in different conditions of miscibility.

Example 2: Contribution of the Acid Gas, H_2S, to the Development of Miscibility

It has been shown experimentally [11] that CO_2 and H_2S mixtures could be more effective flooding agents than CO_2 alone. The injection of H_2S has been proposed [8] for miscible displacement of the

reservoir fluid in the McElroy Field. Using the numerical procedure proposed in the preceding section, this example evaluates the effectiveness of H_2S in contributing to the development of miscibility of CO_2 injection process. The input data to the governing transport equation, namely Equation (15), and the equation of state are exactly the same as those in Example 1, except that the injection gas now contains various amounts of H_2S and CO_2.

The results of this study are summarized via a plot of the predicted MMP versus the mole fraction of H_2S in the injection gas containing CO_2 and H_2S (Figure 10). It is shown from the Figure that as the amount of H_2S increases in the injection gas, the MMP decreases steadily. In other words, the acid gas, H_2S, is beneficial to the development of miscibility in the CO_2 injection processes. This finding is consistent with the conclusion reached by Jacobson [11], based on his slim-tube experiment on a high-gravity reservoir crude from the Rainbow-Zana area of northwestern Alberta. From this example, it is also demonstrated that the simple numerical procedure proposed herein can provide preliminary information on designing and screening miscible displacement projects where several potential miscible agents, such as H_2S, LPG, N_2, etc. are available either from the well stream or nearby sources.

Example 3: Examination of a Condensing-Gas Drive Mechanism via CO_2 Injection Proposed by the AMOCO Research Group

It is interesting to know if a condensing-gas drive mechanism could be operative in a CO_2 recovery process. Generally, it has been recognized that the mechanism responsible for hydrocarbon recovery in the CO_2 process is via vaporization (or extraction) of the hydrocarbon intermediates into the light phase. If a condensing-gas mechanism is to be plausible for the CO_2 process, then the density and volatility ratios of CO_2 versus the particular reservoir fluid at in-situ conditions must be respectively similar to those of C_2-C_5 versus the original oil at conventional condensing-gas-drive conditions. In this regard, the types of reservoir oils and reservoir conditions must be highly selective. The only published data indicating that the condensing-gas drive is responsible for the CO_2 recovery process are those by Metcalfe and Yarborough [15], Leach and Yellig [12] of the AMOCO Production Co. Based on their experimental and simulation results for a slim-tube system containing CO_2 and a synthetic oil, Metcalfe, et al. [15,12] proposes that at low temperature, namely for temperatures in the range of 90°F to about 130°F, condensation of CO_2 into the heavy phase is the mechanism controlling the recovery of oil. The purpose of this example is to examine whether Metcalfe, et al.'s proposition is general to most reservoir fluid systems or is restricted only to their specific synthetic oil.

The component composition and properties of the fluid system, that the above authors employed to arrive at their conclusion of a CO_2 condensing-gas drive mechanism are given in Table 7. The same fluid system had been studied by us previously [14] for different purposes. The single-contact pressure-composition phase envelope of the original fluid versus CO_2 was predicted quite accurately using the Peng-Robinson equation of state at T = 120°F (see Figure 11 reproduced from Reference [14]). In our study here, the equation of state is used to examine the composition paths of the fluids at the front and rear edges of the transition zone. The concept of Hutchinson and Braun [10] is adopted in this particular example to construct the pseudoternary phase diagram. The results obtained from this analysis, therefore, are only qualitative. In the pseudoternary phase-composition diagram of Figure 12, the movement of the liquid phase at the rear and the movement of the gas phase at the front of the transition zone are indicated. According to the phase envelope and the composition path of the gas phase in the front of the transition zone, the front will remain as two-phase fluid for a reasonable length of the core. On the other hand, at the rear edge of the transition zone, the liquid phase is enriched continuously by the injection gas, namely CO_2, and a critical solution is finally formed at composition point c. From this point on, the contact at the rear edge is a single phase miscible process. Based on the description above, the displacement process can be qualified as a condensing gas drive.

Upon further considerations on the shape of the pseudoternary phase envelope and the relative positions of the pseudoternary components in Figure 12, the following points are noted:

(1) The pseudoternary phase-composition relation, shown in Figure 12, is very similar to that of the alcohol-oil-water system presented by Taber, Kamath and Reed [29], in their work on the mechanism of alcohol displacement of oil from porous media. Figure 13, taken from [29], depicts the ternary phase diagram for the fluid system containing isopropyl alcohol (IPA), oil and brine. Because of the similarity of phase-composition relations in Figures 12 and 13, the discussion on the development of miscibility made by Taber, et al. [24] is directly applicable to this example. In Figure 12, the critical point, c, is located to the left of the binodal peak. According to Taber, et al., if the critial point is to the left of the binodal peak for such a ternary phase diagram, the miscibility can be achieved at the rear end of the transition zone.

(2) For the CO_2-crude oil systems at reservoir conditions, the type of pseudoternary phase diagram as shown in Figure 12 is rarely encountered. This is because for the reservoir fluid systems suitable for gas-injection recovery processes, the hydrocarbons from C_2 to C_{7+} fraction generally have complete miscibility (see Figure 8). Furthermore, at the same condition, CO_2 and the C_{7+}

fraction generally have limited miscibility (see Figures 7 and 8). On the contrary for this example, CO_2 and the C_{7+} pseudocomponent are completely miscible at the given condition. A closer examination on the C_{7+} fraction of the fluid given in Table 7 reveals that the API gravity of this fraction is about 63.48° and the C_{12+} material within this fraction is about 10% by mole. These two values of the C_{7+} fraction suggest that the synthetic C_{7+} fraction used by Metcalfe and others [15,12] is unrealistic for a natural reservoir oil suitable for enhanced recovery via gas injection. Here, it is interesting to note that Yellig of the AMOCO Production Company has recently published a paper [32] on the experimental displacement test of CO_2 and a Levelland, West Texas, reservoir oil (API gravity of the separator oil = 18.0°). The experimental temperature was 106°F, which can be qualified as low temperature CO_2 recovery process [18]. Based on the effluent composition profiles, Yellig noted that "these profiles are in marked contradiction to a CO_2-condensing process," proposed by Metcalfe and Yarborough [15]. Furthermore, he concluded that the miscibility was developed by extraction of light and intermediate hydrocarbon from the in-place oil to the light phase. In other words, the condensing gas drive mechanism was not observed for CO_2-crude oil system at low temperature levels.

(3) For the same fluid system discussed here, it may be possible to adjust the pressure and temperature, so that the hydrocarbon components, namely from C_1 to C_{7+}, become completely miscible at the given condition. If this is possible, then the pseudoternary phase diagram will have the interesting shape as shown in Figure 14. According to this Figure, the miscibility could then be developed at both ends of the transition zone.

CONCLUSIONS

The work presented herein consists of two major parts. In the first part, we have demonstrated that a relatively simple equation of state, together with proper characterizations of the crude-oil fractions, can be used to give reasonably accurate predictions of the single-contact fluid properties, such as the CO_2-crude oil swelling factors, and phase envelopes, needed for preliminary screening of potential reservoir crude oils for enhanced oil recovery. Other findings in this part of the our work are

(1) It is inappropriate to derive the differential transport equations governing the compositional processes via gas injection based on the principle of the conservation of volume; and

(2) for the CO_2-Little Knife reservoir fluid system at a reservoir temperature of 240°F, a single-phase fluid could exist in a metastable state without phase splitting for all pressure ranges if the mole fraction of CO_2 in the mixture exceeds about 0.86.

In the second part, a simple procedure is developed to study the development of miscibility at the front of the transition zone of the high-pressure vaporization processes. This procedure is based on a set of explicit finite-difference material conservation equations together with the Peng-Robinson equation. Examples are also provided to

demonstrate the applications of this procedure. Other observations in this part are

(1) For pure ternary systems at fixed temperature and pressure and undergoing continuous gas injection, the minimum miscibility pressure depends solely on the thermodynamic phase behavior and equilibrium interphase mass transfer and is independent of the characteristics of the porous media and rate of injection. On the other hand, for fluid systems having more than three components, the development of miscibility depends on the characteristics of the porous media, the injection rate and the thermodynamic phase behavior.

(2) The classical approach developed by Hutchinson and Braun and Benham, et al., to study the development of miscibility could overestimate the minimum miscibility pressures for high-pressure vaporization processes.

(3) The acid gas, H_2S is beneficial to the development of miscibility in CO_2 injection process.

(4) Regardless of the reservoir temperature, the mechanism responsible for the development of miscibility in the CO_2 injection process is the vaporization, or extraction, of the hydrocarbons to the vapor or the light-liquid phase. The miscibility is developed at the front of the transition zone.

S.T. Lee

Sheng-Tai Lee

John J. Komlenic/FEL

John J. Komlenic

STL:JJK:mam

ACKNOWLEDGEMENTS

We are grateful for the opportunity to have participated in Gulf's Summer Employment Program. Helpful discussions with Mr. J. B. Nolan of the Thermal and Miscible Recovery Processes Section and Dr. C. A. Irani of the Drilling and Production Engineering Section are also gratefully acknowledged.

REFERENCES

1. Benham, A.L., Dauden, W.E. and Kunzman, W.J., "Miscible Fluid Displacement - Prediction of Miscibility," Trans., AIME (1960), Vol. 219, 229-237.

2. Blander, M. and Katz, J., "Bubble Nucleation in Liquid," AICHE J. (Vol. 21, No. 5), September, 1975, 833-848.

2a. Chaudhari, N.M., "Compositional Simulator - User's Manual," Production Research Department, Report No. 441TM192, June 1, 1981, GR&DC.

3. Corey, A.T., "The Interrelation between Gas and Oil Relative Permeabilities," Producers Monthly (Vol. XIX, No. 1), 1954, 38-41.

3a. Corteville, J., Van Quy, N. and Simandoux, P., "A Numerical and Experimental Study of Miscible or Immiscible Fluid in Porous Media with Interphase Mass Transfer," paper SPE 3481, presented at the SPE 46th Annual Meeting, New Orleans, Louisiana, October 3-6, 1971.

4. DeVaney, W.E., "Zabolotny I-3-4A, Little Knife Field, Billings County, North Dakota," Technical Memorandum No. 445TL074, April, 1980, GS&TC.

5. Gardner, J.W., Orr, F.M. and Patel, P.D., "The Effect of Phase Behavior on CO_2-Flood Displacement Efficiency," Soc. of Pet. Eng. J. (November, 1981) 2067-2081.

6. Gibbs, J.W., "The Scientific Papers of J. Willard Gibbs," Volume One: Thermodynamics, pp. 100-133, Dover Publications, Inc. New York (1961).

7. Holm, L.W. and Josendal, V.A., "Discussion of Determination and Prediction of CO_2 Minimum Miscibility Pressures," J. Pet. Tech. (May, 1980), 870-879.

8. Huang, E.T.S. to H.H. Hasiba, "H_2S Injection to the McElroy Field for Miscible Recovery of Oil - A Proposal," Production Research Department Memo. Ref. 4-413SM30, November 14, 1973.

9. Huang, E.T.S., "Miscibility Studies with Little Knife Oil," Technical Memorandum No. 441TJ300, Production Research Department, GS&TC, January 18, 1978.

10. Hutchinson, C.A. and Braun, P.H., "Phase Relations of Miscible Displacement in Oil Recovery," AICHE J. (Vol. 7, No. 1), March 1961, 64-72.

11. Jacobson, H., "Acid Gases and Their Contribution to Miscibility," J. Can. Pet. Tech. (April-June, 1972), Vol. 11, No. 2, 56-59.

12. Leach, M.P. and Yellig, W.F., "Compositional Model Studies - CO_2 Oil-Displacement Mechanisms," Soc. Pet. Eng. J. (February, 1981), 89-97.

13. Lee, S.T., "Applications of the Peng-Robinson Equation of State to Determine Reservoir Fluid Properties and Predict Equilibrium Phase Behavior," Production Research Department Report No. 44ARL186, January 30, 1980.

14. Lee, S.T., "Applications of the Peng-Robinson Equation of State to Equilibrium Calculations of CO_2-Hydrocarbon Mixtures," Production Research Department File Note Ref. 4-416SR02, September 19, 1979.

15. Metcalfe, R.S., Fussell, D.D. and Shelton, J.L., "A Multicell Equilibrium Separation Model for the Study of Multiple Contact Miscibility in Rich Gas Drives," Trans. AIME (1973), Vol. 225, 147-155.

15a. Metcalfe, R.S. and Yarborough, L., "Effect of Phase Equilibrium on the CO_2 Displacement Mechanism," Soc. Pet. Eng. J. (August, 1979), 242-252.

16. Modell, M. and Reed, R.C., "Thermodynamics and Its Applications," Chapters 5, 7, Prentice-Hall, Englewood Cliffs, New Jersey, (1974).

17. Mulliken, C.A. and Sandler, S.I., "Prediction of CO_2 Solubility and Swelling Factors for Enhanced Oil Recovery," Ind. Eng. Chem. Process. Des. Dev. 1980, Vol. 19, 709-711.

18. Orr, F.M., Yu, A.D. and Lien, C.L., "Phase Behavior of CO_2 and Crude Oil in Low Temperature Reservoirs," Soc. Pet. Eng. J. (August, 1981), 480-492.

19. Peng, D.-Y., and Robinson, D.B., "A New Two-Constant Equation of State," Ind. Eng. Chem. Fundam. (1976) Vol. 27, 59-64.

20. Peng, D.-Y. and Robinson, D.B., "A Rigorous Method for Predicting the Critical Properties of Multicomponent Systems from an Equation of State," AICHE J. (Vol. 23, No. 2), 1977, 137-144.

21. Prigogine, I., Bellamans, A. and Mathot, V. "The Molecular Theory of Solutions," Chapter 1, North-Holland Publishing Co., Amsterdam (1957).

22. Prigogine, I. and Defay, R., "Chemical Thermodynamics," Chapters XV, XVI, trans. by D.H. Everett, Longmann, Green and Co., New York (1952).

23. Raimondi, P., Warren, J.E., "Discussion of Bannif's Proposed Miscible Displacement Project in Rainbow Keg River, Canada," Technical Memorandum No. 441T8104, September 12, 1968, Production Division, GS&DC.

24. Rowlinson, J.S., "Liquids and Liquid Mixtures," Chapter 5, Butterworth, London (1969).

25. Sage, B.H., Lacey, W.N., "Some Properties of the Lighter Hydrocarbons, Hydrogen Sulfide and Carbon Dioxide," Monograph on Research Project 37, API (1950).

26. Simon, R. and Graue, D.J., "Generalized Correlations for Predicting Solubility, Swelling and Viscosity Behavior of CO_2-Crude Oil Systems," J. Pet. Tech., January 1965, 102-206.

27. Smith, R.L. and Watson, K.M., "Boiling Points and Critical Properties of Hydrocarbon Mixtures," Ind. Eng. Chem. (Vol. 29, No. 12), 1937, 1408-1414.

28. Soave, G., "Equilibrium Constants from a Modified Redlich-Kwong Equation of State," Chem. Eng. Sci. (1977) Vol. 27, 1197-1203.

29. Taber, J.J., Kamath, I.S.K. and Reed, R.L., "Mechanism of Alcohol Displacement of Oil from Porous Media," Soc. Pet. Eng. J. September, 1961, 195-207.

30. Treybal, R.E., "Liquid Extraction," Chapter 7, McGraw-Hill Book Co., Inc., New York, 1963.

31. Williams, C.A., Zana, E.N. and Humphrys, G.E., "Use of the Peng-Robinson Equation of State to Predict Hydrocarbon Phase Behavior and Miscibility of Fluid Displacement," Paper SPE 8817, presented at the 1st Joint SPE/DOE Symposium on Enhanced Oil Recovery at Tulsa, Oklahoma, April 20-23, 1980.

32. Yellig, W.F., "CO_2 Displacement of a West Texas Reservoir Oil," Paper SPE 9785, presented at the 1981 SPE/DOE Joint Symposium on Enhanced Oil Recovery, Tulsa, Oklahoma, April 5-8, 1981.

33. Yellig, W.F., Metcalfe, R.S., "Determination and Prediction of CO_2 Minimum Miscibility Pressures," J. Pet. Tech. February, 1980, 160-168.

TABLE 1

Compositional Analyses of Two Reservoir-Fluid Samples from the Little Knife Field.

Little Knife A Sample [9]
Reservoir Temperature = 240°F

Component	Mole Percent
N_2	0.98
C_1	35.36
CO_2	1.54
C_2	9.93
H_2S	7.99
C_{3-5}	17.46
C_{6-12}	17.77
C_{12+}	8.97

Little Knife B Sample [4]
Reservoir Temperature = 245°F

Component	Mole Percent
N_2	0.93
C_1	34.01
CO_2	1.20
C_2	9.87
H_2S	4.91
C_3	6.55
i-C_4	1.32
n-C_4	1.32
i-C_5	3.68
n-C_5	1.35
n-C_5	1.74
C_6	3.02
C_{7+}	31.42

Properties of the Heptane Plus (C_{7+}) Fraction:

Sp. Gr.	0.8370
API Gravity	37.6
Molecular Wt.	190.0

TABLE 2

Comparison of Experimental and Predicted Saturation Pressures, P_s, of CO_2 and Little Knife B Fluid Mixtures, T = 245°F.

Mole Percent of CO_2 in the Mixture	Experimental P_s, Psia	Calculated P_s, Psia	Rel. Deviation (%)*
0	2700	2694	-0.22
9.93	2927	2871	-1.91
19.88	3150	3089	-1.94
30.00	3375	3328	-1.39
40.00	3604	3585	-0.53
50.00	3822	3863	+1.07

$$* \quad \frac{P_s(\text{Calc.}) - P_s(\text{Exp.})}{P_s(\text{Exp.})} \times 100$$

TABLE 3

Comparison of Experimental and Predicted Swelling Factors for CO_2-Little Knife B Mixtures, T = 245°F.

Pressure (psia)	Mole Percent CO_2 in the Mixture					
	0.0		30.0		50.0	
	Exp.	Prediction	Exp.	Prediction	Exp.	Prediction
P_s			1.2205	1.2208	1.5301	1.5108
3000	0.9926	0.9911				
3600	0.9798	0.9739	1.2099	1.2070		
4200	0.9688	0.9597	1.1867	1.1804	1.4992	1.4827
4800	0.9590	0.9478	1.1679	1.1580	1.4612	1.4434
5400	0.9505	0.9366	1.1519	1.1388	1.4329	1.4093
6000	0.9426	0.9277	1.1383	1.1218	1.4089	1.3827
Avg. Abs. Dev.%*	0.94		0.70		1.46	
Maximum Dev. %	-1.58		-1.44		-1.84	

$$* \quad \frac{\sum_{i=1}^{n} \frac{|\text{Exp}(i) - \text{Prediction}(i)|}{\text{Exp}(i)}}{n}$$

TABLE 4

Volume Change upon Mixing for CO_2 and Little Knife B Fluid System, T = 245°F

Molar Volume ℓ/g-mole	Pressure (psia)	3000.0	3600.0	4200.0	4800.0	5400.0	6000.0		
V^m	Mixture No. 1	0.1329	0.1306	0.1287	0.1271	0.1256	0.1244	Component Composition	
V^m	Mixture No. 2	--	0.1133	0.1108	0.1087	0.1069	0.1053	Mixture No. 1	Mixture No. 2*
V_i^o	CO_2	0.1076	0.0898	0.0788	0.0715	0.0662	0.0623	0.0120	0.30000
	N_2	0.1685	0.1433	0.1255	0.1123	0.1021	0.0940	0.0093	0.00659
	C_1	0.1498	0.1266	0.1106	0.0990	0.0902	0.0834	0.3401	0.24100
	C_2	0.1067	0.0953	0.0879	0.0827	0.0787	0.0756	0.0987	0.07000
	H_2S	0.0589	0.0549	0.0522	0.0501	0.0486	0.0473	0.0491	0.03480
	C_3	0.0992	0.0948	0.0915	0.0888	0.0867	0.0849	0.0655	0.04640
	iC_4	0.1106	0.1076	0.1051	0.1030	0.1013	0.0998	0.0132	0.00935
	nC_4	0.1072	0.1047	0.1027	0.1009	0.0994	0.0981	0.0368	0.02607
	iC_5	0.1226	0.1205	0.1187	0.1172	0.1158	0.1147	0.0135	0.00956
	nC_5	0.1218	0.1199	0.1183	0.1169	0.1156	0.1145	0.0174	0.01230
	nC_6	0.1387	0.1371	0.1357	0.1345	0.1334	0.1324	0.0302	0.02140
	C_{7+}	0.2487	0.2476	0.2467	0.2458	0.2450	0.2442	0.3142	0.22260
								1.0000	1.00007
Mixture No. 1	$\Sigma V_i^o X_i$ =	0.1652	0.1547	0.1474	0.1420	0.1378	0.1345		
	V^m =	0.0323	0.0241	0.0187	0.0149	0.0122	0.0101		
	V^m/V (%) =	24.3	18.5	14.5	11.72	9.71	8.14		
Mixture No. 2	$\Sigma V_i^o X_i$ =	0.1454	0.1358	0.1274	0.1214	0.1173	0.1135		
	V^m =	--	0.0225	0.0166	0.0127	0.0104	0.00817		
	V^m/V (%) =	--	19.8	15.0	11.7	9.73	7.76		

*Mixture No. 1 = Little Knife B fluid sample.
Mixture No. 2 = 30 mole % CO_2 + 70 mole % Little Knife B fluid sample.

TABLE 5

General Distinctions of the Two Gas Injection Processes

	General Characteristics Required for the Fluid System				
	Reservoir Fluid In-Place	Injection Fluid	The Multiple-Contact Mechanism Involved	Approximate Applicable Pressure Ranges, psia	Existing Empirical Correlations in the Literature to Predict the Development of Miscibility
High-Pressure Gas Drive	Reservoir fluid is rich in the intermediate hydrocarbons	Gas can vaporize the intermediate hydrocarbons from the heavy phase	Gas phase is enriched by the intermediate hydrocarbons in the displacement front	1000-* 4000	Two graphical correlations are available to calculate the minimum miscibility pressure, MMP: 1. Yellig and Metcalfe correlation [33]: MMP=f(reservoir temperature) 2. Holm and Josendal correlation [7]: MMP=f(reservoir temperature molecular weight of C_{5+})
Condensing Gas Drive	Reservoir fluid is lean in the intermediate hydrocarbon	Gas is rich in intermediate hydrocarbons	Liquid phase is enriched by the intermediate hydrocarbons at rear edge of the transition zone	1000-3500	The correlation of Benham, et al. [1] is the only easily applied approach to calculating the necessary enrichment of lean gas for miscible displacement. Their graphical correlation is expressed mathematically as: maximum permissible methane in injection gas = f(reservoir temperature molecular weights of C_{2-4} and C_{5+}).

* In the recent low-temperature CO_2 flooding projects mostly in the West Texas area, the applicable pressure region has been extended to as low as 1200 psia [32]. As a consequence, the traditional high-pressure gas drive should be termed simply vaporizing gas drive or lean gas drive.

TABLE 6

General Information on the CO_2-Little Knife A Reservoir Fluid Slim-Tube Experiment [9].

1. Porous Medium:

Permeability:	1.78 Darcy
Porosity:	0.424
Length:	20 ft
Internal Diameter:	0.65 inch
Relative Permeability*:	$k_{re} = S_{oe}^4$
	$k_{rg} = (1-S_{oe})^2 (1-S_{oe}^2)$
	where $S_{oe} = \frac{S_o - S_{or}}{1 - S_{or}}$
	$S_{or} = 0.20$

2. Displacement Condition:

Injection Rate:	2 ft/day
Temperature:	240°F

3. Fluid Characterization:

Composition of the Original Reservoir Fluid:

(See Table 1)

4. Numerical Simulation Characteristics:

$$\frac{\Delta x}{\Delta t} = \frac{1}{50}\frac{cm}{sec} = \frac{2.36}{1}\frac{ft}{hr}$$

*See Equations (5)-(7) of Reference [3].

TABLE 7

Hydrocarbons Compositions of Synthetic Oil[15]

Component	Mole Fraction
C_1	.3332
C_2	.0310
C_3	.0405
C_4	.0596
C_5	.0408
C_6	.0308
C_7	.0500
C_8	.0500
C_{10}	.3109
C_{14}	.0533

C_{14} Properties	
Molecular Weight	198.30
Critical temperature, °F	235.0
Critical pressure, psia	1,250.69
Specific gravity (60°F/60°F)	0.7658
Acentric factor	0.642

FIGURE 1

PRESSURE-COMPOSITION DIAGRAM FOR CO_2-LITTLE KNIFE A MIXTURES AT 240°F

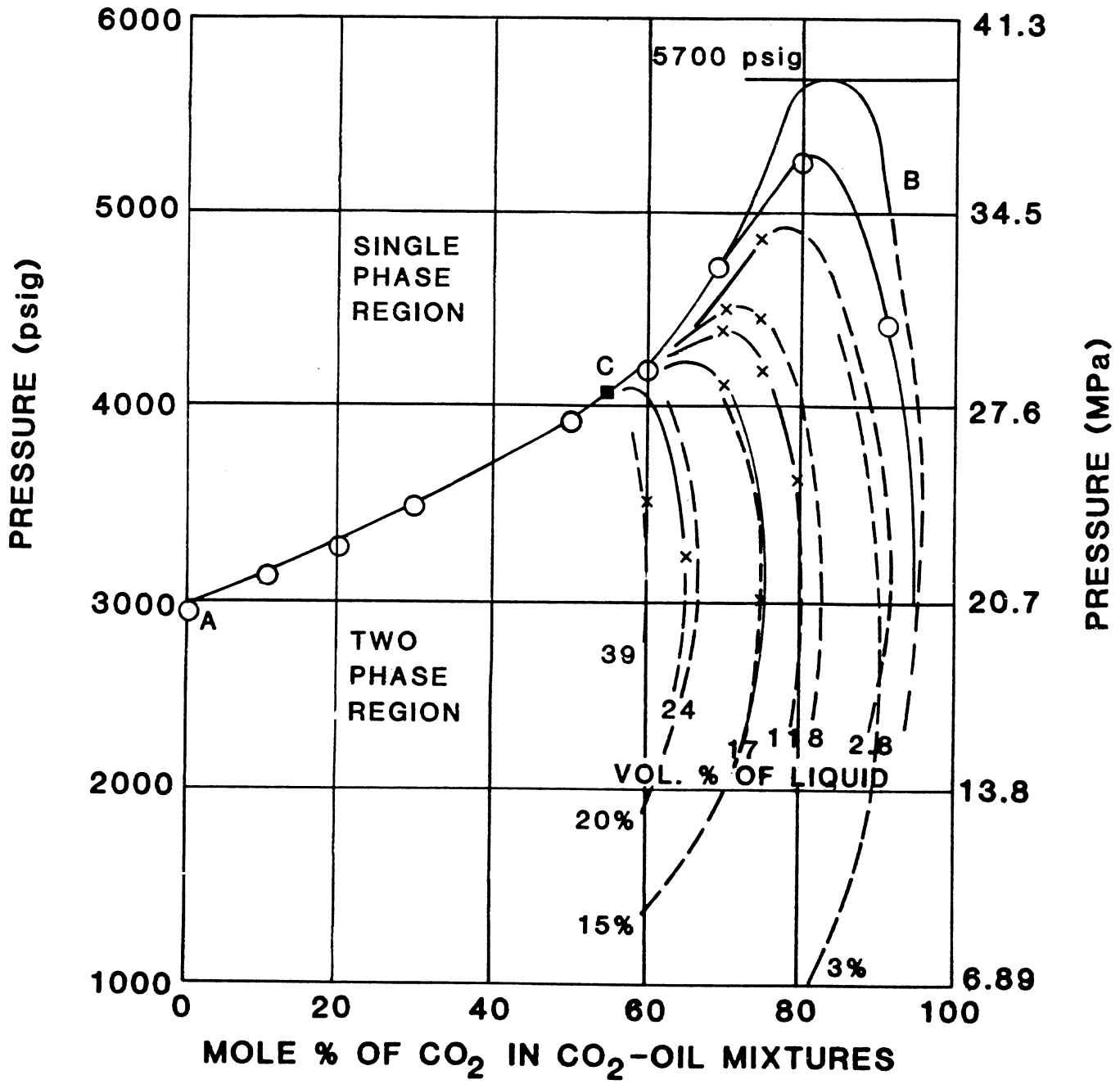

——— EXPERIMENTAL PHASE ENVELOPE [9]

○ PREDICTED PHASE ENVELOPE

■ PREDICTED CRITICAL POINT

— — — PREDICTED CONSTANT LIQUID VOLUME CURVE

×-×-× EXPERIMENTAL CONSTANT LIQUID VOLUME CURVE [9]

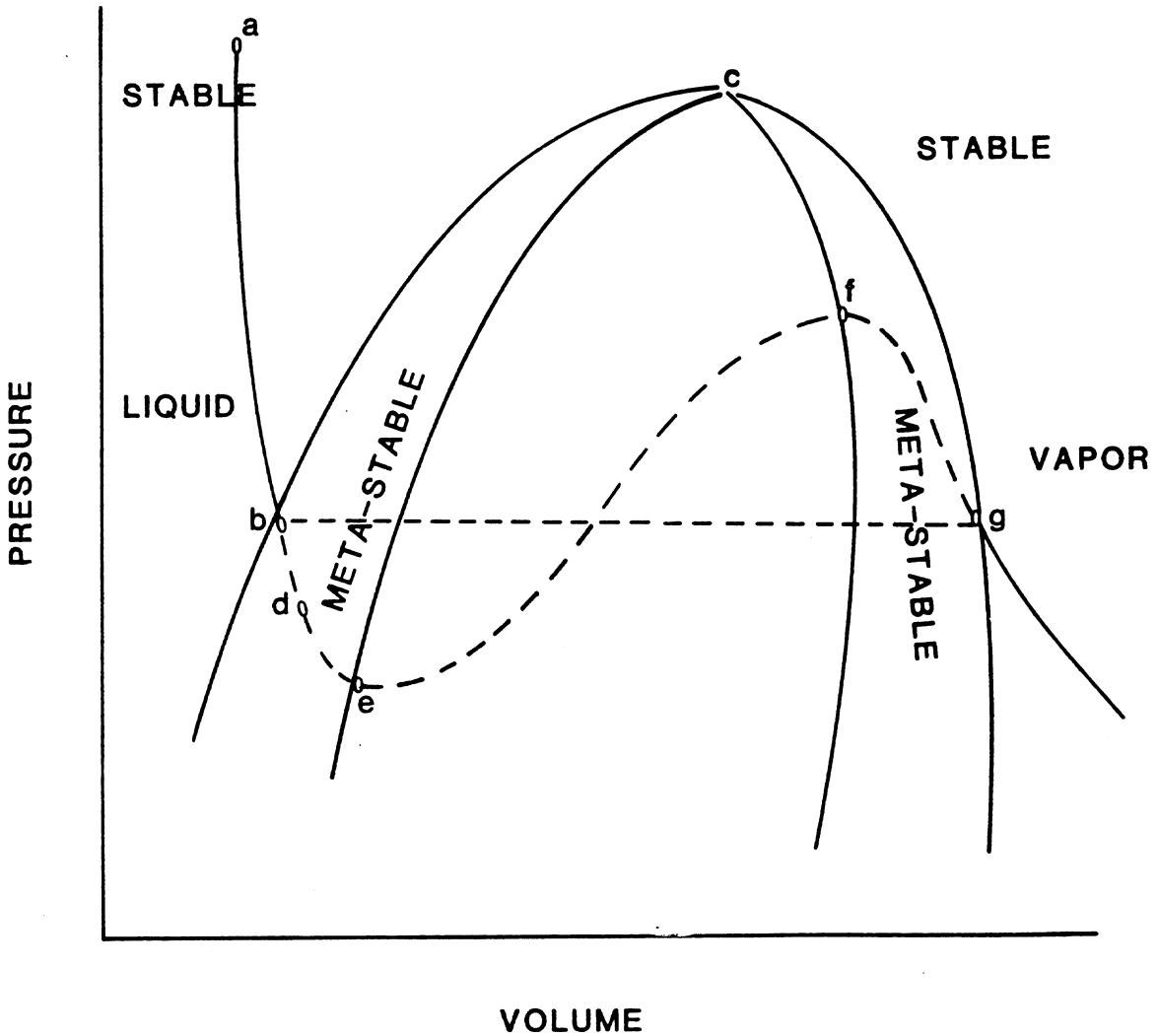

FIGURE 2

STABLE, META-STABLE AND UNSTABLE STATE OF A PURE SUBSTANCE

FIGURE 3

PREDICTION OF PHASE STABILITY FOR CO_2-LITTLE KNIFE A RESERVOIR FLUID SYSTEM, T = 240°F

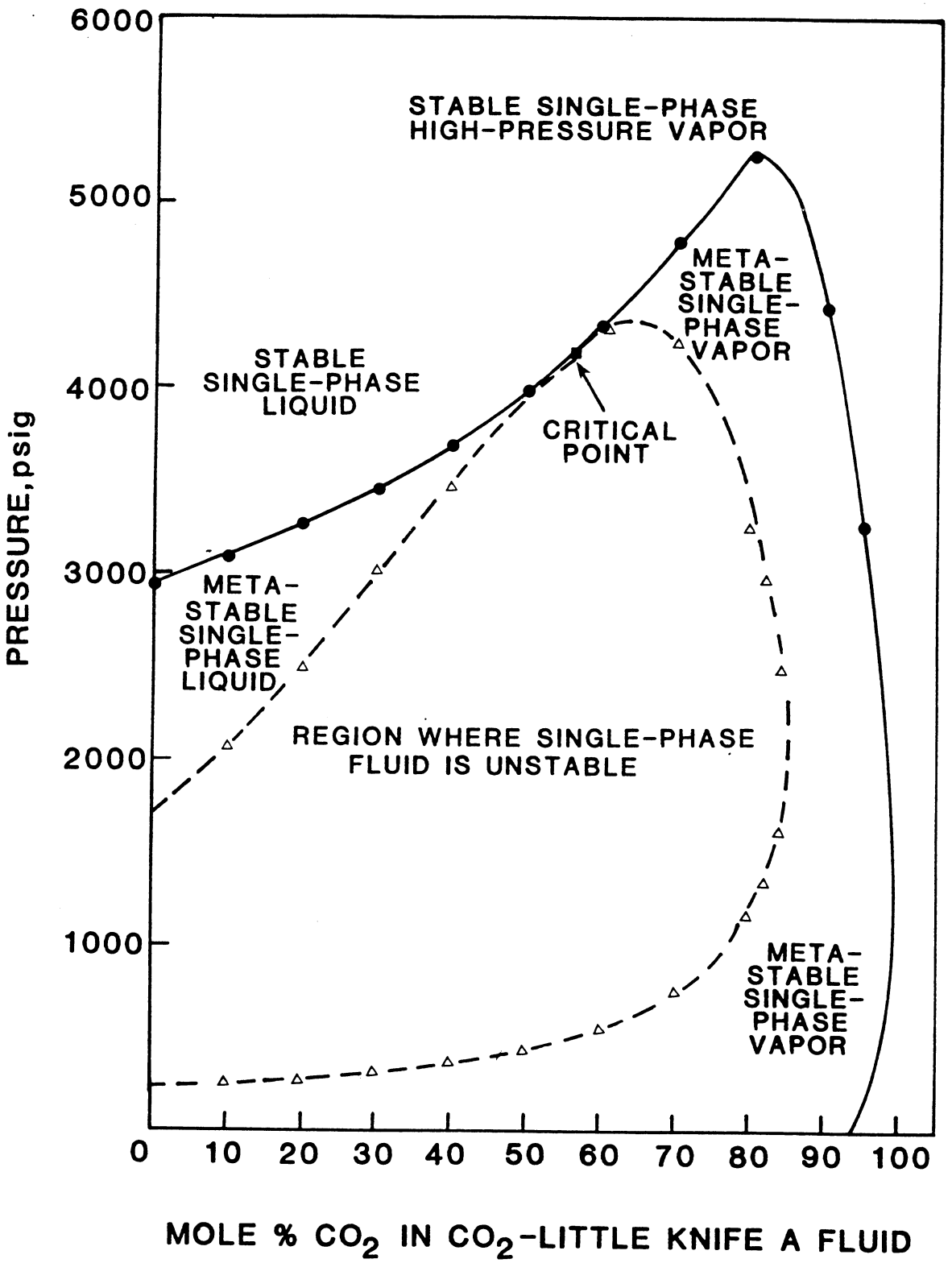

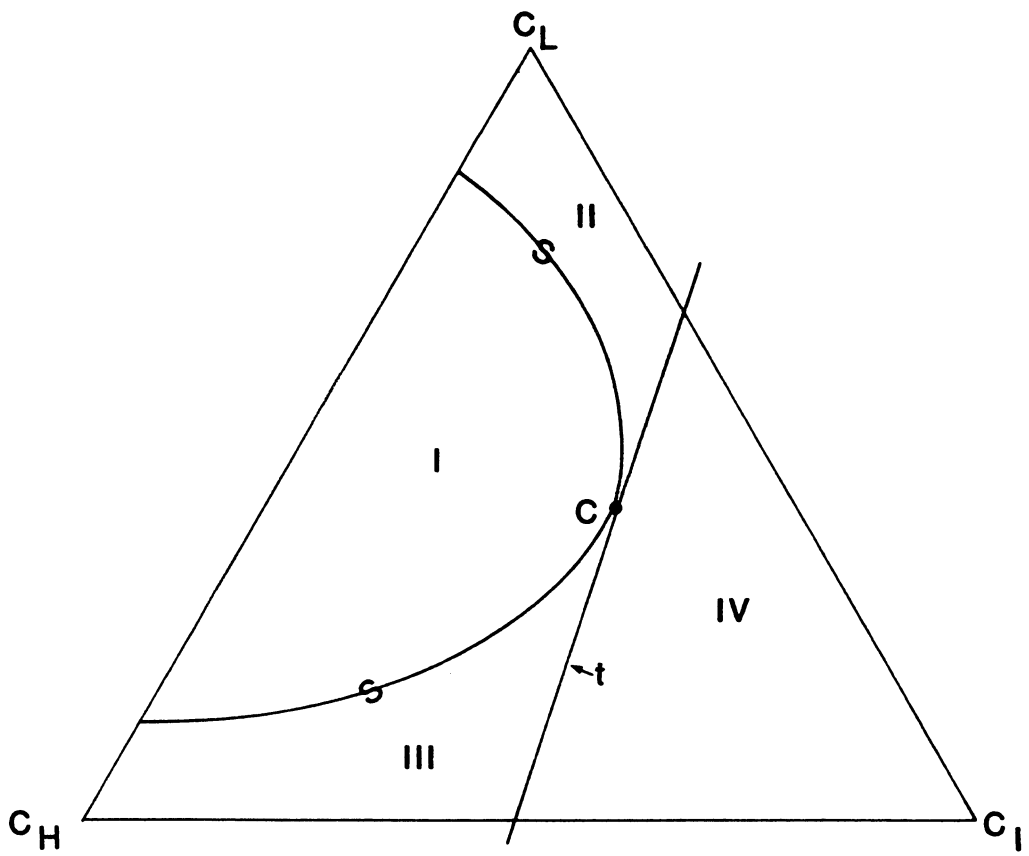

FIGURE 4

TRIANGULAR REPRESENTATION FOR A PURE TERNARY SYSTEM, AT SPECIFIED TEMPERATURE AND PRESSURE

FIGURE 5

TETRAHEDRAL REPRESENTATION OF A FOUR-COMPONENT SYSTEM AT FIXED TEMPERATURE AND PRESSURE

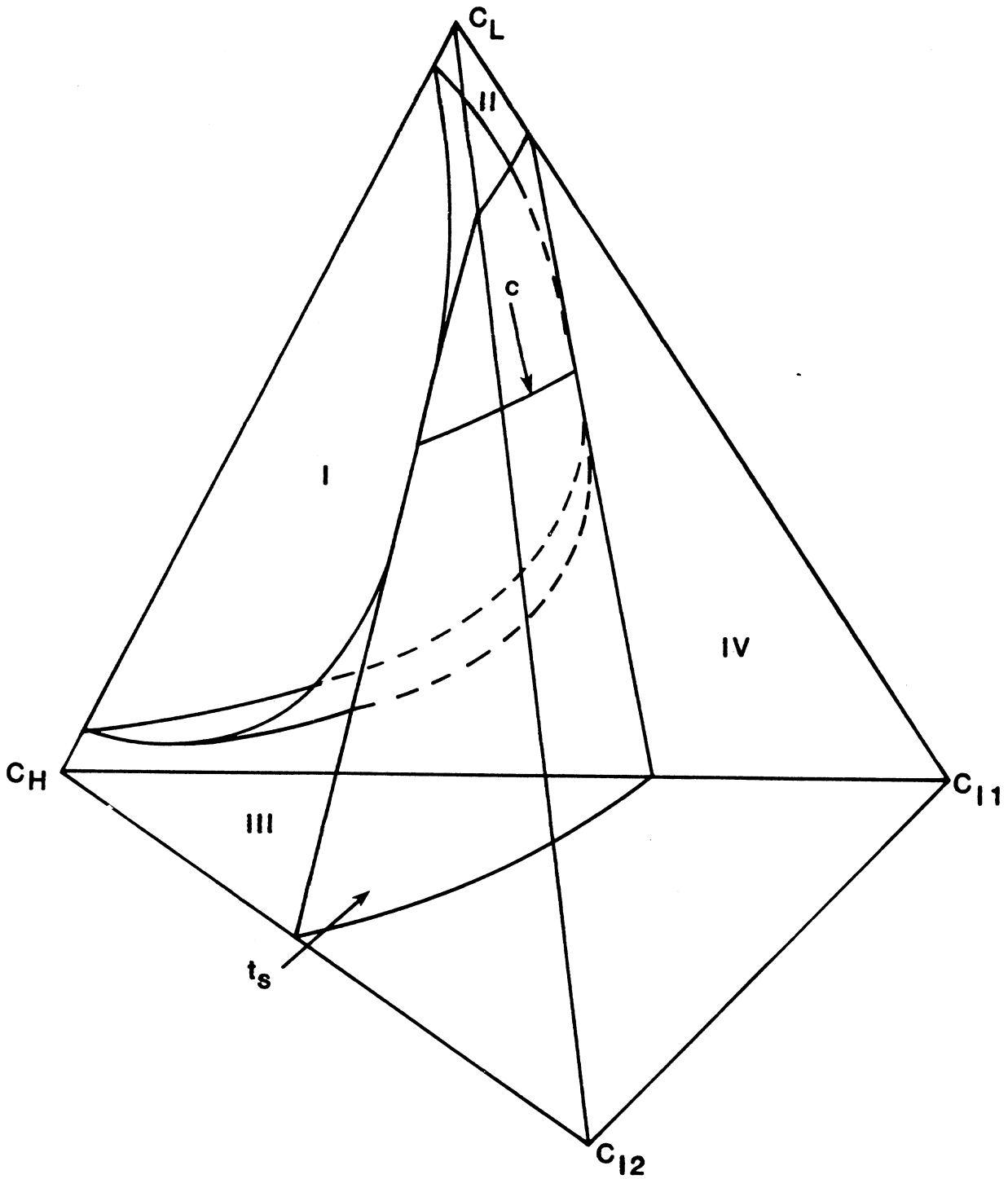

FIGURE 6

PSEUDO-TERNARY PHASE-COMPOSITION REPRESENTATION OF A FOUR-COMPONENT SYSTEM

(a) C_{I1} AND C_{I2} DISSIMILAR

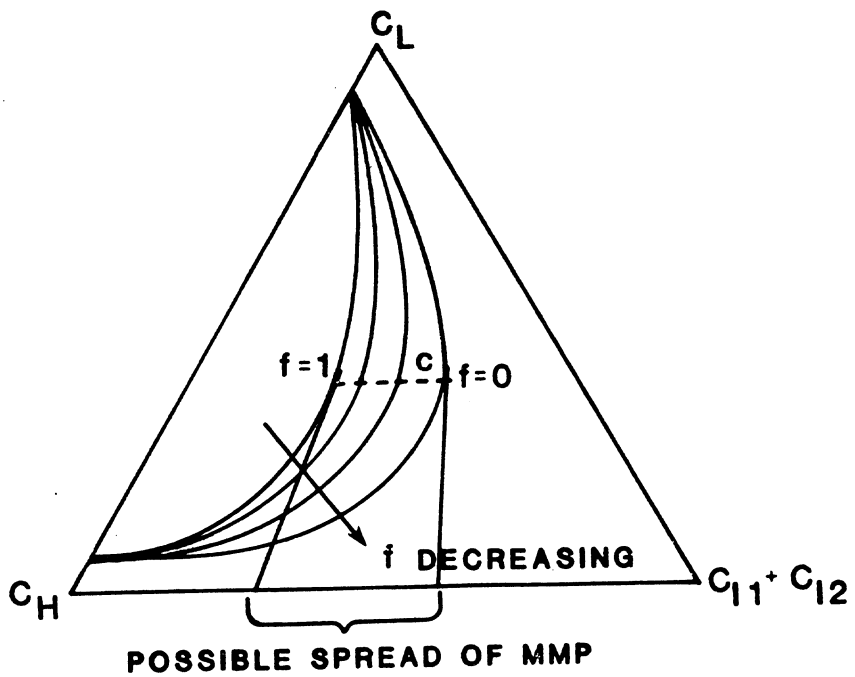

(b) C_{I1} AND C_{I2} SIMILAR

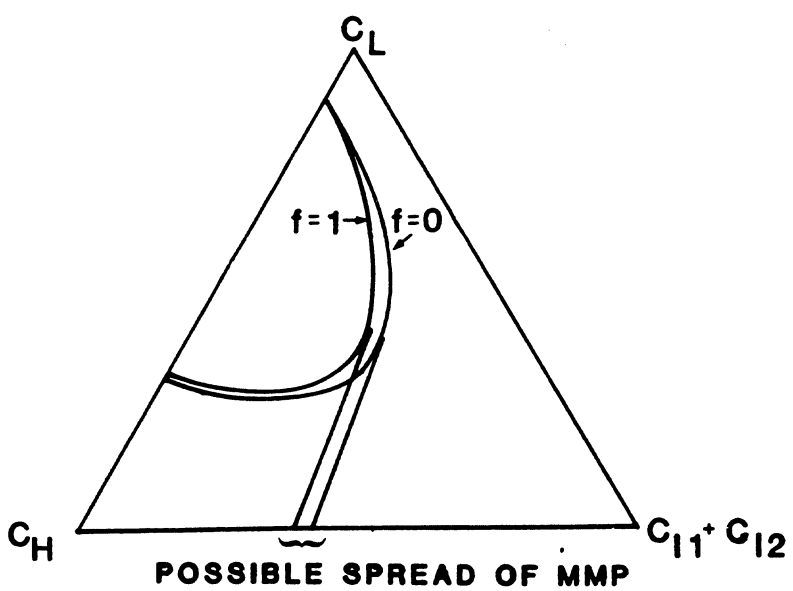

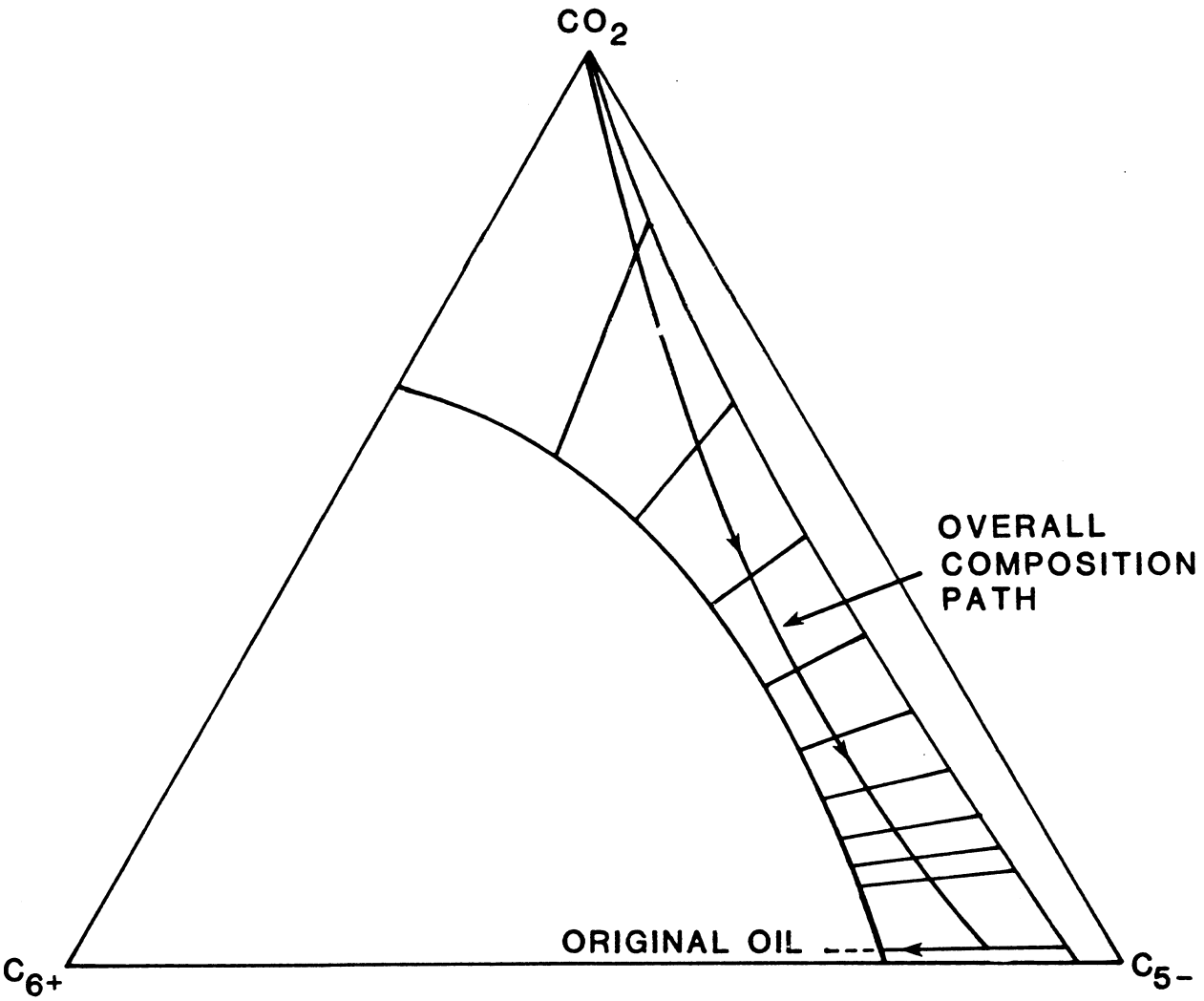

FIGURE 7

SLIM-TUBE MULTIPLE CONTACT PROCESS:
COMPOSITION PATH AT THE FRONT OF
THE TRANSITION ZONE
P= 3200 psia, T= 240°F

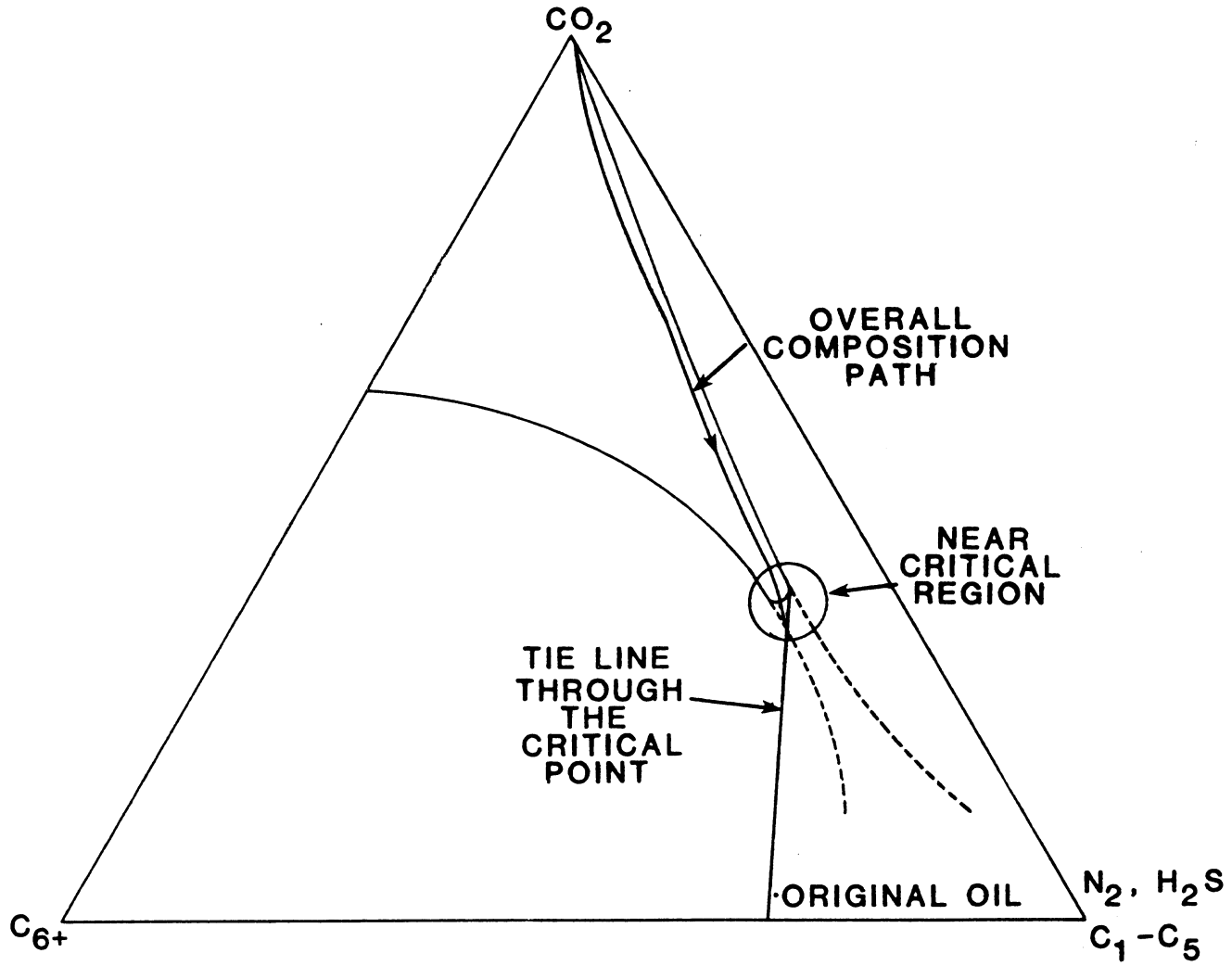

FIGURE 8

SLIM-TUBE MULTIPLE CONTACT PROCESS:COMPOSITION PATH AT THE FRONT OF THE TRANSITION ZONE

——— PHASE ENVELOPE WITH RELATIVE-PERMEABILITY EFFECT

- - - - - PHASE ENVELOPE WITHOUT RELATIVE-PERMEABILITY EFFECT

T = 240°F, P = 3480 psia

FIGURE 9

EFFECT OF MIXING RATIO ON THE MINIMUM MISCIBILITY PRESSURE(MMP) USING HUTCHINSON AND BRAUN'S APPROACH

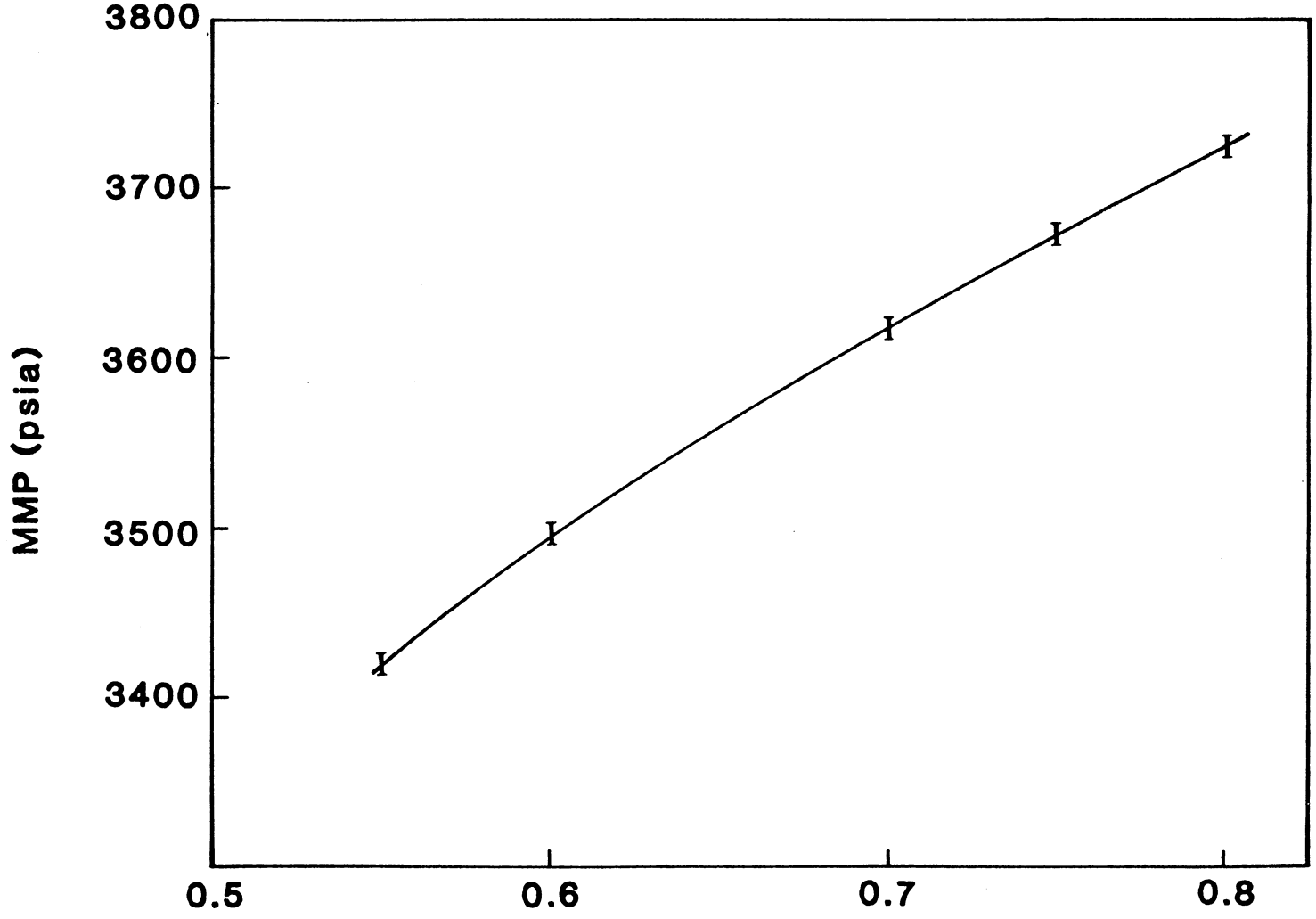

$$R = \frac{\text{(AMOUNT OF DISPLACING FLUID)}}{\text{DISPLACING FLUID + ORIGINAL RESIDING FLUID}}$$

FIGURE 10

EFFECT OF H_2S ON MMP FOR CO_2-INJECTION PROCESS

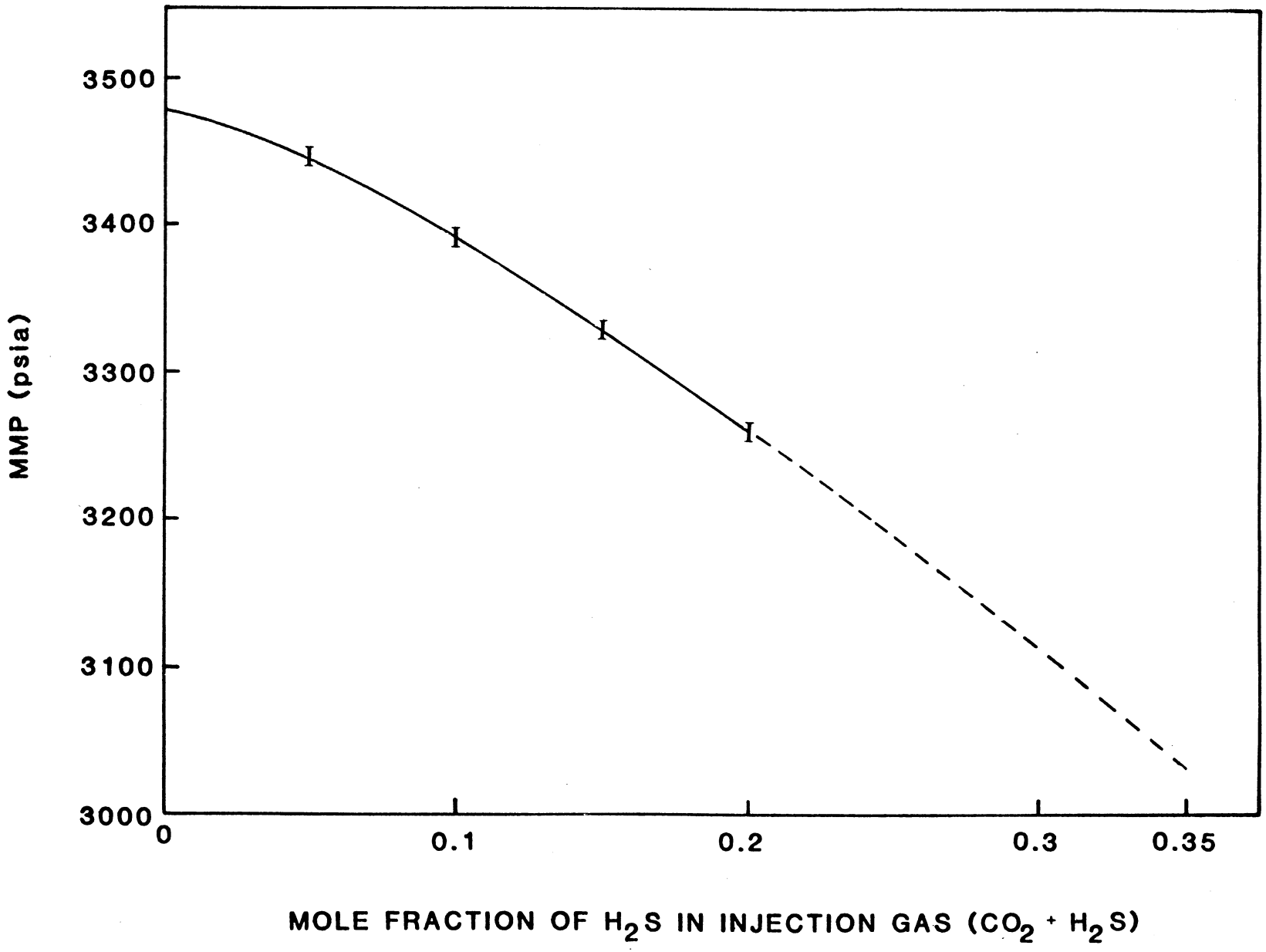

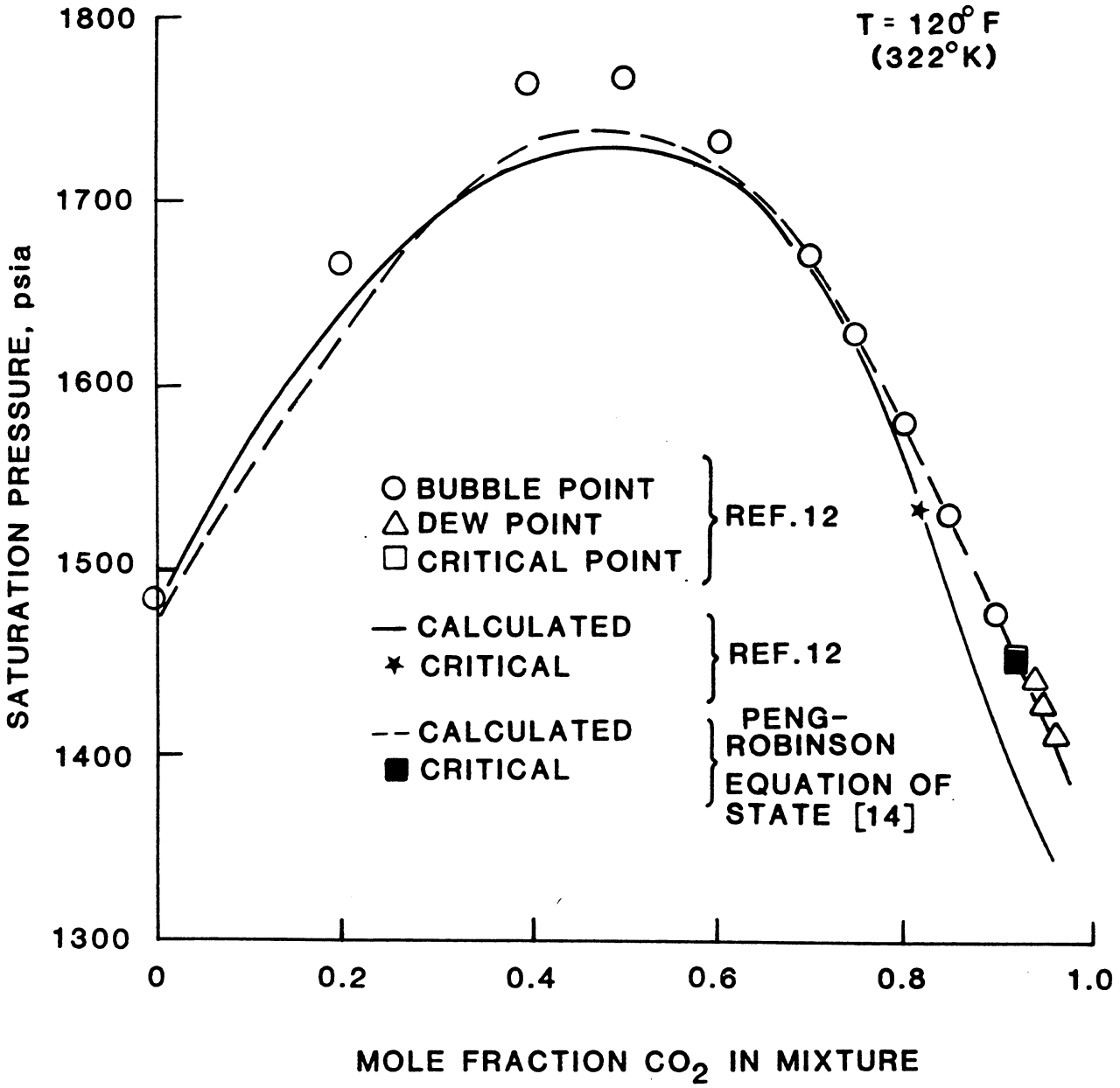

FIGURE 11

PRESSURE-COMPOSITION DIAGRAM FOR CO_2-SYNTHETIC OIL SYSTEM

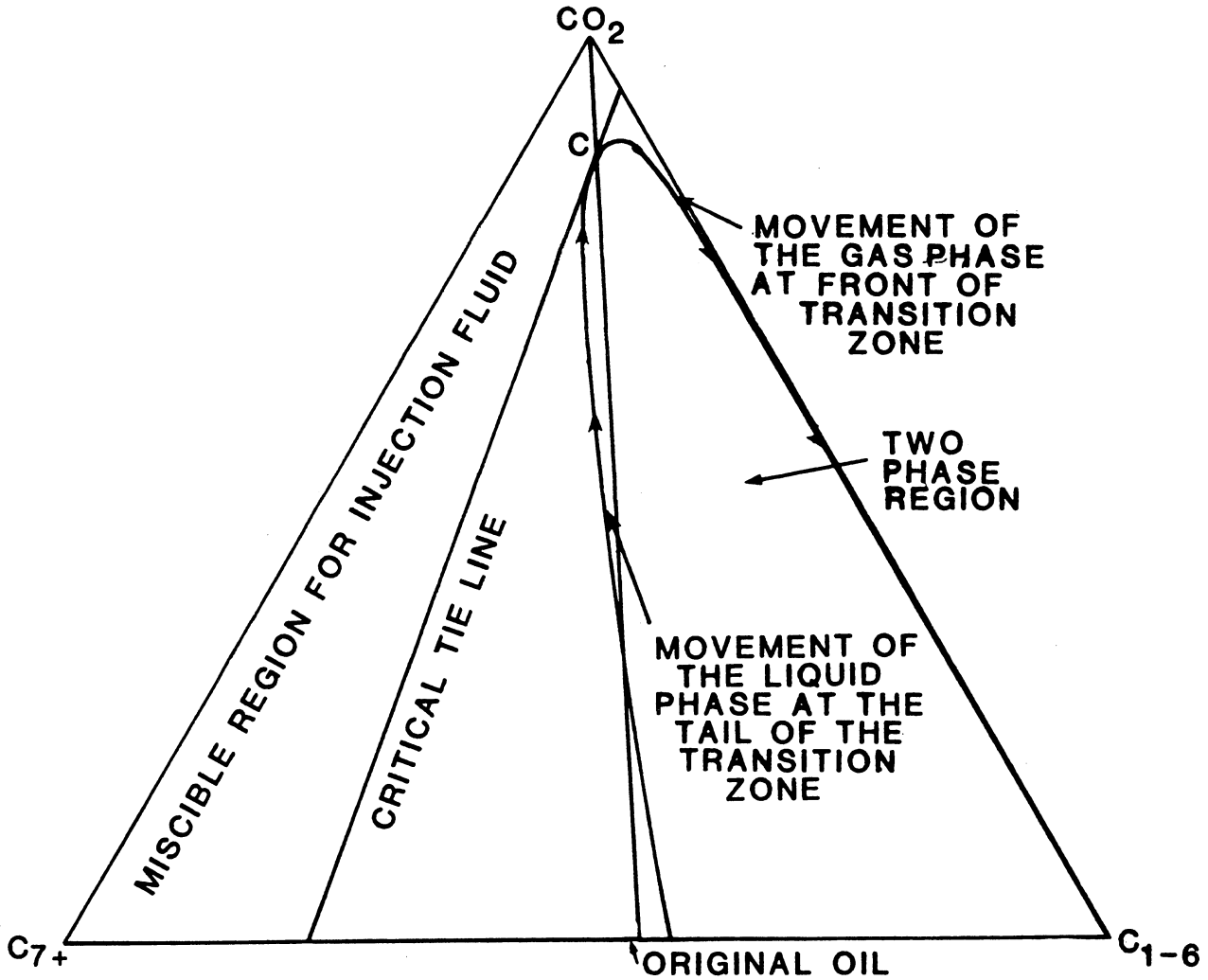

FIGURE 12

PSEUDO TERNARY REPRESENTATIONS OF COMPOSITIONAL PATH FOR FLUID AT FRONT AND REAR ENDS OF TRANSITION ZONE USING METCALFE ET. AL.'S DATA [15]

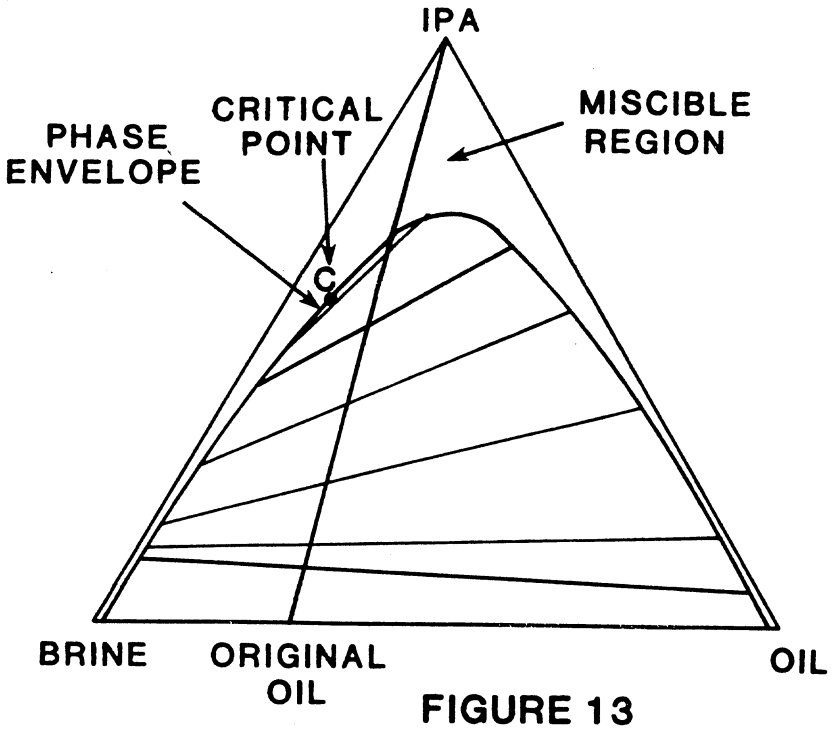

FIGURE 13

TERNARY PHASE ENVELOPE FOR IPA-BRINE-OIL SYSTEM [29]

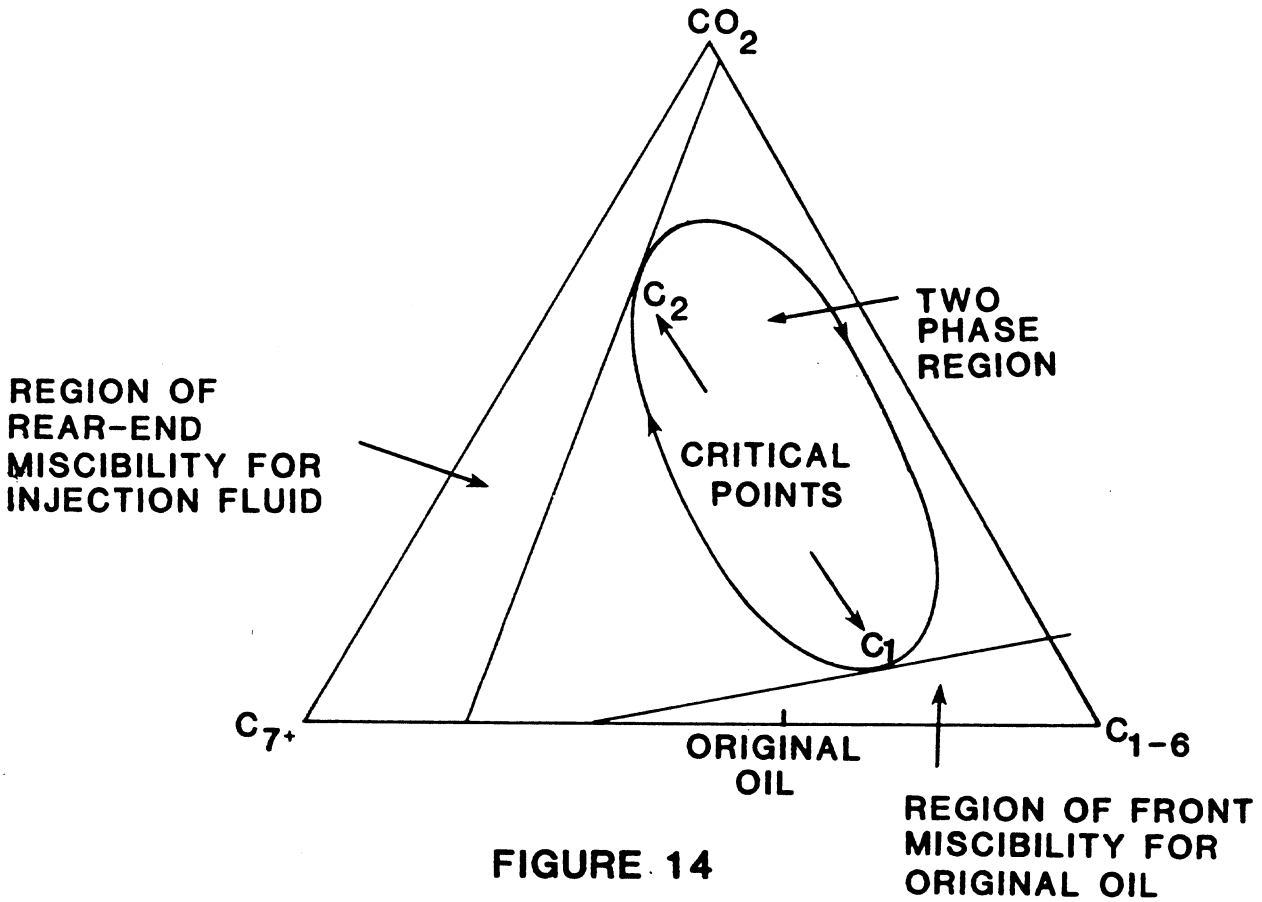

FIGURE 14

DUAL CRITICAL-POINT PSEUDO TERNARY PHASE ENVELOPE

APPENDIX 45

ANALYSIS OF OBSERVATION WELL SATURATION DATA

By

R. Ehrlich

Production Research Department
Gulf Research & Development Company
Pittsburgh, Pennsylvania

TABLE OF CONTENTS

	Page
Abstract	332
Introduction	332
Sequence of Events in Observation Wells	333
General Trends	334
Discussion	335
Conclusions	337
References	338
Sub-Appendix A	342
Sub-Appendix B	384
Sub-Appendix C	387

LIST OF FIGURES

Figure		
1	Well Placement	339
2	Arrival Times of Alcohol Tracers and CO_2	340
3	Pressure Core Analysis - Zabolotny Observation #4	341
A-1	Zabolotny Observation #1 (3/9/81)	342
A-2	Zabolotny Observation #1 (3/24/81)	343
A-3	Zabolotny Observation #1 (4/7/81)	344
A-4	Zabolotny Observation #1 (5/18/81)	345
A-5	Zabolotny Observation #1 (6/1/81)	346
A-6	Zabolotny Observation #1 (6/15/81)	347
A-7	Zabolotny Observation #1 (6/29/81)	348
A-8	Zabolotny Observation #1 (7/13/81)	349
A-9	Zabolotny Observation #1 (7/27/81)	350
A-10	Zabolotny Observation #1 (8/10/81)	351
A-11	Zabolotny Observation #1 (8/25/81)	352
A-12	Zabolotny Observation #2 (3/23/81)	353
A-13	Zabolotny Observation #2 (4/22/81)	354
A-14	Zabolotny Observation #2 (5/5/81)	355
A-15	Zabolotny Observation #2 (5/19/81)	356
A-16	Zabolotny Observation #2 (6/2/81)	357
A-17	Zabolotny Observation #2 (6/16/81)	358
A-18	Zabolotny Observation #2 (6/30/81)	359
A-19	Zabolotny Observation #2 (7/14/81)	360
A-20	Zabolotny Observation #2 (7/28/81)	361
A-21	Zabolotny Observation #2 (8/11/81)	362
A-22	Zabolotny Observation #2 (8/25/81)	363
A-23	Zabolotny Observation #2 (9/16/81)	364
A-24	Zabolotny Observation #3 (5/5/81)	365
A-25	Zabolotny Observation #3 (5/20/81)	366
A-26	Zabolotny Observation #3 (6/3/81)	367
A-27	Zabolotny Observation #3 (6/16/81)	368

LIST OF FIGURES (cont'd.)

Figure		Page
A-28	Zabolotny Observation #3 (6/30/81)	369
A-29	Zabolotny Observation #3 (7/14/81)	370
A-30	Zabolotny Observation #3 (7/29/81)	371
A-31	Zabolotny Observation #3 (8/11/81)	372
A-32	Zabolotny Observation #3 (8/25/81)	373
A-33	Zabolotny Observation #3 (9/17/81)	374
A-34	Observation #1, 9810 Ft	375
A-35	Observation #1, 9813 Ft	376
A-36	Observation #1, 9817 Ft	377
A-37	Observation #2, 9860 Ft	378
A-38	Observation #2, 9863 Ft	379
A-39	Observation #2, 9867 Ft	380
A-40	Observation #3, 9840 Ft	381
A-41	Observation #3, 9843 Ft	382
A-42	Observation #3, 9847 Ft	383
B-1	Pressure Volume Relationship	385
B-2	CO_2 Solubility in Distilled Water	386
C-1	Idealized Geometry for Dispersive Mixing Estimate	388
C-2	Concentration Profiles vs Dimensionless Time	388
C-3	Transverse Dispersion Correlation From Perkins & Johnston	388

ANALYSIS OF OBSERVATION WELL SATURATION DATA
LITTLE KNIFE CO_2 PROJECT

ABSTRACT

Changes in oil, water and gas saturations determined by monitor logs in the observation wells during the Little Knife CO_2 project were analyzed for what could be learned about CO_2 displacement mechanisms. Three distinct mechanisms important in defining the total amount of oil displaced from the project area were identified: (1) waterflooding, (2) waterflooding accompanied by CO_2 swelling of oil where CO_2 is transported in solution, and (3) simultaneous CO_2-water displacement where a vapor phase is present. Displacement efficiency is highest for (3) where multiple-contact miscibility can be developed, lowest for (1) and intermediate for (2). Vertical sweep efficiency is highest for (1)--essentially complete over the X, Y and Z zones. A lower vertical sweep is seen for zones in which (2) occurs, and lower still where (3) occurs.

INTRODUCTION

In the Little Knife CO_2 flood project, alternating slugs of CO_2 and water were injected into a single injection well offset by three observation wells on an approximately five-acre circle (Figure 1). Logs were used to follow changes in oil, water and gas saturations in these observation wells during the course of the project. In this memorandum, we have attempted to analyze this saturation data for what can be learned about CO_2 flood displacement mechanisms operative in the Little Knife project and to use this analysis to test perceptions derived from laboratory and simulation studies about how CO_2 miscible flooding has worked in Little Knife.

The project was begun on 12/11/80 with preinjection of water followed on 1/7/81 by alternating slugs of CO_2 and water (1:1 ratio on a reservoir volume basis). CO_2 injection was terminated on 3/25/81 and drive water injection was continued to 9/24/81. A pressure core well (Observation #4) was spudded on 5/9/81. Pressure coring in the Mission Canyon formation was begun on 7/2/81. Based on the pore volume of the high porosity sections of the Mission Canyon D zone (designated as zones X, Y and Z in the simulation work) within the five-acre area, CO_2 injection has been 17.5% PV and total water including preinjection and drive water has been 183% PV. Details of the operational aspects of the project have been given by Desch et al.[1]

The cased hole monitor log program has been described by Svor and Globe.[2] In this, a dual spaced pulsed neutron tool which measures capture cross section and near-to-far detector count ratio was used. Because these respond in different ways to changes in water and gas filled porosity, a triangulation method could be used to obtain oil, water and gas saturations.

In Observation Wells #1, #2 and #3, base log measurements were obtained before injection was started and then periodically during the test. Data from these measurements for the depth interval where changes seem to be occurring are shown in Figures A-1 through A-33 in Appendix A. These show from left to right: porosity, a comparison of the present and original oil saturations and gas saturation. The latter represents the total amount of gas present including that dissolved in oil and water. An estimate of the free gas saturation was made and is also shown. The assumptions made in this calculation and the uncertainties associated with it are given in Appendix B. Appendix A also contains a series of Figures (A-34 to A-42) in which oil, water, gas and free gas saturation changes at selected depths are shown vs. time.

Fluid samples were also taken from these observation wells. Water was analyzed for alcohol tracer content--the preinjection water contained 500 ppm isopropyl alcohol and the water injected with CO_2 contained 500 ppm n-propyl alcohol. Separator gas samples were analyzed for CO_2 content and the C_{13}/C_{12} isotope ratio which was related to the percent injected CO_2 in the gas--the injected and naturally occurring CO_2 had different isotope ratios. These data are shown in Figure 2 taken from Reference 1.

SEQUENCE OF EVENTS IN OBSERVATION WELLS AS INDICATED BY LOG ANALYSIS

Observation #1 (X, Y, Z zones: 9809-9825 ft)

Oil saturation decreased in the X, Y and Z zones through 4/7 with only trace amounts of gas indicated. The lowest oil saturation at that point was about 49% PV. A definite oil bank arrived between 4/7 and 5/18 and passed through over the period 5/18 through 6/1. Between 6/1 and 6/15, a gas bank arrived, resulting apparently in significant oil saturation reduction. Average oil saturation in the high porosity interval on 6/15 was 41% PV. Average oil saturation in the interval containing significant gas (9809-9820 ft) was 36% PV and the average gas saturation in that interval was 11% PV. Free gas was indicated only over a 2-foot zone (9813-14 ft). Oil saturation in that interval averages 29% PV.

Oil saturations changed relatively slowly after 6/15. Average oil saturation in the X, Y and Z zones on 8/25 was 40% PV. The gas-saturated interval is essentially unchanged (now 9810-9819 ft). Average oil and gas saturations in that interval were 29% PV and 13% PV respectively. Only the same 2-foot zone was indicated to contain free gas on 8/25. Average oil saturation in that zone was 19% PV.

Observation #2 (X, Y, Z zones: 9857-9872 ft)

Oil saturation in the X, Y and Z zones is low in the initial monitor log on 3/23 suggesting that this well may have been substantially watered out at that point. Throughout the monitoring period, oil saturation steadily decreased and gas saturation steadily increased with no indication of bank formation.

Average oil saturation in the X, Y and Z zones on 9/16 was 29% PV. Significant gas saturation existed over the interval 9860-9866 ft. Oil and gas saturations in that interval averaged 11% PV and 13% PV respectively. Free gas was indicated over most of that interval on 9/16.

Observation #3 (X, Y, Z zones: 9838-9853 ft)

Oil saturation in the X, Y and Z zones was relatively high in the initial monitor log on 5/5--59% PV average--but decreased sharply between 5/5 and 5/20, primarily as a result of water displacement. From 5/20 through the end of the monitoring period, oil saturation slowly increased as gas saturation increased with no evidence of bank formation.

Average oil saturation in the X, Y and Z zones on 9/17 was 37% PV. Within the X, Y and Z zones, significant gas saturation existed over the interval 9842-9847 ft. (Gas also has penetrated the interval 9836-9839 ft but does not appear to have resulted in much oil displacement.) In that interval, oil and gas saturations average 20% PV and 12% PV respectively. Free gas was indicated over approximately that same interval on 9/17.

GENERAL TRENDS

A number of general trends in the observation well saturation data are significant.

Displacement Sequence and Vertical Sweep Efficiency:

The sequence and general characteristics of the displacement process are qualitatively the same in each well. Water invasion generally occurs first and is limited primarily to the high porosity X, Y and Z zones although it is fairly complete over those zones. Invasion by fluids containing, by our estimates, dissolved CO_2* follows and is ultimately over somewhat less of the vertical interval than for water. Vertical sweep efficiency by free gas, when it arrives, is significantly less than that of water and dissolved gas. On average for the three observation wells, vertical sweep by CO_2 in any form is about half that of water, and vertical sweep by free CO_2 is about half that of CO_2 in any form.

Final gas saturations (Figures A-11, A-23 and A-32) are more or less the highest that have occurred in those wells. The expected gas saturation reduction has not been seen yet despite the large volume of drive water injected.

Correlation of Oil Saturation Changes With Changes in Gas And Water Saturations:

Where water displacement has occurred in the absence of significant gas, oil saturation is reduced on average to about 40% PV although values as low as about 30% PV are seen at some depths (This can be seen in the Injection #1 residual oil determination[3] as well as in Observation #2 on 3/23).

*Tracer data (Figure 2), although somewhat uncertain because of the use of nitrogen in gas lifting, strongly suggest that the gas saturation is in all cases CO_2.

When significant gas (no less than 5-10% PV) is present together with high water saturation, lower oil saturations--in the 20-30% PV range--are obtained. Very low oil saturations in the zero to 20% PV range are reached only when free gas is present. These trends are most clearly seen in Figures A-34 through A-42.

Vertical Expansion of Low Oil Saturation Zone With Time--Comparison of Observation #2 and Observation #4 (pressure core) Saturation Data:

A low oil saturation-free gas zone, once formed, does not seem to expand rapidly in the vertical direction with time. This is seen in Figures A-1 through A-33 and also in a comparison of Observation #2 and Observation #4 data. Figure 3 shows Observation #4 pressure core saturation data (taken from References 4 and 5). Within the significant uncertainty of the pressure core data, this matches Observation #2 saturation data at the time the pressure core was taken (Figures A-18 and A-19), particularly in the thickness of the very low oil saturation zone. This is despite the fact that Observation #4 is closer to the injection well and would have seen CO_2 earlier.

DISCUSSION

Displacement Efficiency

CO_2 is not miscible on first contact with Little Knife crude oil at pressures that existed in the pilot area. Laboratory tests have shown that multiple contact miscibility can be developed at these pressures and can result in very low residual oil saturations. This mechanism, however, requires a mobile free CO_2 saturation. The correspondence of very low saturation zones with the presence of free gas in those zones is consistent with this mechanism. The fact that very low oil saturations--as low as a few percent pore volume--are obtainable in the presence of high water saturation is also consistent with laboratory results. The fact that oil saturations higher than this are present together with free gas suggests that displacement was not yet complete when the project was terminated.

Where no free gas saturation exists, mechanisms for reduction of oil saturation below waterflood residual are (1) displacement of oil by CO_2 swollen oil followed by water displacement and/or (2) waterflooding to residual oil followed by contacting with CO_2 saturated water resulting in swelling and partial mobilization of that oil. In either case, the lowest achievable residual oil saturation is related to the CO_2 swelling factor and is discussed in Appendix B. If a waterflood residual oil saturation of 40% PV is assumed, then the minimum residual oil would range from 27% PV at 3700 psi to 30% PV at 3500 psi. These values are consistent with oil saturation data in Appendix A where gas saturation is less than that needed to form a free gas saturation.

Vertical Sweep Efficiency

Reasons for incomplete vertical sweep by free CO_2 could have been that permeability trends caused channeling, that insufficient CO_2 was available at the observation wells to form free CO_2 over the entire interval, and/or that the free CO_2 swept interval represents an instability (a finger). Permeability variation does not seem to have been completely responsible--if it were, there should also have been an effect on vertical sweep by water. Insufficient CO_2 does not seem to have been responsible--the same type of vertical sweep seems to have occurred in Observation #4 (where more CO_2 would presumably be available) as in Observation #2.

Instability, possible augmented by some permeability variation appears to be the most likely explanation. Although instabilities of small dimension are generally considered to be damped by dispersive mixing in miscible systems[6], the effect of dispersion in a multiple contact miscible system will only be to equalize CO_2 partial pressure (more properly fugacity). It will not affect a saturated vapor finger through saturated liquid.

CO_2 Transport

CO_2 transport and consequent oil displacement in this project has been very different from that seen in linear laboratory systems. Even after 146% PV drive water injection, CO_2 saturation at the observation wells was, for the most part, still increasing or at least was not decreasing, and oil saturation in some places was still decreasing. This behavior may indicate that there was still a net flow of CO_2 at the observation wells at the time of the last monitor logs.

With incomplete vertical sweep (for whatever reason), oil will be bypassed. Large quantities of CO_2 can accumulate in solution in this oil (primarily) and also in water as a result of convective and dispersive mixing and will move only at a rate related to the flow of these fluids. Appendix C shows that transverse dispersion may be important over the times and vertical distances involved in this project and may be an important factor causing this CO_2 accumulation.

An important benefit of the alternating slugs of water injected with CO_2, in addition to any mobility control effect, may have been to reduce the capacity of these bypassed fluids to retain CO_2. Because of the much lower CO_2 solubility in water than in oil at reservoir conditions, waterflooded zones above and below CO_2 swept zones would retain less CO_2 than if those zones had not been waterflooded.

Overall Project Performance

The departures from ideal miscible flood behavior seen in this project do not indicate that a CO_2 flood at Little Knife will respond any less favorably than other successful carbonate reservoir CO_2 floods. Incremental recoveries over waterflooding for CO_2 floods have been reported[8] as ranging from 3% PV to 12% PV with most in the 7% PV to 10% PV range. Non-

idealities such as we have seen here would be necessary to explain recoveries of this magnitude considering the very high displacement efficiency associated with multiple-contact miscible CO_2 flooding in laboratory systems and, in fact, may be a natural consequence of CO_2 flooding in real reservoirs.

CONCLUSIONS

1. Three distinct displacement mechanisms appear to be operative in the Little Knife CO_2 project: (1) waterflooding, (2) waterflooding accompanied by CO_2 swelling of oil where CO_2 is transported in solution, and (3) simultaneous CO_2-water displacement where a vapor phase is present. All are important in determining the total amount of oil displaced from the project area.

2. Displacement efficiency is highest where water and gaseous CO_2 displacement occurs--oil saturations in the zero to 20% PV range are reached. Displacement by CO_2 in solution is less efficient, giving 20-30% PV oil saturations. Waterflooding alone is less efficient still, giving oil saturations which are mostly in the 40% PV range. The very low gaseous CO_2-water residual oil saturations are in agreement with laboratory tests which showed that multiple contact miscibility could be achieved at reservoir conditions and that high water saturation would not interfere with miscibility development.

3. Vertical sweep efficiency is highest for water displacement, less for displacement by CO_2 in solution and lowest for vapor phase CO_2 displacement.

R. Ehrlich

RE:pj
Attachments

REFERENCES

1. J. B. Desch, W. K. Larsen, R. F. Lindsay, R. L. Nettle: "Enhanced Oil Recovery by CO_2 Miscible Displacement in the Little Knife Field, Billings County, North Dakota", SPE/DOE 10696, SPE/DOE Enhanced Recovery Symposium, Tulsa, (1982).

2. T. R. Svor, M. P. Globe: "A Three-Phase Quantitative Monitoring Method for CO_2 Floods", SPE/DOE 10684, SPE/DOE Enhanced Recovery Symposium, Tulsa (1982).

3. T. R. Svor, J. M. Price: "Results of Water Injection From Cased Hole Log Analysis in the Zabolotny Injection Well No. 1, Little Knife Field CO_2 Pilot Test, North Dakota", GR&DC HTSC Technical Memorandum No. 4455TL084 (August, 1980).

4. A. Whiting: "CO_2 Mini-Test Pressure Core Well" HTC Technical Memorandum No. 446TN022 (February, 1982).

5. R. Ehrlich: "Analysis of Observation Well #4 Pressure Core Data" GR&DC Production Research Department Technical Memorandum No. 441TN388 (June, 1982).

6. T. K. Perkins, O. C. Johnston, R. N. Hoffman: "Mechanics of Viscous Fingering in Miscible Systems", SPEJ (December, 1965) 301-317.

7. W. E. DeVaney: "GOEP-US Zabolotny 1-3-4A, Little Knife Field, Billings County, N.D., CO_2 Swelling Test" GR&DC HTSC Technical Memorandum No. 445TL074 (April, 1980).

8. F. I. Stalkup: "Carbon Dioxide Flooding: Past, Present and Outlook for the Future", JPT (August, 1978), 1102-1112.

9. W. S. Dodds, L. F. Stutzman, B. J. Sollami: "Carbon Dioxide Solubility in Water", I&EC Chem. & Eng. Data, (1956) 1, 92-95.

10. H. R. Crawford, G. H. Neill, B. J. Bucy, P. B. Crawford: "Carbon Dioxide--A Multipurpose Additive for Effective Well Stimulation", JPT (March, 1963), 237-242.

11. J. Crank: The Mathematics of Diffusion, Oxford University Press, London (1956).

12. T. K. Perkins, O. C. Johnston: "A Review of Diffusion and Dispersion in Porous Media" SPEJ (March, 1963).

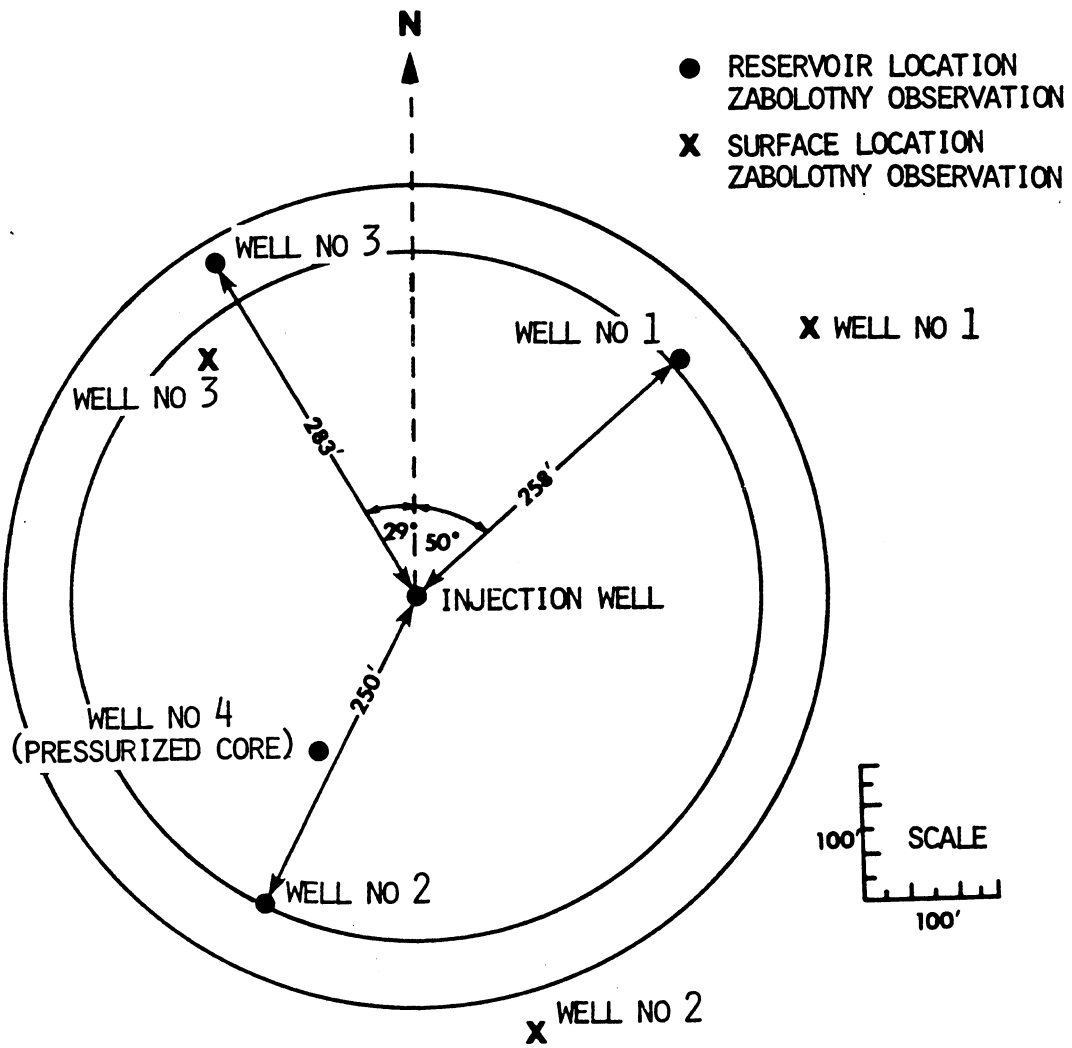

FIGURE 1
LITTLE KNIFE - CO_2 MINITEST
WELL PLACEMENT

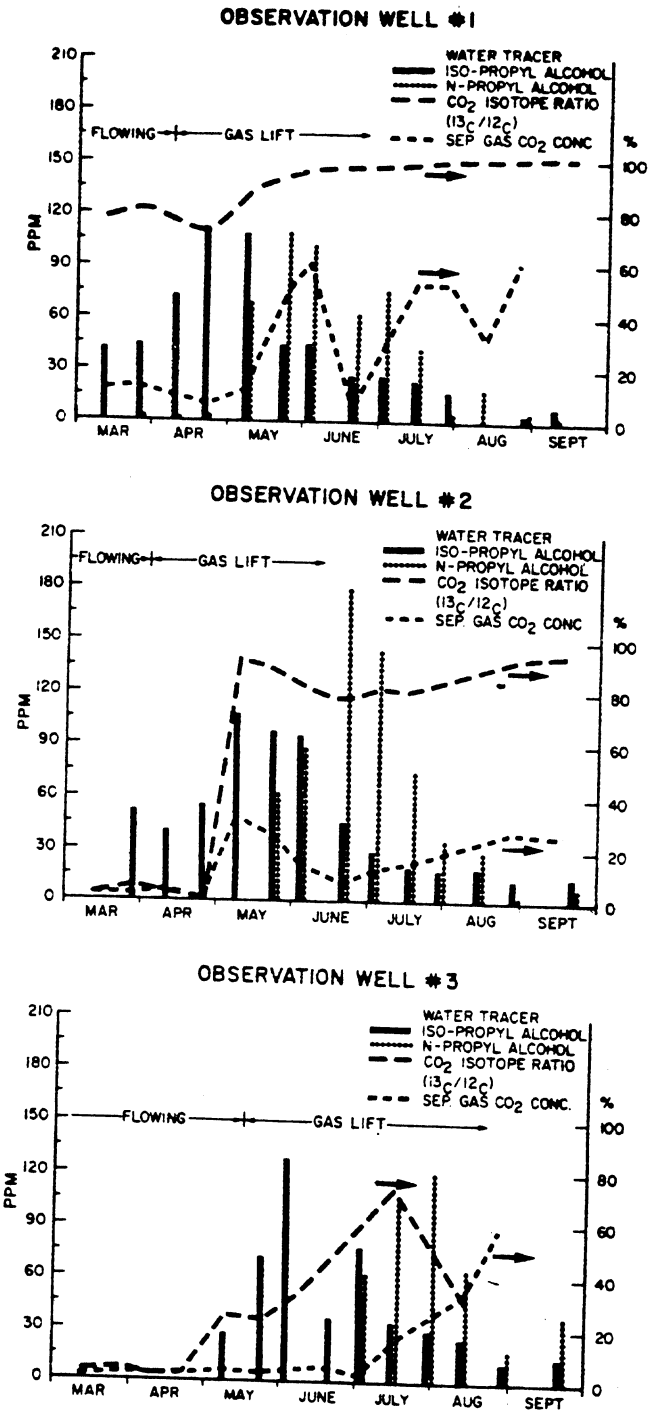

Fig. 2.— Arrival Times of Alcohol Tracers and CO_2 at Each Observation Well.

FIGURE 3

LITTLE KNIFE CO_2 PROJECT

ZABOLOTNY OBSERVATION #4 PRESSURE CORE ANALYSIS

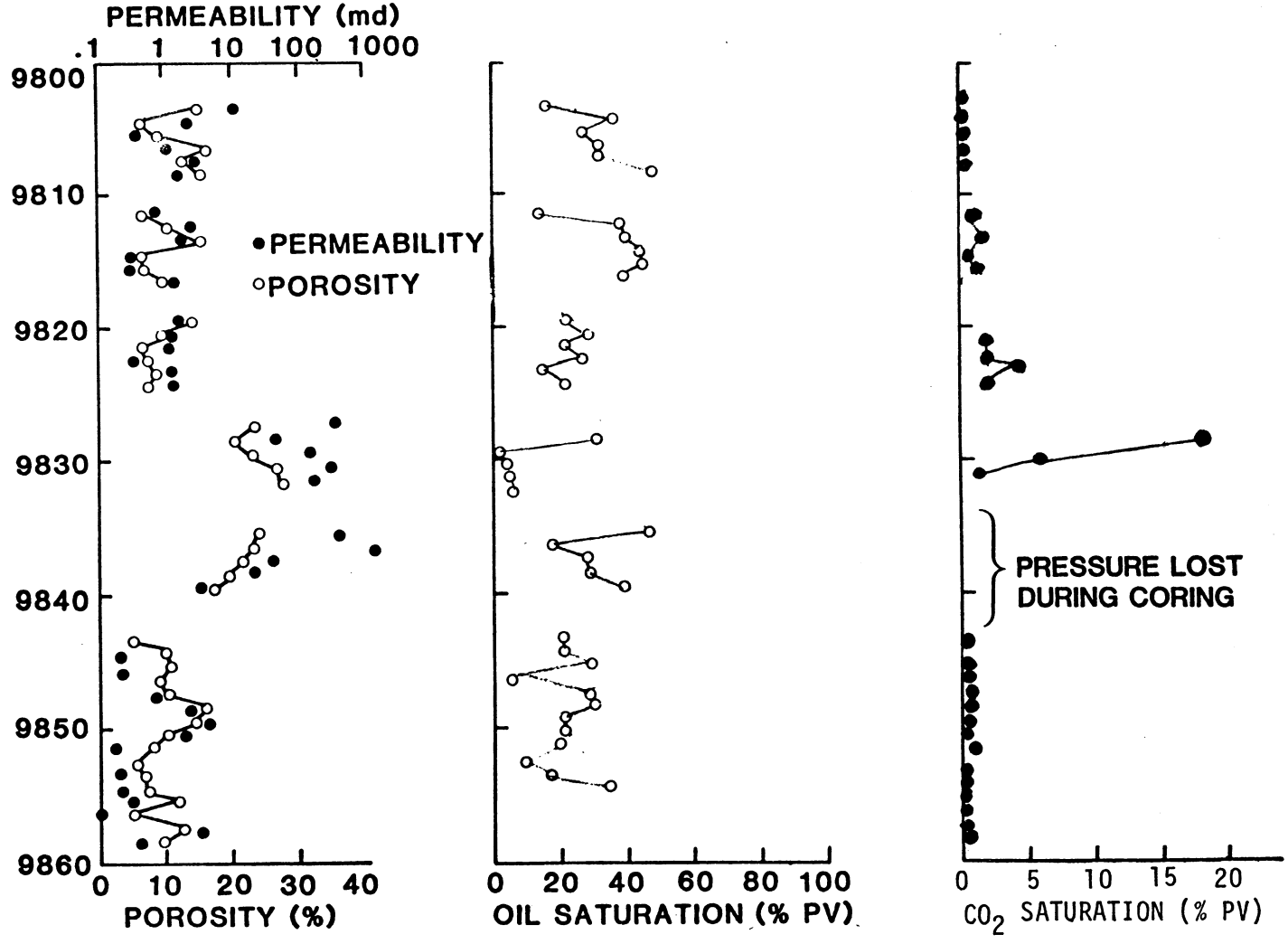

SUB-APPENDIX A

LOG-DERIVED SATURATION

DATA FOR OBSERVATION WELLS

#1, #2 AND #3

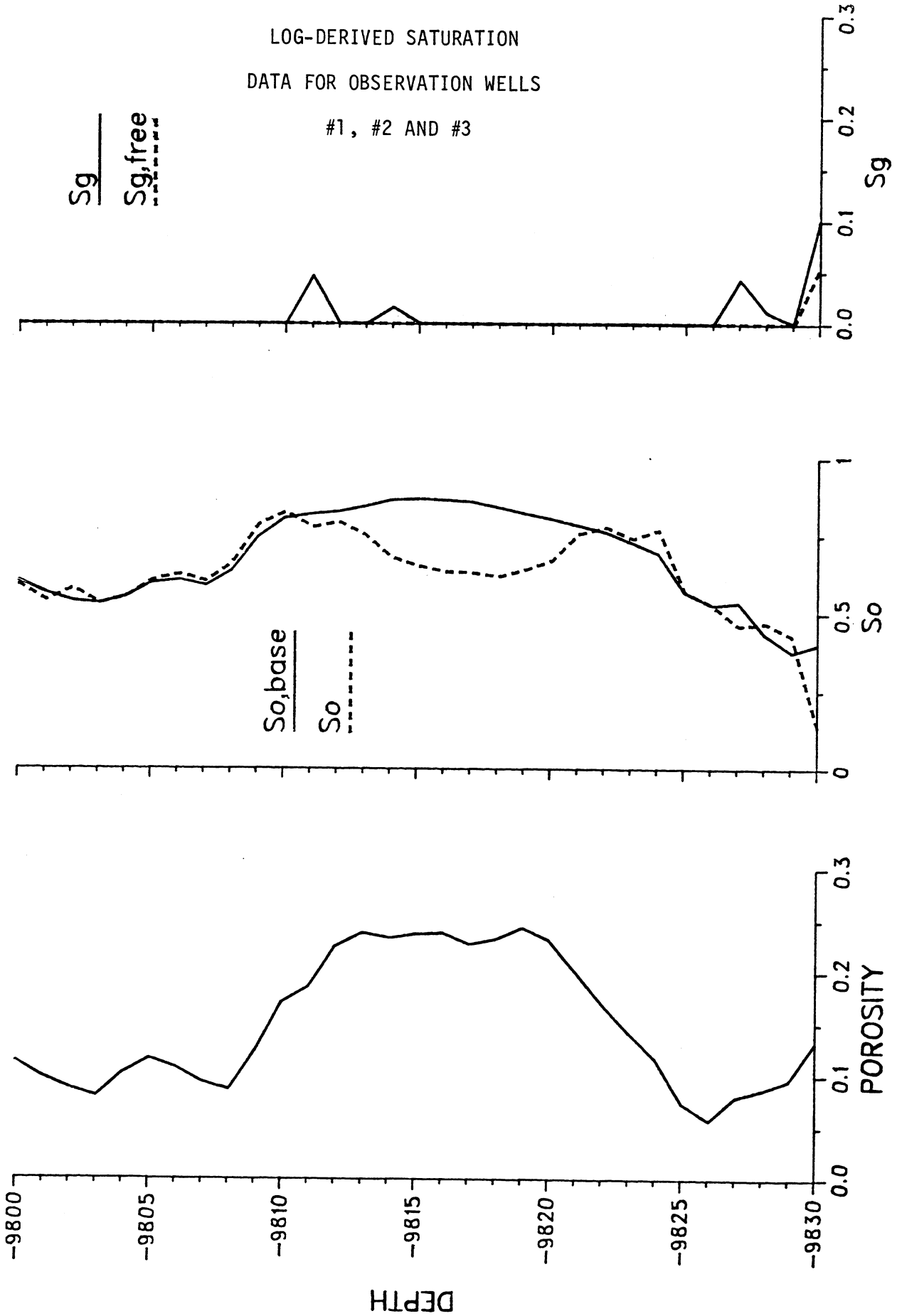

FIGURE A-1 Zabolotny Observation – 1 3/9/81

FIGURE A-2 Zabolotny Observation – 1 3/24/81

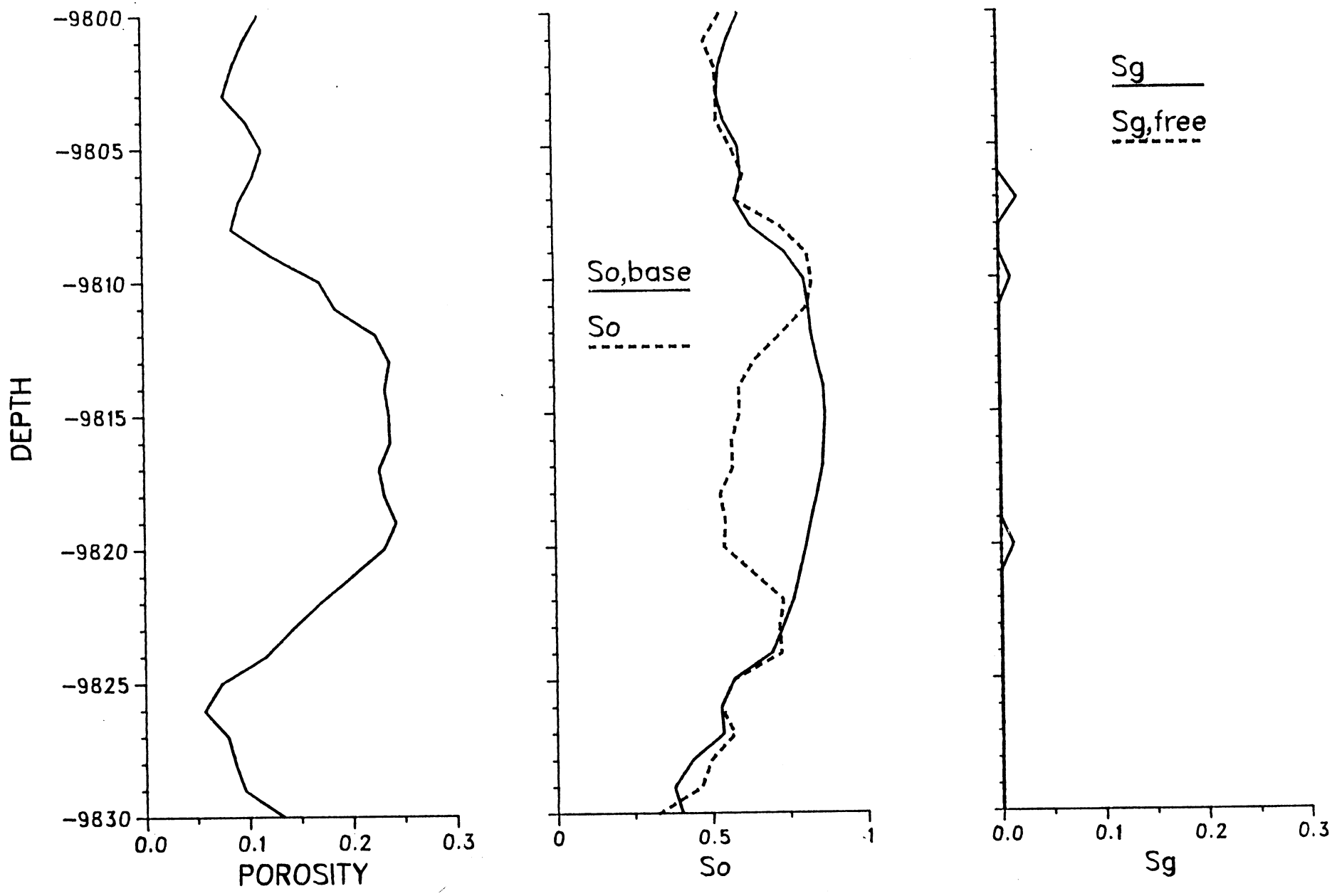

FIGURE A-3 Zabolotny Observation – 1 4/7/81

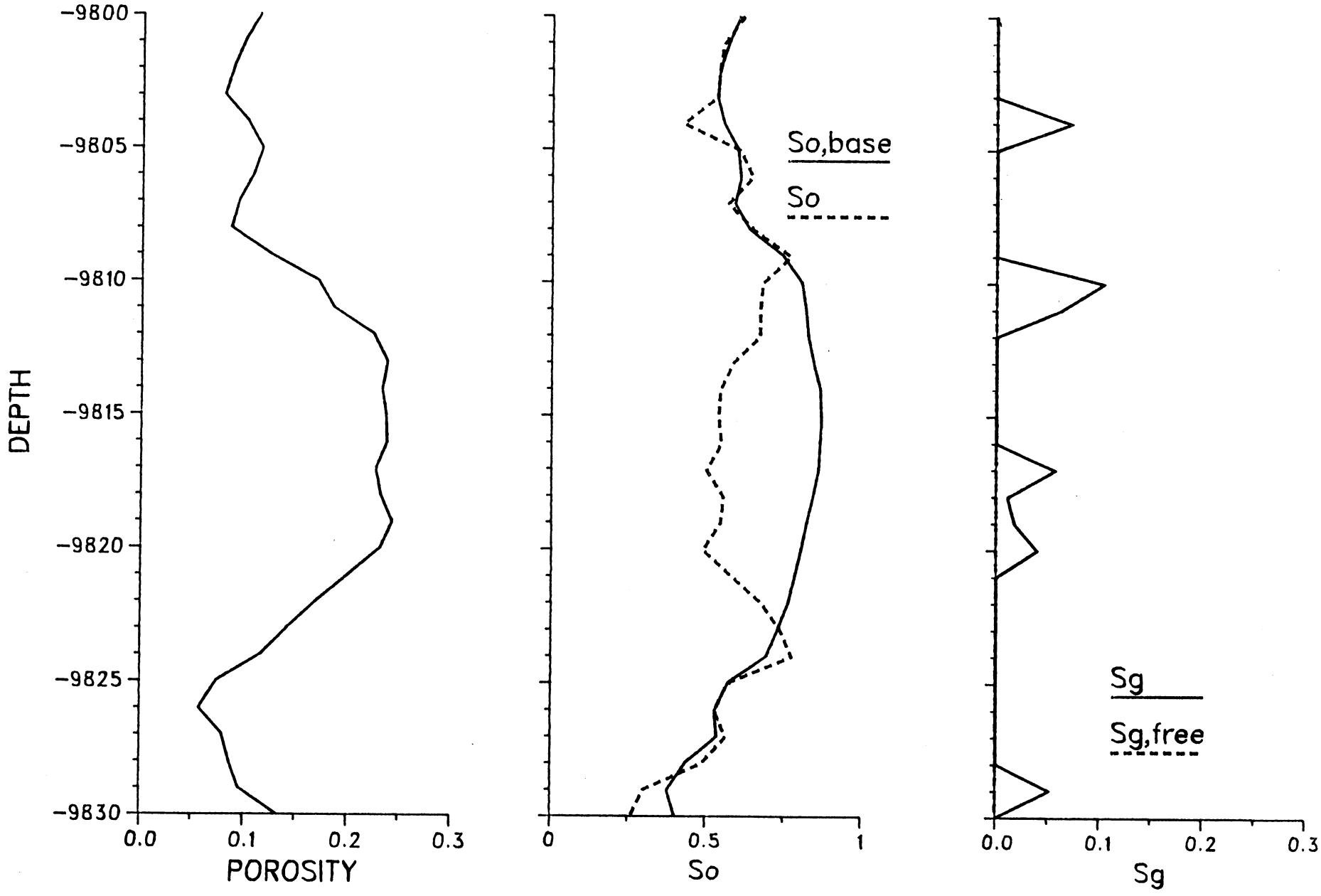

FIGURE A-4 Zabolotny Observation – 1 5/18/81

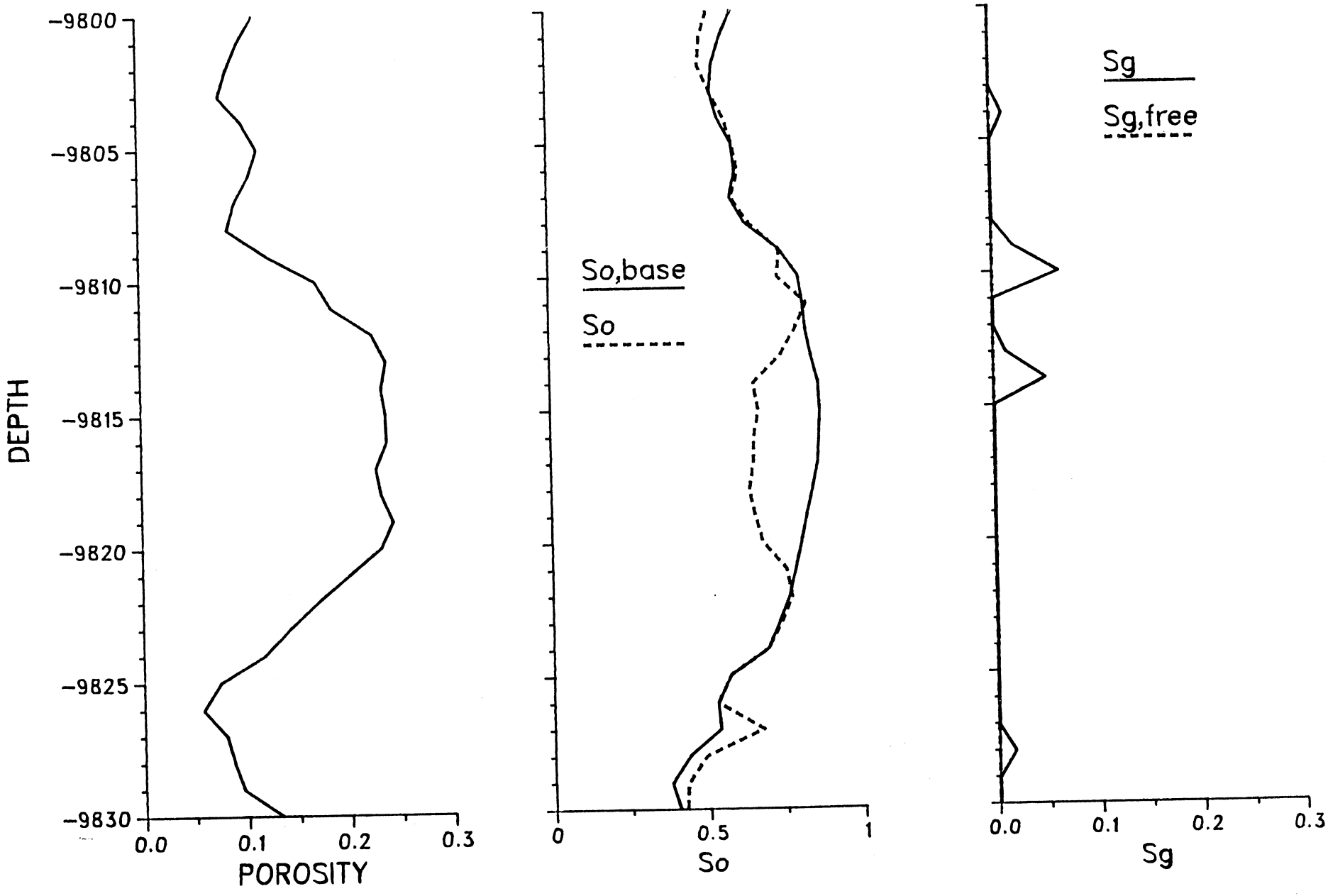

FIGURE A-5 Zabolotny Observation – 1 6/1/81

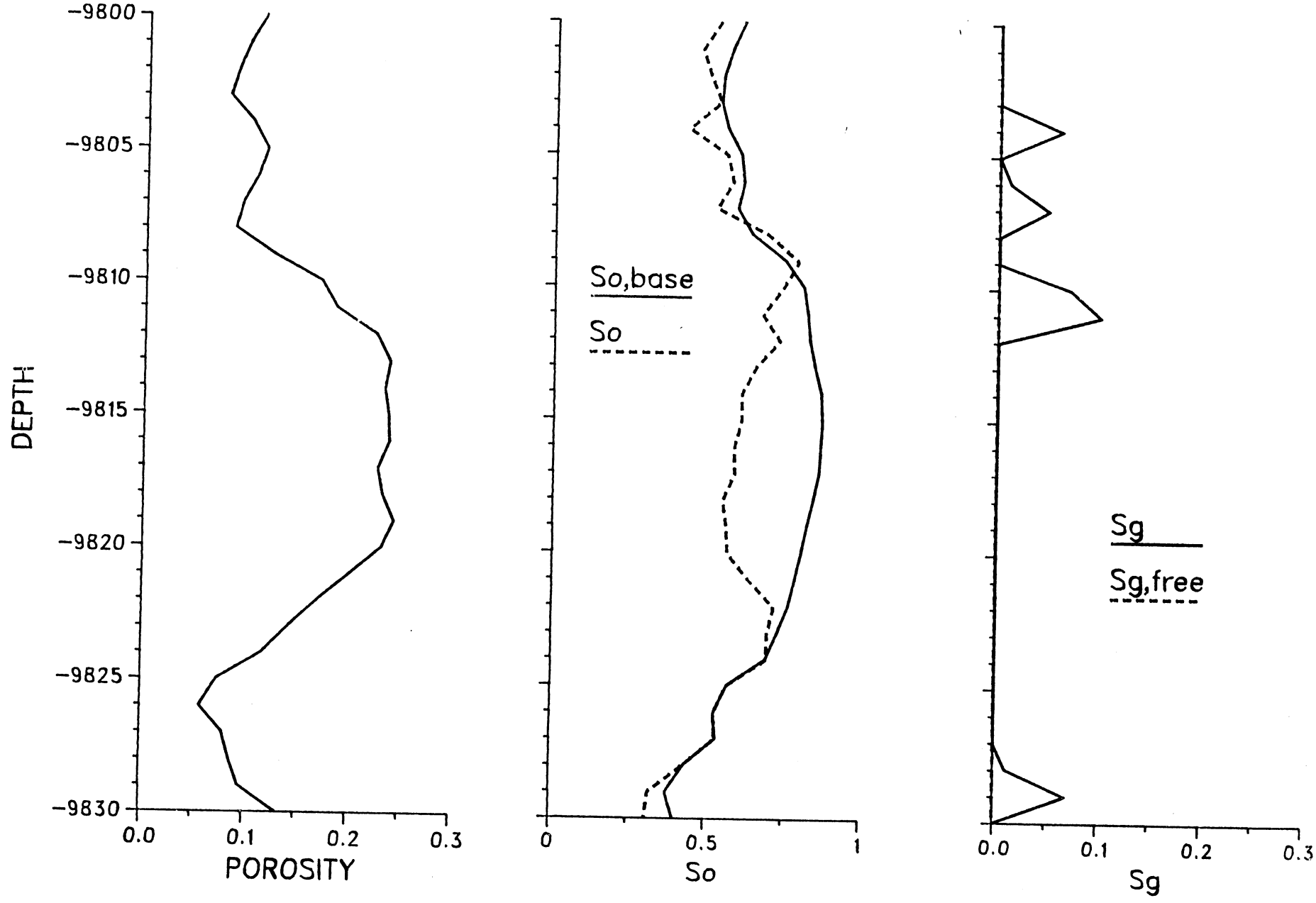

FIGURE A-6 Zabolotny Observation – 1 6/15/81

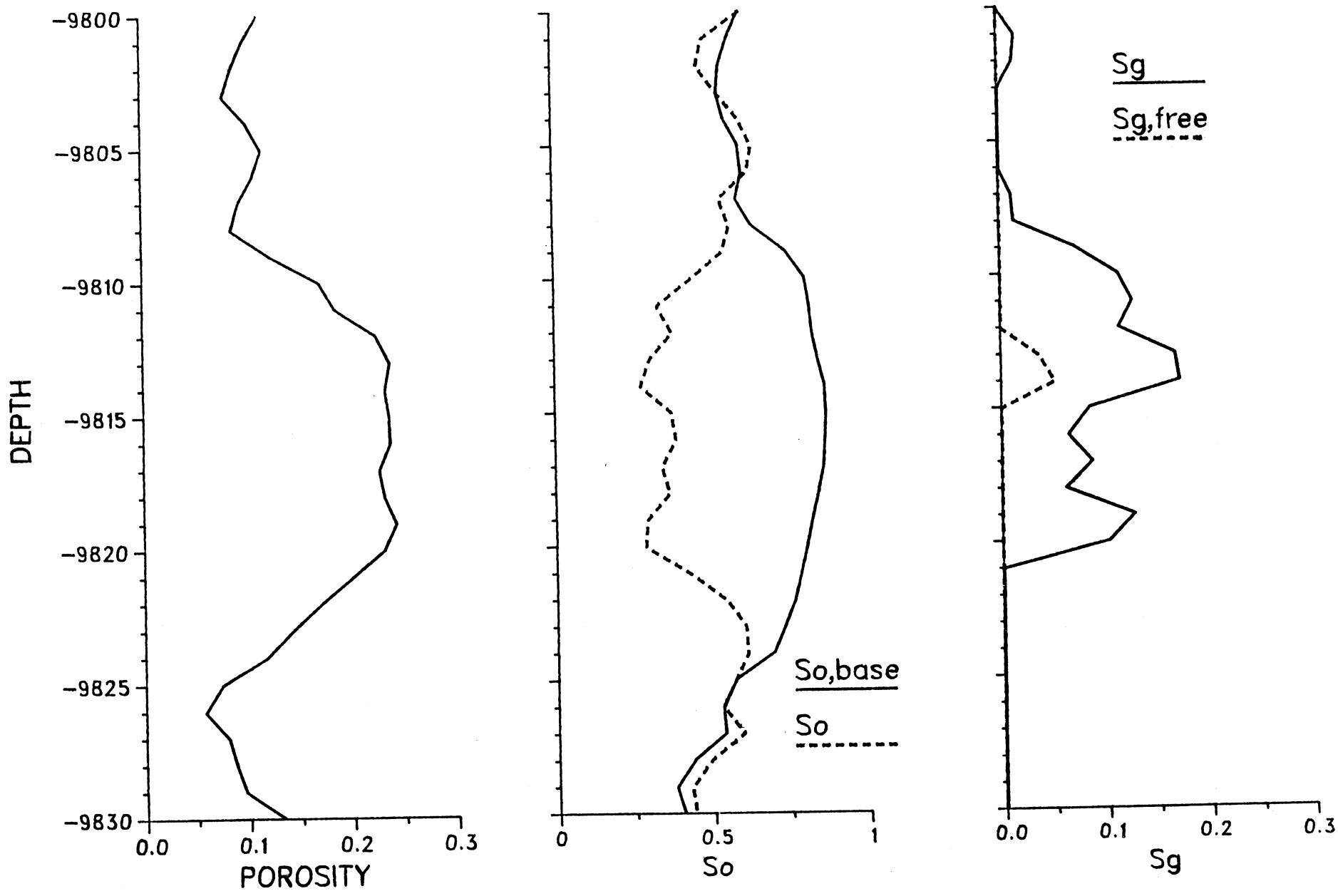

FIGURE A-7 Zabolotny Observation – 1 6/29/81

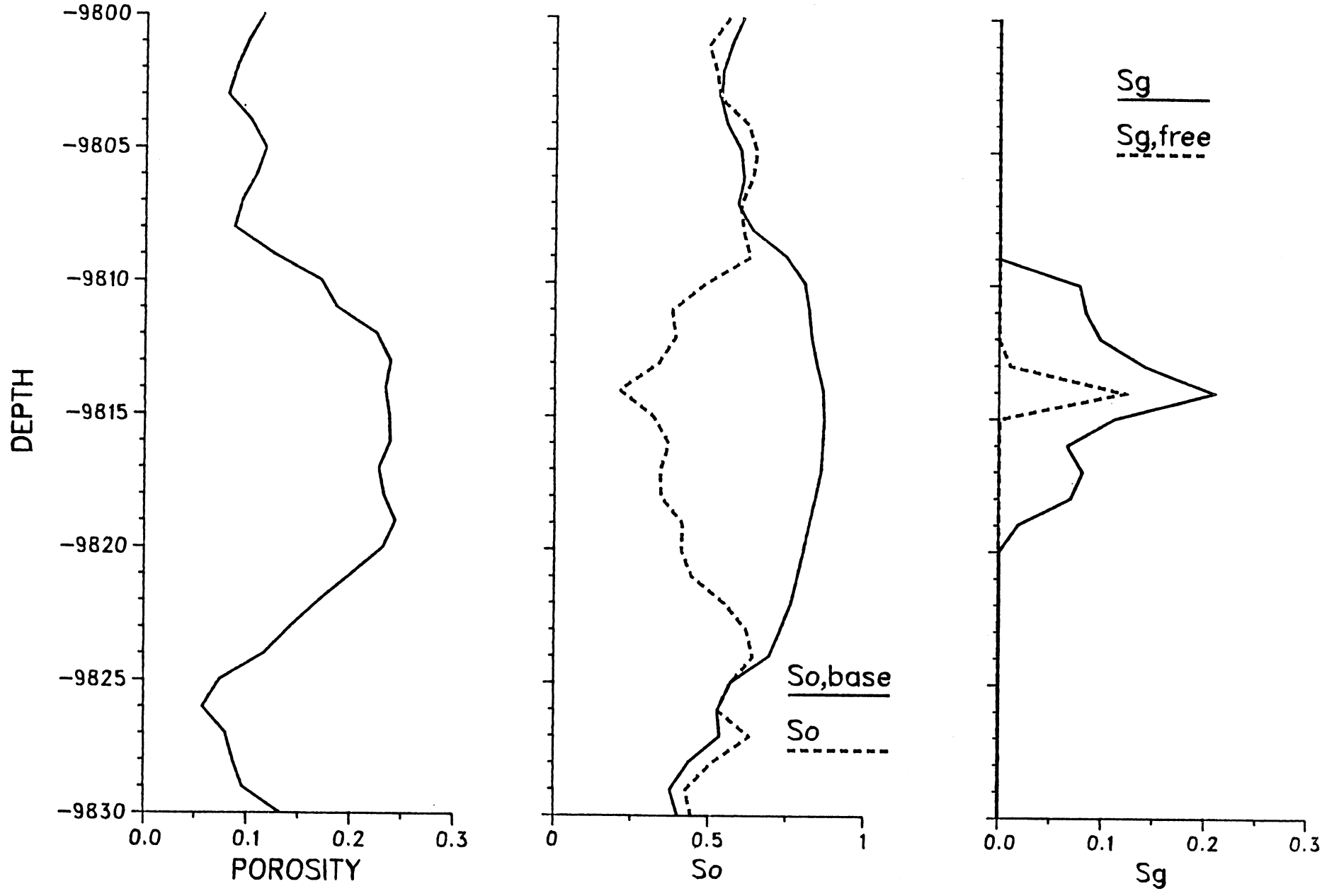

FIGURE A-8 Zabolotny Observation – 1 7/13/81

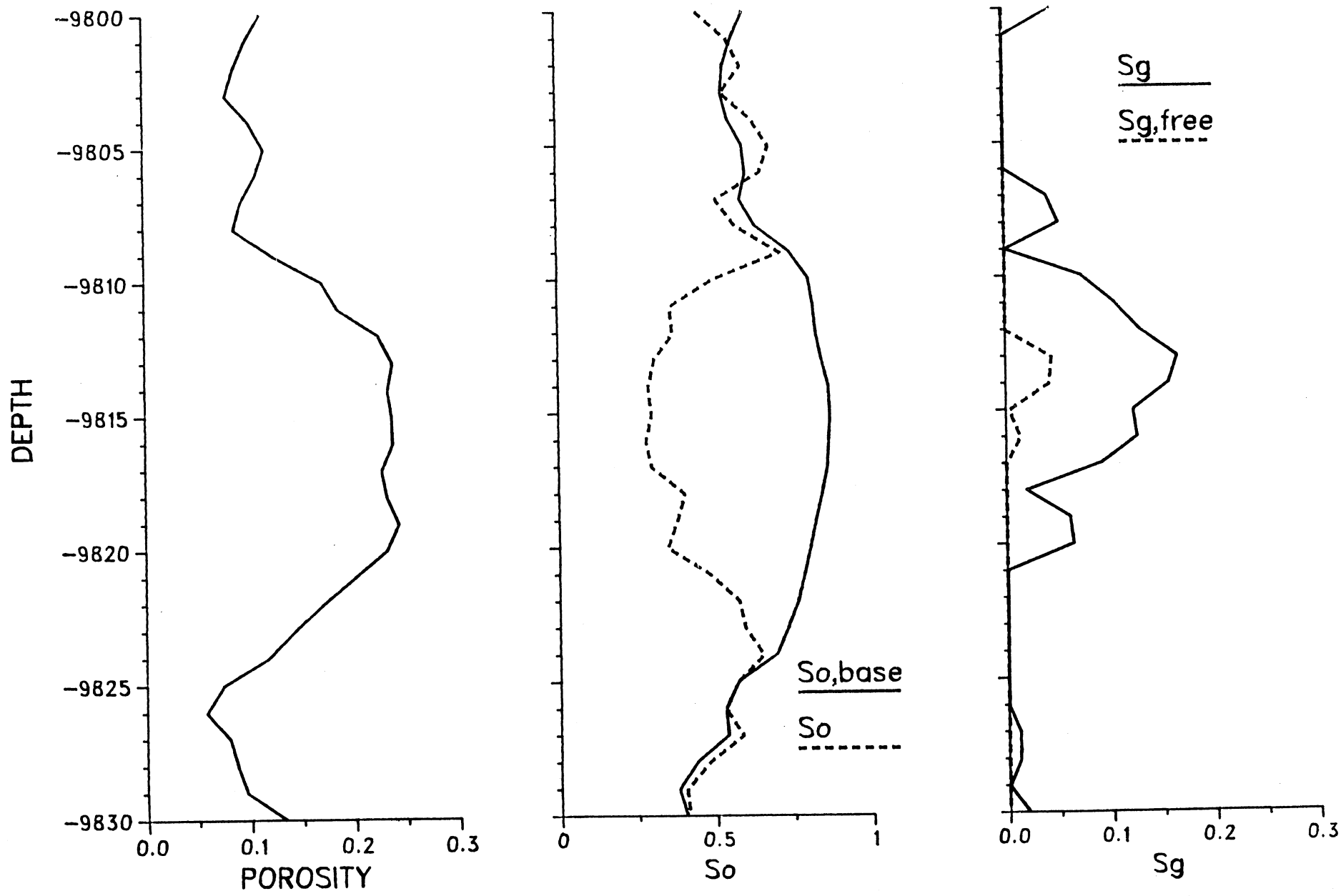

FIGURE A-9 Zabolotny Observation – 1 7/27/81

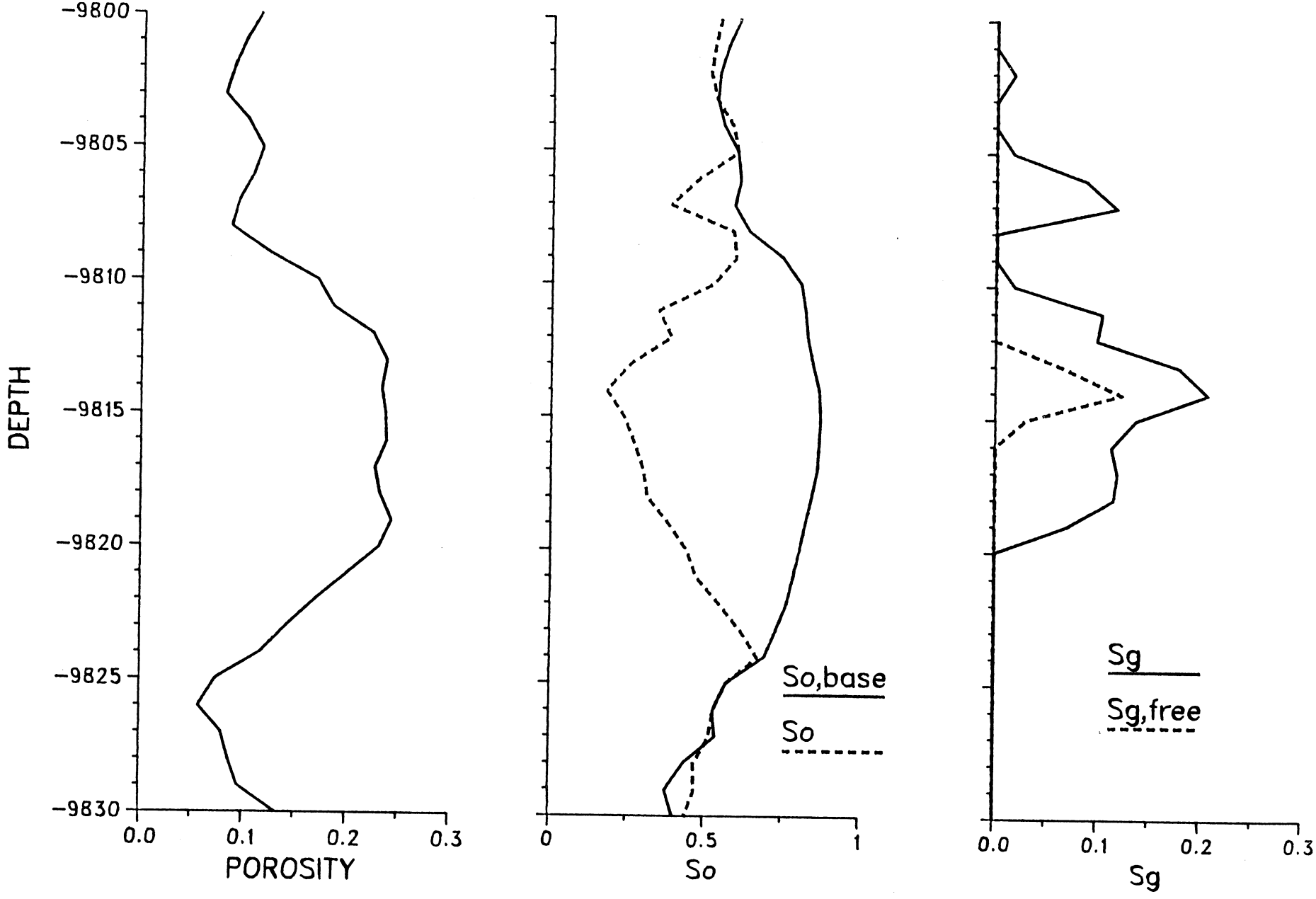

FIGURE A-10 Zabolotny Observation – 1 8/10/81

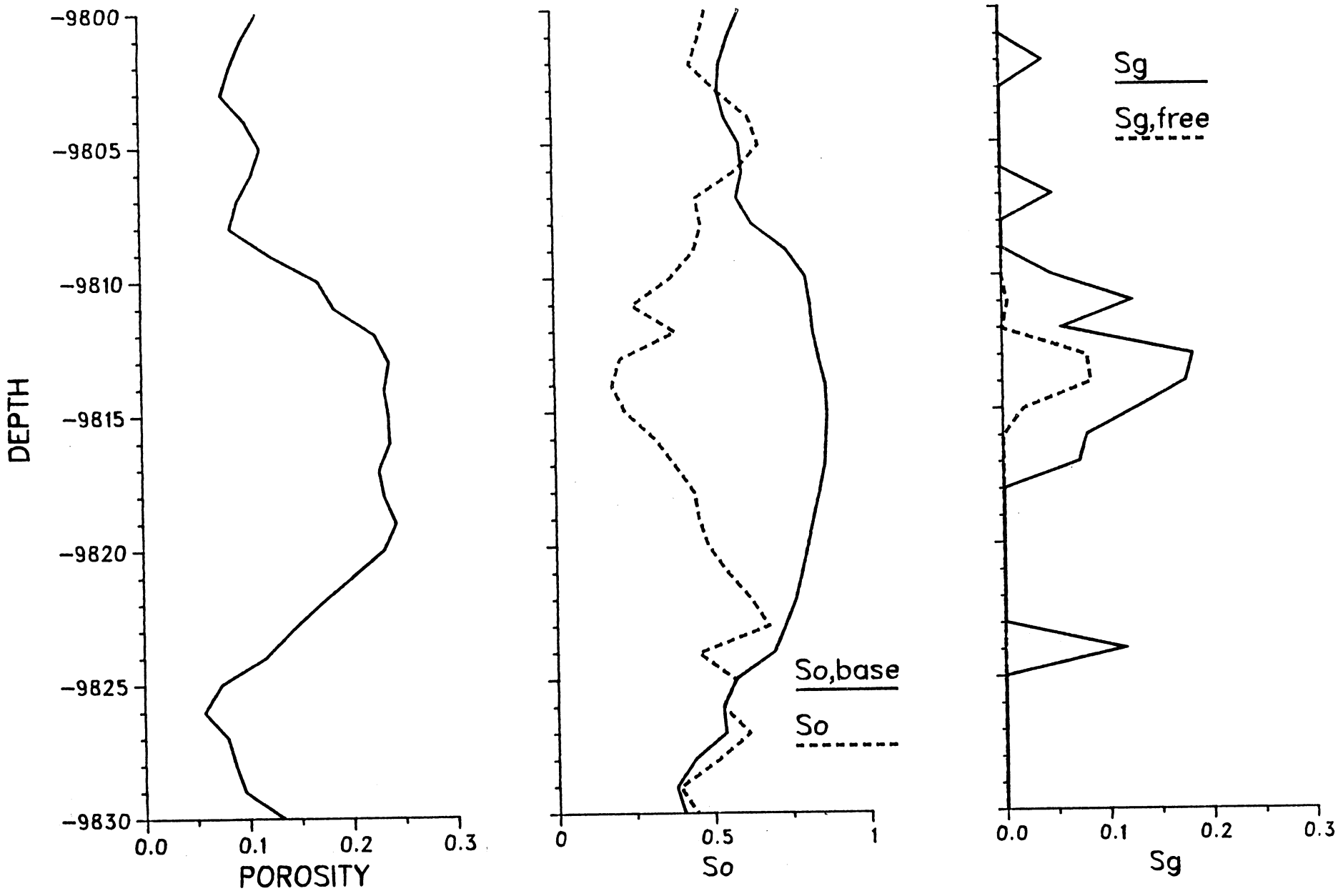

FIGURE A-11 Zabolotny Observation – 1 8/25/81

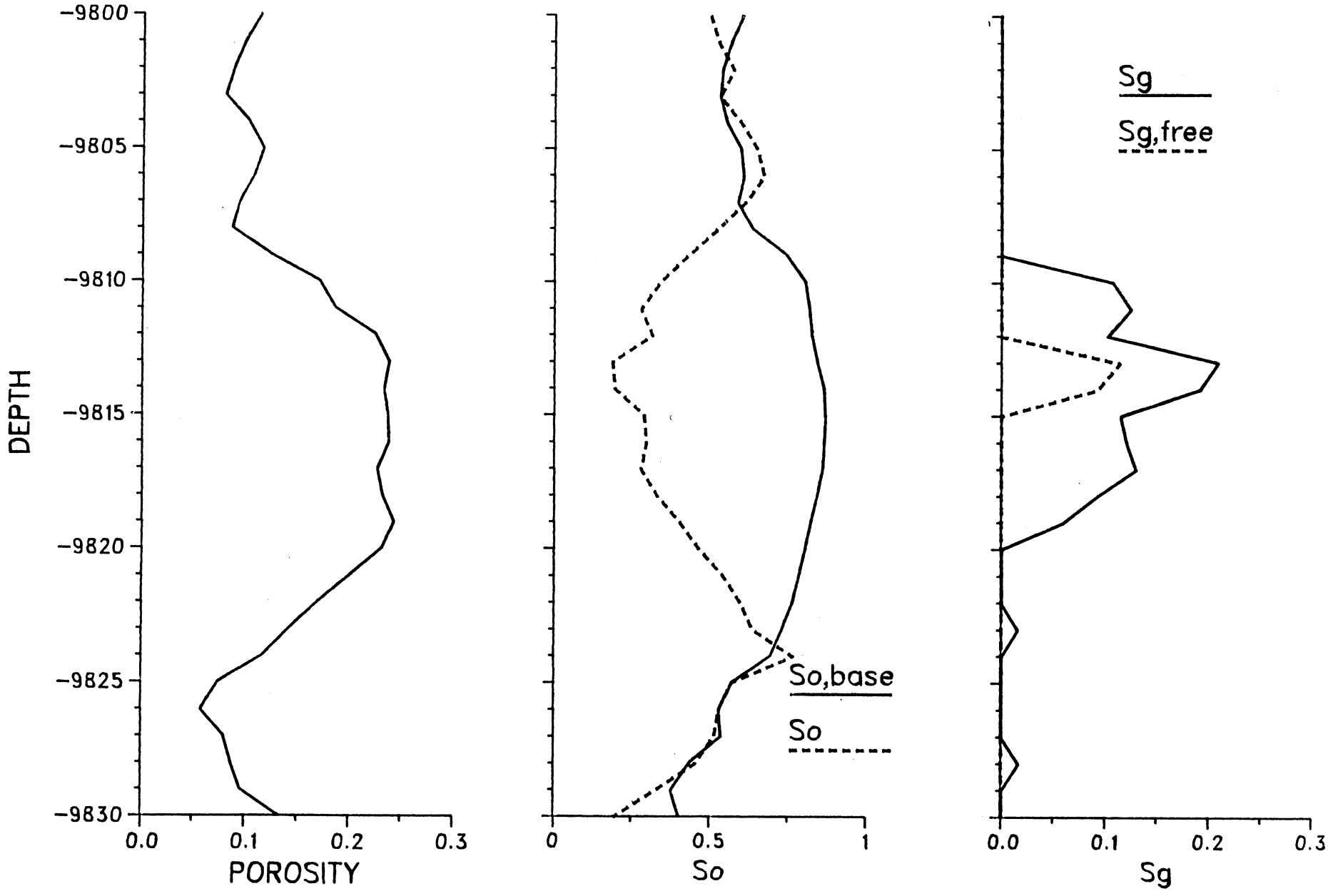

FIGURE A-12 Zabolotny Observation – 2 3/23/81

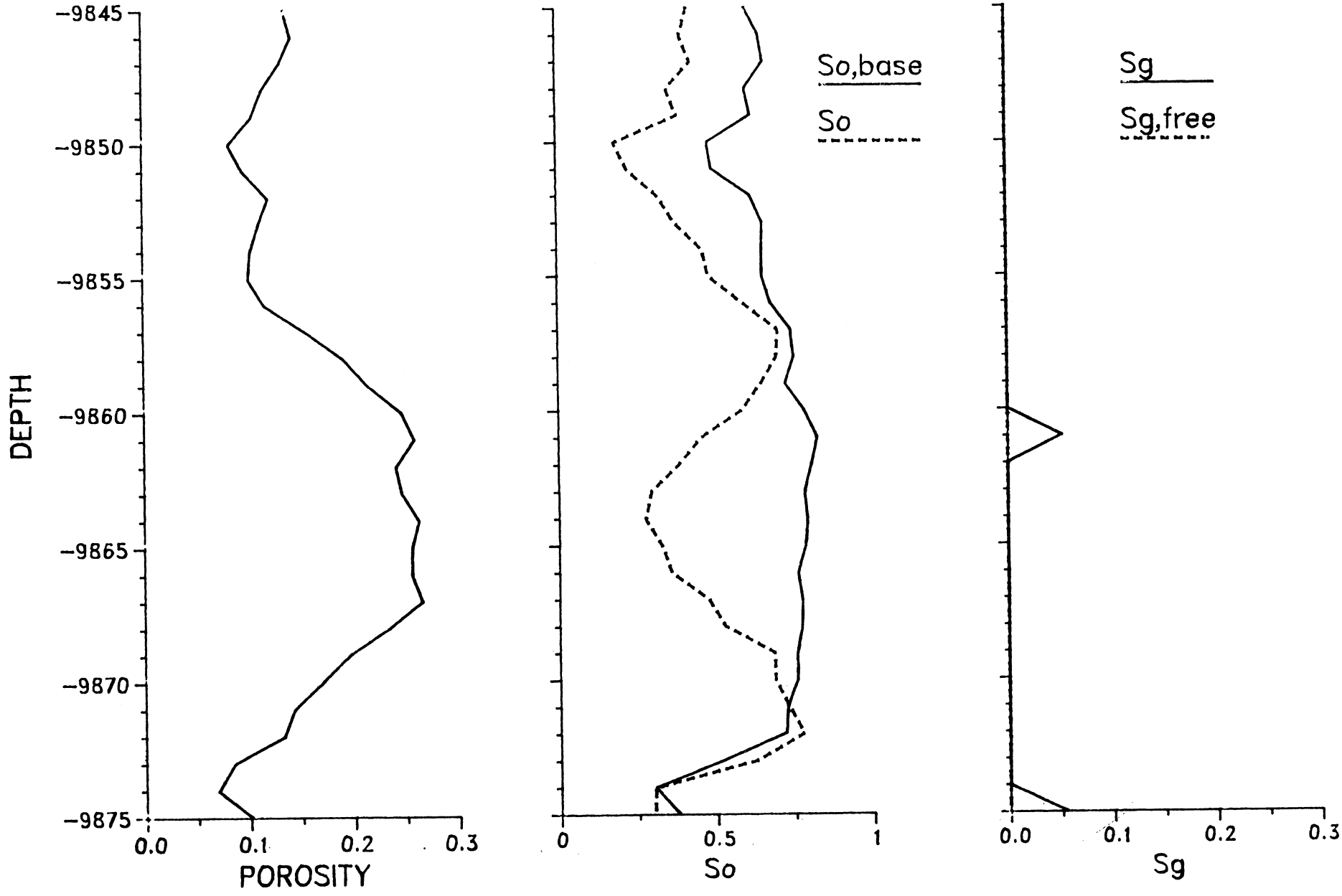

FIGURE A-13 Zabolotny Observation – 2 4/22/81

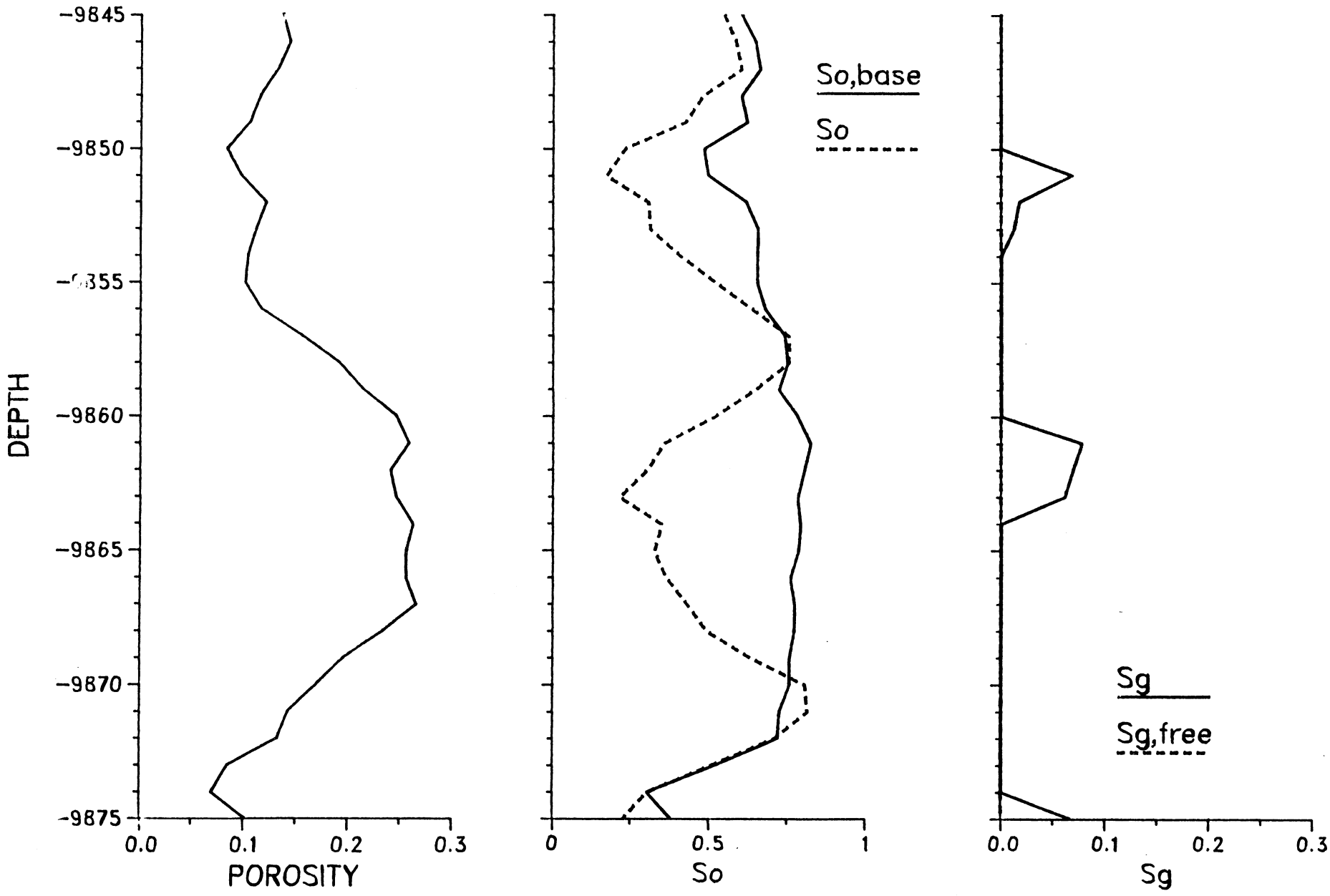

FIGURE A-14 Zabolotny Observation – 2 5/5/81

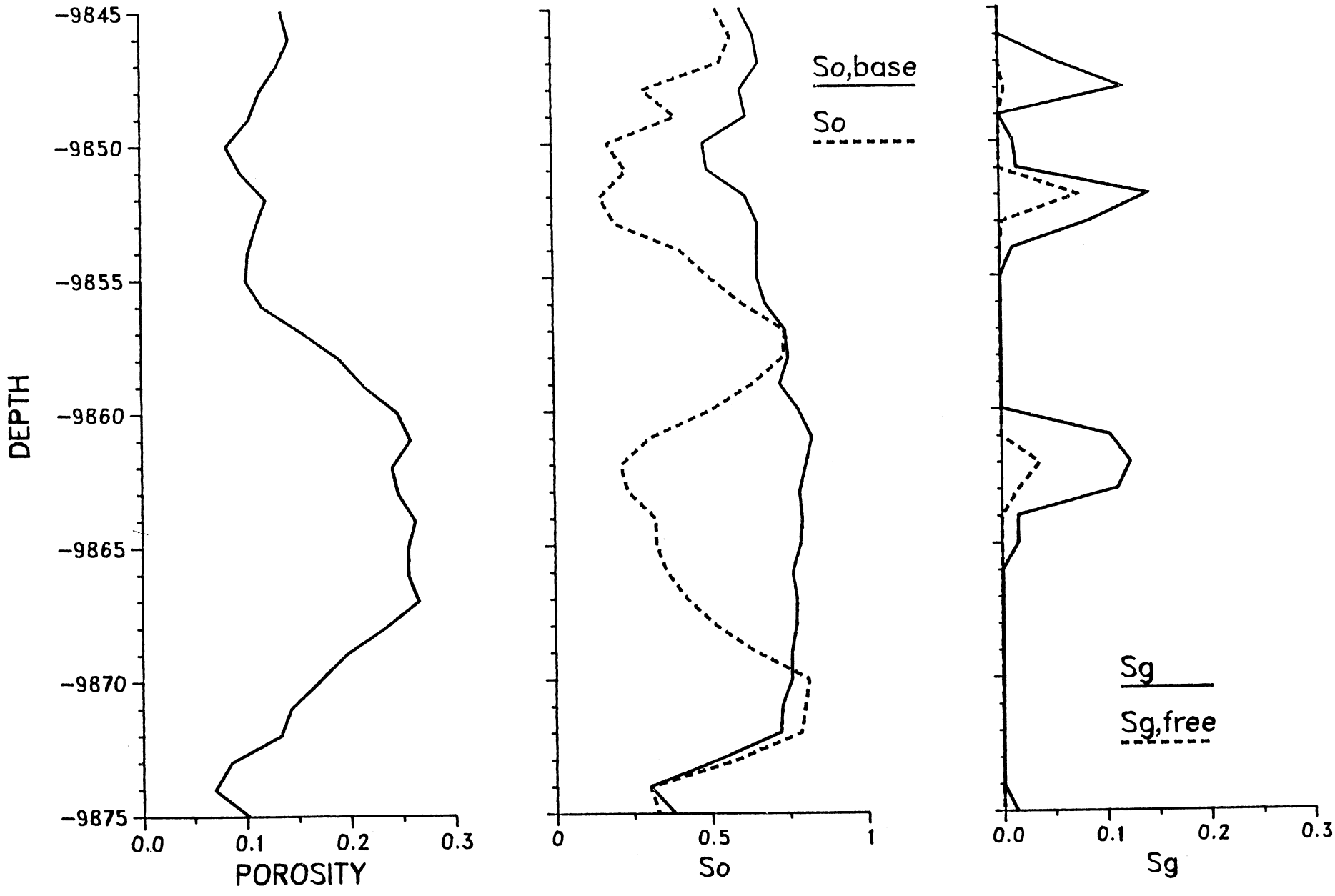

FIGURE A-15 Zabolotny Observation – 2 5/19/81

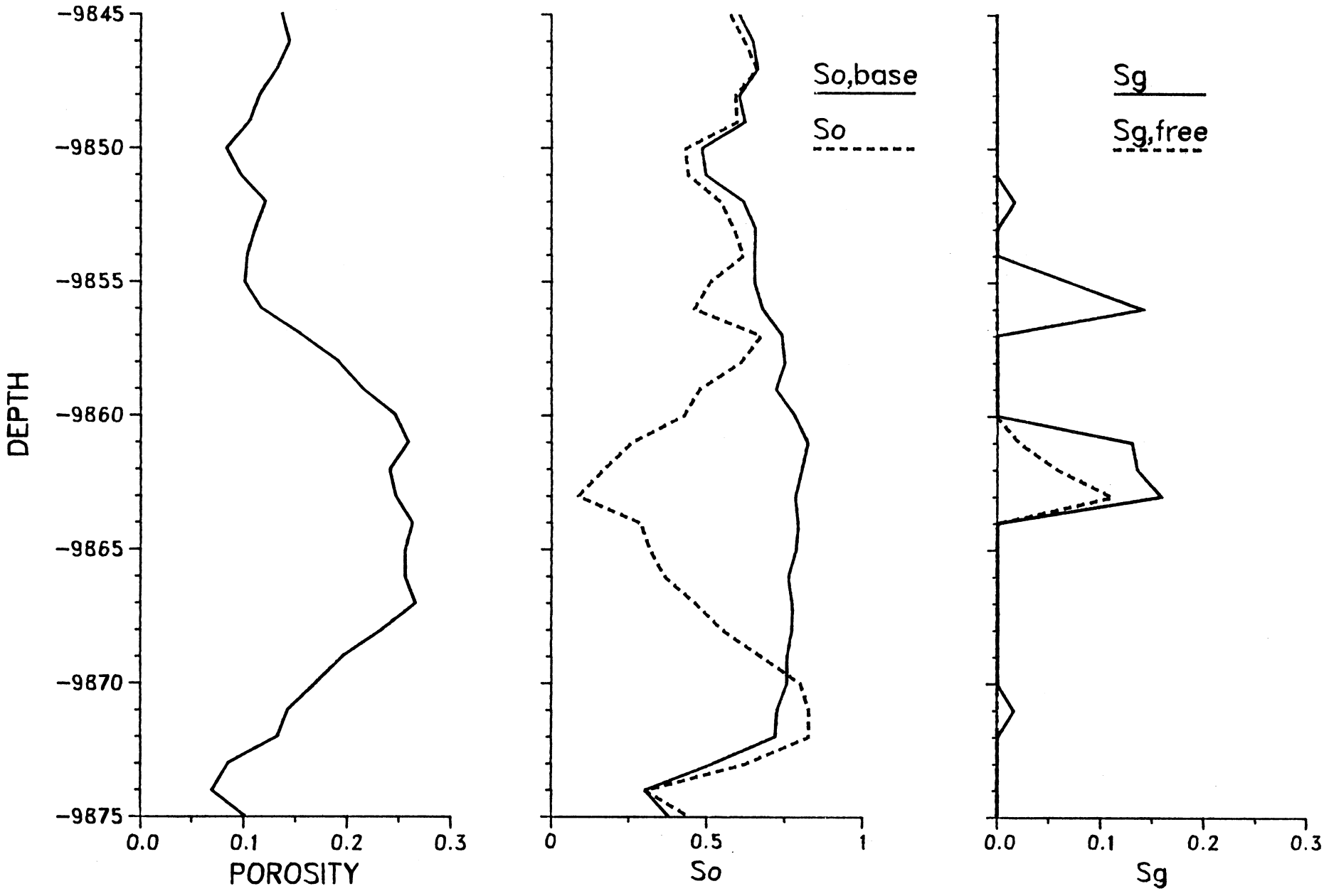

FIGURE A-16 Zabolotny Observation – 2 6/2/81

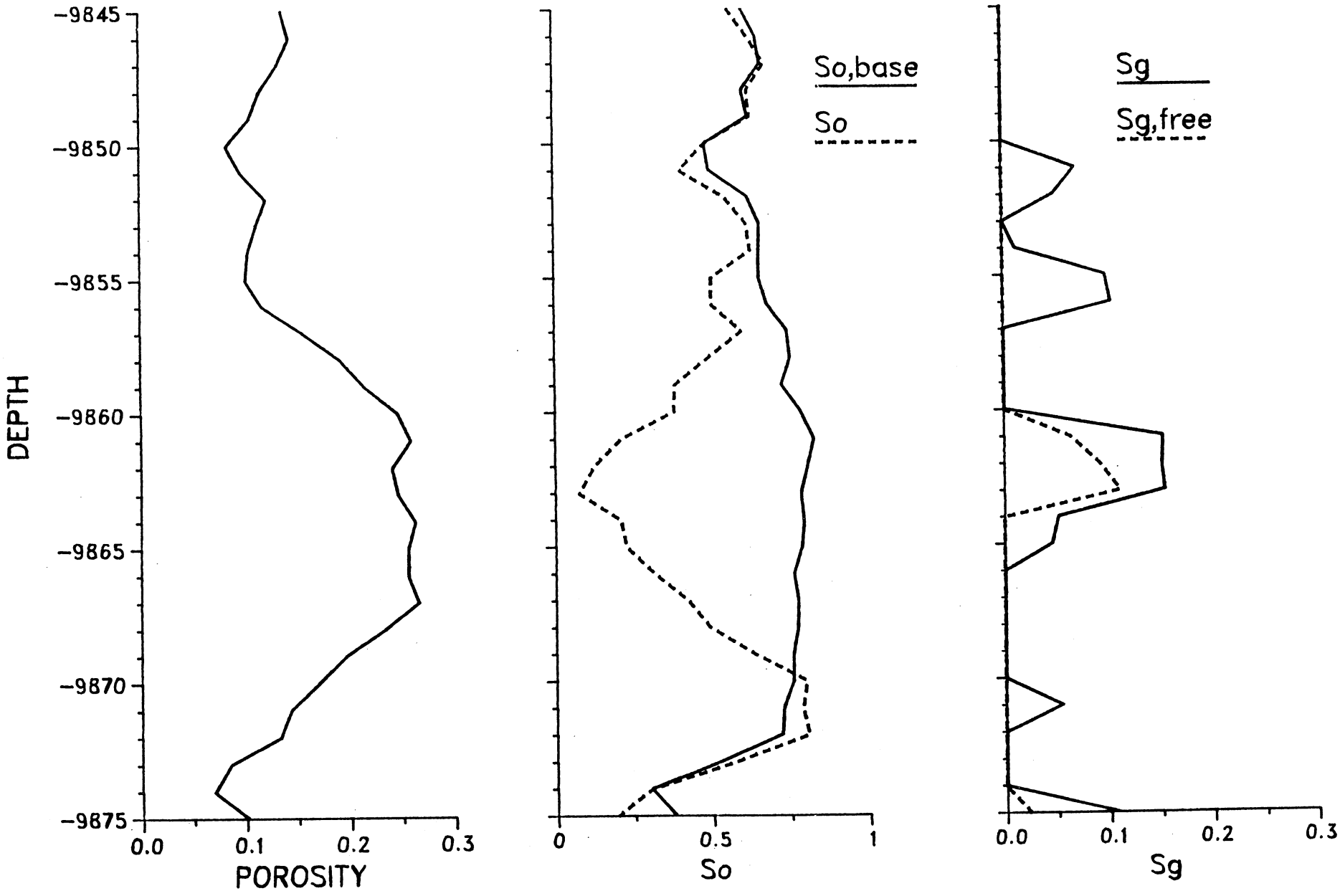

FIGURE A-17 Zabolotny Observation – 2 6/16/81

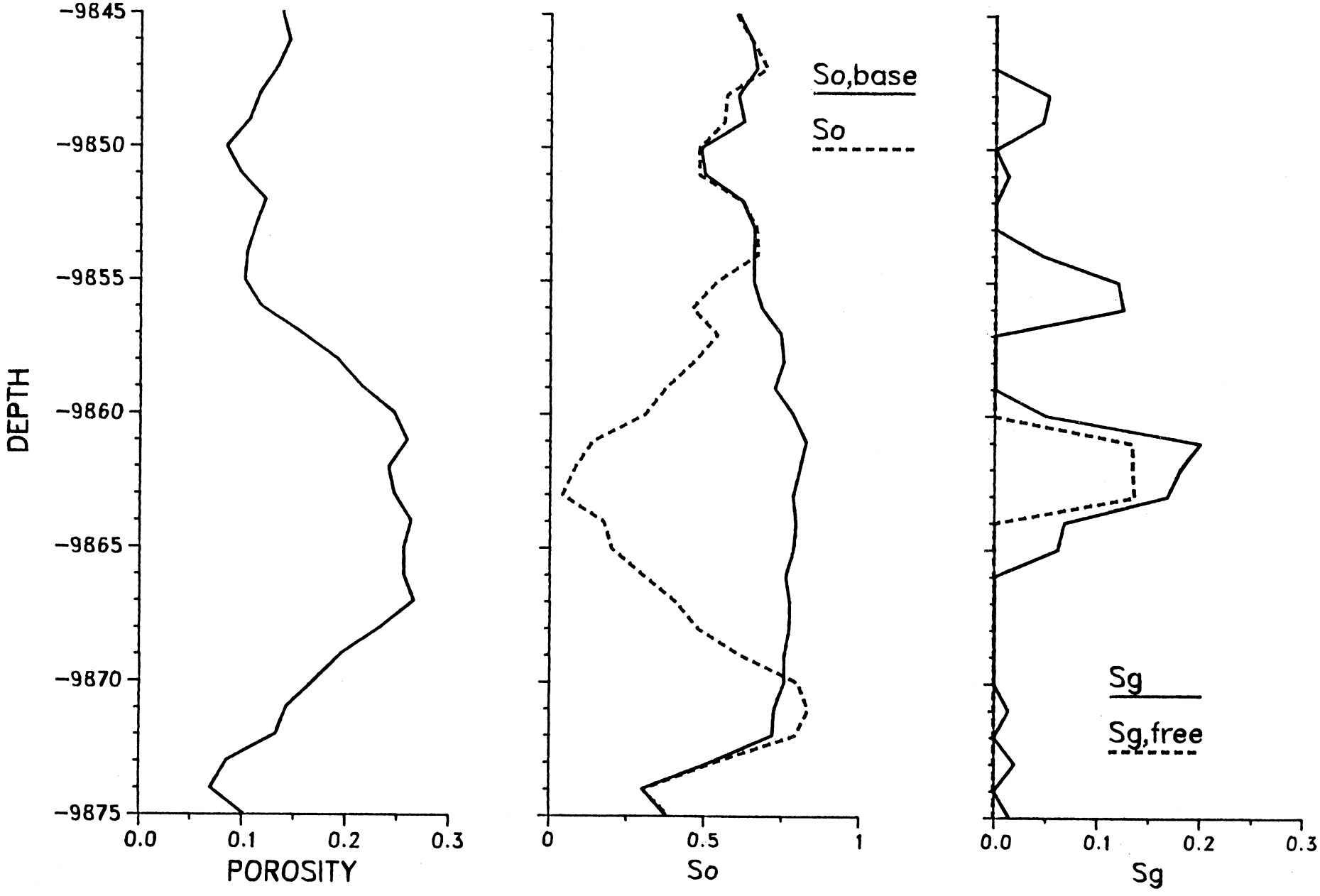

FIGURE A-18 Zabolotny Observation – 2 6/30/81

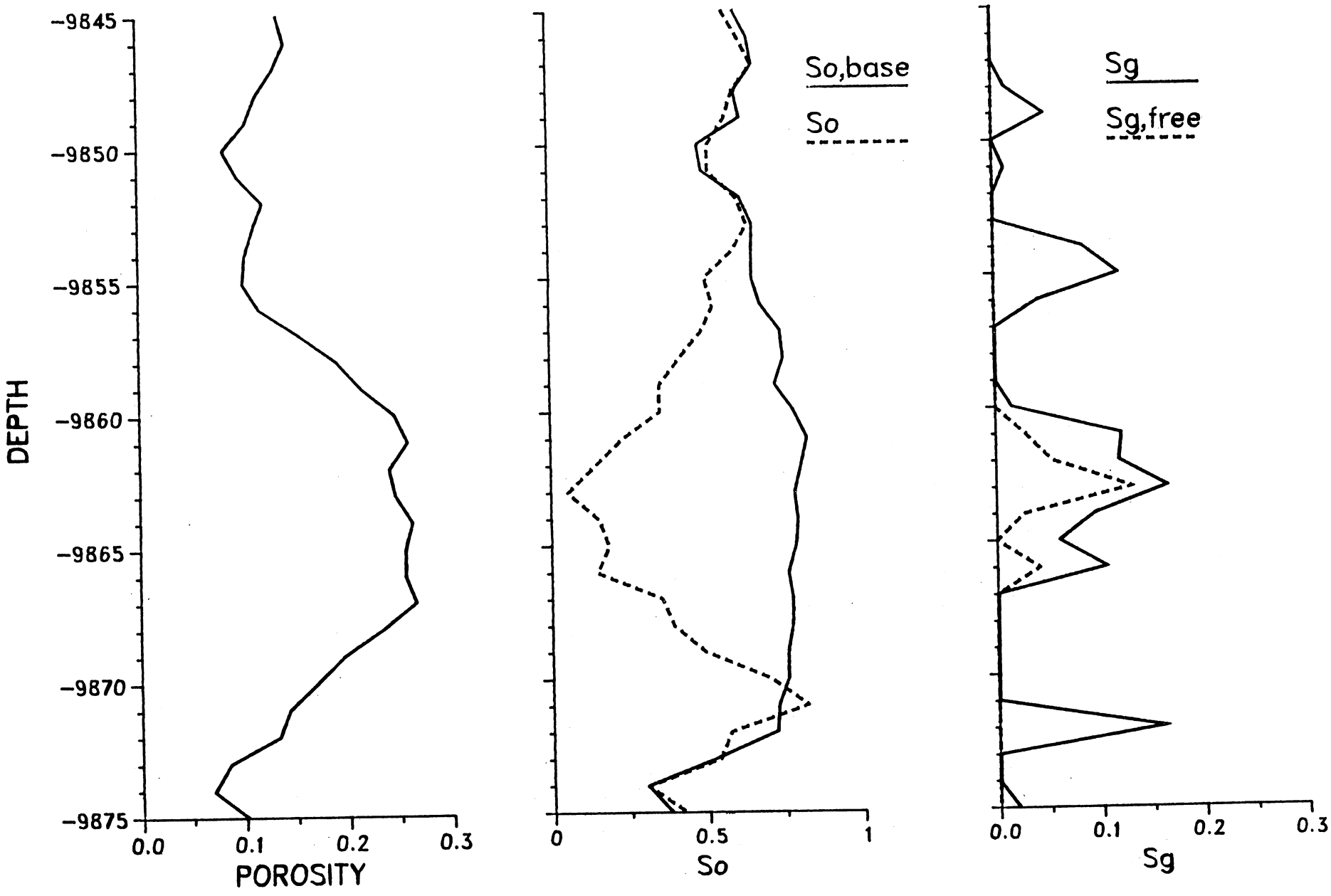

FIGURE A-19 Zabolotny Observation – 2 7/14/81

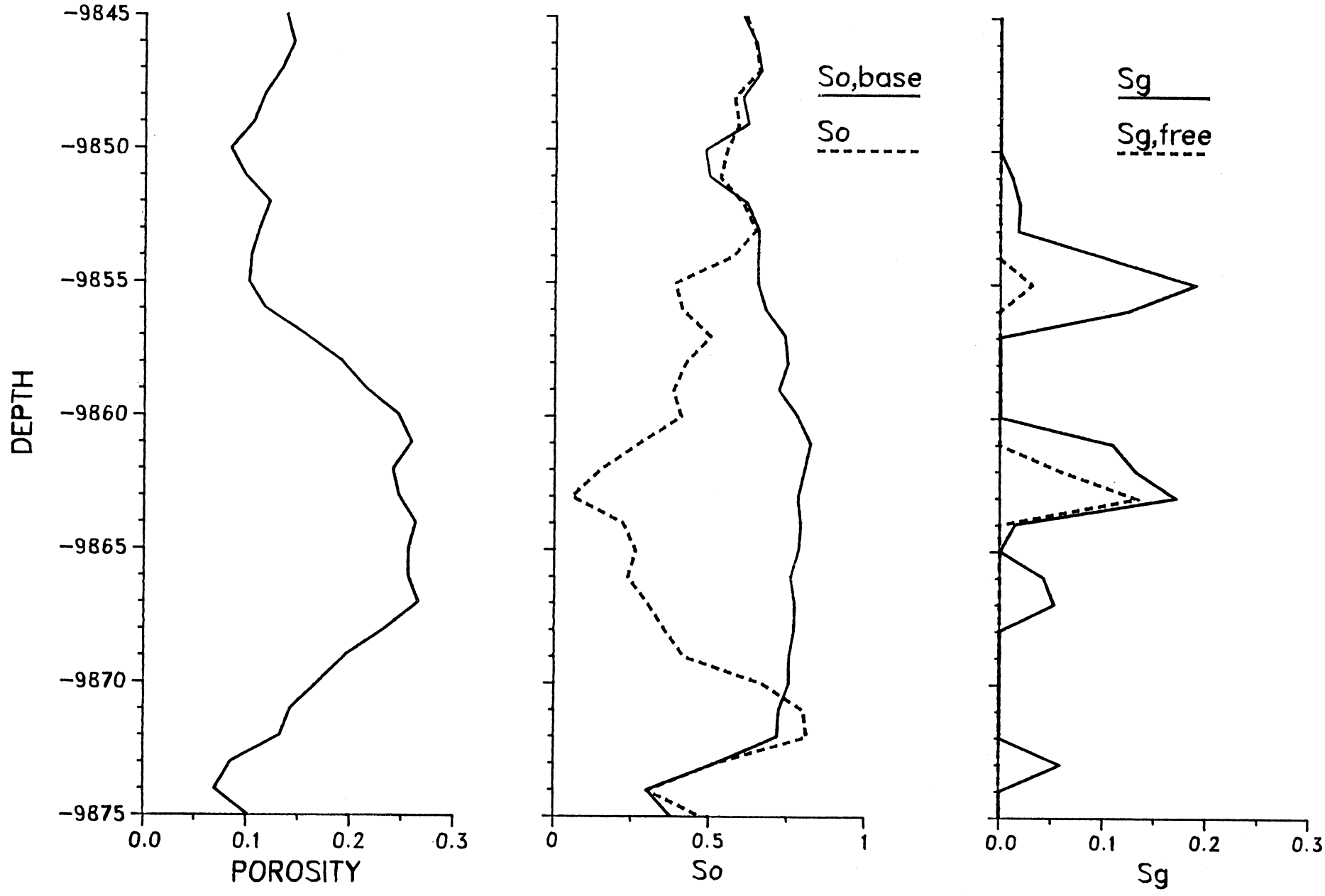

FIGURE A-20 Zabolotny Observation – 2 7/28/81

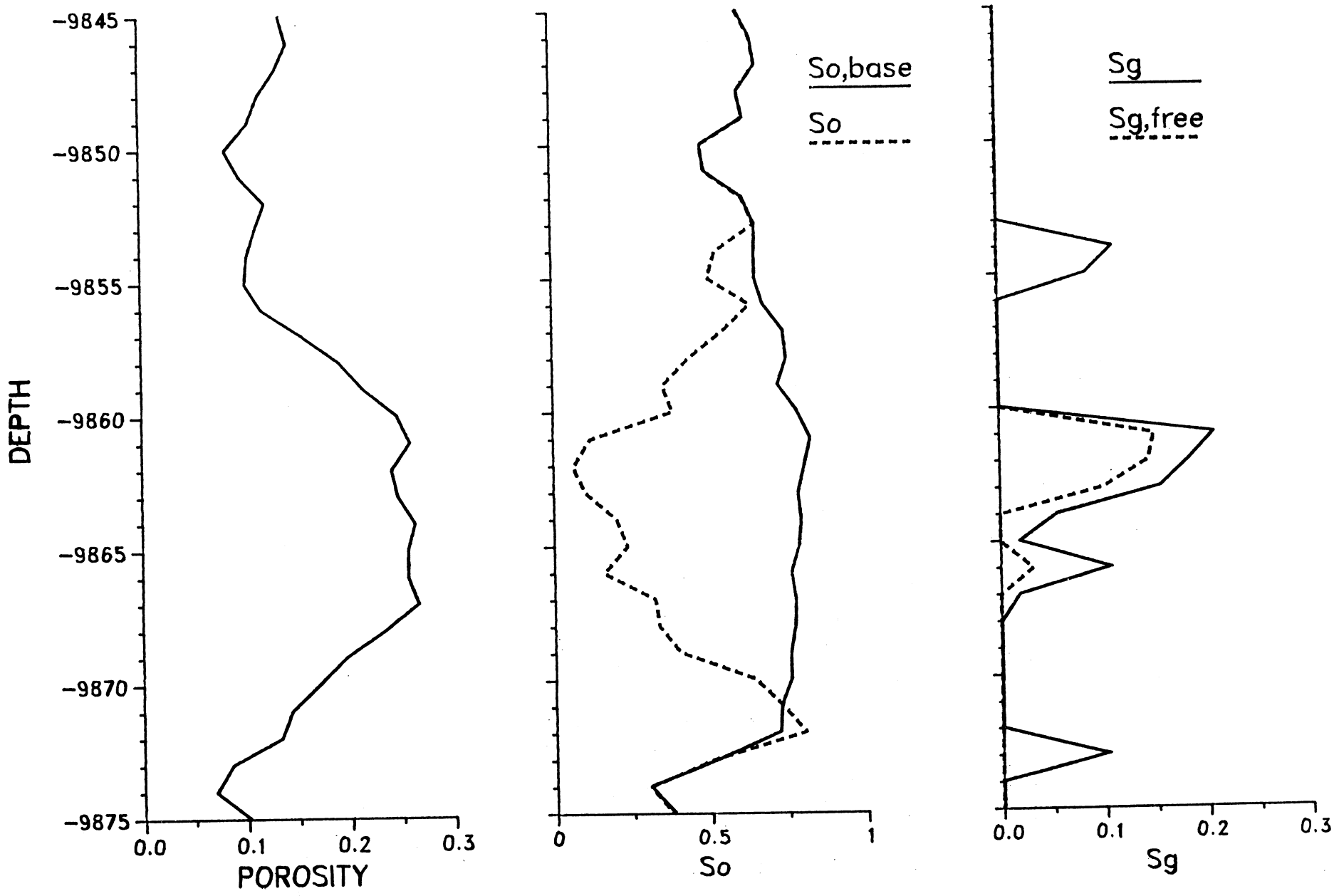

FIGURE A-21 Zabolotny Observation – 2 8/11/81

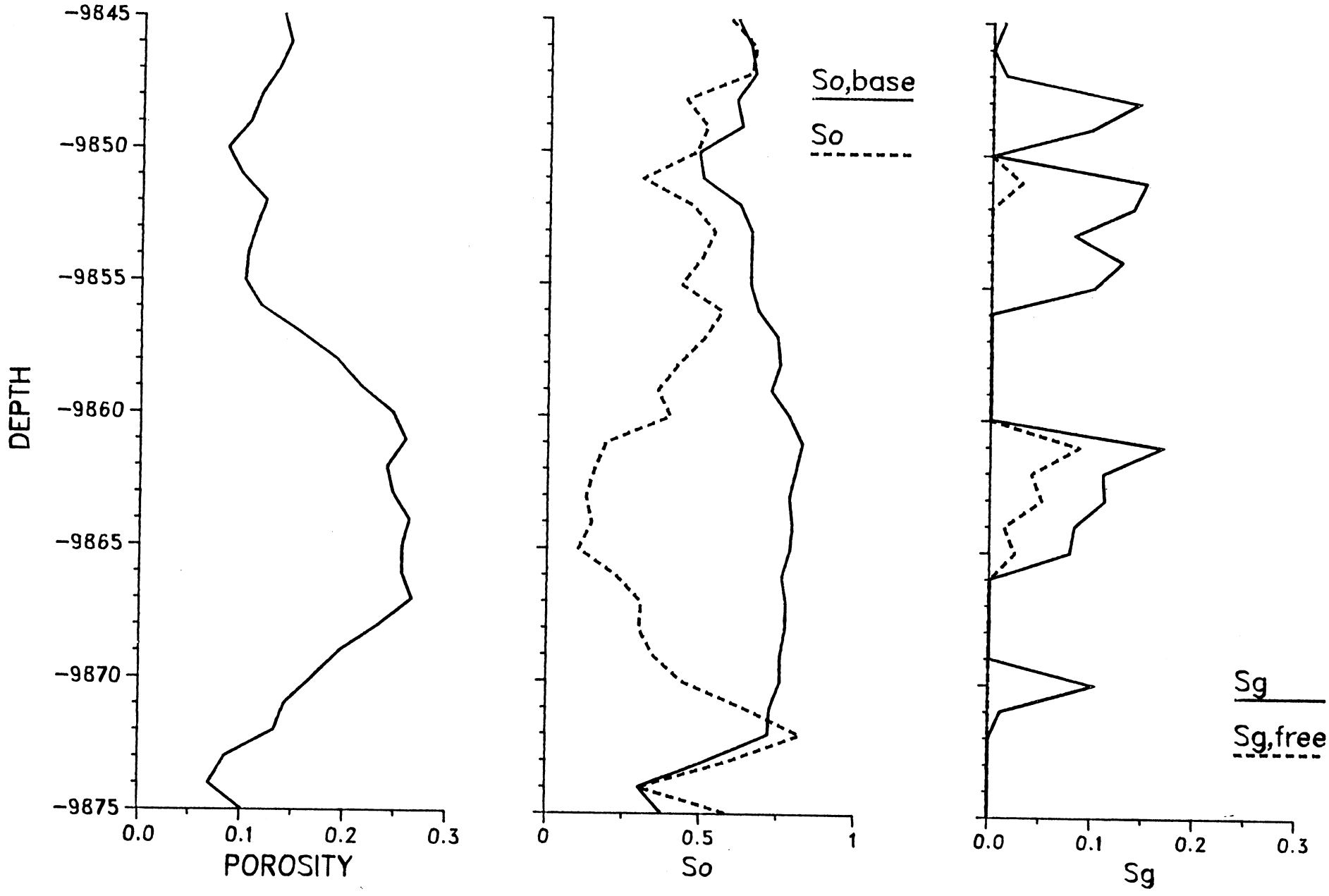

FIGURE A-22 Zabolotny Observation – 2 8/25/81

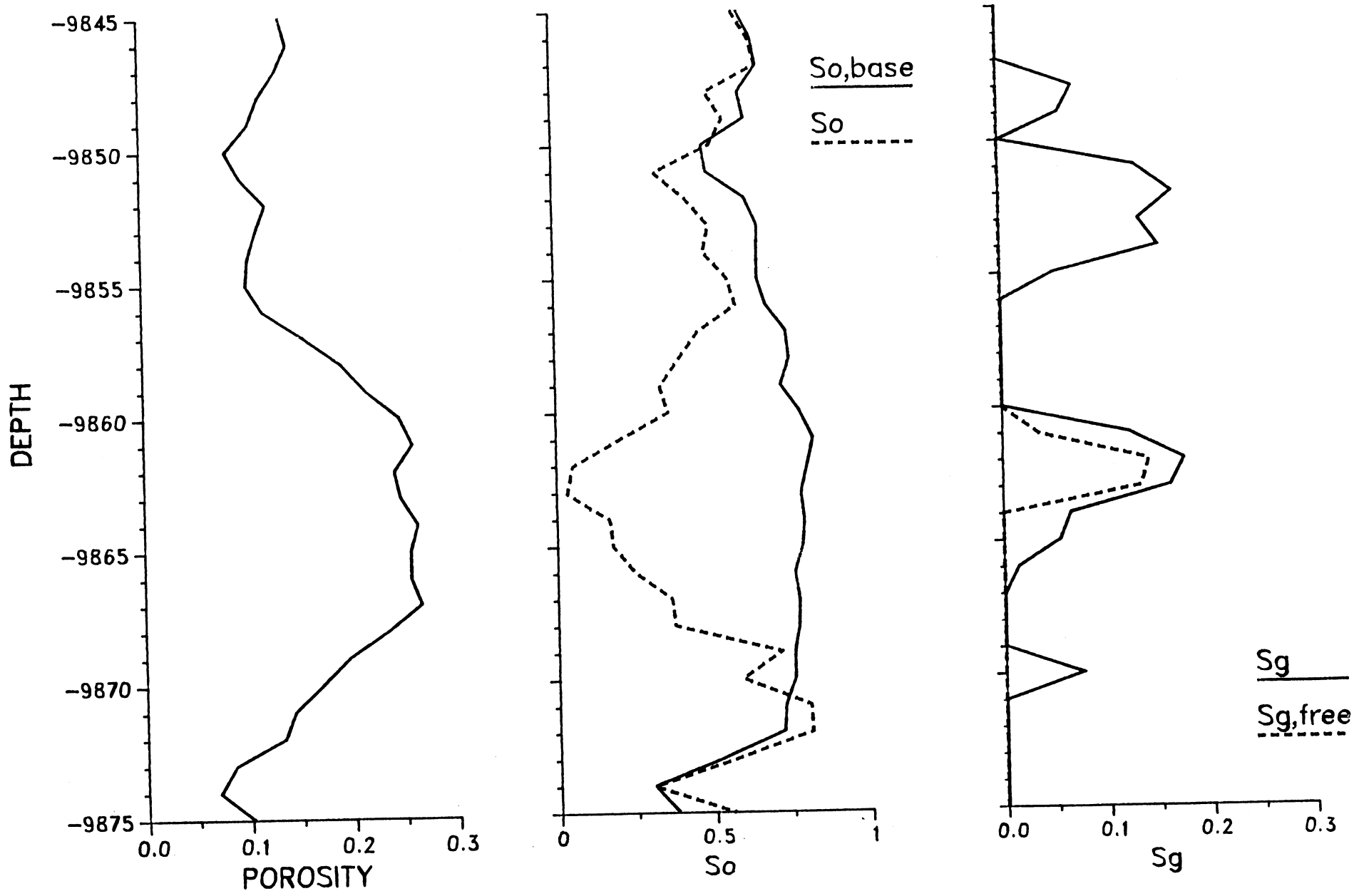

FIGURE A-23 Zabolotny Observation – 2 9/16/81

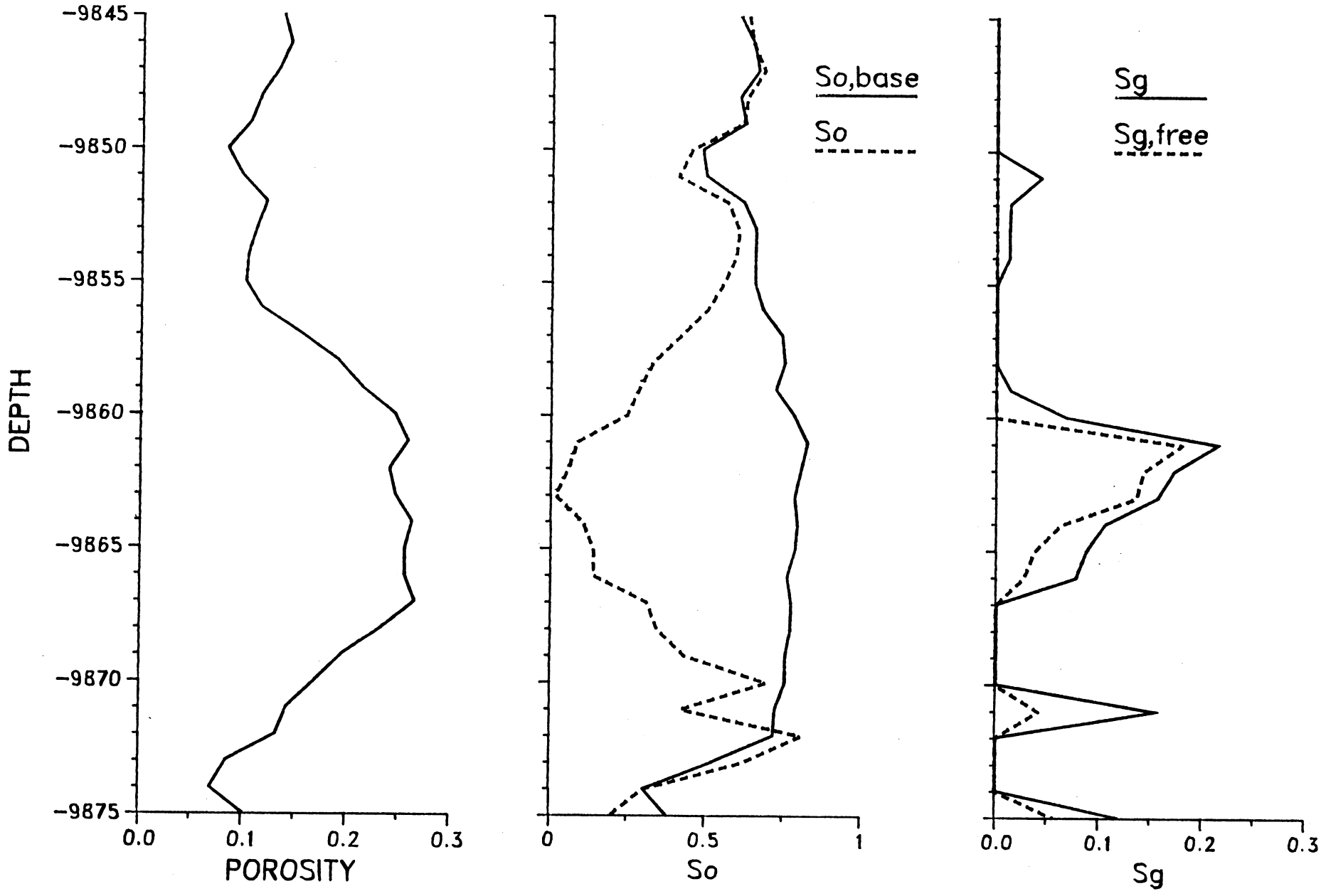

FIGURE A-24 Zabolotny Observation – 3 5/5/81

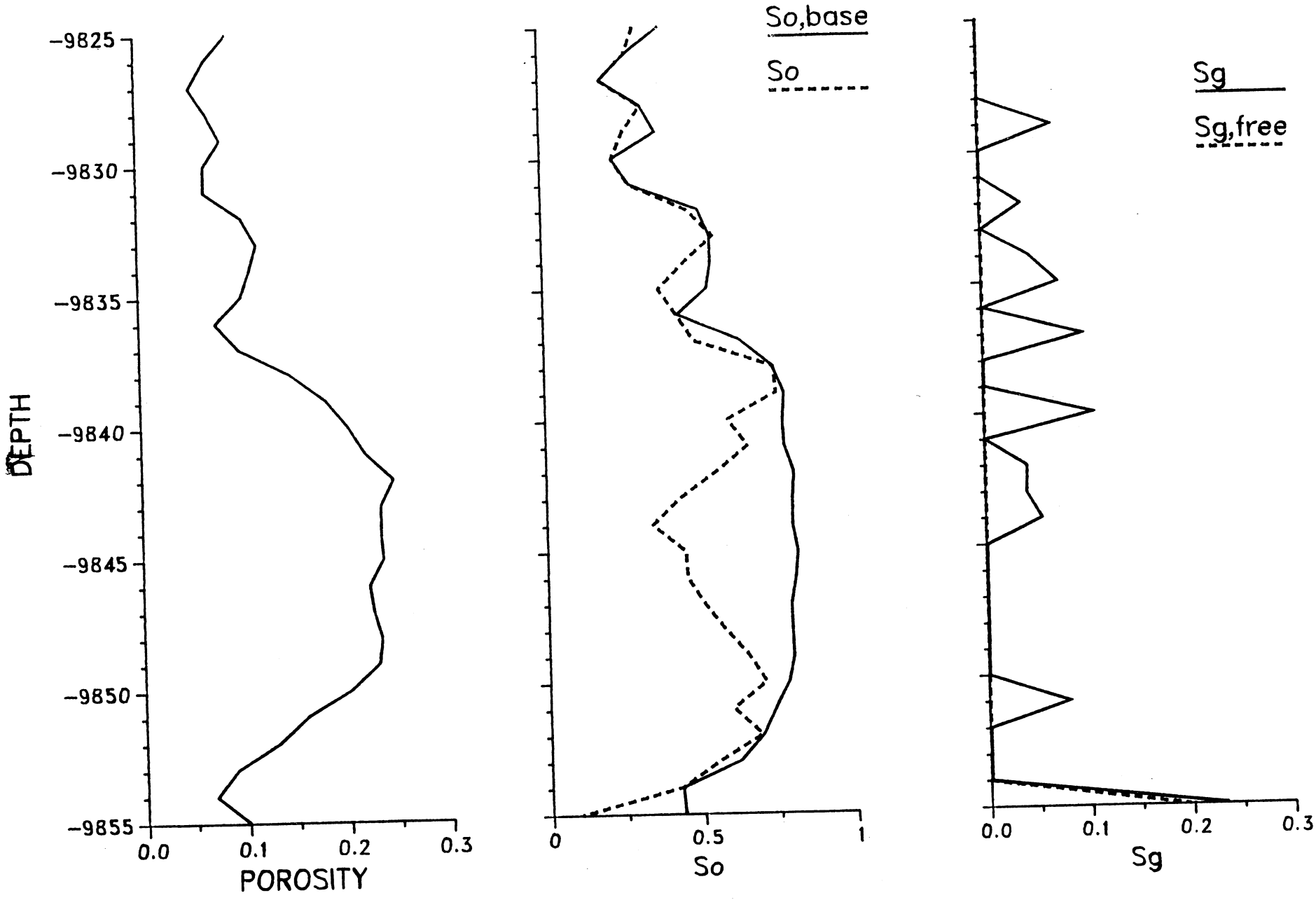

FIGURE A-25 Zabolotny Observation – 3 5/20/81

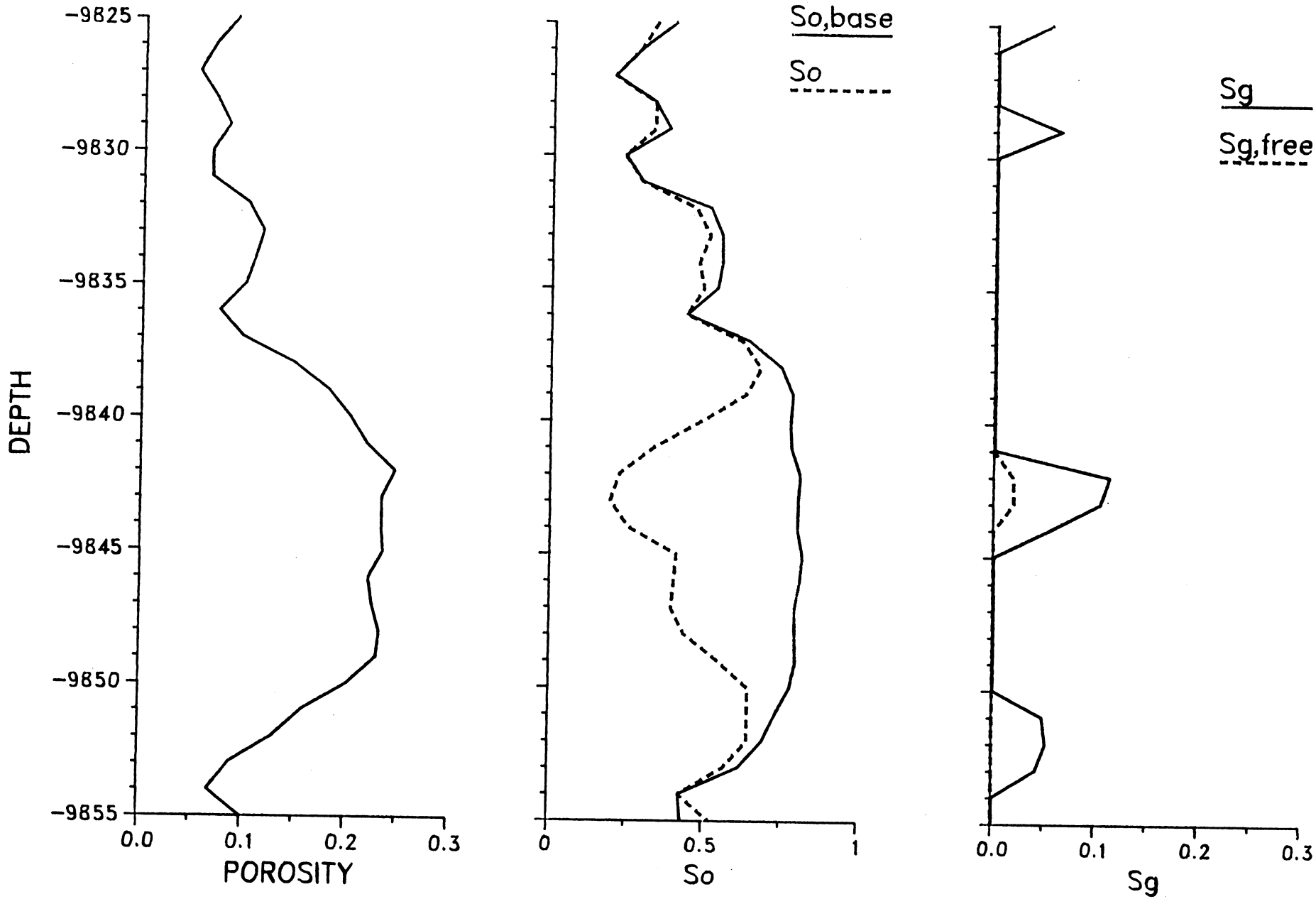

FIGURE A-26 Zabolotny Observation – 3 6/3/81

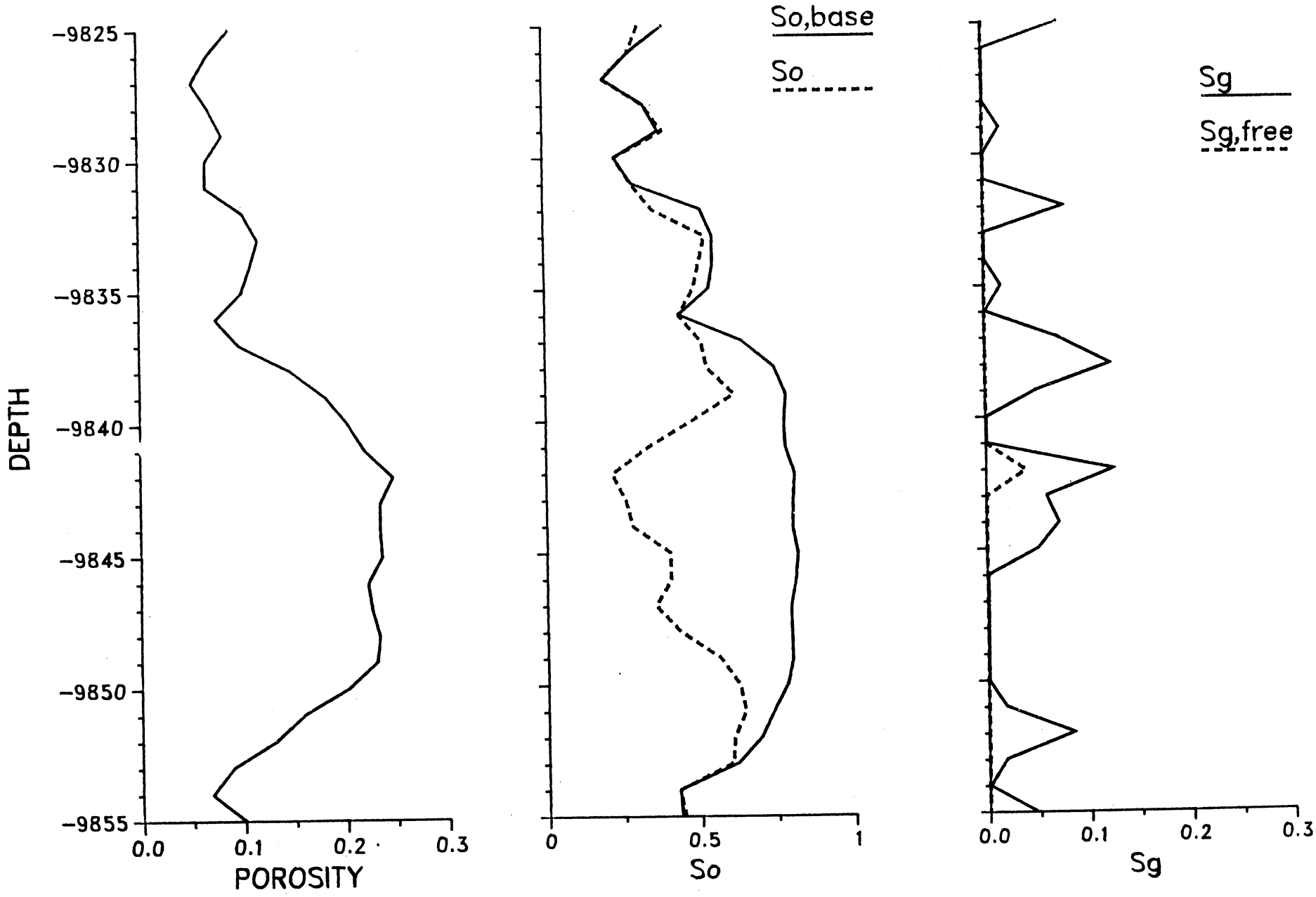

FIGURE A-27 Zabolotny Observation – 3 6/16/81

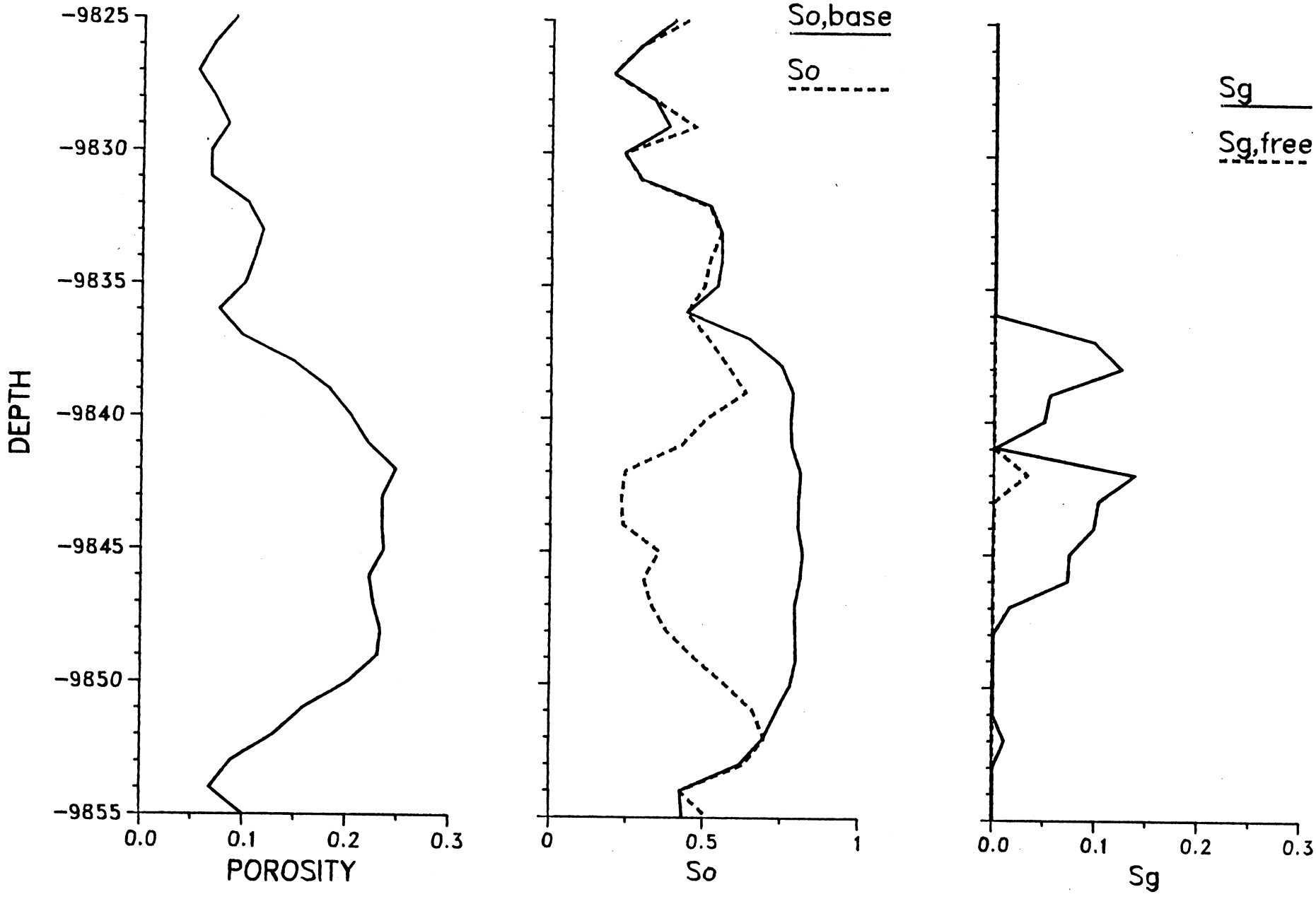

FIGURE A-28 Zabolotny Observation – 3 6/30/81

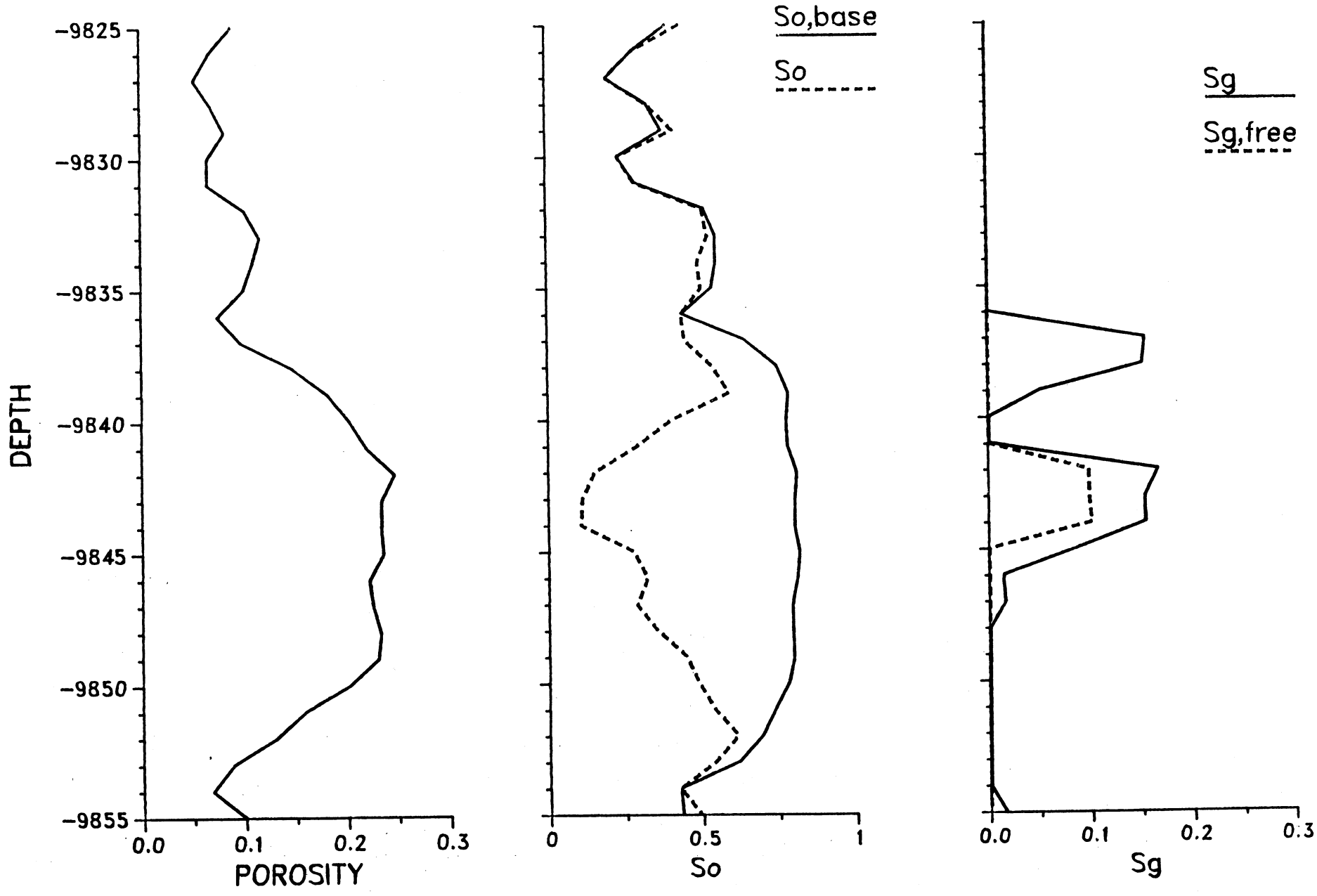

FIGURE A-29 Zabolotny Observation – 3 7/14/81

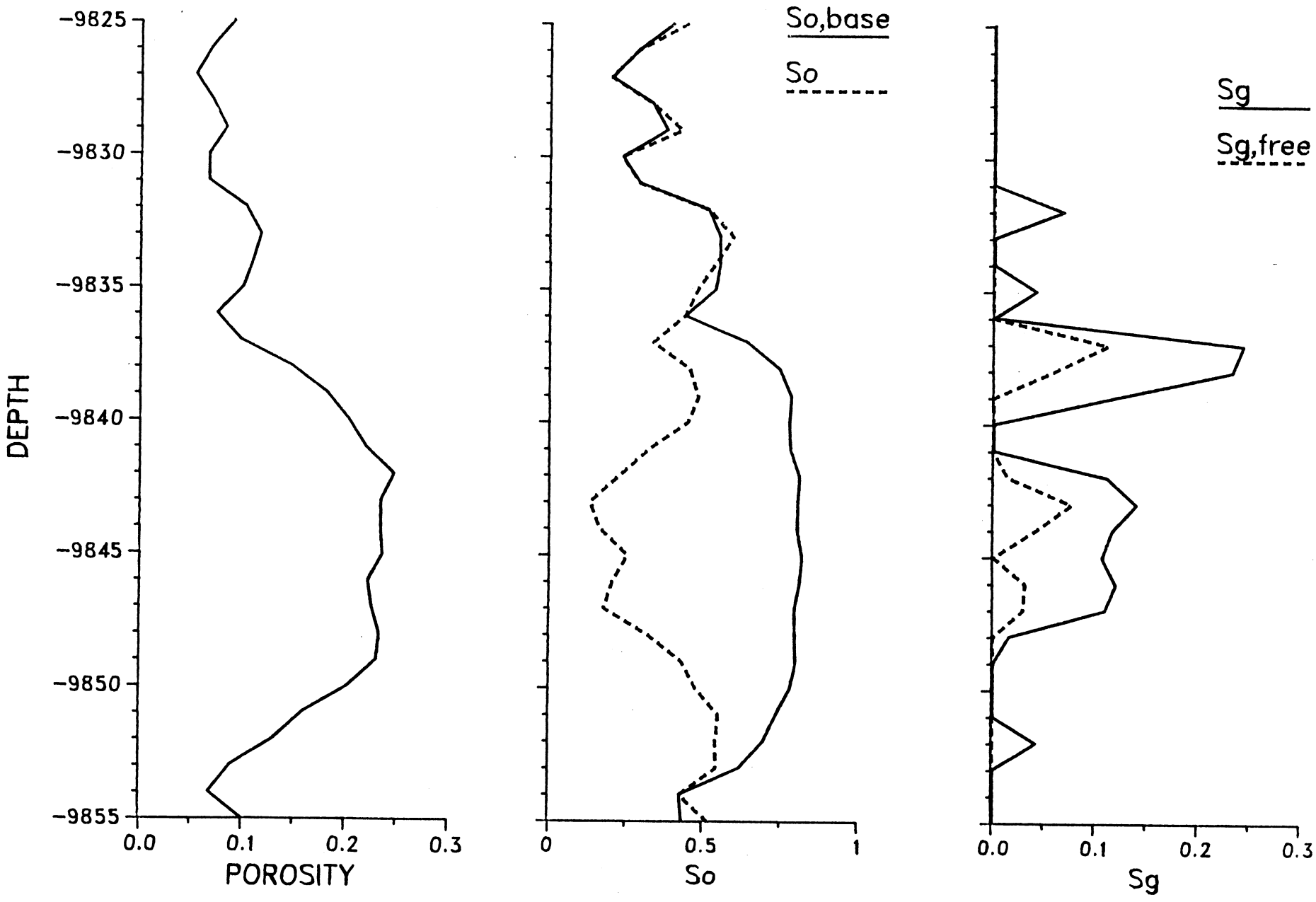

FIGURE A-30 Zabolotny Observation – 3 7/29/81

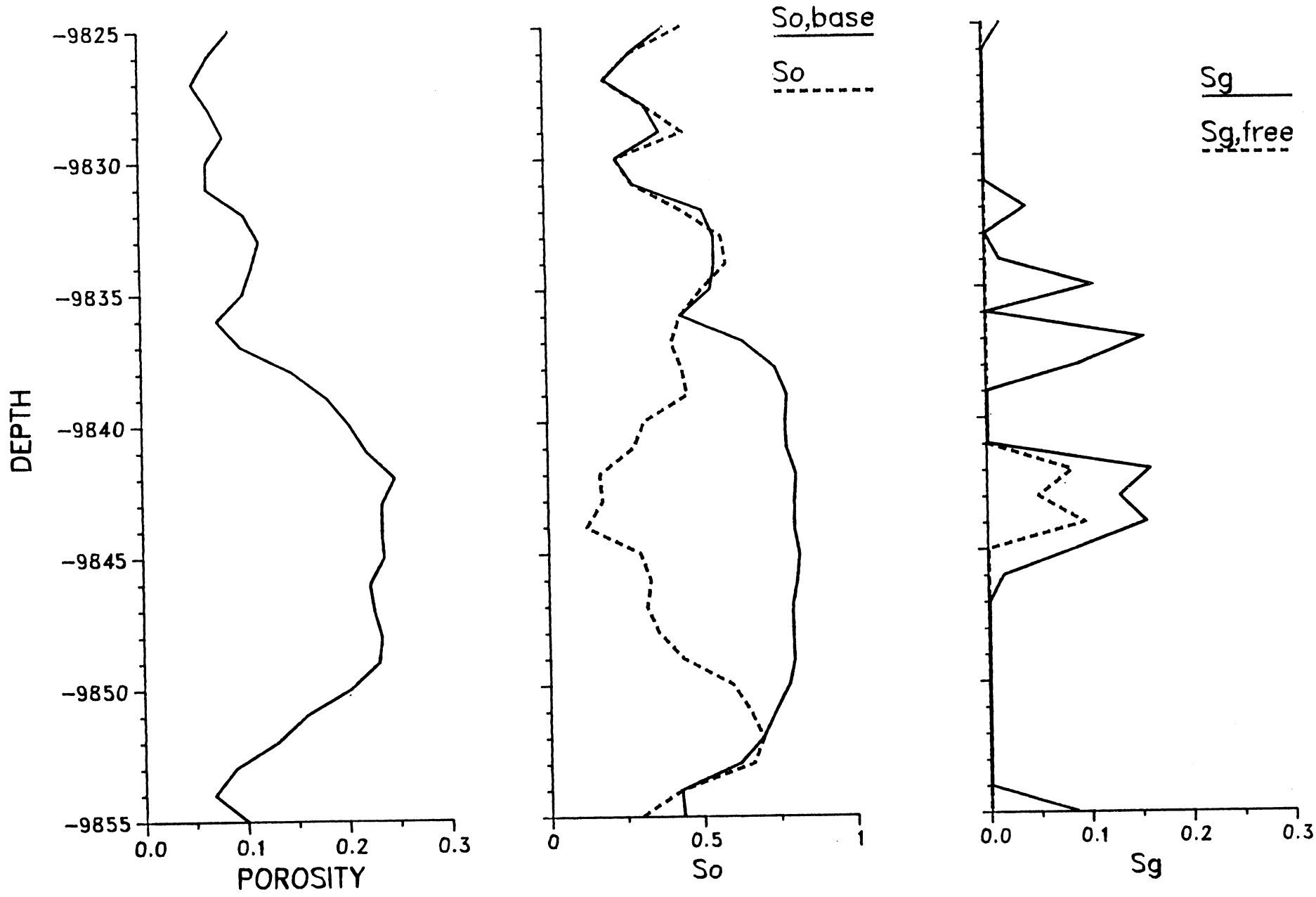

FIGURE A-31 Zabolotny Observation – 3 8/11/81

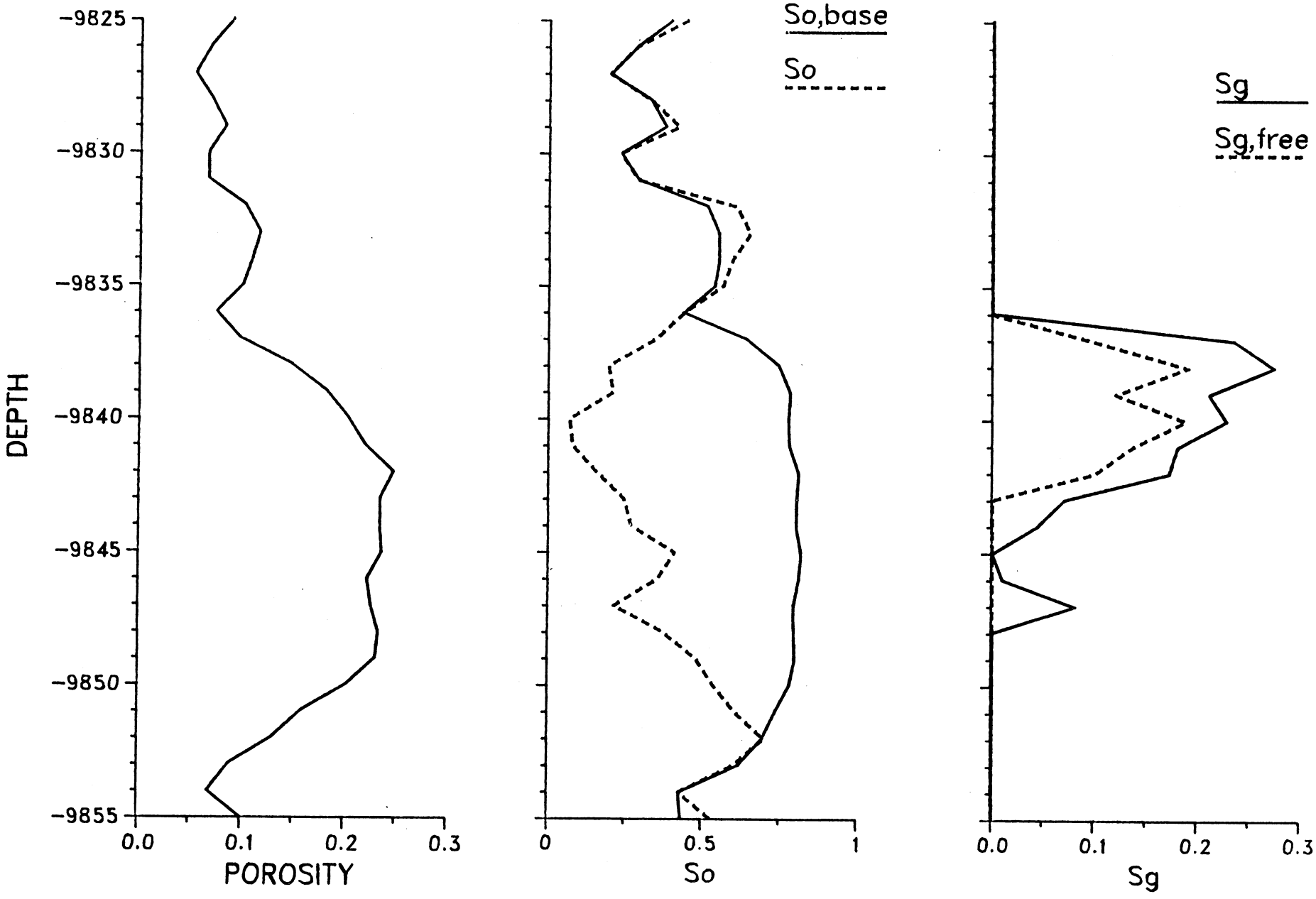

FIGURE A-32 Zabolotny Observation – 3 8/25/81

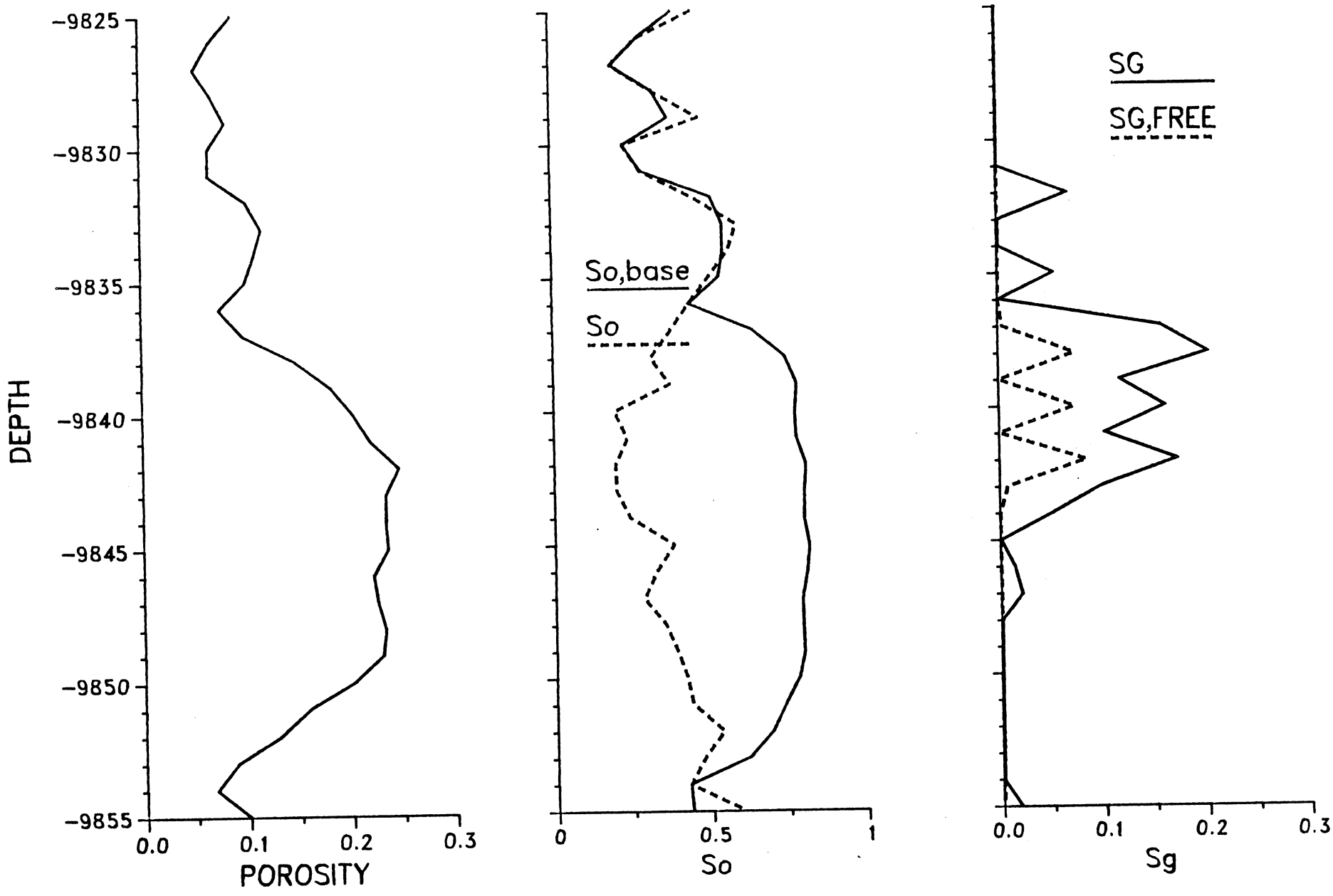

FIGURE A-33 Zabolotny Observation – 3 9/17/81

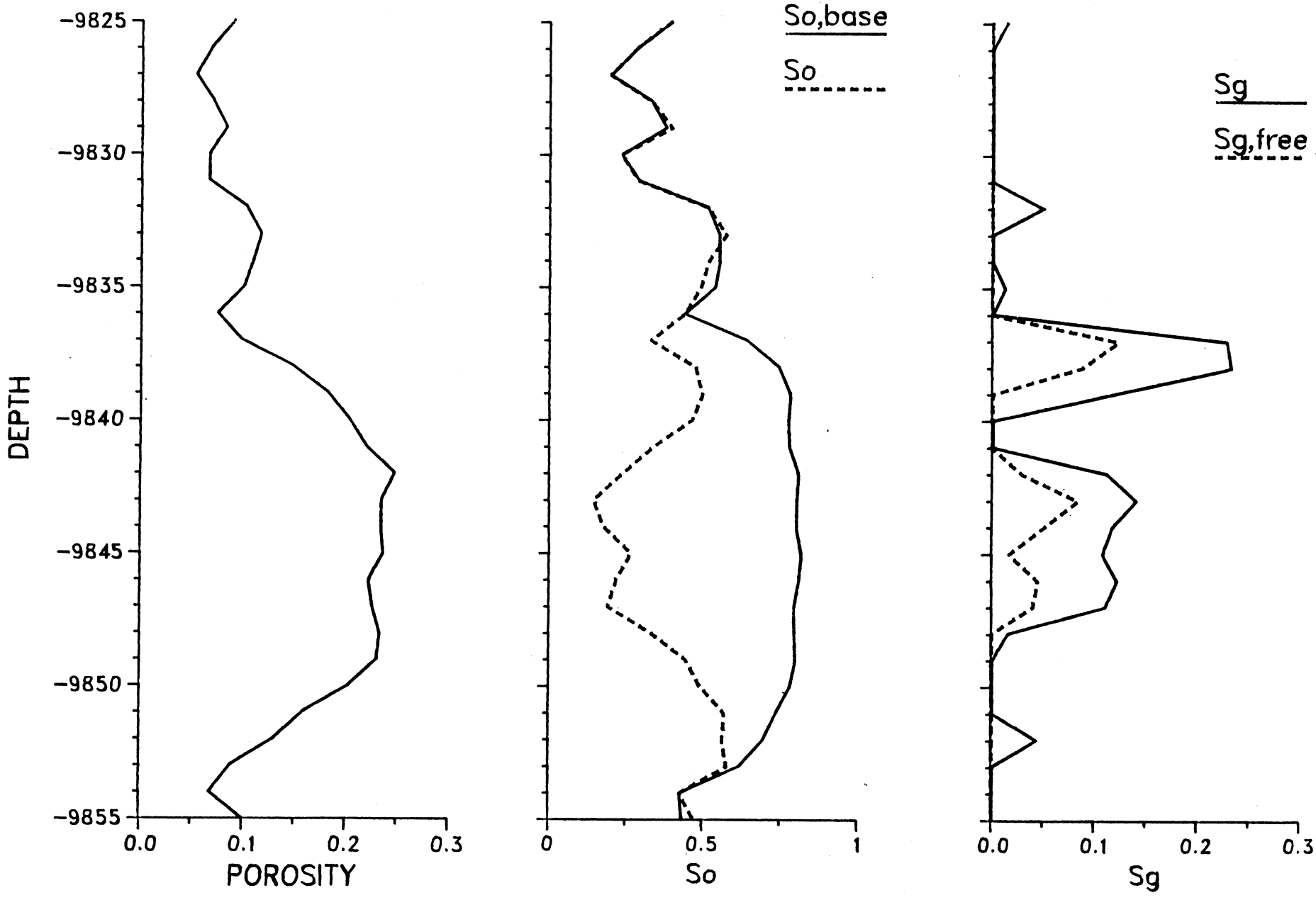

FIGURE A-34 **OBSERVATION #1 9810 FT**

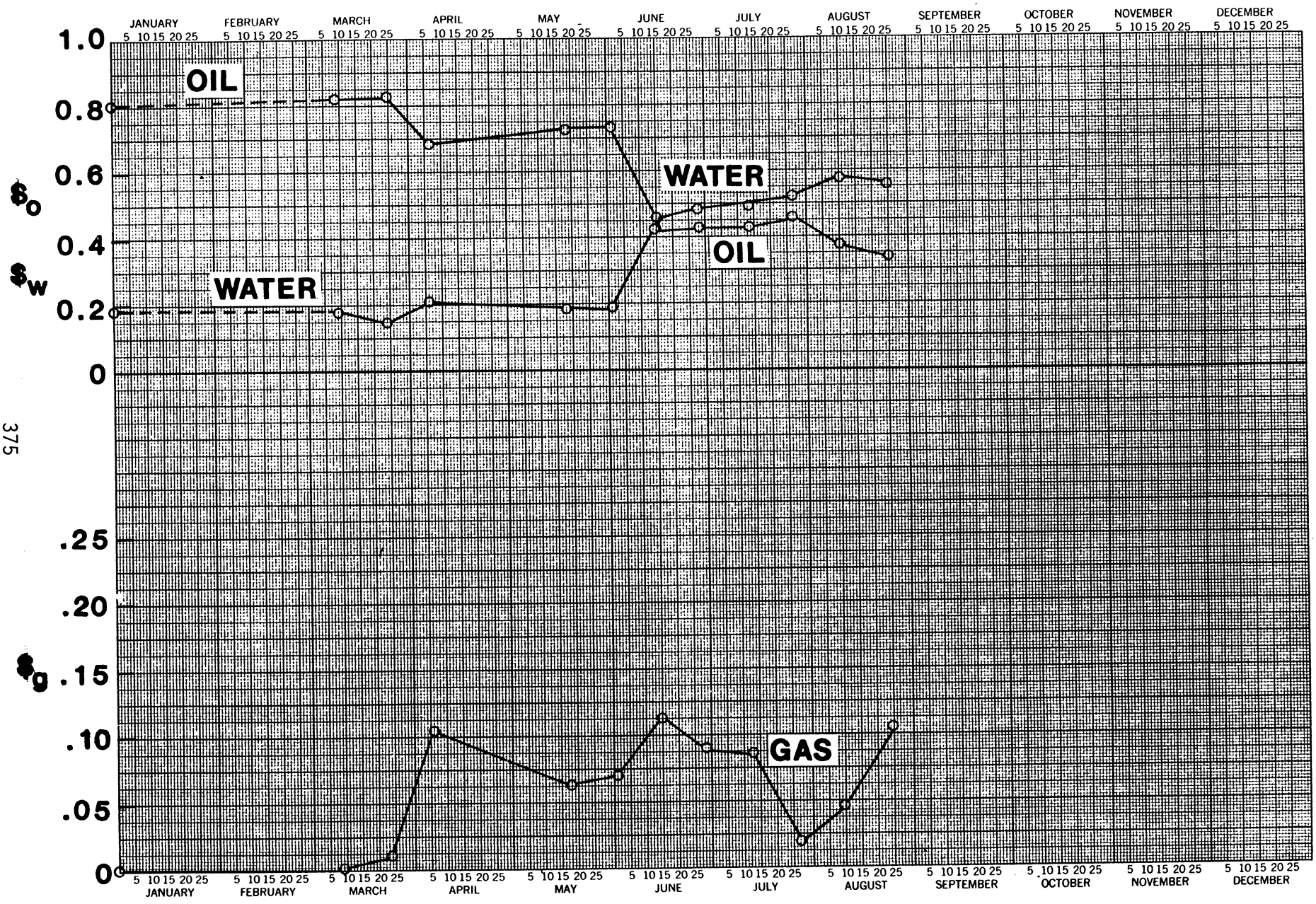

FIGURE A-35 **OBSERVATION #1 9813 FT**

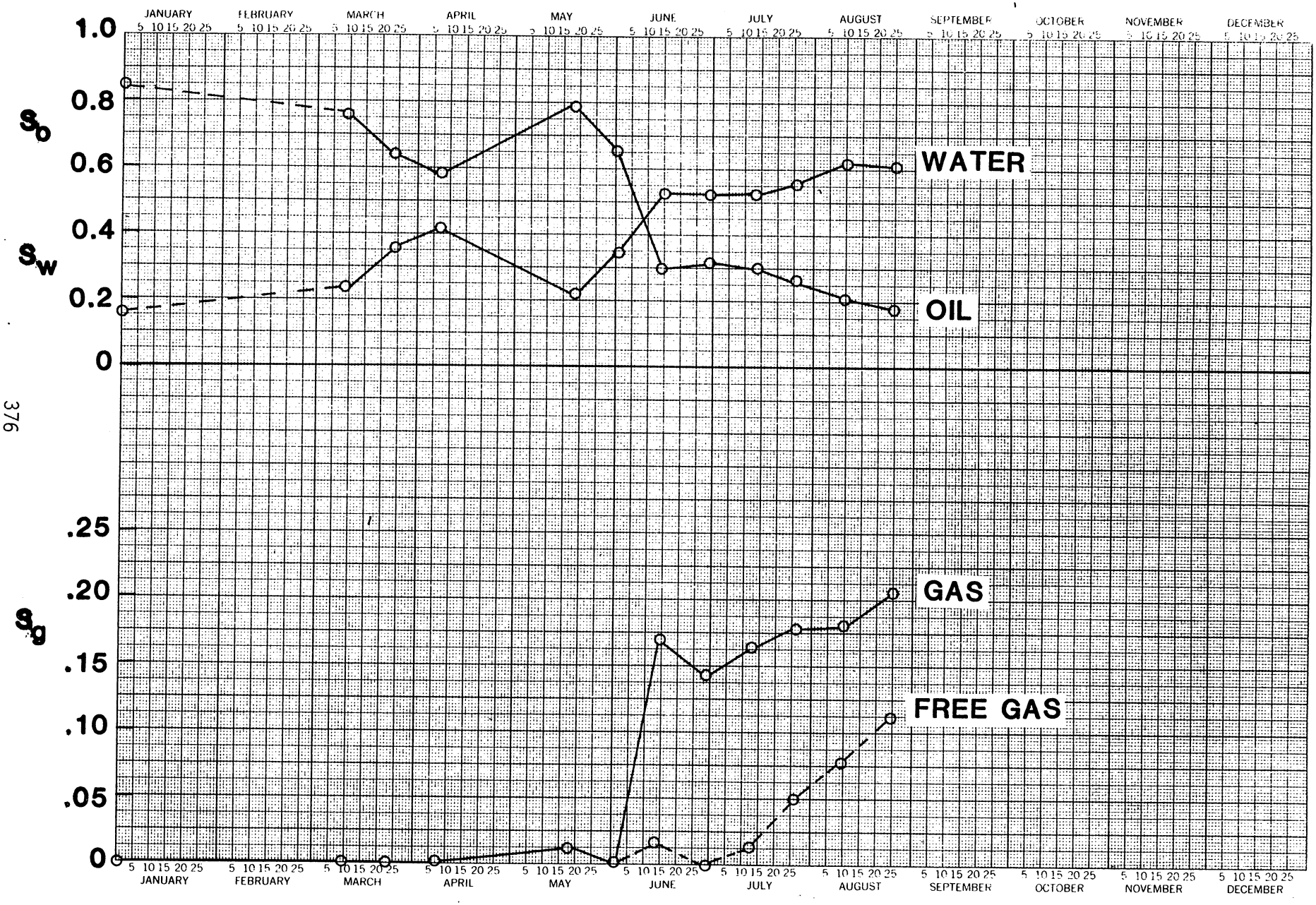

FIGURE A-36 **OBSERVATION #1 9817 FT**

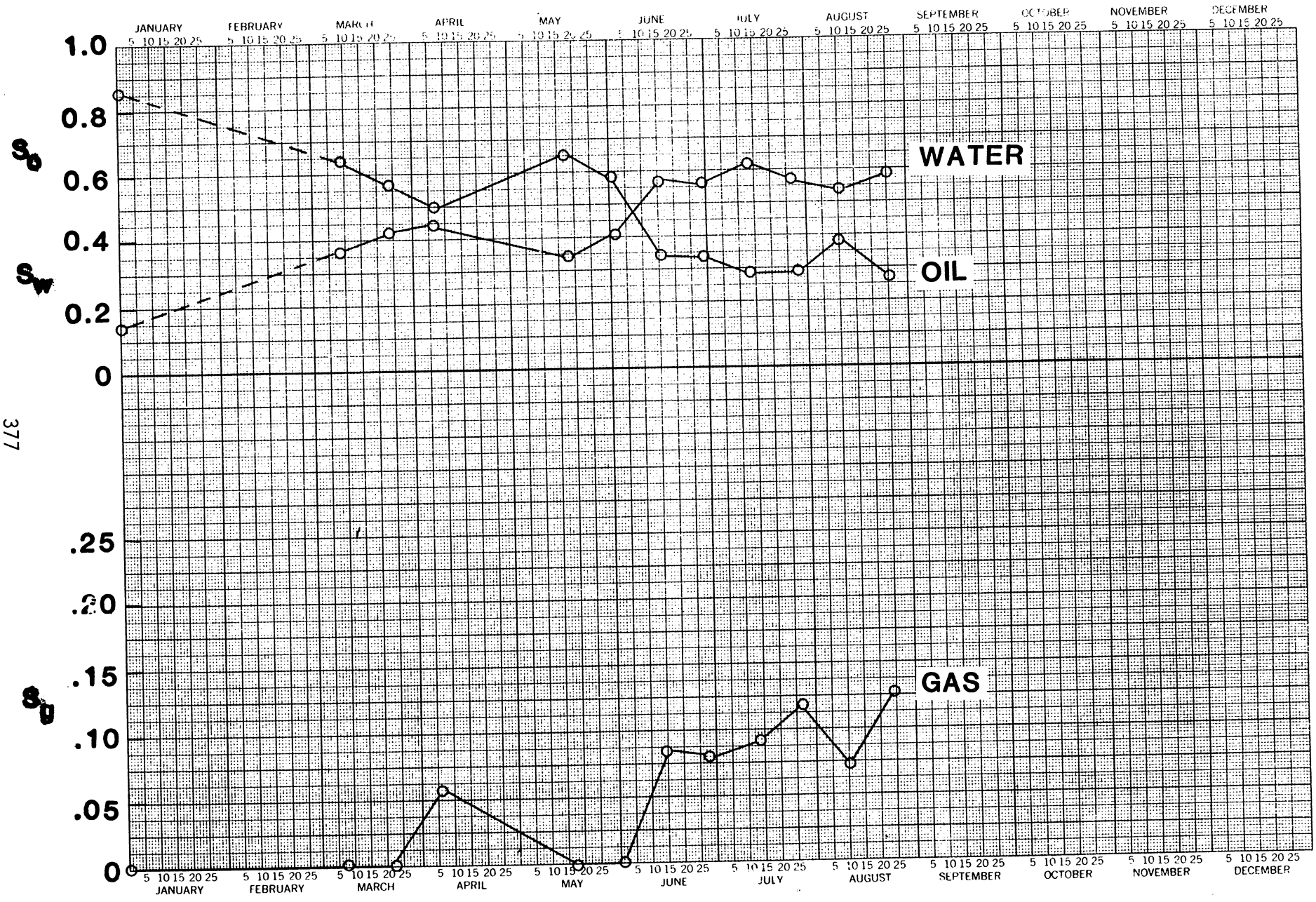

FIGURE A-37 **OBSERVATION #2 9860 FT**

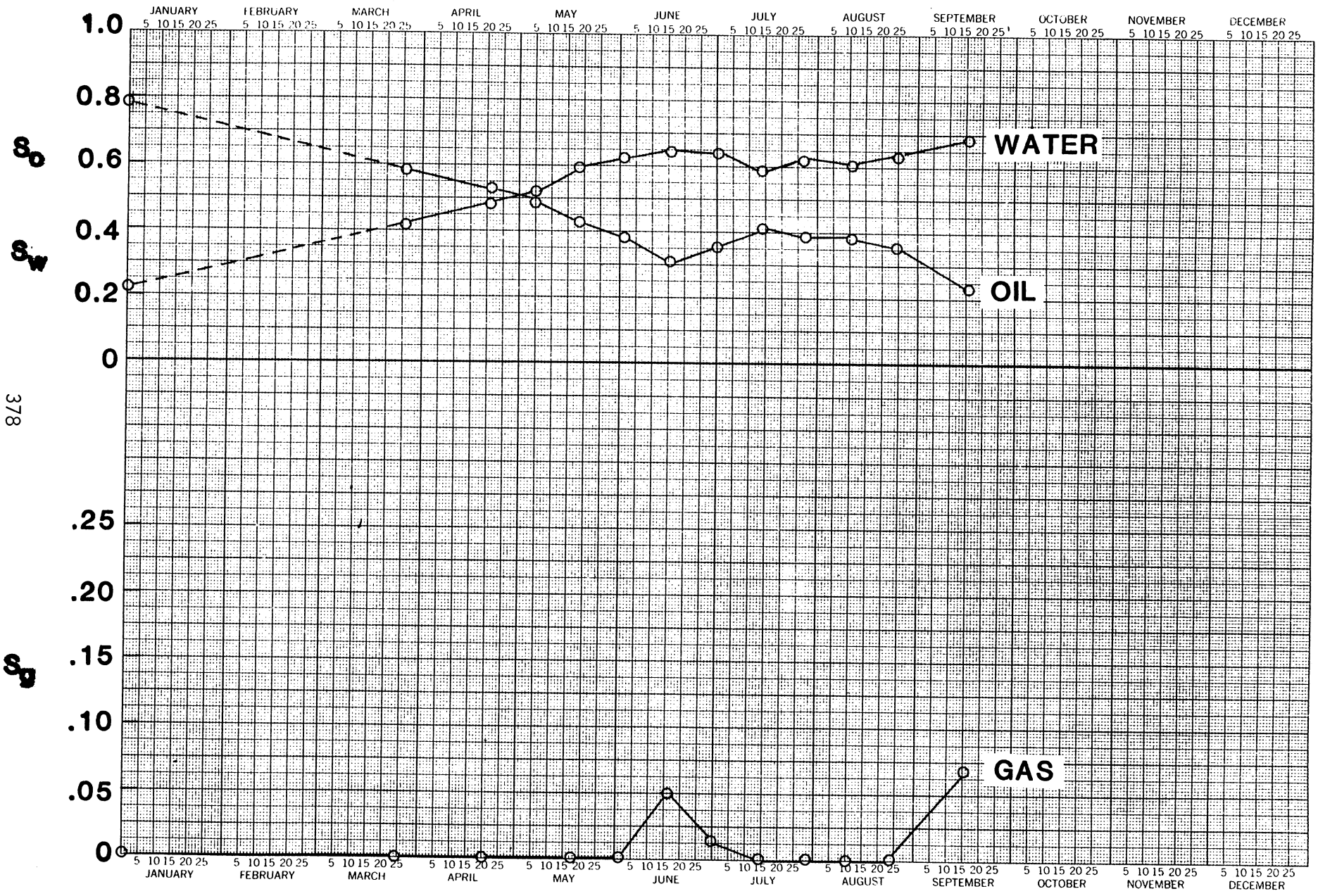

FIGURE A-38 **OBSERVATION #2 9863 FT**

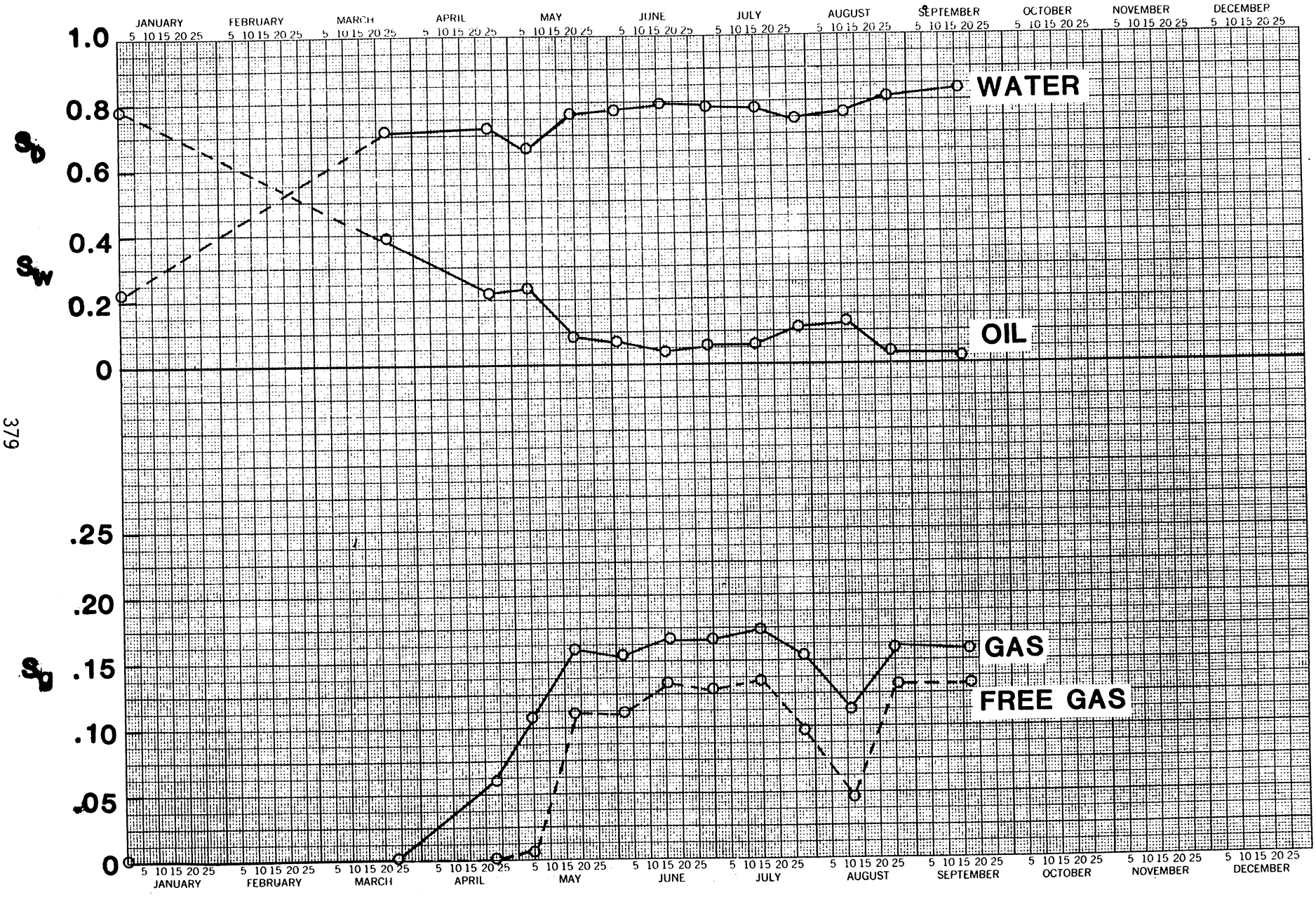

FIGURE A-39 **OBSERVATION #2 9867 FT**

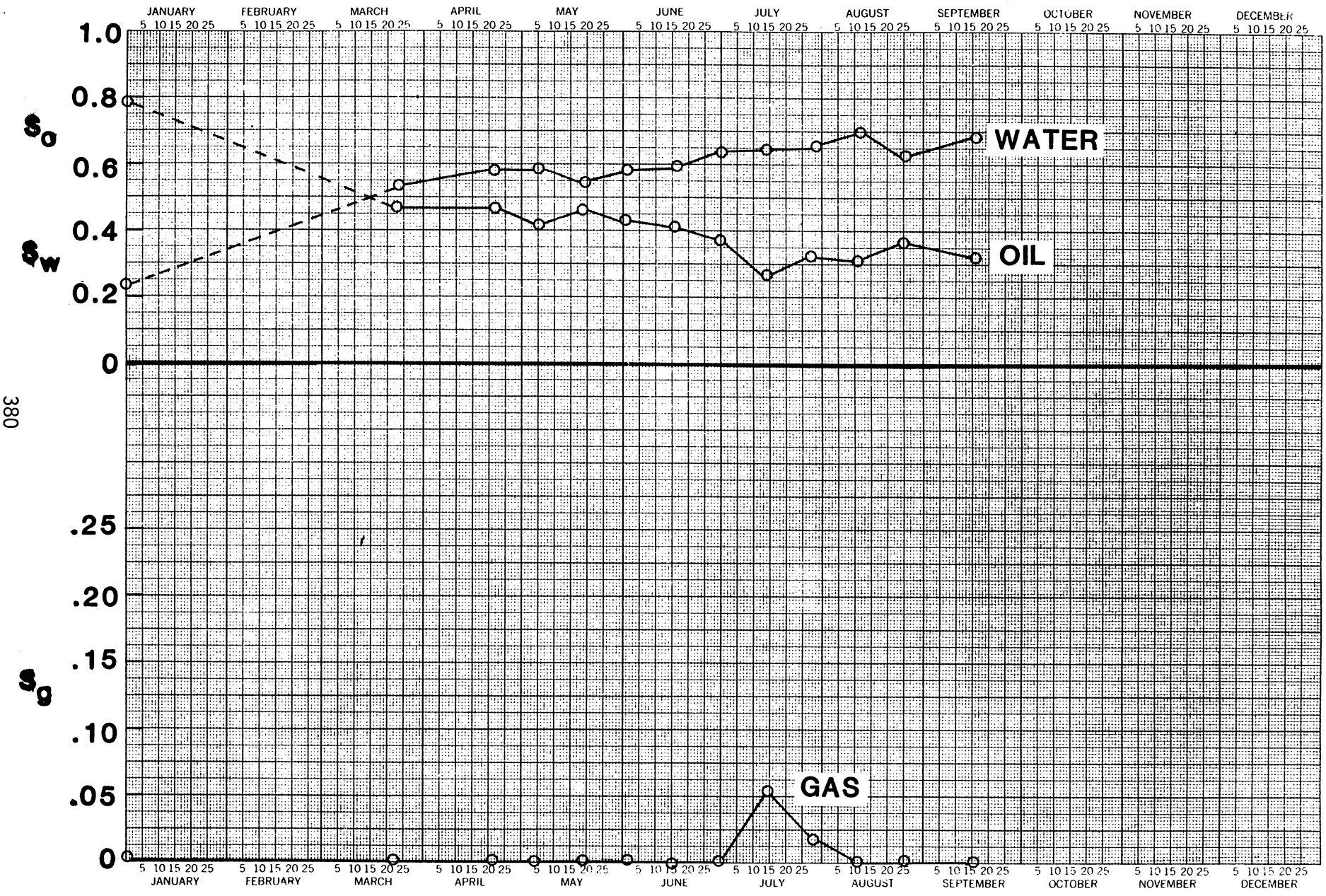

FIGURE A-40 **OBSERVATION #3 9840 FT**

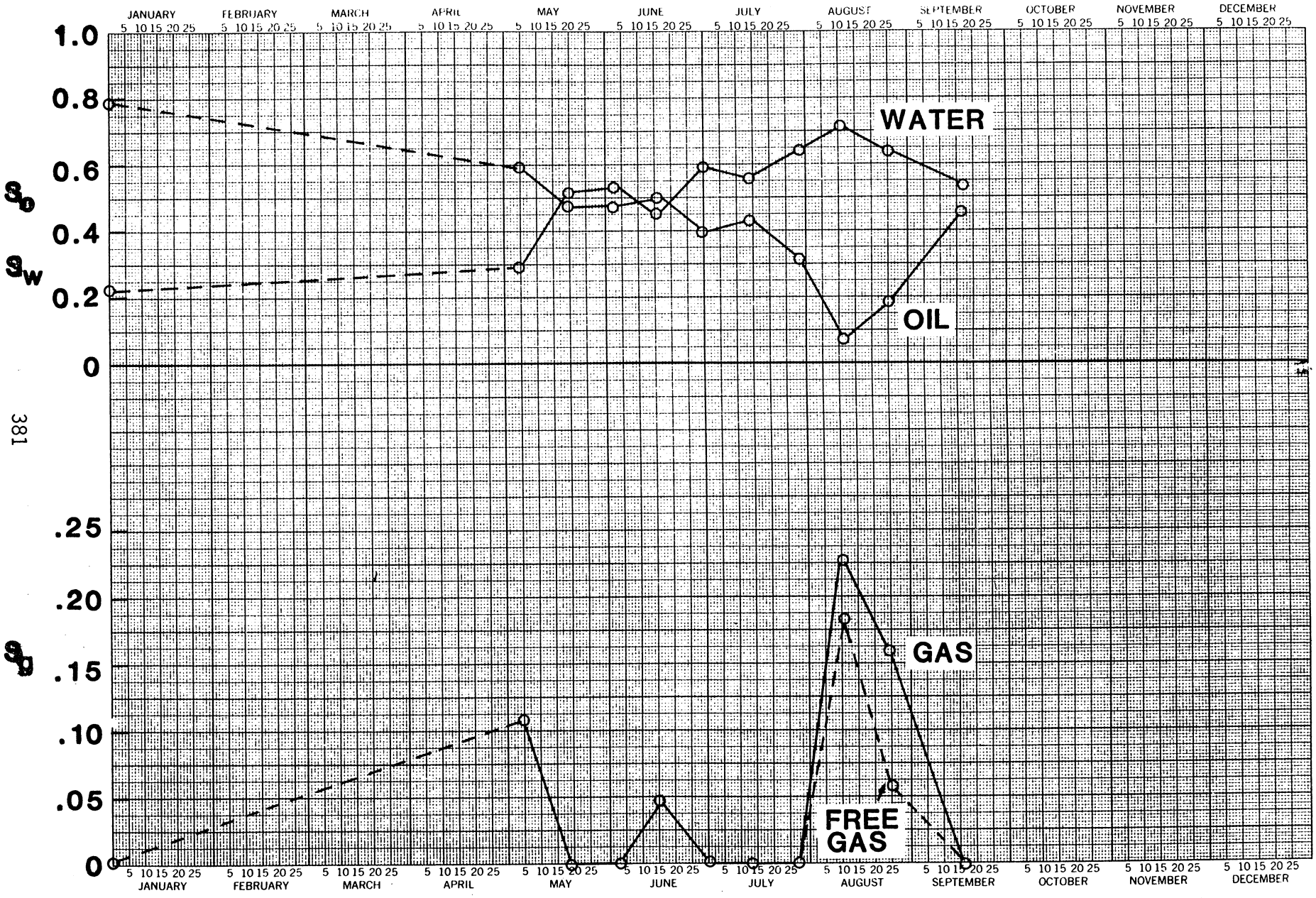

FIGURE A-41 **OBSERVATION #3 9843 FT**

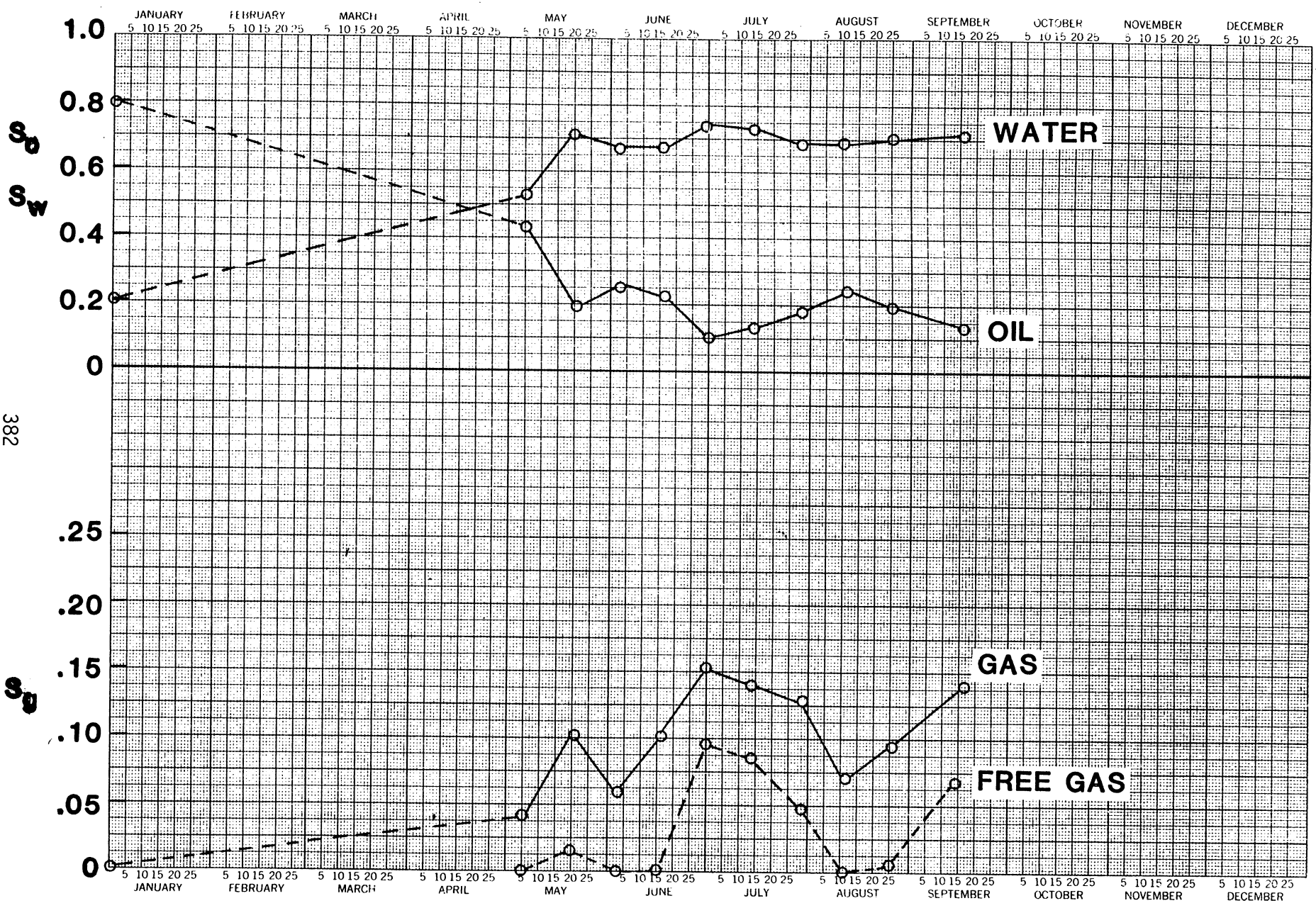

FIGURE A-42 **OBSERVATION #3 9847 FT**

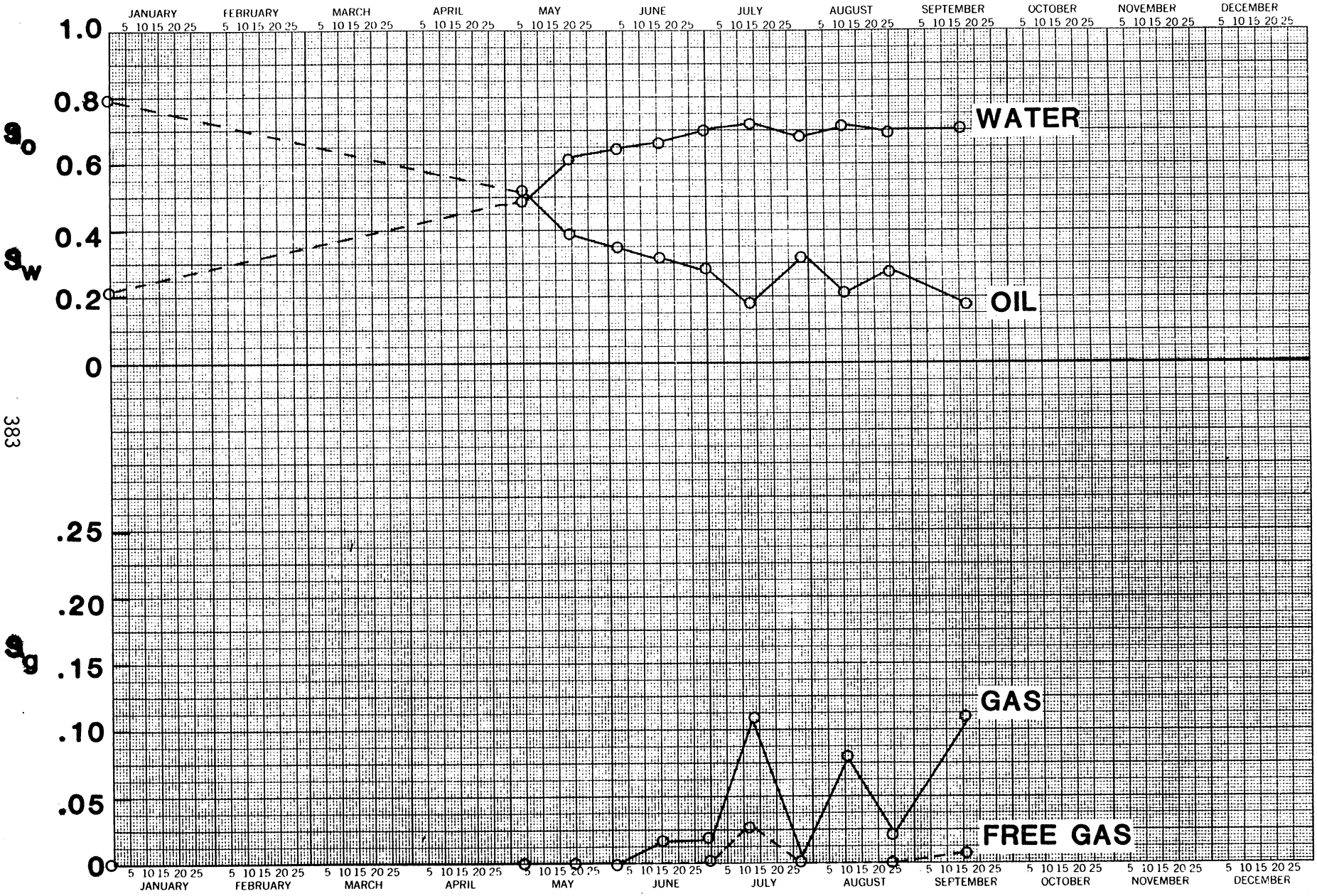

SUB-APPENDIX B

a) Estimation of Free Gas Saturation

The log-derived gas saturations given in Appendix A is actually a measure of reduction in average hydrogen index of the reservoir fluids from some initial value.[2] This will represent dissolved CO_2 to the extent that oil and water are diluted by it as well as free CO_2 gas. To estimate a "free gas" saturation, we assume that oil and water must be saturated with CO_2 at reservoir pressure before a gas phase can form, and that free gas is the excess of the log-indicated gas saturation over that necessary to saturate the oil and water present.

Figure B-1 taken from Reference 7 shows the extent to which CO_2 at various concentrations and pressures swells Little Knife oil. Volumes are relative to the original bubble point. At a given pressure, the ratio of the relative volume on the bubble point curve to the relative volume on the zero percent CO_2 line is the CO_2 swelling factor (F_o).

Data equivalent to that in Figure B-1 are not available for CO_2 in Little Knife brine. Figure B-2, however, shows the effect of temperature, pressure and salinity on CO_2 solubility in water. At Little Knife conditions (245°F, 3600 psi, 240,000 ppm TDS), CO_2 solubility is roughly 2% by weight (60 SCF/bbl). If we assume that CO_2 in aqueous solution has approximately water density, the CO_2 swelling factor for brine (F_w) is 1.02. (Although this is only an estimate, it will not have an important effect on the free gas calculation.)

Free gas saturation is then calculated from:

$$S_{g,free} = \begin{cases} 0 & S_g \leqslant (F_o-1)\,S_o + (F_w-1)\,S_w \\ S_g-(F_o-1)\,S_o -(F_w-1)\,S_w & S_g > (F_o-1)\,S_o + (F_w-1)\,S_w \end{cases}$$

The magnitude of $S_{g,free}$ may not be precisely correct because of compositional effects. The presence or absence of free gas should, however, be correctly predicted by the above equation.

b) Estimation of Residual Oil Saturation for Dissolved CO_2 Displacement

If the magnitude of waterflood residual hydrocarbon phase saturation is unchanged when oil is swollen with CO_2, then the minimum oil saturation that can be obtained with CO_2 where no free gas is formed is:

$$S_{o,min} = S_{or,wf}/F_o$$

FIGURE B-1

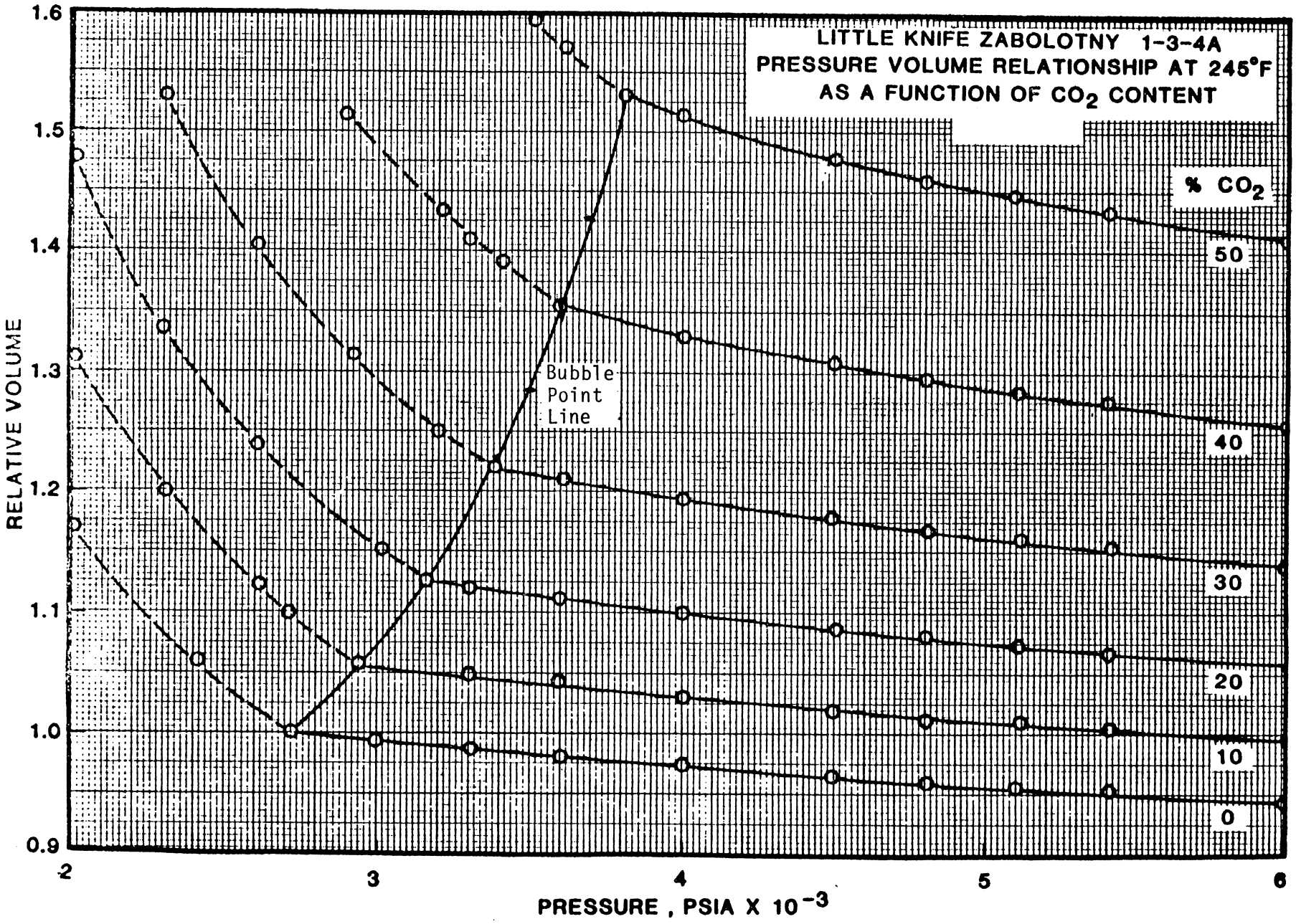
LITTLE KNIFE ZABOLOTNY 1-3-4A
PRESSURE VOLUME RELATIONSHIP AT 245°F
AS A FUNCTION OF CO_2 CONTENT
% CO_2
50
40
30
20
10
0
Bubble Point Line
RELATIVE VOLUME
1.6
1.5
1.4
1.3
1.2
1.1
1.0
0.9
2
3
4
5
6
PRESSURE , PSIA X 10^{-3}

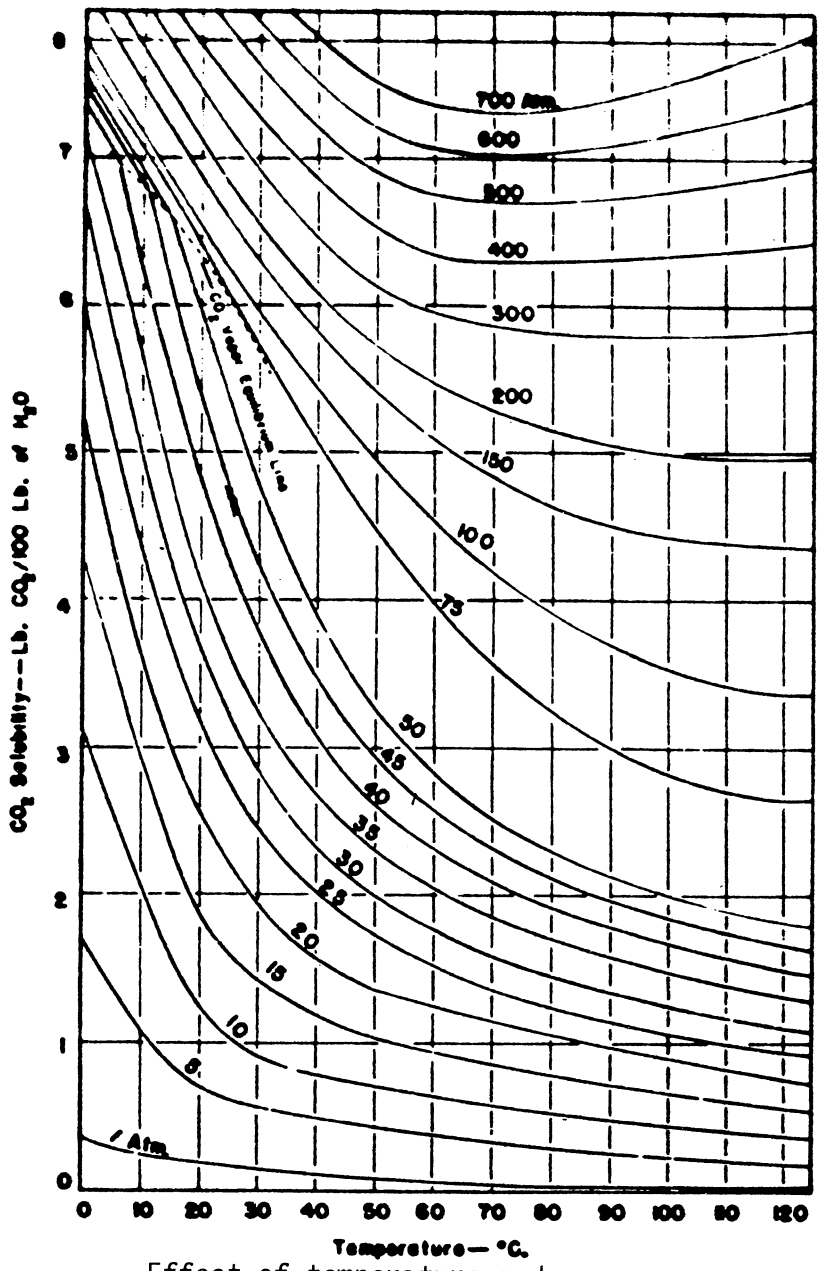

Effect of temperature and pressure upon the solubility of CO_2 in water

FIGURE B-2: CO_2 SOLUBILITY IN DISTILLED WATER (REF. 9) AND BRINE CORRECTION FACTOR FOR CO_2 SOLUBILITY (REF.10)

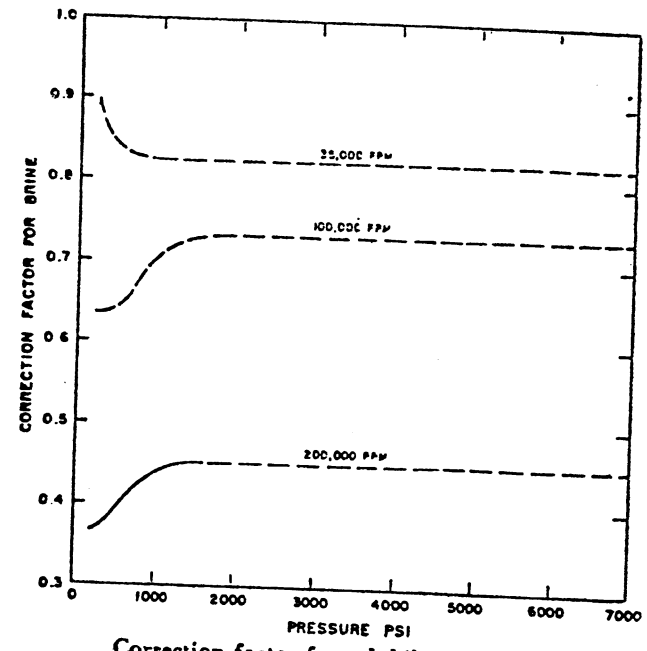

Correction factor for solubility of CO_2 in brine.

SUB-APPENDIX C

Estimation of the Importance of Dispersive Mixing of CO_2 in Oil and Water at Little Knife Conditions

The importance of dispersive mixing at Little Knife conditions can be assessed by looking at a simple system. Figure C-1 shows a layer of the Mission Canyon D zone which initially contains CO_2 (or a fluid containing dissolved CO_2) bounded above and below by layers which contain oil and water only. This might result from a permeability contrast or from instability. We will assume that fluids in all the layers are moving horizontally at the same rate and that the bounding layers are larger than the initially CO_2-saturated layer.

Crank (Ref. 11, pp 13-14) gives an analysis of this system. Figure C-2 shows concentration profiles vs. dimensionless time for a coordinate system moving with the fluids. In Figure C-2, $-1 \leqslant x/h \leqslant 1$ is the initially CO_2-saturated layer. C_o is the initial CO_2 concentration in that layer, and D in this case is the transverse dispersion coefficient.

A correlation allowing estimation of the transverse dispersion coefficient has been given by Perkins and Johnston[12] and is shown in Figure C-3. Any reasonable assumptions for conditions at Little Knife gives values of the dimensionless group $U\sigma d_p/D_o$ in the range of 0.1 - 1.0. The transverse dispersion coefficient will, therefore, be (from Figure C-3) about one-third the molecular diffusion coefficient, depending on the formation resistivity factor, or about 10^{-2} ft^2/day.

In the system of Figure 1 with an initially CO_2-swept layer 4 ft thick (h = 2 ft), dispersive mixing would spread CO_2 vertically into the adjacent layers giving a profile corresponding to $(Dt/h^2)^{1/2} = 1/4$ after 25 days, $(Dt/h^2)^{1/2} = 1/2$ after 100 days, and $(Dt/h^2)^{1/2} = 1$ after 400 days. The time between first CO_2 injection and shut-in at Little Knife was 261 days.

This calculation suggests that dispersive mixing is significant over distances of 4 ft or less at Little Knife conditions although the result is only qualitative because of the idealized geometry. Over much greater distances, dispersive mixing will not be significant as can be seen from Figure C-2.

Figure C-1: Idealized Geometry For Dispersive Mixing Estimate

Figure C-2: Concentration Profiles vs. Dimensionless Time From Crank[11]

Figure C-3: Transverse Dispersion Correlation From Perkins and Johnston[12]

Figure C-1

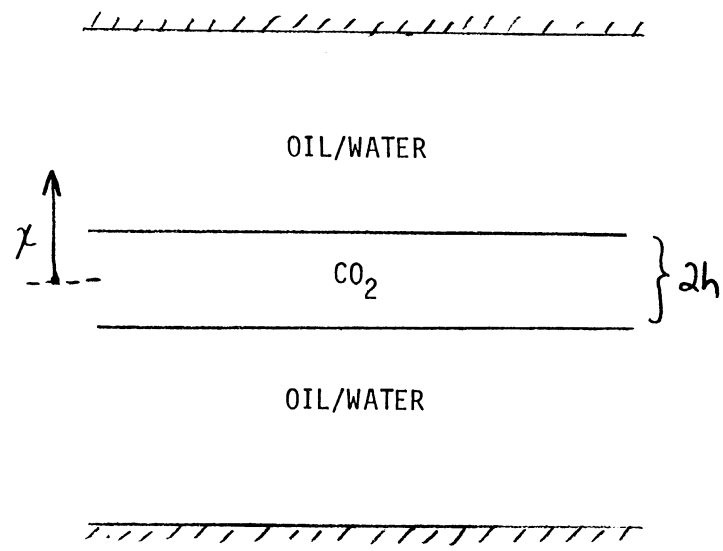

Figure C-2

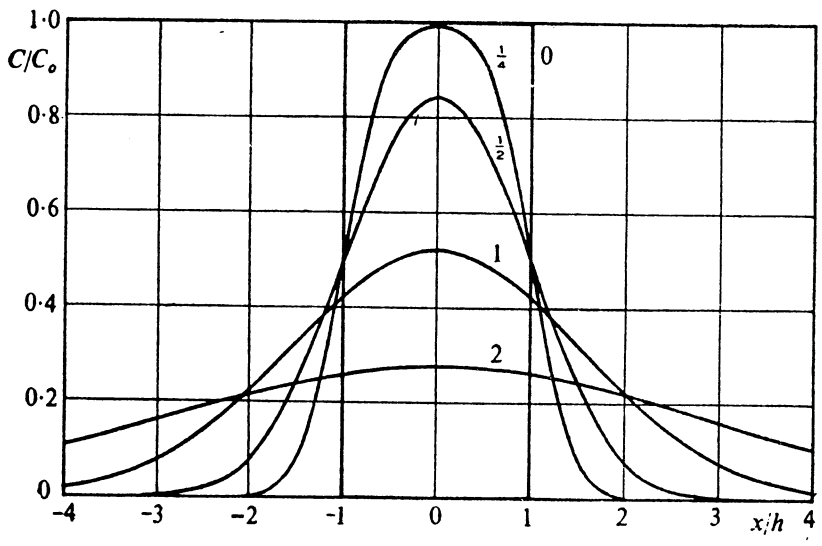

Concentration-distance curves for an extended source of limited extent. Numbers on curves are values of $(Dt/h^2)^{\frac{1}{2}}$.

Figure C-3

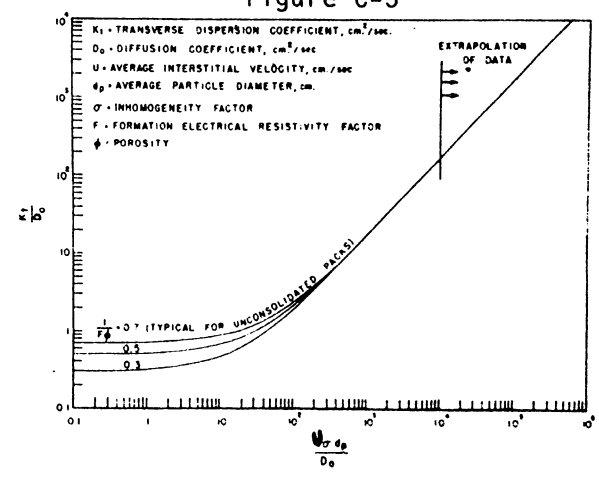

TRANSVERSE DISPERSION COEFFICIENTS FOR POROUS MEDIA.

APPENDIX 47

CORROSION STUDY FOR LITTLE KNIFE CO_2 MINITEST

By

R. A. Morris
S. D. Larkin

Gulf Research & Development Company
Houston Technical Services Center
Houston, Texas

TABLE OF CONTENTS

	Page
Laboratory Investigation	391
Material Selection	392
Field Investigation	392
Discussion	394
References	396

LIST OF TABLES

Table		
1	Water Analysis	397
2	Physical Properties of Reservoir Fluid	398
3	Autoclave Corrosion Tests	399
4	Material Recommendations	401
5	Equipment Corrosion Analysis	402
6	Corrosion Results	403
7	Zabolotny Observation #3 - Visual Inspection	408
8	Pit Depth Corrosion Analysis of Corrosion Nipples in Zabolotny Observation Wells 2 and 3	408

LIST OF FIGURES

Figure		
1	Wellhead Schematic Injection Well	409
2	Wellhead Schematic Observation Well	410
3	Downhole Detail	411
4	Corrosion Sample of C-75	412
5	Corrosion Sample of L-80	412
6	Corrosion Sample of N-80	413
7	Corrosion Sample of N-80 w/Ni	413
8	Corrosion Sample of 316 SS w/Ni	414
9	Corrosion Sample of 316 SS	414

CORROSION STUDY FOR LITTLE KNIFE CO_2 MINITEST

The potential corrosion problems involved in the Little Knife CO_2 Minitest have been investigated in the laboratory and field. The information gained from such studies aids in the selection of materials and the design of well completions for future, effective large scale operations.

LABORATORY INVESTIGATION

For the laboratory investigation, the corrosive environment during CO_2 injection in the Little Knife Minitest was assumed to be a saturated salt brine solution containing about 7000 ppm potassium, 19,000 ppm calcium, 2800 ppm magnesium, 136 ppm sulfate, 300 ppm bicarbonate, and 10 ppm iron in the presence of 10-60 volume percent CO_2, 5-10% H_2S, and the remainder methane.[1*] This environmental description was based on the water analysis and physical properties of typical reservoir fluids obtained from Little Knife wells (Tables 1 and 2).

Autoclave tests (Table 3) designed to simulate representative field environments were performed on various materials to evaluate their potential use in a CO_2 flood. The materials evaluated included the following: 17-4PH, L-80 casing, Incoloy 825, Hastelloy C-276, Inconel 625, Cast 410 stainless steel, K-Monel, and 316 stainless steel. The test results showed that the high nickel-chromium-molybdenum metals, such as Inconel 625, Incoloy 825, and Hastelloy C-276, had the lowest corrosion rates. Although somewhat inferior to the more exotic alloys, 316

---

* References are listed at the end of report.

stainless, K-Monel, and 17-4 PH gave moderate corrosion resistance to CO_2-H_2S-water environments. As expected, carbon steel (L-80) and 410 stainless steel had the highest corrosion rates in the simulated minitest environment.

MATERIAL SELECTION

Based on the guidelines of corrosion resistance and availability of material at the time of selection, the material recommendations for the Little Knife project were made (Table 4)[2]. The wellhead and subsurface completions for the injection and production wells are shown in Figures 1-3.

FIELD INVESTIGATION

Analysis of Equipment Corrosion

Following the termination of the CO_2 minitest, the surface and downhole tubulars and equipment involved in the operation were visually inspected (Table 5) in the field for evidence of corrosion. This inspection indicated that all the equipment appeared to be in relatively good condition.

A tubing inspection for corrosion in all four 2 7/8 in. tubing strings has been completed by service company personnel. According to preliminary field reports, results of the inspection indicate that the coatings (TK-2 and TK-7) were chipped or cracked in the box and pin end areas of numerous joints; otherwise, the integrity of the coatings over the remainder of the pipe appeared to be satisfactory.

In discussion with field personnel, the defects in the coatings are attributed to wireline and logging tool work performed through the tubing during the pilot test. As expected, corrosion was evident in the areas where the coating was

chipped from the tubing wall. Further corrosion analysis will be performed on sectioned joints from the field.

Analysis of Corrosion Coupons

Several two- and four-inch surface coupon racks were placed at various locations in the injection and production lines of the observation and offset wells. A total of twenty-two racks containing metal and coated coupons were evaluated for corrosion resistance. The results of these tests (Table 6)[4,5,6] showed that the corrosion rates were generally low for all materials tested. For example, corrosion for C-75 in various surface locations ranged from only 0.008 to 0.9 mils per year, while no corrosion was detected on 316 stainless steel.

Metal and plastic-coated corrosion coupons were also evaluated in six flow-through type downhole racks in the minitest observation and offset production wells. The downhole rack in the CO_2 injector was not recovered because of well problems. These test results (Table 6)[4,5,6] indicated very low downhole corrosion rates, i.e., 0.1-0.7 mils per year for C-75 and less than 0.07 mils per year for 316 stainless. Of the coated coupons, TK-7 performed best in the more severe downhole production well environments.

In addition to the downhole racks, several downhole corrosion nipples (subs) from Zabolotny Observation Well Nos. 2 and 3 were analyzed for corrosion by visual inspection, pit depth measurements, and photomicrograph analysis of the nickel plating integrity and microstructure of the stainless steels. Corrosion of these nipples was found to vary from zero to moderate on 316 stainless steel and C-75, respectively. Results of the visual inspection of the tubing subs by HTC personnel are shown in Table 7. For comparison, photographs of the samples are

shown in Figures 4 through 9. Moderate corrosion was evident on the C-75 and L-80 nipples as indicated by pit depth measurements performed by an independent laboratory (Table 8). The photomicrograph analysis of the nickel plating showed that the integrity of the nickel plating on the 316 stainless steel and N-80 was satisfactory. No inclusions or deformation of the plating were found on any of the subs. The photomicrograph also revealed no corrosive attack on unplated 316 stainless steel.

DISCUSSION

Overall performance of the materials selected and used in the Little Knife CO_2 project was good. This is evident from field inspection of equipment and the low corrosion rates determined by coupon analysis. Because of insufficient production in the minitest observation wells and the low water cuts (<30%) and low CO_2 production (<1%) in the offset wells, the field test results are not totally conclusive for this particular project. Based on past field experience and laboratory testing, significant corrosion of carbon steel in CO_2-oil-water mixtures does not occur until the water cut approaches about 50%. Apparently, under such conditions, the oil phase provides sufficient protection to the metallic surface to inhibit corrosion at the lower water fractions.

Of all the plastic coatings tested, TK-7 performed best in the production wells where H_2S was present. According to our tests, TK-7 gave better corrosion protection than TK-2 in a water-wet, high temperature, H_2S environment. This finding also has been confirmed by Tuboscope. The failure of TK-7 coating in the Zabolotny Observation Well No. 2 was positively identified from the spectrographic analysis of the ash content in the recovered debris[3] and was attributed primarily to

mechanical operations in the well. Probably because of insufficient H_2S concentration, no visual evidence of TK-2 failure in the injection well was detected.

The only other evidence of failure to date was the recovery of several pieces of Hydril C-B rings from several of the observation wells. Upon examination of the tubing string, it was apparent that the problem was depth related, i.e., poorer condition of rings at greater tubing depths. This problem may be a function of temperature on the Hydril C-B ring material (teflon).

Corrosion rates in the observation wells probably would have been much greater than were actually measured if those wells had been continuously produced, thus, providing a more severe and, possibly, more representative corrosive environment as a result of higher water and CO_2 fractions. Since downhole environments are likely to differ appreciably from one field to another, the results of this study should be used cautiously in predicting corrosion and selecting materials for other CO_2 floods. The corrosion potential for any given CO_2 prospect should always be determined separately.

R. A. Morris

R. A. Morris

S. D. Larkin

S. D. Larkin

APPROVED:

R. D. Shelton

R. D. Shelton
Director
Completion-Production Section

July 6 1982

DATE

REFERENCES

1. R. A. Morris to N. H. Harrison, "Corrosion Testing - Little Knife CO_2 Miniflood," File Note, Reference 4452ST27-07, March 14, 1979.

2. R. A. Morris to J. C. Funderburk, "Materials Recommendations for Little Knife CO_2 Minitest," Internal Correspondence, Reference 4452ST27-07, August 21, 1979.

3. R. V. Brodine to J. L. Goolsby, "Debris from Zabolotny Observation Well No. 2 - Little Knife," Internal Correspondence, Reference 4455AK90-27, April 1, 1981.

4. R. V. Brodine to J. L. Goolsby, "Little Knife Corrosion Tests," Internal Correspondence, Reference 4455AK90-27, March 25, 1981.

5. J. O. Carter to O. E. Stoner, "Little Knife Minitest Corrosion Coupon," Internal Correspondence, Reference 4455AK-90-27, January 11, 1982.

6. R. V. Brodine to J. L. Goolsby, "Little Knife Corrosion Tests," Internal Correspondence, Reference 4455AK90-27, June 5, 1981.

Table 1

Water Analysis - Little Knife Field, North Dakota

Well	P. Glovatski	Kostelnak-State	USA	Fed.Land BF-Gulf	Lind 2	Dolezal 1	Zabolotny 3-3-2B	Hlebechuk
Sample Date	3/24/78	3/24/78	3/24/78	3/24/78	3/24/78	3/24/78	3/24/78	3/24/78
pH	5.9	5.7	5.8	5.6	5.6	5.6	4.1	5.5
Dissolved Solids, ppm	376,000	313,000	346,000	349,000	346,000	341,000	259,000	292,000
Sodium, ppm	125,000	101,000	111,000	110,000	111,000	108,000	71,500	92,200
Calcium, ppm	16,400	18,000	20,000	21,600	18,800	20,400	18,400	17,200
Magnesium, ppm	2,920	1,700	2,190	1,940	2,670	2,190	6,560	2,430
Chlorides, ppm	231,000	192,000	212,000	214,000	212,000	209,000	162,000	180,000
Sulfate, ppm	135	131	135	135	131	135	155	135
Bi-carbonates, ppm	307	254	293	259	405	444	(?)	268
Iron, ppm	18	4	10	8	8	8	12	12

TABLE 2

PHYSICAL PROPERTIES OF RESERVOIR FLUID
LITTLE KNIFE, ZABOLOTNY 1-3-4A

Saturation Pressure	2698 psia
Coefficient of thermal expansion at 4000 psia from 69°F to 245°F	7.2×10^{-4} vol/vol/°F
Density of oil at 2698 psia and 245°F	0.6043 g/ml
Specific volume at 2698 psia and 245°F	0.0265 cu. ft./lb.

Hydrocarbon Analysis

Component	Mole %	Volume %
Nitrogen	0.91	0.27
Carbon Dioxide	1.12	0.51
Hydrogen Sulfide	5.73	2.09
Methane	33.34	15.03
Ethane	9.85	7.01
Propane	6.66	4.88
iso-Butane	1.35	1.18
n-Butane	3.85	3.24
iso-Pentane	1.49	1.45
n-Pentane	1.96	1.89
Hexanes	3.42	3.74
Heptanes-plus	30.32	58.71
Total	100.00	100.00

Properties of Heptanes-plus Fraction

Sp. Gr. (60/60)	0.8390
API Gravity	37.2
Molecular Weight	192

TABLE 3

LITTLE KNIFE CO_2 MINITEST

AUTOCLAVE CORROSION TESTS

Source of Water	Dunn Co., ND	McKensie Co., ND	Synthetic Brine[1]	Dunn Co., ND	McKensie Co., ND
VAPOR COMPOSITION					
Carbon Dioxide, %	35	35	35	85	85
Hydrogen Sulfide, %	15	15	15	15	15
Nitrogen, %	50	50	50	--	--
Temperature, °F	236	240	240	235	240
Pressure, psig	4000	3600	3550	2800	2750
CORROSION RATES, MPY					
17-4 PH	4.9	2.7	6.4	5.2	5.8
L-80 Casing	7.5	6.7	8.0	9.4	8.2
Incoloy 825	0.2	1.3	0.9	1.0	1.1
Hastelloy C-276	0.3	1.2	0.6	3.1	1.0
Inconel 625	0.0	0.8	0.5	1.1	0.9
Cast 410 SS	7.8	10.3	26.6	11.5	9.4
K-Monel	6.9	8.5	5.4	7.2	6.8
316 SS	1.3	4.3	3.1	6.5	1.9
L-80 Casing (Vapor)	--	--	--	--	11.1

1. Synthetic Brine Composition: NaCl 250,000 Mg/L, $CaCl_2$ 50,000 Mg/L, Distilled H_2O.

TABLE 3 (continued)

LITTLE KNIFE CO_2 MINITEST

AUTOCLAVE CORROSION TESTS

Source of Water	Dunn Co., ND diluted 1:1 w/distilled water*	Dunn Co., ND diluted 20:1 w/distilled water*
Vapor Composition		
Carbon Dioxide, %	85	85
Hydrogen Sulfide, %	15	15
Nitrogen, %	0	0
Temperature, °F	240	232
Pressure, psig	2250	2300
Corrosion Rates, MPY		
17-4 PH	4.1	3.6
L-80 Casing	10.0	11.0
Incoloy 825	0.6	1.6
Hastelloy C-276	0.5	0.8
Inconel 625	0.4	0.6
Cast 410 SS	11.4	3.4
K-Monel	7.1	7.8
316 SS	3.6	1.6

* Autoclave O_2 purged w/CO_2

TABLE 4

MATERIAL RECOMMENDATIONS[2]

LITTLE KNIFE FIELD, NORTH DAKOTA

Equipment	Material
Surface Water Injection Line	Standard 2 in. schedule 80 line pipe internally coated with TK-75, couplings coated with Ryton coupling guard
Surface CO_2 Injection Line	Standard 2 in. schedule 80 line pipe with no internal coating (water-free CO_2 to be used)
Injection and Production Wellheads	316 Stainless Steel internally cladded with Inconel 600. Master and wing valves w/ internally cladded Inconel bores and 17-4 PH trim.
Injection Tubulars	2 7/8 in. OD C-75 Hydril CS-CB tubing internally coated with TK-2
Production Tubulars	2 7/8 in. OD C-75 Hydril CS-CB tubing internally coated with TK-7
Landing Nipples	Inconel 718; X-750, heat treated to MR01-75
Downhole Pressure Monitor and Chamber	Chamber containing Hydril CS-CB tool joints, internally coated with TK-2 (injector) and TK-7 (producer).
Gas Lift Valves	Heat treated mandrel, internally coated with TK-7, 303 stainless steel valve, Viton O-rings, stainless gasket, monel seat and latches
Packer	Baker FB-1 with G-22 locator sub and sealbore extension, internally and externally coated with TK-7, mandrel to conform to C-75 specs.

TABLE 5

EQUIPMENT CORROSION ANALYSIS

LITTLE KNIFE FIELD, NORTH DAKOTA

Equipment	Material	Visual Inspection	Comments	Current Status
Surface water injection line	2 in. schedule 80 line pipe internally coated with TK-75	Good condition	No visible pitting	Pipe used in field for other purposes
Surface CO_2 injection line	2 in. schedule 80 line pipe	Good condition	No visible pitting	Pipe used in field for other purposes*
Injection and production wellheads	316 stainless steel internally cladded w/ Inconel, 17-4 PH valve trim	--	--	Sent to manufacturer (Gray Tool). Report to be issued.
Injection tubulars	2 7/8 in. OD C-75 Hydril CS-CB with TK-2	--	--	Tubing inspection report by Tuboscope to be issued.
Production tubulars	2 7/8 in. OD C-75 Hydril CS-CB with TK-7	Coating failure[3] in one string	Failure possibly due to mechanical damage	Tubing inspection report by Tuboscope to be issued.
Landing nipples	Inconel 718	Excellent condition	No evidence of corrosion	Analysis procedure to be determined.
Downhole pressure monitor and chamber	Chamber containing tool joints internally coated with TK-2 in injector and TK-7 in producer	Good	No apparent evidence of corrosion	To be inspected with tubing. Returned to stock.
Gas lift valve	Internally coated with TK-7, 303 SS valve, Viton O-rings, SS gasket, monel seat and latches	Good	--	Sent to manufacturer (Baker). Report to be issued.

* Corrosion rates from coupons -- .03-.04 mpy

TABLE 6

CORROSION RESULTS[4,5,6]

LITTLE KNIFE FIELD, NORTH DAKOTA

Downhole Flow-Through Racks

Rack No.	Location	Material	Coating	Corrosion Rate (mils per year)	Remarks
1	B. Zabolotny	C-75		0.2	
		N-80		0.2	
		316 SS		0.0	
			TK-2		One large blister.
			TK-7		Good. No defects.
			TK-69		Numerous blisters.
			TK-77		Good. No defects.
2	E. E. Miller	C-75		0.7	
		N-80		0.3	
		316 SS		0.07	
			TK-2		Blisters, some broken.
			TK-7		Many small cracks, but intact.
			TK-69		Numerous blisters, some broken.
			TK-77		Coating missing over 4 large areas.
3	Hurinenko	C-75		0.1	
		N-80		0.1	
		316 SS		0.0	
			TK-2		Numerous small blisters.
			TK-7		Good. No defects.
			TK-69		Numerous blisters, some broken.
			TK-77		Evident disbonding.
4	Sabrosky	C-75		0.1	
		N-80		0.1	
		316 SS		0.0	
			TK-2		Three small blisters.
			TK-7		Good. No defects.
			TK-69		Good. No defects.
			TK-77		One large blister.

TABLE 6 (continued)

CORROSION RESULTS[4,5,6]

LITTLE KNIFE FIELD, NORTH DAKOTA

Downhole Flow-Through Racks

Rack No.	Location	Material	Coating	Corrosion Rate (mils per year)	Remarks
5	Zabolotny	C-75		0.3	
		N-80		0.5	
		316 SS		0.07	
			TK-2		Blisters, one large holiday.
			TK-7		Good. No defects.
			TK-69		Blistered, disbonded.
			TK-77		Good. No defects.
6	J. Tachenko	C-75		0.1	
		N-80		0.1	
		316 SS		0.0	
			TK-2		Blisters, cracks.
			TK-7		Good. No defects.
			TK-69		A few small blisters.
			TK-77		Several blisters, disbonding.

4-inch Surface Racks

Rack No.	Location	Material	Coating	Corrosion Rate (mils per year)	Remarks
1	Downstream of high pressure Scrubber CTB#2	C-75		0.05	
		L-80		0.06	
		4140		0.03	
		316 SS		0.0	
2	Downstream of Treater #1 at CTB #2	C-75		0.1	
		L-80		0.2	
		4140		0.1	
		316 SS		0.0	

TABLE 6 (continued)

CORROSION RESULTS[4,5,6]

LITTLE KNIFE FIELD, NORTH DAKOTA

4-inch Surface Racks

Rack No.	Location	Material	Coating	Corrosion Rate (mils per year)	Remarks
3	Bad oil (recycle) line at CTB #2	C-75		0.6	
		L-80		1.9	
		4140		0.8	
		316 SS		0.0	
4	Downstream of Treater #3 on Water Leg-CTB #2	C-75		0.2	
		L-80		0.3	
		4140		0.2	
		316 SS		0.0	
5	Downstream of Treaters on oil Line going into boot-CTB #2		TK-2		Good. No defects.
			TK-7		Good. No defects.
			TK-69		Good. No defects.
			TK-77		Good. Mechanical damage.
6	Downstream of Low Pressure Scrubber CTB #2		TK-2		Good. No defects.
			TK-7		Good. Mechanical damage.
			TK-69		Good. No defects.
			TK-77		Good. Color change.
7	Upstream of Pressure Scrubber CTB #2		TK-2		Good. No defects.
			TK-7		Good. No defects.
			TK-69		Good. No defects.
			TK-77		Good. Color change.
8	Downstream of Treater #2 on Water Leg-CTB #2		TK-2		Good. No defects.
			TK-7		Good. No defects.
			TK-69		Good. No defects.
			TK-77		Good. Mechanical damage.

TABLE 6 (continued)

CORROSION RESULTS[4,5,6]

LITTLE KNIFE FIELD, NORTH DAKOTA

2-inch Surface Racks (Metal Coupons)

Rack No.	Location	Exposure Time (Days)	Material	Corrosion Rate (mils per year)
164	Downstream of Casing Valve Tedrow 1-11-1A	518	C-75 L-80 4140 316 SS	0.4 0.6 0.3 0.0
165	Downstream of casing choke on pumping well Tedrow 6-12-2A	225	L-80 4140 316 SS	0.0 0.0 0.0
167	CO_2 injection system line	95	C-75 L-80 4140 316 SS	0.04 0.04 0.03 0.00
168	Salt water injection line	341	C-75 L-80 4140 316 SS	To be calculated
175	Recycle-Bad Oil Line - CTB #2	237	C-75 L-80 4140 316 SS	0.009 0.009 0.03 0.00
176	Downstream of Casing Valve Tedrow 6-12-2A Gas Line	238	C-75 L-80 4140 316 SS	0.9 1.2 1.0 0.0
177	Downstream of Casing Valve L. Kostelnak 2-29-1D Gas Line	238	C-75 L-80 4140 316 SS	0.008 0.006 0.02 0.00

TABLE 6 (continued)

CORROSION RESULTS[4,5,6]

LITTLE KNIFE FIELD, NORTH DAKOTA

2-inch Surface Racks (Metal Coupons)

Rack No.	Location	Exposure Time (Days)	Material	Corrosion Rate (mils per year)
178	Downstream of Casing Valve-Kostelnak State 1-36-2B Gas Line	238	C-75	0.02
			L-80	0.02
			4140	0.03
			316 SS	0.00

2-inch Surface Racks (Coated Coupons)

Rack No.	Location	Exposure Time (Days)	Coating	Remarks
169	Downstream of Casing Valve-S. Burian 1-22-1A	427	TK-2	Good. No defects.
			TK-7	Good. No defects.
			TK-69	Good. Mechanical damage.
			TK-77	Good. No defects.
170	Downstream of Casing Valve-D. Dolezal 1-17-1A	517	TK-2	Good. Color change.
			TK-7	Good. No defects.
			TK-69	Good. No defects.
			TK-77	Poor. Failed at edges.
171	Downstream of Casing Valve-State 1-16-2B	519	TK-2	Good. No defects.
			TK-7	Good. No defects.
			TK-69	Good. No defects.
			TK-77	Good. No defects.
172	Downstream of Casing Valve-A. Zabolotny 1-4-4C	517	TK-2	Good. No defects.
			TK-7	Good. No defects.
			TK-69	Good. No defects.
			TK-77	Good. No defects.
173	CO_2 injection system line	95	TK-2	Good. Minor mechanical damage.
			TK-7	Good. Minor mechanical damage.
			TK-69	Good. Minor mechanical damage.
			TK-77	Good. Minor mechanical damage.
174	Saltwater Injection Line	341	TK-2	Good. No defects.
			TK-7	Good. No defects.
			TK-69	Good. Color change.
			TK-77	Poor. Failed at one end.

Table 7

ZABOLOTNY OBSERVATION #3

VISUAL INSPECTION

2 7/8 in. O.D. tubing subs

Material	Remarks
C-75	Moderate corrosion, some pitting
L-80	Moderate corrosion, some pitting
N-80	Slight corrosion
N-80 w/ Ni plating	Very slight corrosion
316 SS w/ Ni plating	No corrosion evident
316 SS	No corrosion evident

Table 8

PIT DEPTH CORROSION ANALYSIS OF CORROSION NIPPLES

IN ZABOLOTNY OBSERVATION WELLS 2 AND 3

SAMPLE	PIT DEPTH (INCHES)	
C-75	.017	
	.0004	
	.0105	AVG. = .0101
	.010	
	.0125	
L-80	.010	
	.0155	
	.007	AVG. = .0123
	.013	
	.016	

NOTE: Depth was measured on the 5 deepest-appearing pits on the inside surface. Exposure time was approximately one year. General corrosion was not accounted for by localized measurements.

FIGURE 1
WELLHEAD SCHEMATIC
INJECTION WELL

ALL TUBING CONNECTIONS TO BE IN ACCORDANCE WITH NACE STANDARD MR-01-75 WITH 7 CR-4 NiPH TRIM WITH INTERNAL COATING OF TK-2, BOTTOM HEAD CONNECTION TO BE 2-7/8 HYDRIL CS–CB THREAD PIN.

CASING CONNECTIONS
TO BE STANDARD.

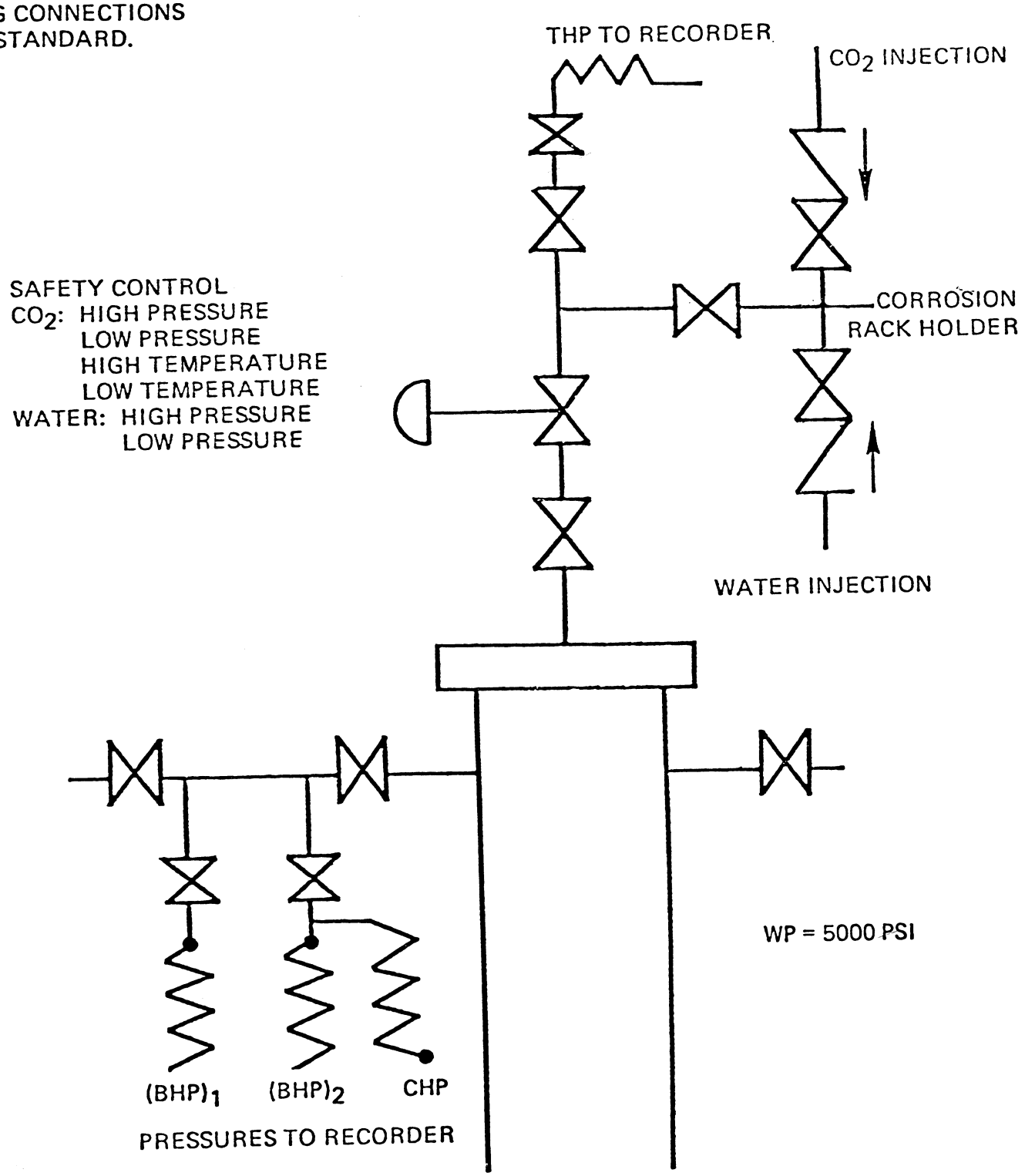

FIGURE 2

WELLHEAD SCHEMATIC
OBSERVATION WELL

ALL TUBING CONNECTIONS TO BE IN ACCORDANCE WITH NACE STANDARD MR–01–75. TRIM WILL BE 17CR–4NiPH. INTERNALLY COAT WITH TK-7. BOTTOM HEAD CONNECTION TO BE 2 7/8"HYDRIL-CS–CB THREAD PIN.

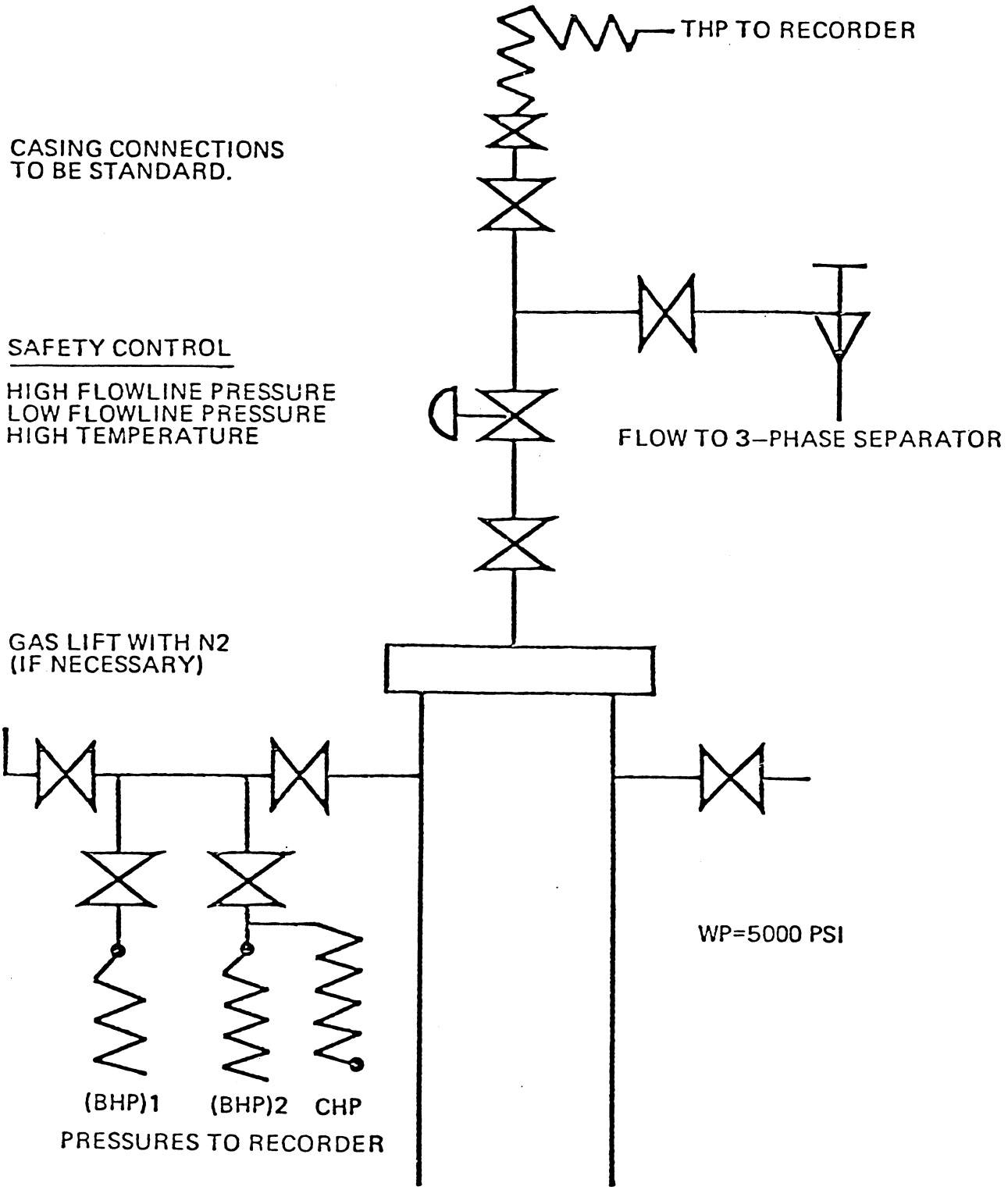

FIGURE 3
DOWNHOLE DETAIL

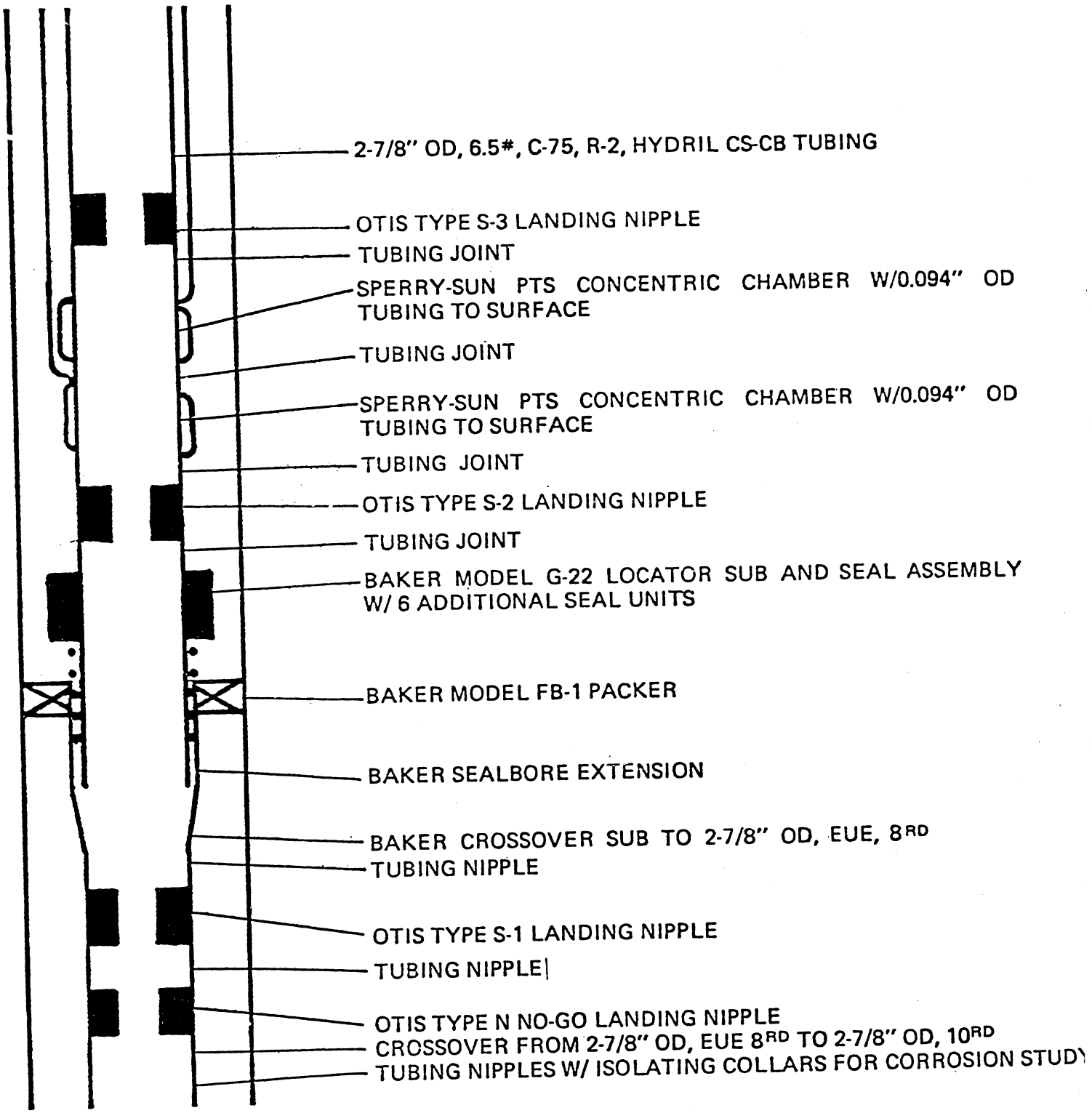

FIGURE 4

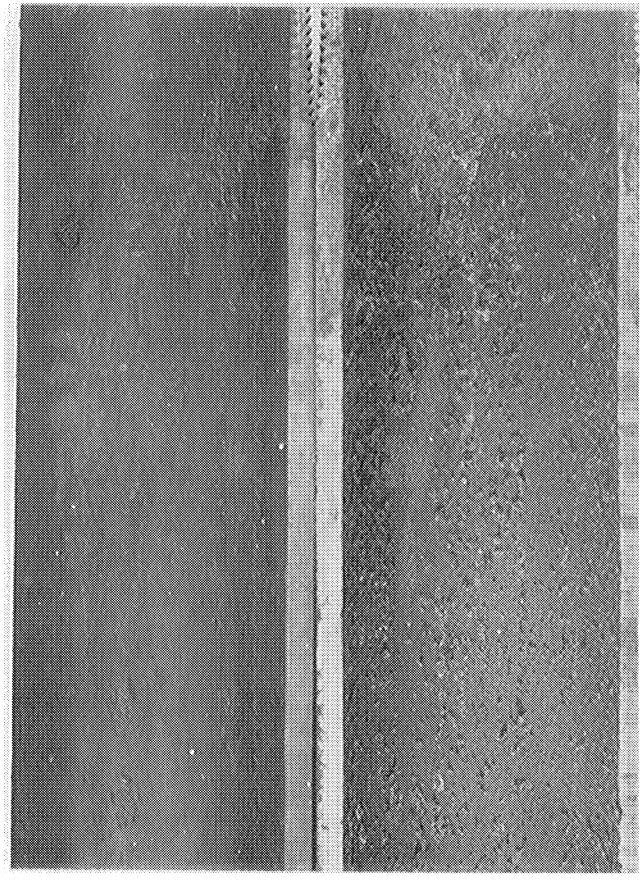

CLEANED AS RECEIVED

C-75

FIGURE 5

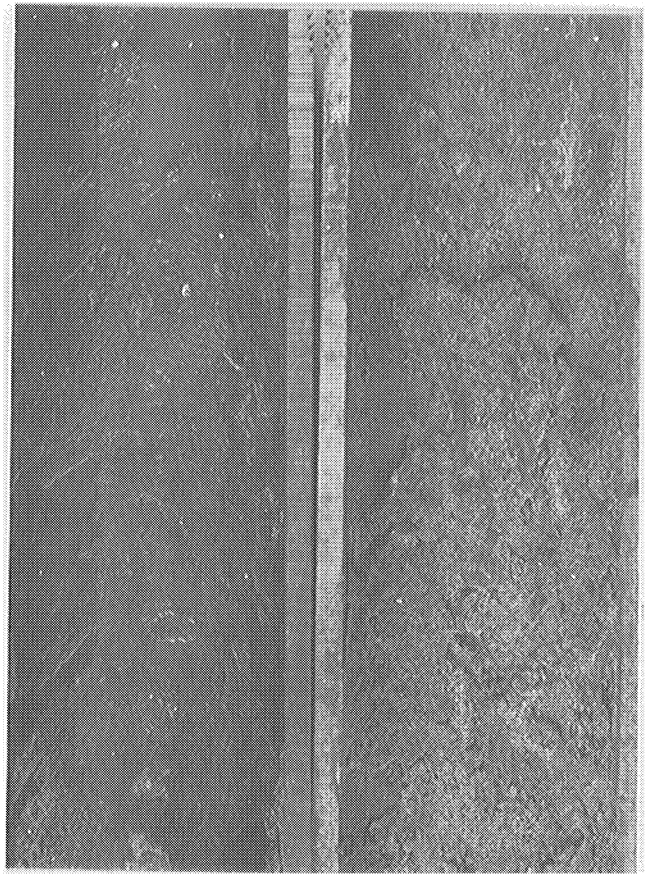

CLEANED AS RECEIVED

L-80

FIGURE 6

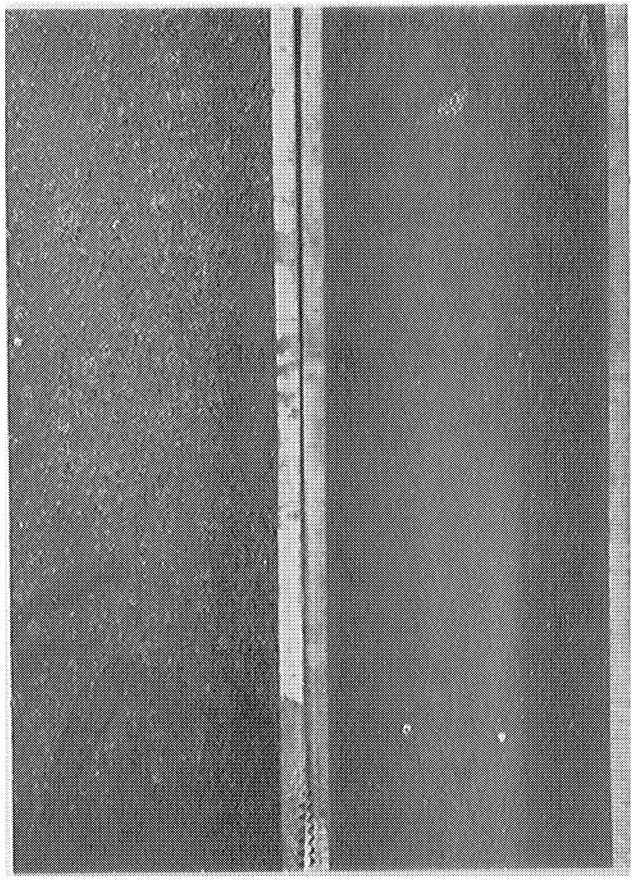

CLEANED AS RECEIVED

N-80

FIGURE 7

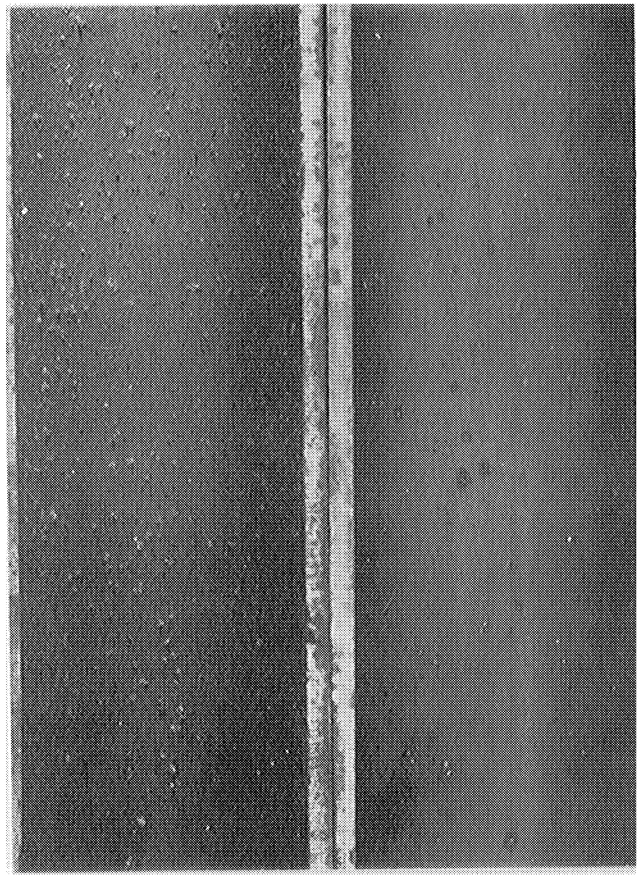

CLEANED AS RECEIVED

N-80 w/Ni

FIGURE 8

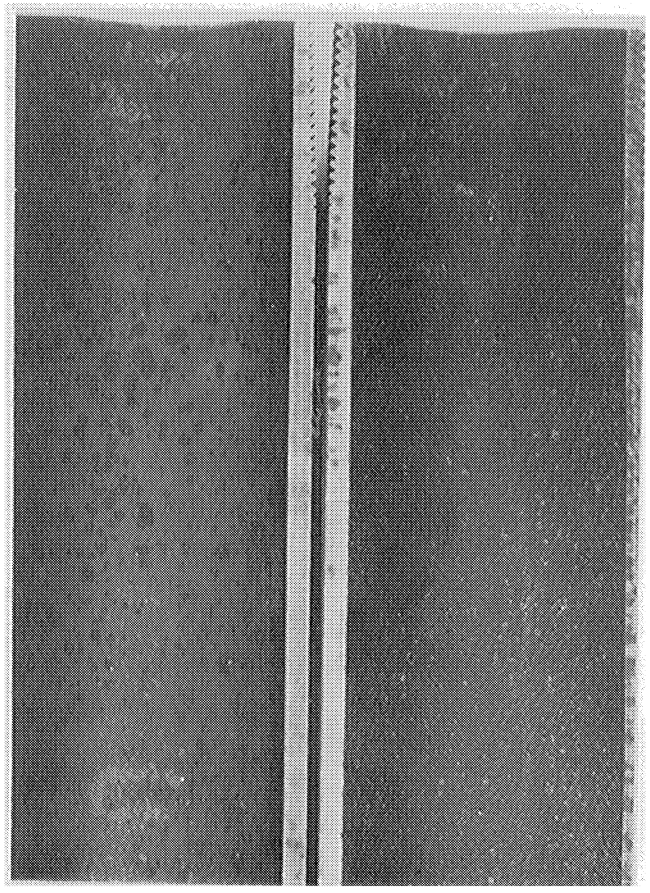

CLEANED AS RECEIVED

316 SS w/Ni

FIGURE 9

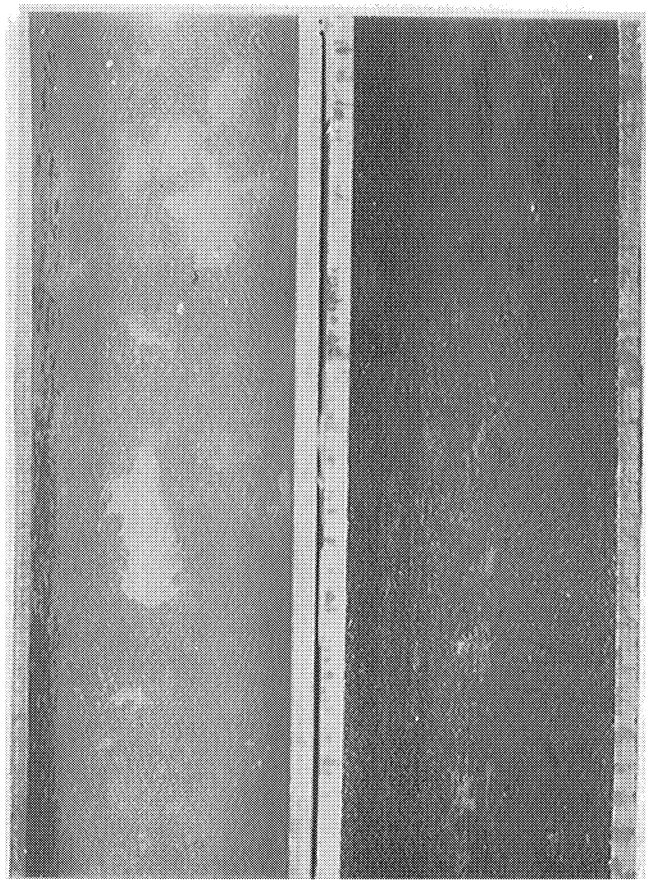

CLEANED AS RECEIVED

316 SS

☆U.S. GOVERNMENT PRINTING OFFICE: 1983- 669-030/37